

TECHNICAL VOLUME

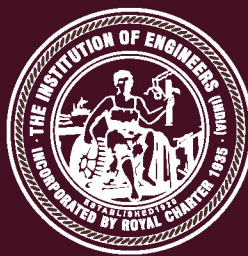


31st Indian Engineering Congress

Kolkata, December 15-18, 2016

Theme

**SMART Technologies for Natural Resource
Conservation and Sustainable Development**



The Institution of Engineers (India)

8 Gokhale Road, Kolkata 700 020

Technical Volume



31st Indian Engineering Congress

THEME

**SMART Technologies for
Natural Resource Conservation
and Sustainable Development**

Technical Volume



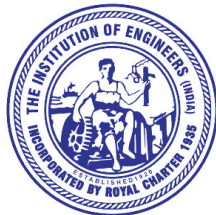
31st Indian Engineering Congress

Kolkata, December 15–18, 2016

THEME

**SMART Technologies for
Natural Resource Conservation
and Sustainable Development**

The Institution of Engineers (India)



8 Gokhale Road, Kolkata 700020, India



ALLIED PUBLISHERS PVT. LTD.

New Delhi • Mumbai • Kolkata • Lucknow • Chennai
Nagpur • Bangalore • Hyderabad • Ahmedabad

ALLIED PUBLISHERS PRIVATE LIMITED

1/13-14 Asaf Ali Road, **New Delhi**–110002

Ph.: 011-23239001 • E-mail: delhi.books@alliedpublishers.com

87/4, Chander Nagar, Alambagh, **Lucknow**–226005

Ph.: 0522-4012850 • E-mail: appltdlko9@gmail.com

17 Chittaranjan Avenue, **Kolkata**–700072

Ph.: 033-22129618 • E-mail: cal.books@alliedpublishers.com

15 J.N. Heredia Marg, Ballard Estate, **Mumbai**–400001

Ph.: 022-42126969 • E-mail: mumbai.books@alliedpublishers.com

60 Shiv Sunder Apartments (Ground Floor), Central Bazar Road,
Bajaj Nagar, **Nagpur**–440010

Ph.: 0712-2234210 • E-mail: ngp.books@alliedpublishers.com

F-1 Sun House (First Floor), C.G. Road, Navrangpura,
Ellisbridge P.O., **Ahmedabad**–380006

Ph.: 079-26465916 • E-mail: ahmbd.books@alliedpublishers.com

751 Anna Salai, **Chennai**–600002

Ph.: 044-28523938 • E-mail: chennai.books@alliedpublishers.com

Hebbar Sreevaishnava Sabha, Sudarshan Complex-2

No. 24/1, 2nd Floor, Seshadri Road, **Bangalore**–560009

Ph.: 080-22262081 • E-Mail: bngl.books@alliedpublishers.com

3-2-844/6 & 7 Kachiguda Station Road, **Hyderabad**–500027

Ph.: 040-24619079 • E-mail: hyd.books@alliedpublishers.com

Website: www.alliedpublishers.com

© 2016, The Institution of Engineers (India)

No part of the material protected by this copyright notice may be reproduced or utilized in any form or by any means, electronic or mechanical including photocopying, recording or by any information storage and retrieval system, without prior written permission from the copyright owners. The views expressed in this volume are of the individual contributors, editor or author and do not represent the view point of the Centre.

ISBN: 978-93-85926-15-0

Published by Sunil Sachdev and printed by Ravi Sachdev at Allied Publishers Pvt. Ltd.,
(Printing Division), A-104 Mayapuri Phase II, New Delhi-110064

The Institution of Engineers (India)



President

- ▶ H.C.S. Berry

President-Elect

- ▶ N.B. Vasoya

Members, Technical Committee

- ▶ Arup Kr. Mishra
- ▶ Jitendra Singh
- ▶ G.S. Yadava
- ▶ D.J. Doke
- ▶ T. Ananthapadmanabha
- ▶ S.K. Bandyopadhyay
- ▶ Sudip Kr. Roy
- ▶ Partha Bhattacharya
- ▶ Swapan Kr. Ghosh
- ▶ Swapan Kr. Goswami
- ▶ Pradip Kr. Das
- ▶ Siddartha Ray
- ▶ Pinaki Bhattacharya

Printed by

Allied Publishers Pvt. Ltd.
A-104, Mayapuri Phase II
New Delhi 110064
Tel.: 011-41845133/28113682
Fax: 011-28116584
E-mail: editorials@alliedpublishers.com

Chairman, Technical Committee

- ▶ N.R. Bandyopadhyay

Ex-officio Members

- ▶ Sisir Kr. Banerjee, *Chairman—Organizing Committee*
- ▶ Maj. Gen. S. Bhattacharya, *VSM (Retd.), Organizing Secretary and Secretary & Director General, The Institution of Engineers (India)*

Editorial Team

Nilanjan Sengupta, *Convener, Technical Committee and Director (Technical), The Institution of Engineers (India)*

- | | | |
|--------------------------|-------------|---------------------|
| ▶ S. Chaudhury | ▶ K. Sen | ▶ S. Ghosh |
| ▶ T. Chakraborty | ▶ A. Dutta | ▶ S.B. Sett |
| ▶ Partha Mukhopadhyay | ▶ T. Roy | ▶ H. Roy |
| ▶ A. Basu | ▶ T. Biswas | ▶ Tarun Chakraborty |
| ▶ S. Bagchi | ▶ P. Nath | ▶ N. Sikdar |
| ▶ Prosenjit Mukhopadhyay | ▶ A.K. Roy | ▶ S. Dey |

Technical Department, The Institution of Engineers (India)

Tel.: 033-40106213, Fax: 033-22238345

Email: technical@ieindia.org

Technical Volume Website

www.ieindia.org



Copyright Information

For Authors

As soon as an article is accepted for publication, authors will be requested to assign copyright of the article (or to grant exclusive publication and dissemination rights) to the Organiser. This will ensure the widest possible protection and dissemination of information under copyright laws. More information about copyright regulations for this Technical Volume is available at: www.ieindia.org

For Readers

While the advice and information in this Technical Volume is believed to be true and accurate at the date of its publication, neither the authors, the editors nor the publisher can accept any legal responsibility for any errors or omissions that may have been made. The publisher/organizer make no warranty, express or implied, with respect to the material contained herein. All articles published in this Technical Volume are protected by copyright, which covers the exclusive rights to reproduce and distribute the article (e.g., as offprint), as well as all translation rights. No material published in this Technical Volume may be reproduced photographically or stored on microfilm, in electronic data bases, on video disks, etc., without first obtaining written permission from the organizer (respective the copyright owner). The use of general descriptive names, trade names, trademarks, etc., in this publication, even if not specifically identified, does not imply that these names are not protected by the relevant laws and regulations. For permission to reuse our content please send request addressed to: Director (Technical), The Institution of Engineers (India), 8 Gokhale Road, Kolkata 700020 (Tel.: 033-40106213 or Email: technical@ieindia.org)

Copyright

As per By-Law 118, Copyright of each paper published in the Institution journals or proceedings in full or in abstract at its Centres shall lie with the Institution.

© The Institution of Engineers (India) 2016

The Institution of Engineers (India) has exclusive rights and license to publish and distribute the print as well as online edition of proceeding worldwide. The views expressed in this publication do not necessarily reflect those of the Institution. All rights reserved. No part of this publication may be reproduced, stored in a retrieval system or transmitted in any form or by any means, without prior written permission of The Institution of Engineers (India).

The Institution of Engineers (India)

AN ISO 9001: 2008 CERTIFIED ORGANISATION

(Established 1920, Incorporated by Royal Charter 1935)

8, GOKHALE ROAD, KOLKATA 700020

Mr H C S Berry, FIE
President



“97 years of Relentless Journey towards Engineering Advancement for Nation-Building”

Message

It is my proud privilege to learn that **31st Indian Engineering Congress** of The Institution of Engineers (India) on the theme “**SMART Technologies for Natural Resource Conservation and Sustainable Development**” is scheduled to be organized by the West Bengal State Centre of the Institution during December 15–18, 2016 at Kolkata.

Nowadays, everyone is aware of his own impact on the environment, thus definition of conservation has expanded to address the effects of human consumption. We have now started encouraging the philosophy, “*reduce, reuse, recycle, buy local and reduce carbon footprint*”. The ultimate aim of these measures is to conserve the natural resources, such as, water and energy required for the human race to survive. To promote more resource efficient, greener and to make more competitive economy, it is clear that significant innovation is required with respect to sustainable growth that needs to go hand in hand with smart growth in order to reap the full benefits of green economy. India needs to reinforce synergies between development and sustainable growth to deal with the climate change, environment and energy demands as well as growing scarcity of natural resources. We need to change our policy currently based on overuse of natural resources into innovation-driven green policies.

I am quite confident that this Congress will provide a common platform to the engineers and other stakeholders for interactions and deliberations on SMART technologies to check the depletion of natural resources in a sustainable manner. I am grateful to all the engineers, technocrats and policy makers of the country and to the foreign delegates for participating in this event to make it a grand success.

I am sure that the papers presented during the Congress and published in this Technical Volume will create great impact towards advancement of engineering and technology in the country.

Jai Hind


(H.C.S. Berry)

The Institution of Engineers (India)

AN ISO 9001: 2008 CERTIFIED ORGANISATION

(Established 1920, Incorporated by Royal Charter 1935)

8, GOKHALE ROAD, KOLKATA 700020

Mr N B Vasoya, FIE
President-Elect



“97 years of Relentless Journey towards Engineering Advancement for Nation-Building”

Message

I am very glad to know that The Institution of Engineers (India) is organizing the **31st Indian Engineering Congress** on the theme “**SMART Technologies for Natural Resource Conservation and Sustainable Development**” hosted by the West Bengal State Centre during December 15–18, 2016 at Kolkata.

Over the last few decades, the world has witnessed phenomenal economic growth with the dissemination of new innovative technologies, accelerated globalization of the economy and implementation of various Government policies. Recent economic liberalization policies have seen new strides in technology up-gradation, cleaner fuels, efficiencies in production and environmentally sound practices. The planning process also seeks to diversify the economy further into industrial and service sectors, while accelerating the growth rate. Development has to be long-standing and inclusive, involving both the private and public sectors as partners. The national planning process emphasizes promotion of people’s participatory institutions and social mobilization, particularly through empowerment of women and other disadvantaged sections of the society, for ensuring environmental sustainability of the development process. Socio-economic development consists of increase in the production, distribution, sale and consumption of food, goods and services. The planning process in India seeks to increase wealth and thereby human welfare and provides a safety net to the environment.

I believe that deliberations during the 31st Indian Engineering Congress will certainly enlighten us about SMART technologies in the current scenario of economic condition with respect to sustainable development.

I wish the Congress a grand success.

Wishing you all Merry Christmas and Happy New Year 2017 well in advance.

Jai Hind


(N.B. Vasoya)



सत्यमेव जयते

प्रो. आशुतोष शर्मा
Prof. Ashutosh Sharma



सचिव
भारत सरकार
विज्ञान और प्रौद्योगिकी मंत्रालय
विज्ञान और प्रौद्योगिकी विभाग
Secretary
Government of India
Ministry of Science and Technology
Department of Science and Technology



23rd November, 2016

Message

I am glad to know that The Institution of Engineers (India) is organising, the **31st Indian Engineering Congress** at Kolkata during 15–18 December 2016 with the theme as “**SMART Technologies for Natural Resource Conservation and Sustainable Development**”.

Debates on conservation of natural resources and promotion of sustainable and inclusive development are incomplete without a comprehensive understanding of issues of Science, Technology and Innovation (STI). Access to smart and appropriate technologies will leverage steady improvements in living conditions, which will be a blessing for the most vulnerable populations, and drive productivity gains which ensure economic stability.

In this context, I welcome and appreciate the efforts made by The Institution of Engineers (India) for choosing such an apt theme for the Congress, which shares so much in common with the vision of policy-makers across the globe in conserving as well as replenishing natural resources of the planet while dignifying the lives of the future generations.

I am sanguine that all the emerging issues will be discussed during the Congress in its right perspective. I am happy to note that the edited **Technical Volume of the Congress** with ISBN No. will also be brought out on the occasion which will benefit the scientists, engineers, technologists, policy makers, academicians and others.

I wish the Congress a grand success.


(Ashutosh Sharma)

The Institution of Engineers (India)

AN ISO 9001: 2008 CERTIFIED ORGANISATION

(Established 1920, Incorporated by Royal Charter 1935)

8, GOKHALE ROAD, KOLKATA 700020

Dr N R Bandyopadhyay, FIE, FAScT

Chairman, Technical Committee

31st Indian Engineering Congress

The Institution of Engineers (India)

and

Professor

School of Materials Science and Engineering

Indian Institute of Engineering Science & Technology

(IEST), Shibpur, Howrah 711103, India



Prologue

We are currently at the early but secure and irreversible stage of a remarkable and far reaching technological revolution. The mastery and control of advanced technologies are dominating several high technology field and major segments of manufacturing which emerged as a science based knowledge intensive high technology area with serious implications for technical change, competitiveness, growth in employment, trade patterns, location of manufacturing activities and global division of labour. Innovation driven growth is no longer the prerogative of the prosperous nations; some developing countries have achieved significant economic growth through the creation and deployment of smart and sustainable technologies. Issues of Science, Technology and Innovation need to be more participatory and inclusive, so that, there is public interface in the scientific endeavour from the entire gamut of social actors. Aligning our interest in synchronization with nature through adoption of smart technologies is a challenge which will keep motivating the entire scientific community.

India has emerged as an economic and industrial power. As a member of the Group of Twenty (G20) and BRICS, it has now a rapidly growing economy facing challenges in social and environmental issues. The accelerated growth in all sectors and urban development in particular has thrown a challenge towards its natural resources. Modern protocols and treaties on environmental protection and natural resource management are highly technology dependent. Adoption and application of Sustainable, Manageable, Appropriate, Rational and Transferable (SMART) Technologies in all sectors of development will be the most befitting action for effective Natural Resource Management in a sustainable manner.

Pursuant with this mission, the **31st Indian Engineering Congress** of The Institution of Engineers (India) is being organized on the theme “**SMART Technologies for Natural Resource Conservation and Sustainable Development**” at Kolkata during December 15–18, 2016.

The Congress assumes huge response from the engineering fraternity across the country and abroad and is all set to discuss all the relevant issues pertaining to the theme of the Congress in its right perspective. There are also concurrent Technical Sessions where peer-reviewed papers, encompassing various engineering disciplines from academic and industrial sector across the country, will be presented. On this momentous occasion, this **Technical Volume of the Congress** with ISBN no. is published containing the above mentioned presented papers. I am confident that this **Technical Volume of the 31st Indian Engineering Congress** will benefit all practicing engineers, technocrats, policy makers, researchers and academicians in all respect.

Let the Congress have its take-off! Meanwhile I extend my sincere thanks and gratitude to all the members of the Technical Committee as well as the team of Technical Department of The Institution of Engineers (India) whose untiring effort and relentless contributions have made this Technical Volume a reality. My sincere thanks are also due to the persons behind the scene, but for whose silent contributions this publication would not have been a success.

A handwritten signature in blue ink, appearing to read "N.R. Bandyopadhyay".

(Prof. N.R. Bandyopadhyay)



Contents

<i>Editorial</i>	v
<i>Message from Mr. H.C.S. Berry (President)</i>	vii
<i>Message from Mr. N.B. Vasoya (President–Elect)</i>	viii
<i>Message from Prof. Ashutosh Sharma</i>	ix
<i>Prologue from Prof. N.R. Bandyopadhyay (Chairman)</i>	x

GROUP A

Agriculture Engineering

1. Estimation of Deep Drainage under Subsurface Drip Irrigation by using RETC Software	3
<i>Ashish Patil and K.N. Tiwari</i>	
2. Drip Irrigation Benefits Small and Marginal Farmers: APMIP Experiences	7
<i>K. Yella Reddy, L. Narayan Reddy, G. Paavan Kumar Reddy and Ch. Sneha</i>	
3. Impact of Floods on Sustainable Development and its Management in Bihar	14
<i>Mitthan Lal Kansal, Kumar Abhishek Kishore and Prashant Kumar</i>	

Architecture Engineering

4. Enhancing Facade Durability through Organosilane Nanotechnology	21
<i>Anupam Shil</i>	

Civil Engineering

5. Identification of Stiffness and Damping Parameters at Element Level	26
for Structural Health Monitoring Utilizing Time Domain Dynamic Response Data	
<i>A. Debnath and S. Chakraborty</i>	
6. An Efficient Response Surface Method Based Finite Element Model Updating	32
of Composite Structures	
<i>T. Islam, S. Chakraborty and C. Ray</i>	
7. Composite Concrete Filled Square Steel Hollow Sections	38
<i>Pathik Debmallik and Pramit Debmallik</i>	
8. Spatial Technology and Modeling for Planning of Transportation Infrastructure	43
<i>A. Narayana Rao, M. Madhavi and K.M. Lakshmana Rao</i>	
9. Torsional Behaviour of Reinforced Concrete Beam Strengthened with FRP Materials	53
<i>S.B. Kandekar, R.S. Talikoti and S.B. Kolhe</i>	
10. Durability Study on Sugarcane Bagasse Ash as an Admixture in M ₃₀ Grade Concrete	57
<i>P.V. Rambabu, G. Aditya and G.V. Ramarao</i>	



Environmental Engineering

11. Challenges due to Change in Land Use and Rain Fall Pattern 63
for Storm Water Collection, Treatment and Disposal
Rajendrakumar V. Saraf
12. Innovative Solutions for Development of Water Resources: 69
How to Utilize Underground Aquifer as a Natural Lake-cum-Reservoir
M.K. Ghosh Roy
13. Severe Contamination of Large Quantity of Groundwater by Bleaching and Dyeing Effluents 73
at Maheshtala Textile Cluster, West Bengal: Seasonal Assessment by Multivariate Approach
Biman Gati Gupta, Jayanta K. Biswas and Kamallesh M. Agrawal
14. Application of Minimalist “SMART” Tools and Techniques for Improving Water Productivity 79
in Industrial Sector with Special Reference to Steel Plants
S. Mitra Mazumder, A.K. Jha, K. Bhattacharjee, M. Choubey and A. Gupta
15. Tackling Corrosion and Bio-Film Formation in Water Distribution Systems 87
for Sustainable Supply of Water
D. Bhaskar and G. Singh

GROUP B

Computer Engineering

16. Reduction in Sub Diaphragmatic Activity in Myocardial Perfusion Imaging 95
with the intake of Water
Gopal Sonai Muthu and Sujata Mitra
17. A New Technique for Extraction Based Text Summarization 99
Goutam Sarker
18. An Intelligent Home Automation System Using Internet of Things Framework 105
Arindrajit Pal and Amitava Nag
19. Statistical Relevance of Sweat on Bloodstain Pattern Documented on Linen Surface 109
Nabanita Basu
20. Color-Based Segmentation of Thin Blood Smear Image 115
to Detect Malaria Parasite using Unsupervised Clustering
Sanjay Nag and Nabanita Basu

Electrical Engineering

21. Cybernetics in Dynamic Data-Driven Identification of the Interactions 122
of Runoff-Rainfall Dependent State Variables for Hourly Monitoring
of Flows of a Fast Flowing River Systems for Hydro-Power Generation
A.S. Chaudhuri
22. Smart Grid Prospects and Implementation in India: A Pathway towards 126
Sustainable Development
M. Alam
23. PEM Fuel Cell Technology Demonstration at NLC India Ltd, Neyveli, Tamil Nadu, India 132
M. Coumarane, K. Ramya, R. Balaji and N. Rajalakshmi



24. The Intelligent Power Grid with Internet of Thing (IoT) Technology	136
<i>Debasish Mondal</i>	
25. Towards Sustainability in Power	141
<i>Ashok K. Jain and Ranjit Sinha</i>	
26. Substation Automation: A Case Study	144
<i>D.J. Patowary</i>	
27. A Novel Non-Intrusive Load Monitoring Technique for Domestic Applications	149
<i>Soumyajit Ghosh, Arunava Chatterjee and Debashis Chatterjee</i>	
28. Economic Analysis and Technical Feasibility of Right to Electricity Act (REA) in India	154
<i>Sreenath Sukumaran and K. Sudhakar</i>	

Electronics and Telecommunication Engineering

29. Increase Digital Data Transmission Speed and Storage Place on Reducing Total Bit Count of a Set of Binary Data Using Interlaced Binary Search	158
<i>Aloke Sarkar</i>	
30. Expounding the Complications and Mitigations for Indian Military Force Related Communication Issues	162
<i>Akarsh Goyal, Nikhil Chaudhari, K. Naresh and V. Balasubramanian</i>	
31. Study on 2.45 GHz Microwave Propagation in an ECR Plasma Enhanced Film Deposition System	167
<i>Soumik Kumar Kundu, Samit Karmakar, Mili Sarkar and G.S. Taki</i>	
32. Design and Development of Multi-Junction Solar Cell on Silicon	171
<i>Anindya Ghosh, Suchandra Mukherjee and Payel Das</i>	

GROUP C

Marine Engineering

33. Improving Competitiveness of Indian Shipbuilding: Intelligent Applications of Systems, Technologies and Economics	177
<i>M.K. Ghosh Roy</i>	

Mechanical Engineering

34. Performance Analysis of a Solar Hydrogen Supported Hybrid Cold Storage	181
<i>R.K. De and A. Ganguly</i>	
35. Trimming Combustion by CO/CO ₂ Measurement	187
<i>Shaji Jose and P. Sathees Chandra</i>	
36. Experimental Investigation on a 660 MW Supercritical Boiler with MOIS Technology	193
<i>Anuj Tomar and Vinod Kumar</i>	
37. Design and Kinematic Simulations of 3-PRS Spatial Parallel Mechanism	198
<i>R. Sai Kiran Kumar and J. Srinivas</i>	
38. Relation between SIF and Crack Geometry	204
<i>Prerna Rai and Shalendra Kumar</i>	



39. Design and Fabrication of Industrial Robot for the Automotive Industry	209
<i>E. Bhaskaran</i>	
40. The Use of a Multilevel Arrangement for Photovoltaic Power Generation	215
<i>Antariksha Sarkar and Bidyut Kumar Bhattacharyya</i>	
41. Surface Roughness and Tool Wear Optimization in Hard Turning Using Taguchi	219
Based Utility Concept during Comparative Assessment of Inserts	
<i>K. Venkata Subbaiah, Ch. Suresh and Ch. Raju</i>	

Production Engineering

42. Multi Response Optimization of the Performance Characteristics in Stir Casting Process	224
for Fabrication of Red Mud Based Aluminium Metal Matrix Composite	
<i>Amit Sharma, R.M. Belokar and Sanjeev Kumar</i>	
43. Reduction in GHG Emission in Iron Ore Sintering Process	233
<i>Subhra Dhara, S.K. Jha and A. Arora</i>	

GROUP D

Metallurgy and Material Engineering

44. Investigation of Tribological Performance of Hybrid Aluminium Metal Matrix Composites	241
<i>R.S.S. Raju, M.K. Panigrahi, R.I. Ganguly and G.S. Rao</i>	
45. Advanced High Strength Steel for Structural Applications	246
<i>B. Chaudhuri and A.K. Samanta</i>	
46. Effect of Ceria (CeO ₂) and Yttria (Y ₂ O ₃) Coating on High Temperature	252
Corrosion Resistance of 2.25 Cr-1 Mo Steel in SO ₂ + O ₂ Atmosphere	
<i>D. Ghosh, S. Das and S.K. Mitra</i>	
47. Engineering Practices for Failure Analysis of Boiler Tube Failures in Power Plants:	258
A Case Study	
<i>Pranab Ray, Debashis Sarkar and B. Chaudhuri</i>	
48. Synthesis and Characterization of Perovskite BaSnO ₃ by Variable Methods:	267
A Comparative Study	
<i>Asima Adak (Maity), Soumya Mukherjee, Mahua Ghosh Chaudhuri and Siddhartha Mukherjee</i>	
49. Mechano-Chemical Synthesis of Nanocrystalline Hydroxyapatite from Egg Shells	274
and Phosphoric Acid	
<i>Anindya Pal, Shubhadeep Maity, Sumit Chabri, Supriya Bera, Amit Roy Chowdhury, Mitun Das and Arijit Sinha</i>	

Mining Engineering

50. Sustainable Rural Development through Responsible Mining	278
of Natural Resources of Kotah Stone in Rajasthan	
<i>S.C. Agarwal</i>	
51. Initiatives for Mine Reclamation in Central Coalfields Limited to Save Environment	284
<i>Rajeev Singh and Alok Kumar Singh</i>	



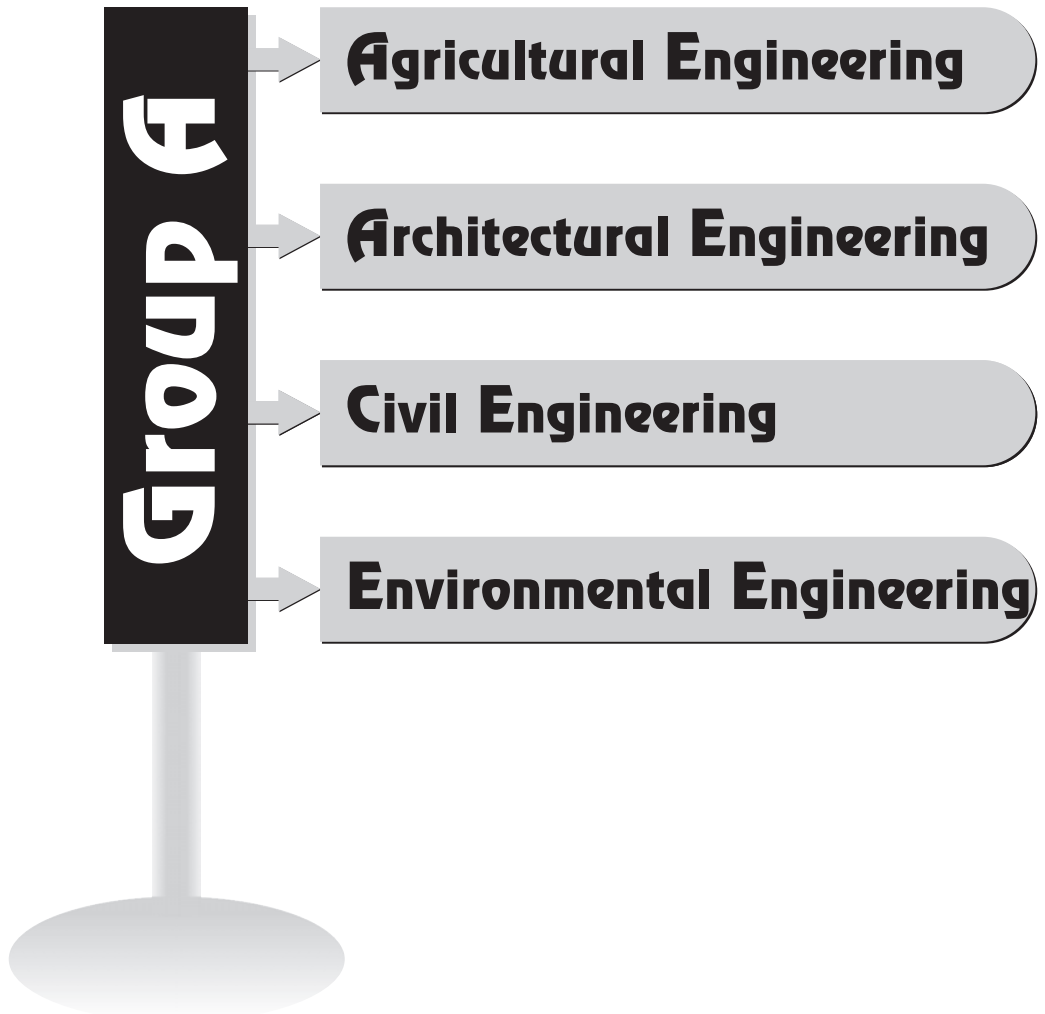
GROUP E

Chemical Engineering

52. Transesterification of Mixture of Edible and Non-Edible Vegetable Oils 293
using Heterogeneous Catalyst Developed from Marble Slurry
Jharna Gupta, Madhu Agarwal and A.K. Dalai
53. Physicochemical Studies of TiO₂/Fe₂O₃/ZnO Heterostructure Assemblies 297
for Electrochemical Water Splitting/Dye Degradation Applications
Dilip Kumar Behara, M. Sudha Maheswari and T. Jalajakshi
54. Biodiesel Synthesis from Soybean Oil in a Tubular Reactor: Numerical Study 303
D. Madhurima Reddy and Nanda Kishore
55. Synthesis, Characterization, Stability Evaluation and Release Kinetics 311
of Trehalose-Encapsulated Bioactive-Nanocapsules
Surashree Sen Gupta and Mahua Ghosh
56. Bio-Nanotube and Regenerative Medicine: A New Look to Molecular Engineering Design 317
N.K. Brahma

Textile Engineering

57. Bio-Engineering Approach to Control River Bank Erosion 323
T. Sanyal
58. Development of Eco-Friendly and Sustainable Feminine Hygiene Products 328
form Lignocellulosic Jute Fibre
S.N. Chattopadhyay, R.K. Ghosh, S. Bhattacharyya and S. Bhowmick
- Author Index** 335





Estimation of Deep Drainage under Subsurface Drip Irrigation by using RETC Software

Ashish Patil^{*1} and K.N. Tiwari¹

Abstract: Interest in subsurface drip irrigation has dramatically increased in recent years because of growing concern about the quality and quantity of soil and water are being adversely affected due to flood irrigation. Relatively very little or no information is available on the distribution of soil water under subsurface drip emitters. A better understanding of the water movement in unsaturated zone of soil through subsurface drip will provide efficient water management practice. RETC (RETension Curve) is a computer program used which describes hydraulic properties of unsaturated soils and involves soil water retention curve, the hydraulic conductivity function and the soil water diffusivity function. For quantifying deep drainage under subsurface drip irrigation, soil water retention function is used which depends upon seven independent parameters, i.e. the residual water content, the saturated water content, the pore connectivity parameter, saturated hydraulic conductivity and the shape factors α , n and m . A field experiment was conducted in a coarse textured lateritic sandy loam soil (Haplustalf) of Kharagpur, India. Okra crop was grown in this soil and irrigated with subsurface drip irrigation system. The Maximum Allowable Depletion (MAD) of 20% was maintained under subsurface drip irrigation to investigate the amount of deep drainage. Maximum Root length of the okra crop for 0 to 45 days after sowing was considered as 30 cm. and 60 cm. after 46 to 93 days after sowing. Water drained beyond 30 cm. and 60 cm. soil depths during 0 to 45 days and 46 to 93 days after sowing of crop was considered as deep drainage. The total seasonal water requirement of okra crop was estimated and found as 642 mm. Average water distribution during okra crop growing season in the soil profile was 42.9 mm. at 0 to 20 cm. soil depth, 44.36 mm. at 20 to 40 cm. soil depth, 42.78 mm. at 40 to 60 cm. soil depth and 40.28 mm. beyond 60 cm. soil depth. Cumulative deep drainage throughout the okra crop growing season was 0.44 mm, which proved effective storage of irrigation water with in the crop root zone due to application of water through drip emitters.

Keywords: Subsurface Drip Irrigation; Hydraulic Conductivity; Lateritic Soil; Maximum Allowable Depletion.

Introduction

Interest in subsurface drip irrigation has dramatically increased in recent years because of growing concern about the quality and quantity of soil and water are being adversely affected by surface irrigation methods. Subsurface drip irrigation (SSD) improves uniformity of water application and water use efficiency for number of crops by applying a low volume of water to the crop root zone. By applying water below the soil surface, water is conserved due to water application directly to the crop root zone and reduced evaporative water loss. In subsurface drip irrigation systems, emitters are placed below the soil surface so water seeps from the emitters into the soil and spreads out in the root zone due to capillary forces. A subsurface drip irrigation method has high water use efficiency [1]. However, application efficiency is affected due to water application

volume and by system design parameters such as the depth, emitter discharge rate and duration of water application, which influence the extent of deep drainage water loss. Very little or no information is available on the distribution of water and deep drainage loss under subsurface drip emitters. It can be determined theoretically using number of models, such as HYDRUS, SWMS-2D and APRI [2]. These models are complex in nature. This study aims in estimating deep drainage under subsurface drip irrigation by using RETC software. RETC (RETension Curve) is a computer program, which describes the hydraulic properties of unsaturated soils uses soil water retention curve, the hydraulic conductivity function and the soil water diffusivity function. The RETC code is a descendent of the SOHYP code previously documented by van Genuchten (1978). As before, soil water retention data are described with the equations of Brooks and

¹Department of Agricultural and Food Engineering, Indian Institute of Technology Kharagpur, India. ✉* ashishpatilifs@gmail.com



Corey (1964) and van Genuchten (1980), whereas the pore-size distribution models of Burdine (1953) and Mualem (1976) are used to predict the unsaturated hydraulic conductivity function [3]. In this study, deep drainage under subsurface drip was estimated by using the Van Genuchten equation (1980), RETension Curve involves, unsaturated hydraulic conductivity function which depends upon seven independent parameters i.e. the residual water content, the saturated water content, the pore connectivity parameter, saturated hydraulic conductivity and the shape factors α , n and m .

Materials and Methods

The field experiment was conducted during February to June 2016 at the Experimental Farm of Precision Farming Development Centre, Agricultural and Food Engineering Department, Indian Institute of Technology Kharagpur, located at 22° 19' N latitude and 87° 19' E longitude at an altitude of 48 m above mean sea level. The soil at the experimental field is coarse textured lateritic sandy loam (Haplustalf). A field plot of 28 m long \times 4 m wide was divided into four equal strips. Each strip was named as R1, R2, R3 and R4 of size 1 \times 13 m² with a buffer strip of 2 m left in the middle. The Miss Okra-18 (F1 hybrid) variety of okra was selected and the seeds were sown at a spacing of 0.6 m \times 0.3 m in the last week of February. Standard agronomic practices such as fertigation and plant protection measures were applied during the crop period. The fertilizer dose of 100 kg N, 50 kg each of P and K were applied to meet nutritional requirement of crop. Okra crop was grown in this soil and irrigated with subsurface drip irrigation system. The lateral lines were buried at 0.08 m depth and laid parallel to the crop rows and each lateral served two rows of crop. The laterals had 'in line' emitters of 4 Lh⁻¹ discharge capacity at 0.3 m interval. Each emitter served the irrigation water requirement of two plants, assuming each emitter wets a strip of 0.6 m \times 0.6 m. In this arrangement there may be a possibility of overlapping of moisture front in the longitudinal direction. Prior to initiate irrigation treatment, the soil profile was saturated and then allowed to bring at field capacity. The maximum root length of the okra crop up to 45 days after sowing was assumed as 0.3 m. After 45 days, the soil profile was watered up to field capacity to refill a depth of 0.6 m considering maximum root length of the okra crop is 0.6 m. The maximum allowable depletion (MAD) of 20% was maintained throughout the crop season. The amount of water estimated to refill the plant-root zone to field capacity was computed using the equation $SWR = CWU - P$; where, SWR = Soil water requirement (mm) and P = Precipitation (mm). Design depth of irrigation (DD) = $WHC \times RZ \times Pw \times f$; where, WHC = Water holding capacity (mm m⁻¹), RZ = Rooting depth (m), Pw = Percentage of wetted soil surface (%) and f = water

depletion factor (%). The Soil Water Requirement (SWR) was calculated based on the Crop Water Use (CWU) and Precipitation (P). The CWU was determined from the moisture loss due to crop ET. Daily P data were recorded for fall crop season. The Okra ET values were calculated based on Penman Monteith equation. The Design Depth (DD) indicated the water depletion level between irrigation events and was determined from soil Water Holding Capacity (WHC), crop Rooting Depth (RZ), water depletion factor (f), and percentage of wetted soil surface (Pw) maintained at 100% according to a FAO guidelines for drip irrigation [4]. Each irrigation event was scheduled at DD values calculated with 20% water depletion of field capacity (f value). Irrigation water was applied when cumulative value of the daily SWR equaled DD. The DD with lower f value corresponded to a higher irrigation frequency events and smaller quantity of water input during each application.

During the experimental period, the deep percolation loss was computed from the unsaturated hydraulic conductivity as a function of the prevailing moisture content and time period. The unsaturated hydraulic conductivity was estimated using Van Genuchten, (1980) equation,

$$K(S_e) = K_s S_e^l [1 - (1 - S_e^{1/m})^m]^2$$

where, S_e is the relative saturation given by,

$$S_e = \frac{\theta - \theta_r}{\theta_s - \theta_r}$$

where, K_s = Saturated hydraulic conductivity (mm/day), θ = Volumetric soil water content (mm³ mm⁻³), θ_s = Saturated volumetric water content (mm³ mm⁻³), θ_r = Residual volumetric water content (mm³ mm⁻³), l = Pore connectivity/tortuosity parameter and m = van Genuchten parameter. These were obtained from the soil moisture characteristic curve, field measurements and hydraulic parameter optimization using software RETC. For estimating the deep drainage loss, $K(S_e)$ of soil layer below the root zone (30–60 cm) during 0 to 45 days was considered. From 46 to 93 days $K(S_e)$ of soil layer below the root zone (60–90 cm) was considered. Assuming a unit hydraulic gradient, the deep percolation becomes equivalent to the hydraulic conductivity value averaged for the time interval under consideration [5]. Thus, the equation for estimation of deep percolation loss (DP) becomes,

$$DP = q\Delta t = K(S_e)\Delta t$$

where, q = Mean volumetric flux density, mm/day, Δt = Time period, days, $K(S_e)$ as defined above for the two layers below the root zone (30–60 cm) for 0 to 45 days and (60–90 cm) for 46 to 93 days. The total seasonal water requirement of okra crop was estimated from the depletion of soil water storage in the root zone taking into account



rainfall, irrigation and deep percolation, and computing the water balance given by Equation,

$$WR = \int_{t_1}^{t_2} dsdt + (R + I) - DP$$

where, WR = Crop water use, mm, ds = Change in soil water storage in the root zone, mm, R = Rainfall, mm, I = irrigation applied, mm, DP = Deep percolation loss, mm and (t_1-t_2) = Start and end of the time interval under consideration, days.

Results and Discussion

Analyses of soil samples, collected from experimental plots are given Table 1. The soils in the root zone depth (0–60 cm) is acidic in nature (pH = 5.2) and with sand content varies between 45.6 to 59.4%. The soil profile depth is characterized as sandy loam with medium bulk density of 1.63 g cm^{-3} and saturated hydraulic conductivity of soil varies between 0.34 to 9.84 cm day^{-1} . Field capacity and wilting point of soil profile varies from 0.24 to $0.28 \text{ cm}^3 \text{ cm}^{-3}$ and 0.10 to $0.13 \text{ cm}^3 \text{ cm}^{-3}$. Top 15 cm soil contains low available N (214 kg ha^{-1}). The total seasonal water requirement of okra crop was estimated and found as 642 mm. In order to assess soil moisture variation with time under different treatments, soil moisture was measured in 0–20, 20–40, 40–60, and 60–90 cm soil layers by using FDR probe (Figure 1). The temporal variations of soil moisture in the root zone and below the root zone of the experimental crop were affected by irrigation treatment. In all soil layers the temporal variations in soil moisture followed cyclic trend with larger variations in the shallow layers of 0–20 cm layers than in 20–40 cm, 40–60 cm, and 60–90 cm soil layers.

In 60–90 cm soil layer, the change in soil moisture was minimum under the entire irrigation events. Figure 1 also reveals that the depletion in soil moisture was relatively rapid in 0–20 cm layer whereas it was gradual 20–40 cm, 40–60 cm and 60–90 cm soil layers. The soil moisture variation within root zone of the crop was greatly influenced

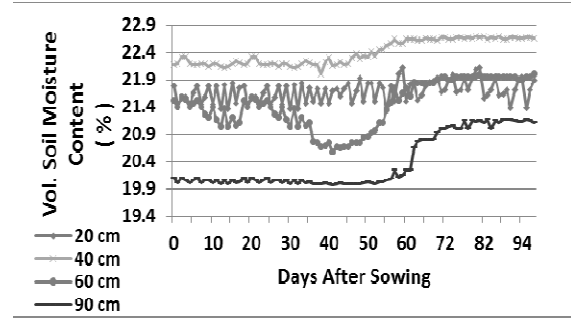


Fig. 1: Temporal Variation of Soil Moisture in Okra Crop at 20% MAD

by the crop water extraction during various stages of crop growth. The data on soil moisture also indicated that the amplitude of cyclic variation was more prominent in 0–20 cm soil profile because major part of the applied irrigation water was lost through evaporation from the soil surface beside the transpiration. In addition to this, a portion of the applied irrigation water percolated to the lower layers also. Major shift of soil moisture was observed after 45 days after sowing because design depth (DD) of irrigation water was 8.9 mm for 0 to 45 days and 17.85 mm for 46 to 93 days. Average soil water content during okra crop growing season in the soil profile of 0–20 cm, was 42.9 mm, 44.36 mm at 20–40 cm soil depth, 42.78 mm at 40–60 cm soil depth and 40.28 mm beyond 60 cm soil depth. The values of K_s (saturated hydraulic conductivity), θ (volumetric soil water content), θ_s (saturated volumetric water content), θ_r (residual volumetric water content), l (pore connectivity/tortuosity parameter) and m were obtained by soil moisture characteristic curve, field measurements and hydraulic parameter optimization using RETC software (Table 2) which were required for determining deep drainage. Cumulative deep drainage throughout the okra crop growing season was only 0.44 mm, which proved effective storage of irrigation water with in the crop root zone due to application of water through subsurface drip.

Table 1: Physical Properties of Soil

Soil Depth	Particle Size Distribution, %			Bulk Density, g cm^{-3}	Saturated Hydraulic Conductivity, cm d^{-1}	Field Capacity, $\text{cm}^3 \text{ cm}^{-3}$	Wilting Point, $\text{cm}^3 \text{ cm}^{-3}$
	Clay	Silt	Sand				
0–15 cm	14.3	26.2	59.5	1.69	9.84	0.26	0.10
15–30 cm	21.0	19.3	59.7	1.56	6.72	0.24	0.10
30–45 cm	27.3	20.2	52.5	1.59	0.89	0.25	0.10
45–60 cm	28.6	19.2	52.2	1.63	0.74	0.26	0.12
60–90 cm	29.7	24.7	45.6	1.69	0.34	0.28	0.13



Table 2: Estimation of Parameters by Using RETC Software

Days after Sowing	Depth, cm	$\theta_r, \text{cm}^3 \text{cm}^{-3}$	$\theta_s, \text{cm}^3 \text{cm}^{-3}$	$K_s, \text{cm d}^{-1}$	l
0 to 45 days	30–60	0.0418	0.3699	0.815	0.5
46 to 91 days	60–90	0.0447	0.3581	0.34	0.5

Conclusion

RETC (RETension Curve) software is simple and reliable source for determining the hydraulic properties of unsaturated soils such as θ_s (saturated volumetric water content), θ_r (residual volumetric water content), l (pore connectivity/tortuosity parameter) and m (Van Genuchten parameter) by using hydraulic parameter optimization technique. It requires only physical properties of the soil as input parameters for determining the hydraulic properties. It is having the flexibility to change the appropriate input parameters after validation by using field experiments. RETC (RETension Curve) computer program is a potential and reliable source to determine the deep drainage and distribution of soil water under subsurface drip emitters. Subsurface drip irrigation is found to be effective for irrigation water application to okra crop at 20% MAD as it retains maximum irrigation water within the crop root zone.

Acknowledgement

The authors are thankful to Information Technology Research Academy, Ministry of Communications and

Information Technology, Govt. of India for providing funds for this research.

References

- [1] Singh, S.D. and Singh, P., Value of drip irrigation compared with the conventional irrigation for vegetable production in hot arid climate, *Agronomy J.*, 70(6), 945–947 (1978).
- [2] Zhou, Q.Y., Kang, S.Z., Zhang, L. and Li, F.S., Comparison of APRI and Hydrus-2D models to simulate soil water dynamics in a vineyard under alternate partial root zone drip irrigation, *Plant Soil*, 291, 211–223 (2007).
- [3] Genuchten, M. Th. van, Leij, F.J. and Yates, S.R., The RETC Code for Quantifying the Hydraulic Functions of Unsaturated Soils, *U.S. Environmental Protection Agency* (1991).
- [4] Sharmasarkar, F. Cassel, Sharmasarkar, S., Miller, S.D., Vance, G.F. and Zhang, R., Assessment of drip and flood irrigation on water and fertilizer use efficiencies for sugar beets, *Agricultural Water Management*, 46, 241–251 (2001).
- [5] Home, P.G., Panda, R.K. and Kar, S., Effect of method and scheduling of irrigation on water and nitrogen use efficiencies of Okra (*Abelmoschus esculentus*), *Agricultural Water Management*, 55, 159–170 (2002).



Drip Irrigation Benefits Small and Marginal Farmers: APMIP Experiences

K. Yella Reddy^{*1}, L. Narayan Reddy¹, G. Paavan Kumar Reddy¹ and Ch. Sneha¹

Abstract: Micro irrigation ranks near the top of measures and achieve efficiencies as high as 95%. The Andhra Pradesh Micro Irrigation project (APMIP) has designed various micro irrigation systems for different crops by considering the field requirements, adaptability by the farmers and also hydraulics and economic parameters. These measures have helped in confidence building and lead to greater demand for micro irrigation in the state. In the present study an attempt has been made to conduct detail field investigations and evaluate the implementation performance of 10% of MI system installed in Ananthapuram district in 2014–15. The study indicates that 67.1% of MI installations were owned by small farmers, 19.7% by big farmers and remaining 13.2% by marginal farmers and in terms of category 56.8% of the MI systems were owned by BC farmers, 33.1% by OC farmers, 6.3% by SC farmers and 3.7% of them by ST farmers.

Keywords: APMIP, Micro Irrigation, Drip Irrigation, Impact Assessment.

Introduction

Agriculture's principal challenge has been raising land productivity—getting more crops out of each hectare of land. In Micro Irrigation water is carried through small tubing and delivered to the plant near its stem to gradually seep towards the root zone. Micro-irrigation technologies adopted at six different locations in Kullu district of Himachal Pradesh under the Farmer's Participatory Action Research Programme (Singh and Sharma, 2013), resulted in a yield increase of 20–90% and water saving of 30–80% over surface methods of irrigation and helped improve the economy of the farmers.

Cost-effectiveness analysis of four water-saving irrigation techniques that are widely implemented in China (Xiaoxia Zou *et al.*, 2013) finds that water-saving irrigation is cost-effective in cropping with climate change, and has benefits for climate change mitigation and adaptation, and for sustainable economic development. Micro irrigation has the highest marginal cost for adaptation, followed by sprinkler irrigation and low-pressure pipe irrigation, but when considering the revenues from improved adaptation, all of the measures assessed are economically feasible. The results suggest that for mitigation and adaptation objectives, micro-irrigation performs best.

Drip irrigation has long been promoted as a promising way to meet today's world water, food and poverty challenges. In most scientific and policy documents, drip irrigation is

framed as a technological innovation with definitive intrinsic characteristics—that of efficiency, productivity and modernity. Based on evidence from North and West Africa as well as South Asia, Venot *et al.* (2014) showed that there are multiple actors involved in shaping this imagery, the legitimacy of which largely stems from an engineering perspective that treats technology and potential as 'truths' that exist independently of the context of use.

A National Task Force Committee, appointed by the Government of India (GOI) in 2003, has recommended that 69 million ha area is suitable for micro irrigation in India. Realizing the importance for economic use of precious ground water for irrigation, Government of Andhra Pradesh (GoAP) has launched the APMIP, first of its kind in the world on 3rd November 2003. The project was aimed at bringing 0.25 million hectares (Mha) area under micro irrigation in 22 districts of undivided AP, with financial outlay of ₹ 11763 million for 5 years. Implementing agencies have been setup at state level and district level for discussing policy issues and for implementation of the project. Govt. of AP has taken up number of measures for promoting micro irrigation, like:

- Providing subsidy of the system cost,
- Creation of separate project cells in the districts,
- Positioning of qualified technical persons,
- Organizing exposure visits and capacity building training programs,

¹ Water and Land Management Training and Research Institute (WALAMTARI), Hyderabad, India.

✉ *yellark@gmail.com



- Guarantee of the MI equipment against manufacturing defects,
- Quality check of equipment through CIPET,
- Monitoring and Evaluation through third party agencies, and
- Providing agronomic and extension services.

The project prepares annual plans for coverage of Micro Irrigation in the state based on the requirements and demands. The annual state wise coverage of drip irrigation in the year 2014–15 is 31386 ha.

Methodology

In the present study, Ananthapuram district was taken as a case study. The total geographical area is 19.13 lakh ha. and the predominant soil is red soil. It is the second lowest rainfall receiving district in India and the annual average rainfall is 553 mm. The coverage of drip irrigation system in the year 2014–15 is 8514 ha.

The scope of the study was,

- Present status of MI system installed in the farmers fields,
- Correctness in deliveries of Mi equipment with reference to Bill of Quantities (BOQ),
- Training and Capacity building to farmers,
- Impact assessment on crop productivity, reduction in labor cost for weeding, fertilizer application and irrigation,
- Reduction in fertilizer use, and
- Increase in area of cultivation.

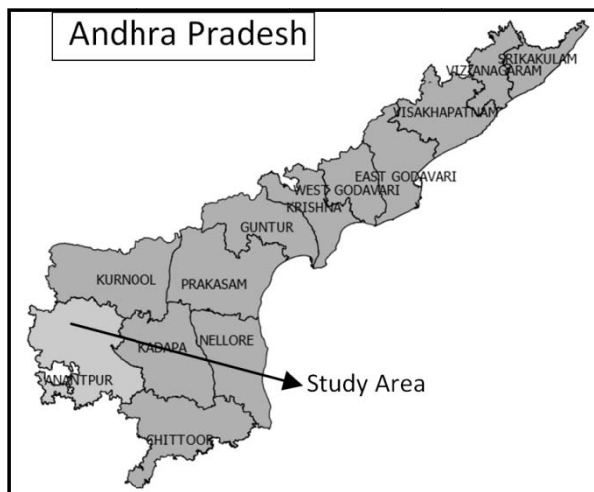


Fig. 1: Map Showing Study area District in Andhra Pradesh

Data questionnaire was prepared to cover all aspects of MI system installation process like general information of the farmer, landholding, status of MI system and Impact of MI

system. The Interns (students of final year B. Tech. Agri. Eng) from college of Agricultural Engineering, Bapatla and Madakasira conducted detailed field survey and verification. The investigators were grouped into two teams of four members each under execution of one program coordinator. A tentative weekly schedule was prepared for conducting detailed field investigation. The farmer’s details were studied and based on that farmers were contacted before visiting the field. The survey team visited each field. The coordinates at the Head Control Unit (HCU) were checked and compared with the Bench mark survey report to know if the field belonged to that farmer. Every day each team has covered 8 MI installed fields. The survey team interviewed the farmer and obtained required feedback and entered in the desired format Plate 1. The area of the field was measured using **Field area measure application** Plate 2. The order of HCU, control valves, flush valves were inspected and the lateral to lateral and emitter to emitter spacing were checked if they confirmed to the National Mission for Sustainable Agriculture (NMSA) guidelines Plate 3. The collected data was analyzed using **Statistical Package for Social Sciences (SPSS)**. The coordinates taken at HCU are placed in Ananthapuram district map by using **Quantum Geographical Information System (QGIS)**.



Plate 1: Farmer Describing about his MI System



Plate 2: MI Field Polygon Generated through GPS



Plate 3: Measuring Lateral Spacing

Fig. 2(Plate 1-3): Field Study

Results and Discussions

The collected data in the prescribed format, was entered in excel format required for analysis using SPSS package. The different components analyzed were:

- Particulars of farmer
- Water source
- MI system details
- Bill of quantities (BOQ) of MI system
- Status of MI system
- Impact assessment of MI system.

However, among different components studied, certain parameters relevant to the theme of the paper are presented here:

Particulars of Farmers

The farmers' details pertaining to gender, category and social status were analyzed in this head.

Gender Distribution of the Farmer

The analysis was carried out to find out the gender distribution from the list provided by the PD Office.

Table 1: Gender Distribution of the Farmers Having MI Systems

S. No.	Sex	Farmers	
		Number	Percentage
1	Male	517	74.2
2	Female	180	25.8
Total		697	100.0

The study indicates that 74.2% of MI systems were owned by male farmers and 25.8% by female farmers as shown in Table 1.

Social Status of the Farmer

The analysis was carried out to find out the farmer distribution according to the social status from the list provided by the PD Office.

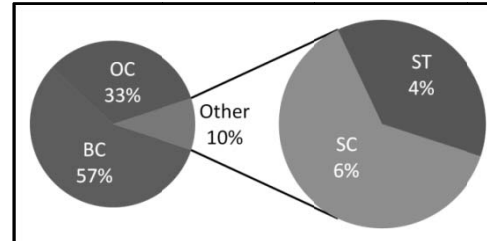


Fig. 3: Social Status of the Farmers having MI Systems

The study indicates that, 56.8% of the MI systems were owned by BC farmers, 33.1% by OC farmers, 6.3% by SC farmers and 3.7% of them by ST farmers as shown in Figure 3.

Type of the Farmers

The type of the farmers is classified in to three divisions based on the Land ownership as Marginal farmer (MF) (<1 ha) Small farmer (SF) (1–2 ha) and Big farmer (BF) (>2 ha). This classification is based on the reference quoted vide Ref. 4.

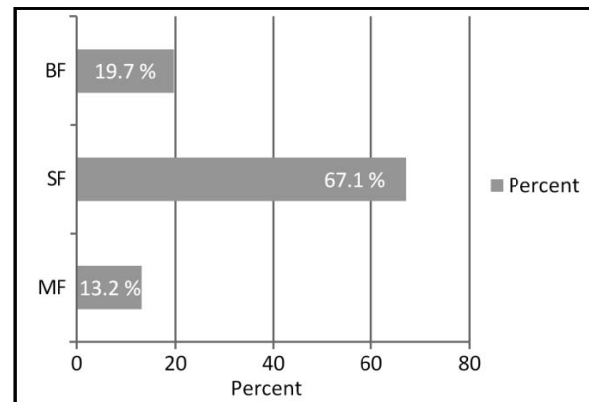


Fig. 4: Category of the Farmers

The study indicates that, 67.1% of the MI installations were owned by small farmers, 19.7% by big farmers and remaining 13.2% by marginal farmers as shown in Figure 4.

Verification of Status of MI Systems

Presence of HCU, water carrying system and other equipment were physically verified in the fields and farmers were also interviewed and obtained their response. Wherever the MI system was not present in the field, the farmers response was obtained in writing and based on feedback of farmers the reasons of non-existence were recorded.

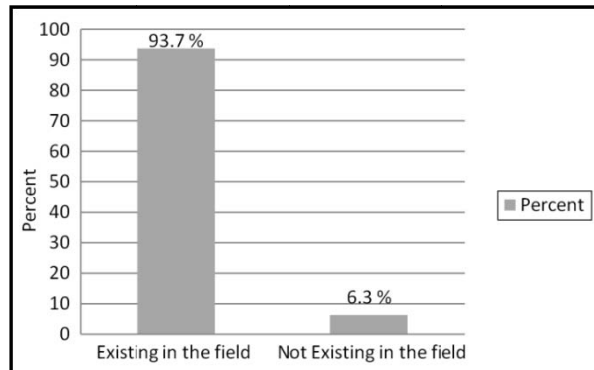


Fig. 5: Status of MI System based on Existence

Out of the total 697MI installations verified, it was found that systems were existing in 653 (93.7%) cases in the fields and in the remaining 44 (6.3%) cases no MI system was found. Based on the feedback of the farmers various reasons were listed for non-existence of MI systems in the field and summarized in the Figure 5.

Impact Assessment of MI System

Among 653 Existing cases, impact assessment of MI system was carried out only for 628 farmers. As, 25 farmers are not available at the time of survey. The details about the water saving, increase in crop productivity, reduction in labor cost, fertilizer usage, pesticide usage and saving on power consumption were assessed and presented in following tables.

Water Saving

By use of drip irrigation system water saving can be realized as irrigation is given near the plants rather than the soil. The farmers were interviewed to assess whether water saving was realized by use of drip of MI system. The data collected is shown in the Table 2.

Table 2: Water Saving with Use of MI Systems

S. No.	Category of the Farmer	Water Saving				Total
		0–25%	26–50%	51–75%	76–100%	
1.	MF	43.0	41.7	12.7	2.6	100
2.	SF	38.4	36.8	21.0	3.8	100
3.	BF	34.4	43.2	16.8	5.6	100

The table shows that the Micro Irrigation has contributed to saving of water. Among marginal farmers 43% realized water saving in the range of 0–25 %, 41.7% farmers in the range 26–50%, 12.7% farmers in the range of 51–75% and remaining 2.6% saved water in between 76–100%. Among small farmers 38.4% farmers realized water saving in

between 0–25% followed by 36.8% farmers in 26–50%, 21% in the range between 51–75% and remaining 3.8% farmers in between 76–100%. Among big farmers 43.2% realized water saving in the range of 26–50% followed by 34.4% farmers in 0–25%, 16.8% in 51–75% and remaining 5.6% farmers in between 76–100%.

Crop Productivity

Drip irrigation increases crop productivity by efficient utilization of water and fertilizers. Farmer’s feedback on increase in crop productivity on use of drip irrigation was obtained as shown in the Table 3.

Table 3: Crop Productivity Increase with Use of MI Systems

S. No.	Category of the Farmer	Increase in Crop Productivity				Total
		0–25%	26–50%	51–75%	76–100%	
1.	MF	73.4	21.5	3.8	1.3	100
2.	SF	71.2	20.1	8.5	0.2	100
3.	BF	71.2	21.6	5.6	1.6	100

The table indicates that the Micro Irrigation has contributed to increase in crop productivity. Among marginal farmers 73.4% farmers observed increase in productivity in the range of 0–25 %, 21.5% farmers in the range 26–50%, 3.8% farmers in the range of 51–75% and remaining 1.3% farmer increased productivity in between 76–100%. Among small farmers 71.2% farmers observed increase in productivity in between 0–25% followed by 20.1% farmers in 26–50%, 8.5% farmers in the range between 51–75% and remaining 0.2% farmer in the range of 76–100%. Among big farmers 71.2% farmers observed increase in productivity in the range of 0–25% followed by 21.6% farmers in 26–50%, 5.6% farmers in 51–75% and remaining 1.6% farmers in between 76–100% increase in MI installations.

Reduction of Labor Cost

Generally reduction in labor cost is noticed by use of drip irrigation in terms of labor requirement for weeding, fertilizer application and irrigation. Information was obtained from farmers regarding in labor cost with use of MI system and the data is presented Table 4.

Table 4: Reduction in Labor Cost with Use of MI Systems

S. No.	Category of the Farmer	Reduction in Labor Cost				Total
		0–25%	26–50%	51–75%	76–100%	
1.	MF	62	24.1	10.1	3.8	100
2.	SF	54.9	32.7	11.2	1.2	100
3.	BF	56	33.6	8	2.4	100

The table indicates that the Micro Irrigation has contributed to reduction in labor cost. Among marginal farmers 62% farmers observed reduction in labor cost in the range of 0–25%, 24.1% farmers in the range 26–50%, 10.1% farmers in the range of 51–75% and remaining 3.8% farmers reduced labor cost in between 76–100%. Among small farmers 54.9% farmers observed reduced labor cost in the range of 0–25% followed by 32.7% farmers in 26–50%, 11.2% farmers in 51–75% and remaining 1.2% farmers in between 76–100%. Among big farmers 56% farmers observed reduction in labor cost in between 0–25% followed by 33.6% farmers in 26–50%, 8% farmers in the range between 51–75% and remaining 2.4% farmers in the range of 76–100%.

Reduction in Fertilizer Use

Fertilizer use efficiency increases with use of MI system as fertilizer in small quantities is applied along with irrigation water. Farmer’s feedback was obtained regarding reduction in fertilizer use with use of MI system and the data is presented in Table 5.

Table 5: Reduction in Fertilizer with Use of MI Systems

S. No	Category of the Farmer	Reduction in Fertilizer Use				Total
		0–25%	26–50%	51–75%	76–100%	
1.	MF	77.2	15.2	6.3	1.3	100
2.	SF	73.6	18.9	6.8	0.7	100
3.	BF	72	23.2	4	0.8	100

The table indicates that the Micro Irrigation has contributed to reduction in fertilizer use. Among small farmers 77.2%

farmers observed reduction in fertilizer use in the range of 0–25%, 15.2% farmers in the range 26–50%, 6.3% farmers in the range of 51–75% and remaining 1.3% farmers reduced fertilizer use in between 76–100%. Among small farmers 73.6% farmers observed reduced fertilizer use in the range of 0–25% followed by 18.9% farmers in 26–50%, 6.8% farmers in 51–75% and remaining 0.7% farmer in between 76–100%. Among big farmers 72% farmers observed reduction in fertilizer use in between 0–25% followed by 23.2% farmers in 26–50%, 4% farmers in the range between 51–75% and remaining 0.8% farmer in the range of 76–100%.

Increased Area of Cultivation

With use of micro irrigation more area can be brought under cultivation as more area can be irrigated with limited water available. The feedback obtained from the farmers has been analyzed and presented in pie chart to show the influence of MI systems on area of cultivation.

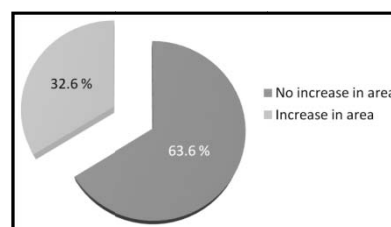


Fig. 6: Influence of MI System on Area of Cultivation

The Pie chart shows that in 63.6% of Installations farmers did not cultivate additional area after installation of MI systems and in 32.6% installations farmers brought additional area to cultivation.

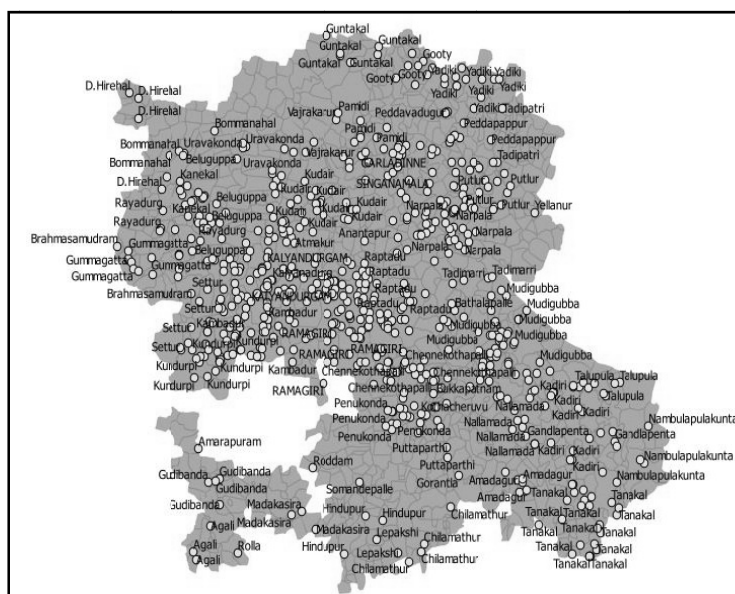


Fig. 7: Map showing Distribution of MI Systems Studied in Ananthapuram District



Farm Size and Area under MI

Table 6 shows that majority of the farmers adopting MI in Ananthapuram (67.9%) are small farmers. Even though the return is high under micro-irrigation, farmers are reluctant to expand the area due to other constraints like high initial capital cost, lack of technical knowledge in the operation and maintenance of the systems and type of crops grown.

Table 6: Farm Size and Area Irrigated by MI Systems

Sl. No.	Type of Farmer	Percentage of Farmers	Average Farm Size, ha	Average Sanctioned Area under MI, ha	% of Sanctioned Area under MI
1.	MF	12.4	0.76	0.72	95.26
2.	SF	67.9	1.52	1.14	75.00
3.	BF	19.7	3.5	1.24	35.43

Cost and Returns MI

The cost of the micro-irrigation system and farmers share after subsidy varied across the farm sizes. It is comparatively lower in the big farmers as compared to the other farms due to economics of scale (Table 7).

Table 7: MI Cost and Returns

Sl. No.	Type of Farmer	Average Total System Cost Invested by Farmer	Net Profit Value	BC Ratio	IRR, %
1.	MF	90000	90388.69	1.93	22
2.	SF	160000	153007.1	1.91	21
3.	BF	280000	190634.4	1.65	15

Even though micro-irrigation could pay for micro-irrigation investment– farmers still expect the subsidy for micro-irrigation because of the following reasons:

1. Micro-irrigation capital investment as it varies from 70,000 to 1.3 lakh/ha depending upon the crops and type of micro-irrigation system and farmers are reluctant to make this investment quickly,
2. Farmers knowledge in the operation and maintenance of the micro-irrigation systems is much limited as often the systems are facing a lot of problems in terms of clogging of the filters, drippers; also the required pressure from the pumps is not always maintained due to poor conditions of the pump sets resulting in low pump discharge;
3. Except for wide spaced and commercial crops, micro-irrigation is not suitable for all crops and spacing.

Except in groundwater overexploited regions, farmers in other regions do not see micro-irrigation as an immediate need. Hence, providing incentives in terms of subsidy helps the farmers to introduce the micro-irrigation system in their farms and save water. The table indicates that the benefit cost ratio and internal rate of return are comparatively higher in marginal (1.93 and 22%) and small farmers (1.91 and 21%) as compared to big farmers (1.65 and 15%).

Conclusion

Spread of micro-irrigation India has been widely noticed in the last 10 years. Andhra Pradesh has expanded the area under micro-irrigation. The study revealed that reached the maximum expectation particular due to policy of government. Further, helped in saving of water, increased in area, reduction in fertilizer use and labor cost.

- The majority of the farmers adopting micro-irrigation in Ananthapuram (67.9%) are small farmers.
- The study indicates 56.8% of the MI systems were owned by BC farmers.
- The study reveals farmers lack of technical knowledge in operation and maintenance of MI system.
- The 32.6% installations farmers brought additional area to cultivation.
- The benefit cost ratio and internal rate of return are high in small and marginal farmers as compared to big farmers.

The recommendations are as follows:

- Farmers need practical training on effective use of fertigation system.
- Field staff should have basic knowledge on MI system.
- The effective implementation of MI systems can be achieved to increase in area by creating credit facilities, after sales services, marketability, and capacity building trainings to farmers.

Acknowledgment

The authors acknowledge the financial support received from the Govt. of Andhra Pradesh and the Water and Land Management Training and Research Institute for giving support to conduct survey at Ananthapuram district.

References

- [1] Anonymous (2012–2013). Annual Report of AP Micro Irrigation Project. Government of Andhra Pradesh, India: Dept of Horticulture.
- [2] Horticulture Department – Andhra Pradesh Micro Irrigation Project – Annual Action Plan 2015–16 – Definition of Beneficiary Farmer categories.



- [3] Anonymous (2014). National Mission for Sustainable Agriculture, Government of India.
- [4] Palanisami, K. (2012). Micro-Irrigation Economics and Outreach.
- [5] Reddy, K.Y. and Tiwari, K.N. (2006). Economic Pipe Size Selection Based on Optimal Flow for trickle irrigation system. *Agricultural Engineering Journal*, 15 (2-3): 109-121.
- [6] Singh, D. and Sharma, V. (2013). Impact of micro-irrigation practices on farmers' economy of Kullu District in Himachal Pradesh. *Progressive Horticulture* 45(2).
- [7] Venot, J.-P., Zwarteveen, M., Kuper, M., Boesveld, H., Bossenbroek, L., Van Der Kooij, S., Wanvoeke, J., Benouniche, M., Errahj, M., De Fraiture, C. and Verma, S. (2014). Beyond the promises of technology: a review of the discourses and actors who make drip irrigation. *Irrigation and Drainage*, Special Issue: First World Irrigation Forum 63(2): 186-94.
- [8] Yella Reddy, K. Micro Irrigation in Participatory Mode Pays Huge Dividends – APMIP Experiences, India. *Irrig. and drain.* 65:72-78 (2016).
- [9] Zou, X., Li, Y., Cremades, R., Gao, Q., Wan, Y. and Qi, X. (2013). Cost-effectiveness analysis of water-saving irrigation technologies based on climate change response: a case study of China. *Agricultural Water Management*, 129 (2013): 9-20.



Impact of Floods on Sustainable Development and its Management in Bihar

Mitthan Lal Kansal¹, Kumar Abhishek Kishore² and Prashant Kumar²

Abstract: Flood causes enormous damage to life, property and infrastructure which affects the social, economic, and environmental aspects of sustainable development. India is one of the highly flood prone countries in the world. Bihar is one of the important states of the India which falls under Ganga river basin and is subject to frequent flooding. The entire North Bihar is crisscrossed by some of the major rivers like Kosi, Gandak, Bagmati, Mahananda, etc. meeting the river Ganga on its left bank. All these rivers originate in Nepal and Tibet which meet the river Ganges in the lower reach. In this reach, the velocity of flow reduces, whereas, the spread of water increases causing flooding in large plains of Bihar. Additionally, as the velocity of flow reduces, it causes the problem of siltation. Siltation in various rivers has increased the bed of rivers, thereby, reducing the carrying capacity which in turn has again increased the spread of flood waters covering a larger area under flood. The flooding in Bihar has affected the all spheres of life and thereby the sustainable development in the state. This study highlights the severity and characteristics of flood in Bihar and its socio-economic impacts during recent times. Further, it discusses the required actions to manage floods through structural (embankment construction and channel improvement, etc.) and non-structural measures like land-use planning, flood plain zoning, silt management, flood forecasting and warning, etc.

Keywords: Floods in Bihar, Sustainable Development, Flood Management, Structural and Non-structural Measures.

Introduction

Water is needed for various human activities, and therefore, most of the civilisations have developed on the banks of rivers. However, as the density of people increases, the flood plains are encroached for various anthropogenic activities. As a result, flooding in such rivers has affected the people in its flood plain to a great extent. It has affected all spheres of life in such areas and has caused adverse impact on sustainable development. Here, sustainable development means that development which meets the needs of the present without compromising the ability of future generations to meet their own needs (*World Commission on Environment and Development, Our Common Future, 1987*). The flooding in rivers has not only affected the needs of the present generation but also affected the ability of the future generation to meet their needs. The conception of sustainable development has been developed beyond initial intergenerational framework to much focus on the goal of “socially inclusive and environmentally sustainable economic growth” since the Brundtland Commission Report (1987). According to the principles of the UN Charter, the Millennium Declaration identified the principles

and treaties on sustainable development encompassing the economic and social development with environmental protection as show in Figure 1.

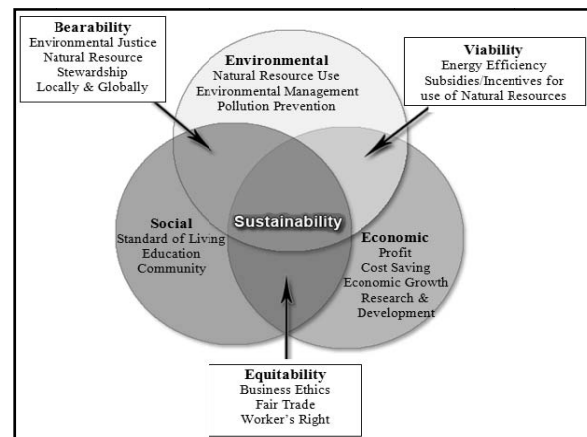


Fig. 1: Scope of Sustainable Development

The term sustainable development as stated by the UN incorporates the issues of land development along with

¹JPSS Chair Professor, Department of Water Resources Development & Management, Indian Institute of Technology Roorkee, India.
✉ mitthan@gmail.com

²PG Students, Department of Water Resources Development & Management, Indian Institute of Technology Roorkee, India.

human development in terms of education, public health, and the general standard of living.

Floods are frequent phenomenon causing huge losses to lives, livelihood, infrastructure and public properties affecting the sustainable development of the region. The rivers carries significant sediment load from the upper part of catchments. These sediments in addition to inadequate carrying capability of the rivers cause floods. Flood is a state of hydrological extreme of high water level in a stream channel that results in inundation of land that isn't ordinarily submerged. Flood is an attribute of physical environment and thus is an important component of hydrological cycle of drainage basin. The National Flood Commission (1976) has reported that about 40 MHa out of total area of 329 MHa in the country is flood affected. This report, thus, revealed a rapid increase in flood proneness in just over a decade. Most of these area falls under Ganga and Brahmaputra basins. The most flood prone basins are those of the Gang and Brahmaputra in Uttar Pradesh, Bihar, West Bengal and Assam. These five states are the most flood prone. The commission analyzed the share of damage went up from 25 to 50 percent of the total and chronically flood prone Bihar area has been increasing.

General Consequences of a Flood

Flash flood causes immediate and huge impacts, whereas gradually occurring floods allows much time for evacuation and protection of properties. Impacts of flood depend on maximum duration and depth of flooding, the extent of inundation in the floodplains, flow velocity and rate of rise of flood levels (Gautam, *et al.*). Flood impacts have social, economical and environmental consequence which affect the sustainable development of any region.

Flood Status in Bihar

Three fourths of Bihar's area and population lie in the natural floodplains of the Ganga and its Himalayan tributaries. About 6.880 million hectares out of 9.416 million hectare comprising 73.06 percent of the state is flood affected which accounts for approximately one-sixth of the flood prone area in India. Major rivers flowing through North Bihar originates from Nepal and the Tibetan region of China. About 65% of the catchment area of Bihar's rivers falls in Nepal and Tibet and only 35% of the catchment areas lie in Bihar (Sinha *et al.*). The upper part of catchment is liable for the morphological activities within the downstream reaches. It carries huge sediment load with its flow every year which is responsible for change in morphological behaviour of the stream. The matter of the flooding is implicitly guided by sedimentation in river. This sedimentation has gradually reduced the capability of the

river to drain extreme flows leading to flooding within the plains.

The Ganga River, which serves as the main drainage system for the state, flows from west to east and stretches 432 km across Bihar, dividing the state into two.

The plain of North Bihar is mainly drained by two River Gandak & Kosi (Figure 2) along with Ghaghara, Burhi-Gandak and Mahananda. Major part of the catchment of these rivers falls in Himalayan glacial region of Nepal and Tibet hence these are snow-fed and perennial rivers. During the monsoon period the flow in these rivers increases 50 to 90 times, leading to flooding in the plains of Bihar. The southern rivers comprising the Karmanasa, Sone, Punpun, Kiul, Badua and Chandranare mainly rain-fed and are either dry or carry little flow during the non-monsoon months (NDMA, 2008).

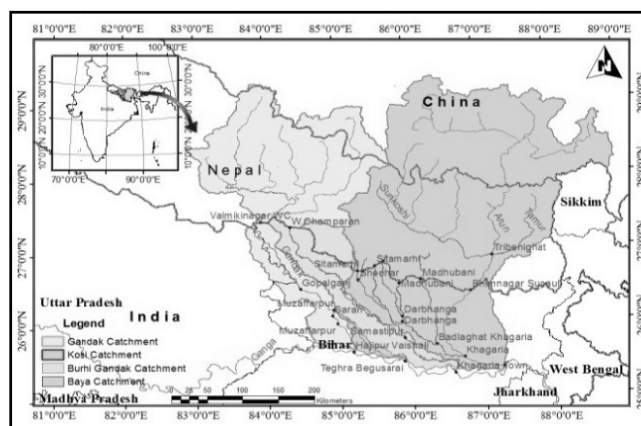


Fig. 2: River Basin System in Bihar

The plains of Bihar, adjoining Nepal, are drained by rivers that carry high discharge and very high sediment loads. Gradients of these rivers vary from 22 cm per km to 7.5 cm per km. at Indo Nepal boundary and at point of confluence with the Ganga respectively (Sinha *et al.*, 2012). So, the rivers reach the plains and lose momentum and begin to meander. Rivers like the Kosi are notorious for changing course. As per the records it is evident that during 1736 to 1953 the river Kosi has shifted its course through a distance of approximately 112 Km. towards westward (Kumar D., 2015). Further Kosi embankment was constructed with a series of spurs on both banks confining the course of river Kosi (Figure 3).

Floods and Growth in Bihar

Agriculture is the backbone of Bihar's economy, employing 78% of the workforce and generating nearly 30% of the State Domestic Product (CSO, 2015). According to government of Bihar 73% of the farmers are small and marginal farmers,



who not only cultivate their land but serves as agricultural labour. So, sustainable development of Bihar principally depends upon agriculture sector.

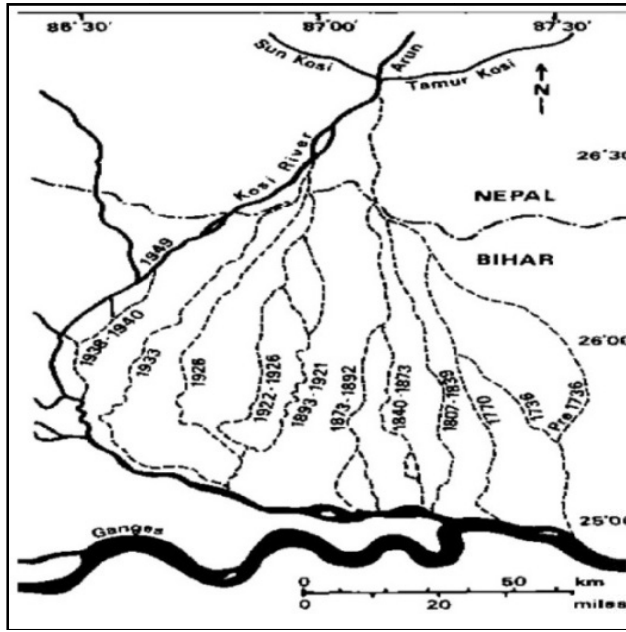


Fig. 3: Kosi River Course
(Source: Kumar D., 2015)

One of the major problems of agriculture development in particular and economic backwardness in general of Bihar is occurrence of frequent flood every year. Flood is a severe issue along the river Ganga and its tributaries. In addition to this flood also affect life, livestock, livelihood, productivity, utilisation and security of investments, education as well as a disincentive for additional investments in Bihar. As a result the development of state is continuously lagging behind the national average (Figure 4a & 4b).

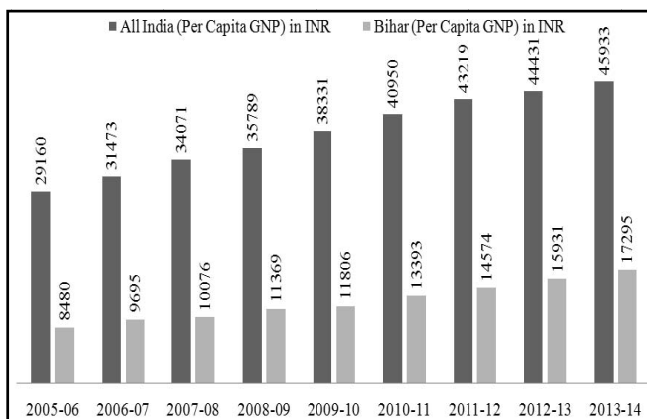


Fig. 4a: Per Capita GNP and GSDP of Bihar
(Source: CSO, 2015)

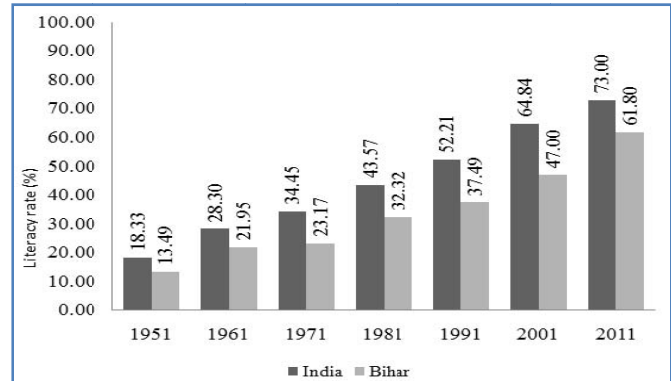


Fig. 4b: Literacy Rate in India and Bihar
(Source: CSO, 2015)

In August 2010, the International Growth Centre (IGC) held a national level meeting in Patna, Bihar on the topic of 'Floods and Growth in Bihar' to explore the multiple causal issues around Bihar's floods and the multiple impacts floods have on the economic growth of the state. The workshop report clearly states that there is a connection between the incidence of floods in Bihar and economic growth, particularly with respect to two factors: agriculture and embankments (IGC, 2010). Agriculture is a major factor as more than 80 percent of Bihar's population is engaged in agriculture as their main source of livelihood; however, floods tend to devastate agriculture lands, particularly in river basins where silt deposits from floods leaves the land uncultivable and therefore forces farmers and their families to relocate or seek alternative livelihoods. The second issue is that of costs associated with embankments—building, maintaining, and repairing—once breaches and damages occur to the infrastructure. According to the IGC report, it is estimated that the cost of managing embankments is far higher than building them (IGC, 2010).

A recent example of this adverse economic impact is the 2008 Kosi floods where more than 500 villages were inundated in the districts of Supaul, Madhepura, Purnea, Saharsa, and Araria. According to Government of Bihar figures, 236,632 homes were either completely or partly. According to the Government of Bihar and the World Bank's Kosi Post Disaster Needs Assessment report of 2010, the estimated damage is ₹ 5,935 million (GoB 2010). Approximately 1800 kilometres road including paved and unpaved and 1100 nos. bridges and culverts were destroyed during this flood. Intensive damage to flood protection structures and irrigation network was reported including damage of Kosi Barrage. Main Eastern Kosi canal was damaged in a length of more than 6 km. Branch canal was also got damaged in a length of 4 km while distributaries and sub-distributaries in more than 150 km. Around 151 canal bridges, and 138 regulators were fully or partially damaged.



Around 154,000 Ha of paddy, 6,300 Ha of maize and 28,000 Ha of other crops were badly affected. This impact on agriculture affected nearly five lacks farmers of the region. Approximately 15000 livestock including 10000 milk animals were lost their lives in this flood (GoB 2010).

In addition to those sectors, major damages were caused to the social, health, livelihoods, education and environment sectors. Among the flood affected population about 90% were dependent on agricultural livelihood. Educational infrastructure was severely affected in all 5 districts. Regular curative and preventative health services also got disrupted in these areas. Further 50,000 Ha of cultivable land has been rendered fallow due to silt deposition causing a long term impact on agriculture, and livelihoods. So, the floods caused a makeable decline in the agricultural production due to sediment deposition and loss of livestock, working capital and other farm assets.

Flood Impacts on Sustainable Development in Bihar

Thus frequent flood have been responsible for many problems in Bihar. Major one is the soil erosion and flooding rendering the fertile cultivable land unsuitable for crop production due to deposition of silt on the surface of variable depth. This is the most severe environmental degradation caused by floods, which in turn is threatening the sustainable agriculture productivity (Figure 5).

Second is low and very fluctuating nature of growth over the successive periods. Next, diversion of funds to flood control measures leading to restricted investment in agricultural sector. So flood plays a vital role in miserable growth rate of state. Observation on growth rate in various sectors in last decade shows the highly unsustainable pattern (Figure 6). Its further study prevails that north Bihar which is major flood affected part of the state is significant contributor of poor development (Figure 7a & 7b). However in some districts of

North Bihar prevails the comparatively high per capita GSDP like in Begusarai district due to refineries and Bhagalpur due to Silk industries there.

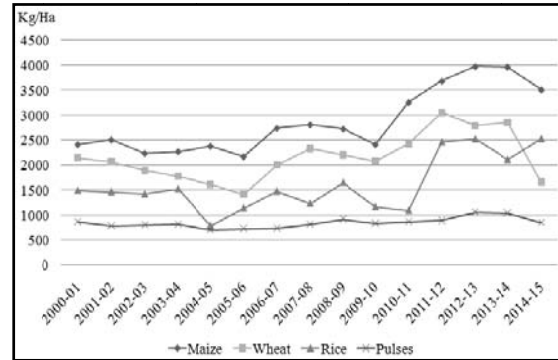


Fig. 5: Productivity of Some Important Crops in Bihar over Last 15 Years

(Source: Directorate of Statistics and Economics, Bihar)

Flood Management in Bihar

In the above context, to minimize negative consequences and ill effects of flooding to maintain the sustainable growth of the state, there is a need of planning for flood management. Planning for flood management doesn't involve absolute control over flood but management of floods in such a way to achieve the most beneficial result within the circumstances. Flood management measures may be classified into two categories, (i) structural involving like construction of embankments, flood retention walls, flood levees and channel improvements, detention basins, etc., and (ii) non-structural including land-use planning, zoning of flood prone lands, redevelopment of flood-prone areas, compensation of incentives, insurance, silt management policy and flood forecasting & warning. Both the measures are not mutually exclusive rather complementary to each other.

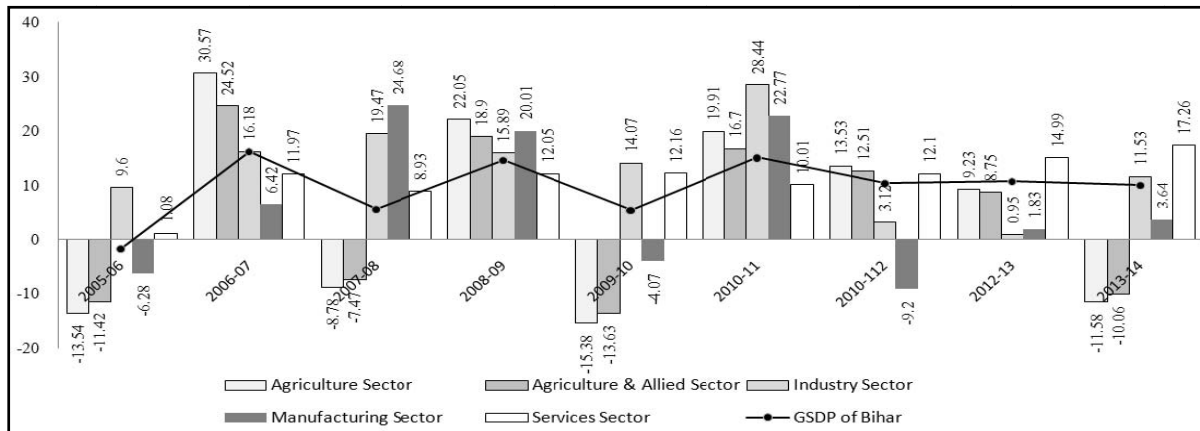


Fig. 6: Percentage Growth in Various Sectors in Bihar

(Source: Directorate of Statistics and Economics, Bihar)

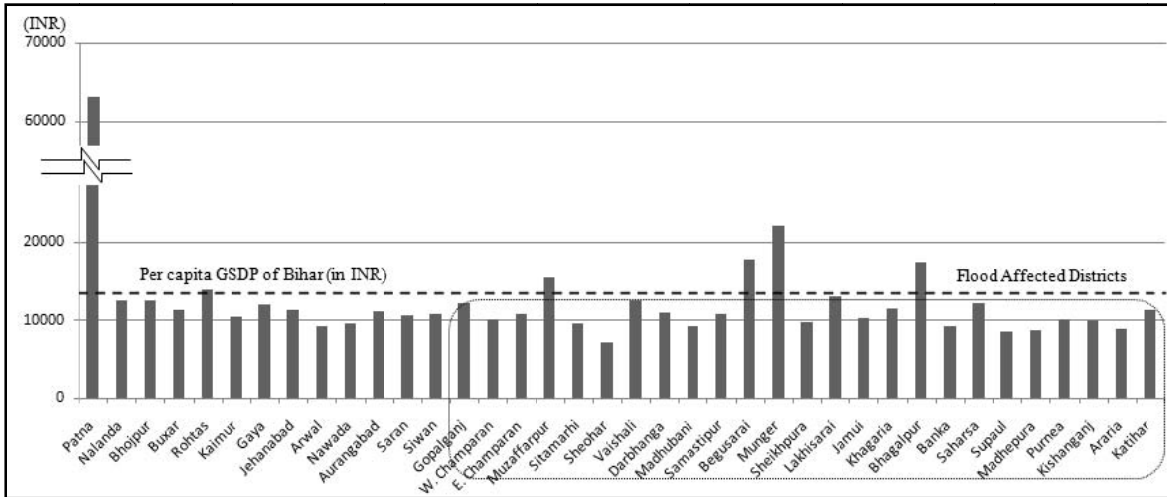


Fig. 7a: Per Capita Gross State Domestic Production Different Districts of Bihar
(Source: Directorate of Statistics and Economics, Bihar)

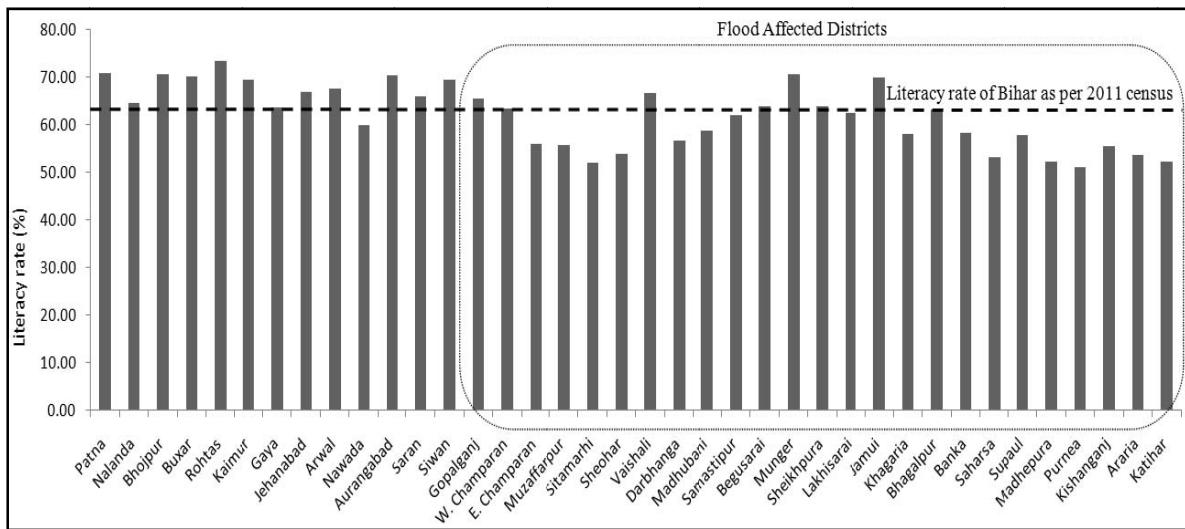


Fig. 7b: Literacy Rate in Different Districts of Bihar
(Source: Directorate of Statistics and Economics, Bihar)

Structural Measures

Flood management works to this point enforced in Bihar comprise of construction and maintenance of embankments. It falls under short-term structural measures. These are generally in practice not due to its effectiveness rather due to low-cost and faster to construct. In Bihar 3732 km embankment has been constructed till March, 2013 and another 1555 kilometre is under construction and likely to be completed by next year. (WRD, Govt of Bihar 2014). Aggradations of river in Bihar necessitates raising and strengthening of the embankments. However this raising stream bed levels, decreases their carrying capability and leading to drainage congestion in countryside.

To overcome such problems, the strategy of developing the channel by de-silting and dredging is a better solution. But due to involvement of high cost and other associated problems this method is in very limited practice.

Non-structural Measures

Losses in recent years contemplate that structural measure alone can't solve the problem. So it is felt necessary to adopt non-structural measure along with structural measures as an integrated approach to efficiently mitigate flood impacts (Kansal *et al.*, 2016). These non-structural measures includes the following.



Land-Use Planning

Land-use coming up with at the local or municipal level is often a useful tool in reducing future flood damages. Use of land in flood prone area should be given consideration to master plan or governing laws.

Zoning of Flood-Prone Lands

Zoning can be used to scale back damages from flooding and must be so flexible to acknowledge that different types of land use are compatible. As in flood prone areas having water velocities are low and not causing serious erosion, agricultural use of lands is acceptable. Particularly in case of Bihar, where agricultural land is limited so in view of self sufficiency in food supply, flood prone lands can judiciously be used as agricultural lands.

Redevelopment of Flood-Prone Areas

A major flood disaster can be taken as opportunity to correct past planning errors. Removal of flood-prone development as well as conversion of the land to a defined and restricted use is an option to be considered. Post 2008 flood development of Kosi catchment is good example.

Compensation and Incentives

Compensation aims at eliminating the negative consequence of flood as earliest. The funds must to be centered on relocation and public education on the risks and their consequences of living on flood-affected area instead of merely paying for damages.

Insurance

Flood insurance can be used to reduce the flood impact and its losses. In case of flood insurance the losses will be paid by insuring agency from the accumulated premiums of policy holders instead of relief funds. Hence it basically works on the principle of distributing impact over a large segment of society.

Silt Management

The Lower reach of river Kosi and its contributing tributaries are severely affected floods every year. As the Kosi with its tributaries like Adhawara group, Bagmati and Kamla Balan originates from the hills and reaches to plains of Nepal Terai and Bihar, their flow velocity drops significantly. It results in increase of depth of flow and hence silt carrying capacity reduces. Due to this, silts get deposited at river bed resulting rise of river bed and consequently erosion of banks. The mouth of the channels oftenly gets obstructed and hence shifting of river course takes place taking new area under threat of flood. Therefore it needs watershed management

with an effective silt management policy to resolve such issue.

Flood Forecasting and Warning

Flood forecasting and early warning system is a predominant non-structural flood protection measure. On the basis of mathematical modeling, experts can convert the past information like discharge, stage and inundation area from data base to present on the basis of rainfall, moisture and snow cover. Accurate forecasting is necessary as well as its formulation into reliable warning and effectively disseminated to the communities at risk to take necessary steps and reduce losses.

Conclusion

Flooding is a perennial problem in the state of Bihar with negative impacts on the lives and livelihood of people. The impact of flood on life and property is devastating. The damage to infrastructure severely affects the economy and hence development of state. Flood event also shows negative impacts on environmental sector. Thus flood affects all spheres of sustainable development i.e. social, economical and environmental. Agricultural sector is worst affected in the event of flood. However it continues to play the primary role in the state's development and the mainstay to our large growing population. However, due to recurrent floods in the state, agriculture and allied sector has accounted miserable growth rate but still plays a vital role in the development of Bihar.

It is not possible to guarantee absolute safety from flood so there is a chance of paradigm is needed. It is required to be aware and live with floods. So, it is very important to build flood risk awareness among public. Even if a safest design have been adopted but any how there is always a risk for greater flood than designed, inducing losses.

Despite the critiques of structural flood protection measures like embankments are absolutely required to safeguard the existing developments, in particular in urban areas. There is a need to efficiently adopt the non-structural measure with structural measure as an integrated approach to conform the spirit of sustainable development (Kansal, *et al.*, 2016).

Non-structural measures for flood management such as land use planning, flood plain zoning, re-development of flood prone areas, compensation and incentives, flood insurance, silt management, flood forecasting and warning, etc. should be adopted. The awareness among the community at risk of flooding should be raise and maintained, with a clear understanding of their role in responding to emergency situations appropriately. They need to be developed so as to adaptation to the flood risk and living with them in flood



plains and simultaneously permitting vacating the same for use by the river whenever the situation demands as integrated approach along with structural measures to minimize the adverse impacts of flood. Among the communities living in flood plains under the recurrent threat of flood awareness should be developed with clear understanding of their role if an emergency situation arises.

References

- [1] Brundtland Report (1987). The World Commission on Environment and Development (WCED), October 1987.
- [2] Central Statistical Organization (CSO) (2015) Ministry of Statistics and Programme Implementation, Government of India, New Delhi, <<http://mospi.nic.in>>.
- [3] Directorate of Economics & Statistics Department of Planning & Development Government of Bihar (2015) Analysis of Budgetary Transactions of Bihar, Patna
- [4] Gautam, K.P. and Hoek, E.E. (2003). Literature Study on Environmental Impacts of Flood, Delf Cluster Publication, June 2003.
- [5] Govt. of Bihar (2010). Kosi Flood 2008: Needs Assessment Report, World Bank, Global Facility for Disaster Reduction and Recovery, Patna, June, 2010.
- [6] Kansal, M.L., Kishore, K.A. and Kumar, P. (2016). Flood Impacts and Its Management in Bihar, *32nd National Convention of Civil Engineers on Role of Civil Engineers in Sustainable Development of India*, Goa, October 21-22, 2016.
- [7] Kansal, M.L., Kumar, P. and Kishore, K.A. (2016). Flood Impacts and Its Management in Bihar, *National Conference on Water Resources and Flood Management with Special Reference to Flood Modelling*, Surat, October 14–15, 2016.
- [8] Kumar, D. (2015). International Water Resources Association, *XVth World Water Congress*, Edinburgh, Scotland, May 25–29, 2015.
- [9] National Disaster Management Authority (2008). Government of India, National Disaster Management Guidelines, Management of Floods, New Delhi, India.
- [10] Sinha, R., Burton, M., and Tiwari., G. (2012). Strengthening the Institutional Framework for Flood and Water Management in Bihar, International Growth Centre, London.
- [11] Water Resources Department (2013). Flood Report 2013, Flood Management Improvement Support Centre (FMISC), Water Resources Department, Government of Bihar, Patna, <<http://fmis.bih.nic.in/publications.html>> (2013).
- [12] United Nations (1992). “Declaration of the 1992 Rio Conference on Environment and Development”, Rio de Janeiro, Brazil, April 1992.



Enhancing Facade Durability through Organosilane Nanotechnology

Anupam Shil¹

Abstract: Every building commands its value in market by virtue of the appearance of its exterior face, whether well or ill maintained. No matter how good the interiors could be, without maintaining the exteriors neither the construction of a single structure nor of an entire town commands its appreciative value from its assessors. Here in this paper, we refer typically to Façade systems that are designed with conventional affordable building materials, like, bricks, silica mortar, fare-faced concrete, natural stones, etc. and how affordable organosilane nanotechnology can be used to maintain them effectively. These days many architects restrict use of these natural siliceous materials on the outer faces of a structure for the only reason being its questionable maintainability. Organosilane nanotechnology works by creating a hydrophobic zone over any façade substrate by penetrating and reacting with the inherent Silanol groups at a nano level. This makes the surface water resistant (tested by RILEM method to sustain Category 1 Hurricane) without compromising the breathability of natural cementitious/siliceous building materials. Apart from protecting the façade it makes the exterior walls damp resistant preventing seepage of water inside the building and creating aesthetic and habitability concerns for its occupants.

Keywords: Nano; Silane; RILEM; Siliceous.

Introduction

In context to habitable structures, it would at the outset become essential to understand what causes ageing of cementitious/siliceous structures. What results in aesthetic and structural disintegration of that strong envelope which we build to protect ourselves from forces of nature? Because it is understood that all the source of cement, sand, stones, aggregates or iron shall not last forever, life extension of these materials is important not only from the perspective of façade maintenance but also for creating a culture that perceives sustainability as a way of life.

How/Why Concrete Ages/Cracks?

It is evident for a causal onlooker that more cracks surfacing over any concrete structure endorses its degeneration. It displays its ageing. Factors that influence the life of a concrete structure and causes that attribute to appearance of a crack can be divided into two time zones, Pre-construction and Post-construction as shown in Figure 1. Till the time a structure gets completely erected, can be termed as the Pre-construction time zone. During this period, conceptualizing, meticulous engineering, procurement of quality raw materials and synchronized construction process gets implemented. These can be termed as the basic deciding

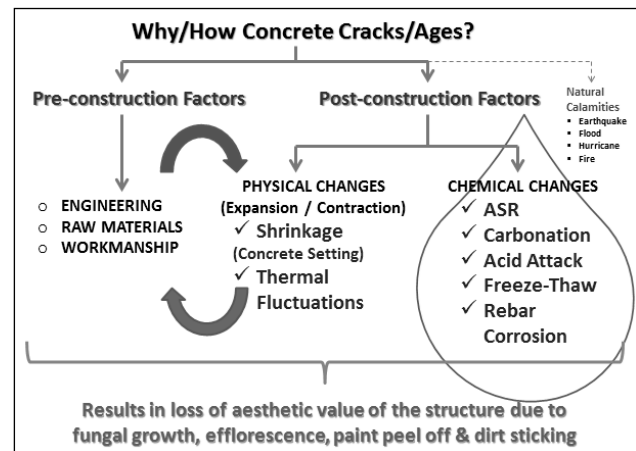


Fig. 1: Concrete Crack

factors and a deviation from scientifically established norms shall have its effect in the integrity of a structure and its consequential fate. But, even structures that are well designed and systematically constructed with best quality materials does age and crack. This is attributed to changes taking place within the concrete which can be either, physical (dimensional) and/or chemical by nature, at the same time they are co-operational, i.e. chemical changes resulting in

¹Technical Head, Waterproofing & Paints Division, Zydex Industries, Vadodara, Gujarat, India. ✉ anupamshil@zydexindustries.com



generation of physical forces to bring about a permanent change in the constitution of the cementitious mass.

Physical (Dimensional) Changes

During the initial years, the following physical (dimensional) changes take place that results in occurrence of surface cracks:

1. *Shrinkage Cracks*: The process of hydration (chemical reaction between cement and water) completes 90–95% in first 28 days (typical setting time of concrete). Some part of it however continues in subsequent years causing volumetric shrinkage of the structure due to consumption of trapped moisture within it. This phenomenon results in appearance of plastic shrinkage cracks on the surface within first few years of construction, till the structure stabilizes.
2. *Thermal Cracks*: Such cracks develop due to differential expansion and contraction of several elements that are incorporated within a concrete super structure. The cement paste, coarse and fine aggregates, steel rebar, etc. each one has a different coefficient of thermal expansion when subjected to fluctuation in atmospheric temperature, induces internal stresses causing surface cracks in a limited surface area.

Both the above stated phenomenon can be mitigated considerably, if not completely eliminated, by appropriate designing, selection of proper raw materials and following a methodical system of construction. However, since such effects cannot be eliminated completely they must be attended periodically as a part of routine maintenance plan, as these cracks are the potential entry points for external environmental elements, like, water, moist air, contaminant salts, etc. to penetrate inside a structure.

Chemical Changes

Water, while on one hand sustains life and nurtures the nature; on the other it also acts as the most destructive element that has the power to disintegrate matter back to its elemental form. Construction materials, by nature, are water-loving. Whether it is soil or cement plaster or bricks or RCC it has a tendency to absorb water. Such ingress of water inside concrete results in various chemical changes within a structure that eventually results in its degeneration and ageing. Some of these chemical reactions are:

- *ASR (Alkali Silica Reaction)*: One of the most detrimental chemical reactions that take place in an alkaline environment within the concrete with its fine or coarse aggregates is ASR. This results in conversion of the amorphous silica to a gel form which not only creates internal stresses within the structure due to volumetric expansion but also acts as moisture

reservoirs due to its inherent tendency of absorbing moisture.

- *Carbonation*: Sometimes also referred as the corrosion of concrete, is a chemical reaction occurring between calcium hydroxide present inside the cement with Carbonic acid (formed by reaction of atmospheric carbon dioxide with moisture/water). This results in formation of Calcium Carbonate (Chalk) and free water. Even though this transformation forms a compound that has significant compressive strength, it reduces the pH environment (state of passivity) within concrete, making the rebar more prone to corrosion.
- *Acid Attack*: Due to fast pace urban development and increasing industrial emissions the atmosphere contains a large reserve of SO_x and NO_x pollutants. These combine with moisture in the atmosphere (clouds) to form various acids, like, Sulphuric/Sulfurous acids, Nitric/Nitrous acids, etc. Upon coming in contact with concrete during rains, it initiates an acid-alkali reaction, resulting in breaking down of the crystalline lime within concrete.
- *Freeze-Thaw*: In colder regions, due to atmospheric temperature dropping to subzero levels, water trapped inside concrete expands while it freezes. This causes internal stresses and such repeated cycles cause cracking and eventually spalling of concrete chunks, thus, disintegrating the structure.
- *Rebar Corrosion*: Water ingress into concrete acts as an electrolyte resulting in ionic exchange between iron rebar and oxygen. This results in corrosion of the rebar, reducing its flexibility and strength, while at the same time causing volumetric stress due to physical swelling of the rebar.

A closer look will reveal to us that ALL the above five concerns are mainly due to entry of water through the labyrinth of micro and nano-size pores inside a concrete structure. Water absorption by a concrete surface starts with primary deterioration of its aesthetic value by formation of fungus; inducing efflorescence; attracting dirt on the surface and causing paint peel off due to repeated dry & wet cycles. The maintenance of a façade starts with protection of its aesthetic value, at the same time; long term structural deterioration caused due to water induced damage must be dealt with equal importance.

How Water Enters Inside Concrete?

Although concrete is porous in nature (Figure 2), yet the pore sizes are much larger than size of a smallest water droplet (size of a water drop when in a cloud is 1,00,000 nm or 0.1 mm). What then results in further break down of this water droplet so as to allow its penetration? Concrete, Bricks, Soil, Sand, Fly Ash, etc., most of all building



materials are siliceous, having high content of silicates. Silica being one of the most stable materials is ideal for construction due to retention of its molecular integrity when subjected to long term weathering conditions of fluctuating temperatures, UV rays, humidity and physical forces. It won't be wrong if we say, "Earth is nothing but a ball of Silica". Though internally silica is strongly bound together by polar covalent bonding of Si-O-Si, each particle of silica at its outer periphery contains a hydroxyl ion (Silanol group). This hydroxyl ion when comes in contact with water, forms a hydrogen bond with the water molecule, resulting in energy release and breaking the water droplet further into much smaller parts. Spread of these surface hydroxyl ions at the surface, breaks down the natural water droplet into extremely tiny parts and it gets sucked into micro and nano pores of the siliceous substrate. This phenomenon, with naked eyes, we witness as the absorption of water over siliceous substrates.

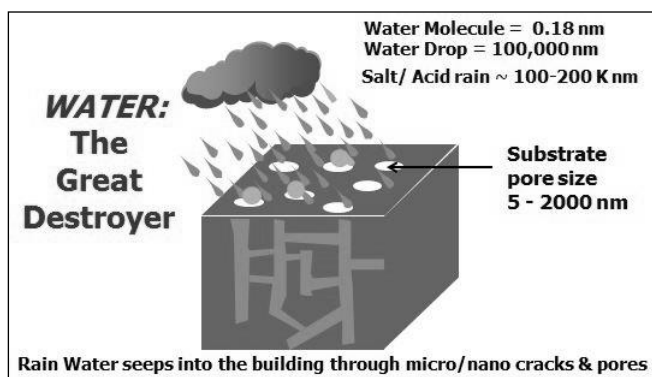


Fig. 2: Rain Water through Nano Crack

History of Silane

In second half of last century, as Silicon was discovered and found its wide acceptance in the consumer market, its Silane derivatives were used in developing composite materials. This was due to its inherent capability to bond well with both organic as well as inorganic materials. It helped in imparting strength to organic formulations by reinforcing them with inorganic fillers, where Silane would act as a coupling agent. During this period, introduction of organosilane chemicals for treatment of siliceous building materials in order to attain water resistivity became popular with the mass production of silicon and its augmentative byproducts. Even though they did address the purpose, it lacked focused research in terms of providing a solution that is, easy to use, affordable and eco-friendly. Most formulations that were marketed required skilled manpower and protective surveillance due to its inflammability and high VOC content, which resulted in high end user costs. Nevertheless, from the 1970s till beginning years of 21st century Silane proved its mettle as an effective technology which can be used to protect siliceous building materials.

Organosilane of this Millennium

The new generation Organosilane has addressed all the issues which prevented widespread use of the solvent-based Silane technology for mass consumption. Salient features of this new formulation are:

- Silane became Water dilutable (instead of Solvent), at 20 times its volume (reducing transportation cost).
- UV stable (UV stability upto 20 years).
- Became easy to apply (high dilution ability allows flooding, eliminating misapplication).
- Eco-friendly (meets the toughest Californian VOC norms).
- Affordable for masses (high water dilution, spreadability and ease of application reduced material and labour costs significantly, placing it for low-cost mass housing consumption).

How Organosilane Nanotechnology Works?

Silane, in itself is a synonym for Nanotechnology (meaning that the molecule size of this material is always smaller than 100 nm). Silicon in its smallest molecular form, that is, as a monomer, would contain one atom of Silicon bonded with other elements to form a molecule (usually < 10 nm). In this state it is referred as Silane. When a few similar Silane molecules polymerize together to form a slightly bigger molecule (usually between 50 to 100 nm), it forms an oligomer, referred as Siloxane. As the degree of polymerization increases they join together to form much larger size molecules that popularly are known as Silicon. Here it is important to understand that when sizes of these molecules change through polymerization, their combined physiochemical property also completely changes. When the surface area to volume ratio crosses beyond a certain limit, a material does not any more follow the principals of classical physics, rather it falls within the purview of quantum physics. Which is why, an elementally similar but constituted differently, material shall display different characteristics. In these lines, Silane, Siloxane and Silicon should not be misconstrued as one, even though they all are made up of similar fashioned silicon atoms. A Silicon atom (Atomic no. 14; Electronic configuration – 2, 8, 4) due to the presence of four valence electrons shall make four bonds. Based on the functionality of these bonds, they are termed as, mono-functional, bi-functional, tri-functional or tetra-functional. The new generation organosilane molecule comprises of an alkylalkoxy structure where one is an alkyl group long chain organic molecule (referred as R in Figure 3).

The rest of the three belong to alkoxy groups which when in contact with siliceous materials, like, concrete, bricks, soil, plaster, etc. replaces the Silanol (OH⁻) ion at the surface and bonds the Silane molecule to the substrate. As these three

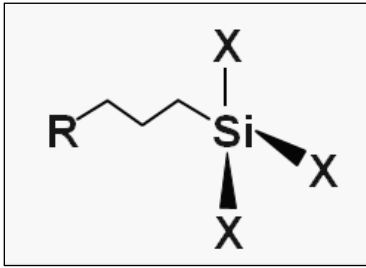
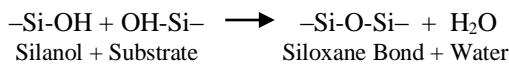


Fig. 3: Alkylalkoxy Structure

groups bond with the substrate, the non-functional R group acts as an umbrella providing a hydrophobic nano layer over the surface. The structure of this long chain organic hydrophobic R group is well researched (4/8/12/16/18 Carbon) in order to make it long lasting against UV rays and wind driven torrential rains. The reaction with the substrate is shown below in a simplified manner; however, it usually takes place in two steps. First, the alkoxy group hydrolyses to form a Silanol (Si-OH) group separating away the alkoxy (X-OH) element, and then the hydrolyzed Silane reacts with the substrate to permanently bond with it forming a Si-O-Si bond. Reaction with a Siliceous Substrate,



The treatment results in a permanent polarity change of the surface turning its nature from hydrophilic to hydrophobic.

Life Expectation

Apart from the reactive chemistry, Silane also has a major size advantage. Since the molecular size of this organosilane ranges from 4–6 nm, it actually can penetrate into the smallest pores, micro cracks and nano capillaries. Since the pore size of building materials (Figure 4) range from 5–2000 nm, a molecule size as small as 4–6 nm ensures penetration into the substrate resulting in forming successive layers of nano molecules, that prevents ingress on water into the structure.

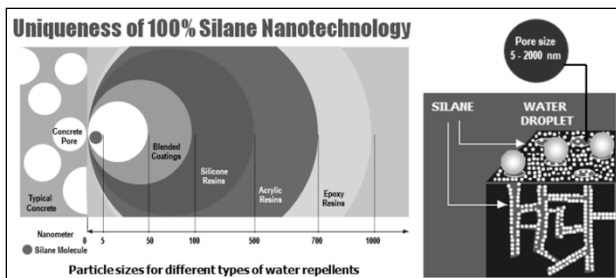


Fig. 4: Particle Sizes in Several Kind of H₂O

Life of any rain water ingress prevention technology has a major concern with respect to its stability against UV rays.

This formulation is tested against UV (as per ASTM G-154) and is estimated to have a stability of 20 years.

Logic also tells us that the most detrimental UV ray (around the wavelength of 300 nm) photons only travel in a straight line. They cannot take a curvaceous path that is taken by liquids. This tells us that only the surface molecules of the reacted organosilane shall get affected by the UV exposure. Molecules that has penetrated and bonded 1 mm deep inside the surface shall remain unaffected. By this logic, a treatment with nanotechnology organosilane has a potential to protect a concrete structure for 100 years (considering an expected 1 mm deep reactive hydrophobic transformation of the substrate against a globally accepted erosive loss rate of 0.1 mm per decade).

How to Reduce Façade Maintenance?

In today's context the popularly prevailing simplistic approach is – 'COVER-IT-UP' (Figure 4). We cover up the siliceous facades with various available material coatings striking a balance between availability and affordability; while always ending up with this coatings deteriorating (cracking, debonding or peeling-off) resulting in water ingress into the structure. Reason for this is due to gradual increase in permeability of these coatings. UV rays from the sun being most detrimental, breaks down the polymeric structure of any coating. This with the passing time allows more rain water across its film thickness to get absorbed by the siliceous substrate on which they are applied.

While it is advised to continue this approach, less has been done to extend the useful service life of these coatings. Through penetrative nanotechnology the basic nature of the structure can be changed from hydrophilic to hydrophobic. In fact, all areas of a concrete structure that shall see direct water should be pre-treated with penetrative nanotechnology before covering them up. This will ensure that whenever due to UV rays, atmospheric forces and/or physical abrasion the film breaks-up; there will be a strong water resistance original surface, which will prevent lateral travel of water across the line of contact of the film and the substrate thus, preventing its premature debonding. This shall result in optimum resource preservation through significant extension in lifespan of these 'cover-ups', like, silicon coatings, paints and waterproofing membranes.

Application and Tests

The organosilane chemical is applied by diluting with potable water (TDS < 1000) at 20 times its volume and spray flooding on the surface upto saturation i.e., till the surface stops absorbing any more. This normally is achieved by spraying 3–4 rounds within a gap of 30–60 seconds, till we see the water dripping down. Application is followed by

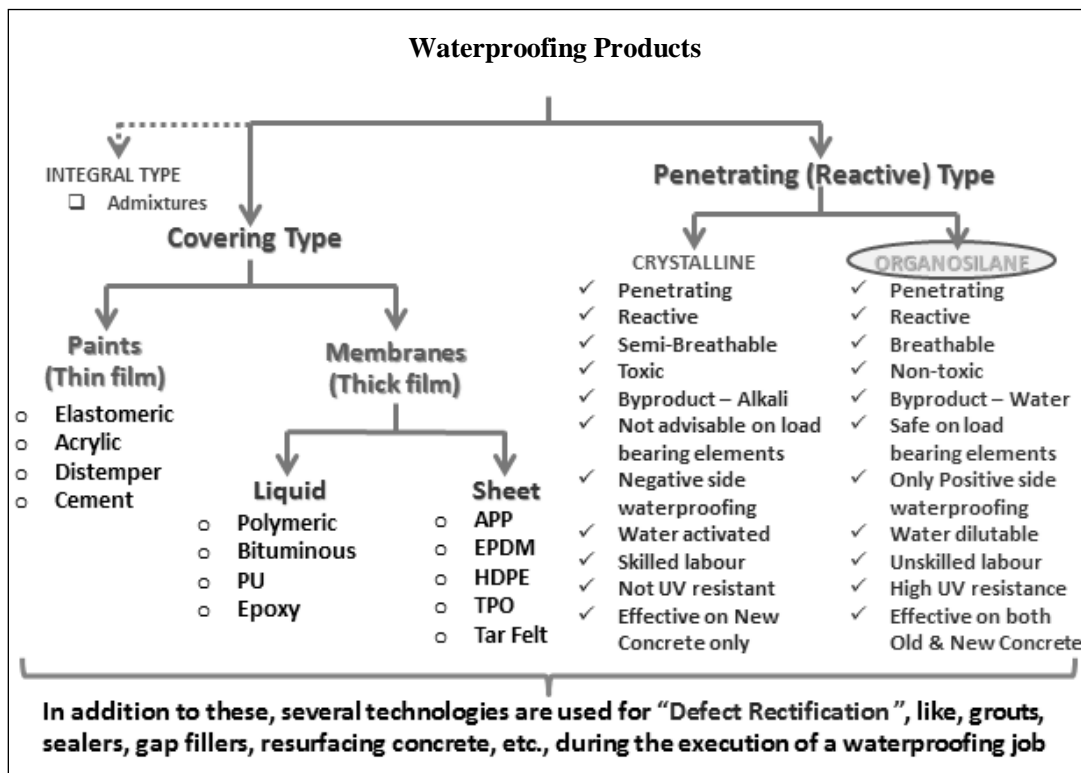


Fig. 5: Waterproofing Strategy

allowing complete drying of the substrate, till all the moisture gets fully evaporated out. Water penetration tests are conducted under laboratory conditions according to ASTM E-514. This test uses a sheet of water cascading down the face of a brick assembly. Additionally, tests to check water absorption on architectural stone, masonry mortar and structural clay tiles are conducted through ASTM 1195, ASTM 1403 and ASTM C67 tests respectively. RILEM tests can be carried out on the treated surfaces in order to test achievement of complete water insulation on the treated areas. Treated building materials with this technology shall meet the above ASTM tests and RILEM 11.4 test to resist Category 1 Hurricane. A tropical storm becomes a Category 1 hurricane when its winds near the center reach 120 km/hr. The RILEM test requires attaching a graduated tube on the treated outer surface on the structure which is filled with a water column. Also, a Scratch test to check the depth of penetration can be done on a treated surface.

Conclusion

With this water soluble 21st century Organosilane, we can redefine sustainability of façade structures, construction materials, paints, waterproofing membranes and also reduce

C&D wastes (1.3 billion ton of solid C&D waste per year, globally). It can restrict usage of expensive glass and aluminium on building facades through encouraged use of natural siliceous building materials. Most importantly, the technology extends useful service life of valuable resources extracted from mother earth, thus, preserving a more likable planet for our future generations.

References

- [1] Arkles, B., "Tailoring Surfaces with Silane," Chemtech, Vol. 7, 1977, pp. 766-778.
- [2] Crissinger, Joseph L., "Measuring Moisture Resistance to Wind-driven Rain Using a RILEM Tube," pp. 4-11, RCI Inc., November 2005.
- [3] PCA (Portland Cement Association), "Types and Causes of Concrete Deterioration". R&D Sr. No.2617, 2002
- [4] Zhuravlev, L.T., "The surface chemistry of amorphous Silica", pp. 1-4, February 2000.
- [5] Space Math @ NASA, "Cloud Droplets and Rain Drops" Lesson 84.
- [6] CSE (Centre for Science & Environment), "Construction and Demolition Waste", pp. 1-4, 2014.
- [7] Wacker Publications, "Silicones – Compounds & Properties", Germany, pp. 1-13.



Identification of Stiffness and Damping Parameters at Element Level for Structural Health Monitoring Utilizing Time Domain Dynamic Response Data

A. Debnath¹ and S. Chakraborty²

Abstract: *The Structural Health Monitoring has attracted significant attentions worldwide utilizing dynamic response data. The application of time domain data based System Identification (SI) algorithms to identify stiffness properties at element levels are well known. The present study attempted to identify the stiffness as well as damping parameters at element level of existing structures utilizing time domain data. For this, the equation error based SI algorithm, found to be efficient for identifying element properties directly is readily developed in the framework of Finite Element Method to determine the element level damage stiffness and damping properties. The algorithm is demonstrated for a number of simulated damage scenarios utilizing artificially generated dynamic response data. The consistency and robustness of the algorithm is further studied by the Monte Carlo simulation based error sensitivity analysis.*

Keywords: Structural Health Monitoring, Stiffness and Damping, Element Level Identification, Time Domain Data.

Introduction

The conventional Non-Destructive Test (NDT) can assess the damage but they are 'local' inspection approaches and cannot quantify the damage scenarios. The need for quantitative global damage detection methods has led to the continued research. Extensive research has been made to develop methods for identifying damage in structures. These methods can generally be categorized as either dynamic or static responses based techniques. Dynamic-based techniques are developed using both the free-vibration and the forced-vibration response in frequency domain and time domain as well. An excellent review article by Doebling *et al.* [1] summarized the various VBDD methods published up to 1996. Chang *et al.* [2] reviewed the literature related to SHM of civil infrastructures mainly buildings and bridges. Sohn *et al.* [3] reviewed the SHM literature in a wider range for papers published between 1996 and 2001. The literature on damage detection based on the modal data have been scattered over various areas i.e. instrumentation for sensing and recording data, system identification and damage localization algorithm, effect of error in measured response etc. The basic approaches are frequency shift, changes in the mode shapes i.e. comparison of changes in the MAC values and also COMAC values. FRF data usually involve data reduction and feature extraction during the transformation of recorded data in time domain to features in frequency domain.

The process may cause loss of information related to damage dynamics. This disadvantage could be avoided by directly using time response data. Another advantage of using time domain features is that non-linearity of responses raised by damage in a structure could be preserved further facilitating diagnostics. Numerous researchers demonstrated the potential of using time responses for identification of structural changes [4–10]. In this regard, the equation error approach is found to be efficient for identifying the element properties directly without iterations [11,12]. The application of the method is restricted to free vibration data to identify the damage stiffness only [11–14]. It has been seen that the element properties can be directly attained without iterations and the solution has unique and global minimal. The present study explored the equation error approach to identify the stiffness as well as damping parameters at element level of existing structures utilizing time domain data. For this, the equation error based SI algorithm, is readily developed in the framework of FEM to determine the element level damage stiffness and damping properties. The algorithm is demonstrated for a number of simulated damage scenarios. The consistency and robustness of the algorithm is further studied by the MCS based error sensitivity analysis.

¹Department of Civil Engineering, Meghnad Saha Institute of Technology, Kolkata, India. ✉ atanudebnath04@gmail.com

²Department of Civil Engineering, Indian Institute of Engineering Science and Technology, Shibpur, Howrah, India.



The Identification Algorithm

The general equation of motion for a multi-degree of freedom system is:

$$[M]\{\ddot{u}\}+[C]\{\dot{u}\}+[K]\{u\} = \{F\} \quad \dots (1)$$

Where, [M], [C] and [K] are mass, damping and stiffness matrix respectively. $\{u\}$, $\{\dot{u}\}$ and $\{\ddot{u}\}$ are displacement, velocity and acceleration vector respectively. $\{F\}$ is force vector. For a damped MDOF system described by Eq. (1), the identification problem can be stated as the minimization of a nonnegative error norm 'ε' defined as, Minimize,

$$\varepsilon = \sum_{t=0}^T \{([M]\{\ddot{u}\} + [C]\{\dot{u}\} + [K]\{u\}) - \{F\}\}^2 \quad \dots (2)$$

Assuming Rayleigh-type damping, the damping matrix [c_i] for ith element is expressed as,

$$[c_i] = \alpha_i[m_i] + \beta_i[k_i] \quad \dots (3)$$

Where, [m_i] and [k_i] are the mass and stiffness matrix of ith finite element, α_i and β_i are the real scalars. If the damping ratios ξ₁ and ξ₂ corresponding to the first two modal frequencies are known, the value of α_i and β_i are obtained by solving the following equation:

$$\frac{1}{2} \begin{bmatrix} 1/\omega_1 & \omega_1 \\ 1/\omega_2 & \omega_2 \end{bmatrix} \begin{Bmatrix} \alpha \\ \beta \end{Bmatrix} = \begin{Bmatrix} \xi_1 \\ \xi_2 \end{Bmatrix} \quad \dots (4)$$

Where, ω₁ and ω₂ is the first and second modal frequency. The global damping matrix for the entire structure is thus obtained as,

$$[C] = \sum_{i=1}^n [L_i] (\alpha_i [m_i] + \beta_i [k_i]) [L_i]^T \quad \dots (5)$$

In Eq. (5), n is the total number of elements. [L_i] is an N × ndel matrix that connects the local dofs to global dofs of ith element, where ndel is the dofs of a local element, N is the total dofs of the whole structure. Substituting [C] in equation (2),

$$\varepsilon = \sum_{t=0}^T ([M]\{\ddot{u}\} + \alpha[M]\{\dot{u}\} + \beta[K]\{\dot{u}\} + [K]\{u\} - \{F\})^2 \quad \dots (6)$$

Assuming conventional linear element, the stiffness of ith damaged element can be expressed as,

$$[K_{d,i}] = (g_i)[K_{u,i}] = (1 - \delta_i)[K_{u,i}] \quad \dots (7)$$

Where, [K_{d,i}] and [K_{u,i}] are the damaged and undamaged stiffness of the ith element and g_i is the parameter quantifying the damage of the ith element. Then the damaged stiffness matrix can be expressed,

$$[K] = \sum_{i=1}^n [L_i][k_{d,i}][L_i]^T = \sum_{i=1}^n (g_i)[L_i][k_{u,i}][L_i]^T \quad \dots (8)$$

Obviously [L_i], [k_{u,i}] are independent of the unknown stiffness parameter g_i. Using equation (8), the following can be easily derived,

$$[K]\{u\} = \left[\sum_{i=1}^n (g_i)[L_i][k_{u,i}][L_i]^T \right] \{u\} = [P_t]\{g\} \quad \dots (9)$$

Where,

$$[P_t] = [L_1][k_{u,1}][L_1]^T \{u\} \quad [L_2][k_{u,2}][L_2]^T \{u\} \\ \dots \dots \dots [L_n][k_{u,n}][L_n]^T \{u\}$$

[P_t] = [P₁] {P₂} ... {P_n} and {g} = [g₁ g₂ ... g_n]^T Again, using the results of equation (9), the following can be obtained,

$$\beta[K]\{\dot{u}\} = [\sum_{i=1}^n (\beta_i g_i) [L_i][k_{u,i}][L_i]^T] \{\dot{u}\} = [Q_t]\{\beta g\} \\ = [Q_t]\{h\} \quad \dots (10)$$

Where,

$$[Q_t] = [Q_1] \{Q_2\} \dots \{Q_n\} \text{ and } \{h\} = [\beta_1 g_1 \quad \beta_2 g_2 \dots \beta_n g_n]^T \\ \alpha[M]\{\dot{u}\} = [\sum_{i=1}^n (\alpha_i) [L_i][m_i][L_i]^T] \{\dot{u}\} = [S_t]\{\alpha\} \quad \dots (11)$$

Where,

$$[S_t] = [[L_1][m_1][L_1]^T \{\dot{u}\} \dots [L_n][m_n][L_n]^T \{\dot{u}\}] \\ = [\{S_1\} \{S_2\} \dots \{S_n\}], \{\alpha\} = [\alpha_1 \alpha_2 \dots \alpha_n]^T$$

The multiplication of mass matrix and acceleration are considered as a vector {R_t} and subtracted from force vector to define {W_t} i.e. [M]{\ddot{u}} = {R_t} and {F_t} - {R_t} = {W_t}. Substituting the results of equation (9) to (11) and {W_t} the error function becomes,

$$\varepsilon = \sum_{t=0}^T ([P_t]\{g\} + [Q_t]\{h\} + [S_t]\{\alpha\} - \{W_t\})^2 \quad \dots (12)$$

The unknowns are {g}, {h} and {α}. The minimum value of ε can be obtained by

Setting $\frac{\partial \varepsilon}{\partial \{g\}} = 0$, $\frac{\partial \varepsilon}{\partial \{h\}} = 0$ and $\frac{\partial \varepsilon}{\partial \{\alpha\}} = 0$ leads to following

equations:

$$\sum_{t=0}^T ([P_t]^T [P_t] \{g\} + [P_t]^T [Q_t] \{h\} + [P_t]^T [S_t] \{\alpha\} - [P_t]^T \{W_t\}) = 0 \quad \dots (13)$$

$$\sum_{t=0}^T ([Q_t]^T [P_t] \{g\} + [Q_t]^T [Q_t] \{h\} + [Q_t]^T [S_t] \{\alpha\} - [Q_t]^T \{W_t\}) = 0 \quad \dots (14)$$

$$\sum_{t=0}^T ([S_t]^T [P_t] \{g\} + [S_t]^T [Q_t] \{h\} + [S_t]^T [S_t] \{\alpha\} - [S_t]^T \{W_t\}) = 0 \quad \dots (15)$$

Those can be expressed in matrix form as,

$$\sum_{t=0}^T \begin{bmatrix} [P_t]^T & [P_t] & [P_t]^T & [Q_t] & [P_t]^T & [S_t] \\ [Q_t]^T & [P_t] & [Q_t]^T & [Q_t] & [Q_t]^T & [S_t] \\ [S_t]^T & [P_t] & [S_t]^T & [Q_t] & [S_t]^T & [S_t] \end{bmatrix} \begin{Bmatrix} \{g\} \\ \{h\} \\ \{\alpha\} \end{Bmatrix} = \sum_{t=0}^T \begin{Bmatrix} [P_t]^T \\ [Q_t]^T \\ [S_t]^T \end{Bmatrix} \{W_t\}$$

$$\text{i.e. } [A]\{X\} = \{b\} \quad \dots (16)$$

Above equation can be solved to obtain {g}, {h} and {α} for each element using time domain response data.



Numerical Study

The proposed SI algorithm is demonstrated through numerical example of a one story one bay plane aluminium frame as shown in Figure 1.

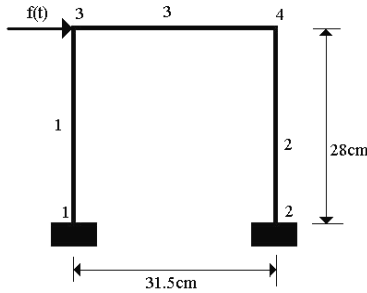


Fig. 1: Simple Plane Frame

The theoretical responses of the numerical model are first calculated using the Numark’s β method from known mass, stiffness and damping matrix. The cross sectional area of both beam and column are 1.32 cm^2 . The mass per unit length of all the beams and columns is 3.564 gm/cm . To generate response data artificially, the damping ratio has been taken corresponds to the first two modes is 1% and .5% i.e. $\xi_1 = 1\%$ and $\xi_2 = 0.5\%$. Using Eq. (4) the (α) and (β) are obtained. The first and second modal frequencies of undamaged structure are 179.1 rad/s and 615.75 rad/s respectively. Now from Eq.(4) the calculated α and β are 8.7952 and 2.8011×10^{-6} respectively. The defect free frame is excited by a harmonic force $f(t) = 4.44 \text{ Sin}(40t) \text{ N}$.

The theoretical responses of the frame are calculated using MATLAB. The theoretical and identified stiffness of the

three elements are shown in Table 1 for different damage cases. The damping identification results are shown in Tables 2 and 3. The results clearly indicate that the algorithm can identify the stiffness and damping parameters very well for various damage scenarios.

To study the performance of the proposed algorithm under noisy responses, the noise free response data are further polluted by adding numerically generated noise following equation below:

$$X_{ij} = X_{ij}^0 (1 + \gamma \zeta_{ij}) \quad \dots (17)$$

In the above, γ is the relative magnitude of the error and ζ_{ij} is uniform random variate in range $[-1, 1]$, X_{ij}^0 is the response in the i^{th} degree of freedom at the j^{th} time step with no error.

The standard MCS is performed to extract the statistical properties of the identified damage parameters to study the effect of errors in response data on the parameter identification process. The MCS is now performed with 1000 simulation to obtain the mean value and percentage of error of various identified parameters. Table 4 shows the values of the identified damage parameters.

It can be readily noted from the results that though the response data is noisy, the algorithm can detect the defect member and damage intensity. It can be also observed that percentage of error in identified parameters is small for the level of noise considered which establishes the robustness of the algorithm. The algorithm also identifies the mass and stiffness proportional damping coefficient from noisy time domain dynamic data. The results are shown in Tables 5 and 6.

Table 1: g Identification under Sinusoidal Load

Damage Case	Identified Damage Parameters in Each Member		
	g_1	g_2	g_3
Damage free	1.00	1.00	1.00
5% damage in member 1	0.95	1.00	1.00
5% damage in member 1 & 10% in 2	0.95	0.9	1.00
5% damage in member 1 & 10% damage in 2 & 3	0.95	0.9	0.9
10% damage in member 1 & 15% damage in 2 & 3	0.9	0.85	0.85

Table 2: α Identification under Sinusoidal Load

Damage Case	Input Mass Proportional Damping Coefficient (α)	Identified Mass Proportional Damping Coefficients in Each Member		
		α_1	α_2	α_3
Damage free	8.7952	8.7952	8.7952	8.7952
5% damage in member 1	8.7097	8.7097	8.7097	8.7097
5% damage in member 1 & 10% in 2	8.5353	8.5353	8.5353	8.5353
5% damage in member 1 & 10% damage in 2 & 3	8.4305	8.4305	8.4305	8.4305
10% damage in member 1 & 15% damage in 2 & 3	8.1978	8.1978	8.1978	8.1978



Table 3: β Identification under Sinusoidal Load

Damage Case	Input Stiffness Proportional Damping Coefficient (β)	Identified Stiffness Proportional Damping Coefficients in Each Member		
		$\beta 1$	$\beta 2$	$\beta 3$
Damage free	2.8011×10^{-6}	2.8011×10^{-6}	2.8011×10^{-6}	2.8011×10^{-6}
5% damage in member 1	2.8280×10^{-6}	2.8280×10^{-6}	2.8280×10^{-6}	2.8280×10^{-6}
5% damage in member 1 & 10% in 2	2.8845×10^{-6}	2.8845×10^{-6}	2.8845×10^{-6}	2.8845×10^{-6}
5% damage in member 1 & 10% damage in 2 & 3	2.9228×10^{-6}	2.9228×10^{-6}	2.9228×10^{-6}	2.9228×10^{-6}
10% damage in member 1 & 15% damage in 2 & 3	3.0058×10^{-6}	3.0058×10^{-6}	3.0058×10^{-6}	3.0058×10^{-6}

Table 4: Identification of g using Noisy Response Data

	Damage Case	Identified Damage Parameters in Each Member		
		$g1$	$g2$	$g3$
No noise	Damage free	1.00	1.00	1.00
2% noise		1.009	1.0004	1.0014
Percentage of error		0.09%	0.04%	0.14%
5% noise		1.0031	1.0030	1.0020
Percentage of error		0.31%	0.30%	0.2%
No noise	5% damage in member 1 & 10% damage in 2	0.95	0.9	1.00
2% noise		0.9508	0.9007	1.000
Percentage of error		0.084%	0.078%	0.0%
5% noise		0.952	0.901	1.001
Percentage of error		0.21%	0.11%	0.11%
No noise	5% damage in member 1 & 10% damage in 2&3	0.95	0.9	0.9
Noise 2%		0.9495	0.8996	0.8994
Percentage of error		0.053%	0.044%	0.067%
5% noise		0.9533	0.9037	0.9024
Percentage of error		0.35%	0.41%	0.27%

Table 5: Identification of α using Noisy Response Data

	Damage Case	Identified Mass Proportional Damping Coefficients in Each Member		
		$\alpha 1$	$\alpha 2$	$\alpha 3$
No noise	Damage free	8.7952	8.7952	8.7952
2% noise		9.255	9.0967	8.6351
Percentage of error		5.23%	3.42%	1.82%
5% noise		9.5914	9.5695	8.4175
Percentage of error		9.05%	8.8%	4.3%
No noise	5% damage in member 1 & 10% damage in 2	8.5353	8.5353	8.5353
2% noise		8.7229	8.6853	8.4638
Percentage of error		2.2%	1.76%	0.84%
5% noise		9.3447	9.1885	8.1823
Percentage of error		9.5%	7.65%	4.13%
No noise	5% damage in member 1 & 10% damage in 2 & 3	8.4305	8.4305	8.4305
Noise 2%		8.544	8.5476	8.3636
Percentage of error		1.35%	1.39%	0.8%
5% noise		9.2175	9.1816	8.0927
Percentage of error		9.33%	8.9%	4.0%



Table 6: Identification of β using Noisy Response Data

	Damage Case	Identified Stiffness Proportional Damping Coefficients in Each Member		
		β_1	β_2	β_3
No noise	Damage free	2.8011×10^{-6}	2.8011×10^{-6}	2.8011×10^{-6}
2% noise		2.637×10^{-6}	2.763×10^{-6}	2.793×10^{-6}
Percentage of error		5.86%	1.36%	0.3%
5% noise		2.883×10^{-6}	2.753×10^{-6}	2.821×10^{-6}
Percentage of error		2.92%	1.72%	0.71%
No noise	5% damage in member 1 & 10% damage in 2	2.8845×10^{-6}	2.8845×10^{-6}	2.8845×10^{-6}
2% noise		2.863×10^{-6}	2.874×10^{-6}	2.89×10^{-6}
Percentage of error		0.74%	0.364%	0.2%
5% noise		2.789×10^{-6}	2.816×10^{-6}	2.874×10^{-6}
Percentage of error		3.31%	2.4%	0.36%
No noise	5% damage in member 1 & 10% damage in 2 & 3	2.9228×10^{-6}	2.9228×10^{-6}	2.9228×10^{-6}
Noise 2%		2.941×10^{-6}	2.912×10^{-6}	2.918×10^{-6}
Percentage of error		0.62%	0.36%	0.16%
5% noise		3.120×10^{-6}	2.902×10^{-6}	2.969×10^{-6}
Percentage of error		6.74%	0.71%	1.58%

It may be seen that the error in the identified damping parameters is larger than that of stiffness parameter identification. Figure 2 shows the change of COV of identified stiffness parameters with the change of input percentage of noise. It can be observed that the COV of the identified damage parameter is almost equal to the input percentage of noise which shows the robustness of the identification algorithm. Figure 3 shows the change of percentage of variation of identified stiffness parameter ($((\text{percentage of variation} = \text{actual value} - \text{mean value})/\text{actual value}) \times 100$) with the change of input percentage of noise.

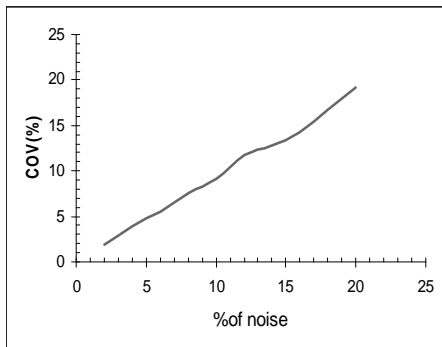


Fig. 2: Change of COV (%) of (g) with the Change of Percentage of Noise during Damage Case

It is observed from the graph that the change of percentage of variation is very low with respect to the change of input percentage of noise.

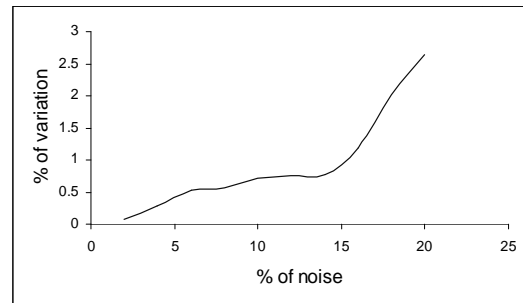


Fig. 3: Change of Percentage of Variation of (g) with the Change of Percentage of Noise during Damage Case

Conclusion

The equation error based SI approach is proposed in present study to identify the damage stiffness and damping properties of MDOF dynamic system at element level using time domain data. The consistency and robustness of the algorithm is studied by MCS based error sensitivity analysis.

The identified damages and damping parameters show excellent agreement with actual parameters. It is found that in most cases the percentage of error is below 10% for the considered level of error percent in input data even for large damage intensity, which establishes the robustness of the algorithm. Results are shown only for few selected cases, however the observation for other damage cases are same. In present work, the case studies are limited to two dimensional frames only. The method can be extended to include various



forms such as beam, plate, etc. It needs to study further when a structural behavior becomes non-linear due to inception of damage. More general type of viscous damping model needs to be investigated further for identification of parameters by the proposed approach. The method should also be verified with real measurements.

References

- [1] Doebling, S.W., Farrar, C.R., Prime, M.B. and Shevitz, D.W., Damage Identification and Health Monitoring of Structural and Mechanical System from Changes in Their Vibration Characteristics a Literature Review, TR No. LA-13070-MS UC-900, University of California, 1996.
- [2] Chang, P.C., Flatau, A. and Liu, S.C., Review Paper: Health Monitoring of Civil Infrastructure. *Structural Health Monitoring*, 2(3), 257–267 (2003).
- [3] Sohn, H., Farrar, C.R., Hemez, F.M., Shunk, D., Stinemates, D.W., Nadler, B. R. and Czarnecki, J.A. Review of structural health monitoring literature: 1996–2001, *Los Alamos National Laboratory Report*, LA-13976-MS. (2004).
- [4] Agbabian, M.S., Masri, S.F., Miller, R.K. and Caughey, T.K., System identification approach to detection of structure changes, *Journal of Engineering Mechanics*, ASCE, 117(2), 370–390, (1991).
- [5] Wang, D. and Halder, A., Element level system identification with unknown input information, *J. of Eng. Mech.*, 120(1), 159–176 (1994).
- [6] Cavaleri, L., Papia, M., A new dynamic identification technique: application to the evaluation of the equivalent strut for infilled frame, *Engineering structure*, 25, 889–901 (2003).
- [7] Yang, J.N. Lei, Y., Lin. S. and Huang, N., Hilbert-Huang Based Approach for Structural Damage Detection, *Journal of Engineering Mechanics*, ASCE, 130, (1), 85–95 (2004).
- [8] Kathuda, H., Martinez, R. and Haldar, A. (2005). Health assessment at local level with unknown input excitation. *Journal of Structural Engng.*, ASCE, 131(6), 956–965 (2005).
- [9] Li, J. and Zang, Y., Prediction error method second-order structural identification algorithm in stochastic state space formulation. *Earthquake Engng Struct. Dyn.*, 35(6), 761–779 (2006).
- [10] Perry, M.J. and Koh, C.G., Output-only structural identification in time domain: Numerical and experimental studies. *Earthquake Engng Struct. Dyn.*, 37, 517–533 (2008).
- [11] Liu, P., Identification and damage detection of trusses using modal data, *J. of Structural Engng.*, ASCE, 121(4), 599–607 (1995).
- [12] Liu, P. and Chain, C., Parametric identification of the truss structures using static strain, *J. of Structural Engng.*, ASCE, 123(7), 927–933 (1997).
- [13] Roy, S., Chakraborty, S. and Sasrkar, S.K., Damage detection of coupled bridge deck-girder system, *Finite Elements in Analysis and Design*, 42, 942–949 (2006).
- [14] Chakraborty, S. and Roy, S., Element Level Identification of a Viscously Damped System. *International, Journal of Acoustics and Vibration*, 15(3), 113–120 (2010).



An Efficient Response Surface Method Based Finite Element Model Updating of Composite Structures

T. Islam¹, S. Chakraborty² and C. Ray²

Abstract: *The composite material properties are usually available from manufacturers as a whole rather than specific properties of various components. Thus, proper identification of composite parameter is important for overall assessment of behaviour and health monitoring. The present study deals with the application of the Finite Element Model Updating (FEMU) technique to identify the parameters of composite structures. In doing so, the Moving Least Square Method (MLSM) based Response Surface Method (RSM) for FEMU technique using dynamic responses are attempted here for identifying the structural parameters. A comparative study between least square method (LSM) and MLSM based RSM is performed to study the effectiveness of the MLSM based RSM for identifying the parameters of the composite structures. In doing so, an error sensitivity study is also performed to realise the robustness of the RSM based approaches. A Fibre Reinforced Plastic (FRP) bridge deck panel made of E-Glass/Epoxy symmetric cross-ply laminate is considered to elucidate the proposed FEMU algorithm. In general, it is noted that the MLSM based RSM identify the model parameters much better than the LSM based RSM approach. The error sensitivity study also indicates the more robustness of the MLSM based algorithm compare to the LSM based FEMU algorithm.*

Keywords: Health Monitoring; Composite Structures; Finite Element Model Updating; RSM.

Introduction

Composite materials like fibre reinforced polymers, Glass Fibre Reinforced Polymers (GFRP), Carbon Fibre Reinforced Polymer (CFRP), etc. are widely used in the aeronautical, automotive, marine and wind turbine blade industries mainly due to their high strength to weight and stiffness to weight ratios. A major problem of such composite structures is on Non-Destructive Testing (NDT) or in-situ identification of developed non-visible damage under real loading conditions. Thus, proper identification of composite parameter is important for overall assessment of behaviour and health monitoring of composite structures. The FEMU, basically an inverse problem used to identify the parameters of a Finite Element (FE) model found to be useful in this regard. The technique actually updates the uncertainty parameters in the initially assumed FE model based on the measured responses so that a more realistic or refined model can be achieved. The present study deals with the application of FEMU technique to identify the parameters of composite structures.

The development of non-iterative and iterative FEMU methods based on dynamic and static data is well known [1–4].

However, the sensitivity based iterative methods involving determining local gradients are not only computationally intensive, but also has convergence difficulty. For large FE model of structures, the large number of computations involved can rule out many approaches due to expense of carrying out many runs. This problem can be overcome by using an approximate surrogate meta model in place of FE model. Response Surface (RS) is one of the commonly used meta model. In case of structural FEMU, once the RS of structure is constructed, updating the model is reduced to the task of finding the smallest value on the RS. Over the years, the LSM based RSM for model updating has gained momentum [5]. Several successful applications of LSM based RSM in FEMU using dynamic or static data or both combined can be found in [6–10]. RS model obtained by using the LSM are based on global approximation, seems to be a major sources of error in prediction of RS model. The MLSM, basically a local approximation approach, is found to be more efficient in this regard. However, the application of MLSM based RSM in FEMU is scarce [11–12].

The MLSM based RSM for FEMU technique using dynamic responses are attempted here for identifying the parameters

¹Department of Civil Engineering, Techno India University, Kolkata, India. ✉ tawhidul.iest@gmail.com

²Department of Civil Engineering, Indian Institute of Engineering Science and Technology, Shibpur, Howrah, India.



of composite structures. A comparative study between LSM and MLSM based RSM is performed to study the effectiveness of the MLSM based RSM for identifying the parameters of the composite structures. In doing so, an error sensitivity study is also performed to realise the robustness of the RSM based approaches. A FRP bridge deck panel made of E-Glass/Epoxy symmetric cross-ply laminate is considered to elucidate the proposed FEMU algorithm. In general, it is noted that the MLSM based RSM identify the model parameters much better than the LSM based RSM approach. The error sensitivity study also indicates the more robustness of the MLSM based algorithm compare to the LSM based FEMU algorithm.

RSM Based FEMU

The RSM is a set of mathematical and statistical techniques designed to gain a better understanding about the overall response by design of experiments (DOE). The RS equation is simply a polynomial regression to a data set. The basic process consists of calculating predicted values of the response features at various sample points in the parameter space by performing an experiment at each of those points.

LSM based RSM

If there are n response values y_i corresponding to n numbers of observed data, x_{ij} (denotes the i^{th} observation of the input variable x_j in a DOE), the relationship between the response and the input variables can be expressed by the following,

$$y = X\beta + \varepsilon_y \quad \dots (1)$$

In the above multiple non-linear regression model X , y , β and ε_y are the design matrix containing the input data from the DOE, the response vector, the unknown co-efficient vector and the error vector, respectively. Typically, the quadratic polynomial form used in the RSM is as following:

$$y = \beta_0 + \sum_{i=1}^k \beta_i x_i + \sum_{i=1}^k \beta_{ii} x_i^2 \quad \dots (2)$$

The LSM of estimation technique is usually applied to obtain the unknown polynomial coefficient by minimizing the error norm defined as:

$$L = \sum_{i=1}^n \left(y_i - \beta_0 - \sum_{i=1}^k \beta_i x_i - \sum_{i=1}^k \beta_{ii} x_i^2 \right)^2 = (y - X\beta)^T (y - X\beta) \quad \dots (3)$$

And the least squares estimate of β is obtained as,

$$\beta = [X^T X]^{-1} \{X^T y\} \quad \dots (4)$$

Once the polynomial coefficients β are obtained from the above equation, the response y can be readily evaluated for any set of input parameters.

MLSM based RSM

The MLSM based RSM is a weighted LSM that has varying weight functions with respect to the position of approximation. The weight associated with a particular sampling point x_i decays as the prediction point x moves away from x_i . The weight function is defined around the prediction point x and its magnitude changes with x . The least-squares function $L_y(x)$ can be defined as the sum of the weighted errors as following,

$$L_y(x) = \sum_{i=1}^n w_i \varepsilon_i^2 = \varepsilon^T W(x) \varepsilon = (y - x\beta)^T W(x) (y - x\beta) \quad \dots (5)$$

Where, is the diagonal matrix of the weight function. It can be obtained by utilizing the weighting function such as constant, linear, quadratic, higher order polynomials, exponential functions, etc. [13]. In the present study, following form [14] of weight function is considered,

$$w(x - x_i) = w(d) = \frac{e^{-\left(\frac{d}{c}\right)^{2k}} - e^{-\left(\frac{1}{c}\right)^{2k}}}{1 - e^{-\left(\frac{1}{c}\right)^{2k}}}, \text{ if } d < D; \text{ else } 0 \quad \dots (6)$$

Where, c and k are free parameters to be selected for better efficiency. Common values suggested in the literatures are $c = 0.4$, $k = 1$. The parameter d represents the distance of the point where approximate response is required to the origin of the approximating domain. It should be selected at any point of interest such that it contains sufficient numbers of DOE points to avoid singularity. By minimizing the least-squares estimators $L_y(x)$, the coefficients $\beta(x)$ can be obtained as,

$$\beta(x) = \left[x^T W(x) x \right]^{-1} x^T W(x) y \quad \dots (7)$$

It is important to note here that the coefficients $\beta(x)$ are the function of location x , where the approximation is sought.

Model Updating Procedure

The updating of parameters consistent with the structural response is basically minimization of a nonnegative error function i.e. the residuals between the responses obtained from the solution of the FE model of the structure and the measured responses from the actual structure. In the present study, the updating procedure start with replacing the evaluation of FE response quantity f_k (natural frequency herein) by RSM. The optimization problem for parameter updating is posed as following,

Minimize,

$$\varepsilon = \sum_{k=1}^r \left(1 - \left| \frac{\omega_{fk}(x)}{\omega_k} \right| \right)^2 \quad \dots (8)$$



where $\omega_{fk}(x)$ and ω_{ik} are the RS metamodel data and experimental data of natural frequencies respectively.

The implementation of the proposed FEMU procedure using dynamic response is a three-stage interlinked procedure, viz.: i) Analysis of the FE model at the DOE points to obtain the response necessary to construct the RS, ii) Evaluation of the RS function, $f(X)$ following the MLSM based RSM during the iteration of the optimization process utilizing the computed responses as per the DOE in step (i) and (ii). Finally checking the convergence of the optimization solution and obtaining the desired updated model parameters. It is important to note that for each update of the parameters during the iteration process, the MLSM based RSM is re-called and new approximation function is formed which is not the case for LSM based RSM where a single approximation function $f(X)$ gets operated throughout the iteration process.

Numerical Study

A simply supported FRP bridge deck panel ($4\text{ m} \times 1\text{ m} \times 0.25\text{ m}$) made of E-Glass/Epoxy symmetric cross-ply $[0^\circ/90^\circ/90^\circ/0^\circ]$ laminate of thickness 0.025 m has been considered. The baseline values of the material properties used for numerical study are: $E1 = 41\text{ GPa}$, $E2 = E3 = 12\text{ GPa}$, $\nu12 = \nu13 = 0.28$, $\nu23 = 0.5$, $G12 = 5.5\text{ GPa}$, $G13 = 5.5\text{ GPa}$, $G23 = 3.5\text{ GPa}$ and $\rho = 2100\text{ kg/m}^3$. This deck panel was modelled in ANSYS Parametric Design Language (APDL) using eight noded layered SHELL281 element having 8 nodes with 6 degrees of freedom at each node. The FEMU algorithm needs measured response from the actual structure as input (i.e. ω_{ik}). However, no experimental investigation was done in the present study. The FE analysis is performed in ANSYS software to obtain the structural response with these reduced parameters values and used as the necessary input response of the FEMU algorithm.

With the baseline values of the material properties the first three natural frequencies are 24.656 Hz , 27.708 Hz and 67.910 Hz . For developing the second degree polynomial RS models, $E1$, $E2$, $G12$, $G13$, (ρ) and $\nu12$ are the six model parameters represented as $X1$, $X2$, $X3$, $X4$, $X5$ and $X6$, respectively. Twenty DOE points have been generated within 30% (+ and -) of baseline values by Latin hypercube sampling design method. Once the DOE points are generated, the frequencies are obtained with the aid of FE model. The first three natural frequencies are used to find out the coefficient β using eqn. (4) and (7) for LSM and MLSM based RS model, respectively.

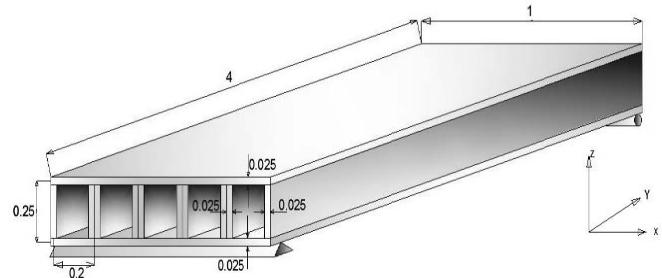


Fig. 1: FRP Bridge Deck Panel (Dimensions in m)

Model Parameter Identification

For different cases the identified model parameters by LSM and MLSM are represented in Table 1. It can be noticed that though both the approaches can identify the predefined parameters well; the MLSM based method identifies the parameters better even beyond the range of data points.

Error Sensitivity Study

The error sensitivity of LSM and MLSM based RSMs in FEMU are further performed. The six model parameters of the FRP bridge deck panel are identified by introducing certain amount of predefined error in the response as following,

$$y_{error} = y + (r \times p \times y) \quad \dots (9)$$

Where, y_{error} and y are the erroneous and the frequency without error, respectively, p is the percentage of error, r is a uniformly distributed random numbers between $+1$ to -1 . A set of 5000 erroneous y are generated. With these values of y , the model parameters are identified by optimizing equation (8) and the mean and standard deviation (SD) of the identified parameters are obtained accordingly. The model parameters shown in Table 1 for Case 2 are identified by considering varying percentage of errors (i.e. 5 to 20%) in frequency data. For 20% error, the SD of the identified parameter $X1$ with respect to the number of simulation is shown in Figure 2. It can be seen from the figure that the SD of MLSM based RSM is lesser than LSM based RSM approach. Other identified parameters also show similar pattern.

The mean values of the identified parameters for different percentage of errors in frequency data are studied. The results for 5% and 15% are shown in the Table 2. Again both the LSM and MLSM based algorithms identify the parameters with good accuracies. But MLSM based method is more robust. Further, the values of the coefficient of variation (COV) of the model parameters are also calculated and shown in Table 3.

It can be observed that the COV increases with the increase in error in frequency and LSM based method yields higher



COV compared to MLSM based method indicating that the MLSM based RSM updates the model parameters better with more confidence. Based on the 5000 identified parameter sets, 5000 sets of first three natural frequencies are calculated for both LSM and MLSM based on FEMU using

eqn. (2) and comparative graphs of its mean are shown in Figures, 3, 4 and 5. It can be readily noted that with increasing errors in response, error in the updated natural frequencies increases.

Table 1: Parameter Identification Results by LSM and MLSM based RSMs without Error in Response Input Data

	Parameter	Predetermined Parameter Values	Parameter Obtained by LSM	Parameter Obtained by MLSM
Case 1 10% less	X1	3.690E+10	3.631E+10	3.659E+10
	X2	1.080E+10	1.074E+10	1.077E+10
	X3	4.950E+09	5.073E+09	4.998E+09
	X4	4.950E+09	4.952E+09	4.951E+09
	X5	1890	1878.689	1887.391
	X6	0.252	0.2514	0.2516
Case 2 20% less	X1	3.280E+10	3.214E+10	3.25E+10
	X2	9.600E+09	9.524E+09	9.574E+09
	X3	4.400E+09	4.451E+09	4.382E+09
	X4	4.400E+09	4.395E+09	4.398E+09
	X5	1680	1714.229	1710.975
	X6	0.224	0.2237	0.2242
Case 3 30% less	X1	2.870E+10	2.861E+10	2.863E+10
	X2	8.400E+09	8.189E+09	8.239E+09
	X3	3.850E+09	3.816E+09	3.792E+09
	X4	3.850E+09	3.788E+09	3.801E+09
	X5	1470	1584.653	1580.461
	X6	0.196	0.1962	0.1964

Table 2: Parameter Identification Results with Varying Error in Frequency for Case 2

% of Error	Parameter	Predetermined Parameter Values	Parameter Obtained by LSM	Parameter Obtained by MLSM
5	X1	3.280E+10	3.272E+10	3.275E+10
	X2	9.600E+09	9.373E+09	9.568E+09
	X3	4.400E+09	4.487E+09	4.342E+09
	X4	4.400E+09	4.342E+09	4.386E+09
	X5	1680.00	1730.407	1719.989
	X6	0.224	0.22295	0.22420
15	X1	3.280E+10	3.261E+10	3.279E+10
	X2	9.600E+09	9.367E+09	9.406E+09
	X3	4.400E+09	4.491E+09	4.332E+09
	X4	4.400E+09	4.344E+09	4.320E+09
	X5	1680.00	1747.482	1721.076
	X6	0.224	0.22291	0.22303



Table 3: COV of the Updated Parameters for Erroneous Response Input

% of Error	Method Applied	COV of X1 (%)	COV of X2 (%)	COV of X3 (%)	C.O.V of X4 (%)	C.O.V of X5 (%)	C.O.V of X6 (%)
5	LSM	1.922	1.788	1.940	0.576	4.983	0.481
	MLSM	1.797	0.465	2.577	0.411	4.434	0.465
15	LSM	3.506	3.476	6.240	1.574	14.368	1.349
	MLSM	3.065	1.985	8.626	1.681	12.595	1.256

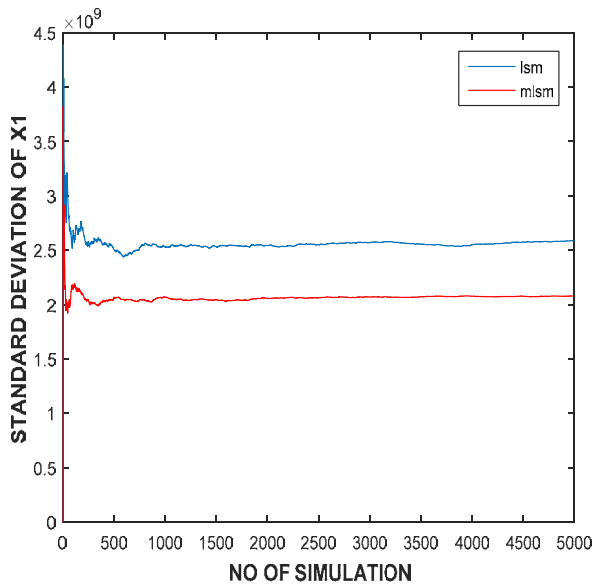


Fig. 2: SD of the Model Parameter X1

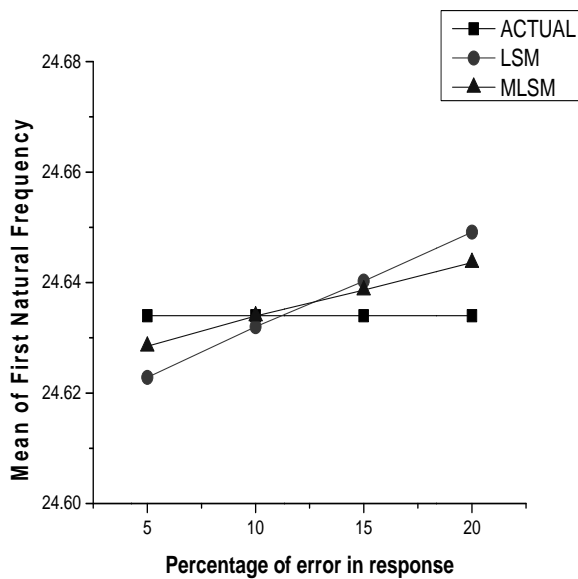


Fig. 3: Identified First Natural Frequency

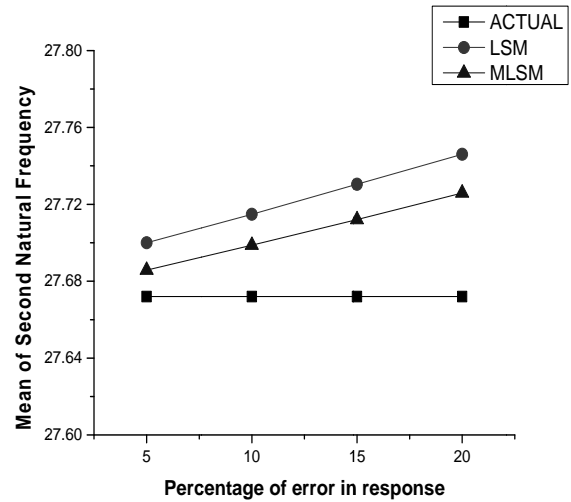


Fig. 4: Identified Second Natural Frequency

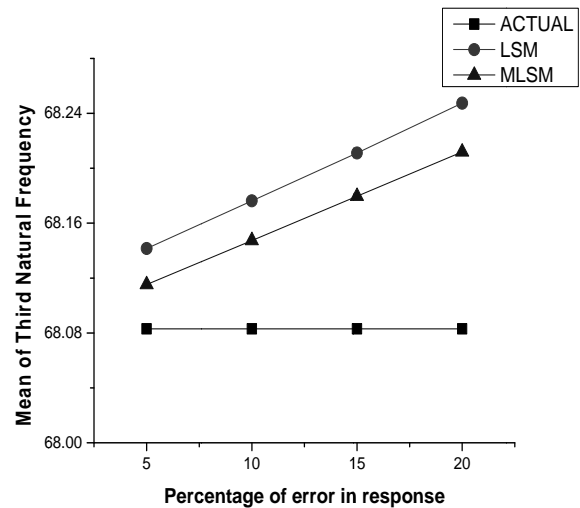


Fig. 5: Identified Third Natural Frequency

Summary and Conclusion

An efficient RSM based FEMU of a FRP bridge deck structure is presented here. The parameter identification is



being made by LSM and MLSM based RSM using natural frequency data. In general, the LSM based RSM can update the model parameters successfully. But, the MLSM based RSM updates with improve accuracy. The error sensitivity study shows that with increase in percentage of error in responses, the efficiency of parameter identification decreases. The COV of updated model parameters generally increases with the increase in percentage of error in frequency data. Based on the comparison of COV values of updated model parameters, it can be observed that for all the parameters MLSM based RSM has better efficiency of parameter identification than the LSM based RSM. The updated natural frequency as obtained by the LSM and MLSM based FEMU method, it is noted that both the approaches are capable to update parameter with reasonable accuracy; but the MLSM based approach is better. In present study FEMU using LSM and MLSM based RSMs are studied for simulated dynamic frequency data. However, experimental study with actual measured response data is needed to prove the superiority of the MLSM over the LSM technique for real situation. This study can also be extended for combined static (like strain) and other dynamic (like mode shape, frequency response function) responses of structures.

References

- [1] Friswell, M.I., Mottershead, J.E. and Ahmadian, H., Finite-element model updating using experimental test data: parametrization and regularization, *Phil. Trans. R. Soc. Lond. A*, 359, 169–186 (2001).
- [2] Gladwell, G., *Inverse problems in vibration*, Dordrecht: Springer, 2005.
- [3] Mottershead, J.E., Link, M. and Friswell, M.I., The sensitivity method in finite element model updating: A tutorial, *Mechanical Systems and Signal Processing* 25, 2275–2296 (2011).
- [4] Jaishi, B. and Ren, W.X., Finite element model updating based on eigenvalue and strain energy residuals using multi-objective optimisation technique, *Mechanical Systems and Signal Processing* 21, 2295–2317 (2007).
- [5] Marwala, T., *Finite-element-model updating using computational intelligence techniques*, London: Springer, 2010.
- [6] Ren, W.X., Fang, S.E. and Deng, M.Y., Response Surface-Based Finite-Element-Model Updating Using Structural Static Responses, *Journal of Engineering Mechanics* 137(4), 248–257 (2011).
- [7] Fang, S.E., Ren, W.X. and Perera, R., A stochastic model updating method for parameter variability quantification based on response surface models and Monte Carlo simulation, *Mechanical Systems and Signal Processing* 33, 83–96 (2012).
- [8] Shan, D., Li, Q., Khan, I. and Zhou, X., A novel finite element model updating method based on substructure and response surface model, *Engineering Structures* 103, 147–156 (2015).
- [9] Deng, L. and Cai, C.S., Bridge Model Updating Using Response Surface Method and Genetic Algorithm, *Journal of Bridge Engineering*, 15(5), 553–564 (2010).
- [10] Ren, W.X. and Chen, H.B., Finite element model updating in structural dynamics by using the response surface method, *Engineering Structures*, 32(8), 2455 –2465 (2010).
- [11] Chakraborty, S. and Sen, A., Adaptive response surface based efficient Finite Element Model Updating, *Finite Elements in Analysis and Design* 80, 33–40 (2014).
- [12] Rathi, A.K. and Chakraborty, A., Adaptive Response Surface based FE Model Updating for Operational Modal Analysis of RC Road Bridge, *4th Optimization & Stochastic Days*, Bangalore (2014).
- [13] Kim, C. and Wang, S., Efficient response surface modelling by using moving least-squares method and sensitivity, *AIAA J.* 43(1) 2404–2411(2005).
- [14] Taflanidis, A.A. and Cheung, S.H., Stochastic sampling using moving least squares response surface approximations, *Probabilistic Engineering Mechanics* 28, 216–224 (2012).



Composite Concrete Filled Square Steel Hollow Sections

Pathik Debmallik¹ and Pramit Debmallik²

Abstract: A significant amount of research has been conducted worldwide on the behaviour of concrete filled steel tubes. Composite columns especially of steel hollow sections filled with concrete, offer great advantages in major architectural and structural applications and offers economic advantages. Possible variations of sections to loading without external dimension changes can be achieved by use of Square or Rectangular Hollow Section (SHS/RHS) the use of concrete filled SHS in multi-storied buildings allows variation in thickness in relation to the load reduction as the level rises without any alteration to outside column dimension. Concrete filled composite section retards damage due to fire, leading safe evacuation of the occupants contrary to bare RHS/SHS. Though some application of this concept has been used in a few places in India, the understanding of the concept is still in its nascent stage because of non-availability of larger size hollow sections and also due to non-availability of a code of practice for such composite hollow sections. Insignificant work has been done in India, particularly with concrete in-filled Square or Rectangular Hollow Sections (SHS/RHS). Concrete in filled SHS/RHS can cut down construction time as frames can be made ready and concrete can be poured later, thus eliminating the need for formwork. This study focuses on the understanding of the behaviour by experimental investigation of concrete filled Steel Hollow Sections. Tests performed to determine the effect of different structural parameters on the load carrying capacity of same sized SHS filled with different grades of concrete, indicates significant capacity increase when the Hollow core of Square sections (SHS) were filled with various grades of concrete. However, the use of higher strength concrete infill does not significantly contribute in terms of increased structural parameters. The benefits of the concrete compressive strength was fully exploited due to confinement effect provided by the steel Square Hollow Section resulting in increased load carrying capacity and improved structural parameters. It was also noted that the rate of loading has an effect on the load-deformation behaviour. It is interesting to note that the in filled concrete is able to provide adequate enhancement of strength without much sacrificing the ductility and toughness properties of steel section. Thus these in-filled SHS seem to be a feasible option for seismic resistant structural element.

Keywords: SHS; Hollow; Infill; Seismic.

Introduction

Composite columns especially of steel hollow sections filled with concrete, offers a great deal of advantages in major architectural and structural applications and also offers a great deal of economic advantages. The concrete filled hollow sections are being increasingly used now in structural buildings. The applications of composite concrete filled steel tubular sections have increased phenomenally in the recent times due to availability of large and jumbo sized Structural Hollow Sections (SHS). Concrete or grout filling of structural hollow sections requires no special equipment and the filling operation may be integrated into other concreting operations. The enhancement in the overall efficiency obtained by filling a steel structural hollow section with concrete allows the designer a wider choice of application. Filled hollow section columns combine the advantages of

economy in the use of materials with the construction advantages of the use of steelwork. The steel tube acts as both erection steel and form work for the composite column during construction, thus a considerable amount of labour, materials and construction time and cost can be avoided. Concrete filled tubular columns i popularity in supporting heavy loads in high rise buildings, bridges and offshore structures.

Columns, whether externally fire-protected or not, will usually arrive to site as fully finished elements with make-ups only at column splice joints, if any. Concrete filling of the hollow section columns can take place on or off site. If filling takes place on site, then the steel column and its connections are designed to carry all construction loads so that the operation of filling the columns can be taken off the planning critical path. In larger buildings, the best economy

¹Assistant Professor, University of Engineering and Management, Kolkata, India. ✉ pathik249@hotmail.com

²Construction Engineering Department, Jadavpur University, Kolkata, India. ✉ pramit_97@hotmail.com

is obtained by planning for the simultaneous working of different trades at different levels or plan positions. The steel structure is visible and allows a pretentious architectural design with various colourings. The costs for painting as well as the cost of corrosion protection are low due to small external surface area of the columns. SHS acts as casing as well as reinforcement for the concrete (No confining links like stirrups and there is no requirement for cover). Lifts or dowels as in reinforced concrete are avoided. One of the most significant advantage is that core of the concrete filled hollow steel sections increases the fire resistance time of the steel sections which would otherwise exhibit rapid loss of strength after a temperature rise of around 350° Celsius. Reinforcement concrete filled SHS can reach 90 minutes of fire resistance time was reported. No external fire protection is therefore necessary. The enhancement of structural properties of concrete filled SHS is due to the composite action between the constituent elements. The steel shell acts as longitudinal and transverse reinforcement. The shell also provides confining pressure to the concrete, which puts the concrete under a tri-axial state of stress. On the other hand, the steel tube is stiffened by the concrete core. This can prevent the inward buckling of the steel tube, and increase the stability and strength of the column as a system. It is known that the ultimate strengths of concrete filled SHS columns are influenced by their constituent material properties such as the compressive strength of the concrete and the yield strength of the steel. In addition, the ultimate strengths of concrete filled SHS columns are also influenced by the concrete confining pressure and the geometric properties of the tubes such as the shape of the cross section, the width-to-thickness ratio, and the spacing and the diameter of the reinforcing ties. Today the producers have been able to see the potential of these sections and have started producing right kind of sections confirming to IS: 4923:1997. Hence it seems that the optimal confining effect on the in-filled concrete by these superior types of SHS was not fully exploited.

Objective

The objective of this work is to report the experimental findings of concrete in-filled cold rolled Square Hollow section (SHS) under compressive loading. The experimental study of linear and non-linear behaviour, failure mechanism, ductility and toughness of these composite materials has been narrated. Thinner steel tubes may be used since the concrete core forces all local buckling modes outwardly delaying the onset of local buckling and the tube prevents concrete spalling which increase the member ductility in precast members. Most importantly, the concrete filled columns display a greater ductility and strength than the sum of the individual ductility's and strength of constituent materials due to interaction between steel and concrete.

Critical Remarks

Concrete-filled tube columns can provide excellent seismic resistant structural properties such as high strength, high ductility, and large energy absorption capacity. The extraordinary earthquake resistance property of the concrete filled hollow section columns were demonstrated during the South Hyogo earthquake on January 11, 1995 in Japan.

Experimental Setup

A frame with a device to hold the specimens (concrete filled SHS) tightly was fabricated by welding heavy steel plates. The frames also had protruding fins to accommodate the strain gauge as shown in Figure 1. The sensor for strain measurement is a linear variable displacement transducer commonly known as LVDT, a type of electrical transformer used for measuring linear displacement. The Gauging sensor (Figure 2) has a plunger guided in plain bearings and fitted with return spring. Measurement probes are primarily used for the measurement and inspection of work-piece geometry.



Fig. 1: Strain Gauge Setup



Fig. 2: Gauging Sensor

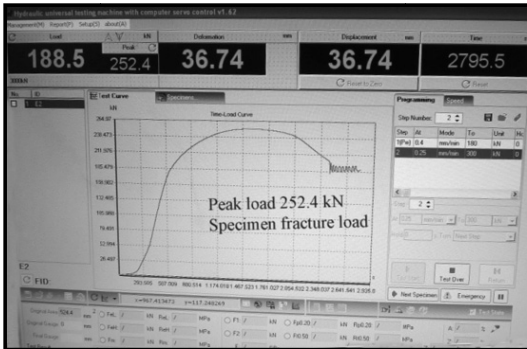


Fig. 3: Loading Output

The strain controlled compression testing machine was capable of testing any structural element for a compressive load up to 3000 kN with a least count of 1 KN. SHS filled with various grades of concrete was placed exactly at the middle of the compression testing machine and the verticality was checked. The compressive load was slowly applied and the load increase vs. deformation was noted from the console connecting the strain gauge for strain measurement. The least count for the strain gauge mentioned above is 0.001 mm. Loading was applied and the deformation recorded for every 10 KN. All samples were tested until specimen fracture notification prompt from the strain controlled compression testing machine was obtained. Failure of the specimen was considered to have occurred when the specimen column, shed off any additional load increment. The axial load was permitted to increase until ultimate load was reached. Readings were tabulated up to, dropping of the load after the attainment of peak load (Figure 3). Tests were repeated with other samples and the test results for the repeated tests were close to their first test values. The small differences between the repeated test values and their first test value demonstrated the reliability of the test results. It is shown that the failure modes at the ultimate load of the columns were all buckling. The failure modes were determined by the deformed test specimens at ultimate load. The concrete filled hollow steel sections specimens were considered to experience two stages of load sustenance under axial loading until failure. In the first stage: the concrete and steel tubes work together initially; until local buckling occurs. In the second stage namely post-buckling stage, the specimen continues to resist the load. At the end of the second stage (after attainment of peak load), the load could not increase and large deformations of the steel tubes were observed. Strain gauges were used to measure the strain of specimens during tests. Though the load-strain curves were used to determine the local buckling load, it was however difficult to determine the local buckling load based on the load-strain curves since the local buckling may not occur always in the location where strain gauges were attached.

Discussions

The experimental results and theoretical calculations of SHS in-filled with different grades of concrete are discussed below.

IS: 456: 2000 Clause 39.3 states that for Short Axially Loaded member the member shall be designed by considering the assumptions given in clause 39.1 and when the minimum eccentricity as per clause 25.4 does not exceed 0.05 times the lateral dimension, the members may be designed by the following equation:

$$P_u = 0.4f_{ck} \cdot A_c + 0.67f_y \cdot A_{sc}$$

Where, P_u = ultimate axial load on the member

f_{ck} = characteristic compressive strength of concrete,

A_c = area of concrete,

f_y = characteristic strength of the compression reinforcement, and

A_{sc} = area of longitudinal reinforcement for columns.

It is assumed that this short column is a reinforced concrete column having longitudinal reinforcement in form of the box SHS with clear cover missing. The confinement by stirrups in normal RCC has been replaced here with the box SHS skin.

Hence with the above logical assumption we can calculate the design ultimate axial load P_u for an axially loaded SHS filled with concrete. (As per IS: 456:2000)

With M 15 concrete infill: $P_{u15} = 177$ KN

With M 20 concrete infill: $P_{u20} = 181$ KN

With M 25 concrete infill: $P_{u25} = 186$ KN

Predicted Strength of Composite Section

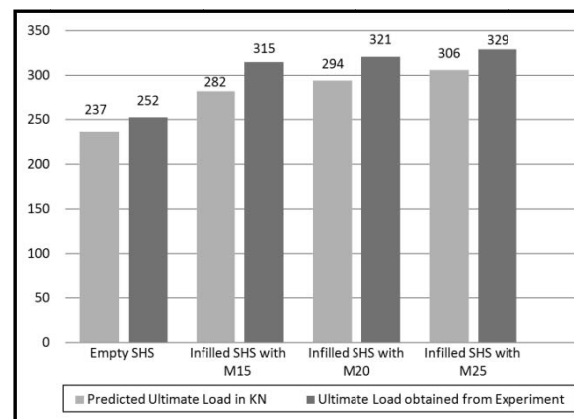


Fig. 4: Predicted Load Capacity against Experimental Load Capacity

The predicted ultimate load vs. the ultimate load obtained from experiment has been shown in the Figure 4 above. In all the cases it was observed that the Predicted load carrying capacity based on the ultimate value of each individual



material of the composite when added up, was exceeded during experimental investigation. Moreover from the above graph it can also be concluded that there will be higher ultimate load carrying capacity of the composite (around 3%) than that predicted by adding up each individual components ultimate load capacities.

Based on the analysis of all the graphs from the experiments it appears that the nature of infilled SHS are of same character. The comparison of structural parameters are given in Table A.

Table A: Comparison of Structural Parameters

	Empty Core without Fill. E2	CF2-15	CF3-20	CF2-25
Load at Yield (P_y), kN	160.00	229.00	235.00	241.00
Ultimate load (P_u), kN	252.40	314.00	321.00	328.45
Load at Failure (P_f), kN	195.65	224.00	235.95	252.00
Deformation at Yield (Δ_y), mm	2.07	4.30	4.12	4.36
Ultimate Deformation (Δ_u), mm	8.33	11.02	10.21	10.05
Deformation at failure (Δ_f), mm	16.67	33.87	33.33	28.84
P/Δ (KN/mm)	77.42	53.26	57.04	55.28
Ductility Ratio = (Δ_f/Δ_y)	8.06	7.88	8.09	6.61
Toughness (Area under the Graph)	3089.60	8642.57	8856.91	8767.50

The purpose of axial load-deflection measurements was to identify the point of yielding, maximum (Peak) load and post buckling behaviour of the stub columns (SHS) empty and concrete filled (composite). From the axial load-deflection diagrams, it is seen that the columns behaves fairly linearly before the ultimate load is reached. By comparing the hollow columns and concrete filled steel columns, the latter columns are much stiffer than the former columns. However, when they approach the ultimate strength, the stiffness of the concrete filled steel columns decreases much more gradually than the hollow steel columns. The failure modes of the columns mainly illustrate overall buckling or global instability. However, this has also been followed by local instability of the slender cross-sections, which have very high plate slenderness. It seems that due to the gradual development of internal micro cracks in the concrete core, the rate of lateral expansion of the concrete increases and exceeds its initial Poisson's ratio. Once the dilation of concrete exceeds Poisson's ratio of the steel, confinement pressure is developed at the interface between the tube and the concrete. As the column was reaching the maximum load, the steel tube yielded and the concrete core failed in shear. The friction within the diagonally fractured concrete core, which is confined by the steel tube, became the major load resistance mechanism.

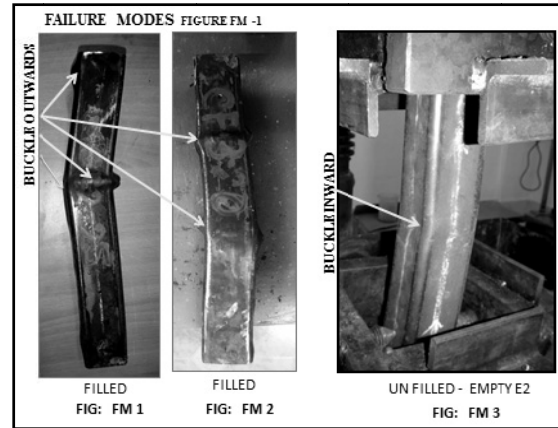


Fig. 5: Failure Mode at Various Loads

It is believed that compressive pressure induces tension in the tube (SHS), changing the stress state from uniaxial to biaxial in the steel and from uniaxial to tri-axial in the concrete. None of the experiment with concrete in-filled composite sections revealed sudden failure without any local buckling. Such occurrences otherwise would have been undesirable for seismic loading.

A composite sample was deliberately subjected to low strain rate in contrary to the strain rate applied on other samples. The parameters were measured and a comparison has been drawn between the same grades of concrete in filled sample subjected to higher strain rate. When the strain rate is low, the P/Δ , P_y , P_u and P_f values are higher (comparison table and graph for two kinds of strain rate provided) (Table B). In addition there is a zone of load resisting, fluctuation. Which may be due to post buckling behaviour of the steel tube (SHS).

Table B: CF1-15 Strain Rate 0.2 mm/min C2-15 Strain Rate 0.4 mm/min

	Low Strain Rate	High Strain Rate
Load at Yield (P_y), KN	245	229
Ultimate Load (P_u), KN	326	314
Load at Failure (P_f), KN	274	224
Deformation at Yield (Δ_y), mm	4.62	4.30
Ultimate Deformation (mm) Δ_u	12.95	11.0
Deformation in mm at failure Δ_f	35.31	33.87
P/Δ (KN/mm)	77.42	53.26
Ductility Ratio = Δ_f/Δ_y	8.06	7.88

The failure mechanism is characterized by partial steel yielding, crushing of the concrete on the compression face,



and concrete cracking on the tensile face, which are caused by the induced bending moment in the column as it deforms laterally.

Conclusion

Based on the above study the following conclusion may be drawn:

- Composite columns of steel hollow sections filled with concrete, offers a great deal of advantages in major architectural and structural applications along with economic advantages. Lighter, airier design can be achieved with the excellent buckling and lateral stability with smaller number of joints.
- Concrete in-filled SHS can cut down construction time as frames can be made ready and concrete can be poured later, thus eliminating shuttering. The use of concrete filled SHS in multi-storied buildings allows variation in thickness without alteration to outside column dimension.
- Due to concrete fill, the composite section retards damage due to fire, leading to safe evacuation of the occupants contrary to bare SHS as reported.
- The SHS in-filled with concrete exhibits significant improvement of different structural properties. However, the grade of in-filled concrete does not have any significant contribution on the enhancement of strength and other properties.
- The gain in strength by the in-filled concrete is mainly due to the confining effect as provided by the SHS

around it. The rate of loading has an effect on the load-deformation behaviour, which is quite normal for any material.

- The in-filled concrete is able to provide adequate enhancement of strength without sacrificing the ductility and toughness properties of steel section. Thus these in-filled SHS seem to be a feasible option of seismic resistant structural element.

References

- [1] Bergmann, R., Matsui, C., Meinsma, C. and Dutta, D., Design Guide for Concrete filled Hollow Sections under static and Seismic Loading - Verlag TUV Rheinland GmbH, Koln, 1995, ISBN 3-8249-0298-2.
- [2] Debmallik, Pathik "Study of Concrete Filled Square Hollow Sections, November 2014, Masters Degree Thesis., Jadavpur University Department of Construction Engineering, Kolkata 700064.
- [3] Ge, H. and Ushami, T. (1992). "Strength of concrete filled thin walled steel box columns: Experiments" *Journal of Structural Engineering*, ASCE, 118(11), 3036–3054.
- [4] IS: 4923-1997-Hollow Steel Section for Structural Use-Specification (second revision).
- [5] Mamaghani, I.H.P. and Packer, J.A., Seismic design and ductility issues in concrete filled steel tubular structures by: Tubular Structures X—*Proceedings of the 10th International Symposium on Tubular Structures*, 18–20 September 2003, Madrid, pp. 561–566.
- [6] Shakir-Khalil and J Zeghiche Experimental behaviour of Concrete filled rolled rectangular hollow section columns.— *The Structural Engineer*, Vol. 67, No. 19, pp. 345–353.



Spatial Technology and Modeling for Planning of Transportation Infrastructure

A. Narayana Rao^{*1}, M. Madhavi¹ and K.M. Lakshmana Rao²

Abstract: Planning of supportive infrastructure with third dimension mapping through the leads of spatial technologies is essential. Most of the failures in functionality of bridges, culverts, retaining walls, approach conduits and natural drains are creating transportation mobility and economic losses in the catchment area and neighborhood places. A study is framed with GIS as supportive tool to develop the catchment area of the culvert or water flow leads for every 2 km² along the highway. Third dimension data base will be created with spatial technologies and create a data base of elevations over a space. Modeling through p-Median will be attempted to identify the optimal locations of the culverts by taking water flow patterns into account. Modeling will work with minimizing the impedances and enhancing the demand potential for optimal utility of the supportive infrastructure. Outcome of this research will evaluate for any highway in reference to supportive infrastructure on their locations and reasons for failure in functionality. Culvert failures can be subdued with proper treatments on water flow diversions. Control of floods and its impact on culverts can be handled by locational modeling and profile corrections at longitudinal and transverse leads on the study area. Deliverable will be the analytics of spread distribution water and its integration with culvert location.

Keywords: Locational Modeling, Spatial Spread, p-Median, Culvert Analytics.

Problem Contesting

The major problem witnessing on NH67 is a lack of proper highway drainage system mainly during monsoon season. The travel demand is increasing day by day in this particular route as it runs from Nagapattinam, Tamil Nadu to Gunlupet in Karnataka. This resulted in congestion and formation of potholes due to stagnation of water on the road. Due to a long-standing demand of the people of Tiruvarur and Nagapattinam, the vehicular are enduring a bumpy, slow ride on the damaged stretch, with accidents, particularly, at night causing another concern for people. As the number of vehicles increases manifold every year, the road became too congested. The problems are mounting for road users due to traffic congestion too. As the traffic on the damaged stretch became a bitter experience to the road users. Journey time is also increasing as four railway crossings on the narrow route from Needamangalam to Tiruvarur clamp down on speed, as many vehicles have to wait at the gates. However, National Highways Authority of India (NHAI) has proposed for laying a two-lane road on the existing stretch has been prepared.

Highway drainage is one of the parameters that have to be kept in mind while designing national highway. Highway

drainage system is made effective by disposing rain water quickly by storm water drains along the road length and locating of culverts at regular intervals. The water disposed of is transferred to the nearby water tanks and lakes through culverts, feasible locations for culverts on National Highways are identified and placed by following the standard recommendations. Thus there is a need to understand the present problems and feasible location for locating a culvert has to be identified.

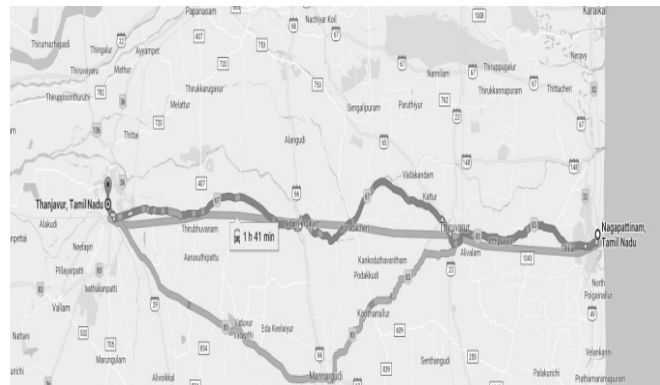


Fig. 1: Study Area

¹Engineer, Engineering Branch, Dr. B.R. Ambedkar Open University, Road. No. 46, Jubilee Hills, Hyderabad-500 033, India.

✉ anrao2k@gmail.com; anrao2k@rediffmail.com

²Professor and Head, Department of Civil Engineering, JNTUH, Kukatpally, Hyderabad-500072, India. ✉ kmlraoin@yahoo.com



Objective

By analyzing the problem witnessing at study area NH67, the objective chosen for this study is optimally locating supportive infrastructure for NH67 by using p-median methodology using GIS as an interface. This study is focused mainly on highway drainage system. Hence from highway drainage system only supportive infrastructure like culvert are taken as the main parameter.

Methodology

The methodology opted for this study is P-Median methodology from location modeling. Using p-median methodology, optimal location of the provision of a culvert in the study area is identified. The necessary data needed to run the p-median program is extracted from Arc GIS software and GPS visualizer webpage. Available Road network drawing a plan of the NH67 has been taken for data extraction. The process involved in data processing and data extraction is explained below in a step-wise manner.

Step 1: Exporting the Data

The road plans data available in CAD dwg. The file is exported to the ArcMap 10.1 for carrying out the further data extraction process. Once the data gets exported the layers are saved as shapefiles for data manipulation.

Step 2: Creating Fishnet

Generate a FISHNET grid with cell width of 50 m for the complete road length of 80 kms.

Step 3: Digitizing a Polyline

- Create a shape file of the polyline and name it accordingly.
- Measure the length of 2 kms vertically on fishnet.
- Digitize vertical lines with construction points spaced at an interval of 50 m on fishnet of length 2 kms continue this process for 80 kms of road length.
- Convert the shape file to kml. Format.

Step 4: GPS Visualizer

- Add the converted kml file.
- Export the kml to text format.
- Download the output text file containing Latitude and longitude values along with elevation values generated.

P-Median Methodology

The data generated from the GPS visualize web page is exported to excel sheet. From the data, an elevation matrix E for every 1 km of road stretch is generated. By assuming a

lead point for every 1 km of road stretch a distance of separation D_{ij} matrix is generated. The distance of separation is the distance between the assumed node point 'i' to the standard node point 'j'. Here the node points are nothing but the construction points generated while digitizing.

Considering the elevations generated from digitized lines an elevation matrix E of size $(m \times n)$ and distance of separation matrix D_{ij} of size $(m \times m)$ is generated. Now calculate the p-value using the formula,

$$p\text{-value} = \sum_j^n E d_{ij}$$

P-median matrix is obtained by multiplying the distance of separation matrix with elevation matrix. The p-value corresponding to the least value is considered as an optimal location.

Data Processing

The actual data processing and calculation for the road length of 80 km is very huge. For the purpose of better understanding, the processing of data and the methodology implementation is explained in a case example provided in this work.

Case Study

Application

A study area of 1 km^2 i.e., from 3 km to 4 km road length is selected using ARC GIS 10.1 as a tool. The area is further divided into grids of $50 \text{ m} \times 50 \text{ m}$ size. The center points are marked inside the grid cells which are considered as the node points. From the digitized data of the study area, numbers of nodes are obtained. Each grid contains one node at center. Using GPS Visualizer elevation values and latitude and longitude values for the nodes are identified. Out of all the nodes, a sample of 8 nodes is identified. The distance of separation between each node is identified for all the selected eight nodes and recorded in the form of a matrix. The p-median methodology is applied to obtain the optimal location to the grids.

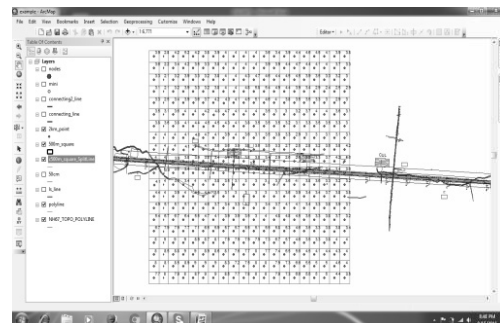


Fig. 2: Marking of Points in the Middle of the Grid

Matrix A (Distance of Separation)

Nodes	A	B	C	D	E	F	G	H
A	0	0.47	0.12	0.17	0.28	0.22	0.45	0.28
B	0.47	0	0.35	0.61	0.2	0.51	0.33	0.32
C	0.12	0.35	0	0.29	0.15	0.26	0.36	0.22
D	0.17	0.61	0.29	0	0.44	0.18	0.63	0.35
E	0.28	0.2	0.15	0.44	0	0.39	0.25	0.25
F	0.22	0.51	0.26	0.18	0.39	0	0.62	0.2
G	0.45	0.33	0.36	0.63	0.25	0.62	0	0.5
H	0.28	0.32	0.22	0.35	0.25	0.2	0.5	0

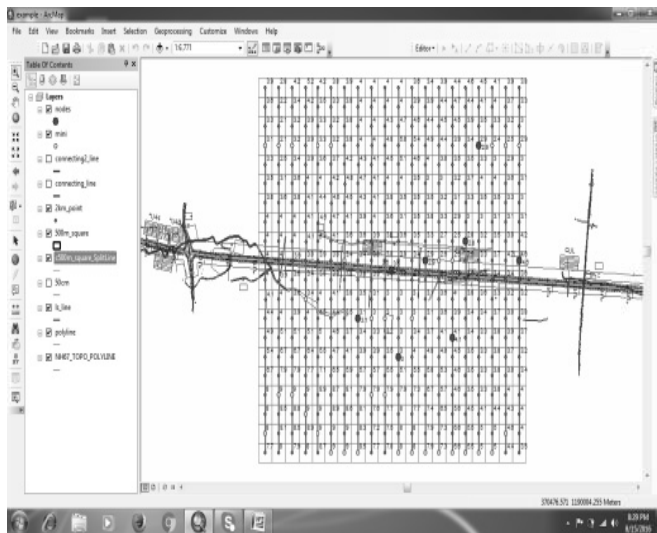


Fig. 3a: Selected Nodes Points for Calculation

Calculation

The feasible location for locating a culvert is identified by using the formula elevation values of the nodes E_1, E_2, E_3, \dots multiplied by the distance of separation d_{ij} between the node to node. Where, 'i' is the node point which is connected to 'j' (i.e., for eg. 1 to 2, 1 to 3, here $i = 1, j = 2$).

$$p\text{-value} = \sum_{j=0}^n E d_{ij}$$

In the p-median method, the minimum value obtained from the result will be taken as the optimal value or the p-value for the location the facility. The facility chosen here is culvert that has to be located in the study area. The matrix method is adopted for calculating the result.

Two matrices are developed from the data gathered out of which one matrix A of 8×8 size is generated for a distance of separation d_{ij} while the other matrix B of size 8×1 is generated for elevation values of the 8 node points.

Matrix B (Elevations)

A	3.6
B	4.6
C	2.9
D	3.1
E	2.8
F	3
G	2.9
H	4.1

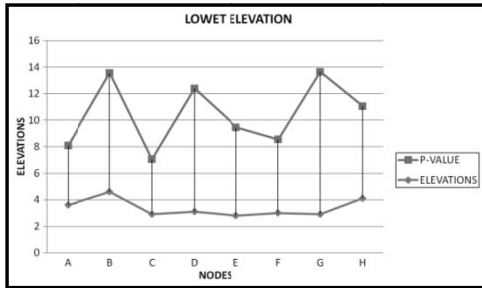
p-value or minimum value = $A \times B$

A	4.481
B	8.957
C	4.141
D	9.293
E	6.647
F	5.542
G	10.745
H	6.953

From the result values, obtained values are sorted from low to high.

Table 1: Result

Ranking from Least to High	
C	4.141
A	4.481
F	5.542
E	6.647
H	6.953
B	8.957
D	9.293
G	10.745



Graph 1: Difference between Actual Elevation and P-value

According to the rule of p-median, the minimum value obtained will be considered as the optimal value or p-value for locating a culvert.

Result

From the result obtained the node point c is carrying the least value of 4.141 out of all the 8 node points taken. Hence it will be taken as the p-value where the facility can be located. Comparing with the graphical real-time data the node point 3 stands in third place, hence can be taken as the feasible location for locating a culvert.

Similarly, the p-median methodology is used for the data of the total study area covering a length of 80 kms. Matrices A and B are generated for every 1km of road length. the p-median program has been run for the matrices developed in the excel. From the result, minimum p-value will be taken as the optimal p-value or feasible location for locating a culvert.

Generation of Matrices in Ms Excel

Consider the elevation lines digitized along with the fishnet, each line consists of 42 intermediate/construction points for which lat and long values along with elevation are generated using GPS Visualizer. Using the lat and long data distance of separation matrix D_{ij} with size 42×42 (i.e., $m \times n$) is generated for every digitized elevation line. Elevations along with lat and long values are also arranged as elevation matrix E of size 42×1 . The following Figure 3b shows the arrangement of matrices in excel.

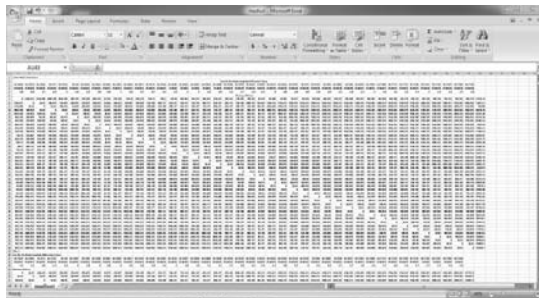


Fig. 3b: Arrangement of Elevation Matrix and Distance of Separation Matrix in Excel

Matrices are developed for each digitized line. Around 1450 matrices are generated as a total of 1450 lines have been digitized covering the total road length of 80 km.

The two matrices are multiplied in excel, the result will be a 42×1 matrix which is considered as the desired p-values. Of the 42 p-values, the least value will be taken as the optimal value for that kilometer length of the road. A similar method is followed for the rest of 1449 matrices, of all the p-values least values are listed out along with latitude and longitude values denoting them as the optimal locations for the study.

Table 2: Optimal p-Values

Title	Longitude	Latitude	Lowest p-Value
1	79.81604834	10.7647486	56840.9446
2	79.81650381	10.76520246	58611.3178
3	79.81559111	10.76474686	58651.2902
4	79.81695928	10.76565631	62497.0372
5	79.81513387	10.76474511	62797.0908
6	79.82520005	10.76297492	64582.135
7	79.78815717	10.76464089	100038.286
8	79.80827892	10.76381462	100799.1499
9	79.80644999	10.76380759	102244.3538
10	79.78861621	10.76419057	102598.7703
11	79.78769994	10.76463911	104339.0563
12	79.79364394	10.76466228	104549.3184
13	79.8224391	10.76748564	105005.4718
14	79.80599276	10.76380583	105304.9168
15	79.79089875	10.7651037	105749.4364
16	79.79044332	10.76464982	105924.4541
17	79.79501563	10.76466761	106544.7476
18	79.78724091	10.76508942	108059.7233
19	79.80553553	10.76380407	109155.6226
20	79.77671916	10.76640444	110999.8373
21	79.80279035	10.7642456	111420.9565
22	79.77397761	10.7659415	111724.8638
23	79.77443484	10.76594331	112094.9375
24	79.77169146	10.76593246	112404.8723
25	79.75889094	10.76542939	137493.6876
26	79.75843371	10.76542756	137648.6948
27	79.75751926	10.7654239	137768.6243
28	79.75797648	10.76542573	138103.711
29	79.77031794	10.76637912	139759.6263
30	79.76986071	10.76637731	143860.3401
31	79.76940348	10.7663755	144055.3546
32	79.76894442	10.76682579	144425.3965



Title	Longitude	Latitude	Lowest p-Value
33	79.72779976	10.76530343	145083.3357
34	79.72825888	10.76485321	145653.4308
35	79.7287142	10.76530718	148078.8604
36	79.73648696	10.76533894	148169.2706
37	79.73145942	10.76486631	149504.2174
38	79.75020366	10.76539451	150100.3624
39	79.73694418	10.7653408	150574.6976
40	79.74974457	10.76584477	151555.5787
41	79.73602974	10.76533707	152549.9711
42	79.74928548	10.76629502	153875.9147
43	79.75066088	10.76539635	154246.0904
44	79.7374014	10.76534266	157495.8724
45	79.69259795	10.76425285	163308.9998
46	79.69259795	10.76425285	163308.9998
47	79.71728563	10.76480802	163760.6275
48	79.69305516	10.76425478	164134.1427
49	79.69305516	10.76425478	164134.1427
50	79.68848109	10.76468757	165134.0142
51	79.68848109	10.76468757	165134.0142
52	79.71774285	10.76480991	166246.0861
53	79.69351237	10.7642567	166664.5224
54	79.69351237	10.7642567	166664.5224
55	79.70860043	10.76431988	166735.5736
56	79.70814322	10.76431798	167100.587
57	79.68802387	10.76468563	167154.2791
58	79.71682841	10.76480613	167691.2544
59	79.71180095	10.76433319	169211.1375
60	79.67110708	10.76461362	169513.5262
61	79.67110708	10.76461362	169513.5262
62	79.72460112	10.76483819	169652.0694
63	79.71225816	10.76433509	170341.3263
64	79.67064988	10.76461166	170523.6672
65	79.67064988	10.76461166	170523.6672
66	79.67156429	10.76461558	171498.8527
67	79.67156429	10.76461558	171498.8527
68	79.70402828	10.76430082	172186.083
69	79.70402828	10.76430082	172186.083
70	79.70357107	10.76429891	172206.0772
71	79.70357107	10.76429891	172206.0772
72	79.68756471	10.76513579	172254.9932
73	79.70494657	10.76340045	173496.3538
74	79.70494657	10.76340045	173496.3538
75	79.70448743	10.76385064	173681.3499

Title	Longitude	Latitude	Lowest p-Value
76	79.70448743	10.76385064	173681.3499
77	79.66459658	10.78945071	175843.9613
78	79.66505183	10.78990477	176629.0735
79	79.67202348	10.76416545	176659.5868
80	79.67202348	10.76416545	176659.5868
81	79.66836383	10.76460186	177109.3922
82	79.66836383	10.76460186	177109.3922
83	79.66882104	10.76460382	177265.4607
84	79.66509171	10.78086311	177384.2044
85	79.66459858	10.78899863	177429.1782
86	79.66927825	10.76460578	177789.5288
87	79.68710749	10.76513385	177795.7523
88	79.66462251	10.78357364	178769.3683
89	79.66458261	10.79261529	178804.3632
90	79.70540379	10.76340236	178977.2113
91	79.66973546	10.76460774	179049.7419
92	79.66458062	10.79306738	179539.4891
93	79.66464843	10.77769655	180799.6288
94	79.66464644	10.77814864	180999.6593
95	79.66465042	10.77724447	181669.7512
96	79.66790662	10.76459989	182205.0518
97	79.68665028	10.76513192	182701.4805
98	79.68665028	10.76513192	182701.4805
99	79.66513153	10.77182144	183660.072
100	79.66457862	10.79351946	184310.1136
101	79.70585907	10.76385636	185278.2117
102	79.6646763	10.77136739	187325.4538
103	79.66744942	10.76459793	187881.0125
104	79.68619307	10.76512998	189057.3553
105	79.66699221	10.76459596	191711.2872
106	79.6852806	10.76467402	191777.6687
107	79.68482339	10.76467208	191987.6723
108	79.66457662	10.79397154	195566.6471
109	79.65085303	10.79526827	200056.2311
110	79.65131028	10.79527026	201886.4062
111	79.65039578	10.79526627	207552.109
112	79.64582124	10.79569837	213102.4949
113	79.62661883	10.79516163	223802.0455
114	79.64216324	10.79568233	223898.4873
115	79.63165059	10.79473184	223997.581
116	79.62707608	10.79516365	224422.211
117	79.63485132	10.79474598	225077.9999
118	79.62616158	10.79515959	225447.2586



Title	Longitude	Latitude	Lowest p-Value
119	79.64170802	10.79522825	225453.71
120	79.63439204	10.79519604	226143.1036
121	79.62250361	10.79514333	231317.599
122	79.60924353	10.795084	233266.5674
123	79.62387535	10.79514943	233677.9967
124	79.61198699	10.79509632	234151.9139
125	79.6124463	10.7946463	234652.0321
126	79.62296086	10.79514536	234693.09
127	79.61152974	10.79509427	235252.0281
128	79.62341811	10.7951474	236998.3372
129	79.57952504	10.79449689	277473.119
130	79.57906781	10.79449479	277548.1263
131	79.5799844	10.79404692	279463.4277
132	79.57861057	10.79449269	281748.5009
133	79.57724099	10.79403431	293184.4617
134	79.57678375	10.79403221	296389.7577
135	79.57632652	10.79403011	297134.7879
136	79.57586928	10.794028	297874.7803
137	79.55940243	10.79530798	300047.9057
138	79.58226422	10.7954136	300065.8335
139	79.55985966	10.79531011	300127.9783
140	79.56031689	10.79531224	300728.1053
141	79.55894519	10.79530585	301117.9306
142	79.56077413	10.79531436	301268.2175
143	79.55848796	10.79530372	304638.2037
144	79.53334246	10.79473345	305735.0284
145	79.53562641	10.79519634	306335.3751
146	79.53516918	10.79519417	308390.4526
147	79.55803073	10.79530159	309238.5796
148	79.53379969	10.79473562	309460.4003
149	79.55757134	10.79575152	312378.8149
150	79.53151355	10.79472477	317075.6988
151	79.53105633	10.7947226	319090.7598
152	79.53014187	10.79471826	320240.7678
153	79.5305991	10.79472043	320435.8316
154	79.54842668	10.79570874	327473.8469
155	79.51733735	10.79510922	328234.5715
156	79.51688012	10.79510703	328294.5108
157	79.5164229	10.79510484	329399.5225
158	79.54796945	10.79570659	331349.3546
159	79.54888174	10.79616295	331709.4233
160	79.54979621	10.79616724	331809.5689
161	79.51367955	10.79509167	335079.5532

Title	Longitude	Latitude	Lowest p-Value
162	79.51322455	10.79463742	339459.7868
163	79.50910955	10.79461761	340979.3039
164	79.50865233	10.79461541	341969.2931
165	79.50453733	10.79459554	369420.5715
166	79.50408011	10.79459333	370350.5485
167	79.50362289	10.79459112	372960.6807
168	79.59370572	10.79320544	378680.6777
169	79.59324849	10.79320336	378715.6625
170	79.59416086	10.79365958	380335.969
171	79.46338783	10.79439388	381719.4106
172	79.45881571	10.79437114	382288.6366
173	79.46475947	10.79440069	382684.6976
174	79.4583585	10.79436886	382718.5482
175	79.46521668	10.79440296	383454.7551
176	79.45790129	10.79436658	383603.4694
177	79.60468361	10.79235098	384788.0901
178	79.60194019	10.79233859	385027.7163
179	79.60148504	10.79188446	385192.6262
180	79.45744408	10.7943643	385838.5237
181	79.59553467	10.79321374	386946.7554
182	79.45698687	10.79436202	387823.5605
183	79.59599191	10.79321582	388777.2053
184	79.47253209	10.79443917	391986.5855
185	79.47207488	10.79443691	395241.6217
186	79.47481817	10.79445045	396422.2359
187	79.47298931	10.79444142	397076.8824
188	79.44829989	10.79431857	403792.7412
189	79.44555663	10.79430479	405087.2673
190	79.44509943	10.7943025	405127.1506
191	79.44875709	10.79432086	406508.0409
192	79.43778411	10.79426564	412551.1465
193	79.4373269	10.79426333	413396.0439
194	79.43824132	10.79426795	414006.242
195	79.43138323	10.79423325	416219.9821
196	79.43092603	10.79423093	417799.959
197	79.42498237	10.79420073	418448.8273
198	79.42543958	10.79420306	420308.9664
199	79.43046882	10.79422861	420614.9783
200	79.41949594	10.79417275	437238.3242
201	79.41995314	10.79417508	437933.4311
202	79.41903874	10.79417041	438813.3309
203	79.41675273	10.79415872	439857.8183
204	79.41080674	10.79458027	466347.3706



Title	Longitude	Latitude	Lowest p-Value	Title	Longitude	Latitude	Lowest p-Value
205	79.41035192	10.79412589	468757.2849	248	79.33450297	10.78559034	741777.2353
206	79.40989472	10.79412354	470607.2139	249	79.33084561	10.78557064	759260.6944
207	79.40943752	10.79412119	471092.1757	250	79.33038844	10.78556818	765615.3764
208	79.41126632	10.79413059	473212.6008	251	79.32993127	10.78556571	773055.0398
209	79.40898032	10.79411884	474612.1499	252	79.3294741	10.78556324	774164.9494
210	79.39252119	10.79403375	475833.4363	253	79.31758273	10.7864029	802059.8136
211	79.40760872	10.79411178	476221.9215	254	79.31072523	10.78636555	803687.1755
212	79.39389278	10.79404088	477893.8305	255	79.3111824	10.78636804	803852.2615
213	79.39297839	10.79403613	477923.6013	256	79.31163957	10.78637054	804707.5285
214	79.392064	10.79403138	478778.3922	257	79.30661075	10.78634307	806835.4547
215	79.39434998	10.79404325	480528.9631	258	79.31712556	10.78640041	808749.489
216	79.39755275	10.79360782	480844.6798	259	79.29975583	10.78585347	812287.6024
217	79.39480957	10.7935936	485999.1569	260	79.30021046	10.78630799	812677.8191
218	79.39709555	10.79360545	487854.7398	261	79.31301106	10.78637802	813472.7074
219	79.39526677	10.79359597	489594.3613	262	79.29564138	10.78583085	815245.9615
220	79.50180296	10.79277406	503569.3159	263	79.3180399	10.78640538	815514.8395
221	79.49311584	10.79273188	509597.6968	264	79.29929867	10.78585096	815632.3753
222	79.49357306	10.7927341	510067.7993	265	79.29244125	10.78581321	835213.9552
223	79.49265863	10.79272965	511762.7362	266	79.28329807	10.78576265	836130.1628
224	79.49403028	10.79273633	513773.2223	267	79.28375523	10.78576518	837240.3051
225	79.48031384	10.79266926	543466.7148	268	79.28421495	10.78531571	837315.4531
226	79.47985662	10.79266702	544151.6678	269	79.29426735	10.7862753	837554.5891
227	79.48077105	10.79267151	544856.8928	270	79.28284091	10.78576011	838839.8522
228	79.47939941	10.79266477	552077.0179	271	79.29106977	10.78580565	839293.3307
229	79.37838936	10.78627537	596866.5801	272	79.29061261	10.78580312	839393.0585
230	79.37793218	10.78627298	600996.5131	273	79.27095743	10.78524195	868843.2498
231	79.377475	10.78627058	605536.3891	274	79.27050027	10.7852394	869598.1138
232	79.37701782	10.78626818	609041.3235	275	79.27141458	10.7852445	870223.3767
233	79.37427473	10.78625379	614540.5382	276	79.27004312	10.78523684	872667.6578
234	79.37381755	10.78625139	614650.3892	277	79.26501443	10.7852087	884234.9024
235	79.37336037	10.78624899	615035.2722	278	79.26547159	10.78521126	887370.0639
236	79.37198884	10.78624178	615484.8989	279	79.26684304	10.78521894	888890.6606
237	79.35415892	10.78614749	660779.5125	280	79.26638589	10.78521638	890945.276
238	79.3537042	10.78569305	664844.3599	281	79.2577	10.78516762	909690.4224
239	79.35233022	10.78613777	665208.9248	282	79.25724285	10.78516505	912145.0847
240	79.35187304	10.78613533	665453.7878	283	79.24489982	10.78509532	918044.0174
241	79.34912999	10.78612072	697532.7928	284	79.24535697	10.78509791	918529.1642
242	79.34867282	10.78611828	700722.6158	285	79.24352838	10.78508754	918798.2672
243	79.34684412	10.78610852	704926.9926	286	79.2567857	10.78516248	919034.5305
244	79.34821565	10.78611584	705017.4063	287	79.24444267	10.78509273	919118.6446
245	79.3340458	10.78558788	735132.102	288	79.2549571	10.78515217	921373.5369
246	79.33999149	10.78516779	735734.348	289	79.23941406	10.78506417	945594.6732
247	79.33358863	10.78558542	738956.9164	290	79.23895691	10.78506157	945764.4372



Title	Longitude	Latitude	Lowest p-Value
291	79.23667118	10.78504856	952532.8839
292	79.23712833	10.78505116	953983.0579
293	79.22341401	10.78497277	970770.0947
294	79.23027116	10.78501204	971068.6225
295	79.22295687	10.78497014	974139.5581
296	79.22021402	10.78495439	1001241.36
297	79.21518547	10.78492544	1001683.621
298	79.21198282	10.78535896	1002111.977
299	79.22570237	10.78453389	1003824.043
300	79.21335424	10.78536687	1004082.436
301	79.21564261	10.78492807	1005903.688
302	79.21152568	10.78535632	1006896.227
303	79.21107121	10.78490169	1009256.112
304	79.21061407	10.78489905	1012185.586
305	79.20146863	10.78529805	1017215.311
306	79.20192577	10.78530071	1017570.454
307	79.20009722	10.78529008	1018164.433
308	79.19415715	10.78480349	1019705.961
309	79.19964278	10.78483544	1019773.977
310	79.19370002	10.78480082	1024180.332
311	79.19324019	10.78525013	1029079.929
312	79.18684301	10.78476074	1031345.95
313	79.18501448	10.78475002	1050368.259
314	79.18455735	10.78474734	1059072.247
315	79.18364309	10.78474198	1064741.235
316	79.18318596	10.7847393	1064891.12
317	79.17587187	10.78469629	1091424.389
318	79.17541474	10.78469359	1094738.793
319	79.17404335	10.78468551	1097632.722
320	79.17450048	10.78468821	1097673.034

From the above table, the optimal p-values listed along with lat and long values are ranked from lowest p-value in ascending order. A total of 320 optimal values is generated which represents that on an average of 4 culverts can be located for 1km length of the road. The better analysis can be done by displaying of the locations in map from which the result can be analyzed in a better way.

Mapping the Result

The result generated is displayed in the Arc Map for checking out the locations and to specify necessary recommendations.

Once all the options are set automatically all the points are located accordingly with respect to the longitude and latitude values spread along the study area. The p-values located on the map after adding the data are shown in the figures below.

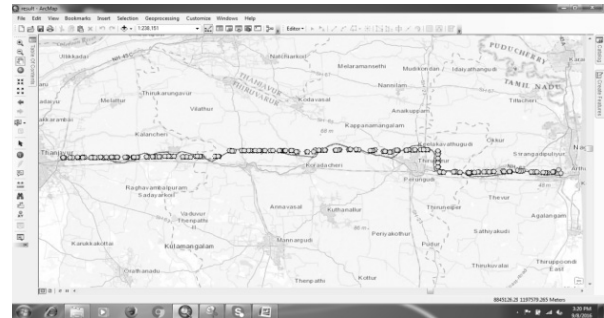


Fig. 4: Points Located on the Map

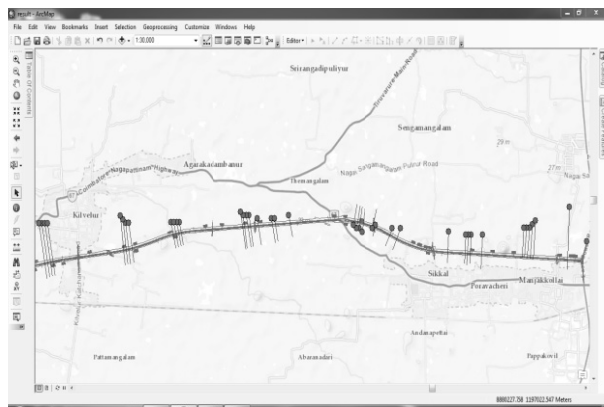


Fig. 5: Points Located on the Map

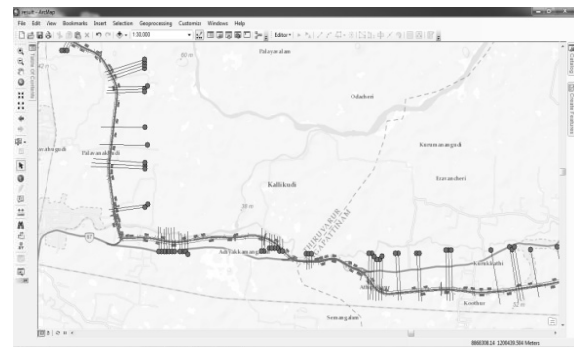


Fig. 6: Points Located on the Map

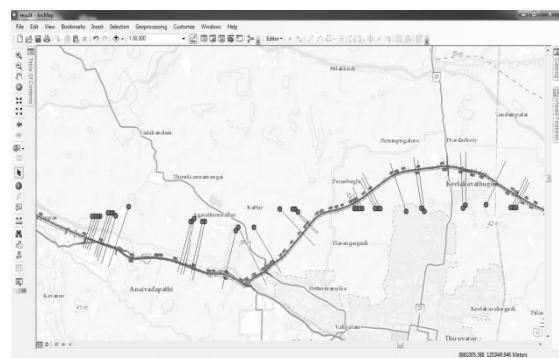


Fig. 7: Points Located on the Map

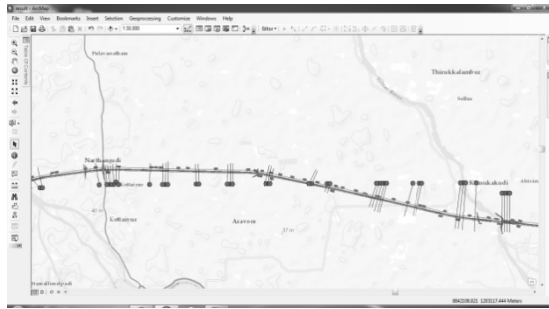


Fig. 8: Points Located on the Map

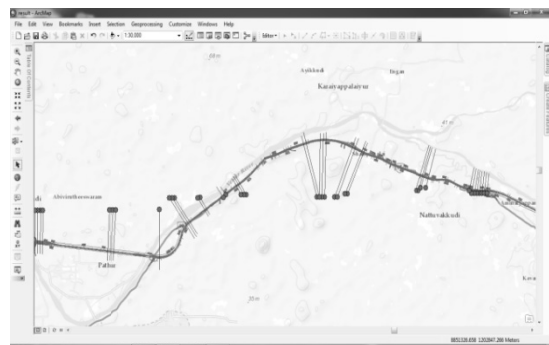


Fig. 9: Points Located on the Map

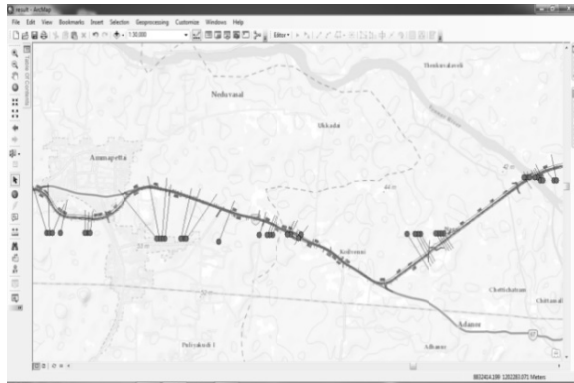


Fig. 10: Points Located on the Map

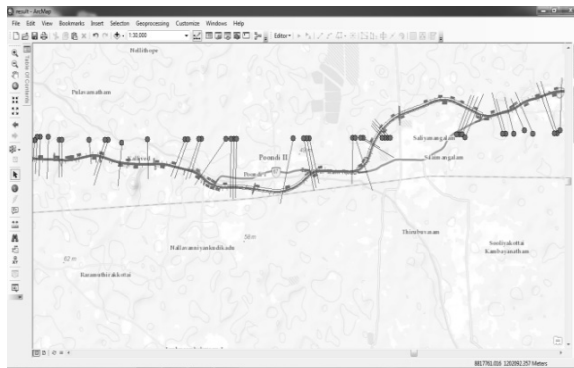


Fig. 11: Points Located on the Map

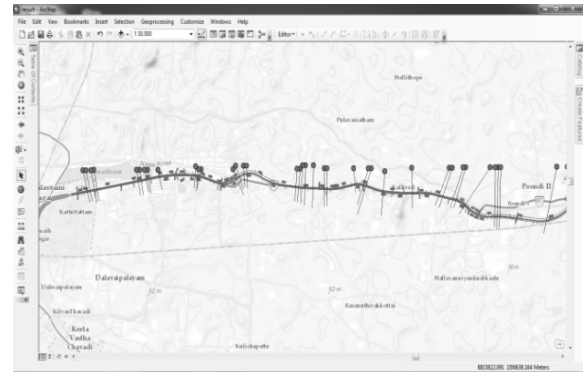


Fig. 12: Points Located on the Map

Conclusion

Reducing stagnation of rain water, quick disposal of the rain water is achieved by providing the cross drainage or culverts is the objective that has been accomplished in the study. For the complete road of length 80 kms elevation values along with distance and lat and long readings are estimated for calculating the p-value or optimal value for locating a culvert. The p-values needed is calculated by multiplying the distance of separation matrix and elevation matrix.

For the study area, NH67 on an average of 320 p-values are generated that means 4 culverts are located for every kilometer of road data. From the figures shown in the previous chapter the p-values when located on the map, they appeared at some distance away from the road since the road is a treated structure they have to be a bit far away from the road. While at the time of designing and construction the treatment of water flow should be placed with lower level gradient and is longitudinally intersected to the road storm water drains. Cross drainage system is an important feature that has to be given importance while designing a road to immediately dispose the water flow from the road surface, as water shows adverse effects on the materials and design like wearing, rupture, reducing of skid resistance, etc. stagnation of water on highways is showing adverse effects like traffic congestion, reduction of traffic density, road user characteristics and vehicular characteristics. By providing the effective cross drainage system these affect can be reduced on the highways.

References

- [1] Sharkia, S. and Haque, M.N., Structural condition assessment of bridges and culverts in national highway N7: Roads and Highways Department, Dhaka 1000, Bangladesh, M.S.K. Bhuiya Hifab International AB, Dhaka, Bangladesh.
- [2] Florentiu Damian, Improving Cross Drain Culvert Spacing with GIS Interactive Design Tool: College of Forest Resources, University of Washington, Seattle WA 98195, evenflo@u.washington.edu



- [3] Historic Stone Highway Culverts in New Hampshire Asset Management Manual, New Hampshire Department of Transportation, Bureau of Environment, Concord, September 2009.
- [4] Drainage of Highway Pavements WSDOT Hydraulics Manual M 23-03.03 June 2010.
- [5] Francisco Daniel B. de Albuquerque, Evaluating the Cost-Effectiveness of Roadside Culvert Treatments, University of Nebraska-Lincoln, dbenicio@huskers.unl.edu Dean L. Sicking University of Nebraska-Lincoln, dsicking1@unl.edu, Ronald K. Faller University of Nebraska-Lincoln, rfaller1@unl.edu Karla A. Lechtenberg University of Nebraska - Lincoln, kpolivka2@unl.edu
- [6] Mr. Dipanjan Mukherjee B.Tech in Civil Engineering, Highway Surface Drainage System and Problems of Water Logging In Road Section West Bengal University of Technology; West Bengal, India.
- [7] Gis and modeling overview, Michael f. good child, national center for geographic information and analysis, university of California Santa barbara, California.
- [8] Scott D. Bryant, P.E., Kenneth, A. Carper, P.E. and John Nicholson, Ph.D., GIS Tools for Proactive Urban Watershed Management.
- [9] R L Church, Location modeling, and GIS.
- [10] http://www.gpsvisualizer.com/convert_input?convert_add_distance=1&convert_add_slope=1&form:add_elevation=auto
- [11] www.michigan.gov/documents/MDOT_MS4_Chap_9172_5_7_05_Drainage_Manual.pdf
- [12] www.dot.ny.gov/divisions/operating/oom/transportation-maintenance/repository/CulvertInventoryInspectionManual.pdf
- [13] <http://www.hyuan.com/java/how.html>
- [14] Integrating Future Hydrologic Models into Transportation Management in North Cascades National Park, North Cascades National Park Service Complex Sedro-Woolley, WA.
- [15] Kadiyali, L.R., *Traffic and Transport Planning*, Khanna Publishers, New Delhi, 1987.
- [16] Nguyen Ngoc Quang, Mark Zuidgeest and Mark Brussel, *Development of an Integrated Gis-Based Land Use and Transport Model for Studying Land-Use Relocation in Hanoi, Vietnam*.
- [17] Nooradelena Mohd Ruslim, Noraida Abdul Ghani. *An Application of the P-Median Problem with Uncertainty in Demand in Emergency Medical Services*.
- [18] Ndiaye, Fagueye; Ndiaye, Babacar Mbaye and Ly., Idrissa. *Application of The P-Median Problem in School Allocation*.



Torsional Behaviour of Reinforced Concrete Beam Strengthened with FRP Materials

S.B. Kandekar¹, R.S. Talikoti² and S.B. Kolhe³

Abstract: During its whole life span, nearly all engineering structures ranging from residential buildings, an industrial building to power stations and bridges faces degradation or deteriorations. The main causes for those deteriorations are environmental effects including corrosion of steel, gradual loss of strength with ageing, variation in temperature, freeze-thaw cycles, repeated high intensity loading, contact with chemicals and saline water and exposure to ultra-violet radiations. This problem needs development of successful structural retrofit technologies. Carbon fiber and Aramid fiber as an external reinforcement is used extensively to deal with the strength requirements related to flexure in structural systems. But the strengthening of members subjected to torsion is explored recently. Torsional failure is an undesirable brittle form of failure which should be avoided specially in the earthquake prone areas. In the present work, the behaviour and performance of rectangular reinforced concrete beams strengthened with externally bonded Carbon and Aramid fiber subjected to torsion is studied.

Keywords: Retrofit, Carbon Fiber, Aramid Fiber, Torsional Failure, Externally Bonded.

Introduction

The maintenance, rehabilitation and upgrading of structural members, is perhaps one of the most crucial problems in Civil Engineering application. Moreover, a large number of structures constructed in the past using the older design code in different part of the world are structurally unsafe according to new design codes. Since replacement of such deficient elements of structures incurs a huge amount of public money and time, strengthening has become the acceptable way of improving their load carrying capacity and extending their service lives. Infrastructure decay caused by premature deterioration of building and structure has led to the investigation of several processes for repairing or strengthening purpose. One of the challenges in strengthening of concrete structure is selection of a strengthening method that will enhance the strength and serviceability of the structure while addressing limitation such as constructability, building operation and budget.

Torsional Strengthening of Beams

Early efforts for understanding the response of plain concrete subjected to pure torsion revealed that the material fails in tension rather than shear. Structural members curved in plan, members of a space frame, eccentrically loaded beams, curved box girders in bridges, spandrel beams in buildings,

and spiral stair-cases are typical examples of the structural elements subjected to torsional moments and torsion cannot be neglected while designing such members. Structural members subjected to torsion are of different shapes such as T-shape, inverted L-shape, double T-shapes and box sections. These different configurations make the understanding of torsion in RC members a complex task.

In addition, torsion is usually associated with bending moments and shearing forces, and the interaction among these forces is important. Thus, the behaviour of concrete elements in torsion is primarily governed by the tensile response of the material, particularly its tensile cracking characteristics. Spandrel beams, located at the perimeter of buildings, carry loads from slabs, joists, and beams from one side of the member only. This loading mechanism generates torsional forces that are transferred from the spandrel beams to the columns. Reinforced Concrete (RC) beams have been found to be deficient in torsional capacity and in need of strengthening. These deficiencies occur for several reasons, such as insufficient stirrups resulting from construction errors or inadequate design, reduction in the effective steel area due to corrosion, or increased demand due to a change in occupancy.

Similar to the flexure and shear strengthening, the FRP fabric is bonded to the tension surface of the RC members

¹ Research Scholar, Department of Civil Engineering, Late G.N. Sapkal College of Engineering, Nashik, India. ✉ sbkandekar@gmail.com

² Professor, Department of Civil Engineering, Late G.N. Sapkal College of Engineering, Nashik, India.

³ Assistant Professor, Department of Civil Engineering, Amrutvahini College of Engineering, Sangamner, Maharashtra, India.



for torsion strengthening. In the case of torsion, all sides of the member are subjected to diagonal tension and therefore the FRP sheets should be applied to all the faces of the member cross section. However, it is not always possible to provide external reinforcement for all the surfaces of the member cross section. In cases of inaccessible sides of the cross section, additional means of strengthening has to be provided to establish the adequate mechanism required to resist the torsion. The effectiveness of various wrapping configurations indicated that the fully wrapped beams performed better than using FRP in strips.

Aramid Fiber

Aramid fiber is a strong, heat-resistant fiber formed of polymers with repeating aromatic groups branching from a carbon backbone. In the polyamide fibers, at least 85% of the amide linkages are attached directly to two aromatic rings. Two types of aramid materials are used in Meta aramid paper which is used for making honeycomb core materials required for sandwich construction. The oriented Para substituted aromatic units provide a rod like polymer. The rod like structure results in a high glass transition temperature and poor solubility. They are not spinnable by conventional process and hence they are made by the dry-jet wet spinning of liquid crystalline polymer solutions.

Carbon Fiber

Due to outstanding mechanical properties, Carbon fiber can be used to rehabilitate and strengthen those zones where the structure is exposed to high mechanical or cyclic loading and severe environmental conditions. Only the outer part of the older structure get wrapped which will improve the strength of concrete; instead of disturbing other parts of structures. Therefore, this conceptual idea will greatly improves the serviceability and life-cycle costs reduction of the structures contributes significantly towards increasing the stiffness and strength of the structure under flexure and torsion.

A Unidirectional Carbon Fiber is one in which the majority of carbon fibers run in one direction only. A small amount of carbon fiber runs in other directions with the main intention being to hold the primary carbon fibers in position.

To manufacture the carbon fibers, Carbonizing polyacrylonitrile yarn at high temperatures process is used. Long thin strand of carbon atoms are bonded together in a Graphene which is a honeycomb crystal lattice. Some of the Graphene layers are folded around each other in random orientations but most are aligned parallel to the long axis of the strand. This makes the fiber incredibly strong along the axis of the strand. The strands are usually wound into a yarn then woven into a fabric. The fabric is then wrapped around the beam or the structure stick with epoxy.

Methodology

Total Eighteen numbers of reinforced concrete rectangular beams were cast of M30 grade of concrete. Three are taken as controlled beam, three beams are design for torsion and other twelve beams are strengthened using Aramid and Carbon fiber. In this, three beams were fully wrapped and three beams were wrapped with 100mm Aramid and Carbon fiber strips.

Beam Specimen for Testing

All beams were of the same geometry 150 mm × 300 mm × 1000 mm size, 3 Nos-8 mm diameter bars were used for tension reinforcement at the bottom of each beam, 2 Nos-8 mm at the top of each beam as an anchor bar and 6 mm diameter shear reinforcement spaced 150 mm center to center. The reinforcement details of beam used for experiment are shown in Figure 1.

Preparation of Test Specimen

The detail of test specimen is given in Table 1. The surface of the beam was cleaned using polish paper to remove dust on surface of beam. Each of these beams was wrapped with Aramid and Carbon fibers by using epoxy resin at all faces of the beam as per the procedure given by the manufacturer.

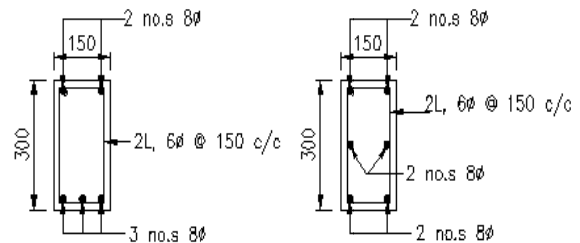


Fig. 1: Reinforcement Detailing of Controlled Beam and Beam Designed for Torsion

Table 1: Specimen Designation

Type of Beam	Beam Designation	No. of Specimen
Controlled Beam	C	3
Design for Torsion	T	3
Fully wrapped with Carbon fiber	FC	3
Fully wrapped with Aramid fiber	FA	3
Wrapped with Carbon strip	SC	3
Wrapped with Aramid strip	SA	3

Test Setup

All beams were tested under lever arm loading. The load was applied by using Universal Testing Machine of capacity



100 kN. During testing twisting moment is measured by using dial gauge having a least count of 0.02 mm with every load increment. Cracks formed on the surface of beam were observed and marked.



Fig. 2: Test Set-up for Testing of Beam

Failure Pattern

The torsional cracks develop in spiral direction at torsional loading in controlled beam. Vertical cracks develop in beam which is designed for torsion and wrapped with strip. The wrap pattern of FRP around beam and twisted shape of wrapped beam is shown in Figures 3 and 4.

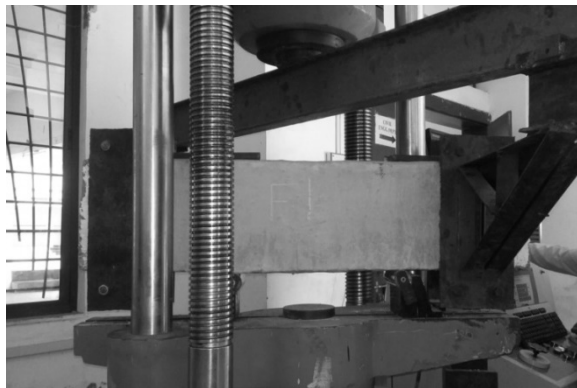


Fig. 3: Test Set-up for Aramid Fiber Full Wrapped Beam

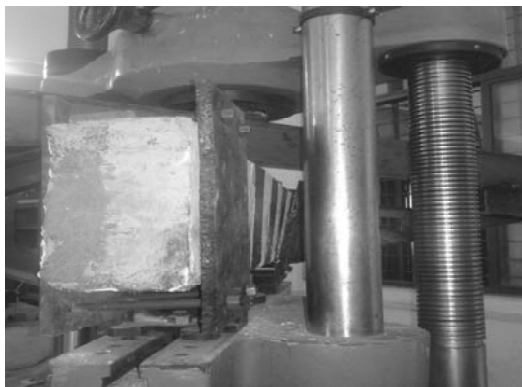


Fig. 4: Test Set-up for Carbon Fiber Beam Wrapped with Strip

Result and Discussions

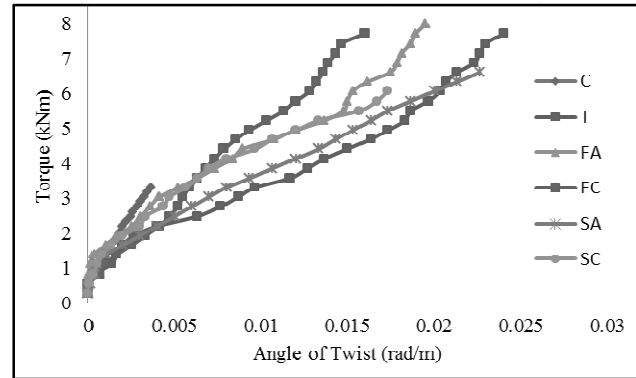


Fig. 5: Relation between Angle of Twist and Torsional Moment

Before yielding of reinforcement, all strengthened specimens exhibited limited deformation and cracks. The initial cracks were initiated and progressed towards upward direction from bottom of beam. The results of retrofitted beam with Carbon fiber were compared with Aramid fiber retrofitted beam and controlled beam for its torsional behavior.

Table 2: Ultimate Load and Nature of Failure for Beams

Set No.	Type of Beam	Beam Designation	Torsional Moment (kNm)	
			At Initial Crack	Ultimate
I	Controlled Beam	C1	2.61	3.3
		C2	2.34	2.88
		C3	2.61	3.16
II	Design for Torsion	T1	6.32	7.70
		T2	6.87	8.52
		T3	7.15	8.25
III	Fully wrapped (Carbon)	FC1	5.78	7.15
		FC2	6.33	7.7
		FC3	6.32	7.7
IV	Wrapped Carbon strip	SC1	4.68	6.05
		SC2	4.4	5.78
		SC3	4.95	6.05
V	Fully wrapped (Aramid)	FA1	6.32	7.97
		FA2	7.15	8.52
		FA3	7.42	8.25
VI	Wrapped Aramid strip	SA1	5.22	6.60
		SA2	4.67	6.05
		SA3	5.22	6.32



Conclusions

Based on experimental results following conclusions are drawn:

- The torsional capacity of strengthened beams was enhanced as compared to the controlled beam.
- Reinforced concrete beams strengthened with Aramid fiber sheets exhibited significant increase in its ultimate strength.
- Initial cracks appear for higher loads in case of strengthened beams. The load carrying capacity of the strengthened beam fully wrapped with Aramid fiber was found to be maximum compare to all the beams.
- The load carrying capacity of the strengthened beam wrapped with Carbon fiber strip was found to be equivalent to beams designed for torsion.
- The load carrying capacity of the strengthened beam fully wrapped with Aramid fiber was found to be 11% greater than beam fully wrapped with Carbon fiber.
- The load carrying capacity of the strengthened beam wrapped with Carbon fiber strip was found to be 7% lesser than the beam wrapped with Aramid fiber strip.
- Carbon fiber increases strength of retrofitted beam 45% to 140% more than normal beam; but Aramid fiber material is approximately 6% to 15% more effective than Carbon fiber; although economically both are nearly same.

References

- [1] Ghobarah, A., Ghorbel, M.N. and Chidiac, S.E., Upgrading torsional resistance of reinforced concrete beams using fiber-reinforced polymer, *Journal of Composites for Construction*, 6, 257–263 (2002).
- [2] Zojaji, A.R. and Kabir, M.Z., Analytical approach for predicting full torsional behavior of reinforced concrete beams strengthened with FRP materials, *Scientia Iranica, Transactions A: Civil Engineering*, 19, 51–63 (2012).
- [3] Deifalla, A. and Ghobarah, A., Full torsional behavior of RC beams wrapped with FRP: Analytical Model, *Journal of Composites for Construction*, ASCE, 14, 289–300, (2007).
- [4] Deifalla, A., Awad, A. and Elgarhy, M., Effectiveness of externally bonded CFRP strips for strengthening flanged beams under torsion: An experimental study, *Engineering Structures*, 56 2065–2075 (2013).
- [5] Chalioris, Constantin E., Torsional strengthening of rectangular and flanged beams using carbon fibre-reinforced-polymers – Experimental study, *Construction and Building Materials*, 22, 21–29 (2008).
- [6] Obaidat, Yasmeen Taleb, Structural retrofitting of reinforced concrete beams using carbon fibre reinforced polymer, dept. of Construction sciences, *Structural Mechanics*, 129, 3–5 (2010).
- [7] Chalioris, Constantin E., Analytical model for the torsional behaviour of reinforced concrete beams retrofitted with FRP materials, *Engineering Structures*, 29, 3263–3276 (2007).
- [8] Jassal, M. and Ghosh, S., Aramid Fiber—an Overview, *Indian Journal of Fiber and textile Research*, 27, 290–306 (2002).
- [9] Jariwalaa, Vishnu H., Patelb, Paresh V. and Purohit, Sharadkumar P., Strengthening of RC beams subjected to combined torsion and bending with GFRP composites, *Procedia Engineering*, 51, 282–289 (2013).
- [10] Ameli, Mehran; Ronagh, Hamid R. and Dux, Peter F., Behavior of FRP strengthened reinforced concrete beams under torsion, *Journal of Composites for Construction*, 11, 192–200 (2007).
- [11] Santhakumar, R., Dhanaraj, R. and Chandrasekaran, E., Behaviour of retrofitted reinforced concrete beams under combined bending and torsion: A numerical study, *Electronic Journal of Structural Engineering*, 7, 1–7 (2007).



Durability Study on Sugarcane Bagasse Ash as an Admixture in M₃₀ Grade Concrete

P.V. Rambabu¹, G. Aditya² and G.V. Ramarao³

Abstract: This investigation is focused on the partial replacements of Portland cement by sugarcane bagasse ash in concrete. The utilization of industrial and agricultural waste produced by industrial process has been the focus of waste reduction research for economical, environmental and technical reasons. Sugarcane bagasse is a fibrous waste product of sugar refining industry. This waste product is already causing serious environmental pollution, which calls for urgent ways of handling the waste. Bagasse ash mainly contains aluminum ion, silica, iron and calcium oxides. The ash therefore becomes an industrial waste and poses disposal problems. So few studies have been reported that sugarcane bagasse ash as good pozzolanic material in partial replacement of cement. In this project objective is to study the influence of partial cement replacement with sugarcane bagasse ash in concrete subjected to different curing environments. Experimental investigation is based on acid resistance of concrete in HCL, H₂SO₄ and sulphate resistance of concrete in Na₂SO₄, MgSO₄ solution. The variable factors considered in this study were concrete grade of M30 and curing periods of 28 days, 60 days and 90 days of the concrete specimens. The parameter investigated was the time in days to cause strength deterioration factor of fully immersed concrete specimens in 1%, 3%, 5% on acid resistance of concrete in HCL, H₂SO₄ and sulphate resistance of concrete in Na₂SO₄, MgSO₄ solution. Bagasse ash has been chemically and physically characterized and partially replaced in the ratio of 0%, 5%, 10%, 15%, 20%. Hardened concrete tests like compressive strength at the age of 28 days, 60 days, 90 days was obtained.

Keywords: Durability, M₃₀ Concrete, Sugarcane Bagasse Ash.

Introduction

For a long time concrete was subjected to highly aggressive environments, Building of concrete structures in highly polluted urban and industrial areas, aggressive marine environments, harmful sub-soil water in coastal area and many other hostile conditions, and other materials of construction are found to be non-durable [1, 2]. In the past only strength of concrete was considered in the concrete mix design procedure assuming strength of concrete is an all pervading factor for all other desirable properties of concrete including durability. On other hand, cement both in mortar or concrete is the most important element of the infrastructure and can be a durable material [3–5]. However, the environmental aspects of cement has become a growing concern, as cement manufacturing is responsible for about 2.5% of total worldwide waste emissions from industrial sources. Sugarcane bagasse is a fibrous waste product of the sugar refining industry. This waste product is already causing serious environmental pollution. Bagasse ash mainly

contains aluminum ion, silica, iron and calcium oxides. The ash therefore becomes an industrial waste and poses disposal problems. So few studies have been reported sugarcane bagasse ash as good pozzolanic material in partial replacement of cement [6–9].

In the present experimental investigation sugarcane bagasse Ash has been used as partial replacement of cement in concrete mixes. On replacing cement with different weight percentages of SCBA the compressive strengths are studied at different ages of concrete cured in different environments like 0%, 1%, 3%, 5% HCL and H₂SO₄, Na₂SO₄ and MgSO₄ added to water [11–14].

Materials

Cement Ordinary Portland cement of 53 Grade from a single batch was used for the entire work and care has been taken such that it has been stored in airtight containers to prevent it from being affected by the atmospheric and monsoon

¹ Assistant Professor, SRKR Engineering College, Bhimavaram, Andhra Pradesh, India.

² PG Student, SRKR Engineering College, Bhimavaram, Andhra Pradesh, India. ✉ adityaagurram122@gmail.com

³ Professor, Andhra University, Visakhapatnam, Andhra Pradesh, India.



moisture and humidity. The cement procured was tested for physical requirements in accordance with IS: 12269–1987 and for chemical requirements in accordance with IS: 4032–1985. The details are given in Table 1, the cement confirms to 53 Grade.

Table 1: Physical Properties of Portland Cement (53 Grade)

S. No.	Property	Test Result
1.	Normal consistency	31%
2.	Setting times	
	Initial (Minutes)	174
	Final (Minutes)	286
3.	Specific Gravity	3.10
4.	Soundness (Le-Chatlier Exp.)	1.30 mm
5.	Compressive strength of cement (28 days)	53 Mpa
6.	Specific surface area	320 m ² /Kg

Fine Aggregate

The river sand, passing through 4.75 mm sieve and retained on 600 μ sieve, confirming to Zone II as per IS: 383–1970 was used as fine aggregate in the present study. The sand is free from clay, silt and organic impurities. The aggregate was tested for its physical requirements such as gradation, fineness modulus, and specific gravity and bulk modulus in accordance with IS: 2386–1963.

Coarse Aggregate

Throughout the investigations, a crushed coarse aggregate of 20 mm procured from the local crushing plants was used. The aggregate was tested for its physical requirements such as gradation, fineness modulus, specific gravity and bulk density, etc. In accordance with IS: 2386–1963 and IS: 383–1970.

Water

Fresh potable water free from organic matter and oil is used in mixing the concrete. Water in required quantities were measured by graduated jar and added to the concrete. The rest of the materials for preparation of the concrete mix were taken by weight batching. The pH value should not be less than 6.

Sugarcane Bagasse Ash

Sugarcane bagasse consists of approximately 50% of cellulose, 25% of hemi-cellulose of lignin. Each ton of sugarcane generates approximately 26% of bagasse (at a moisture content of 50%) and 0.62% of residual ash. The residue after combustion presents a chemical composition dominated by silicon-dioxide (SiO₂). In spite of being a material of hard degradation and that presents few nutrients; the ash is used on the farms as a fertilizer in the sugarcane harvests. The sugarcane bagasse ash was collected during the cleaning operation of a boiler in the Andhra sugar factory, located near Tanuku, Andhra Pradesh.

Durability Studies on Cement Conventional Concrete and SCBA Concrete

Concrete is the most versatile material of construction in the world over. It is achieved that the distinction of being the “largest man-made material” with the average per capita consumption exceeding 2 kg. Concrete is the material of choice for a variety of applications such as housing, bridges, highway pavements, industrial structures, water carrying and retaining structures, etc. The credit for this achievement goes to well-known advantages of concrete such as easy availability of ingredients, adequate engineering properties for a variety of structural applications, adaptability, versatility, relative low-cost etc. Moreover, concrete has an excellent ecological profile compared with other materials of construction. With the continuing expansion of infrastructure and housing construction, especially in the developing countries of Asia, Africa, and South America, the rate of consumption of cement and concrete is rising and is bound to go further. In India, concrete construction scenario has been witnessing considerable growth in recent years.

Table 2: Physical and Chemical Properties of SCBA

S. No.	Physical Properties		Chemical Composition	
	Property	Test Result	Characteristic	Test Results %
1.	Density	575 Kg/m ³	(SiO ₂) + Al ₂ O ₃ Fe ₂ O ₃ % by mass	85.14
2.	Specific Gravity	2.2	SiO ₂ % by mass	60.20
3.	Mean particle size	0.1–0.2 μm	MgO % by mass	2.48
4.	Min specific surface area	250 m ² /Kg	Total sulphur as SO ₃ % by mass	0.10
5.	Particle shape	Spherical	Available alkali as sodium oxide (Na ₂ O) % by mass	4.32
6.			Loss of ignition % by mass	5.10



Table 3: Properties of Na₂SO₄, MgSO₄ and H₂SO₄

S. No.	Na ₂ SO ₄		MgSO ₄		H ₂ SO ₄	
	Chemical	Volume (%)	Chemical	Volume (%)	Molecular Formula	H ₂ SO ₄
1.	Loss on drying (at 130°C)	1.0	pH (5% water)	6.3	Molar mass	98.079 g/mol
2.	Chlorides	0.001	Free Alkali sol. (as NaOH)	0.008	Appearance	Clear, colorless, odorless liquid
3.	Nitrates	0.02	Free Acid (as H ₂ SO ₄)	0.01	Density	1.84 g/cm ³ , liquid
4.	Iron	0.01	Chlorides	0.02	Melting point	10°C; 50°F; 283 K
5.	Potassium	0.1	Heavy metals (Pb)	0.0005	Boiling point	337°C; 639° F; 610 K (When Sulphuric acid is above 300°C, it will decompose slowly.
6.			Arsenic	0.0002	Solubility in water	Miscible
7.			Iron (Fe)	0.01	Acidity (pK _a)	-3, 1.99

Problem of Durability

While the spectacular growth has been occurring in concrete production, the problem of early deterioration of some of the reinforced and pre-stressed concrete structures has also come to the forefront in recent years. It has been observed that some recently constructed structures—even those built conforming to the latest specifications—has shown early signs of distress and damage, sometimes within a few years of commissioning, while quite a few structures built more than half a century ago are still in a good serviceable condition. The phenomenon of early deterioration of concrete structures is tending to assume alarming proportions in some countries, especially those spacing hostile weather conditions. The seriousness of the problem is reflected with the high cost of repairs in these countries. It has been estimated that in the USA alone, the overall cost of repairing and replacing all deteriorated concrete structures would a staggering \$200 billion! In the most of the advanced countries, nearly 40% of the construction industries budget is spent on repair, restoration and strengthening of the damaged concrete structures. All this has tarnished the image of concrete as a “durable, maintenance-free” material. Thus, durability of concrete has become an important issue today.

The durability tests have been conducted to check the durability parameters to withstand for the environmental attacks. So, in the present thesis work the test was conducted on Sodium Sulphate (Na₂SO₄), Magnesium Sulfate (MgSO₄), Sulfuric Acid (H₂SO₄) and Hydrochloric acid (HCL) attack.

Results and Discussion

The properties of materials determined based on the various laboratory tests are presented in this work. The strength and durability characteristics of SCBA have also been presented

in this work on the replaced concrete are studied and discussions on the results obtained from the tests are done.

Compressive Strength and Durability Charecteristics of SCBA Replaced Concrete

In accordance with IS-516 the compressive strengths of SCBA replaced concrete in different percentages cured in water and different percentages of Na₂SO₄, MgSO₄ and HCL, H₂SO₄ for 28, 60, 90 days are determined by testing the cube specimens in compression testing machine.

Compressive Strength of SCBA Cubes Cured in Water

The SCBA replaced concrete cubes are prepared in the moulds for estimating the compressive strength values. The tests were conducted as per IS-516. Cube specimens were prepared using cement, replaced with varying percentages of SCBA. The tests were conducted after 28, 60 and 90 days of curing.

The compressive strengths of SCBA replaced concrete increased with increase in curing period for all the percentages of replacements. Graph 1 infers that compressive strengths of SCBA replaced concrete cubes cured in water for all curing periods’ increases up to 10% replacement and a decrease in compressive strength is observed at 15% and 20% replacement.

Sodium Sulphate Effect on SCBA Replaced Concrete Cubes

Graphs shows the results for SCBA concrete cubes exposed to 1%, 3% and 5% Na₂SO₄, MgSO₄, H₂SO₄ and HCL solution. From the graphs it can be seen that the compressive strength of SCBA replaced concrete cubes increases with



increase in the period of exposure for all percentages of replacement. For different periods of curing an increase in compressive strength is observed up to 10% replacement and a decrease in strength is observed at 15% and 20% replacement.

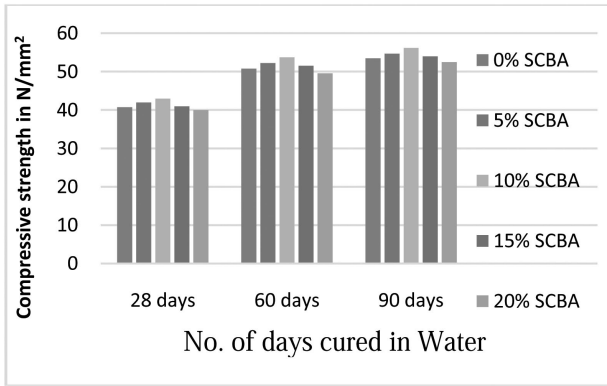


Fig. 1: Compressive Strength Results of SCBA Concrete Cured in Normal Water

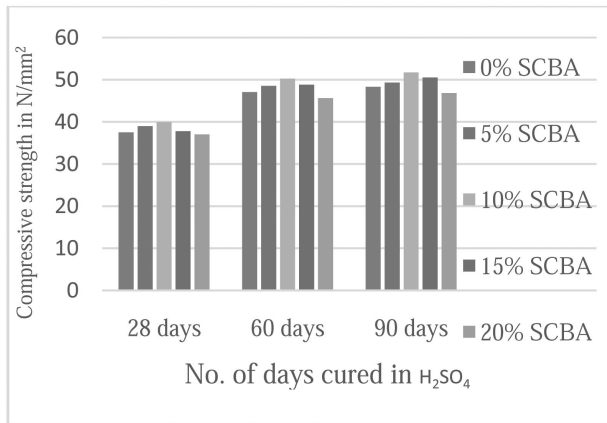


Fig. 2: Compressive Strength Results of SCBA Concrete Exposed to 1% by Weight of H₂SO₄ Solution

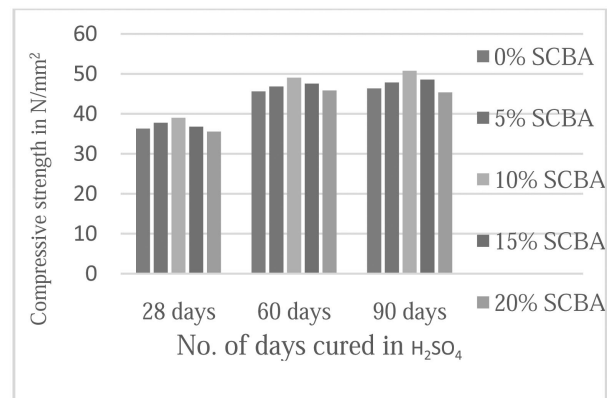


Fig. 3: Compressive Strength Results of SCBA Concrete Exposed to 3% by Weight of H₂SO₄ Solution

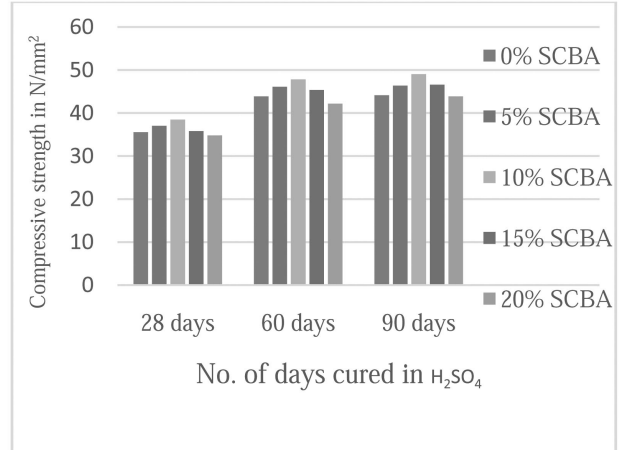


Fig. 4: Compressive Strength Results of SCBA Concrete Exposed to 5% by Weight of H₂SO₄ Solution

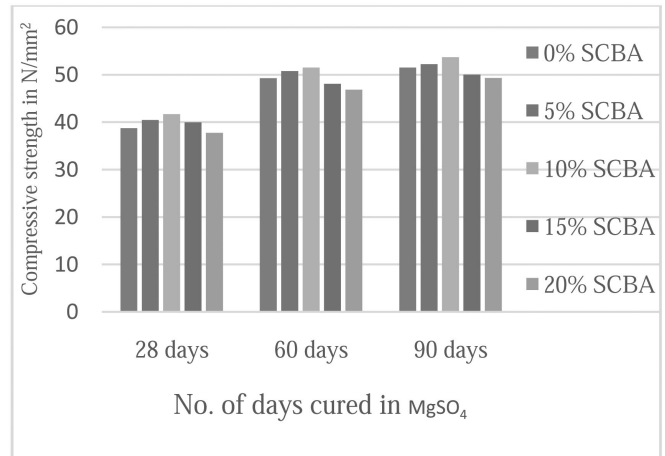


Fig. 5: Compressive Strength Results of SCBA Concrete Exposed to 1% by Weight of MgSO₄ Solution

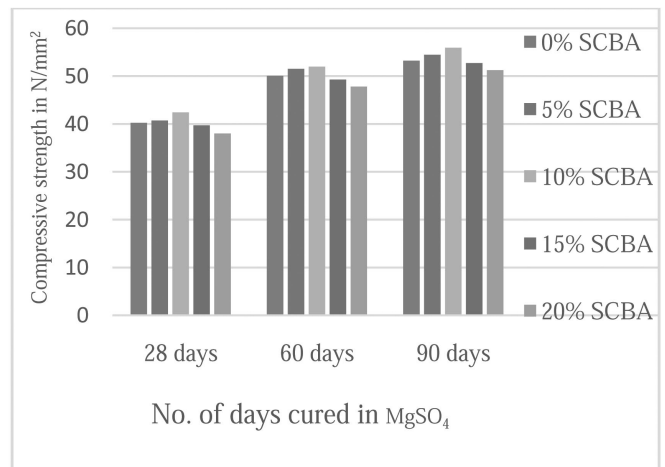


Fig. 6: Compressive Strength Results of SCBA Concrete Exposed to 3% by Weight of MgSO₄ Solution

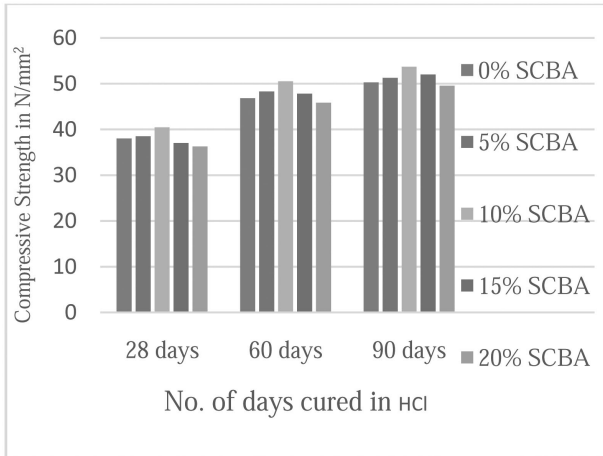


Fig. 7: Compressive Strength Results of SCBA Concrete Exposed to 1% by Weight of HCl Solution

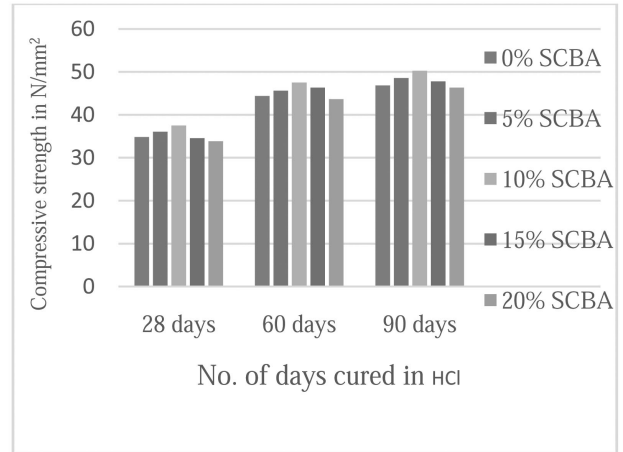


Fig. 10: Compressive Strength Results of SCBA Concrete Exposed to 5% by Weight of HCl Solution

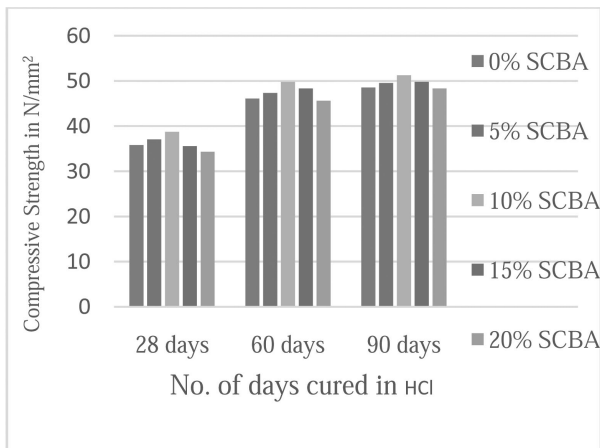


Fig. 8: Compressive Strength Results of SCBA Concrete Exposed to 3% by Weight of HCl Solution

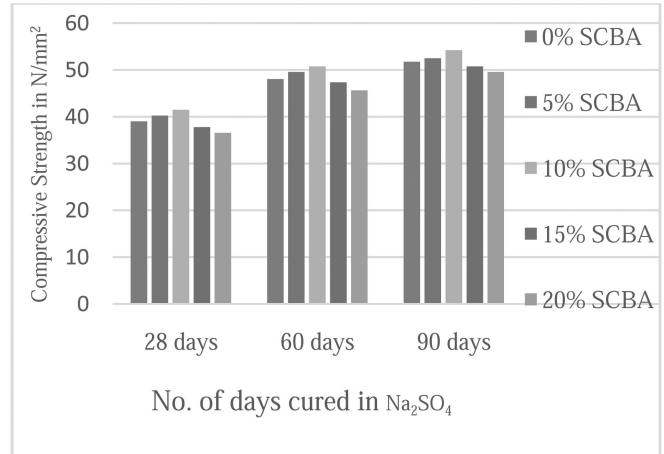


Fig. 11: Compressive Strength Results of SCBA Concrete Exposed to 1% by Weight of Na₂SO₄ Solution

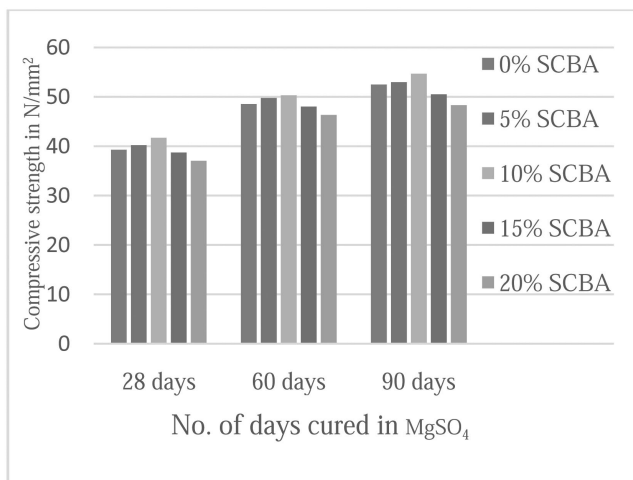


Fig. 9: Compressive Strength Results of SCBA Concrete Exposed to 5% by Weight of MgSO₄ Solution

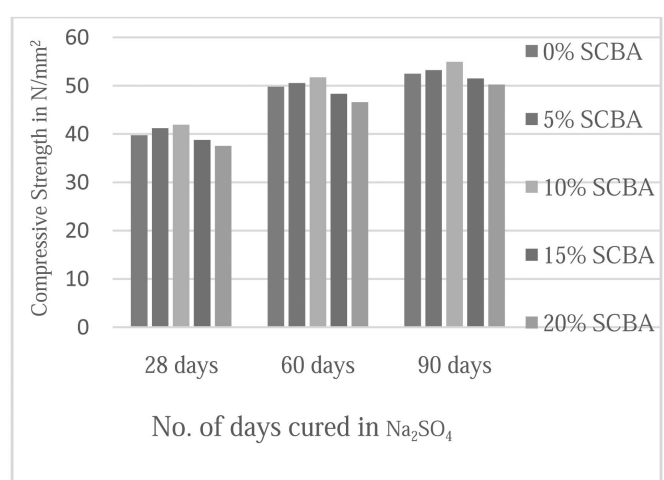


Fig. 12: Compressive Strength Results of SCBA Concrete Exposed to 3% by Weight of Na₂SO₄ Solution

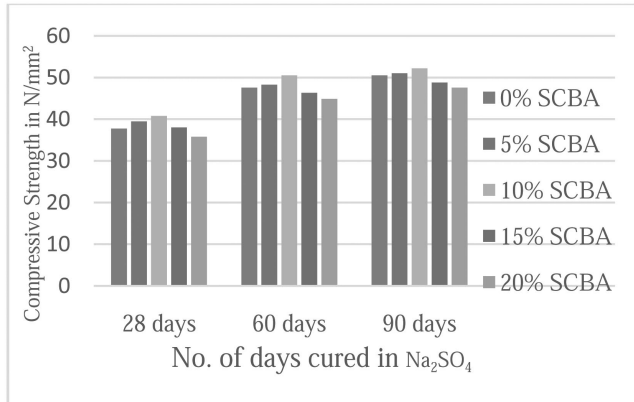


Fig. 13: Compressive Strength Results of SCBA Concrete Exposed to 5% by Weight of Na₂SO₄ Solution

Conclusion

The following conclusions have been made based on the work carried out:

- The compressive strengths of SCBA replaced concrete cubes cured in water increased with increase in curing period for all percentages of replacements. An increase in compressive strength is observed at 10% replacement and a decrease in strength is observed at 15% and 20% replacement for all curing periods.
- The compressive strengths of SCBA replaced concrete cubes exposed to Sodium sulphate concentrations of 1, 3 and 5 percentage solutions increases with the increase in period of exposure for all percentages of replacements. For different periods of curing an increase in compressive strength is observed up to 10% replacement and a decrease in compressive strength is observed at 15% and 20% replacements.
- The compressive strengths of SCBA replaced concrete cubes exposed to Hydrochloric acid solution of 1, 3 and 5 percentage solutions increases with the increase in period of exposure for all percentages of replacements. For different periods of curing an increase in compressive strength is observed up to 10% replacement and a decrease in compressive strength is observed at 15% and 20% replacements for all curing periods.
- Due to slow pozzolanic reaction, the sugarcane bagasse ash concrete achieves significant improvement in its mechanical properties at later ages.
- The partial replacement of SCBA in cement is not only enhances the strength to the concrete but also prevent it from the attack of sulphates and also provides resistance against acids.
- It was clearly shown that SCBA is a pozzolanic material that has the potential to be used as partial cement replacement material and can contribute to the environmental sustainability.

References

- [1] Murthi, P. and Sivakumar, V., Studies on Acid Resistance of Ternary Blended Concrete, *Asian Journal of Civil Engineering (Building and Housing)*, Vol. 9, No. 5 (2008), pp. 473–486.
- [2] Maroliya, M.K.; Parghi, Anant; Modhera, C.D. and Patel, Bhavin A., Physio-Mechanical Behaviour of Reactive Powder Concrete under Aggressive Environment of Contaminated Soil, *33rd Conference on Our World in Concrete and Structures: 25–27 August 2008, Singapore*.
- [3] Beulah, Prallahada M.C., Effect of Replacement of Cement by Metakalion on The Properties of High Performance Concrete Subjected to Acid Attack, *i-manager's Journal on Civil Engineering*, Vol. 2 1, No. 3, 1 June–August 2012.
- [4] Ogork, Egbe-Ngu Ntui; Uche, Okorie Austine and Elinwa, Augustine Uche, A Study on Groundnut Husk Ash (GHA)–Concrete under Acid Attack, *IJMER*, ISSN: 2249–6645, www.ijmer.com, Vol. 4, Iss. 7, July 2014, 30.
- [5] Chatveera, B. and Lertwattanaruk, P., Durability of conventional concretes containing black rice husk ash, *Journal of Environmental Management*, 92 (2011) 59e66.
- [6] Abdulkadir, T.S., Oyejobi, D.O. and Lawal, A.A., Evaluation of Sugarcane Bagasse Ash as a Replacement for Cement in Concrete Works, *Acta Tehnica Corviniensis – Bulletin of Engineering Tome VII [2014] Fascicule 3 [July – September]* ISSN: 2067-3809.
- [7] Aigbodion, V.S., Hassan, S.B., Ause, T. and Nyior, G.B., Potential Utilization of Solid Waste (Bagasse Ash), *Journal of Minerals and Materials Characterization and Engineering*, Vol. 9, No. 1, pp. 67–77, 2010.
- [8] Shafana, T. and Venkatasubramani, R., A study on the Mechanical Properties of Concrete with partial replacement of Fine aggregate with Sugarcane bagasse ash, *International Journal of Advanced Structures and Geotechnical Engineering*, ISSN 2319–5347, Vol. 03, No. 01, January 2014.
- [9] Ganesan, K., Rajagopal, K. and Thangavel, K., Evaluation of bagasse ash as supplementary cementitious material, *Cement and Concrete Composites*, 29 (2007), 515–524.
- [10] Marcos Oliveira de paula, Ilda DE Fátima Ferreira Tinôco, Conrado DE Souza Rodrigues, Jairo Alexander Osorio Saraz, Sugarcane Bagasse Ash as A Partial-Portland-Cement-Replacement Material, Received for review August 6th, 2008, accepted March 19th, 2009, final version March, 20th, 2009.
- [11] Attiogbe, Emmanuel K. and Rizkalla, Sami H., Response of Concrete to Sulfuric Acid Attack, *ACI Materials Journal Technical Paper Title no. 85-M46*.
- [12] Reddy, B. Madhusudhana; Rao, H. Sudarsana and George, M.P., Effect of Hydrochloric Acid (HCl) on Blended Cement (Fly Ash based) and Silica Fume Blended Cement and their Concretes, *International Journal of Science and Technology*, Vol. 1, No. 9, September, 2012.
- [13] Noor-UL-Amin, Mardan, Chemical Activation of Bagasse Ash in Cementations System and its Impact on Strength Development, *J. Chem. Soc. Pak*, Vol. 32, No. 4, 2010.
- [14] Srinivasan, R. and Sathiya, K., Experimental Study on Bagasse Ash in Concrete, *International Journal for Service Learning in Engineering*, Vol. 5, No. 2, pp. 60–66, Fall 2010, ISSN: 1555-9033.



Challenges due to Change in Land Use and Rain Fall Pattern for Storm Water Collection, Treatment and Disposal

Rajendrakumar V. Saraf¹

Abstract: *There is urgent need to consider Storm water management as a part of Town planning and development. Urban storm water is surface run off from roofs, roads, footpaths, car parks and all open spaces like gardens, parks etc. Storm water has been traditionally collected by storm water drains and transported through pipes and channels to creeks, rivers, the harbor and ocean. In the earlier days there used to be a combined sewerage system that carries sanitary wastewater and storm water together. For Municipal Authorities provision of storm water sewers is always the last priority. In most of the urbanized area Storm water flows on the road, through the open gutter or the storm water sewer if provided. Due to Urbanization Land use pattern changes and natural drainage system is vanished, altered, encroached and being used as dumping site during non-rainy days. Rain water gushes directly because natural obstructions and percolation are drastically reduced in urbanized area. Despite of the best efforts by the municipal authority, chaos takes place during rainy season e.g. flood like situation in Mumbai, Chennai, etc. The statistic shows that the rain fall pattern is not changed much. However it is definite that duration of rain fall is becoming shorter. The excess rain fall always becomes excuse for failure of storm water drainage system. Therefore there is need of understanding different aspects of Storm water management and its integration with Water supply and Sewerage system. Geological and topographical conditions, Land use pattern, Hydrogeology and the rain fall are not same all over therefore approach and guidelines are to be developed for site specific conditions. Urbanization changes the original landscape and increases the surface run off rate. Excess water if it does not find way, it creates the problems of manmade flood like situation. Therefore storm water needs a proper design and planning. Carefully engineered and dedicated storm water system is required. The storm water is highly contaminated because it carries all the discharges of liquid and solid waste on and above the ground along with it, to the receiving water bodies. Attention is to be given to the impact and mitigation measures. Runoff into storm sewers can be minimized by including sustainable or low impact development or green infrastructure practices into municipal plans. Direct use of rain water will increase Green water Foot Print of Urbanized population. The wetland can be developed to reduce the peak flow of Strom water and to have green cover over the land and enhance ground water recharge. Rain water harvesting in urbanized area needs critical evaluation. SOP is to be prepared for storm water management system during rainy and dry days. Finally people involvement and participation needs to be built up to take care and maintain natural and manmade drainage system for their safety. Hence Smart Technologies and engineering solutions are required to take up the challenges due to Change in Land use and Rain Fall Pattern for Storm water Collection Treatment and Disposal.*

Keywords: Urbanization, Land Use Pattern, Rain Fall, Storm Water Management.

Introduction

After independence there is shift of population from rural to urban area. According to 1901, 2001 and 2011 census population residing in urban area in India was 11.4%, 28.53% and 31.16% respectively. Growth rate of urban population was 2.76% per annum during 2001–2011. It is anticipated that more than 50% population will be urban by 2050 [1, 2]. Under the urban sprawl change is from **Village → Out Growth → Urban Agglomeration → Census**

Towns → Statutory Towns → Municipal Corporation. In Annual report 2015–16 Ministry of Urban Development acknowledged that this transition to urban society, has not been accompanied by a appropriate increase in the supply of basic urban services like water supply, sewerage and drainage network, garbage disposal facilities, citywide roads, public transport, and public safety systems like street lighting and pedestrian pathways. The supply of land and housing has not kept pace with the increase in urban population. Water

¹Chairman, Viraj Envirozing India Pvt. Ltd., Pune, India. ✉ sarafrv@virajenvirozing.com



supply and sanitation is a State subject and the State Governments/Union Territories and Urban Local Bodies are responsible for providing water supply and sanitation services through planning, design, implementation, operation and maintenance [3]. However more thrust is given on Water Supply. Sewerage system is not yet provided in most of the urban areas. Storm water management is yet waiting to get in the list of priorities. It is commonly observed that, these expanding urban areas receive increased water supply through network of pipelines, but do not have a well defined sewerage systems or storm water drainage systems. Proper storm water drainage system is always put on the last priority while planning new developments. Urban storm water is surface run off from roofs, roads, footpaths, car parks and all open spaces like gardens, parks, etc. Storm water has been traditionally collected by storm water drains and transported through pipes and channels to creeks, rivers, the harbor and ocean. In the earlier days there used to be a combined sewerage system that carries sanitary wastewater and storm water together. For Municipal Authorities provision of storm water sewers is always the last priority. In most of the urbanized area Storm water flows on the road, through the open gutter or the storm water sewer if provided.

Change in Land Use Pattern Due to Urbanization and its Impact on Storm Water

Surface runoff is the flow of water that occurs when excess storm water, melt water, or other sources flows over the Earth's surface. This might occur because soil is saturated to full capacity, rain arrives more quickly than soil can absorb it or impervious areas (roofs and pavement) send their runoff to surrounding soil that cannot absorb all of it. Surface runoff is a major component of the water cycle. Soil characteristics, plants and animals, and slope angle are among the natural factors controlling the proportion of precipitation that is converted to runoff in a given landscape, and the time it takes for runoff to enter a stream. Human changes to these landscape features has greatly influence runoff. Before the urbanization the land is agricultural where surface run off rarely exceed 25%. Due to urbanization, large magnitude of virgin land is being converted into residential and commercial centers. It changes the surface and topographic characteristics of the area by 'grading and re-grading. The roads and buildings increase the impervious surfaces that subsequently increase the storm water runoff rate and volume. Natural drainage patterns are encroached, altered or redirected. This leads to Localized flash flooding, increased frequency of flooding on the downstream, scouring of banks of natural streams, silting, loss of ground water recharge, lower dry weather flows in the streams, habitat destruction and pollution of natural streams. When land-use changes Routing factor increases i.e. time taken for the runoff to reach the water inlet decreases thus resulting in

higher peak flows. The increase in runoff coefficient causes larger volume of flow in the drains and lower volume percolate into the ground.

Change in Rain Fall Pattern and its Impact on Storm Water

The Indian summer monsoon (June–September) rainfall is very crucial for the economic development, disaster management and hydrological planning of the country. The July rainfall has shown decreasing trends over most parts of central India. However, June and August rainfall has shown increasing trend over the central and south western parts of the country. Contribution of July rainfall is decreasing in central and west peninsular India. But contribution of August rainfall is increasing in all these areas. Significant increasing trend is also observed in the annual rainfall for the sub-divisions Konkan and Goa, Madhya Maharashtra, North Interior Karnataka, Rayalseema, coastal Andhra Pradesh, Gangetic West Bengal, Assam and Meghalaya and Jammu and Kashmir [4]. Nearly 75 to 90% of the total average annual rainfall in India occurs during the four months from June to September. As such storms of heavy to moderate rain are common phenomena during this period in most parts of India. The extreme rainfall event of 994 mm on 26 July 2005 has been a lesson for Mumbai and it has indicated the perils of rapid development in highly concentrated urban areas. Hyderabad in August 2008 received over 150 mm of rainfall in less than 14 hours within a span of two days. It is second highest in four decades. On 15 to 16th of Nov. 2015, Chennai city and neighboring areas got 246.5 mm of rain precipitation. These examples indicate that change in rain fall pattern is making the scenario worst. Urban floods are becoming common since 2005. Intergovernmental Panel on climate Change (IPCC) in its report released in January 2001 has concluded that most of the warming observed over the last 50 years is attributable to human activities (especially emissions of heat trapping gases from fossil fuels which is likely to double the risks). Further, deforestation, urbanization, industrialization, increase in automobiles, etc. add to the fury. These changes are having a lot of influence on meteorological parameters. Rao, Jaswal and Kumar (2004) studied the effects of urbanization on meteorological parameters over fifteen cities (with a population of more than one million) and concluded that in general bright sunshine hours, wind speed, total cloud amount and radiation values were showing a decreasing trend while relative humidity and rainfall had an increasing trend [7,8]. It is observed that average rain fall remains almost same. However the duration of rain fall is decreasing. Probability of having +50 mm rain fall in one hour duration is more. It happened in Pune, Mumbai and Nagpur, etc. Conditions become worst due to increase surface runoff rate due to change in land use pattern. Alone in Chennai due to urban flood the losses are

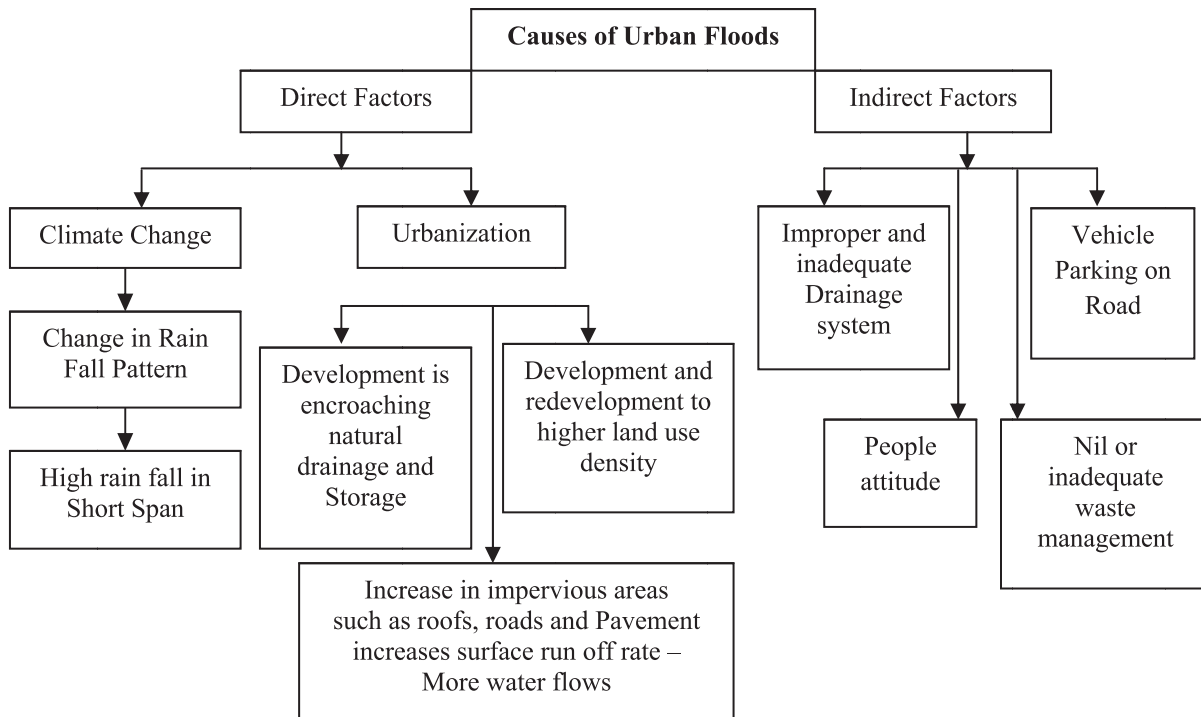


Fig. 1: Cause of Urban Floods

accumulating from Rupees 50,000 crores to 100,000 crores. The automobile sector’s losses alone were estimated between 8,000 crore [5]. Thus floods in urbanized area caused the damages to the tune of thousands of million rupees in India and will continue to happen till storm water management is considered seriously. Thus an integral approach is required for storm water design for reduction in peak flow and total flow of storm water runoff. Direct and Indirect causes of urban floods are summarized in Figure 1.

Need of Storm Water Management

Increased urban population obviously creates pressure on available urban infrastructure for land, water, shelter and put forth higher demands for housing, transportation, industrial and commercial developments. Unplanned urban growth causes illegal encroachments on natural drainages. Water management in urban area always play vital role in city development. In addition to water supply and sewerage distribution network, management of storm water is getting a prime importance. By default we assume that storm water will find its way. It was true prior to the change in land use by urbanization. Improper storm water management increases flood and water logging potential of city, create serious threats to underground and surface water resources available. Therefore storm water needs a proper carefully engineered design appropriate planning and dedicated storm water management. Sustainable urban drainage systems

ensure planning of storm water drainage network with environmental considerations and use of green technologies for storm water management. It has potential for economic use of costly water resources and also to reduce the cost of water pollution control and abatement. It will also reduce the associated health hazards, increase green cover and improve air quality and increases aesthetic values of the city. Essential planning considerations, technology options and innovations in storm water management to be considered for “Smart City” concept.

Strom Water Quality, its Impact and Mitigation Measures

The storm water carries all the discharges of liquid and solid waste on and above the ground along with it to the receiving water bodies. It is highly contaminated. Yet attention is not given to the impact and mitigation measures. Urban storm water contains pollutants that deteriorate water quality and adversely impact aquatic habitat. Pollutants found in storm water include suspended solids, heavy metals and a broad spectrum of organic compounds including pesticides, nutrients, petroleum compounds, pathogen indicators and other by-products of urban activities. Urban storm water has also been shown to alter water quality parameters such as pH, oxygen demand, specific conductance, temperature and turbidity. Urbanization modifies the hydrologic properties of a land that generally leads to increase volumes of runoff



from a given amount of precipitation, and a more rapidly developing runoff peak. These pollutants and hydro-modifications can directly result in negative impacts to biota and degrade ecosystems. The samples of Storm water joining Mutha River were collected during heavy rains in August 2016. The results are given in Table 1. Similar are the findings by Nivedita and Rawal [6] for the sample collected from Kothrud Basin in Pune. It can be concluded from the Table 1 that Storm water quality in natural drains is very poor and is comparable to that of dilute to medium strength sewage. It means the Storm water shall be treated before the disposal in to water bodies.

Table 1: Storm Water Quality

Parameters	1	2	3	4	5
Suspended Solids, Mg/l	240	320	235	198	210
COD Mg/l	315	192	145	295	188
BOD, Mg/l	122	90	78	145	102

Rain Water Harvesting

Fate of rain water is given in Figure 2. Four products of rain water are humidity, natural storage (ponds, Lake, etc.), surface runoff, ground water recharge and bound water. As discussed earlier after construction the due to increase in impervious areas surface runs of increases from 25% to 85%. To increase ground water recharge Pune, Chennai and many other cities have made Rain water harvesting compulsory. However practically it is difficult to put entire rain water or water equivalent to difference of surface run off before and after the construction. At present storm water gushes out on roads or through the storm water drainage system. Storm water drainage system can be integrated with Rain water harvesting by providing the recharge pits and the obstructions to the flow. As per the studies carried out by R.V. Saraf [9] rainwater before touching the ground is devoid of soluble solids and has tendency to leach out calcium and solids from all the rocks commonly found in aquifers. It indicates that Magnesium and other solids based on and heavy metal present in rock can be leached out with rainwater. Enhance rate of percolation and recharge can cause drastic change in ground water quality. It is observed that excessive pumping of ground water has lowered down the ground water table. This is due to imbalance between natural recharge and draw of ground water. Vice versa if the recharge of ground water is enhance by rainwater harvesting then it may increase the ground water table and cause the serious problem of increase in salinity of soil and change in soil flora and fauna. Similarly if rainwater directly comes in contact with lower strata of soil and rock it can change water quality and weather the rock at faster rate. Over period of time it may change the geochemistry [9].

Organic and inorganic chemicals emitted due to vehicular traffic and other domestic and industrial activities can get deposited on rooftop and leach out with rooftop water. These chemicals may present in micro level can contaminate the underground water over period of time. Therefore rainwater harvesting is to be critically evaluated and carefully implemented to avoid any adverse impact due to collision of human activities with the nature to have more water [9,10]. No doubt at present Rainwater harvesting offers a small-scale best management practice to reduce storm water runoff and the problems associated with it.

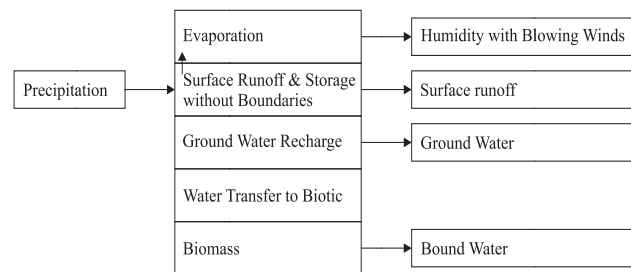


Fig. 2: Fate of Rain Water

Retention Basins

Retention basins offer a viable solution to the problem of urban storm water runoff in developing countries. In rural India, retention basins have been used for centuries for holding rainfall to augment drinking water and irrigation supply. Percolation tanks are among the most common runoff harvesting structures in India. It is an artificially created surface water body submerging a highly permeable land area so that the surface runoff is made to percolate and recharge the ground water storage.

Retention basins filter pollutants such as metals, nutrients, sediments, or organics by sedimentation. Further removal of pollutants is achieved through algal and wetland plant uptake as well as bacterial decomposition. Case studies have been reported from various parts of India including Hyderabad, Surat and Karnataka [11]. Due to financial constraints and lack of infrastructure, wastewater management systems are not well equipped to treat sudden increase in hydraulic load due to rain or floods. Retention basins offer an inexpensive and sustainable drainage solution to this problem. Instead of Retention basins ponds can be used for storage of storm water for longer time. This allows natural processes, using bacteria and sunlight, to break down pollutants before the water eventually flows into downstream watercourses. Ponds can also be a welcome addition to urban areas, encouraging plants and wildlife. Studies show that incorporating retention basins to conventional drainage networks can prevent flooding in receiving bodies and transport of oil, organics and toxic metals through storm water runoff (CIDCO 2013).



Retention basins or holding ponds have been constructed in coastal Navi Mumbai to avoid water logging of low lying areas and prevent pollutants to flow into the creek. In Mumbai, retention basin was effective in storm water flooding and reducing the total suspended solids [10–12]. Silting of Pond and mangroves growth is the main problem observed with Retention Basin constructed in Navi Mumbai. Ponds act as retention basin in normal condition and storage tank during high tide. It helps in avoiding water logging.

Sustainable Urban Drainage Systems

Sustainable Urban Drainage Systems (SUDS) mimic nature and typically manage rainfall close to where it falls. It involves sequence of followings management practices.

- Transport of surface water with reduction in surface run off before it joins the natural water body to ensure reduction in urban floods and protection of natural flow regimes in watercourses.
- Encourage natural groundwater/aquifer recharge.
- Provide opportunities for natural evaporation from surface water and evapo-transpiration from vegetation.
- Reduction of pollution from storm water to protect water quality.
- Ensures minimal or no long-term detrimental damage on manmade structures and natural environment.
- Provide storage for storm water for natural treatment to enhance percolation for ground water recharge and usage of water in non rainy days. It will be also an attractive habitat for wildlife in urban watercourses.
- Create safe and better places to live, work and play.

A SUDS is done in three stages as shown in Figure 3. It begins with Source control at Individual Buildings, Site control for larger area of residential complex, roads and parks and finally Regional Control at downstream of Site control and before it joins the natural water conveyance (Streams, Nala and river) Rainwater that passes through small SUDS can feed into larger SUDS which deal with the gathered run-off from a wide area. It is best to connect the flows between SUDS components with swales, filter drains or ditches and avoid the use of pipes.

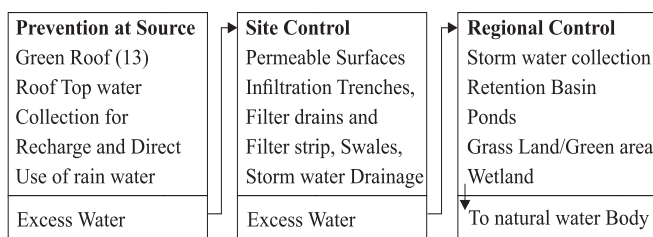


Fig. 3: Three Stages of Sustainable Urban Drainage Systems

Integration of Storm Water for Wetland Development

Storm water can be stored on the open land before it joins the natural drainage. The wetland can be developed to reduce the peak flow Storm water and developed the green cover over the land. It will also add to the ground water recharge. It also satisfy urban design objectives, such as providing passive recreational and landscape value, wildlife habitat, flood control and control of the physical changes in a stream due to urban development. Existing ponds or wetlands to treat run-off shall never be used. Always create new ponds to avoid damaging or disturbing the wildlife that is already in the area. Contrary to common practice, vegetation should be established perpendicular to the direction of flow to optimize interaction between wetland vegetation and polluted water. Most pollutants from urban area are transported during storm events. Therefore physical processes are more important in trapping pollutants at these times. Biological processes become important under low flow conditions, when previously trapped materials are transformed and recycled. Small suspended particles adhere to plant surfaces, which act as filters. Plants also provide a surface on which photo-synthetic organisms such as algae can grow. These epiphytic algae remove both fine particles and dissolved pollutants from the water column. The proper design of constructed wetlands for treatment of urban storm water is a multi-disciplinary task. Early planning, identification and prioritizing of the various beneficial uses are vital in ensuring a sustainable urban storm water management and urban design system. The creation of constructed wetlands requires the coordination of civil works and wetland vegetation establishment [14]. The functions of vegetation during storm-event flow and base flow conditions in wetlands are summarized in Table 2.

Table 2: Function of Wetland during Base Flow and Storm Event Flow

During Base Flow	During Storm Event Flow
Provides surface area for epiphytes Epiphytes take up materials from the water and introduce them to sediments, as cells dislodge from plant surfaces and settle. This is a short-term process occurring over hours to weeks.	<ul style="list-style-type: none"> • Increases hydraulic roughness • Promotes uniform flow • Enhances sedimentation of particles
Takes up nutrients from the sediments Nutrients in the sediment are transformed into plant biomass. This is a medium-term process occurring over weeks to years	<ul style="list-style-type: none"> • Provides surface area for small-particle adhesion
Control of surface sediment redox Plant root-zones generally help maintain an oxidized sediment surface layer preventing chemical transformation of settled pollutant	<ul style="list-style-type: none"> • Protects sediments from erosion



Operation and Maintenance of Storm Water Drainage

The storm water system is to be operated only during rainy season and rest of the year it remain idle. As such there is no SOP available for storm water management system during rainy and dry days. There is need of Storm water quality monitoring to ensure the treatment and protect the receiving water body.

Guidelines or Standards for Storm Water Management

Detail Guidelines standards are not yet available in India. There is one standard called as Guidelines on Urban Drainage Published by Indian Roads Congress [15]. There is need to prepare Guidelines and standards for Storm Water Management general and specific to site condition.

Public Involvement and Participation

Natural drainage system is encroached by or changed for human habitation. It is observed that storm water manholes are used for dumping the solid waste. Sewage is connected to the storm water line. This results into the unsafe conditions. People involvement and participation needs to be built up to take care and maintain natural and manmade drainage system for their safety.

Conclusion

Sustainable Storm Water Management is to be considered on top priority to avoid urban floods and loss of money due to damages. There is definite impact of change in land use and rainfall pattern on storm water generation. It is to be integrated with site specific geological and metrological factors. There is a need of planning of storm water drainage network with environmental consideration and use of green technology. Prevention at resource, reduction and control at site followed by control at region will reduce the impact of pollution, peak flow and gushing water in the storm water drain. The rain water harvesting, retention pond and wetland development are to be incorporated in planning. The wetland will reduce the pollution, peak load impact and will increase percolation of water. The water in the tank can be used during non rainy season and will also attract the wild life. Public involvement and participation is must to protect the natural drainage and avoid the encroachment or dumping of solids. Specifications and guidelines are to be prepared for sustainable storm water drainage system. It will reduce the cost of water pollution control and abatement, associated health hazards and urban flood. It will increase green cover and aesthetic values of the city. Essential planning

considerations, technology options and innovations in storm water Management are required for “Smart City” concept.

References

- [1] Emerging Pattern of Urbanization in India, R.B. Bhagat, August 20, 2011, Vol. XVI, No. 34, EPW Economic and Political Weekly.
- [2] Urbanisation in India–Wikipedia, https://en.wikipedia.org/wiki/Urbanisation_in_India.
- [3] Annual Report 2015–16 Ministry of Urban Development, Govt. of India.
- [4] Guhathakurta and Rajeevan, M., Trends in the rainfall pattern over India, *International Journal of Climatology*, 28: 1453–1469 (2008), Published online 6 November 2007 in Wiley Inter Science.
- [5] Rafiq, Farhat; Ahmed, Sirajuddin; Ahmad, Shamshad and Khan, Amir Ali, *Urban Floods in India International Journal of Scientific and Engineering Research*, Vol. 7, Issue 1, January 2016.
- [6] Gogate, Nivedita G. and Rawal, Pratap M. Sustainable Storm water Management in developing and Developed Countries: A Review, *Proc. of Int. Conf. on Advances in Design and Construction of Structures 2012*.
- [7] De, U.S., Dube, R.K. and Rao, G.S. Prakasa, Extreme Weather Events over India in the last 100 years, *J. Ind. Geophys. Union (July 2005)*, Vol. 9, No. 3, pp. 173–187.
- [8] Climate Change 2014. Syntheses Report The Inter governmental Panel on Climate Change, ISBN 978-92-9169-143-2.
- [9] Saraf, Er. Rajendrakumar V., Rainwater Harvesting – Critical Evaluation, Rain Water Harvesting Practices, 2008, UNESCO and IEI.
- [10] ZOPE, P. and Sawant, P. (2008). Characterization of Urban Storm Water Runoff. In: *Journal of Environmental Research and Development* 3, 523–530. Bhopal: Jerad Publications.
- [11] National Policy on Disaster Management (2009). Government of India Ministry of Home Affairs.
- [12] Retention Basin, factsheet – Indo-European Project NaWa Tech- “Natural Water Systems and Treatment Technologies to cope with Water Shortages in Urbanized Areas in India”, Compiled by: Pranav Nagarnaik (CSIR-NEERI), Girish R. Pophali (CSIR-NEERI), Pawan Labhasetwar (CSIR-NEERI).
- [13] Lennin Antonelli Living Design–Green Roofs Nov 2008. <http://www.dublincity.ie/sites>.
- [14] Managing Urban Storm water Using Constructed Wetland, Tony H F Wong, Peter F. Breen, Nicholas L G Somes, and Sara D. Lloyd, Industry Report 98/7, Second Edition, September 1999.
- [15] Guidelines on Urban Drainage Published by Indian Roads Congress 2013 IRC: SP: 50–2013.



Innovative Solutions for Development of Water Resources: How to Utilize Underground Aquifer as a Natural Lake-cum-Reservoir

M.K. Ghosh Roy¹

Abstract: India is beset with some real water problems with frequent floods in some states and recurrent drought in some other States arising out of unpredictability of the monsoon. There are also some serious problems in the distribution of river water between neighbouring States, as exemplified by the Cauvery River Water disputes between Karnataka and Tamil Nadu, and also Mahanadi River water dispute between Odissa and Chhattisgarh. To remove the maldistribution of water resources over the States, there are some proposals of interlinking of rivers, which solutions are hugely costly and time consuming. The paper recommends systematic use of groundwater which is generally available in all States. To build a reservoir or other surface infrastructure, huge investments are required to be made. Similarly to create a network of canals to distribute irrigation water calls for using up large areas of land and heavy investment to create the associated infrastructure. On the other hand the underground aquifer may be made to serve as natural reservoir or lake which already exists. No new water infrastructure needs to be built, other than recharging. An agriculturist shall be allowed to draw all reasonable water by pumping to maximize agricultural production. But there will be a condition that all excess water that remains after wetting the soil shall be returned to the underground to help recharging the aquifer. The excess water must not be allowed to remain on the soil surface getting evaporated or running off to the waterway, without creating any economic value. During the rainy season, the same millions of recharging facility will recharge the aquifer to the full, making up the actual consumption for irrigation.

Keywords: UNESCO, Siklomanov, McKinsey.

Introduction

India has a large number of rivers. India also gets reasonably good amount of rainfall of 1100 mm on the national average. The problem arises because of uneven space and time distribution of the water resources. In some river basin Brahmaputra-Barak, there is considerable excess of water unutilized and flowing out to the sea. In south India the rivers are generally rain-fed and there is enough water in the rivers only during four months of monsoon. In some parts of Rajasthan in western India, the annual rain fall is as low as 100 to 300 mm. Further, the major rainfall occurs for only three to four months in a year leading to low utilization of the available water. To make the matter worse, the Indian population is steadily increasing from about 400 million in 1950 to 1200 million in 2012.

PART-I: Present Water Resource Status

Water is vital for life, to grow food, to run industries, to save the environment, to sustain biodiversity. Saving water is

really serving the nature. The development, conservation and sustainability of water resources are of strategic importance for India and the world.

Global Stock of Water—Static Stock and Renewable Stock

To fully understand the problem of water resources, it is advisable that we examine water resource with a global perspective. For water is a globally shared resource with local variations of availability. Based on water exchange characteristics, two concepts of water are used in hydrology and water management to assess the water resources in a region: static storage component and renewable water component. The total globe stock of water is 1400 million km³ (Table 1), of which total fresh water is 37.8 million km³, most of which is frozen in icecaps and glaciers. Hence the maximum available freshwater is only 0.14 million km³ or 14,000 km³.

The stock of water undergoes recirculation through the annual hydrological cycle of evaporation, and precipitation

¹Former Senior Professor, Indian Institute of Technology Madras, Chennai, India. ✉ mkghoshroy@gmail.com



(Table 2 and Figure 1). Table 2 shows excess precipitation (i.e. rainfall) of 42,700 km³ on land, which is called the renewable stock of water.

A small part of the excess water at 2100 km³ infiltrates into the underground aquifer, leaving an available surface water of 42,700 km³ annually for human use.

Table 1: Global Stock of Water Resources

Sources	Quantity, Million km ³	Percentage, %
Ocean Water	1362.2	97.3
Fresh Water	37.8	2.7
Total Water	1400.0	100.0
Breakup of Total Fresh Water		
Icecaps and Glaciers	29.18	77.2
Groundwater and Soil Moisture	8.46	22.4
Lakes and Swamp	0.13	00.3
Atmosphere	0.02	00.05
Streams and Rivers	0.01	00.03
Total Fresh Water	37.80	100.00
Available Fresh Water		
Lakes and Swamps	0.13	00.3
Streams and Rivers	0.01	00.03
Total Available Fresh Water	0.14	00.33

Sources: UN Waters.

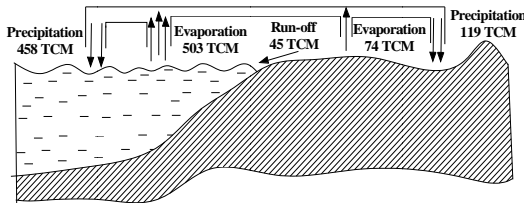


Fig. 1: Cycles of Evapo-Transpiration and Precipitation (Siklomanov, UNESCO)

Table 2: Renewable Fresh Water – Evaporation and Precipitation

Areas	Evaporation, km ³	Precipitation, km ³	Difference, km ³
Sea	-502,800	+458,000	-44,800
Land (Surface Water)	-74,200	+119,000	+42,700
Groundwater (recharge)	-	-	+2,100
Balancing Total	-577,000	+577,000	

Source: UNESCO Water Report (Prof. Siklomanov), 1998, State Hydrological Institute, St. Petersburg.

Table 3: Demand Supply Position (Business as Usual)

Water User Sectors	Water User Demand 2000		Water User Demand 2030 (Projected)		Current Supply 2000		
	Km ³	%	Km ³	%	Water Sources	Km ³	%
Domestic	600	14	900	12	Surface Water	8500	83
Industry	800	16	*1500	22	Ground Water	700	17
Agriculture	3100	70	**4300	66	Surplus Water	-100	-
Total	4500	100	6900	100	Total	4100	100

* Increase in consumption is driven by Chinese conspicuous consumption of 365 km³ for Electricity generation.

** Increase is driven by conspicuous Indian consumption of 1195 km³ for higher food production.

UNESCO Report: Supply and Demand

As already stated, the UNESCO estimates the annual renewable freshwater at 42,700 km³ from the global hydrological cycle (see Table 2 and Figure 1). The global average withdrawal as per UN Waters is about 3750 km³. This scenario does not therefore highlight water scarcity, at least at the global level.

McKinsey Report: Supply and Demand

However, the McKinsey Report highlights the relative global scarcity more realistically from more detailed consideration of demand and supply. It shows a deficit of 400 km³ in 2000 rising likely to 2800 km³.

The McKinsey data show that the water withdrawal at present is 4500 km³, which is higher than the UNESCO (Siklomanov) estimate of 3750 km³. However, we may use the higher figure of McKinsey to play safe. In any case it does not affect our hypotheses regarding the innovative solutions of water problems.

Summarizing the Water Resource Problem

Summarizing the relevant parts of the reports of UNESCO Report and McKinsey Consortium,

- Global Stock of Fresh Water : 140,000 bcm
- Renewable Fresh Water at : 42,700 bcm
- Annual Withdrawal : 3,750 bcm (UN)
- 4,200 bcm (McKinsey)

Why then is the big water crisis?

Though the actual available global stock of fresh water is fairly large at 140,000 km³, it constitutes only 0.3% of the total global fresh water stock of 37.8 million km³; it may be noted that the total stock of fresh water is 2.5 times the annually renewable 42,700 km³ and 28.5 times the estimated withdrawal of water at 3750 km³.



But the problem of water scarcity arises as we have been emphasizing, for water is very unevenly distributed in the world and worse still, the distribution is totally unrelated to the areas of human habitation. This utter mal-distribution of water has given rise to high scarcity of water, especially in major part of the developing world. In particular, water is indeed very scarce in arid zones of North Africa and the Middle East Arab Peninsula. Worsening the scarce situation of water there is wasteful use of water in agriculture, industry and municipalities, lack of sanitation and unprecedented pollution of water. All in all, it appears that the water resource position is unsustainable and calls for radical reform and development.

Indian Scenario of Water Resources

Without displaying statistics and data, we are able to describe Indian water resource scenario as grim as under:

1. Extensive floods in many parts of the country during monsoon;
2. Severe drought in many parts of the country leading to suicides of many farmers in the summer.
3. River Water distribution problems, exemplified by Cauvery River Water disputes between Karnataka and Tamil Nadu.
4. Regional Water Distribution problem, calling for hugely expensive Inter-linking of rivers projects Innovations in Water Management are thus highly necessary for India as to storage, conservation, scientific distribution and modern economic irrigation.

Part-II: Innovative Solutions of Water Resources

Treat Underground Aquifer as a Natural Lake-cum-Reservoir

Taking cognizance of difficult water situation in India, it is felt that for India some innovative thinking in water resource is called for. In any case, we venture here to submit some innovative solution proposals, which are applicable globally and is basically low-cost. The basic philosophy of the recommendations is to treat underground aquifer a natural lake-cum-reservoir.

Groundwater as an Effective Source of Water Resource

Groundwater is available in most areas of the world. But there are genuine concerns about the over-exploitation of groundwater. However, we recommend more use of groundwater to produce more crop and food. How this should be possible? Firstly, treat the groundwater as the

natural underground reservoir, river or canal. In building a reservoir or other surface water infrastructure, huge investments are required to be made. Similarly, to create a network of canals to distribute irrigation water also calls for using up huge areas of land and investing large funds to create the necessary infrastructure. The underground aquifer serves as natural reservoir or lake which already exists. No new water infrastructure needs to be built, other than recharging. An agriculturist shall be allowed to draw all reasonable water by pumping to maximize agricultural production. But there will be a condition that all excess water that remains after wetting the soil shall be returned to the underground to help recharging the aquifer. The excess water must not be allowed to remain on the soil surface getting evaporated or running off to the waterway, without creating any economic value. During the rainy season, the same millions of recharging facility will recharge the aquifer to the full, making up the actual consumption for irrigation.

Implementation of “Underground Natural Lake” Project

How such a system could be implemented? All agriculture pumping systems will be required to be licensed. License will be granted only when the recharging networks of field channels are provided for and recharging pit is built. Perhaps several farmers in the neighbourhood are needed to be organised together owing a larger pump and a large recharging pit. And each farmer needs to excavate their own shallow channels. The design of such a scheme of water management is displayed in Figure 2. In Figure 2 is shown the schematic design of a network of field channels watering scheme which provides most economic but comprehensive use of water with very high agricultural productivity. The water is sourced from ground water serviced by a pumping well at the left of the field. The excess water flows through the channels to a groundwater recharging well on the right. The author has seen similar scheme working in China during his industrial-cum-business tour some years ago. The lush green fields in China were found so well watered with the

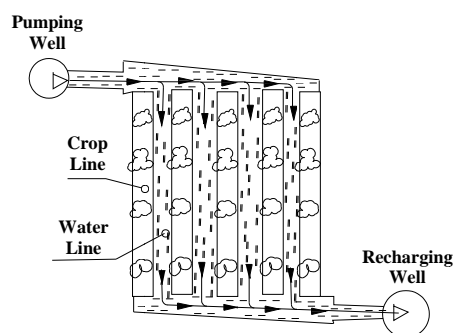


Fig. 2: Agricultural Field Watering Channels



above scheme, naturally achieving high productivity. The above scheme can be enlarged to cover up an entire village or several villages by using piped supply water and piped return water instead of digging canals as schematically illustrated in Figure 3.

The above system commends itself for another vital reason. This water scheme does not depend on the monsoon or other rain on the immediate basis. Even if the rainy season is bad in one year, the natural reservoir of underground aquifer is capable of supply vital agro-water, necessary recharging can be implemented as and when good rain arrives.

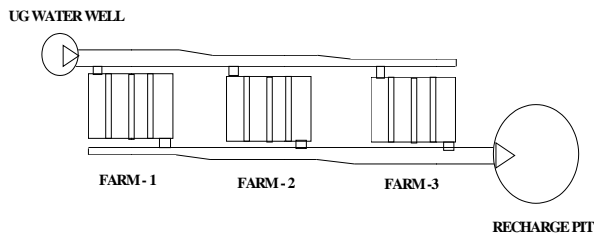


Fig. 3: Enlarged Multi-Farm Irrigation with UG Water

Continuous and Intensive Recharging

Two proposals have been made above to save water on the agro-fields and use that to recharge underground aquifers. Now it has been mentioned that there are many projects at the national and sub-national levels of recharging aquifers sponsored by the governments and civil societies. We would like to augment the above recharge systems by methods of continuous recharges by drilling recharge wells inside lakes, rivers, canals and ponds, to the extent practicable. While the recharge wells inside the river may be kept active throughout the year, diverting part of the run-off to underground, the other recharge wells inside lakes, reservoir canals and ponds shall be kept active at least during the rainy seasons.

Extra Storage Reservoir of Water

Now, on the expenditure side of water budget, there are two losses-Evaporation and river Run-off (less minimum environmental flow). On the receipt side we have renewable water from precipitation, which is variable and active. The role and cause of storage is not that much highlighted or given importance. The underground aquifers are natural storage spaces of unlimited capacities. By augmenting, activating and popularizing the underground storage systems, water supply and use equation can be truly transformed solving water scarcity to a very substantial extent. Today, we have a high ratio of evaporation, nearly equal to the

precipitation. By increasing storage, the usage factor goes up and the evaporation ratio comes down. High storage also brings down the run-off.

Minimizing Evaporation of Water by Solar Panel Coverage

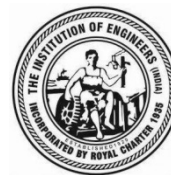
Here is another innovating proposal in future water management, which the author first heard from a lecture of Shri Narendra Modi, the then Chief Minister of Gujarat and presently the Prime Minister of India. Evaporation causes heavy losses of water, much more than the losses by way of run-off. If evaporation can be reduced, more water will be available for agriculture and domestic water. There are large networks of canals all over the country. If the canals could be covered by solar panels, protecting the canal water from direct solar radiation, the evaporation will come down substantially and at the same time large amount of photovoltaic electricity will be available to augment national productivity of services and goods, ushering in economic prosperity.

Other Water-Saving Proposals

There is several low-water irrigation technologies like drip water irrigation, which is widely practiced in Israel. The use of this technology leads to large saving of water for the same or more crops per drop. It is well known that rice cultivation is highly water-intensive. But newer method of rice cultivation like “Systems of Rice Intensification (SRI)”, promoted by UN-FAO and used in Japan, which requires much less water than the flooding method of paddy culture followed still today in India.

References

- [1] IFC Biswas, A.K. (2007). Lecture on Water Management in 21st Century at the Indian Institute of Technology, Kharagpur, India, published by Third World Centre for Water Management, Atizapan, Mexico.
- [2] FAO (AQUASTAT 1998–2003, 2005).
- [3] Roy, M.K. (2011). Sustainable Development–Environment, Energy and Water Resources, Ane Books, New Delhi and CRC Press, USA.
- [4] Ghosh Roy, M.K. (2015). Water Resources–Strategic Overview for Global Sustainability, MedTech, Scientific International, New Delhi.
- [5] McKinsey Co., Coca Cola Co, Nestle *et al.* (2000). International Consortium “Charting Our Water Future”.
- [6] Luvovitch/Baumgartner (1974). USSR Water Balance Report and Monograph.
- [7] UNESCO Study (1998). Director Prof. Siklomanov, State Hydrological Institute, St. Petersburg.



Severe Contamination of Large Quantity of Groundwater by Bleaching and Dyeing Effluents at Maheshtala Textile Cluster, West Bengal: Seasonal Assessment by Multivariate Approach

Biman Gati Gupta¹, Jayanta K. Biswas^{*1} and Kamalesh M. Agrawal²

Abstract: The study was conducted for four years (2012–2016) to assess the contamination of groundwater due to the discharge of huge quantity of hazardous effluent (2000 MLD) from small scale (SSI) textile bleaching, dyeing units (800 No.) located at Kalikapur and Mahispota under Maheshtala textile cluster (22.290N, 88.110E), 24-Parganas, West Bengal. The large quantity of water required for textile processing is drawn from groundwater by pumps. An enormous quantity of effluent is directly discharged to the nearby open land (60%), nallah (10%) and canal (30%). Apart from effluent, groundwater aquifers also receive sewage and other household wastewater left unattended by treatment infrastructure lacking in the area. The physicochemical analysis of groundwater drawn from 30 m depth and measured as per APHA (2001) reflected pH (8), carbonate (804 mg/l), nitrate (22.2 mg/l), total dissolved solids (4769 mg/l), sodium (1117.6 mg/l), fluoride (0.49 mg/l), iron (0.68 mg/l), lead (0.058 mg/l), SAR (22.5) and EC at 250C (7.9 μ S/cm), all exceeding the maximum permissible limits as laid down by both EPA (2016) and WHO (2003). The multivariate approach of physico-chemical parameters and statistical analyses was used in this study to find out the seasonal groundwater quality variation. Study indicated that quality of groundwater is very poor for domestic, industrial and agriculture uses. Thus, this study reflects the usefulness of the analysis of quality assessment. From the study it also appears that contaminated groundwater requires total treatment to arrest the production of degraded agricultural crops, fruits, vegetable and drinking water required for human consumption to save from epidemic gastrointestinal (GI) disorder, hepatitis, skin allergy, renal disorder etc. in a populated area near Calcutta. The findings of the study will help formulating water treatment processes to generate safe water for domestic, agriculture and industrial uses.

Keywords: Bleaching and Dyeing Effluents; Groundwater; Contamination; Assessment of Seasonal Quality.

Introduction

About 74% of the wells in West Bengal has witnessed decline in water level during 2006 to 2016 as per the study conducted by CGWB (2016). With the continuing business as usual scenario of water uses, it will undoubtedly become more intense and about half of the global population will be affected with severe water crisis by 2030 (UNICEF and WHO, 2010). Among different industries, textile industries draw large quantity of water from different surface and underground sources for process requirement. The wastewater generated from textile industries contains large quantities of dyes and chemicals that create major environmental challenges by degrading surface water, soil,

agricultural land and underground water due to lack of proper infrastructure. Majority of tiny and small scale bleaching and dyeing units discharge textile wastewater to open drains, canals and even lands. Continuous discharge of wastewater over decades impose loads of Biochemical Oxygen Demand (BOD), Chemical Oxygen Demand (COD), Total Dissolved Solids (TDS), Total Suspended Solids (TSS), dyes, nitrate (NO₃), sulphate (SO₄), carbonate (CaCO₃), fluoride (F⁻), sodium (Na), iron (Fe), heavy metals like lead (Pb), Chromium (Cr) that contaminate of surface and ground water resources, soil and air (Vega *et al.*, 1998). The effect of this long time discharge created major environmental risk in the form of loss of agricultural and

¹ Department of Ecological Studies & International Centre for Ecological Engineering, University of Kalyani, Kalyani, West Bengal, India.
✉ *biswajoy2000@yahoo.com

² Department of Environment Management, Indian Institute of Social Welfare & Business Management, College Square West, Kolkata, India.

aqua cultural production, accumulation of heavy metals in fruits and vegetable, non-availability of drinking water (Simenonov *et al.*, 2003) in the study area. The yearly consumption of groundwater has been estimated at 600,000 ML (@2000MLD and 300 working days) at Maheshtala Textile cluster. Decrease in annual rainfall and lack of treatment facilities for reusing of wastewater will create water shortage in the cluster area in near future. Several positive interventions have been adopted in Tirupur Textile cluster in Tamilnadu, India to mitigate the ecological risk in the region. Only oxidation process as operational in the common effluent treatment plant at Tirupur if replicated in the present study area will not be sufficient to get potable and reusable water for bleaching and dyeing industries. Common effluent treatment plant with zero discharge facilities will help purification of ground and underground water (Tchobanoglous and Burton, 1995). Treatment of effluent will save further degradation of water quality, soil, air, agricultural produces and human health through food chain. Considering these facts, the present assessment of untreated ground water and underground water and their effects on the environment will help selection of treatment process to get quality and reusable water for textile industries and to protect the area

from degradation of agriculture produces, soil quality, and change in characteristic of canal, depleting water table and human health risk.

Study Area

Maheshtala (44.77 km²) is an urban area having administrative headquarter at Alipore of South 24-Parganas district of West Bengal lies between 10.450° N latitude to 75.90°E longitudes. Chatta canal running through Chatta and Kalikapur (1.85 km²) is selected for the study. Open land receives maximum effluent from bleaching and dyeing units from these area. Existing canal, nallah and pond also receive sewage and household wastewater and effluent from bleaching and dyeing units from different interconnecting drains of the neighborhood and waste water percolates to the underground water aquifer. The water carrying capacity of Chatta canal is reducing over the years due to improper cleaning and siltation. Collection of underground water samples at station A and B have been set up and collected in summer, rainy and winter seasons. The map of West Bengal and map of South 24-Parganas along with location of Maheshtala are given in Figures 1 and 2 respectively.

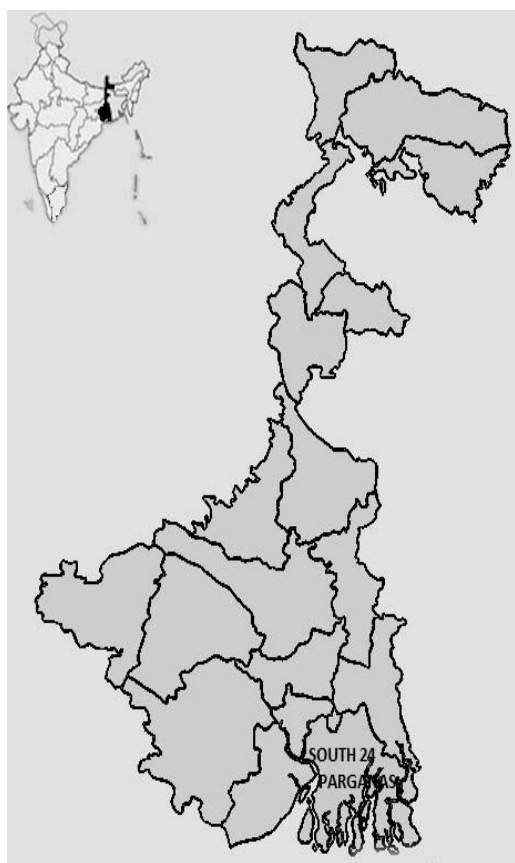


Fig. 1: Map of West Bengal



Fig. 2: Map of South 24-Parganas & Maheshtala



Materials and Method

Collection of Samples

Total 36 underground water samples were collected at two monitoring stations (A & B) in the canal stretch at 500 m apart during summer, rainy and winter seasons every year during 2012–2016. April, May and June are considered as summer season. Similarly, July, August and September have been considered as rainy season and November, December and January months form the winter season. The collection station A was the point of direct collection of raw underground water used in textile industries and near a populated area whereas the station B was the point near the normal flowing stretch of canal at 30 m depth, also being utilized in bleaching and dyeing units.

Methodology

Samples were regularly brought to the laboratory and analyzed using the standard methods as per American Public Health Association (APHA, 2001). Temperature and pH were measured on site by a mercury thermometer having range from 0°C–100°C and with digital portable pH meter respectively. TDS was determined by filtering a measured amount of sample through a standard glass filter. The filtrate (i.e., filtered liquid) was then added to a pre-weighed ceramic dish that was placed in a drying oven at a temperature of 103°C. After the sample dried, the temperature was increased to 180°C to remove occluded water, i.e., water molecules trapped in mineral matrix. TDS, dissolved oxygen, salinity, turbidity were determined by water analyzer (Systronic-371). Alkalinity was measured by titrametric method. Sodium, potassium and calcium were measured by Flame-photometric method. Nitrate was measured by UV spectra photometric screening method with the help of Zuconyl indicator. Heavy metal samples were acidified and were digested with concentrated HNO₃ (0.1%) acid on a hot plate and analyzed after filtration by Whitman filter-paper No. 42. For determination of metal ions atomic

absorption spectrophotometer (OMA 300 process analyzer) was used. For analysis of COD, samples were stabilized by acidifying with H₂SO₄ below 2 and it was measured by dichromate titration method (APHA, 2001).

Results and Discussion

The discharge of effluent from bleaching and dyeing units of the cluster contained very high quantities of chemicals, dyes and heavy metals. The raw effluent was discharged to open land, existing canal, nullah and water bodies due to lack of infrastructure in the cluster. This effluent percolates through the different strata and contaminated the underground aquifer.

Physico-Chemical Analysis

The study shows heavy contamination of underground water as reflected by the physicochemical parameters which exceeded Secondary Maximum Concentration Level (SMCL) specified by United States Environmental Protection Agency (EPA, 2016). EPA sets a Maximum Contaminant Level Goal (MCLG) based on human health effects. The MCLG is the maximum level of a contaminant in drinking water allowing an adequate margin of safety. The pH of underground water is found to vary between 7.5–7.9. High alkalinity of underground water is due to excessive use of salt and acids like sodium carbonate, sodium bicarbonate, sodium hydroxide, sodium silicate, sodium peroxide, sodium bi-sulphate, bleaching powder, sulphuric acid, acetic acid, and tannic acid, detergents in various preparatory and dyeing processes of grey clothes. The maximum TDS (4769 mg/l), carbonate (815 mg/l), Fe (0.68 mg/l), Fl (22.2 mg/l) and sodium (1117 mg/l) ions formed the bulk quantity of the dissolved solids. The seasonal results of underground water are presented in Table 1. The assessment of quality of underground water against SMCL of different chemicals and metals are taken from US-EPA for drinking water and are given in Table 2.

Table 1: Physicochemical Parameters of Underground Water Collected from 30 m Depth at Station A and B

Tube well	Summer		Rainy		Winter		SMCL (pH)	
pH	7.9		7.5		7.62		6.5–8.5	
Unit	TDS	CaCO ₃	NO ₃	BOD	COD	Fe	Fl	Na
	mg/l	mg/l	mg/l	mg/l	mg/l	mg/l	mg/l	mg/l
S1 Summer	4730	804	22.1	3.4	10	0.68	0.49	1117.6
S2 Summer	4769	810	20	2.8	8	0.14	0.37	1100
S3 Summer	4764	815	21	2.6	8	0.15	0.36	1091.2
S4 Rainy	4758	363	10.7	1.8	4	0.35	22.2	1056
S5 Rainy	492	358	11.66	0	0	0.36	18.6	936
S6 Rainy	432	360	13.7	0	0	0.21	17	788
S7 Winter	382	780	2.5	1.1	5	0.48	11	52
S8 Winter	382	788	5.5	2.3	4	0.52	9	51.6
S7 Winter	363	792	22	2.4	2.3	0.55	12	30



Table 2: Seasonal Contamination Level vis-à-vis Condition of Physicochemical Parameters of Underground Water

Parameters	N	M/SMCL* (Summer)	M/SMCL (Rainy)	M/SMCL (Winter)	Allowable M/SMCL ³	Summer Condition ^b	Rainy Condition	Winter Condition
CaCO ₃		3.24	1.44	3.14	1	NA	NA	NA
NO ₃	92	2.1	1.2	1.05	1	NA	NA	NA
Fe	233	1.7	1.1	1.7	1	NA	NA	NA
Fl	86	5.33	9.63	5.33	1	NA	NA	NA
TDS	141	9.51	3.78	0.75	1	NA	NA	NA

* Mean/SMCL indicates the mean value of parameter studied/SMCL. Mean values are given in Table 3.

a. Allowable limit of mean/SMCL = 1.

b. NA indicates not acceptable.

From the seasonal assessment it is evident that the contamination level of carbonate, nitrate, iron, fluoride and sodium are not acceptable during all summer, rainy and winter seasons. Total dissolved solids are also not acceptable in all seasons excepting the winter. As per ground water information booklet, South 24–Parganas issued by Central Ground Water Board, Govt. of India, the iron content of groundwater at Maheshtala varies from 0.44 mg/l to 2.91 mg/l, chlorine level varies from 99 mg/l to 110 mg/l and no significant levels of fluoride, nitrate and sodium are found. But the present study shows that very recently due to heavy industrialization through textile industries the underground aquifer of the study area has been heavily contaminated with higher levels of Fe, Fl, NO₃ and Na content coming from the textile bleaching and dyeing units of that area.

Statistical Analysis

All the data of physiochemical parameters of underground water samples were presented as mean values and were analyzed using descriptive analysis. We used Standard Deviation (SD) for describing the spatiotemporal degree of variations of the observed water quality parameters during different seasons. One-way analysis of variance (ANOVA) showed that for all water quality variables the samples reflected significant differences among the sites ($p < 0.05$). Figure 3 shows the underground water condition during summer, rainy and winter season while the descriptive statistical analysis is presented in Table 3.

Table 3: Descriptive Statistical Analysis of Underground Water for Summer, Rainy and Winter Season

Summer	Unit	Minimum	Maximum	Mean	Median	SD	SMCL	Mean/SMCL
TDS	mg/l	4730	4769	4754.33	4764	17.32	500	9.51
CaCO ₃	mg/l	804	815	809	810	4.49	250	3.24
NO ₃	mg/l	20	22.1	21.03	21	0.85	10	2.10
Fe	mg/l	0.14	0.68	0.32	0.15	0.51	0.3	1.70
Fl	mg/l	9	12	10.66	11	1.52	2	5.33

Rainy	Unit	Minimum	Maximum	Mean	Median	SD	SMCL	Mean/SMCL
TDS	mg/l	432	1758	1894	492	2480	500	3.78
CaCO ₃	mg/l	358	363	360.33	360	2.51	250	1.44
NO ₃	mg/l	10.7	13.7	12.02	11.66	0.88	10	1.20
Fe	mg/l	0.21	0.36	0.33	0.35	0.08	0.3	1.10
Fl	mg/l	17	22.2	19.6	18.6	2.66	2	9.63

Winter	Unit	Minimum	Maximum	Mean	Median	SD	SMCL	Mean/SMCL
TDS	mg/l	363	382	375.66	382	10.95	500	0.75
CaCO ₃	mg/l	780	792	786.66	788	6.11	250	3.14
NO ₃	mg/l	2.5	22	10	5.5	10.5	10	1.05
Fe	mg/l	0.48	0.55	0.51	0.52	0.035	0.3	1.70
Fl	mg/l	9	12	10.66	11	1.52	2	5.33

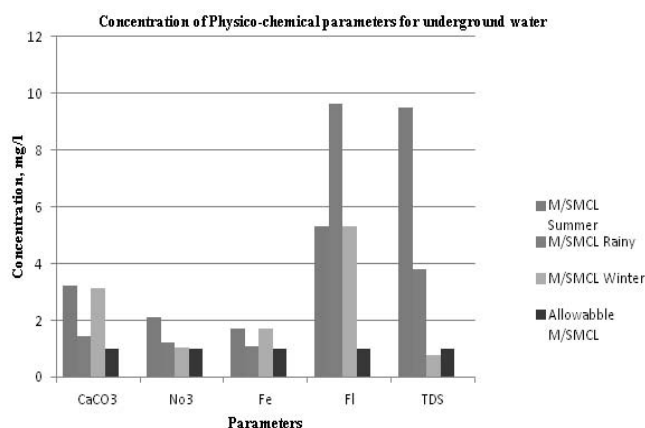


Fig. 3: Underground Water Quality during Summer, Rainy and Winter Season

Seasonal Analysis

Table 3 shows that almost five parameters comprising of TDS (4754.33 ± 17.32 mg/l), CaCO_3 (809 ± 4.49 mg/l), NO_3 (21.03 ± 0.85 mg/l), Fe (0.32 ± 0.51 mg/l) and Fl (10.66 ± 1.52 mg/l) of underground water during summer season exceeded SMCL limits for drinking water quality as per EPA (2016). Similarly, in rainy season concentration of TDS (1894 ± 2480), CaCO_3 ($360 \pm$), NO_3 (12 ± 0.88), Fe (0.33 ± 0.08) and Fl (19.6 ± 2.66) also exceeded beyond their standard limits of EPA for drinking water. Further, in winter season the concentration of TDS (375.66 ± 1.95), NO_3 (10 ± 10.5), CaCO_3 (786 ± 6.11 mg/l), Fe (0.51 ± 0.035 mg/l) and Fl (10.66 ± 1.52 mg/l) also exceeded their limits for drinking water as per EPA standards.

Effect of High Total Dissolved Solids and Nitrate in Water

The high values of pH, TDS, CaCO_3 , NO_3 , Fe and Fl indicate that water quality of underground water is very poor and therefore, adversely affect the domestic uses and agricultural production (Balchandra *et al.*, 2010). Higher concentration of TDS is not suitable for irrigation purpose (Kannan and Thavamani, 1993). High level of hardness creates leaching of calcium and magnesium and other polyvalent cations from soil by natural process. Hardness in water may cause heart diseases (Mason Alma and Ahmed, 2002). High nitrate concentrations in water indicate organic pollution in the water due to heavy industrialization particularly discharging chemicals (Satyr *et al.*, 2003). High total dissolved solids may affect the aesthetic quality of the water, interfere with washing clothes and corroding plumbing fixtures. For aesthetic reasons, a limit of 500 mg/l

has been specified as part of the Secondary Drinking Water Standards (EPA). Nitrate poisoning includes increased heart rate and respiration.

Effect of Higher Level of Iron and Fluoride Content in Water

High level of Fe and Fl in water causes gastro-intestinal disorder, neurological problems, paralysis and carcinogenic affect to human health. Irrigation with poor quality underground water influences reduced germination, root growth, absorption of water and nutrients (Solaimalai and Saravanakumar, 2004). The results of the physico-chemical parameters of underground water from Chatta and Kalikapur area show that six parameters out of 8 parameters analysed crossed the permissible limit of water required for domestic and irrigation purpose. It indicates 75% of the parameter failed to meet the secondary concentration limit specified for domestic purpose. Hence, the underground water is not safe for domestic and agriculture production (Balchandra *et al.*, 2010). The findings and approach adopted in assessing the water quality in the present study can be corroborated with several other studies of textile hubs at Vapid, Gujarat, India (Joshi and Santani, 2012), at Coimbatore, Tamilnadu, India (Balachandran *et al.*, 2010) and at Karur District, India (Kannan *et al.*, 2005).

Conclusion

Both the results obtained from physico-chemical parameters and statistical analysis indicate that the underground water at Chatta, Kalikapur and Mahispota of Maheshtala textile cluster are very poor in summer and poor in rainy and winter season. The underground water is not suitable for drinking, domestic, and agriculture purpose. The time is long overdue to take a hard look at this undesirable and unplanned growth of these bleaching and dyeing units. Further, it requires to take corrective measures through recyclable zero discharge treatment process to prevent environmental risks and depletion of water level around the cluster.

References

- [1] APHA (2005). Standard methods of chemical analysis of water and waste water. 21st edition, American Public Health Association, Washington, USA.
- [2] Balachandra, D., Sundarraj, P., Ruthaavel, M.K. and Kumaraswamy, K. (2010). An investigation of ground water quality and its suitability to irrigated agriculture in Coimbatore district, Tamilnadu, India, A GIS approach. *International Journal of Environmental Science*, 1(2), pp. 176–190.



- [3] CGWB, 2016, Central Ground Water Board, Ground water data in different parts of the Country, India.
- [4] EPA (2016). National primary drinking water contamination. Environmental Protection Agency, United States, available at <http://water.epa.gov/drink/contaminant/upload/mcl-2.pdf>
- [5] Joshi, V.J. and Santani, D.D. (2012). Physicochemical characterization and heavy metal concentration in effluent of textile industry. *Universal Journal of Environmental Research and Technology*, 2/2, pp. 93–96.
- [6] Kannan, V., Ramesh, R. and Sashikumar, C. (2005). Study on ground water characteristic and the effects of discharged effluents from textile units at Karur District, India. *Journal of Environment Biology*, 26(2), pp. 269–272.
- [7] Kannan, V. and Thurman, E.M. (1993). Assessment of industrial ground water pollution potential from correlation of parametric ratio—Dye industry. *Indian Journal of Environmental Protection*, 13(5), pp. 346–348.
- [8] Mason, Alma and Ahmed, A. (2002). Water quality in and around Industrialized city of Delhi East and Sahibabad. *Indian Journal of Environmental Protection*, 22 (8), pp. 900–904.
- [9] Simenon, V., Simenon, P., Samara, C., Zachariadis, G., Vousta, D., Anthemidis, A., Sofonious, M. and Kouimtzi, T. (2003). The assessment of the surface water quality in Northern Greece. *Water Research*, 37(17), pp. 4119–4124.
- [10] Solaimalai, A. and Saravanakumar, R. (2004). Assessment of irrigation water qualities, In Water pollution assessment and management, Daya publishing House, New Delhi, pp 389–395.
- [11] Shastry, C.K., Aboo, A.M., Bhatia, H.L. and Rao, A.V. (1970). Pollution of upperlake and its effect on Bhopal water supply. *Journal of Environmental Health*, 12, pp. 218–238.
- [12] Tchobanoglous, G. and Burton, F.L. (1995). Wastewater Engineering: Treatment, disposal and reuse. TATA- MaGraw Hill Publishing India Limited, New Delhi.
- [13] Vega, M., Pardo, R., Barrado, E. and Deban, L. (1998). Assessment of seasonal and polluting effects on the quality of river water exploratory data analysis. *Water Research*, 32(12), pp. 3581–3592.
- [14] WHO and Unicef (2010). Progress on sanitation and drinking water. Joint monitoring Programme data Published by WHO/Unicef, 2010.



Application of Minimalist “SMART” Tools and Techniques for Improving Water Productivity in Industrial Sector with Special Reference to Steel Plants

S. Mitra Mazumder^{*1}, A.K. Jha¹, K. Bhattacharjee¹, M. Choubey¹ and A. Gupta¹

Abstract: India has 18% of the world’s population and 4% of the water resources. Due to this uneven distribution, it has been predicted that India might be the most water-stressed among G-20 nations by 2025. Consequently, water scarcity and water quality are predicted to be one of the largest economic concerns in the coming decade. This is going to be significant challenge for Indian Industrial sector in general and steel sector in particular because it is estimated that with current growth rate, Indian industrial sector is poised to double its production in next decade. The challenge originates from the fact that continuing economic growth will result in steady rise of both per capita consumption and agricultural requirements of water necessitated by increased demand for food. Under the circumstances, neither sectoral share of water consumption by industry nor pattern of use can change significantly in future. Doubling of industrial production without any significant increase in fresh water intake will require significant improvement in “Water Productivity” of almost all unit operations and unit processes across industrial sector. Out of various ways of increasing water productivity, aspects of reduction in industrial water discharge (commonly referred as zero discharge) is widely acknowledged and is often addressed through adoption of various technologies for recycling, which generally is achieved at high capital cost and significant recurring cost. However, other aspects of increasing water productivity attract less attention. Some of these aspects viz. ensuring minimum possible water consumption per unit of production, maximizing Cycles of concentration, setting benchmarks and application of cascaded recycling etc. have the potential to ensure both reduction in fresh water consumption and volume of discharge. A number of SMART tools and techniques can be adopted to address these in-process aspects of water productivity. These include, conductivity based approach of water management, index based approach of water use, application of physical simulation tools, key parameter based decision making, application of surrogate monitoring techniques and tool based approach to management of cycle of concentration. This work suggests an integrated INTELLIGENT TOOLBOX approach towards increasing water productivity through application of minimalist SMART tools and techniques in industrial sector with special reference to Indian steel plants.

Keywords: Water Productivity, Conductivity, Cycle of Concentration, Recycling.

INTRODUCTION

Concept of Industrial Water Productivity

Water, especially fresh water in a particular region, is a finite resource, unless reused. Productivity of any resource is defined by the efficiency of resource use. In the context of water, the productivity of water used in industry can be defined in terms of the economic value added by industrial production based upon the water withdrawn; i.e., productivity of water can be defined as economic value added in monetary terms per unit of water withdrawn. However, concept is also socio-technological in nature because low level of industrial water productivity may not

mean low level of development; this may indicate a multitude of situations- either water is undervalued, or water is used for low value applications or simply water is abundant in a particular country or region. Although calculation of industrial water productivity in strict sense of the term remains in the domain of economists, from an industrial perspective the factors that directly contribute to improvement in industrial water productivity are:

- improvement in industrial technology
- adoption of water saving measures
- high level of water circulation
- reuse and minimization of water withdrawal.



Need for Improving Water Productivity in Indian Industrial Sector

Indian economy is expected to grow at an average rate of 7% in foreseeable future. Therefore, industrial sector is also expected to grow at a similar or higher rate. Water requirement for industrial sector is a small percentage of total water requirements by various sectors but due to negative environmental consequences of discharge, the impact is widely discussed. Economic growth will entail that while water availability decreases continuously (Figure 1) direct and indirect requirement of water will increase for all sectors including industry sector. However, considering primacy of agricultural requirement it will be significantly difficult to get additional allocation for industrial sector in future. Since industrial water productivity is significantly low in India (Table 1) industrial sector in India has to significantly increase its water productivity before additional allocation is sought.

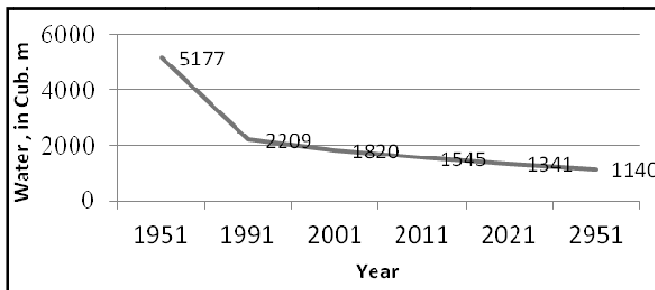


Fig. 1: Per Capita Water Availability, M³/capita/year
(Source: Bulletin of Indian Society of Soil Science, No. 29, 2014)

Table 1: Industrial Water Use and Productivity in some Select Countries

Country	IVA 2001	Ind. Water. use, km ³ /yr	Ind. Water. Productivity, US \$ IVA/m
Japan	1890	16	119.62
Korea	286	3	93.66
UK	340	7	47.28
Netherlands	120	5	25.17
Germany	748	32	23.43
USA	2148	221	9.73
China	594	162	3.67
India	120	35	3.42

IVA: Industrial Value Added, in 1995 constant US \$

Source: Bulletin of Indian Society of Soil Science, No. 29, 2014.

Industry is the second largest user of fresh water. But the actual demand largely depends on the type of industries and the purpose of water withdrawal. The need for improvement in industrial water productivity arises from the fact that in

general water withdrawal by industry is much higher than actual consumption/need of water for industrial applications. Various types of industrial water usages are given in Table 2.

Table 2: Various Large Scale Applications of Water in Industrial Context

Water for Energy	e.g., Large hydro projects
Cooling Water	Cooling in thermal power generation is the largest single use of water for industrial purposes
Process Water	e.g., Use of water to make steam, use in various process or chemical reactions
Water for Products	Many industrial sectors, mostly the food, pharmaceutical and beverage, where water is an ingredient of the end products for human consumption
Water as a Medium for Waste Disposal	Water removes any raw material not used in the manufacturing process as waste and is commonly known as wastewater

Aspects of Water Usage and Reduction in the Context of Steel Industry

It is estimated that with current growth rate Indian steel sector has to double its produce without any significant increase in fresh water intake. This will require significant improvement in “Water Productivity” of almost all unit operations and unit processes across steel sector. Since “water use efficiency” indicates the amount of produce per unit amount of water, “water productivity” essentially becomes related to reciprocal of “water use efficiency”. Although water productivity of a process or operation cannot be benchmarked unless the “theoretical minimum” requirement of an operation or a process is known, improvement in water productivity can be tracked through:

- Minimum possible water consumption per unit of goods or services
- Minimum possible withdrawal of fresh water
- Maximizing cycles of Internal and external recycling of water
- Minimum possible discharge of water to external environment
- Beyond norms of discharge, meet standards of recycling and reuse.

Generic Tools and Techniques of Increasing Water Productivity

Collaborative Cascading

Cascaded use of water is an important tool for achieving the goal of minimal water discharge. However, a structured and



integrated approach for cascading of water has not been reported in available literature in the context of Indian industry in general and steel industry in particular. The effort towards cascading need to cover “maximum possible area” in the vicinity of an industrial unit where cascading will involve both use of incoming water and discharge water. Exhibit elucidates sequential steps of cascaded water use.

Table 3: Sequential Steps of Cascaded Water Use

Sl. No.	Steps of Water Usage
I	Assume unavailability of potable water
II	Consider replacement of all potable water use points with recyclable water
III	Recycle water on-site. Match the quality of water with the quality required by the use.
IV	Use treated municipal and industrial wastewater instead of potable supplies for landscape irrigation, dust control, cooling etc
V	Reuse water sequentially
VI	Treat and reclaim used water

Development and Use of Water Foot Printing as a Key Tool for Benchmarking and Decision Making

Conventional concept of “Foot Print” consists of three components, namely, green, blue and gray water footprints. The green water footprint refers to the consumption of the rain water. The blue water footprint relates to the consumption of surface and ground water. The grey water footprint is the polluted water released by the production system and described as the volume of fresh water that would be required to assimilate the load of pollutants based on existing water quality standards. However, in the particular context of various units and shops of steel plant “water footprint” implies the pattern of use and discharge of particular processes. Therefore there is a need to develop “footprint” of different processes for identifying process inefficiencies and facilitate decision making and benchmarking.

Development and use of Index based Techniques

Water Quality Index (WQI) can be an important tool for improving water productivity through optimization of water use, recycle and discharge. From industry perspective one of the most effective ways to exploit this tool is to use suitable simple indices. Indices are based on the values of various physico-chemical and biological parameters in a water sample. These indices either can be used for quick decision making/information dissemination regarding quality of water (Table 4) or for direct implementation in a control system for recycling and discharge (Table 5).

Table 4: Relative Weight of Water Quality Parameters

Parameter	Water Quality Standard	Assigned Weight (AW)	Relative Weight (RW)
pH	6.5–8.5	2.1	0.109375
DO (mg/l)	5	4.0	0.208333
Turbidity (NTU)	5	2.4	0.125
Conductivity (us/cm)	250	2.7	0.140625
Hardness (mg/l)	100	1.1	0.057292
Alkalinity (mg/l)	100	1.7	0.088542
BOD (mg/l)	3	3.0	0.15625
No3	50	2.2	0.114583
Total		19.2	1

Highest Weight assigned to parameter that has major importance in water quality assessment, while the smallest weight assigned to that parameter that may not be harmful. Weight values can be decided based on ecological impact.

Table 5: Water Behaviour According to LSI and RI

LSI	Water Behaviour	RI
-2/-3	Very strong aggressiveness	>0
1/-2	Strong Aggressiveness	8/9
0/-1	Moderate Aggressiveness	7/8
0	Stable Water	6/7
0/+1	Lightly scaling water	6/5
+1/+2	Moderately Scaling water	5/4
+2/+3	Strongly scaling water	4/3
> 3	Severe scaling	<3

The two most important indexes for measuring the scaling/aggressive tendency of cooling water are Ryznar Stability Index (RI) and Langelier Saturation index (LSI), calculated based on standard numerical relationship between select monitored parameters.

Use of Simulation Tools for Optimization of Water Treatment, Use and Recycling

Although individual effect of many water quality parameters are available in literature, very little technical information is available in public domain about the combined effect of various ionic, surface and particulate properties and quality parameters of water, on water systems. Moreover, since most of the chemicals used for water treatment are proprietary chemicals, scientific data on their real effect on water quality parameters is also not available in public domain. However,



this information is extremely important and crucial for optimization of water treatment, use and recycling. Simulators, of simulation tools, bridge the gap. Application of these simulation tools can help in significantly increasing water productivity.

“Intelligent” Water Grid Management

Technologies such as smart metering, SCADA, GIS, telecommunication sensors allow for the provision of real-time reliable data which can significantly help in improving water management while reducing water losses in the distribution system. To begin with four parameters need to be made part of water grid management system across industries in a particular region. These are:

- Flow
- pH
- Conductivity
- Turbidity.

Application of Expert/Decision Support Systems

Expert/Decision Support Technology can be an extremely effective tool for water management for decision making based on own data as well as learning from data generated by others. For this, all industries need to develop their own structure of water management database. The data should form the back-end of an open architecture expert system framework that would be easy to access and update the learning at any time by responsible industry personnel. With proper security, it must be ensured that data, analysis and decision points are available in a real-time basis. The system should provide a flexible structure that user can define and customize to suit individual requirements.

An Integrated “Smart Toolbox” for Improving Water Productivity in Steel Sector

In steel industry there are a large number of water circuits having significantly varied water quality need. The three major ways of increasing water productivity in steel sector are like in any other sector i.e., reduction in discharge of wastewater, treatment and recycle of wastewater wherever feasible based on application/use need and reduction in makeup water consumption. However, steel industry probably differs from many other industries because of the fact that there exists large number of opportunities for potential application within the plant premises. The need for SMART Toolbox arises from the fact that there exists need for both decision making and treatment optimization for increasing water productivity. The complexity of arises from the complex functional relationship between various water quality parameters, impact parameters and functional aspects of treatment process:

- $\text{pH} = f(\text{Hardness})$
- $\text{pH} = f(\text{Alkalinity})$
- $\text{Scale formation} = f(\text{pH } 7+)$
- $\text{Corrosion} = f(\text{pH } 7-)$
- $\text{Scale formation} = f(\text{TDS})$
- $\text{Coagulation} = f(\text{Alkalinity, pH})$
- $\text{Coagulant dose rate} = f(\text{Turbidity, Alkalinity, Temperature})$
- $\text{Alkalinity} = f(\text{pH, Carbonate Hardness, Non carbonate Hardness})$
- $\text{Scale formation} = f(\text{Alkalinity})$
- $\text{Scale formation} = f(\text{CoC})$
- $\text{Conductivity} = f(\text{pH, temp, Flow})$
- $\text{Metal solubility} = f(\text{Solution Acidity})$
- $\text{Turbidity} = f(\text{Temp, pH, Alkalinity})$.

Adoption of Electro-Kinetic Charge Analysis for Targeted Reduction of Suspended Solids

As per conventional practice, off-line jar test is used for determination of chemical dosing requirement for coagulation/flocculation aimed at reduction in Suspended solids. For example, this test is critical in clarifier water circuit where suspended solids from gas cleaning is required to be removed before the water is recycled. However, often this water is required to be either blown down or need to be mixed with additional make up water to achieve level of recyclability of suspended solids since treatment process does not meet the objective. As per current advancement, in order to identify the optimal dosing point, this can lead to optimal coagulation-flocculation, electro-kinetic charge analysis (Figure 2) (on-line/off-line) can be more effective than visual observation based conventional jar test.



Fig. 2: Electro-kinetic Charge Analysis



In one such circuit while Suspended Solids level even after conventional jar test based optimization was consistently more than 300 mg/l, whereas after electro-kinetic charge analysis based optimization it came down consistently below 100 mg/l. (Figure 3).

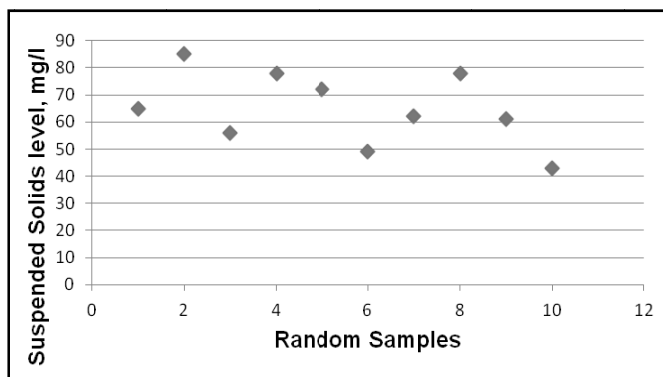


Fig. 3: Optimally Treated Water for Recycling

Improved Control over Closed Loop Water Treatment through On-line Monitoring of Key Water Quality Parameters like, Dissolved Oxygen

Water is the cooling media in all closed loop circuits of steel plants. In many circuits, particularly in iron and steel making processes, water is used at very high pressure. For example, during BOF steelmaking between hood inlet and hood outlet, the gas temperature has to be brought down from 1000°C to about 75°C, where the heat, by radiation and convection, is absorbed by the hood cooling water. Evaporation and other losses of water takes place for which make up water is added to the system.

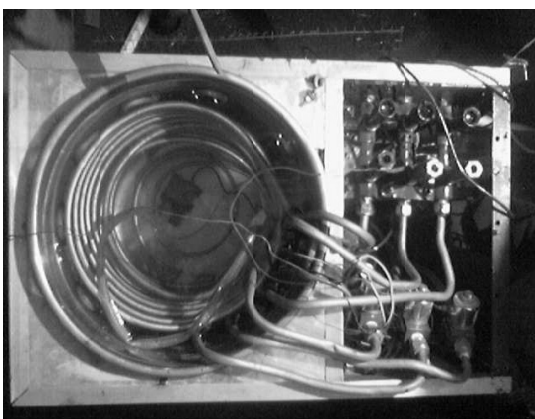


Fig. 4a: Closed Circuit of Water

Make up water adds dissolve oxygen in the circuit. This closed circuit water is maintained at very high pressure and temperature. Under high pressure relatively large quantities of oxygen gets dissolved in water. In cold water, oxygen

normally has little corrosive effect. In contrast, when the water is heated, the oxygen can cause serious corrosion problems. A combination of chemicals is used to remove oxygen from circuit water. Improvement in efficiency as well as monitoring of consistency of this treatment is possible through on-line monitoring of dissolved oxygen (a sample designed circuit is given in photograph) in the cooling water circuit. Such treatment consistency is essential for improving water productivity. Figure 4b shows the DO level in cooling water circuit without (left side) and with (right side) treatment.

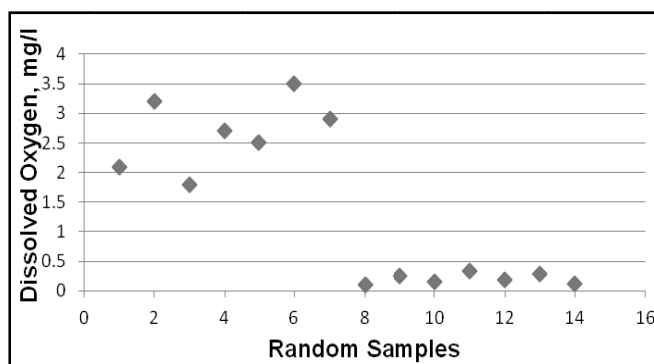


Fig. 4b: DO Level in Cooling Water Circuit without and with Treatment

Dynamic Monitoring of Water Quality Impact Parameters for Monitoring of Effectiveness of Closed Loop Water Treatment

High pressure closed loop water systems in steel plants require continuous chemical treatment to keep corrosion, scaling and bio-fouling under check. There exists no integrated facility to monitor (on-line and in-situ) water quality parameters in such circuits in steel Plants which is required for improved control action. The system is generally maintained through a third party “system maintenance” approach where proprietary chemicals are used for maintaining system water quality with periodic off-line monitoring of water quality parameters (e.g. pH) and target impact parameters (e.g. corrosion). This entailed that Cooling Water System “owner” (i.e. plant) had little or no control over Cooling Water System “Management” in terms of treatment cost as well as water consumption. In order to address this gap, a state-of-the-art composite on-line and in-situ system was conceptualised, designed and implemented for direct and surrogate monitoring of requisite cooling water quality and impact parameters aimed at prevention of water quality related problems like, biocide formation, scale formation, corrosion etc in this closed loop water circuit. The System uses relationship between various water qualities parameters measured through on line analyzers to monitor effectiveness of water treatment. This shifting of paradigm



from third party based “system maintenance” approach to “parametric approach” has, over a period of time has resulted in improved control over water system, as well as reduction in discharge and make up water consumption through gradual increase in Cycle of Concentration (CoC) without negatively affecting the system in terms of scale formation, corrosion or bio-fouling. Figure 6 shows a sample “control” data generated online, i.e. that of maximum corrosion potential of cooling water.

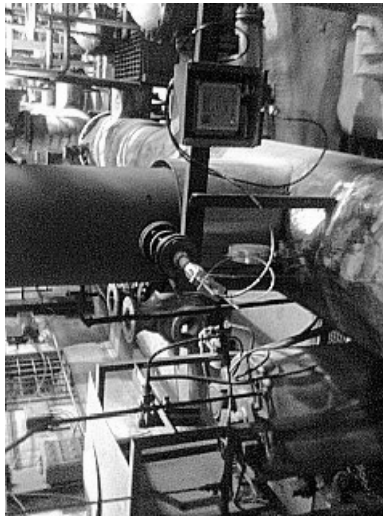


Fig. 5: Section of Installation of Closed Water System

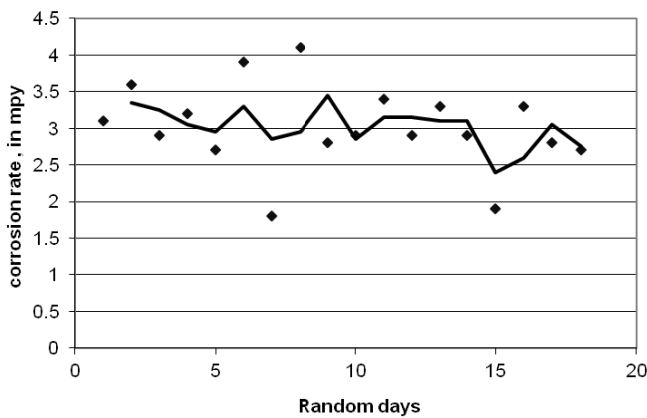


Fig. 6: Maximum Corrosion Potential of Cooling Water

Application of Physical Water Treatment Simulator

Since iron and steel making involves very high temperature processes, steel industry relies on water as a very critical resource. While contact water is recycled and/or discharged to a water body after a series of physico-chemico-biological treatment, closed loop water is continuously recycled, by design, with only a very percentage discharged as blow down and replenished through make up water. The makeup

water consumption and discharge water volume is dependent largely on efficiency of water treatment. The challenges of closed loop circuit water management is thus multi-dimensional that requires taking care of various system stresses arising out of dynamic nature of the processes. The challenges are further increasing because of the increasing need of recycling wastewater internally. Moreover, the problem gets accentuated since with reduction in availability of makeup water.



Fig. 7: Closed Loop Circuit Water Management

Although, individual effect of many water quality parameters are available in literature, very little technical information is available in public domain about the combined effect of various ionic, surface and particulate properties and quality parameters of water on flow loop and system. Since most of the chemicals used are proprietary chemicals, scientific data on real effect on water quality parameters is not available in public domain. The effectiveness of proprietary chemicals vis-a-vis generic chemicals is also not well established. There exists no tool for comparison between various chemicals for their treatment effectiveness. The recirculation water treatment simulator has been conceptualised, designed and developed to bridge this gap (Photograph). Figures 8 and 9 show the data generated in such system which helps in decision making.

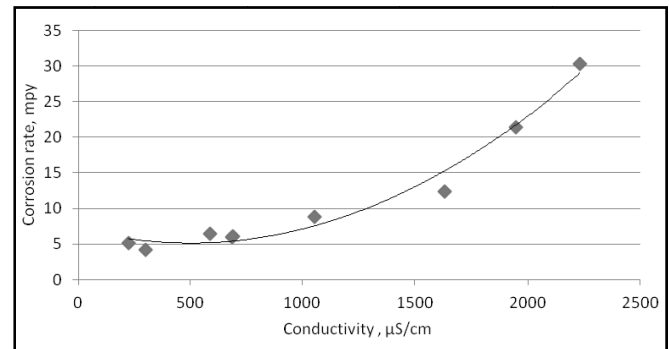


Fig. 8: Closed Loop Conductivity against Corrosion Rate without pH/DO Adjustment

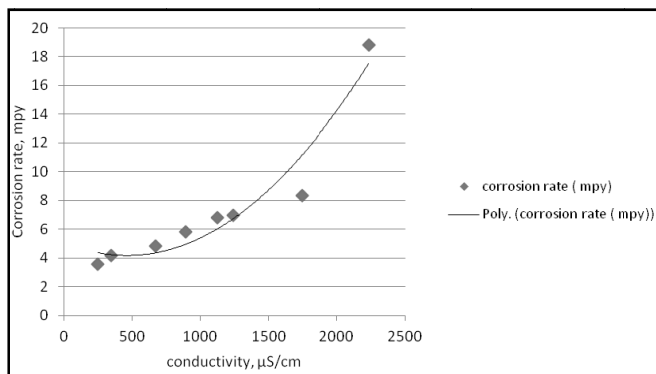


Fig. 9: Closed Loop Corrosion Rate against Conductivity with pH > 8 and DO < 4 mg/l

Development of Application-Specific Algorithm for Scaling/Corrosion Control in Water System for Maximizing Cycle of Concentration and Reducing both Blow Down and Make-up Water Intake

Effectiveness of dosing for reducing deposit forming tendency is dependent on reaching an optimal point of dosing (equivalent to point of zero charge for particles settling) when level of water hardness becomes minimal. However, there exists no defined relationship since optimal dosing rate is non-linearly dependent on many parameters out of which turbidity, conductivity, pH and alkalinity predominates (as per technical literature). This entails that the dosing system can be effective if a large number of in-situ tests and monitoring are carried out at a periodic interval (preferably every hour) using jar test method and dosing rate is manually adjusted based on results. Since the same is practically impossible, there is a requirement of on line determination of optimal dosing based on some intra-parametric relationships based algorithm and system for dosing. An effort has been made to develop an algorithm that uses generic and empirical relationships available along with on-site relationship data so that an integrated control strategy can be developed. This algorithm along with proper maintenance of CoC can be used as a starting point for controlled dosing of any chemical.

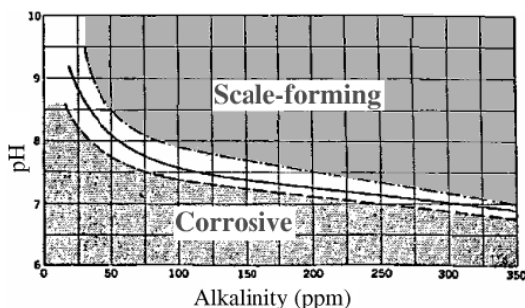


Fig. 10: Snapshot of Standard Relations

On-line Conductivity Analysis based Blow Down for Maintaining Optimal Cycle of Concentration

As water gets evaporated or contaminants get added to the recirculation of water stream, a part of water is required to be blown down to maintain optimal cycle of concentration of contaminants so that system does not get affected. The term Cycle of Concentration (CoC) generally refers level of concentration of contaminants in recirculation of water to that in fresh make up water. Blowing down is the process of removing a portion of this concentrated water and replacing the same with fresh make up water. Higher level of water productivity demands higher level of Cycle of Concentration (CoC). This blow down is generally set at a predetermined safe level so that system impact like, scale formation, corrosion, fouling etc are minimized. However, this limits the Cycle of Concentration. Besides, effect of cycle of concentration also depends on a particular system. i.e., one system may not get affected with a cycle of concentration of 4, while some other system may get affected with a cycle of concentration of 4. This offers the opportunity of increasing cycle of concentration based on on-line monitoring of conductivity and controlling of bleed based on same. This will require setting of a relationship between water quality parameter like hardness (to be monitored off-line) and conductivity of water. A sample of such relationship generated is shown in Figure 7 Once system does not get affected based on bleed set at a particular conductivity level, conductivity level can be gradually set upwards.

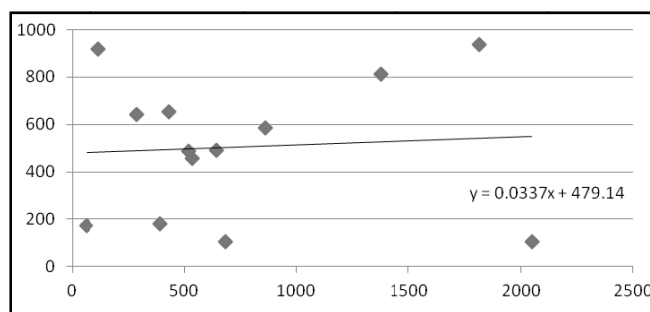


Fig. 11: Inlet Total Hardness against Outlet Conductivity

Off-line Multi-Parametric Optimization of Open Circuit Water Treatment

Water treatment is a key requirement of open recirculation of water circuit. The treatment program comprises dosing of various chemicals for achieving end user needs. The chemical treatment program varies depending on input as well as output water quality and characteristics. Often, there are competing needs. While jar test does help in optimizing the system in terms of suspended solids/turbidity, in practical situations there is an optimal quality requirement in terms of multiple parameters. Since no such apparatus exists an effort



was made to develop an apparatus which could help in optimizing open circuit water treatment. It was established that using the dosage pattern determined off-line for maintaining target parameters using the apparatus, the target parameters in actual circuit could be maintained within 10% range of off-line optimized value.

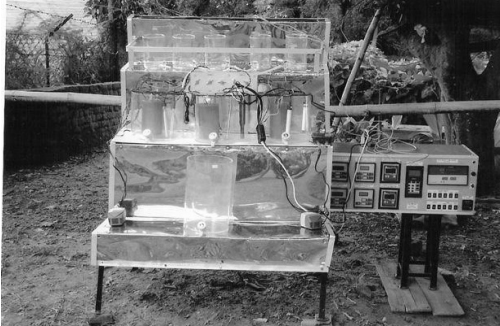


Fig. 12: Chemical Treatment Program

Conclusion

The set of tools suggested and experimented with can significantly contribute to increasing industrial water productivity in not only steel sector but industrial sector in general.

References

- [1] Report of RDCIS project No. 65:49:80 and associated references/technical publications
- [2] Report of RDCIS project no. 65:49:87 and associated references/technical publications
- [3] Report of RDCIS project No. 65:76:03 and associated references/technical publications
- [4] Report of RDCIS project No. 65:76:09 and associated references/technical publications
- [5] Report of RDCIS project No. STA:65:051 and associated references/technical publications



Tackling Corrosion and Bio-Film Formation in Water Distribution Systems for Sustainable Supply of Water

D. Bhaskar¹ and G. Singh^{*1}

Abstract: While the recent internal tussle over sharing water resources on national and international level exemplifies the severity of the water woes in India, the jaundice outbreak earlier this year in Shimla highlighted the urgency to ensure safety of water. Hence, there is an urgent need to balance the efforts for intelligent and fair utilization of water as is the case with the outline for the SMART cities with the efforts to assure potability of the supplied water. Preventing corrosion and biofilms from forming within the water network are the two avenues for effective utilization and safe reuse of water, which have so far been largely over-looked. The role of a healthy water distribution network in assuring the quality and quantity of water supplied to the public is emphasized here with the objectives of preventing wastage of water, ensuring effective utilization of water, and safety of recycled water. This paper highlights that operational factors such as type and dosage of the disinfectant, flow regimes, and pipe material influence the corrosion and biofilm development within the water distribution network. Together they impact the efficacy of water distribution infrastructure adversely by permitting water loss, metal contamination, and pathogen intrusion, re-growth and persistence. Further, a roadmap is laid for research to establish an efficient water model for safely supplying and reusing water to meet the ever-increasing demands.

Keywords: Water Distribution Network, SMART Cities, Sustainable Water, Biofilms, Corrosion.

Introduction

Water is a scarce resource in India and its long term availability cannot be ensured in the urban and peri-urban under the current setup. Additionally, the mismatch between the demand and supply of water is continually aggravated [1]. The ever increasing strain on water in urban and peri-urban region necessitates prevention of water wastage and contamination; the key intervention being proper management of water and water network. Leakages in the water network and subsequent intrusion of nutrients and microbes fail the efforts of disinfection to keep the drinking water clean. The intermittent water supply and subsequent water stagnation, and low hydraulic pipeline pressure further drive the deterioration of water quality. A comprehensive management approach, which encompasses all the stages of the water cycle and is scientifically informed, is urgently needed to ensure adequate quantity and quality of water. In order to successfully conserve water, leak-proof water networks with intelligent distribution and use of water are needed [2, 3]. The serious concern regarding the quality of water also needs to be taken into account. It has been reported that 70-80% of water consumed across the globe does not meet the WHO standards [4]. The current strategies to prevent deterioration of water resources emphasize

development of watersheds, protection, management, and increment of water utilization capacity, and improvement of physical, chemical and biological characteristics of water [2, 5]. In this context the safe reuse of water requires addressing the accumulation of persistent contaminants with every cycle of use [6–8]. The paucity of water and explosion of the population, whose lifestyle is trending towards increasing consumption of resources has thinned out the current interventions of privatization and making conservation of the available water resources imperative [1].

As of now, the integrity of water networks in India (Figure 1) is challenged by: (a) leaky joints in fractured and corroded pipes resulting in the entry of microbes and nutrients within the water network [3]; (b) leaching of heavy metals such as Lead, Copper, Cadmium in water from water supply pipes; often due to corrosion [9]; (c) deterioration in the water quality due to decay of disinfectant in pipelines [3]; and (d) disintegration of pipe due to inappropriate or inefficient water supply regimes that result in sudden changes in water demand, main breaks, or pump outages [3, 10]. These four challenges can be traced back primarily to two phenomenon of corrosion and formation of biofilms. Corrosion literally “opens the doors” for entry of microbes and nutrients into the water distribution network. These microbes along with

¹Department of Civil Engineering, Indian Institute of Technology Roorkee, India. ✉*gargifce@iitr.ac.in



those that survive disinfection often contribute to formation of biofilms. The biofilms trap nutrients and efficiently utilize the additional surface made available by corrosion and permit proliferation of a rich community of heterotrophs [9, 11–13].

Often the ageing and mismanaged water infrastructure of the developing countries allows for intrusion of pathogens in water distribution systems and accelerates the ageing process. To ensure sustainable maintenance of water supply in cities, it is crucial to control contamination via effective monitoring and technical interventions that account for both the chemistry and the microbial ecology of the water in the water network [14]. In this context the establishment of SMART cities with “intelligent” water distribution network presents a unique opportunity to lay down water networks that besides being conducive to monitoring and proportioning of water resources, also incorporates the design and operation elements, which would safeguard against leaks and contamination of water at source, treatment plant, water distribution network, or the point of use [3, 15]. While, the “intelligent” aspect of the water networks of the SMART cities is informed by advancements in public policy, information technology, and related fields, the “sustainability” aspect suffers in want of knowledge about the biochemical factors that enhance or attenuate corrosion and biofilm formation [5, 12]. Any approach proposed for ameliorating the water woes of India need to incorporate interventions for limiting both of them. Thus, the two major scientific challenges facing the water networks in India today are the scientific understanding of various factors that together result in corrosion and biofilm formation.

Biofilms and Corrosion

Biofilms develop within the water networks owing to colonization of microbes that survive the disinfection or intrusion of the microbes that manage to disrupt the integrity of water distribution network. Biofilms can result in numerous problems ranging from Microbial Induced Corrosion (MIC) of water pipelines, to persistence of pathogens in drinking water [12, 16]. Under certain conditions such as slow and interrupted flow regimes [13], at some temperature ranges [13, 17, 18], and when the water networks are comprised biofilms are known to proliferate heterotrophs including pathogens. As a result the traditional water treatment efforts have failed to limit the number of microbes including Coliforms in drinking water [19]. Many urban areas have interrupted supply of water and resulting stagnation that gives increases the water age and encourages growth of microorganisms in drinking water system [20]. The generation of negative hydraulic pressure in case of hilly towns that have elevation difference between pipe ends sucks in the microbes and nutrients through the leaky pipes

from the contaminated vicinity and further encourages biofilm formation. This in turn accelerates the corrosion rate of metallic pipes due to metabolic activity of microorganisms [15, 21, 22]. Though corrosion is largely dependent upon the metal properties, electrochemistry, and bulk water chemistry, the attachment of biofilm to metal surface and colonization of microbial consortium is identified as the foremost source of MIC. Further, the spatial distribution of biofilms affects the microbial corrosion processes and distribution of corrosion events within the water distribution network [23]. Corroded pipes aggravate both the microbiological and chemical quality of water and potentially pose serious health burden in developing countries. The community and functional profile of the microbes residing within the biofilms, availability of nutrients such as assimilable Carbon and dissolved oxygen, type and dosage of the disinfectant, and the flow regime are known to influence the extent and type of corrosion event and biofilm formation [13, 17], [24–29]. Therefore, it can be concluded that both corrosion, an abiotic event and biofilms, a biotic phenomenon persist and proliferate with an unusual symbiotic relationship and are aggravated by a common set of triggers. It is speculated that limiting either of the corrosion or biofilm formation will have a desirable impact on the status of both the corrosion events and heterotrophs population in the drinking water and will improve the health of water distribution network and water quality. Since both of these phenomena share triggers, effective management of the common contributing factors is hypothesized to reduce both frequency of corrosion events and biofilm formation. While disinfection and maintenance of certain level of residual disinfectant has been widely used and promoted as an effective strategy for ensuring the microbiological quality of drinking water, this approach too is neither entirely reliable nor without any repercussions.

Biofilms and Resistance to Disinfection

Disinfection by chlorine has had served as a reliable and effective method to ensure safety of drinking water for many decades [30]. At the same time, chlorination is not without the inherent risk of damaging public and environmental health due to formation of organic halides, and when overdosed directly impacting human health, leading to corrosion, and perhaps even proliferating microbial resistance to chlorination [31–33]. The organic halides, which are disinfection by-products have adverse long term side effects on both the environment and humans [34–37]. Biofilms provide microbes with an enclosure of extracellular polymeric substances that protects them from direct onslaught of disinfectants, traps nutrients in an otherwise oligotrophic environment, and provides a reservoirs for the development of microbial consortia including heterotrophs and potential pathogens [38, 42, 43] Long-term chlorination can encourage resistance



to disinfection within the water microbiome. Subsequently the resistance-conferring genetic elements may be transferred to pathogens [38–41]. Thus, the harsh environment of a water distribution network is quickly transformed into a nutrient rich refuge that is suitable for growth and sustenance of heterotrophs and other microbes. Despite wide-spread use of Chlorine based disinfectants such as bleaching powder, hypochlorous acid, and chloramine in water treatment plant, pathogens are still detected in the drinking water. Apparently mere disinfection cannot ensure safety of drinking water [38, 39, 44, 45]. Probably the biofilms-refuge of the microbes is the source for pathogens and heterotrophs in the drinking water in absence of microbial intrusion. Tachikawa *et al.* showed that the biofilm formation lowered the biocidal efficacy of disinfectant [44]. The potency of HOCl was most markedly affected by biofilm formation among the biocides tested in that study [9]. Dan Li *et al.* (2013) revealed that contrary to the prevalent belief that chlorine reduces the growth and reactivation of bacteria, there was sustained prevalence and re-growth of bacteria including Coliforms and *Enterococcus* after disinfection despite high chlorine dosage i.e. 69 (mg·min)/L in reclaimed water [31]. Disinfection may be efficient for reduction of free floating bacteria but have none or little effect on microbes within the biofilm because of the shielding effect of the biofilm. Codony *et al.*, chlorination permitted growth of biofilms and observed increased resistance of bacteria within the biofilm to Chlorine [46]. The factors which promote the growth and proliferation of microbes within the water distribution networks include the type of pipe material, temperature, water source and age, disinfectant type, storage retention time [9, 12, 13, 18, 26].

Technical Challenges Associated with Urban and Peri-Urban Regions in India

Urban and peri-urban regions in India face nearly all of the multiple challenges enumerated in this paper: 1) The intermittent water supply leads to water stagnation providing more time for the microbes to re-grow inside the distribution system; 2) The cracks and leakage in the often deteriorated water distribution network provide a potential portal for intrusion of contaminants including pathogens and nutrient into the treated drinking water; 3) Often water supply pipelines are laid in proximity with the sewage pipelines. When both the pipelines are compromised the risk of pathogen intrusion into drinking water is very high. It is notable that the fecal pathogens and culturable human viruses have been observed in the soil and water outside the water distribution pipelines; 4) The subsequent intrusion of nutrients and microbes encourages development of biofilm within the water distribution network providing a safe haven for opportunistic pathogens to grow and promote the corrosion of pipe materials; and 5) The shedding of cells after maturation of biofilms causes the dissemination of

microbes within water network providing “seed” for newer biofilms and populate the drinking water. Depending upon the water age and the cycle of water supply, public can be exposed to these microbes, which are released from biofilms. Notably, these microbes might include pathogens.

Substandard information on the magnitude of health burden of water-borne diseases does not allow adequate portrayal of the shortcomings of the current water distribution infrastructure. Little research has been devoted to the disease outbreaks in India in context of the water network in the country. An example of a failing water network is the recent jaundice outbreak in Shimla, which was coincident with the mismanaged and ill-maintained water treatment plants and water distribution network [47]. Hepatitis E Virus (HEV), a fecal-orally transmitted viral infection was discovered in water networks and was suspected to be the major fomite for this outbreak [48]. Ageing infrastructure and inefficient running of sewage treatment plants in Shimla and discharge of improperly treated wastewater into the raw drinking water might have contributed to the intrusion of HEV in the water distribution network [49]. The current strategy of over chlorination of water is expected to clear pathogens off the Shimla’s water network but might have severe repercussions in the long run [50, 51]. Heavy chlorination as currently practiced here is commendable in context of protecting public from exposure to HEV. However, a sustainable solution would require analysis of possible contamination hotspots, the role of various factors that contribute to corrosion and biofilm formation, and the long term impact on environmental and public health of any proposed intervention. Our knowledge of the mechanisms of microbial growth and colonizing behavior within the water distribution network in the presence of disinfectants is superficial, and studying the microbial ecology and metabolism in distribution systems will provide deep insights to resolve the current public health concerns associated with microbial growth in these engineered systems [15].

The current research at the home institute of the authors aims to investigate the factors responsible for corrosion within the water network to prevent deterioration of water distribution network and the water quality. Further, efforts are underway to limit the extent of microbial intrusion, re-growth, and potential for resistance to chlorine disinfection. This study incorporates the contribution of physico-chemical factors such as pipe material, stagnation time, disinfection type, dosage and temperature ranges. Further, the biofilms will be monitored for the prevalence and persistence of pathogens and microbes in general within the water supply systems. The recent outbreak in Shimla serves as a source of inspiration for the experimental design of this project and is intended to assist delineating the factors associated with the water quality in Shimla. A lab scale simulation of water distribution network would establish the proof of concept prior to the field study.

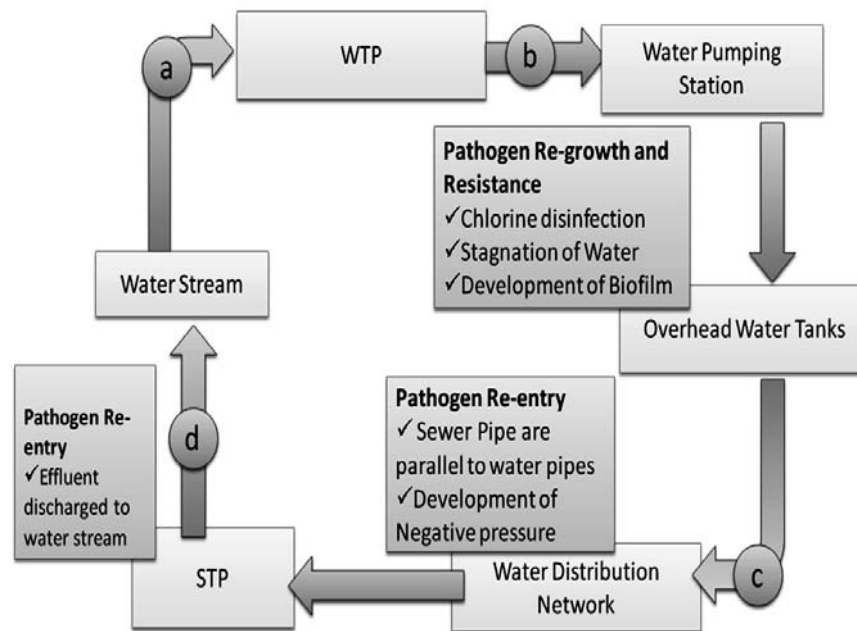


Fig. 1: The Water Network of Shimla

There are four points of chlorination: a) pre-treatment of raw drinking water b) post-treatment of drinking water, c) after storage in water tank, and d) before discharge to stream. The point of pathogen intrusion and re-growth of have been denoted here.

Conclusion

Deficiencies in water distribution systems such as corrosion, intermittent water supply, and poor residual disinfectant, biological and chemical contamination have adversely impacted both the quality and quantity of water in most developing countries. The fast urbanization is a crisis situation given the lack of adequate water infrastructure and as a result the problems associated with the upkeep of the water distribution systems have increased. Poorly operated and maintained engineered systems designed to treat and transport drinking water now serve as the transmission vehicles of pathogens and cause serious disease outbreaks. The primary reason behind the failure of distribution networks may be linked to corrosion and biofilm formation. To ensure effectiveness of any intervention it is quintessential to study the various factors that accelerate deterioration of water networks in context of developing countries. A study such as the one currently being conducted by the authors can provide insights for setting truly sustainable and long-lasting water networks in the proposed SMART cities and elsewhere. The repercussions of such a feat would translate into improved public health and lesser economic and resources losses.

References

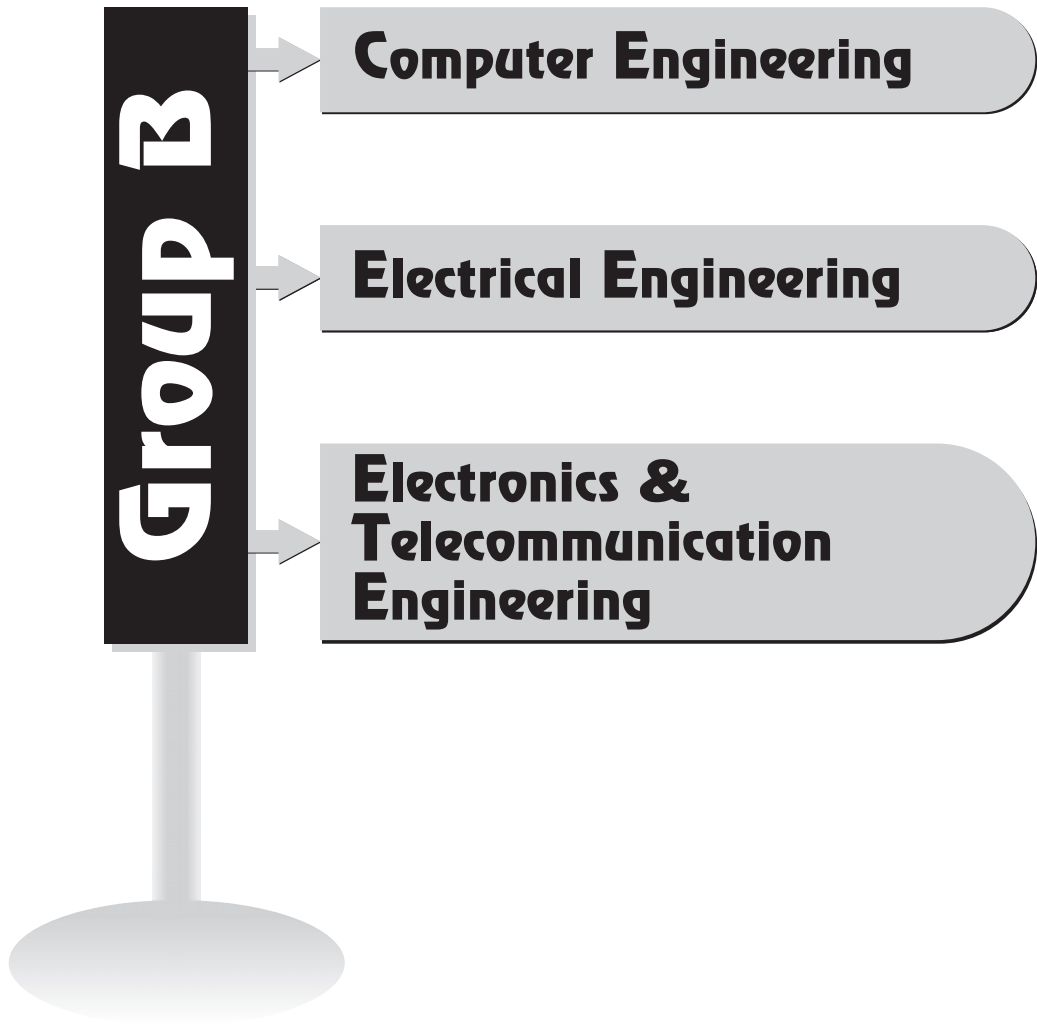
- [1] Carc, A., "For 1 Billion People: Safe Water is Scarce," pp. 1–4, 2016.
- [2] Meanausa, "Kerala Water Resource – Threats and Management Issues," *Meanausa. Org*, 2016.
- [3] Ercumen, A., Gruber, J.S. and Colford, J.M.J., "Water distribution system deficiencies and gastrointestinal illness: a systematic review and meta-analysis.," *Environ. Health Perspect.*, Vol. 122, pp. 651–660, 2014.
- [4] Times of India, "80% of India's surface water may be polluted, report by international body says - Times of India," *Times of India*, pp. 1–34, 2016.
- [5] Hegde, N., "Water scarcity and security in India," *Indian Sci. Congr.*, pp. 1–18, 2012.
- [6] Gabarrón, S., Gernjak, W., Valero, F., Barceló, A., Petrovic, M. and Rodríguez-Roda, I., "Evaluation of emerging contaminants in a drinking water treatment plant using electro dialysis reversal technology," *J. Hazard. Mater.*, Vol. 309, pp. 192–201, 2016.
- [7] Gavrilescu, M., Demnerová, K., Aamand, J., Agathos, S. and Fava, F., "Emerging pollutants in the environment: Present and future challenges in biomonitoring, ecological risks and bioremediation," *N. Biotechnol.*, Vol. 32, pp. 147–156, 2015.
- [8] Leinmiller, B.M., "Smart Water: A Key Building Block of the Smart City of the Future," pp. 10–13, 2016.
- [9] Edwards, M., Pruden, A., Falkinham, J., Brazeau, R., Williams, K., Wang, H., Martin, A. and Rhoads, W., "Relationship between Biodegradable Organic Matter and Pathogen Concentrations in Premise Plumbing," *Water Res Found.*, pp. 111, 2013.
- [10] Lehtola, M.J., Miettinen, I.T., Keina, M.M., Kekki, T.K., Laine, O., Hirvonen, A., Vartiainen, T. and Martikainen, P.J.,



- "Microbiology, chemistry and biofilm development in a pilot drinking water distribution system with copper and plastic pipes," Vol. 38, pp. 3769–3779, 2004.
- [11] Wang, H., Edwards, M., Falkinham III, J.O. and Pruden, A., "Molecular Survey of the Occurrence of Legionella spp., Mycobacterium spp., Pseudomonas aeruginosa and Amoeba Hosts in Two Chloraminated Drinking Water Distribution Systems," *Appl. Environ. Microbiol.*, Vol. 78, pp. 6285–6294, 2012.
- [12] Wang, H., Masters, S., Edwards, M.A., Falkinham, J.O. and Pruden, A., "Effect of disinfectant, water age and pipe materials on bacterial and eukaryotic community structure in drinking water biofilm," *Environ. Sci. Technol.*, Vol. 48, pp. 1426–1435, 2014.
- [13] Rhoads, W.J., Ji, P., Pruden, A. and Edwards, M.A., "Water heater temperature set point and water use patterns influence Legionella pneumophila and associated microorganisms at the tap.," *Microbiome*, Vol. 3., p. 67, 2015.
- [14] Berry, D., Xi, C. and Raskin, L., "Microbial ecology of drinking water distribution systems," *Current Opinion in Biotechnology 2006*, Vol. 17, pp. 297–302, 2006.
- [15] Lee, E.J. and Schwab, K.J., "Deficiencies in drinking water distribution systems in developing countries," pp. 109–127, 2005.
- [16] Simões, L. Chaves and Simões, M., "Biofilms in drinking water: problems and solutions," *RSC Adv.*, Vol. 3, p. 2520, 2013.
- [17] Boulay, N. and Edwards, M., "Role of temperature, chlorine and organic matter in copper corrosion by-product release in soft water," *Water Res.*, Vol. 35, pp. 683–690, 2001.
- [18] Ji, P., Parks, J., Edwards, M.A. and Pruden, A., "Impact of Water Chemistry, Pipe Material and Stagnation on the Building Plumbing Microbiome," *PLoS One*, Vol. 10, pp. 1014–1087, 2015.
- [19] Berney, M., Vital, M., Hlshoff, I., Weilenmann, H.U., Egli, T. and Hammes, F., "Rapid, cultivation-independent assessment of microbial viability in drinking water," *Water Res.*, Vol. 42, pp. 4010–4018, 2008.
- [20] Lautenschlager, K., Boon, N., Wang, Y., Egli, T. and Hammes, F., "Overnight stagnation of drinking water in household taps induces microbial growth and changes in community composition," *Water Res.*, Vol. 44, pp. 4868–4877, 2010.
- [21] Lechevallier, M.W., Gullick, R.W., Karim, M.R., Friedman, M., Funk, J.E. and Funk, J.E., "The Potential for Health risks from Intrusion of Contaminants into distribution system from pressure transients," *J. for Water and Health*, pp. 3–14, 2003.
- [22] Lenhart, T.R., Duncan, K.E., Beech, I.B., Sunner, J.A., Smith, W., Bonifay, V., Biri, B. and Suflita, J.M., "Identification and characterization of microbial biofilm communities associated with corroded oil pipeline surfaces.," *Biofouling*, Vol. 30, pp. 823–835, 2014.
- [23] Sarin, P., Snoeyink, V.L., Bebee, J., Kriven, W.M. and Clement, J.A., "Physico-chemical characteristics of corrosion scales in old iron pipes," *Water Res.*, Vol. 35, pp. 2961–2969, 2001.
- [24] Little, B.J., Lee, J.S. and Ray, R.I., "Diagnosing microbiologically influenced corrosion: A state-of-the-art review," *Corrosion*, Vol. 62, pp. 1006–1017, 2006.
- [25] McNeill, L.S. and Edwards, M.A., "Iron pipe corrosion in distribution systems," *Am. Water Work. Assoc.*, Vol. 93, pp. 88–100, 2001.
- [26] Dudi, M.E.A., "Role of chlorine and chloramine in corrosion of lead-bearing plumbing materials," *J. Am. Water Work. Assoc.*, Vol. 96, pp. 69–81, 2004.
- [27] Wang, H., Masters, S., Falkinham III, J.O., Edwards, M.A. and Pruden, A., "Distribution System Water Quality Affects Responses of Opportunistic Pathogen Gene Markers in Household Water Heaters," *Environ. Sci. Technol.*, Vol. 49, pp. 8416–8424, 2015.
- [28] Nguyen, C.K., Stone, K.R., Dudi, A. and Edwards, M.A., "Corrosive Microenvironments at Lead Solder Surfaces Arising from Galvanic Corrosion with Copper Pipe," *Environ. Sci. Technol.*, Vol. 44, pp. 7076–7081, 2010.
- [29] Edwards, M.A., Ferguson, J.F. and Reiber, S.H., "The pitting corrosion of copper," *J. Am. Water Work. Assoc.*, Vol. 86, 1994.
- [30] Sedlak, David L. and Gunten, Urs von, "The Chlorine Dilemma," *Science*, Vol. 331, pp. 42–43, 2011
- [31] Li, D., Zeng, S., He, M. and Gu, A.Z., "Water Disinfection Byproducts Induce Antibiotic Resistance-Role of Environmental Pollutants in Resistance Phenomena," *Environ. Sci. Technol.*, Vol. 50, pp. 3193–3201, 2016.
- [32] Li, D., Zeng, S., Gu, A.Z., He, M. and Shi, H., "Inactivation, reactivation and regrowth of indigenous bacteria in reclaimed water after chlorine disinfection of a municipal wastewater treatment plant," Vol. 25, pp. 1319–1325, 2013.
- [33] Bougeard, C.M.M., Goslan, E., Jefferson, B. and Parsons, S.A., "Comparison of the disinfection by-product formation potential of treated waters exposed to chlorine and monochloramine," *Water Res.*, Vol. 44, pp. 729–740, 2010.
- [34] Hua, G. and Reckhow, D.A., "Comparison of disinfection byproduct formation from chlorine and alternative disinfectants," *Water Res.*, Vol. 41, pp. 1667–1678, 2007.
- [35] Puget, S., Beno, N., Chabanet, C., Guichard, E. and Thomas-Danguin, T., "Tap water consumers differ from non-consumers in chlorine flavor acceptability but not sensitivity," *Water Res.*, Vol. 44, pp. 956–964, 2010.
- [36] Sun, Y.X., Wu, Q.Y., Hu, H.Y. and Tian, J., "Effect of bromide on the formation of disinfection by-products during wastewater chlorination," *Water Res.*, Vol. 43, pp. 2391–2398, 2009.
- [37] Goslan, E.H., Krasner, S.W., Bower, M., Rocks, S.A., Holmes, P., Levy, L.S. and Parsons, S.A., "A comparison of disinfection by-products found in chlorinated and chloraminated drinking waters in Scotland," *Water Res.*, Vol. 43, pp. 4698–4706, 2009.
- [38] Goel, S. and Bouwer, E.J., "Factors influencing inactivation of Klebsiella pneumoniae by chlorine and chloramine," *Water Res.*, Vol. 38, pp. 301–308, 2004.
- [39] Power, K.N., Schneider, R.P. and Marshall, K.C., "The effect of growth conditions on survival and recovery of Klebsiella oxytoca after exposure to chlorine," *Water Res.*, Vol. 31, pp. 135–139, 1997.
- [40] Cargill, K.L., Pyle, B.H., Sauer, R.L. and McFeters, G.A., "Effects of culture conditions and biofilm formation on the



- iodine susceptibility of *Legionella pneumophila*,” *Can J Microbiol*, Vol. 38, pp. 423–429, 1992.
- [41] Kilb, B., Lange, B., Schaule, G., Flemming, H. and Wingender, J., “Contamination of drinking water by coliforms from biofilms grown on rubber-coated valves,” Vol. 573, 2003.
- [42] Juhna, T., Birzniece, D., Larsson, S., Zulenkovs, D., Sharipo, A., Azevedo, N.F., Mnard-Szczebara, F., Castagnet, S., C.Fliers and Keevil, C.W., “Detection of *Escherichia coli* in biofilms from pipe samples and coupons in drinking water distribution networks,” *Appl. Environ. Microbiol.*, Vol. 73, pp. 7456–7464, 2007.
- [43] Wingender, J. and Flemming, H., “International Journal of Hygiene and Biofilms in drinking water and their role as reservoir for pathogens,” *Int. J. Hyg. Environ. Health*, Vol. 214, pp. 417–423, 2011.
- [44] Tachikawa, M., Tezuka, M., Morita, M., Isogai, K. and Okada, S., “Evaluation of some halogen biocides using a microbial biofilm system,” *Water Res.*, Vol. 39, pp. 4126–4132, 2005.
- [45] Howard, K. and Inglis, T.J.J., “The effect of free chlorine on *Burkholderia pseudomallei* in potable water,” *Water Res.*, Vol. 37, pp. 4425–4432, 2003.
- [46] Codony, F., Morat, J. and Mas, J., “Role of discontinuous chlorination on microbial production by drinking water biofilms,” *Water Res.*, Vol. 39, pp. 1896–1906, 2005.
- [47] IITR, “IITR Report on Shimla STP,” 2016.
- [48] Stories, T.O.P., Modi, P.M., Pak, I. and Shimla, S., “Shimla, Solan under Hepatitis – E threat, all water samples fail test,” pp. 1–3, 2016.
- [49] Chobe, L.P. and Arankalle, V.A., “Investigation of a hepatitis A outbreak from Shimla Himachal Pradesh,” *Indian J. Med. Res.*, Vol. 130, pp. 179–184, 2009.
- [50] World Health Organization, “Water and Public Health Session Objectives,” *Water Public Heal.*, pp. 1–19, 1995.
- [51] Chalmers, T.C. and Angelillo, I.F., “Chlorination, Chlorination By-products, and,” pp. 955–963, 1992.





Reduction in Sub Diaphragmatic Activity in Myocardial Perfusion Imaging with the Intake of Water

Gopal Sonai Muthu^{*1} and Sujata Mitra¹

Abstract: Myocardial perfusion imaging is routinely used to detect and assess the extent and severity of the myocardial damage. Distribution of 99 mTc Methoxy IsoButyl Isonitrile (MIBI) in the myocardium images and the interpretation is made with the Single Photon Emission Computed Tomographic (SPECT) images. Higher uptake of 99 mTc MIBI seen in the sub-diaphragmatic region causes overlap of activity in the inferior wall region of the myocardium and makes the interpretation of images more difficult. This study was undertaken to quantify the reduction in the uptake of 99 mTc MIBI in the sub-diaphragmatic region, in response to the intake of water between injection and image acquisition. This study was done on 117 patients who underwent myocardial perfusion scan. There were two groups of patients, one with intake of water and another without intake of water. The uptake in the sub infero septal, sub infero lateral and myocardial regions were measured in a projection image. Uptake ratios were calculated in both groups and analysed. Administration of water to the patients at the specified time improves the quality of myocardial perfusion SPECT images and facilitates the improved interpretation of the infero-lateral myocardial wall.

Keywords: Myocardium, Sub-Infero Septum, Sub-Inferolateral, Uptake, Ratio.

Introduction

Myocardial Perfusion Imaging is routinely used to detect, assess the extent and severity of the myocardial damage. One day stress, rest protocol is followed in this study with an intravenous injection of a radiopharmaceutical 99 m Technetium labelled Methoxy IsoButyl Isonitrile (99 mTc MIBI). Images are acquired in various projections in the gamma camera. Single Photon Emission Computed Tomographic (SPECT) images are reconstructed that is used for making the interpretation. 99 mTc MIBI binds to mitochondria of the cardiaccells, and the gamma ray emission from 99 mTc is used for imaging. 99 mTc MIBI is also cleared by the liver and excreted by the biliary system. Abdominal activity after rest injection may be elevated because there is no exercise effect to reduce splanchnic activity. When one uses filtered back projection (FBP), image artifacts can be caused by so-called halo and spill over effects [1]. The halo effect is a reconstruction artifact that is associated with the implementation of FBP on attenuated projection images, with focally increased activity in other wise low-count surroundings. This may result in an underestimation of the inferoposteroseptal walls. Spill over of activity into the myocardium, resulting from photon scatter in the patient associated with activity in the liver, bowel, and stomach, may result in an overestimation of this area. Both

artifacts are patient dependent and their severity is hard to predict. Although both halo and spill over are often mentioned in articles on myocardial SPECT, very little information is available on avoidance of these phenomena. An adequate clearance is prerequisite for high quality SPECT. However, by stimulating the clearance, the radio-activity may be transferred to another area. Increased bowel and gastric activity are as great a problem as high liver uptake in the visual and quantitative interpretation of the inferoposteroseptal myocardial walls. Higher uptake of 99 mTc MIBI seen in the sub-diaphragmatic region causes overlap of activity in the inferior wall region of the myocardium and makes the interpretation more difficult (Figure 1).

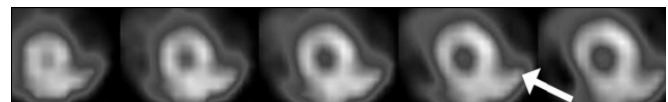


Fig. 1: Short Axis SPECT Images of Myocardium with High Sub-Infero Lateral Uptake

This study was undertaken to quantify the reduction in the uptake of 99 mTc MIBI in the sub-infra septal and sub infero lateral regions, in response to the intake of water between injection and image acquisition.

¹ Department of Nuclear Medicine, Tata Main Hospital, Jamshedpur, India. ✉ gopalsaimuthu@gmail.com

Materials and Method

This study was done on 117 patients who underwent myocardial perfusion scan during January 2016–July 2016. There were 45 patients in Group-1 with no administration water in between injection and the scan acquisition, and there were 72 patients in Group-2 who have had at least 450 mL of water 10 min after the injection in both stress and rest studies (Table 1). There were 22 males with a mean age of 58.7 ± 13.7 years and 23 females with a mean age of 60.7 ± 10.8 years in Group-1. There were 40 males with a mean age of 60.0 ± 5.4 years and 32 females with a mean age of 60.8 ± 11.4 years in Group-2. All the 45 patients in Group-1 did not drink water after the injection in both stress and rest studies. All the 72 patients in Group-2 were advised to drink at least 450 ml of water 10 minutes after the injection in both stress and rest studies.

Table 1: Age and Sex of the Patients

	Group-1 Patients without Water Intake		Group-2 Patients with Water Intake	
	Males	Females	Males	Females
N	22	23	32	40
Mean	58.7	60.7	60.0	60.8
SD	13.7	10.8	5.4	11.4

One day stress-rest protocol was followed in the Myocardial Perfusion Scintigraphy [2]. Stress study was done in a bicycle ergometer similar to Bruce protocol and about 300–400 Mega Becquerel (MBq) of ^{99m}Tc MIBI was injected intra venously at the peak of the exercise. Images were acquired 30–40 minutes after the injection, on a GE Millennium MG dual head gamma camera (Model number H3000ZL, serial Number 51432, manufacturing date 17th October 2006) with a Genieacq image acquisition system and a Xeleris post processing workstation. Rest studies were done the injection for stress studies. About 800–1000 MBq of ^{99m}Tc MIBI was injected 3 hours after for the rest studies and the images were acquired 30 minutes after the injection. SPECT images were reconstructed in the Emery Cardiac Toolbox in the Xeleris workstation, without attenuation correction.

Uptake of ^{99m}Tc MIBI in the myocardial and the sub-diaphragmatic region depend upon many factors including the amount of activity injected, Body Mass Index (BMI), and the clinical condition of the patient. Hence the ratio between uptake of ^{99m}Tc MIBI in the sub-diaphragmatic and myocardial regions was computed in this study to compare the uptake in both groups. Same projection image (image 1 of the detector-1 from the stress image data set, corresponding to the Left Anterior Oblique (LAO) view) was

used in all the patients for measuring the radiation counts (Figure 2). The daily and the periodic QA (uniformity, linearity and Centre of Rotation (COR) as per the National Electrical Manufacturers Association (NEMA) and the Atomic Energy Regulatory Board (AERB) requirements) were within the acceptable levels. The QA for the radiochemical purity of ^{99m}Tc MIBI was done by the paper chromatographic method and was found to be greater than 98% in all the days these scans were performed, where the expected level of purity was greater than 90%.

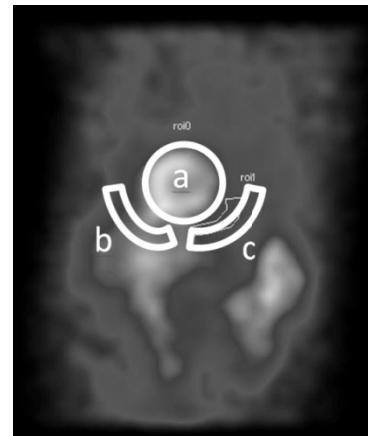
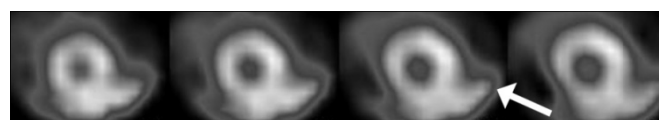


Fig. 2: Regions of Interest: (a) Myocardial, (b) Sub Infero Septal and (c) Sub-Infero Lateral Regions

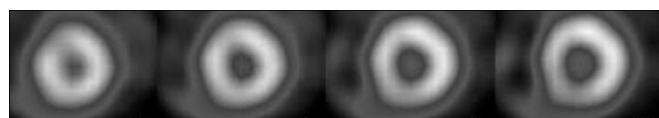
A circular region of interest (ROI) was used for measuring the myocardial activity (M) (Figure 2). Two more ROIs were drawn in the sub infero-septal (SIS) and sub infero-lateral (SIL) regions. The ROIs in SIS and SIL regions were drawn with constant image area of 25 pixels in all the image datasets, to measure the activity in the sub-diaphragmatic region. Radiation counts in the myocardial, sub infero-septal and sub infero-lateral regions were measured. The ratio between the sub infero-septal and myocardial uptake (SIS/M) and the ratio between the sub infero-lateral and the myocardial uptake (SIL/M) were calculated and analysed. This analysis was done in both the groups of patients. Student's-t test was used for statistical significance between the two groups. p-value less than 0.05 was considered as statistically significant.

Result

There is an improvement in the quality of the images in the patients in Group-2, when compared with that in the patients in Group-1. Figure 3a is the SPECT images of a patient who did not drink water between injection and image acquisition. Figure 3b is the SPECT images of another patient who drank water between injection and image acquisition. Images in Figure 3b make the interpretation easier to make an accurate diagnosis.



(a) SPECT Images in a Patient with no Water Intake



(b) SPECT Images in a Patient with Water Intake

Fig. 3: Reconstructed SPECT Images with (a) High and (b) Low Sub-Diaphragmatic Activity

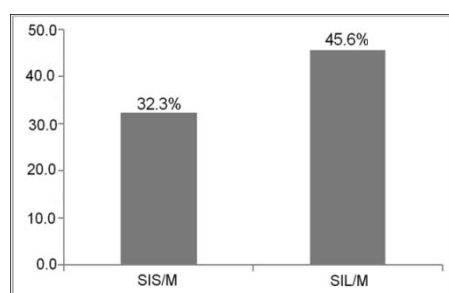
The ratio between the sub infero-septal and myocardial uptake (SIS/M) and the ratio between the sub infero-lateral and the myocardial uptake (SIL/M) in both groups of patients are showing in Table 2.

Table 2: Uptake Ratios

	Group-1 Patients without Water Intake N = 45		Group-2 Patients with Water Intake N = 72	
	(SIS/M)*	(SIL/M)	(SIS/M)	(SIL/M)
Mean	0.34	0.28	0.23	0.15
SD	0.07	0.05	0.06	0.04

*M–Myocardial, SIS–Sub-Infero Septal, SIL–Sub-Infero Lateral.

The ratio between the sub infero-septal and myocardial uptake (SIS/M) has come down from 0.34 in the patients who did not drink water to 0.23 in the patients who drank water. The ratio between the sub infero-lateral and myocardial uptake (SIS/M) has come down from 0.28 in the patients who did not drink water to 0.15 in the patients who drank water. There is a statistically significant reduction of 32.3% and 45.6% of the uptake values in subinfero-septal and sub infero lateral regions in the patients who drank water, when compared with the patients who did not drink water ($p < 0.001$) (Figure 4). Relatively reduced reduction in



M–Myocardial, SIS–Sub-Infero septal, SIL–Sub-infero lateral

Fig. 4: Reduction in Sub-Diaphragmatic Uptake of 99 mTc MIBI in Response to Intake of Water

uptake of 99 mTc MIBI is seen in the sub infero septal region due to the liver uptake that is not diluted with the intake of water.

Discussion

One of the patients had to undergo a repeat study during the period of this study due to very high uptake of 99 mTc MIBI in the sub diaphragmatic region. The first SPECT study on this patient without administration of water showed 2 small perfusion defects with a size of 35 pixels did not show any reversibility and showed an Ejection Fraction of 48%. When repeated with administration of water, the image quality was better and the same patient showed a perfusion defect 128 pixels, reversibility of 56% and an Ejection Fraction of 48%.

Although both halo and spill over are often mentioned in articles on myocardial SPECT, very little information is available on avoidance of these phenomena [3]. The effects of areas of high activity close to the myocardium, as in the liver, can be eliminated by the application of attenuation correction [4]. Some authors state that scatter effects may be more serious on attenuation corrected images because the procedure cannot distinguish between scattered and unscattered photons [5]. Both components are amplified equally during attenuation correction. In addition, iterative reconstruction will eliminate the halo effects but will not diminish scatter. To date, the problems caused by halo and spill over effects can only be partially solved by new imaging techniques. It is necessary to estimate and remove the scatter component from the measured signal and to incorporate the depth-dependent response of the imaging system in the reconstruction algorithms [6].

Several protocols include the use of a fatty meal or intravenous cholecystokinin to stimulate hepatobiliary clearance [7]. Others include giving patients a drink of milk, a milk shake and carbonated lime or water [8–13]. But intake of milk or carbonated lime is restricted in some patients with some known ailments. Water is tried in this study because water intake is not restricted in most of the patients. Intake of water reduces activity in the gastric fundus and speeds up the migration of biliary secreted activity through the bowel [14]. Activity dispersed more diffusely throughout the entire abdomen is less likely to cause reconstruction artifacts. However some patients showed higher liver uptake. Milk can be used in these patients, if not contra-indicated. Scan done 90 minutes post injection also provides good background clearance in some patients.

Conclusion

Administration of water to the patients at the specified time improves the quality of myocardial perfusion SPECT images,



thus facilitating the better interpretation of the infero-lateral myocardial wall.

References

- [1] Middleton, G.W. and Williams, J.H., Significant gastric reflux of technetium-99 m-MIBI in SPECT myocardial imaging, *J. Nucl Med.*, 35, 619–620 (1994).
- [2] Strauss, H.W., Miller, D.D., *et al.*, Procedure Guideline for Myocardial Perfusion Imaging version 3.3, *J. of Nuc Med Tech.*, 3, 155–161 (2008).
- [3] AJ van Dongen and PP van Rijk. Minimizing Liver, Bowel, and Gastric Activity in Myocardial Perfusion SPECT. *J Nucl Med.*, 41, 1315–1317 (2000).
- [4] Nuyts, J., Dupont, P., Van den Maegdenbergh, V., Vleugels, S., Seutens, P. and Mortelmans, L., A study of the liver-heart artifact in emission tomography. *J Nuc Med.*, 36, 133–139 (1995).
- [5] Ficaro, E.P., Fessler, J.A., Shreve, P.D., Kritzman, J.N., Rose, P.A. and Corbett, J.R., Simultaneous transmission/emission myocardial perfusion tomography: Diagnostic accuracy of attenuation corrected Tc-Sestamibi SPECT. *Circulation*, 93, 463–473 (1996).
- [6] Hutton, B.F., Hudson, H.M. and Beekman, F.J., A clinical perspective of accelerated statistical reconstruction. *Eur. JI. Nuc. Med.*, 24, 797–808 (1997).
- [7] Ramin, S. and Vahid, R.D.K. *et al.*, Persistent Sub-diaphragmatic Activity on the Myocardial Perfusion Scan with 99 mTc-Sestamibi, *Iran J. Nucl Med.*, 16(1), 52–56 (2008)
- [8] Garcia, E., Cooke, C.D., Van Train, K.F., *et al.* Technical aspects of myocardial SPECT imaging with technetium-99 m sestamibi., *Am J. Cardiol.*, 66 (suppl), 80E–90E (1990).
- [9] Hurwitz, G.A., Clark, E.M., Slomka, P.J. and Siddiq, S.K., Investigation of measures to reduce interfering abdominal activity on rest myocardial images with Tc-99 m sestamibi., *Clin. Nucl. Med.*, 18, 735–741 (1993).
- [10] Boz, A. and Karayalcin, B., Which is better for inferior wall evaluation: a full or empty stomach. *J. Nuc. Med.*, 37, 1916–1917 (1996).
- [11] Malhotra, G. and Upadhye, T.S., *et al.*, Can Carbonated Lime Drink Intake Prior to Myocardial Perfusion Imaging With Tc-99 m MIBI Reduce the Extracardiac Activity That Degrades the Image Quality and Leads to Fallacies in Interpretation? *Clin. Nuc. Med.*, 35(3), 151–221 (2010).
- [12] Hadi, M., Raheleh, H., *et al.*, The Effect of Milk, Water and Lemon Juice on Various Sub diaphragmatic Activity-Related Artifacts in Myocardial Perfusion Imaging. *Res. Cardiovasc Med.*, 4(4), e29235 (2015). doi: 10.5812/cardiovascmed.29235.
- [13] Sumina, G., Srinivas, B. and DePuey, E.G., Effect of Proton Pump Inhibitors and H₂ Antagonists on the Stomach Wall in 99 mTc-Sestamibi Cardiac Imaging. *Nuclear Medicine Review*, 16(2), 91–94 (2013) 10.5603/NMR.2013.0042.
- [14] Russo, A., Fraser, R. and Horowitz, M., The effect of acute hyperglycaemia on small intestinal motility in normal subjects. *Diabetologia*, 39, 984–989 (1996).



A New Technique for Extraction Based Text Summarization

Goutam Sarker¹

Abstract: Text summarization is the process of reducing a text document with a computer program in order to create a summarized text that retains the most important information of the original text. Text summarization is an area of data mining and in turn Artificial Intelligence. The present work is one new type of extrinsic technique of summarization, which finds a representative subset of the original textual sentence set, and thereby contains the precise and salient information of the original text.

Keywords: Text Summarization, Sentence Weight, Clustering, Redundant Sentence.

Introduction

A summary [1] of a text is produced from one or more texts that conveys important and salient information in the original text(s), and is shorter in length than the original text(s). The goal of automatic or machine generated text summarization is to condense the source text(s) into a shorter version, preserving its content information and overall meaning. A summary can be effectively and efficiently employed either in an indicative way as a pointer to some parts of the original text, or in an informative way to cover all salient and relevant information of the text. In both cases the most important advantage of using a summary is its reduced reading and/or post processing time.

Text summarization [2, 3] methods can be broadly classified under two categories namely extrinsic or extractive summarization and NLP based or intrinsic summarization. An extractive summarization method consists of selecting important sentences, paragraphs etc. from the original text and concatenating them into shorter form by eliminating less important, redundant irrelevant and useless sentences. Intrinsic summarization requires the understanding of the inner meaning of sentences of the text and is thereby more hard and complex. The importance of the sentences are decided based on the weight of sentences. In this paper a new novel technique of extractive text summarization method is focused.

Automatic or machine generated text summarization [4, 5] is the technique, where a computer system summarizes a text. A text is entered in the system and a summarized text is returned as output, which is a non-redundant extract from the original text. A redundant set of sentences is a sentence set having more or less identical meaning of all the sentences in that set.

The technique was originated in the 60's and has been developed through 60 years. Today, with the internet and the worldwide web, the technique has become more important and finds versatile applications.

Text document summarization can be used:

- To summarize news to SMS or WAP-format for mobile phones.
- To let a computer synthetically read the summarized text. Written text can be too long and boring to understand.
- In search engines to present compressed descriptions of the search results (e.g. internet search engine Google).
- In keyword directed subscription of news which are summarized and pushed to the user.
- To search in foreign languages and obtain an automatically translated summary of the automatically summarized text.

In the present novel approach, text document summarization is based on weight of the sentences, where the summarization system calculates how often certain set of keywords appears in the text file and/or a set of text files. The keywords belong to the so called open class words. The summarization system calculates the 'intra' and 'inter' frequency of the key words in the given text set, to ultimately compute the weight of each sentence. Then it arranges the sentences in descending order of weight after eliminating the redundant sentences through clustering. The representative sentences (with minimum sentence length) in the cluster of same-meaning sentences are the most optimal ones with the same meaning as the other sentences in the group or cluster. This improves the quality of summary. A certain percentage of sentences in weight-wise descending order are selected, while others are deselected. Then, the selected sentences are compared with the original text to find

¹Department of Computer Science & Engineering, National Institute of Technology, Durgapur, India. ✉ sarkergoutam@yahoo.co.in



their right order and right position to form a meaningful qualitative summary. After this, the machine generated summarized texts are compared with human generated summaries for those texts to evaluate the summary system in terms of accuracy.

Basic Ideas and Theory of Operation

Text Mining

Text mining [6], also referred to as text data mining [7–10] roughly equivalent to text analytics, refers to the process of deriving high-quality information from text. High-quality information is typically derived through the devising of patterns and trends through means such as statistical pattern learning. Text mining usually involves the process of structuring the input text (usually parsing, along with the addition of some derived linguistic features and the removal of others, and subsequent insertion into a database), deriving patterns within the structured data, and finally evaluation and interpretation of the output. 'High quality' in text mining usually refers to some combination of relevance, novelty, and interestingness.

Text Pre-Processing

Figure 1 presents the steps used for text pre-processing. The first step in text pre-processing is to transform documents, which typically are strings of characters, transformed into a representation suitable for the learning algorithm and the classification task. The text transformation usually is of the following kind:

- Word separation, sentence splitting.
- Remove HTML or other tags.
- Remove stopwords, punctuations.

The stopwords are frequent words that carry no information i.e. pronouns, prepositions, conjunctions, etc.

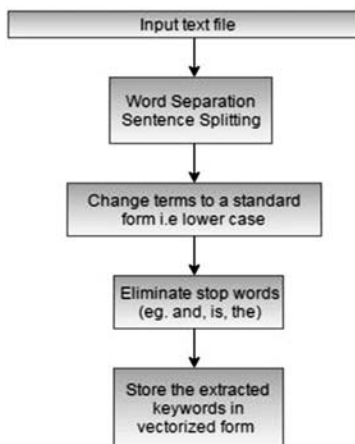


Fig. 1: Schematic of Text Pre-Processing

Multi-Text Summarization

Multi-Text summarization is an automatic procedure aimed at extraction of information from multiple texts written about the same topic. The resulting summary report allows individual users, such as professional information consumers, to quickly familiarize themselves with information contained in a large cluster of texts. In such a way, multi-text summarization systems are complementing the news aggregators performing the next step down the road of coping with information overload.

Overview of Current Approach

In this work, the Extractive method is used to get the summary of the input texts. In order to extract the summary, we use the following features are used:

1. *Content Words or Keywords (w_k):* During preprocessing, after removing the stop words the remaining words are treated as keywords. The total number of keyword is taken during assigning the weight to each term.
2. *Term Frequency (t_f):* The frequency of the keyword which are frequently occurring in the text.
3. *Sentence Feature:* Usually first sentence of first paragraph of a text document are more important and are having greater chances to be included in summary. So in the present system, the inclusion of first sentence and counting the number of sentences in the text has been made. Have been assigned Weights to the keywords to find the weight of the sentence. Sentence weight is calculated according to original text and then sorted in descending order of sentence weight.
4. *Normalized Term Frequent (t_f):* Normalized term frequency of the i^{th} keyword is given by,

$$t_{f_i} = \left(\frac{f_i}{f_1 + f_2 + \dots + f_n} \right) \times w_k,$$

Where f_i = frequency of the keyword for k_i for $1 \leq i \leq n$; and w_k is the Total number of keywords.

5. *Inter Document Frequency (IDF):* Inter Document frequency IDF_i of the keyword k_i is the ratio of the number of text files in which that keyword k_i is occurring (n_i) and the total number of text files (n),

$$\text{Therefore, } IDF_i = \frac{n_i}{n}$$

6. Weight of the keywords k_i in a sentence is assigned by $s_i = (t_{f_i} + IDF_i)$, so that weight of a sentence can be

expressed by the terms $\sum_{i=1}^j t_{f_i} + IDF_i$ where there are j different keywords in sentence s_i . Now the sentences are arranged in descending order of their weights, after



removal of redundant sentences through ‘sentence clustering or grouping’.

Sentence Clustering or Grouping: Here each sentence from the texts are compared with every other sentence in that text file to form a group or cluster [11–14] of similar sentences having same meaning. If a cluster is having cardinality greater than one then normalized weight of all sentences of the clusters are computed by the formula,

$$w_{s_i} = \frac{\text{weight of the sentence}}{\text{length of the sentence}}$$

where, w_{s_i} is the weight of the sentence and s_i is the cluster or group.

Then the sentence s_i in the cluster for which w_{s_i} is maximum, is selected and all the others are deselected and thus are regarded as redundant sentences.

7. **Evaluation:** Evaluation of the system in terms of accuracy is done by comparing the system generated summary with the same benchmark or standard summary usually human generated summary.

Algorithm for Present Technique

The text summarization tasks can be classified into single-document (like images, videos, audios, texts, etc.) and multi-document (like images, videos, audios, texts, etc.) summarization. In single-document summarization, the summary of only one document is to be built, while in multi-document summarization the summary of a whole collection of documents is built. In the paper, different subject texts collected from the internet as the documents to work on has been used.

Algorithm for Single Text File

Input: Text file for summarization, stop words, file for extracting keywords and threshold.

Output: Sorted sentences in descending order of the sentence weight.

Steps:

1. Extract keywords k_i in the text
2. Determine the keywords in the text greater than threshold (th) i.e. $k_i > th$
3. Determine weight of keyword k_i ,

$$w_i = \frac{t_f}{n}$$

4. Determine the weighted sum of all the sentences

$$w_{t_1} = \frac{w_{t_i}}{n} \quad i = 1 \text{ to } n$$

Where, w_{t_s} = effective weight of the sentence.

$w_{t_1}, w_{t_2}, w_{t_3}, \dots, w_{t_n}$ are the weights of individual terms in that sentence. n = total number of terms in that sentence.

5. Finally, arrange the sentences in descending order of weighted sum.

Algorithm for Multiple Text file

Input: Text file for summarization, stop words file for extracting keywords and threshold.

Output: Sorted sentences in descending order of the sentence weight

Steps:

1. Extract keywords k_i
2. Find occurrence of keywords k_i in the text
3. Determine the keywords in the text

$$w_i = \frac{t_f}{n}$$

Where t_f is the term frequency of the keyword greater than threshold (th) i.e. $k_i > th$.

4. Determine weight of keyword k_i ,
5. Compute Inter Document frequency (IDF) as the ratio of the number of text files in which that word is occurring (n_i) and total number of text files (n).

$$IDF = \frac{n_i}{n}$$

6. Compute the weight of the sentence in that text file as,

$$\sum_{i=1}^j t_{f_i} + IDF_i$$

where, “ j ” is the total number of keywords in the given sentence. This is performed in all the text files in the folder.

7. Determine the weighted sum of all the sentences

$$w_{t_1} = \frac{w_{t_1}}{n} \quad i = 1 \text{ to } n$$

Where, w_{t_s} = effective weight of the sentence.

$w_{t_1}, w_{t_2}, w_{t_3}, \dots, w_{t_n}$ are the weights of individual terms in that sentence.

n = total number of terms in that sentence.

8. Cluster all the redundant sentences by comparing each sentences from the text with every other sentence in that text file to represent the sentence having the maximum ratio of the cluster i.e.

$$\max\left(\frac{w_i}{l_i}\right)$$

Where, w_i = weight of the keywords,

l_i = length of the sentences



9. Step 1 to step 8 is repeated for all the text files in the folder.
10. Finally, sequentially arrange the sentences in descending order of weighted sum in all the text files of the folder and select first 25% sentences and deselect the others.

Algorithm for Clustering Meaningful Sentences

Input: Text files for clustering, pre -defined threshold.

Output: A set of sentences with maximum ratio of $(\frac{w_i}{l_i})$.

Steps:

1. Extract weighted sentence, w_s in a text file.
2. Grouping sentences based on commonality of keywords between the sentences, given a pre-defined threshold ‘ th ’.
3. For $1 \leq i \leq n$ $w_s \in G_i$
4. Then, redundancy is removed by keeping the sentence which has maximum ratio i.e. $\max(\frac{w_i}{l_i})$. Where w_i = weight of the key words (k_i) and l_i = length of the original sentences.
5. Finally, meaningful sentences obtained from text file.

Experimental Results

The system is evaluated using an Intel® Xeon® CPU E5645 @2.40 GHz having 8GB RAM and Windows 7 64-bit OS.

The English text file data of different subjects like Accounting, Geography, Biology, Economics, Artificial Intelligence (AI) etc. is collected from internet (www.worldscientific.com, en.wikipedia.org, scienceworld.scholastic.com www.ncert.nic.in/ncerts/textbook/textbook www.textbooksonline.tn.nic.in/books and many more).

Due to lack of benchmark texts with corresponding human generated summaries in the internet, benchmark texts (www.worldscientific.com, en.wikipedia.org, scienceworld.scholastic.com, www.ncert.nic.in/ncerts/textbook/textbook www.textbooksonline.tn.nic.in/books and many more using textsummarization.net/text-summarizer) was used, and human generated summaries for them all was utilized for the purpose of system generated summary evaluation.

It is observed from Table 1 that the time for summarization is affordable. To evaluate the system in terms of accuracy, human generated summary was used, which is usually intrinsic rather than extrinsic and is based on the conceptual meaning of the text. With that also the accuracy of summarization is adequate in most cases and is acceptable for all practical purposes while enjoying the simplicity of design.

Table 1: Performance Evaluation

Sl. No.	Input Folder	Input Text File	No. of Input Texts	Time for Summarization (seconds)	Accuracy of Summarized Text	Average Accuracy
1.	ACC TXT	ACC1.TXT	7	348.36	54.44	38.6
		ACC2.TXT		171.66	64.55	
		ACC3.TXT		1135.5	36.67	
		ACC4.TXT		1054.27	37.78	
		ACC5.TXT		1371.41	28.18	
		ACC6.TXT		184.38	31.42	
		ACC7.TXT		816.52	17.14	
2.	AI TXT	AI1.TXT	6	628.88	54.44	40.96
		AI2.TXT		1167.64	45.71	
		AI3.TXT		1287.47	29.05	
		AI4.TXT		1763.79	41.57	
		AI5.TXT		1358.62	37.27	
		AI6.TXT		1443.6	37.77	



Sl. No.	Input Folder	Input Text File	No. of Input Texts	Time for Summarization (seconds)	Accuracy of Summarized Text	Average Accuracy
3.	BIO TXT	BIOLOGY1. TXT	5	501.36	75	48.9
		BIOLOGY2. TXT		293.76	75	
		BIOLOGY4. TXT		100.84	32.22	
		BIOLOGY5. TXT		386.33	35	
		BIOLOGY6. TXT		1160.42	27.65	
4.	ECO TXT	ECO1.TXT	8	527.31	60	46.34
		ECO2.TXT		931.48	55.45	
		ECO3.TXT		585.78	68.6	
		ECO4.TXT		299.69	26.67	
		ECO5.TXT		618.78	50	
		ECO6.TXT		507.99	35	
		ECO7.TXT		526.06	35	
		ECO8.TXT		575.26	40	
5.	GEO TXT	GEO1.TXT	6	374.44	55.45	53.68
		GEO2.TXT		1791.71	50	
		GEO3.TXT		491.83	60	
		GEO4.TXT		365.29	55.45	
		GEO5.TXT		1445.95	38.57	
		GEO10.TXT		935.77	62.63	

Conclusion

An Extrinsic Summarization System has been designed and developed, which is able to summarize a set of texts based on term frequency and inter document frequency of the keywords of the text set. It is able to deselect the redundant sentences by detecting the presence of same or almost same set of keywords in the sentence set.

Since the summarization is extrinsic and not intrinsic technique, it might happen that the meaning of two or more sentences are same, but different set of keywords are used. Although this situation is rare in a text, those conceptually same or similar meaning redundant sentences remain undetected thereby slightly degrading the quality of summary. Of course, this drawback is resolved in intrinsic summarization at the cost of complicacy of design.

The time for summarization is affordable. Also the accuracy of the system is acceptable for all practical applications if the

simplicity of the design of the present novel system is considered.

References

- [1] Nalini, K. and Sheela, L. Jaba, "Survey on Text Classification," *International Journal of Innovative Research in Advanced Engineering (IJIRAE)* ISSN: 2349-2163, Vol. 1, Issue 6, (July 2014).
- [2] Alguliev, R.M. and Aliguliyev, R.M., "Effective summarization method of text documents," Proceedings of the 2005 IEEE/WIC/ACM International Conference on Web Intelligence (WI'05), France, pp. 264-271, 19-22 September 2005.
- [3] Salton, G., Singhal, A., Mitra, M. and Buckley, C., "Automatic text structuring and summarization," *Information Processing and Management*, Vol. 33, No. 2, pp. 193-207, 1997.
- [4] Jones, K.S., "Automatic summarizing: the state of the art," *Information Processing and Management*, Vol. 43, No. 6, pp. 1449-1481, 2007.



- [5] Deng, J., Hu, J., Chi, H. and Wu, J., “An Improved Fuzzy Clustering Method for Text Mining”, *Networks Security Wireless Communications and Trusted Computing (NSWCTC)*, 2010 Second International Conference on, Vol. 1, pp. 65–69
- [6] Yan, Y., Chen, L. and Tjhi, W.-C., “Semi-supervised fuzzy co-clustering algorithm for document categorization”, *Knowledge Inf. Syst.* 34, No. 1, pp. 55–74, 2013
- [7] Sarker, G., Dhua, S. and Besra, M. (2015). A Learning Based Handwritten Text Categorization, *2015 International Conference on Advances in Computer Engineering and Applications, (ICACEA–2015)*. ISSN: 978-1-4673-6910-7/15/\$31.00 © 2015 IEEE.
- [8] Sarker, G., Besra, M. and Dhua, S. (2015), A Programming Based Handwritten Text Identification, *2015 International Conference on Advances in Computer Engineering and Applications, (ICACEA–2015)*. ISSN: 978-1-4673-6910-7/15/\$31.00 © 2015 IEEE.
- [9] Sarker, G., Besra, M. and Dhua, S. (2015), A Malsburg Learning BP Network Combination for Handwritten Alpha Numeral Recognition, *2015 International Conference on Advances in Computer Engineering and Applications, (ICACEA–2015)*. ISSN: 978-1-4673-6911-4/15/\$31.00 © 2015 IEEE.
- [10] Sarker, G., Dhua, S. and Besra, M. (2015). A New Fuzzy Categorization Technique for Cursive Handwritten Text with Weight Learning in Attributes – ICIEC16. Jan. 2016.
- [11] Shah, K., Chatterjee, N. and Saha, B., “A New Approach to a Single Pass Optimal Clustering Algorithm in Data Mining”, 2004.
- [12] Sarker, G., “A Heuristic Based Hybrid Clustering for Natural Classification”, *International Journal of Computer, Information Technology and Engineering (IJCITAE)*, Vol. 1, No. 2, pp. 79–86, 2007.
- [13] Sarker, G. and Roy, K., “An RBF Network with Optimal Clustering for Face Identification”, *International Conference on Information & Engineering Science-2013 (ICIES-2013)*.
- [14] Sarker, G., Dhua, S. and Besra, M. (2015). An Optimal Clustering for Fuzzy Categorization of Cursive Handwritten Text with Weight Learning in Textual Attributes, *2015 IEEE 2nd International Conference on Recent Trends in Information Systems (ReTIS – 2015)* held at Jadavpur University Kolkata INDIA 9–11 July, 2015, ISSN: 978-1-4799-8349-0/15/\$31.00 ©2015 IEEE, pp. 6–11.



An Intelligent Home Automation System Using Internet of Things Framework

Arindrajit Pal¹ and Amitava Nag²

Abstract: *The advancement of automation technology, life is getting simpler and easier in all aspects. In today's world automatic systems are being preferred over manual system. The rapid increase of the number of users of internet over the past decade has made internet as an essential part of the life, and the Internet of Things (IoT) is the latest and emerging internet technology. In this paper, we develop a home automation system is developed by using the Raspberry Pi, a microprocessor based on-board computer system. Raspberry Pi has ethernet port and some general input-output pins that can connect different home gadgets through internet. Techniques are being developed techniques to operate it by our smart phone and control the devices. In our work, web-cam is also used for capturing the photos and live streaming and watch it through the smart phone.*

Keywords: Internet of Things (IoT), Raspberry Pi, Home Automation.

Introduction

The Internet of Things (IoT), can be looked as an intelligent network [1] which is equipped with a very large number of smart objects. The 'things' in IoT are smart objects such as home appliances, surveillance cameras, monitoring sensors, displays, etc. that have the ability to collect, store and transfer data over internet without manual assistance [2]. It provides the intelligent services such as locating, tracking, monitoring, and managing things [1], [3]. Nowadays, researchers from both industry and academia are focusing on IoT to make the existing domestic appliances more efficient with the help of local networking or by remote control [4]. This paper aims to design a home automation system based on IoT using Raspberry pi. Raspberry pi is a credit card-sized microprocessor based single-board computer with a Linux operating system [5], [6]. This minicomputer can provide all the services of a normal desktop computer [7]. It is now being widely used for various applications such as home automation, robot, smart parking systems, etc. [8]. In this paper, a mechanism is proposed to develop a smart home automation system that uses Raspberry Pi to enabling easy access and interaction with home appliances.

Implementation of Home Automation Model

Working Principles

In this paper, the authors have developed a system which can help user to operate home appliances from far away from

their home through internet with the help of the smartphones. It also helps the physically challenged or elder persons to live independently in their house. This is one of the important applications of IoT. Because, the normal remote control system can work within a room and bluetooth enabled devices can operate within a few meter range. But, the IoT technology can be used anywhere of the world if Internet is available. The user can operate different home appliances by a smart phone. Several applications can be developed regarding this purpose. The sensors of the home appliances should be connected through the Raspberry Pi kit. In this way the physically challenged or elderly persons can monitor their total house and operate on different devices like fans, lights and several home appliances by sitting on a room. Another objective of this application is to develop a security system and a door sensor notification in our home using webcam surveillance and Raspberry pi together. The user can monitor his house through is smart phone or some monitoring devices also from faraway of his home. In absence of the owner of a house, this security system can help to protect that house from intruder. If any unauthorized person may try to enter his house, the proprietor can get an automatic notification or alarm from his house and watch the live stream pictures of his house in the monitor. To establish this security system, the users has to apply the IoT technology. The webcam surveillance and the door sensors are connected with the Raspberry Pi which is an Internet enable device. This Raspberry pi can transmit data to the user's smart phone and he can notify to the security or police.

¹Department of Computer Science and Engineering, Academy of Technology, Aedconagar, Hooghly, India. ✉ arindrajit@gmail.com

²Department of Information Technology, Academy of Technology, Aedconagar, Hooghly, India.



This technology also helps those persons who live alone in their house. So, the objective of this work is to help the different persons in the society to live better and secure life.

Hardware Components

Raspberry Pi It is a microprocessor based single board computer interface with the android module to perform the automation which is shown as Figure 1(a). It has been developed by the Raspberry Pi Foundation, UK. It receives signals from the smart phone and processes it to perform several tasks. There are in two board configurations of Raspberry Pi: a) Broadcom BCM2835 System on a chip (SoC), which includes an ARM1176JZFS 700 MHz processor, Video Core IV GPU and 256/ 512MB of RAM. There is no built in HDD or solid state drive in it. It uses an SD card for booting and storage purpose. Different switches, door sensors and webcam control systems need to be integrated with the Raspberry Pi. It is easy to install and low cost.

Magnetic Door Sensors: This is a reed switch covered in an ABS plastic shell. They are often used to detect when a door is open or close as shown in Figure 1(b). This is connected with Raspberry pi and notifies the status to the pi.

Wifi Router: This device is attached with the Raspberry pi kit and transmits data to the user's smart phone through Internet as shown in Figure 1(c). It actually communicates with the local server or Internet router.

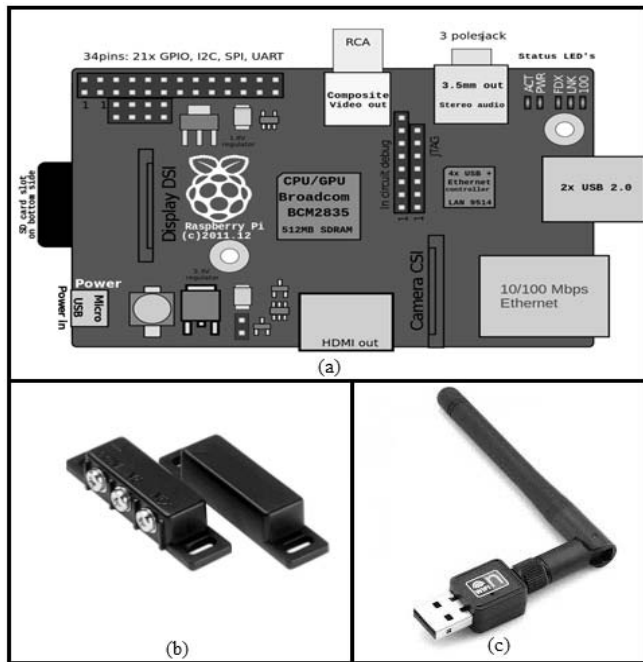


Fig. 1: (a) Raspberry Pi Model B (b) Magnetic Door Sensors (c) WiFi Router

PiCam/Surveillance Camera: It is a high resolution video camera that streams the images in real time and transfer to users monitoring device as shown in Figure 2(a). It is also possible to save the images to the storage unit or clouds. This device can attach with Raspberry Pi through the USB port.

HDMI Monitor This device is used for monitoring the live stream from the surveillance camera as shown in Figure 2(b). It can directly attach with Raspberry Pi through the HDMI port and display the live stream from the surveillance camera.

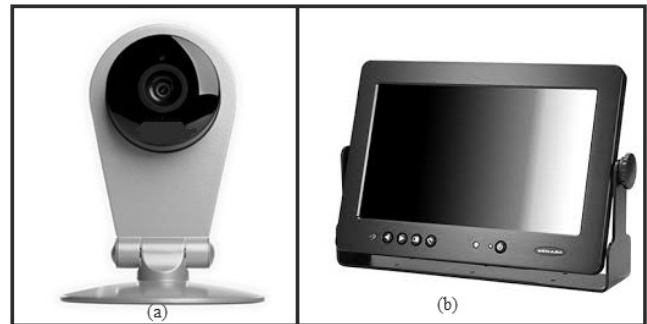


Fig. 2: (a) Surveillance Camera (b) HDMI Monitor

Software Requirements:

1. OS-Rasbian Jesse (version- 4.4)
2. PHP
3. Python 3.0
4. HTML/CSS/JavaScript
5. MJPEG Streamer
6. ngrok.io and pagekite.py for port tunneling.

Proposed System

After preparing the template, now all the development work is integrated to make a complete interface. The user display and the controls are managed by the python code. There are different software packages which provide various views to control. The lights and sensors are connected to the Raspberry Pi. The server and client applications are written in Python to the interface for Raspberry Pi. The application software produces the built in functions as well as user defined methods to the smart phone. An android application can be developed using the Android Developer Tools to run the programs on mobile devices that communicates between pi and home appliances easily.

The operational overview of the proposed work is in Figure 3. Here, the system is divided in two parts namely server side and client side. Server side consists of ON/OFF switches and live-feed button and user interface that allow us to turn ON/OFF a device and to see the live feed also. This is normally the devices used by the user like smart phone,

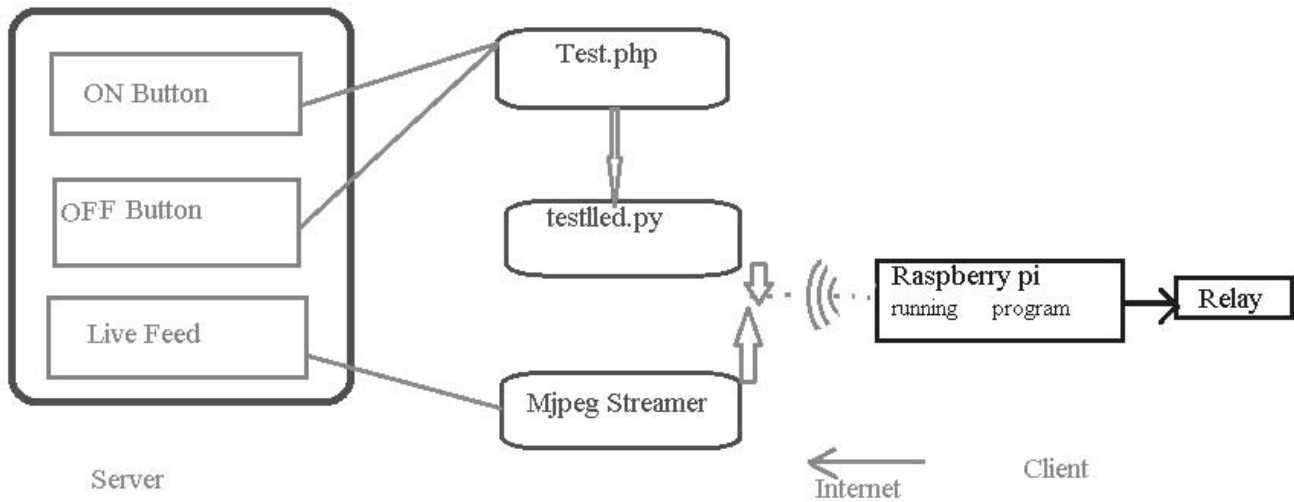


Fig. 3: Operational View of the System

computer etc. It consists of PHP and HTML files and Python modules. The client side has the Raspberry Pi module which consists of relay circuit connected with GPIO pins. In the client side, all the switches, home appliances and routers are connected with the pi. The pi runs a python program for each ON/OFF button. In case of live feed we use picam. Whenever the live feed switch is ON, the Mjpeg Streamer performs the streaming. In Figure 4, the user interface (UI) consists of four switches which are synchronized with each other and a button which gives the live stream. This UI is present in the user's smart phone. User can control the different switches which are connected to the lights or gadgets of his home by this UI. ON/OFF states show the current status of the switches. Figure 5 shows the security system of the house, where the Surveillance camera and sensors are attached to the Raspberry Pi. This security system involves the notification to the smart phone through the Internet and also the live stream to the users monitoring devices.

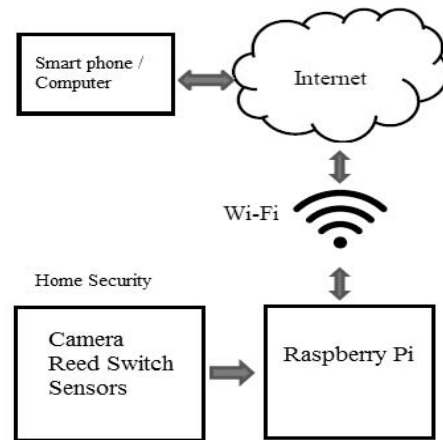


Fig. 5: Security Module Using Surveillance Camera and Sensors

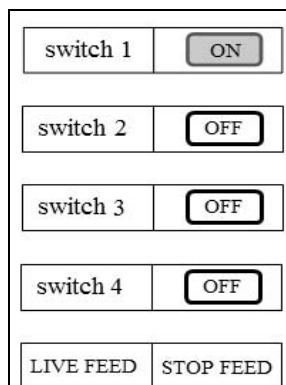


Fig. 4: User Interface in Smart Phone

Conclusion

IoT is an emerging technology in modern science. In present days, internet can be accessed by the common people with a reasonable cost. The people can also access internet through different pocket devices which are not so costly. So, they are trying to live a better comfortable and secure life using these gadgets. So, day-to-day different technologies are invented to serve the societies requirement. The IoT may enhance a new potential by enabling communications between objects and human, making a smarter and intelligent planet. This proposed work can build up easily by using some small devices like Raspberry Pi, few sensors, relays, modules etc. This work can help the user to control the switches, gadgets by his smart phone through the internet. It also helps the disable or older persons to live independently. Our future work is to develop a new technology where the home



automation can be controlled by artificial intelligence system and reduces the human activities.

References

- [1] Moness, Mohammed and Moustafa, Ahmed Mahmoud, "A Survey of Cyber-Physical Advances and Challenges of Wind Energy Conversion Systems: Prospects for Internet of Energy", *Internet of Things Journal IEEE*, Vol. 3, pp. 134–145, 2016.
- [2] Zanella, A., Bui, N., Castellani, A., Vangelista, L. and Zorzi, M., "Internet of Things for Smart Cities," in *IEEE Internet of Things Journal*, Vol. 1, No. 1, pp. 22-32, Feb. 2014.
- [3] Stankovic, J.A., "Research directions for the Internet of Things," *IEEE Internet Things J.*, Vol. 1, No. 1, pp. 3–9, Feb. 2014.
- [4] Gubbi, J., Buyya, R., Marusic, S. and Palaniswami, M., Internet of Things (IoT): A vision, architectural elements, and future directions, *Future Generation Computer Systems.*, Vol.29, No. 7, pp. 1645–1660, Sep. 2013.
- [5] Jain, S., Vaibhav, A. and Goyal, L., "Raspberry Pi based interactive home automation system through E-mail," *Optimization, Reliability, and Information Technology (ICROIT)*, 2014 International Conference on, Faridabad, 2014, pp. 277–280.
- [6] Banerjee, S., Sethia, D., Mittal, T., Arora, U. and Chauhan, A., "Secure sensor node with Raspberry Pi," *Multimedia, Signal Processing and Communication Technologies (IMPACT)*, 2013 International Conference on, Aligarh, 2013, pp. 26–30.
- [7] Raspberry Pi Foundation, Raspberry Pi, [Online]. Available: <https://www.raspberrypi.org>. [Accessed: 30-Apr-2016].
- [8] Gomez, C. and Paradells, J., Wireless homeautomation networks: A survey of architectures and technologies, *IEEE Commun. Mag.*, Vol.48, No. 6, pp. 92–101, Jun. 2010.



Statistical Relevance of Sweat on Bloodstain Pattern Documented on Linen Surface

Nabanita Basu¹

Abstract: Bloodstain patterns are considered as static evidence of dynamic consequences that had occurred at a crime scene. Stain patterns are used in coherence with other circumstantial evidence for reconstruction of crime scene. As compared to non-absorbant, non-porous, smooth surface stains on fabric surfaces are difficult to interpret. Sweat is a natural reaction to human fear and anxiety. The effect of sweat on fabric surface and its effect on the stain pattern formed still remains undocumented within the scientific community. Again, experiments in relation to sweat are difficult to re-create owing to the large variability in sweat composition of different individuals owing to the varied food habits and environmental conditions in which individuals survive. In this work artificial acidic sweat was simulated using industrial standard ISO 3160:2. Experiments show that linen fabric wetted with sweat or hence dried statistically significantly ($p < 0.001$) affect stain patterns form on 100% linen fabric. For the particular sweat composition regular stains almost resembling regular stains were obtained at different angle of impact and fall height, when after being soaked in sweat the fabric was natural air dried before staining.

Keywords: Bloodstain Pattern, Linen, ISO 3160: 2, Sweat, Group Comparison.

Introduction

Bloodstain pattern analysis deals with reconstruction, sequencing of events that had occurred at a crime scene based on bloodstain patterns. Bloodstain patterns are static consequences of dynamic events that had occurred at a crime scene. Fluid mechanics provides the fundamental basis for predictions made from bloodstain patterns [1]. Forces like adhesion, cohesion, gravitation, surface tension and capillary action control the characteristic flow of the pseudo-plastic non-Newtonian fluid blood [1].

Unlike fingerprints, bloodstain patterns are reconstructive evidence. While stain patterns formed on non-porous/non-absorbent, plain, smooth target surface are easier to analyze and interpret (eg. paper), such is not the case with stain patterns formed on porous/absorbent, rough surfaces (e.g. fabric). Stains formed on non-porous/non-absorbent, plain, smooth target surface are mostly regular stains while stains formed as a result of similar physical mechanism on porous/absorbent, rough surface are irregular.

Research undertaken elucidates that sweat glands are stimulated in response to high temperature, exercise, hormone secretion and emotional stress [2, 3]. Again, sweat and threat perception have a complicated relationship [2]. When threatened, intuitively an individual makes a choice of

‘flight’ or ‘fight’. Sweating helps an individual prepare and hence sustain either of the two scenarios, ‘fight’ or ‘flight’ [2].

This research work is aimed to analyze how sweat affects the formation of stain on cloth surface particularly in the case of 70 Lea and 100% Linen shirting fabric. Often it is considered that experiments conducted with sweat in laboratory’s pertaining to different geographical zones are difficult to re-create owing to the fact that sweat composition of different individuals vary. Food habit and environmental conditions that the person is exposed to largely affect the composition of his/her sweat. This variance is also evident in the artificial sweat composition used in the commercial/industrial sector. The artificial sweat used for testing metal corrosion in Japan varies in composition from the Deutsch, International standard. To encompass this variation the experiment designed consists of artificial sweat simulation as per 12 industrial artificial sweat simulation standards.

This paper is only a brief excerpt of the research work undertaken to analyze the effect of sweat on the bloodstains recorded on fabric surface.

Literature Review

Crime scene reconstruction is particularly dependent on the analysis and interpretation of reconstructive evidence in

¹Department of Computer Science & Engineering, University of Calcutta, India. ✉ nabs.basu@gmail.com



coherence with other circumstantial evidence. Bevel and Gardener provide an extensive description of the science that governs the study/interpretation of bloodstain patterns in the reconstruction of crime scene [1]. Daniel Attinger elaborately reviewed the different theories of fluid mechanics that govern blood flow dynamics [4].

In relation to the study of bloodstain patterns on fabric, of particular relevance is the work of White [5] and Slemko [6]. White in his work highlighted that estimation of angle of impact from fabric stain was particularly misleading [5]. The fact that stains formed on new cloth were particularly different from stains formed on worn out cloth was emphasized by Slemko in his work [6]. By use of different types of fabrics Slemko analyzed the effect of velocity, relative distance and chemically treated fabric target surface on the pattern of stains on fabric [6]. Miles *et al.* in their work documented the effect of surface roughness and fall height on the number of satellites formed for a stain recorded on fabric surface [7]. Prior laundering of fabric, fiber content and fabric structure particularly affect the formation of stain pattern on fabric [7]. Castro TC *et al.* identified a significant increase in the stain size on laundered blend fabric [8, 9]. Dicken *et al.* used a micro computed tomography scanner to study bloodstain size and shape throughout fabrics [10]. The study identified impact velocity and fabric structure as important factors that affected bloodstain morphology on fabric [10]. Castro TC *et al.* also identified the age of the fabric as an important parameter that affected the stain pattern on fabric [11].

Though substantial work has been undertaken in understanding the effect of fabric texture, impact velocity, fabric type, laundry wash on the morphology of bloodstain pattern formed on fabric, the impact of human sweat on the stain pattern formed stands particularly unexplored. This work is intended to bridge this particular gap.

Experimental Design

In order to study the effect of sweat on stain patterns on fabric, certain hypotheses were generated. The experiments were designed to examine the validity of the hypotheses based on statistical methods. The hypotheses are:

- H1: Stain patterns recorded on paper surface are distinctly different from the stain patterns developed on new 100% Linen shirting fabric under identical physical mechanisms.
- H2: Stains patterns recorded on new cloth, cloth soaked in sweat and hence dried, cloth wetted with sweat vary even when all the passive drops were formed by the same mechanism and similar atmospheric conditions.

At the very onset, porcine blood was used to recreate stain patterns. This is because porcine blood closely resembles

human blood rheology [12]. Table 1 provides a summary of the properties of porcine blood that was used in the experiments [13].

Table 1: Intra Variability in Porcine Blood that was used in the Experiments [13]

Porcine Blood	Before the Experiment [Blood at 37°C and 60% Humidity]
Age since collection from a pig	1-day-old
PCV	0.39 ± 0.01
Density, ×10 ³ kg/m ³	1.069 ± 0.022
Surface tension, mN/m	62.47 ± 0.71
Whole blood viscosity, mN-s/m ²	4.001 ± 0.008
Plasma viscosity, mN-s/m ²	1.482 ± 0.003

Blood being a non-Newtonian fluid, the environmental conditions as also the temperature of blood at the time of experiment are important parameters that need to be controlled for the experimental setup. Table 2 represents the environmental conditions as also the controlled experiment conditions that were maintained across the lifetime of each experiment.

Table 2: Record of the Atmospheric Conditions and Conditions within the Laboratory at the Time of Experimentation [13]

Atmospheric Conditions	
LABORATORY SETTING	
Temperature	37° C
Humidity	60 %
Wind Condition	Not windy
ENVIRONMENTAL CONDITION (outside the Laboratory)	
Dry Temperature	23°C (approx.)
Wet Temperature	26°C (approx.)
Relative Humidity	77–78% (approx.)
Wind Condition	Not windy
Blood Temperature	37° C

Passive drip stains in particular are bloodstains formed on a target surface as a result of dripping of blood under the action of gravity. As part of the experimental setup, blood was allowed to drip under the action of gravity at varying angle of impact and fall height from a 2.5 ml. subcutaneous syringe without needle. A syringe was used for blood dripping in order to maintain parity in volume of blood flow out. The volume of each blood drop emanated from the syringe was calculated. Table 3 records the different



combinations of angle of impact and fall height used in the study along with the volume of each blood drop from the syringe that fell through under the action of gravity.

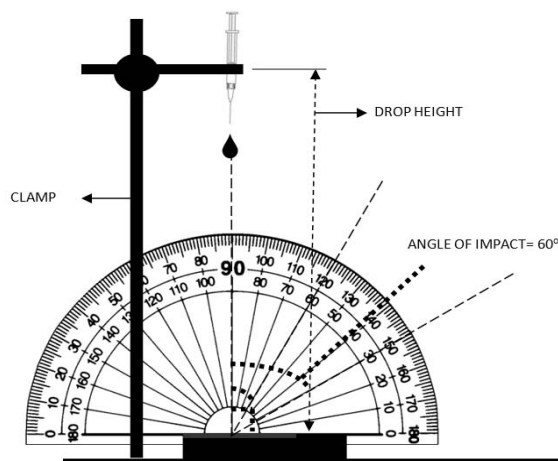


Fig. 1: Experimental setup for creating stain patterns at different angles of impact and fall height. The dotted lines along 30° and 60° represent the position of the target surface for an impact angle of 60° and 30° respectively [13].

Figure 1 represents the experimental setup for a paper target surface. For fabric target surface, same tensile strength of the

target surface was ensured by fixing the target surface on an embroidery frame. This was done to avoid bounce, crease on the target surface and hence make the stain patterns on the target surface comparable.

Linen Shirting cloth (100% Linen, 70 Lea) was cut out into 30.48 cm by 30.48 cm (1 ft by 1 ft) pieces for recording each stain pattern. Three sets of target surface were created. Group 1 consisted of new 100% Linen shirting fabric (70 Lea) cut out into 30.48 cm by 30.48 cm (1 ft by 1 ft) pieces. The different combinations of angle of impact and fall height (refer Table 3) were used to record stain patterns on new 70 Lea 100% Linen shirting fabric. Again the same array of angle of impact and fall height combinations were used to record stains on Group 2, 30.48 cm by 30.48 cm (1 ft by 1 ft) pieces of cloth each of which was uniformly soaked in 100 ml. of artificial sweat simulated as per ISO-3160:2 standard for 20 min and hence air dried. Each 70 lea Linen shirting cloth piece was dried in natural air condition. Group 3 consisted of 30.48 cm by 30.48 cm (1 ft by 1 ft) 100% Linen shirting fabric each of which was uniformly soaked in 100 ml. of artificial sweat simulated as per ISO-3160: 2 for 20 min and dried to a point where the cloth doesn't drip unless twisted and turned. The pieces of fabric that were part of Group 3 were stained as per the angle of impact and fall height combinations in Table 3.

Table 3: Angle of Impact and Fall Height Combination for Dripping of Blood for Control, Group 1, Group 2 and Group 3 Target Surface

Target surface on which stain was recorded	Angle of Impact and Fall Height Combination and the number of stains created for each combination			Target surface on which stain was recorded	Angle of Impact and Fall Height Combination and the number of stains created for each combination				
Paper [Control]	30°	20 cm	1	New 100% Linen shirting fabric soaked for 20 min in 100 ml artificial sweat simulated as per ISO 3160:2 standard and natural air dried (Group 2)[9 pieces each of size 1 by 1 ft ²]	30°	20 cm	1		
		40 cm	1			40 cm	1		
		60 cm	1			60 cm	1		
	60°	20 cm	1		60°	20 cm	1		
		40 cm	1			40 cm	1		
		60 cm	1			60 cm	1		
	90°	20 cm	1		90°	20 cm	1		
		40 cm	1			40 cm	1		
		60 cm	1			60 cm	1		
	New 100 % Linen shirting fabric (Group 1)[9 pieces each of size 1 by 1 ft ²]	30°	20 cm		1	New 100% Linen shirting fabric soaked for 20 min in 100 ml artificial sweat simulated as per ISO 3160:2 standard. The cloth is wet to the point that it does not drip (Group 3)[9 pieces each of size 1 by 1 ft ²]	30°	20 cm	1
			40 cm		1			40 cm	1
			60 cm		1			60 cm	1
60°		20 cm	1	60°	20 cm		1		
		40 cm	1		40 cm		1		
		60 cm	1		60 cm		1		
90°		20 cm	1	90°	20 cm		1		
		40 cm	1		40 cm		1		
		60 cm	1		60 cm		1		
Total Number of Stains Formed – 36 stains [Volume of each Blood drop: 0.04 ml]									



Bloodstain patterns can particularly classified into two groups, namely, Regular and Irregular stains. Regular stains abide by a geometric shape while Irregular stains do not. For regular stains, the best fitting ellipse to a regular stain is estimated and the major and minor axis values for the ellipse are referred to as the length and breadth of a particular stain. For a regular stain, the angle of impact is calculated as $\sin^{-1}(\text{Breadth}/\text{Length})$ (refer Figure 2). However, for an irregular stain the angle of impact cannot be estimated (refer Figure 3).

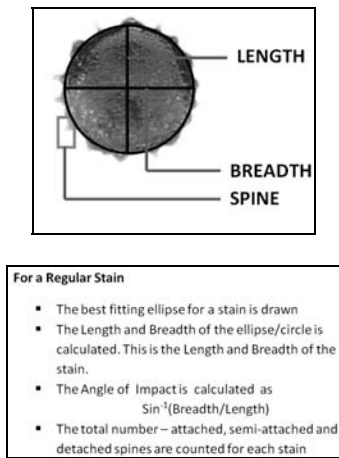


Fig. 2: Graphical Representation of the Accepted Methodology for Calculating the Length, Breadth and Angle of Impact for a Regular Passive Drip Stain. [13]

On similar lines, the length and breadth of the parent stain formed on paper and new 100% Linen shirting fabric (70 Lea) (Group 1) using the same physical mechanism (i.e. environmental conditions, temperature of blood, syringe, combinations of fall height and angle of impact) were calculated. The length and breadth of stains formed on Group 2 and Group 3 fabrics were measured manually and with a computer based program.

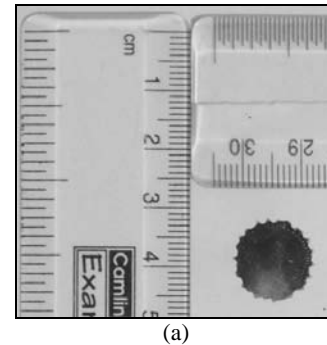


Fig. 3: An irregular stain (i.e. a stain in which an ellipse cannot be fitted) formed on new 100% Linen shirting fabric at an angle of impact 90° and a fall height of 20 cm due to passive dripping of blood from a 2.5 ml. subcutaneous syringe without needle.

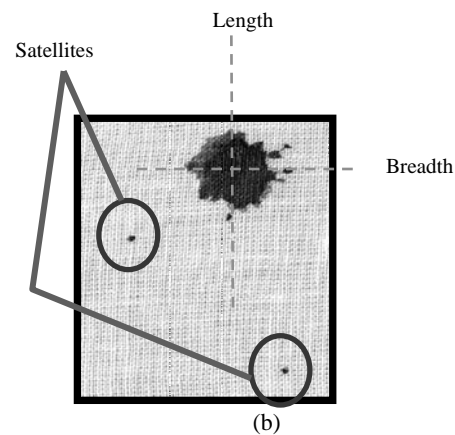
Statistical tests were performed to compare stains on paper to the stains formed on fabrics in Group 1. Statistical tests were performed to compare stains formed on fabrics in Group 1, Group 2 and 3 respectively.

Results and Discussion

Given that the length and breadth value for the stains is not normally distributed, Mann-Whitney U test was performed to compare whether the stain patterns on paper and fabric are similar or part of the same population or not. The p value for the length and breadth parameter of the 18 stains (9 stains on paper and 9 on fabric) being less than $0.001 (< 0.001)$ revealed that there is statistically significant difference between the stains formed on paper and those formed on 100% Linen target surface and it is unlikely that such a difference was merely by chance. While Figure 4a provides the stains formed on paper at 90° angle of impact and 60 cm fall height, Figure 4b provides the stains formed on 100% new linen fabric at the same angle of impact and fall height when emanated from a subcutaneous syringe without needle.



(a)



(b)

Fig. 4: (a) Stain formed on paper at 90° angle of impact and 60 cm fall height. Length of stain – 1.1 cm, Breadth of stain – 1.1 cm, Number of satellites – 0, [13] (b) Stain formed on new 100% Linen shirting fabric at 90° angle of impact and 60 cm fall height, Length – 1.0 cm, Breadth-0.9 cm, No. of satellites – 2.



Owing to the non-normal distribution of the length and breadth values for the stains formed on Group 1, Group 2 and Group 3 fabrics [14], Kruskal Wallis test [15] was performed to compare the stain patterns formed on fabrics belonging to the 3 groups. The Kruskal Wallis Test [15] revealed that there is a statistically significant difference between stain patterns formed on fabrics in Group 1 and those formed on Group 2 and 3 respectively in terms of stain length ($p < 0.001$) and breadth ($p < 0.001$) parameters. The outcome of the Kruskal Wallis test [15] revealed that a statistically significant difference exists between the stains formed on Group 1 fabrics, Group 2 fabrics and Group 3 fabrics in terms of stain length ($p < 0.001$) and breadth ($p < 0.001$) parameters (refer Figure 5).

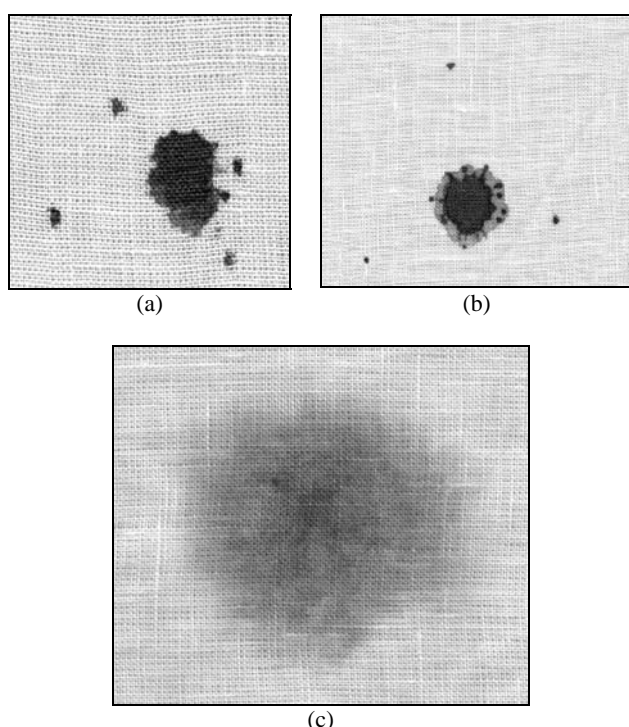


Fig. 5: Bloodstains created at 90° angle of impact and 40 cm fall/drop height (a) target surface- new 100% Linen shirting fabric [part of Group 1] (Length- 1 cm, Breadth-0.9 cm) (b) target surface – new 100% Linen shirting fabric soaked for 20 min in artificial sweat simulated as per ISO 3160: 2 standard and air dried (Length-0.9 cm, Breadth-0.9 cm, Regular stain) [part of Group 2], (c) target surface – new 100% Linen shirting fabric soaked for 20 min in artificial sweat simulated as per ISO 3160: 2 standard and left wet at the time of staining (Length -3.5 cm, Breadth-3.4 cm) [Part of Group 3].

Conclusion

In a crime scene, it is often difficult to interpret bloodstains on fabric. This has been identified and well documented by White in his work. In coherence with Slemko and White's

findings, this work statistically emphasizes the difference in the stain patterns formed on new 100% Linen shirting fabric against a paper control surface. Additionally, the effect of sweat on stain pattern was analyzed in this work. Human sweat was artificially simulated as per ISO 3160: 2 standard. When uniformly soaked and air dried, the stains formed on the same fabric under similar physical conditions were significantly different from the stains formed on the new fabric. Again, stain morphology on cloth soaked in sweat significantly differed from stains formed on new fabric and stains formed on air dried sweat wetted fabric. Only acidic sweat was considered in this particular experiment.

As has been previously mentioned, the composition of sweat varies widely. To overcome this drawback, different standard for artificial sweat simulation shall be used in due course of the research work to analyze the effect of human sweat on bloodstain pattern in fabric. Sweat being a common involuntary reaction to anxiety/fear, this work is focused to provide a deeper understanding on the role of human sweat on bloodstain morphology within a real life scenario.

References

- [1] Bevel, T. and Gardner, R.M. Bloodstain pattern analysis: With an introduction to crime scene reconstruction (3rd ed.), (2002).
- [2] Wilke, K., Martin, A., Terstegen, L. and Biel, S.S. (June 2007). "A short history of sweat gland biology" (pdf). *International Journal of Cosmetic Science*. 29 (3): 169–179. doi:10.1111/j.1467-2494.2007.00387.x. ISSN 1468-2494.
- [3] Folk Jr, G. Edgar and Semken Jr, A. (1 September 1991). "The evolution of sweat glands". *International Journal of Biometeorology*, 35 (3): 180–186. doi: 10.1007/BF01049065. ISSN 0020-7128. Retrieved 18 December 2012.
- [4] Attinger, D., Moore, C.B., Donaldson, A. and Jafari, A.(2013). "Fluid dynamics topics in bloodstain pattern analysis: Comparative review and research opportunities", *Forensic Science International*.
- [5] White, B. (January, 1986), "Bloodstain Patterns on Fabrics: The Effect of Drop Volume, Dropping Height and Impact Angle", *Journal of the Canadian Society of Forensic Science* 19(1): 3–36.
- [6] Slemko, J.A. (December 2003), "BLOODSTAINS ON FABRIC The Effects of Droplet Velocity and Fabric Composition", IABPA News, Retrieved from www.bloodspatter.com/uploads/files/December2003News.pdf
- [7] Miles, H.F., Morgan, R.M. and Millington, J.E. (July 2014). "The influence of fabric surface characteristics on satellite bloodstain morphology", *Science and Justice* 54(4): 262–266.
- [8] de Castro, T.C., Taylor, M.C., Kieser, J.A., Carr, D.J. and Duncan, W., (May, 2015) "Systematic investigation of drip stains on apparel fabrics: The effects of prior-laundrying, fibre content and fabric structure on final stain appearance", *Forensic Science International* 250: 98–109, doi: <http://dx.doi.org/10.1016/j.forsciint.2015.03.004>.



- [9] de Castro, T.C., Nickson, T., Carr, D. and Knock, C. (Jan, 2013). "Interpreting the formation of bloodstains on selected apparel fabrics." *International Journal of Legal Medicine* 127(1): 251–8, doi: 10.1007/s00414-012-0717-3.
- [10] Dicken, L., Knock, C., Beckett, S., de Castro, T.C., Nickson, T. and Carr, D.J. (Dec, 2015). "The use of micro computed tomography to ascertain the morphology of bloodstains on fabric.", *Forensic Science International* 257:369-75. doi: 10.1016/j.forsciint.2015.10.006.
- [11] de Castro, T.C., Carr, D.J., Taylor, M.C., Kieser, J.A. and Duncan, W. (Sep, 2016), "Drip bloodstain appearance on inclined apparel fabrics: Effect of prior-laundrying, fibre content and fabric structure", *Forensic Science International* 266: 488–501. doi: 10.1016/j.forsciint.2016.07.008.
- [12] Raymond, M.A., Smith, E.R. and Liesegang, J. (Jul.–Sep, 1996), "The physical properties of blood-forensic considerations", *Science & Justice* 36(3):153–60, doi: 10.1016/S1355-0306(96)72590-X.
- [13] Basu, N. and Bandyopadhyay, S.K. (Sep, 2016), "Initial data release of regular blood drip stain created by varying fall height, angle of impact and source dimension", *Data in Brief*, 8:1194-1205, doi: 10.1016/j.dib.2016.07.003.
- [14] Shapiro, S.S. and Wilk, M.B., An analysis of variance test for normality (complete samples), *Biometrika* 52 (3–4): 591–611. doi:10.1093/biomet/52.3-4.591. JSTOR 2333709. MR 205384. p. 593 (1965).
- [15] Kruskal, W.H. and Wallis, W.A., Use of Ranks in One Criterion Variance Analysis, *Journal of American Statistical Association*, 47(260): 583–621 doi: 10.1080/01621459.1952.10483441 (1952).



Color-Based Segmentation of Thin Blood Smear Image to Detect Malaria Parasite using Unsupervised Clustering

Sanjay Nag^{*1} and Nabanita Basu¹

Abstract: Malaria is a life-threatening vector-borne parasitic disease. Most often the disease is curable with early detection and proper diagnosis but the disease management often fails and gets out of control with increased number of reported cases within a short period of time resulting in mortality. The 'gold standard' for Malaria diagnosis is the detection of the parasite with a conventional light microscope and blood smear slide stained with giemsa stain. The accuracy is lower due to inter-operator/intra-operator variability as a major drawback. The contemporary digital microscope and the ability to capture image led to the development of CAD software for malaria detection and diagnosis. This research work has proposed a method for cellular segmentation and image analysis using modern 'machine learning based CAD systems'. Unsupervised K-Means clustering has been utilized to perform image segmentation using Lab colour model to represent the image. The image dataset used for experimentation is obtained from MaMic database. In total, a set of 300 images were used for the study. The images were pre-processed prior to segmentation. Statistical analysis was performed on the segmented images to determine the efficacy of the proposed method.

Keywords: Malaria, RBC, Clustering, Segmentation, Unsupervised Learning.

Introduction

Malaria is a life-threatening vector-borne parasitic disease, caused by the protozoan parasites of Genus Plasmodium and is transmitted through the bite of female Anopheles mosquito. Tropical countries in Africa and Asia are mostly affected by the disease though it is also known to cause disease in Mediterranean countries and temperate regions of the world. Most of the known species of Plasmodium that infect humans are relatively less harmful causing extensive suffering to the infected patient but is mostly curable with early detection and proper diagnosis. Mortality is caused due to the infection of the virulent species and/or late detection and to children below the age of five years. Moreover, the disease management often fails and gets out of control with increased number of reported cases within a short period of time. Due to lack of adequate healthcare infrastructure it often results in a serious medical issue with increased mortality rate in underdeveloped nations. This disease got its name 'Malaria' in 1740 meaning 'bad air' in Italian. During that time it was often referred to as 'Roman Fever' and was a key cause of battlefield mortality. The disease originated in Africa and then propagated to Mediterranean Europe, South East Asia, and India. Ancient Indian medical manuscripts of 800 BC by the

Indian sage Dhanvantari, Charaka Samhita written in 300 BC and Susrut Samhita written in 100 BC mentioned about the Malaria-like disease. In modern day medicine history, Sir Ronald Ross (1902), working in India, received Nobel Prize for demonstrating the lifecycle of Malaria parasite.

The malaria parasites belong to Genus Plasmodium and are characterized by the presence of two hosts in the lifecycle with Schizogony (asexual cycle) in humans and Sporogony (sexual cycle) in female Anopheles mosquito gut. There are 5 different species that cause Malaria infection to Human beings, namely, *P. malariae*, *P. vivax*, *P. falciparum*, *P. ovale* and *P. knowlesi*. The parasite infects the human system as Sporozoite which is a minute thread-like protozoon. It then migrates to the liver cells where they multiply and are released into the blood stream. Early infection to Red Blood Cells (RBC) in the form of ring Trophozoites which mature to form Schizonts, that ruptures to release Merozoites and the cycle is repeated. Male and female Gametocyte formation within RBC can also be observed from microscopic images. Further sexual lifecycle is completed within an infected mosquito after a blood sucking event from an infected human host.

Malaria disease management is a global challenge. The World Health Organization (WHO) have taken up this

¹Department of Computer Science & Engineering, University of Calcutta, India. ✉* sanjaynag75@gmail.com



challenge of complete eradication of the disease by the year 2020. It has allocated funds for infrastructure development in underdeveloped countries to effectively fight against the disease. It has heavily invested on eradication of mosquito breeding grounds and preventive measures against mosquito bites in Asian and African continents. However, Malaria still affects 40% of the world's population in more than 100 countries. About 500 million gets malaria infections annually, causing 1–2 million deaths, mostly children in sub-Saharan Africa [1]. Malaria still remains the cause of death and morbidity in tropical and sub-tropical regions with 1–2 million mortality per year [2]. The World Malaria report of 2015 [3] contains data taken from 95 countries that in total reported an approximate 214 million infections worldwide in 2015. An approximate of 438,000 mortality was reported worldwide.

The clinical diagnosis of malaria is performed by a medical practitioner but for the confirmation of the disease laboratory diagnosis of malaria includes the preparation of thick and thin smear slides for the purpose of microscopic examination. Such laboratory tests require experienced technicians. A major drawback of this popular methodology is the identification of parasite at a low level of infection. This methodology of using conventional light microscopy and blood smear slide stained with Giemsa still remains the 'gold standard' for Malaria diagnosis. The accuracy of detection is heavily dependent on the pathologists with inter-operator/intra-operator variability as a major drawback [4]. Several contemporary methods have gained popularity like the use of the rapid diagnostic test (RDT) kits for quickly detecting malaria. They are based on identifying specific antigens proteins produced during parasite and immunological response interaction that happens during the parasitic invasion of the body. However, the reliability of such methods are not always accurate and availability of kits is also a major issue. Modern equipment based on polymerase chain reaction (PCR) that can amplify trace amounts of parasitic DNA, the use of Flow Cytometer device for cell sorting and the use of Mass spectrometry to identify parasitic hemozoin are highly accurate methods for diagnosis. However, they are costly and often impractical for implementation in rural/under-developed regions of the world.

Advanced microscopy technology combined with the use of built-in LED lighting systems with an array of light filters and fluorescent light has transformed the conventional device. The combination of a digital camera fitted with the microscope system and connecting them with a computer system using firmware have led to recording of digital images directly from slide. The images captured by an untrained technician can be archived and remotely shared for analysis by an expert pathologist for diagnosis. Furthermore, image processing algorithms can be developed to create a fully automated intelligent system that will be able to

perform detection and identification of parasites. The development of CAD software for malaria detection and diagnosis is one of many such applications of digital microscopy and contributing towards the era of Digital Pathology. A CAD system will be able to assist pathologists in identifying Malaria infections from slide images. The system will be able to scan the slide and capture images at regular interval. The algorithms will identify possible problem areas as suspected regions for confirmation by pathologists, thus saving valuable time and effort.

This research work intends to propose a method for cellular segmentation and image analysis using 'machine learning based unsupervised learning systems'. A digitized slide image is used as a source for performing image analysis using image processing techniques to obtain image segmentation. The outcome in the form of the segmented image will be further processed by intelligent algorithms to train the system so that the system will derive its own rules to classify the image accordingly.

Literature Review

Advancement in computer technology and subsequent development of new tools to assist medical practitioners, diagnosis process, and disease management play an important role in the fight against Malaria. While research in medical and pharmaceutical domain approach the problem by discovering new products and means to control the disease, intelligent CAD tools will enhance medical infrastructure and ease of diagnosis. A large amount of research work has contributed towards the development of CAD based systems to detect Malaria parasites from blood smear slide image. There are substantial research work that utilizes simple Image Processing algorithms for identifying the malaria parasite from thin smear digitized slide image. While other research work utilizes Machine Learning Technique to segment the image into the cellular component and classify them as normal or infected. Such literature has utilized different feature set to achieve segmentation and classification. The various feature set includes texture-based, geometric and intensity-based features extracted from different colour space like RGB, HSV, and lab colour model.

Some key contributions using simple image processing algorithms are the authors Sio *et al.* [5] proposed 'Malaria Count' an automated software for Parasitaemia estimation using Adaptive Histogram equalization and edge extraction. Edge contours were linked and cell clumping was removed. The paper [6] by Freaan used an open-source ImageJ software [7] on images to estimate Parasitaemia over manual counting as preliminary automation of manual counting. Another notable work by Zheng [8] using a colour mask developed with the 'V' component of HSV colour model and Otsu binarization. The edges were obtained using Canny Edge



detector and finally matching the cell contours with circular rings to establish infected cells. The authors Somasekar *et al.* [9] proposed an intensity based morphological operations to identify infected cells. The citation performed morphological erosion operation to isolate infected cells and achieved sensitivity and specificity value of 94.87% and 97.3%. The research citation by Ghosh *et al.* [10], enhanced the image and used a Laplacian gradient operator to sharpen the edges. Then the authors performed image binarization with empirical thresholding value and morphological operations to achieve an accuracy of 98.125%. Another cell segmentation method was proposed by Ruberto *et al.* [11], using 'Morphological Area Granulometry' on images in HSV colour model to suppress White Blood Cells (WBC) and cell clumping. The classification was done after the process of 'skeletonization' using erosion operation. Chakraborty *et al.* [12] used thick smear slide images to detect the presence of parasite infected RBC. Zack thresholding method was applied to obtain a binary image using HSV model and infected RBC was differentiated using porosity value given by Euler number. A similar method used by Arco *et al.* in the research citation [13] using CLAHE for contrast enhancement, morphological operations for hole filling and parasite enumeration with system achieving an accuracy of 96.46%.

The use of rule-based system showed that the accuracy fell when the system was used with a different dataset as most of them relied on thresholding values and intensity/ colour based rule systems. Substantial research work has been proposed using Machine Learning based techniques to overcome the limitations of the rule-based systems. Some notable works belong to Diaz *et al.* [14], proposed a Parasitaemia estimation method using a luminance-corrected image in RGB colour model and k-NN classifier that labeled each pixel belonging to erythrocyte or background pixel. The authors partitioned the image into blocks and extracted texture, colour and statistical features. The authors then performed a two-stage classification system to differentiate healthy/ abnormal RBC. The infected cells were trained with four learning models each for three different stages of infection and another for the artifact. The authors implemented a Multilayered Perceptron Model (MLP) and Support Vector Machine (SVM) for classification. The SVM classifier achieved a sensitivity of 94% and a specificity of 99.7% in parasite detection.

Similarly, Tek *et al.* [15] proposed a new parasite detection algorithm that modified K-nearest neighbor classifier and validated the performance using a Bayesian method. The authors further performed classification for detection, stage of life cycle and type of infection using a single multi-class classifier. The authors used image processing methods to segment the image followed by Area Granulometry to

generate morphological features. A multi-class k-NN classifier was used with 83 features set with city block distance metrics for distance calculation was used by the authors. The authors performed a 20-class (detection, species, and stage), 16-class (species and stage) and 4-class species and 4-class stage classification. Cross Validation was performed using hold-out and leave-one-out cross-validation methods. For evaluation of the method, Fisher linear discriminant (FLD) and the back-propagation neural network (BPNN) was implemented. The results of the proposed model showed accuracy of 93.3%, sensitivity of 72.4% and specificity of 97.6%.

The authors [16] calculated Parasitaemia using colour, geometrical and statistical feature metrics for the training of the classifier. For classification purpose, a linear SVM was used and the system achieved a sensitivity of 93.12%, and specificity is 93.17%.

There are research works that have utilized Artificial Neural Network (ANN) for classification. The authors Ahirwar *et al.* [17] pre-processed the image using SUSAN and generated morphological, colour based and texture based features and classification was performed using back propagation feed forward (BFF) neural network. The authors in [18] performed similar processing but used Probabilistic Neural Network (PNN) for training and classification. The authors claimed that the system provided a sensitivity of 99%. Razzak in the research citation [19] used GLCM based 28 texture features and Back Propagation Artificial Neural Networks for classification. The authors Bahendwar *et al.* [20] used RGB and HSI features for training and testing and classification using ANN. Similarly, Chayadevi [21] extracted 80 features for training using colour and fractal metrics. The authors compared the performance using four different types of classifiers, namely, Adaptive Resonance Theory (ART) based neural network, Neural Network based Backpropagation Feed Forward (NN-BPFF), Support vector machine (SVM) and k-Nearest Neighbour (k-NN). The authors performed comparative study based on the performance of the different classifiers. The best results obtained were the accuracy of 94.45%, precision 96.41%, specificity 94.68% and sensitivity 94.32%. ROC curve analysis was also performed with the area under the curve of 0.9847.

Methodology

Segmentation of red blood cells/erythrocytes from the white blood cells and platelets in a thin blood smear image is pivotal to Malaria parasite detection. This work is aimed to develop an automatic method for segmentation of erythrocytes from non-RBC particles.



The process of segmentation of erythrocytes from non-RBC particles can particularly be classified into 5 basic steps, namely, Data Acquisition, Image pre-processing, K-means Clustering, De-clumping, and Artifact removal from Clusters.

The dataset for the study consisted of thin blood smear images acquired from the public MaMic database [22]. The images in the dataset developed were acquired at 40X magnification and 25-watt illumination. As a pre-processing step, salt and pepper noise from the images was removed from the images using 2D median filtering with 3 by 3 window size. The window size was empirically calculated. In total the dataset developed consisted of 300 images, 150 of which were thin blood smear images from individuals not suffering from Malaria, while the remaining 150 were thin blood smear images taken from individuals suffering from malaria (refer Figure 1).

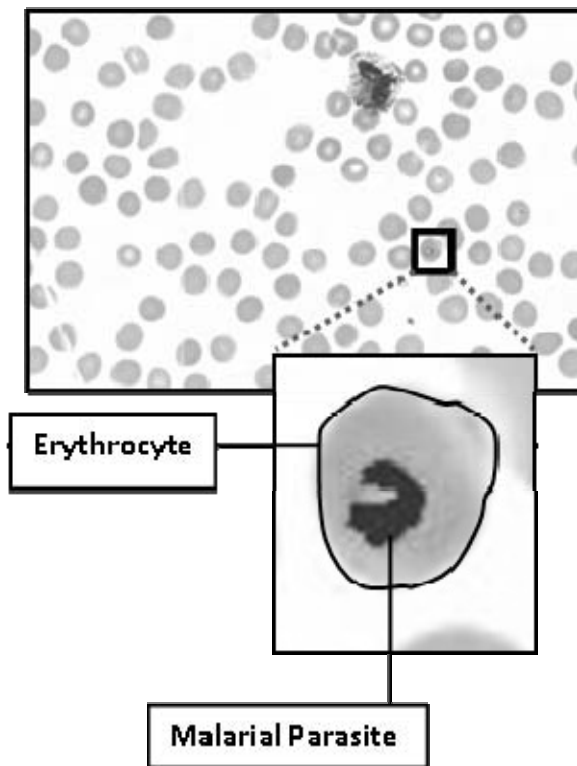


Fig. 1: Thin blood smear image from the MaMic database. The blood smear image is taken from an individual affected with malarial parasite.

There are certain characteristic morphological features that distinctly differentiate an RBC from a non-RBC particle. These morphological features are cell size, shape, absence of nucleus and colour. These morphological features of all connected component were taken into account. So each connected component in a thin blood smear image was defined in terms of the length and breadth value, regular

elliptical shape or absence of the same, presence/absence of nucleus structure and color. Based on these factors unsupervised K-means clustering was performed. Four clusters were developed as a result of K-means clustering. Cluster 4 consisted of background, cluster 2 consisted of red blood cells and cluster 1 consisted only of WBC and cluster 3 consisted of platelets and Malaria parasite (if any). To avoid being stuck at local minima, repeated seed selection, and 100 iterations were performed. However, the method still has certain limitations. The presence of malarial parasite within a clumped erythrocyte group often leads to the labeling of the erythrocyte group as a White Blood Cell. Again, erythrocytes are often connected to a white blood cell and form a single connected component. This group is categorized as a white blood cell on the whole (refer Figure 2). This hinders the enumeration process of red blood cells.

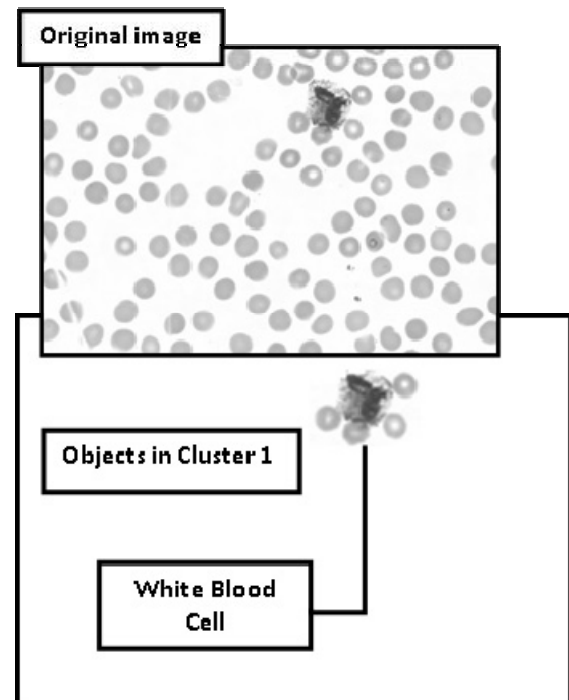


Fig. 2: Each 4-connected component was classified as red blood cell, white blood cell, platelet or background based on the size, shape, presence of nucleus, color etc. When a White Blood cell particle is connected with adjacent red blood cells, the algorithm often treats the whole connected component as a white blood cell particle.

To overcome these limitations, colour based unsupervised clustering technique was developed for segmentation of thin blood smear images into RBC, WBC, Platelets and malarial parasite (if any). The RGB image was converted into L^*a^*b color space. The L, a and b components in the image were used to cluster the different cells in the thin blood smear image. Unsupervised K-means clustering was performed



based on the L, a and b components. Three clusters were generated with K-means clustering (i.e. $K = 3$). While cluster 3 only consisted of the background pixels, cluster 1 consisted of red blood cells and cluster 2 consisted of white blood cells, platelets and Malaria parasite (if any). The edges of the red blood cells in cluster 1 were marked out with a Sobel operator (refer Figure 3). The red blood cell cluster image was eroded emulating a disc structure with a radius value of 3 and neighbourhood size of 4 in order to remove the White Blood cell outline/artifacts from the red blood cell cluster. The radius value and the neighbourhood size was empirically decided based on the dataset at hand.

Next de-clumping of red blood cells was performed in accordance with the methodology put forth by Tek *et al.* [15]. De-clumping of red blood cells was performed to facilitate enumeration of red blood cells.

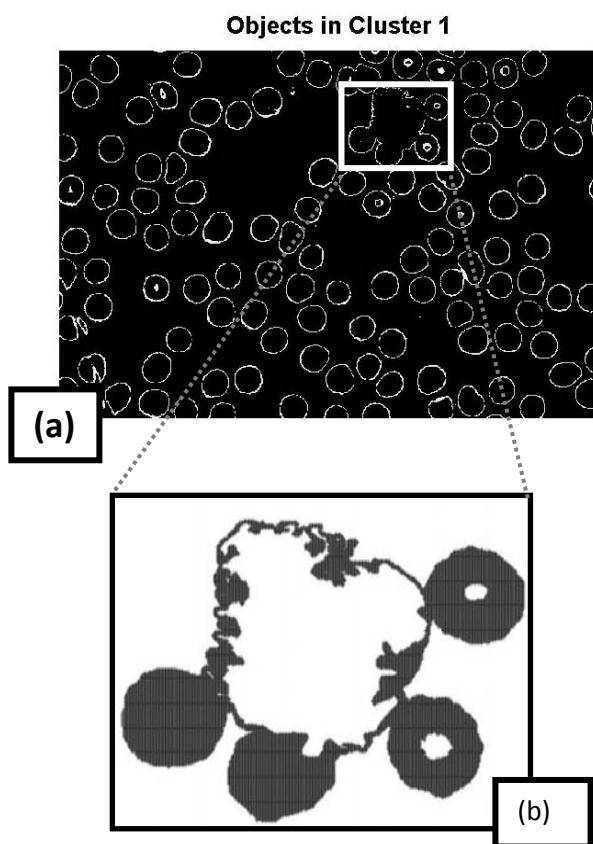


Fig. 3: (a) The Sobel edges of red blood cell cluster formed as a result of 3-means clustering. (b) The image represents the magnified outline of WBC (i.e. WBC artifact) present in the RBC cluster.

Results and Discussion

As opposed to morphology-based clustering, the color based clustering was found to produce better results for the

particular MaMic database. Figure 4 represents the two clusters (i.e. Cluster 1 and 2) formed for a thin blood smear image from the MaMic dataset. However, in removing the artifacts of the white blood cell/s from the RBC cluster, certain RBC cells towards the periphery of the image were often truncated out from the final RBC cluster as demonstrated in Figure 5.

To estimate the performance of the segmentation algorithm, sensitivity and specificity value for the algorithm was calculated. The sensitivity value for an image was calculated in terms of the number of red blood cells correctly identified in the final RBC cluster against the total number RBC particles present in a blood smear image. Any particle other than the RBC particle (i.e. WBC, platelet and malarial parasite) are clustered as one (namely, cluster 2) by the unsupervised 3-means clustering algorithm.

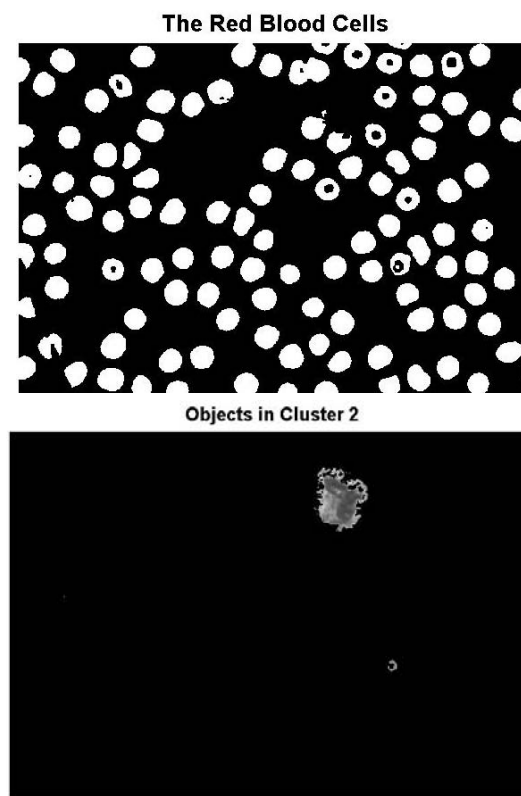


Fig. 4: The Final Cluster 1 and Cluster 2 Extracted from the Original thin Blood Smear Image

Specificity for an image was calculated as the non-RBC particles correctly identified by the algorithm against the total number of non-RBC particles present in the blood smear image. Table 1 documents the Sensitivity and Specificity value for blood corpuscle segmentation for the given image, along with the sensitivity and specificity value across all of the 300 images.

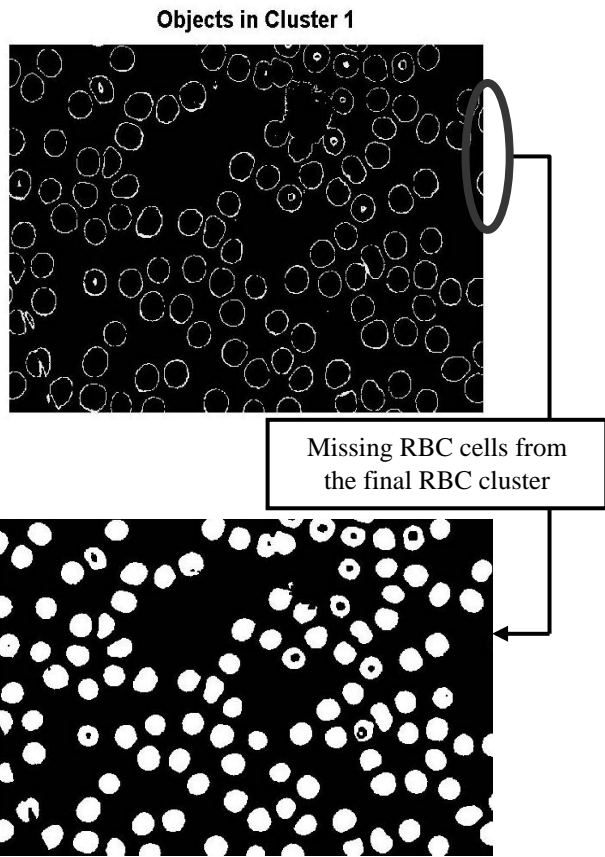


Fig. 5: Disc based erosion is performed to remove artifacts from the red blood cell cluster (Cluster 1). While such erosion helps remove WBC artifacts from a RBC cluster it also removes certain incomplete RBC cells from the thin blood smear image.

Table 1: Sensitivity and Specificity Values Obtained for the k-Means Clustering Algorithm

	Accuracy	Sensitivity	Specificity
For the current image	0.9364	0.9352	1
Across all 300 images	0.9536	0.9528	0.9967

Conclusion

Malaria remains a significant health problem across the world especially in poor under-developed countries that lack proper medical infrastructure. Availability of trained/expert pathologists in such regions as well remote areas requires the intervention of cost-effective technology to provide an adequate solution and prevent mortality. The advent of the digital microscope and the possibility of capturing images have opened new avenues of research in this medical domain where automated software can assist decision making by a pathologist regarding Malaria diagnosis, hence reducing the workload considerably. The key to the development of an effective CAD system for Malaria parasite detection and

analysis is good segmentation of cellular components of blood. In this research paper, a five-step elaborate process is proposed for segmentation using colour images and unsupervised K-means Clustering. Quantitative analysis was performed to test the accuracy of the segmentation results. The algorithm proposed was tested on 300 images from MaMic database where Sensitivity of 95.28% and Specificity of 99.67% was achieved by the proposed method.

References

- [1] Tangpukdee, N., Duangdee, C., Wilairatana, P. and Krudsood, S. (2009). Malaria Diagnosis: A Brief Review. *Korean J Parasitol*, 47(2), 93. doi:10.3347/kjp.2009.47.2.93
- [2] Hartl, D.L. (2004). The origin of malaria: mixed messages from genetic diversity. *Nature Reviews MicroBiology*, 2(1), 15–22. doi:10.1038/nrmicro795
- [3] WHO (2015). WHO, World Malaria Report 2015. Retrieved from WHO website: <http://www.who.int/malaria/publications/world-malaria-report-2015/report/en>
- [4] Payne (1988). Use and limitations of light microscopy for diagnosing malaria at the primary health care level. *Bull World Health Organ.*, 66(5), 621–626.
- [5] Sio, S.W., Sun, W., Kumar, S., Bin, W.Z., Tan, S.S., Ong, S.H., Tan, K S. (2007). Malaria Count: An image analysis-based program for the accurate determination of parasitemia. *Journal of Microbiological Methods*, 68(1), 11–18. doi: 10.1016/j.mimet.2006.05.017
- [6] Frean, J.A. (2009). Reliable enumeration of malaria parasites in thick blood films using digital image analysis. *Malar J*, 8(1), 218. doi:10.1186/1475-2875-8-218
- [7] Point Picker plugin, ImageJ [<http://bigwww.epfl.ch/thevenaz/pointpicker>].
- [8] Zheng, A. (2012). Blood Smear Malarial Parasite Detection. Department of Electrical Engineering, Stanford University.
- [9] Somasekar, J., Reddy, B.E., Reddy, E.K. and Lai, C.H. (2011). An Image Processing Approach for Accurate Determination of Parasitemia in Peripheral Blood Smear Images. *IJCA Special Issue on “Novel Aspects of Digital Imaging Applications”*, DIA, 23–28. doi:10.5120/4153-316.
- [10] Ghosh, P., Bhattacharjee, D., Nasipuri, M. and Basu, D.K. (2011). Medical Aid for Automatic Detection of Malaria. *Communications in Computer and Information Science*, 170–178. doi:10.1007/978-3-642-27245-5_22.
- [11] Di Ruberto, C., Dempster, A., Khan, S. and Jarra, B. (2002). Analysis of infected blood cell images using morphological operators. *Image and Vision Computing*, 20(2), 133–146. doi:10.1016/s0262-8856(01)00092-0.
- [12] Chakraborty, K., Chattopadhyay, A., Chakrabarti, A., Acharya, T. and Dasgupta, A.K. (2015). A Combined Algorithm for Malaria Detection from Thick Smear Blood Slides. *Journal of Health & Medical Informatics*, 06(01), 1–6. doi:10.4172/2157-7420.1000179.
- [13] Arco, J., Górriz, J., Ramírez, J., Álvarez, I. and Puntonet, C. (2015). Digital image analysis for automatic enumeration of malaria parasites using morphological operations. *Expert*



- Systems with Applications, 42(6), 3041–3047. doi:10.1016/j.eswa.2014.11.037
- [14] Díaz, G., González, F.A. and Romero, E. (2009). A semi-automatic method for quantification and classification of erythrocytes infected with malaria parasites in microscopic images. *Journal of Biomedical Informatics*, 42(2), 296–307. doi:10.1016/j.jbi.2008.11.005
- [15] Tek, F.B., Dempster, A.G. and Kale, İ. (2010). Parasite detection and identification for automated thin blood film malaria diagnosis. *Computer Vision and Image Understanding*, 114(1), 21–32. doi:10.1016/j.cviu.2009.08.003
- [16] Savkare S.S., Narote S.P., Automatic Detection of Malaria Parasites for Estimating Parasitemia, *International Journal of Computer Science and Security (IJCSS)*, 2011, Vol. 5, Issue 3, pp 310–315.
- [17] Ahirwar, N., Pattnaik, S. and Acharya, B., Advance Image Analysis Based System for Automatic Detection and Classification of Malarial Parasite in Blood Images, *International Journal of Information Technology and Knowledge Management*, 2012, Vol. 5, Issue 1, pp 59–64.
- [18] Kurer, D.A. and Gejji, V.P., Detection of Malarial Parasites in Blood Images, *International Journal of Engineering Science and Innovative Technology (IJESIT)*, May 2014, Volume 3, Issue 3, pp 651– 656.
- [19] Razzak M. I., Automatic Detection and Classification of Malarial Parasite, *International journal of Biometrics and Bioinformatics*, Vol (2015). 9(1): 1–12.
- [20] Bahendwar Y.S. and Chandra U.K., Detection of Malaria Parasites through Medical Image Segmentation Using ANN Algorithm, *International Journal of Advanced Research in Computer Science and Software Engineering*, July 2015, Vol. 5, Issue 7, pp. 1063–1067.
- [21] Chayadevi, M.L. and Raju, G.T., Usage of ART for Automatic Malaria Parasite Identification Based on Fractal Features, *International Journal of Video & Image Processing and Network Security IJVIPNS-IJENS*, August 2014, Vol. 14, Issue 04, pp. 7–15.
- [22] The MaMic Image Database. (n.d.). Retrieved from <http://fimm.webmicroscope.net/Research/Momic/mamic>



Cybernetics in Dynamic Data-Driven Identification of the Interactions of Runoff-Rainfall Dependent State Variables for Hourly Monitoring of Flows of Fast Flowing River Systems for Hydro-Power Generation

A.S. Chaudhuri¹

Abstract: *The paper presents the identification of the interactions of the runoff dependent state variables for hourly monitoring of flows of a fast flowing river system in the Himalayan mountain region in North Bengal in India with the cybernetical process of multilayer group method of data handling algorithms (GMDH). The dynamic data-driven identification of the interactions of runoff-rainfall dependent state variables has been attempted to monitor the hourly flows of the river with multilayer GMDH algorithms. The GMDH algorithms of applied cybernetics are effective analytical tools for on-line operation and control of hydraulic structures of the river systems and the algorithms exhibit identification robustness adhering to an optimal decision.*

Keywords: River Systems, Runoff-Rainfall, State Variables, Monitoring, GMDH.

Introduction

Cybernetics deals with the purposeful analysis of complex systems with a view to ascertain control mechanism in accordance with an optimally designed decision algorithms. The investigation attracts interest in water resources systems.

The interactions of the runoff dependent state variables for hourly monitoring of flows of a fast flowing river system in the Himalayan mountain region in North Bengal in India has been identified with multi-layer group method of data handling algorithms (GMDH) [2]. The identification of the interactions of runoff-rainfall dependent state variables has been attempted to monitor the hourly flows of the river with multilayer GMDH algorithms. It is evident from the results that the GMDH is capable to give flood warning during storm periods, ahead of the occurrence of the flood, on the basis of flows hourly gauged at the upstream points. The GMDH algorithms are effective analytical tools for on-line operation and control of hydraulic structures of the river systems and the algorithms exhibit identification robustness adhering to an optimal decision.

The river Teesta rising from the Himalayan ranges in North Sikkim and passing through the deep gorges for nearly 160 Kms falls upon the plain of North Bengal near Sevoke. Its average velocity is 6.2 m/s. A brief description of the river is given. The river Lohnak originates from the snow

line in North Sikkim at a height of 6401 metres. The river Poki Chu originates from the Zemu glacier at a height of 4968 meters. These two rivers combine at Lachen, after which it is known as Zemu Chu river. At Chungthang Lachen Chu river joins the Zemu Chu from the north eastern side. This combined flow is augmented by the river Lachung Chu at down-stream of Chungthang to form the river Teesta. At Sankalan the river Taluna Chu originating from the Talung glacier in north western Sikkim at a height of 5873 metres joins the river Teesta. Upto Sankalan the length of the river Teesta from the origin is 70 Kms. and the catchment area is 4200 sq. Kms. From Sankalan the river Teesta flows through the narrow gorges and comes to Singtam. About 15 Kms upstream of Singtam the river Dik Chu joins the Teesta. At Singtam from the eastern side the river Rongni Chu joins the Teesta. Upto Kantitar the length of the Teesta is 114 Kms. from the origin and the catchment area is 4874 sq Kms. from the origin. At Rongpo the river Rongpo Chu from the eastern catchment region joins the Teesta. The length of the Teesta and its catchment area upto Rongpo are 116 Kms and 5405 sq. Kms respectively. At Singla Bazar the river Great Rangit combines with the rivers Ramam and Little Rangit, and flows as the river Great Rangit. This combination of three rivers brings an additional 1956 sq. Kms. of catchment area. At 3 Kms upstream of Teesta Bazar the Great Rangit joins the Teesta. The length and the catchment of the Teesta upto Teesta Bazar are 134 Kms and 7714 sq. Kms. Upto

¹Former Emeritus Fellow, All India Council for Technical Education, New Delhi, India. ✉ chaudhuri1943@live.com



Coronation Bridge the length and the catchment of the Teesta are respectively 158 Kms and 8147 sq. Kms. from the origin. Upto Domohani Bridge the length of the Teesta is 206 Kms. the catchment area is 9432 sq. kms. The main observation stations from which the data for this investigation were collected are Sankalan Bridge, Kantitat, Singla Bazar, Teesta Bazar, Coronation Bridge and Domohani Bridge. The river distance and the travel time from Coronation Bridge to Sankalan Bridge, Kantitar, inglabazar and Teesta Bazar are 84 Kms: 10 hours, 44 Kms: 4 hours, 54 Kms: 4 hours and 22 Kms.: 2 hours respectively. The formulation of the mathematical models of dependence of the up-stream flows and the catchment rainfall on the down-stream flow at a point of the river system can bring out the inherent hydrological characteristics of a river. The hydrologic processes for a short-term flow modelling during a storm period are non-stationary in nature. In the mountain region the hydrologic characteristics for short-term storm period do not obey the principles of superposition. In this situation the linear least square recursive algorithms of the time series analysis will not be useful. The foregoing discussion of the river system gives a brief description of the complex nature of the hydrological characteristics of the Teesta river.

The present investigation exposes the hydrological characteristics of the river in the form of models of polynomials. The past values of runoff and rainfall variables at different catchment regions have been correlated with the river flow at a point in the river system to provide a real-time model which gives one step ahead prediction of river flows.

In Section 2 a mathematical model of optimum complexity of hourly monitoring of river flows has been obtained by multilayer group method of data handling algorithms (GMDH). In Section 3 a rainfall-run off model of flows of the river for the sixth hourly monitoring of flows has been presented by multilayer GMDH.

Prediction of Hourly Flows with Interacting Flow Dependent State Variables by Multilayer GMDH

It has been observed that multilayer GMDH algorithms are capable of handling non-linearity, feed-backs and other stochastic features that are encompassed within the hydraulic process of a fast flowing river systems.

Multilayer Group Method of Data Handling Algorithm

Multilayer group method of data handling is a method of self-organisation of different partial models (Ivakhnenko, 1971). This method involves the generation and comparison of all possible combinations of input output and to select the best possible ones according to an integral performance index known as the criterion of integral squared error (Chaudhuri, 1989).

Brief Description of Multilayer GMDH

In multilayer group method of data handling algorithms, polynomials are used as the basic means of investigation of complex dynamical systems. The polynomials of prediction are regression equations which connect the current values of output with the current and/or past values of input variables. The regression analysis allows to evaluate the coefficients of the polynomial by criterion of minimum integral squared error. Then the polynomials are treated in the same manner as are seeds in the selection process in agriculture, a unique mathematical concept. The salient features of multilayer GMDH as applicable in multilayer selection process which is used in the present investigation are briefly described here. Each output element implements a non-linear function of its inputs. The function implemented is usually a second order polynomial of its inputs. Since each element generally takes two inputs, the implemented function by an element in one of the layers is given by,

$$Y = A_2(x) = a_0 + a_1x_1 + a_2x_2 + a_3x_1x_2 + a_4x_1^2 + a_5x_2^2 \dots (1)$$

Only those elements whose performance indices exceed the thresh-hold at that layer are allowed to pass to the next layer. Therefore, the process represents a feed forward transformation whereby each succeeding layer increases by two the degree of the multinomial fit to the input properties of x . The selection hypothesis employed to select the elements to be used in the succeeding layers involves two basic conclusions; the composite character of a system must be based on the use of the information which controls the totality of the elements of the system, and the long history of the art of selection as observed in the case of plants and animals can be successfully extended to the science of cybernetics. To get plants in the agricultural sense with certain specific properties, a large number of plants are sown which may have these properties, and the plants are crossed. From the harvest of the first generation, the plants are chosen which better the requirements (the first self selection) as compared to others. The seeds of the selected plants are again sown and crossed. From the second harvest certain seeds are selected and the seeds are sown and so on. Rules employed in the process of selection are as follows:

For each generation certain optimal number of seeds are sown. The selection process cannot be completed in a single generation (at least 3 to 4 generations are needed).

In accordance with the selection hypothesis, the simple polynomials of second degree that are easiest are taken. The combination of data are subjected to the first threshold selection in accordance with the integral square error criterion. Only some of the polynomials which fit best are allowed to pass into the second layer where they form more complex combination of polynomials of fourth degree. From the second layer again the polynomials which fit best are



singled out and are allowed to pass into the third layer and so on. The process continues so long as minimum of a selection criterion is obtained. This constitutes multilayer group method of data handling algorithms. Ivakhnenko models the input output relationships of complex process using multi-layer network structure of Rosenblatt's perception type, who designed the model of brain's perception. The GMDH-type polynomial networks have been described where x_i is a i -th input variable, y is an output. The GMDH-type networks are the multi-layered ones.

Since each element generally accepts two inputs, the function (algorithm) implemented by an element in one of the layers is,

$$y = A_2(X) = a_0 + a_1 x_1 + a_2 x_2 + a_5 x_1^2 + a_4 x_2^2 + a_5 x_1 x_2$$

where the subscript in A_2 denotes a second-order transformation of the inputs.

The network is described by a set of the following polynomials:

$$\begin{aligned} & y_2^{(3)} - g_1(y_1^{(2)}, y_3^{(2)}) \\ & y_1^{(2)} - g_2(y_2^{(1)}, y_3^{(1)}) \\ & y_3^{(2)} - g_3(y_1^{(1)}, y_2^{(1)}) \\ & y_1^{(1)} - g_4(x_1, x_4) \\ & y_2^{(1)} - g_5(x_1, x_2) \\ & y_3^{(1)} - g_6(x_2, x_4) \end{aligned}$$

where, g_1, \dots, g_6 are the transfer function of the neurons.

Use of GMDH in Simulating Hourly River Flows

Data were taken for a period commencing from 4.00 hours on the 23rd July, 2006 to 15.00 hours on the 25th July, 2006 for the gauging stations at Coronation Bridge, Teesta Bazar, Rongpo (Teesta), Great Rangit (Singlabazar) and Sankalan. The data are rationalised as,

$$x(k) = \frac{X(k) - X_{\min}}{X_{\max} - X_{\min}} \quad \dots (2)$$

here $X(k)$ = observed data

X_{\max} = the maximum value of the relevant data set

X_{\min} = the minimum value of the relevant data set.

Formulation of the Process Equation

The hourly flow process at Coronation Bridge point can be represented by

$$y_k = f(y_{k-1}, y_{k-2}, \dots, x_{1,k-1}, \dots, x_{7,k-1}, \dots) \quad \dots (3)$$

where y_k denotes the transformed hourly flow at Coronation Bridge, x_1 , the hourly flows at Teesta Bazar, x_2 , the hourly flows at Rongpo, x_3 , the hourly flows at Great Rangit, x_4 , the

hourly flows at Singla Bazar, x_5 , the hourly flow at Sankalan, x_6 , the hourly flow at Kantitar and x_7 , the hourly flow at Pedong. The subscripts $k, k-1, k-2$, refer respectively to the current hour, one hour preceding the current hour, two hours preceding the current hour and so on. All the data are in rationalised unit. The arguments having a strong correlation with y_k are then selected in the process equation on the basis of correlation functions.

The correlation function of hourly flow Coronation Bridge with other gauging stations for different shift of instances of time are shown in Table 1. After such selection of arguments as having strong correlation with the hourly flows at Coronation Bridge, the process equation becomes:

$$y_k = f(y_{k-1}, y_{k-2}, x_{1,k-9}, x_{2,k-3}, x_{3,k-2}, x_{4,k-4}) \quad \dots (4)$$

denoting the arguments as,

$$\begin{aligned} & y_{k-1} = x_1', y_{k-2} = x_2', x_{1,k-9} = x_3', x_{2,k-3} = x_4', x_{3,k-2} = x_5', x_{4,k-4} \\ & = x_6' \text{ and the output } y_k = y, \text{ the process equation becomes.} \\ & y = f(x_1', x_2', x_3', x_4', x_5', x_6') \quad \dots (5) \end{aligned}$$

First Layer Selection

There are ${}^6C_2 = 15$ possible combinations of selections of two arguments at a time out of 6. For every such combinations, the partial regression equation is written in the form,

$$y_a = a_{0a} + a_{1a}x_b' + a_{2a}x_c' + a_{3a}x_b'x_c' + a_{4a}x_b'^2 + a_{5a}x_c'^2 \quad \dots (6)$$

where $a = 1, 2, \dots, 15$, while b and c are indices for all 15 combinations. And these, therefore lead to 15 systems of normal Gaussian equations with matrices of order 6×6 . The coefficients α 's are then estimated by solving normal equation systems constructed from the data set. For estimating the coefficients, it is assumed that the equation error is very small, being distributed with zero mean, constant variance and also not-correlated with the inputs. The second assumption is that for the construction of the model the inputs and outputs are known exactly without any measurement error.

The accuracy of every variable y_a is calculated by using the entire data set. From all variables, seventeen more accurate ones are chosen which give low values of integral square error criterion.

Selection of Other Layers

The intermediate variables of y_a layer chosen from the first layer give 15 combinations of two arguments of y_a layer. Again in second layer these become,

$$z_a = \beta_{0a} + \beta_{1a}y_b + \beta_{2a}y_c + \beta_{3a}y_b y_c + \beta_{4a}y_b^2 + \beta_{5a}y_c^2 \quad \dots (7)$$

where, $a = 1, 2, \dots, 15$ while b and c are indices of all 15 combinations. The calculation of the coefficients β 's and



estimation of the accuracy of z_a are repeated as in the case of y_a . Six z_a variables are then chosen for the next layer u_a .

$$u_a = \Upsilon_{ca} + \Upsilon_{1a} z_b + \Upsilon_{2a} z_c + \Upsilon_{3a} z_b z_c + \Upsilon_{4a} z_b^2 + \Upsilon_{5a} z_c^2 \dots (8)$$

In this way each layer is tested for accuracy by using the entire data set and on the basis of minimum integral square error criterion explained earlier. For all the layers, the variable on the left hand side of the equations is kept equal to the value of the output variable. The minimum integral square error is obtained in the z -layer for $ISE = 7.065E-03$ and afterwards the error starts increasing.

Results

The process of hourly river flows at Coronation Bridge has been identified by the polynomials shown below:

$$\begin{aligned}
 y &= z_5 \\
 z_5 &= -0.0083340 + 0.7145809 y_1 + 0.2874315 y_6 - \\
 & 2.3779436 y_1 y_6 + 1.0833849 y_1^2 + 1.2711237 y_6^2 \\
 y_1 &= -0.5568849 + 0.78741211 x_4' + 1.083384 x_6' - \\
 & 0.7874361 x_4' x_6' - 0.10718708 x_4'^2 + 0.0456246 x_6'^2 \\
 y_6 &= 0.0495098 + 1.0707701 + 0.1782401 x_3' - \\
 & 0.75572243 x_3' x_4' - 0.0494594 x_3'^2 + 0.67454377 x_4'^2 \\
 & \dots (9)
 \end{aligned}$$

Rainfall-Runoff Model of Hourly Flows for a Storm Period

In the present work a dynamic model for sixth hourly prediction of flows correlating the different upstream flows and the rainfall at different gauging stations in the catchment region of the river Teesta with multilayer GMDH has been presented.

Illustration

The sixth hourly flow data were taken for a storm period commencing from 02.30 hours on 30 July, 2006 to 20.30 hours on 31 July, 2006 for the flow measuring stations at Coronation Bridge and Sankalan. The sixth hourly integrated rainfall data were taken for the rainfall measuring stations at Teesta Bazar, Singla Bazar, Pedong and Kantitar for the period mentioned above.

The sixth hourly flows of the river Teesta at Coronation Bridge for the storm period has been identified as a non-linear polynomial.

The minimum integral square error was obtained as 0.089.

Conclusion

The multilayer GMDH has been successfully used for modelling the river flows at Forecasting stations on the basis of measurements at upstream stations. The travel times from Teesta Bazar, Rongpo, Singla Bazar and Sankalan to Coronation Bridge are 2 hours, 4 hours, 4 hours and 10 hours respectively. The highest correlation coefficients for the respective stations however are obtained at lagged instants 1, 3, 2 and 4 hours. Thus, the identified flow process elucidates the hydrologic response of the Teesta basin such as the porosity of the soil, the base flow separation and the ground water charging to the dynamics of river runoff.

References

- [1] Ivakhnenko, A.G., "Polynomial Theory of Complex System", *Transaction of Systems, Man and Cybernetics*, Vol. SMC-1, No. 4, October 1971, pp. 364–379.
- [2] Chaudhuri, A.S., "Observation, Conjecture and Experiment with Group Method of Data Handling Algorithms" *System Analysis Modelling and Simulation* Vol.6 (1989) 11/12, pp. 867–906, Akademia Verlag, Berlin.



Smart Grid Prospects and Implementation in India: A Pathway towards Sustainable Development

M. Alam¹

Abstract: *The Indian power grids are not secure, reliable and up to the mark. Today's electrical grid suffers from a number of problems, including that it is old (the average age of power plants is 35 years), dirty (more than half of our electricity is generated from coal), inefficient (the delivered efficiency of electricity is only 35%, and vulnerable (the worst blackout in the history which affected 620 million people, 9% of the total population of the world occurred on 2012 July 30th and 31st across 22 states of Northern, Eastern and North-eastern India). About 32 GW power was taken offline from the grid. To reduce these deficiencies, the technology of "Smart Grid" (SG) is required. At this moment in time, energy conservation and emission reduction, green energy, sustainable development, safety, reduction of loss and optimal utilization of assets have become the main center of attention. To obtain a flexible, clean, safe, economical, and friendly intelligent grid, Different organizations and countries including India have unanimously accepted SG. SG will facilitate the environment-friendly sustainable development, network planning, operation management, market trading and service enrichment, asset optimization and resource saving, etc. Smart grid (SG) is the only choice to overcome the power system instability in the 21st century considering rapid development. SG has been a common aim of the whole world because of the increasing demand of electrical power grid, safe, steady running, as well as the requirement of high quality and reliable power supply for consumers. In this paper, the key drivers and features of smart SG are outlined. The effects of SG development on different sectors are discussed. A possible framework for the SG architecture and SG technologies is outlined, considering practical constraints. The recent initiatives taken by the Government of India (GoI) related to smart grids are described. Considering the social, economical, political and environmental circumstances, the paper suggests a strategy to implement smart grids in India.*

Keywords: Smart Grid, Information Communication Technology, Demand Side Management, Advanced Metering Infrastructure, Distributed Generation, Outage Management System.

Introduction

Electricity is the major share of total global energy requirement, which is expected to be exponentially growing. As the demand grows steadily, not only will the supply become inadequate, it's transmission and distribution will become inefficient and wasteful. The existing grid infrastructure was not basically designed for today's pace of power transfer. It has not been updated and upgraded in accordance to the pace of increases in power and its delivery.

Considering the 21st century technological innovations and trends, smart grid is the current development of world's electric power system [1]. To obtain a flexible, clean, safe, economical, and friendly intelligent grid, Different organizations and countries including India have unanimously accepted smart grid (SG).

What is Smart Grid?

A **smart grid** is a digitally enabled **electrical grid** that gathers, distributes, and acts on information about the behaviour of all participants (suppliers and consumers) in order to improve the efficiency, reliability, economics, and sustainability of electricity services [1].

A SG [1, 2] employs innovative products and services together with intelligent monitoring, control, communication, and self-healing technologies to:

1. Better facilitate the connection and operation of generators of all sizes and technologies;
2. Allow consumers to play a part in optimizing the operation of the system;
3. Provide consumers with greater information and choice of supply;

¹Department of Electrical Engineering, National Institute of Technology Durgapur 713209, West Bengal, India. ✉ meheubjgec1990@gmail.com



4. Significantly reduce the environmental impact of the whole electricity supply system;
5. Deliver enhanced levels of reliability and security of supply.

Table 1 presents the comparison between present grid and SG.

Table 1: Comparison between Present Grid and SG

<i>Present Status of Electrical Grid</i>	<i>Target for SG</i>
Very limited or one way communication	Both(two way) communication
Electromechanical devices	Digital devices
Limited price information, static tariff	Full price information, dynamic tariff
Manual restoration	Automated restoration, self healing
Limited control over power flow	Pervasive control-substation, feeder and distribution automation
Carbon based generation	Carbon limit and green power credit through significant renewable energy sources
Centralized generation	Centralized as well as distributed generation
Few customer choices	Many customer choices, value added services
Limited or non transparent operation, few sensors	Sensors throughout, wide area monitoring
Sub optimal asset utilization	Asset life extension through condition monitoring

SG Frame Work

General power system consists of generation, transmission, distribution and consumers. markets/business values, intelligent operation and service providers are not included in the typical power systems. The frame work [1] of SG is shown in Figure 1. From the shown frame work, it is observed that all generation, transmission, distribution and consumers are correlated and also inter-dependent.

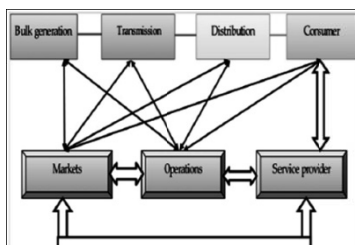


Fig. 1: Smart Grid (SG) Frame Work

Key Drivers: Key drivers [3] of SG are given in pictorial form:

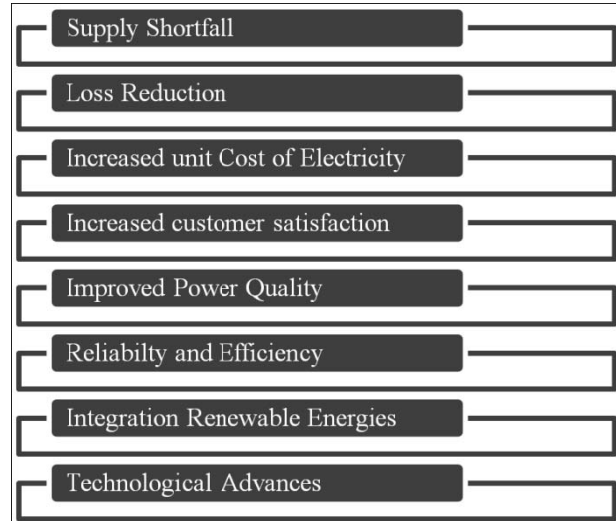


Fig 2: Key Drivers of Smart Grid (SG)

Features

Key features [1,4] of smart grid are:

1. Flexibility and Marketization
 - Expandability for future development
 - Seamless compatibility with various market operation
 - ‘Plug and play capability to accommodate upgraded technologies
 - Active participation of consumer
 - Market liberty to increase transparency and competition
 - Two way communication between consumer and company using smart meter.
2. Resiliency
 - Capable of self recovery from blackouts, network component failures, faults etc.
 - Capable of fast response, protection and restoration without hazards
 - Capable to deliver electricity securely and reliably
 - Overall self healing capability to maintain power system reliability.
3. Sustainability
 - Significant penetration of renewable energy sources (wind, solar etc)
 - Reduce impact on environment by reducing emission
 - Adoption of energy saving and energy storage technologies
 - Mitigation of network congestion.



4. Improved Power Quality

- A smart grid will have high quality of power and reduces the occurrence of distortions of power supply.

5. Supervision

- Faster, reliable operation and supervision done with the help of better computation, measurement, communication, control, protection, maintenance, onitoring, etc.

6. Optimization

- Optimize resource utilization; reduce investment costs and operation and maintenance costs.

play, they are often unable to make the business case for smart grid investments.

- *Lack of Awareness:* There is lack of awareness among stakeholders about the role of smart grids in enabling a low-carbon future.
- *Poor Financial Health of Utilities:* In India, the debt burdened utilities find it difficult to invest in Smart grid initiatives.
- *Skill and Knowledge:* In the longer term, a shortfall is expected in critical skills that will be required to architect and build smart grids.
- *Cyber Security:* Digital communication networks and more granular and frequent Information on consumption patterns raise concerns in some quarters of cyber-insecurity and potential for misuse of private data.

Barriers

Several barriers or challenges [5–9] towards SG implementation are:

- *Political and Regulatory Issue:* In many cases, utilities do not get as far as a business case for the smart grid as there are regulatory and policy barriers in place that either create reverse incentives or fail to create sufficient positive incentives for private sector investment.
- *Technology Maturity and Delivery Risk:* Technologies have significant technology risks associated with them because agreed standards have not emerged.
- *Business Case:* Where policy-makers and utility executives are aware of the role that smart grids can

Smart Grid Technologies

Table 2 presents the brief overview of SG technologies.

The many smart grid technology [3] consisting of sets of individual technologies associated with the entire grid, from generation through transmission and distribution to various types of electricity consumers. Some of the technologies are actively being deployed and are considered mature in both their development and application, while others require further development and demonstration. SG components are presented in Figure 3.

Table 2: Brief Overview of Smart Grid (SG) Technologies

Technology	Hardware	System and Software	Implementation Area
Information and communication technology	Communication equipment (Power line carrier, WIMAX, LTE, RF mesh network, cellular), routers, relays, switches, gateway, computers (servers)	Enterprise resource planning software (ERP), customer information system (CIS)	Generation, Transmission, Distribution, Industrial, Service, Residential
Renewable and distributed generation	Power conditioning equipment for bulk power and grid support, communication and control hardware for generation and enabling storage technology	Energy management system (EMS), distribution management system (DMS), SCADA, geographic Information system (GIS)	Generation, Transmission, Distribution, Industrial, Service, Residential
Wide area monitoring protection and control (WAMPAC)	PMU (Phasor measurement unit) and other Sensors	SCADA, WAMS, WAAPCA etc	Generation and Transmission
Transmission enhancement	Superconductors, FACTS, HVDC	Network stability analysis, automatic recovery systems	Transmission
Distribution grid management	Automated re-closers, switches and capacitors, remote controlled distributed generation and storage, transformer sensors, wire and cable sensors	Geographic information system (GIS), distribution management system (DMS), outage management system (OMS), workforce management system (WMS)	Distribution
Advanced metering infrastructure (AMI)	Smart meter, in-home displays, servers, relays	Meter data management system (MDMS)	Distribution, Industrial, Service, Residential
Demand side management (DSM)	Smart appliances, routers, in-home display, building automation systems, thermal accumulators, smart thermostat	Energy dashboards, energy management systems, energy applications for smart phones and tablets	Industrial, Service, Residential
Electric vehicle charging infrastructure	Charging infrastructure, batteries, inverters	Energy billing, smart grid-to vehicle charging (G2V) and discharging vehicle-to-grid (V2G) methodology	Distribution, Industrial, Service, Residential

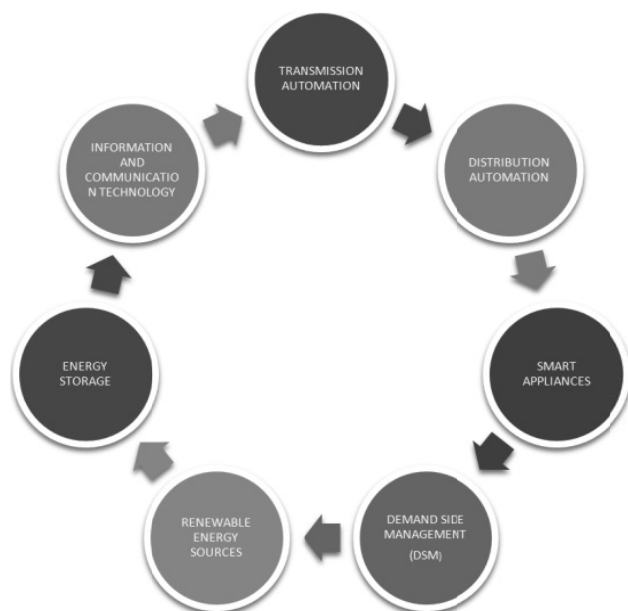


Fig. 3: Smart Grid (SG) Components

GOI Initiatives towards SG

Several initiatives [3, 5, 6] taken by GOI are:

A. India SG Task Force (ISGTF)

The Government of India formed the India Smart Grid Task Force in 2010 and is primarily meant for understanding and advocating policies in smart grid technologies.

Major functions of the ISGTF are:

- Ensure awareness, coordination, and integration of diverse activities related to smart grid technologies
- Promote practices and services for R&D of smart grids
- Coordinate and integrate other relevant intergovernmental activities
- Collaborate on an interoperability framework
- Review and validate recommendations from the India Smart Grid Forum.

Five working groups have been constituted to take up the different task related to SG activities. They are:

- WG1 – Trials/Pilot on new technologies.
- WG2 – Loss reduction and theft, data gathering and analysis.
- WG3 – Power to rural areas and reliability & quality of power to urban areas.
- WG4 – Distribution Generation & renewable.
- WG5 – Physical cyber security, standards and spectrum.

B. India Smart Grid Forum (ISGF)

The Government of India also formulated the India Smart Grid Forum in 2010 with the prime objective of accelerating

development of smart grid technologies in the Indian power sector in an efficient, cost-effective, innovative and scalable manner. The India Smart Grid Forum will coordinate and cooperate with relevant global and Indian bodies to leverage global experience and standards [10] where ever available or helpful, and will highlight any gaps in the same from an Indian perspective.

C. Distribution Reform, Upgrades, and Management (DRUM)

The Ministry of Power, Government of India, and the U.S. Agency for International Development (USAID)–India jointly designed the Distribution Reform, Upgrades and Management (DRUM) Project with the purpose of demonstrating “the best commercial and technological practices that improve the quality and reliability of ‘last mile’ power distribution in selected urban and rural distribution circles in the country.” The overall programmatic goal of the DRUM Project is to demonstrate commercially viable electricity distribution systems that provide reliable power of sufficient quality to consumers and to establish a commercial framework.

D. Re-Structured Accelerated Power Development and Reforms Program (R-APDRP)

Ministry of Power, Govt. of India, as a part of Reforms in the Power Sector, has launched the RAPDRP in the XI Five year Plan. The focus of the program is on the actual demonstrable performance in terms of AT&C loss reduction, establishment of the reliable and automated sustainable systems for collection of base line data, adoption of information technology in the areas of electricity accounting, Consumer care and strengthening of Distribution network of State Power Utilities. Projects under the scheme shall be taken up in two parts. Part-A shall include the projects for establishment of baseline data and IT applications for energy accounting/auditing & IT based consumer service centres. Part-B shall include regular distribution strengthening projects.

Some other initiatives taken by GOI [5] are:

- Launch of the India Smart Grid Knowledge Portal in Jan. 2013.
- Approval of 14 smart grid pilot projects by the India Smart Grid Task Force in 14 States in June 2013 (CESC, Mysore and UGVCL, Gujarat have recently released Smart Grid Pilot Project).
- A committee was constituted by Ministry of Power, under Chairperson, CEA to review Functional Specifications of Low Cost Single Phase Smart Meters and its report was released on 12th June 2013.
- GoI had kept ₹ 200 crores for 20 Smart Grid Pilot Projects in India, for public distribution utilities, with matching contribution from the State utility.



The following mentioned power sector companies in India already took initiatives:

1. NDPL Smart Grid Initiatives.
2. BESCOM Smart Grid Project.
3. West Bengal State Electricity Distribution Company Ltd (WBSEDCL) Smart Grid Project.
4. Smart Grid Customer Demo Center (CDC) by Mahindra Satyam in partnership with Schneider Electric.
5. Smart Mini-Grid System at The Energy and resources Institute (TERI).

Recommendations

Regulators

- Create a regulatory framework which aligns incentives of each member in the value chain.
- Allocate risk and reward efficiently.
- Consider both utilities and customer while making policies.
- Adopt output based regulatory system (Reward/ Penalties) which stresses on utilities to perform better.

Utilities

- Adopt more holistic approach about Smart Grids, so that they can convey its future benefits to the customers.
- Reduce the risk of technology obsolescence by R & D activities.
- Undertake large scale pilot projects and analyze the benefits.
- Transformation from utility-centric investment decision to societal-level decisions.

Vendors

- Required to play important role in policy making process.
- To help utilities to adopt flexible design and compatibility of Smart Grid fast.
- To convince customers about the acceptance of changing trend by product and service offering.

Customers

- Plays critical role by demanding for more flexible service.
- To encourage more players to enter in this field and in order to make the market competitive.
- To help utilities and regulators to set goals and make conducive policies.
- To increase the awareness in society.

Some other recommendations [7] for implementing Smart Grid in India include:

- A governing body (multi-disciplinary) consisting of various stakeholder representatives should be nominated by Govt. of India for the exploration and implementation of Smart Grid in developed countries.
- A central Power Research Institute (CPRI) should be established which may coordinate various regional centres and agencies in this regard.
- The research and technical organizations like IITs, NITs, should be incorporated in this mission.
- Confirm target loss reduction curve for T & D losses DISCOM Energy Conservation awareness among end users through the use of energy efficient devices and mechanisms should be propagated.

CPRI may form subcommittee to implement the tasks. Regulatory committee will facilitate in cooperation in Table 3 Strategy undertaken for implementation of SG SG policy, SG standards, regulations and finance. The committee for Electric Vehicle (EV) or Plug in Hybrid Electric Vehicle (PHEV) will help to promote the fuel efficient electric vehicles.

Strategy to Implement Smart Grid

Indian Government has started implementation of SG and taken a lot of initiatives [3, 6]. Government gives financial support to promote smart grid. Conferences, seminars and workshops are organized in India. Strategy [1, 3] to execute intelligent grid is given in Table 3.

Table 3: Strategy Undertaken for Implementation of SG

Upto 2020		2020–2030	
Case	Action/Implementation	Case	Action/Implementation
Deploy base technology	OMS, DMS system	Mature new services	Expanded SCADA and line services
	Micro grid pilot		Load control with demand response (DR)
	Smart meter installation		PMU placement, increased PHEV adoption
Many smart grid components are initially deployed	HAN, energy management	Energy supply and storage	Significant DER penetration
	PHEV infrastructure pilot		Energy storage through flywheel, advanced battery
Regulatory issue	Proper smart grid standard and taskforce	Advance grid technology	FACTS, HTS (high temperature super conductor)
	Flexible policy		HVDC, DLR (dynamic line rating)
	Dynamic pricing		Self healing grid in reality

Smart Grid: A Pathway towards Sustainable Development

Smart grid plays a crucial role towards sustainable development (Figure 4) in the following way:

1. Better control of power flow through use of OMS, FACTS devices thus improving reliability, efficiency, less outages, etc.
2. Decarbonisation by less dependency on pollution based technologies.

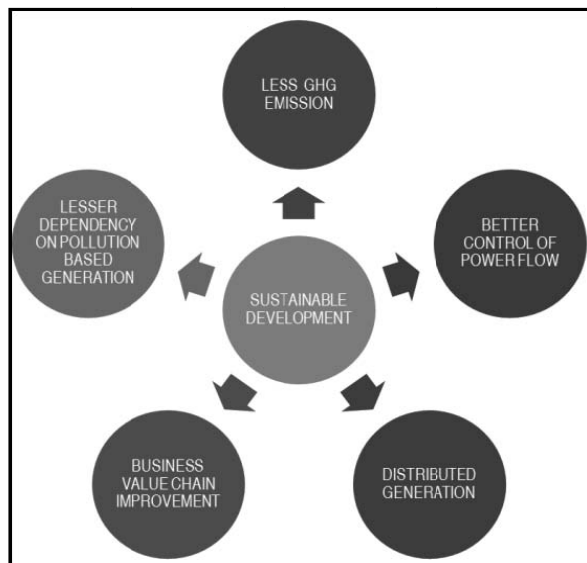


Fig. 4: Smart Grid (SG): A Pathway towards Sustainable Development

3. Significant penetration of distributed generation (Wind, solar, etc.) results into less impact on environment by emission reduction.
4. Evolving of new technologies and materials create a path to business value chain improvement.
5. With the help of Smart appliances, energy storage, demand side management (DSM) load management is possible.

Conclusions

The transition towards a smart grid from the current electric grid is one of the most important decisions to meet for

electric reliability, economy, efficiency and sustainability goals. Only through a well structured grid, efficient, reliable and secure communication technologies and integrated intelligent decision making capabilities associated with the structure, a Smart Grid can evolve. Smart grid project needs to be executed in stages [1, 7]. Awareness about SG for all Indians (i.e. common people and industrialists) is necessary required to strengthen the existing grid using advanced technology instead of going for new construction whenever possible. New technologies should be adopted, but it is also required to keep scope for future compatibility. Increase in customer active participation and awareness is essential. New investment options in power industry needs to be provided. Through the development of renewable energy sectors, optimization of existing resources, extensive use of modern SG technologies, proper planning and government support, a self healing smart grid can be evolved in reality which in turn extends the path of sustainable development.

References

- [1] Acharjee, P., Strategy and implementation of Smart Grids in India, Elsevier, *Energy Strategy Reviews*, pp. 193–204 (2013).
- [2] EPRI Intelligrid, <http://intelligrid.epri.com>.
- [3] 2nd International Convention, Grid world-2013 28–29 May 2013, New Delhi, India.
- [4] Acharjee, P. and Gunda, J., “Development Prospect of Smart Grid in India”, *Power and Energy, IEEE International Conference*, Kuala Lumpur, pp. 953– 957, Nov. 29th 2010–Dec. 1st 2010.
- [5] Batra, Pankaj, Smart Grid–Issues and Prospects for India.
- [6] The Smart Grid Vision for India’s Power Sector: A White Paper published by United States Agency for International Development (March 2010).
- [7] Ali, Sayyad Vajahat *et al.*, Smart grid: An overview and its implementation strategy in India, *International Journal of Development Research*, Vol. 5, Issue, 01, pp. 2985–2987 (January 2015).
- [8] Vivek, K., Context Setting-Smart Grid, India Context and Components, International Workshop on Challenges in Smart Grid and Renewable Resources, Mysore, India, May, 2010.
- [9] McDaniel, P. and McLaughlin, S., Security and privacy challenges in the smart grid, *IEEE J. Security Privacy* 7(3), 75–77 (May Jun. 2009).
- [10] www.nist.gov/smartgrid.



PEM Fuel Cell Technology Demonstration at NLC India Ltd, Neyveli, Tamil Nadu, India

M. Coumarane¹, K. Ramya², R. Balaji² and N. Rajalakshmi²

Abstract: This manuscript is based on the experience gained in the demonstration of a polymer electrolyte membrane system developed at Centre for Fuel Cell Technology, (CFCT), Chennai and demonstrated at NLC India Ltd. (NLCIL), Neyveli. This is an entirely new exercise as the system was demonstrated by International Advanced Research Centre for Powder Metallurgy and New Materials (ARCI) at the industrial site of NLCIL, Neyveli. The resources required for the said demonstration were provided by NLCIL in terms of hydrogen produced through an electrolysis process, coolant water and the required loads. A fully integrated fuel cell system comprising of high performance PEM fuel cell stack with the peak capacity of 5 kW, fuel cell control system and thermal management system with power converters developed by CFCT, ARCI was tested in the premises of NLCIL, Neyveli to demonstrate the PEMFC for stationary applications consisting of ac and dc loads.

Keywords: Fuel Cell, Stack Demonstration, Thermal Power Plant, Alternator, Decentralized, Industry, Environment.

Introduction

Fuel cells are electrochemical devices that convert chemical energy of the fuel into electrical energy where the charged ions pass through the electrolyte to create a voltage difference between the cathode and the anode and the electric current passes through the external circuit. Fuel cells are of several types depending on the electrolyte and the temperature of operation. They are one of the cleanest and efficient methods of production of electricity. The Polymer electrolyte membrane fuel cells (PEMFC) are a type of fuel cell that uses a polymeric electrolyte and operates between ambient to 100°C. PEMFC offers many advantages, like easy start up, low levels of pollution and greenhouse gas emissions, high efficiency and low noise. As a result these devices find application as power source in the stationary, transport and portable sectors. PEMFC can be applied in a wide range of stationary applications like power plants, combined heat and power generating units for household and industrial buildings, for off grid applications and as uninterrupted power sources in back up power sector.

Developing a fuel cell system for commercial exploitation in various applications has been a major challenge both for the developers as well as for the industries. The solution to this problem will require the coordination and interaction of many different disciplines. Although the fuel cell stack is

fundamentally an electrochemical device, the balance of system (BoS) such as the air and water management modules interacts significantly with the stack design. Fluid dynamics, mechanical engineering, and control systems skills are required to develop a properly optimized system. Any organization or set of organizations with a goal of successfully commercializing fuel cells must reflect these interactions and manage these complex interfaces. Fuel cell, owing to the attractive characteristics displayed, is a subject of intense research and development throughout the world. The last five years have seen some major developments in all types of fuel cell technologies.

Due to the easy start up, PEMFC has been the choice of power source in transport sectors with many vehicle developers demonstrating the PEMFC system either as a primary power source or as a range extender or as an auxiliary power source. Recently, there have been some demonstrations of PEMFC as a power source in stationary applications. One of the demonstrations of residential fuel cell unit is the Japan's ENE-FARM program where 120,000 residential fuel cell units have been installed to push the new technology into market place. The units can operate independently when the power grid fails. While many companies participated in the early development and deployment, the main participants now are Panasonic and

¹ Centre for Applied Research and Development, Neyveli Lignite Corporation India Ltd., Neyveli-607803, Tamil Nadu, India. ✉ couma_rane@yahoo.com

² Centre for Fuel Cell Technology, International Advanced Research Centre for Powder Metallurgy and New Material (ARCI), IIT Madras Research Park, II Floor, 6, Kanagam Road, Taramani, Chennai-600113, India.



Toshiba which offer PEM units, and Aisin Seiki, offering SOFC units. PEMFC units have shown 60,000 hrs while cycling on and off to home's response for electricity and hot water with more than double the efficiencies compared to that of grid efficiency. The ENE-FARM program thus demonstrated the fuel cell's capability for power generation to pave a way for transition from petroleum economy to hydrogen economy. Some residential fuel cell units have been deployed in South Korea also with government subsidies. Large stationary PEMFC deployment refers to multi-megawatt units providing primary power to replace the grid or for areas where there is no grid infrastructure or for expansion off grid nodes. Kolon Hydrogenics, a joint venture between Hydrogenics, Canada and Kolon Water and energy, South Korea have installed a fuel cell power plant of 1MW capacity using the hydrogen produced from the refinery.

PEM fuel cells are ideally suited for decentralized power generation, provided hydrogen is made available. In the absence of accelerated methods to test fuel cells, the only option to ascertain the life of the fuel cell systems is to operate them continuously. This is possible only when the hydrogen is available continuously. The purpose of co-operation between Centre for Fuel Cell Technology (CFCT), International Advanced Research Centre for Powder Metallurgy and New Materials (ARCI) and NLC India Ltd. (NLCIL), Neyveli is to forward fuel cell commercialization through research and implementation of practical application of fuel cell technology. Further, being a stationary power project the product size need not be limiting. The co-operation is to evaluate the product that provides maximum possible value in terms of the product durability. Hence, the industrial site that can provide hydrogen was identified at NLCIL, Neyveli.

CFCT, ARCI has developed and demonstrated grid independent fuel cell based power systems in the power range 300–10000 watts. The fuel cell system has besides the fuel cell stack, air moving devices, thermal management systems, humidifier and inverters. Integration of these entire sub units with high efficiency is quite challenging. The other challenges are hydrogen infrastructure in the country. The interaction of the fuel cell system with the fueling infrastructure adds further to the overall complexity of this technology. At Neyveli Lignite Corporation India Limited (NLCIL), Neyveli hydrogen is being produced in a separately in their thermal power plant Hydrogen plant for use in the Alternators for cooling purpose. It was hence, proposed to demonstrate PEMFC system at NLCIL, Neyveli.

For the demonstration a PEM Fuel cell system was continuously and intermittently operated at their site and the generated power from the Fuel cell was connected with decentralized ac and dc loads. The details of results of the

PEM Fuel cell tested in the industrial environment are presented.

Experimental

Fabrication of PEM Fuel Cell Stack

The PEM fuel cell stack developed for this demonstration program consists of 50 cells of active electrode area 770 cm². The solid polymer electrolyte membrane used is Nafion®, DuPont. Anode and cathode contains a layer of carbon supported platinum catalyst. Exfoliated graphite plates (430 × 330 mm) are used as bipolar plates. Copper plate is used as current collector. All the cells are clamped between two aluminum end plates, using nuts and bolts. The fuel cell stack has inlet and outlet ports for H₂ and air and for cooling water. Stack has positive and negative terminals to which the load can be connected.

Operation of PEM Fuel Stack with BoP Components

For effective operation of the fuel cell stack, H₂ gas has to be humidified. A bottle bubbler type gas humidifier was used to humidify H₂ gas before it enters the fuel cell stack. This gas humidification system has been externally attached to the PEMFC stack. Mass flow meter was used for measuring the H₂ gas flow to fuel cell stack. Un-reacted H₂ gas escapes out of the stack via port provided. Air blower was used for feeding air to the fuel cell stack. A controller was provided and used to control the DC voltage of blower for required air flow. Un-reacted air and product water escapes out from the stack via the ports provided in the stack. Since heat is also produced during operation of fuel cell stack, cooling plates are also incorporated in the stack assembly through which water can be circulated. A radiator-fan assembly is used to cool the stack and to maintain the stack temperature at or below 52°C. To operate the fuel cell system, hydrogen is a major commodity. Hence the hydrogen available at the plant can be utilized to generate power.

The activities for demonstration includes site preparation for gas manifold and coolant cycle at NLCIL site, development of PEMFC stack at CFCT, ARCI, development of Balance of systems at CFCT, ARCI, integration of stack with BoP components and get the baseline performance at CFCT, ARCI, transportation of the system to NLCIL, integration with hydrogen supply system at NLCIL site, demonstration at the NLCIL site using available hydrogen, data collection and analysis, documentation and training NLCIL personnel. It is understood that NLCIL plant produces around 8.8 Nm³ of hydrogen, which is convenient to generate power upto 8 kWh. The byproduct hydrogen available was found to be at low pressure as well contains moisture and chlorine at a particular level. Moisture may not be an issue. However



chlorine and low pressure hydrogen may be an issue, which needs to be addressed. If they are quantified, then one can take remedial measures. The time frame set is for 3 months which includes installation, integration, demonstration and data collection.

CFCT, ARCI planned, designed the entire power supply system and fabricated the required components by proprietary processes developed in house. CFCT, ARCI worked with its identified collaborators and develop required power controllers and system controllers. The power controller would also include required safety features for smooth operation of the fuel cell stack. The system consists of 1 Module of PEMFC stack, Fuel management system (Rotometers/Mass flow controllers, H² sensors, pressure transmitters), Air supply units (Blowers, controllers), Fuel cell control system, and Power conditioners (dc to ac conversion, single phase) Control Monitoring system for safe operation. The site requirement for system demonstration includes a footprint space of 1 m³ and 1 m space around the system on all the sides in a well-ventilated room.

Results and Discussion

The PEMFC system developed is shown below.

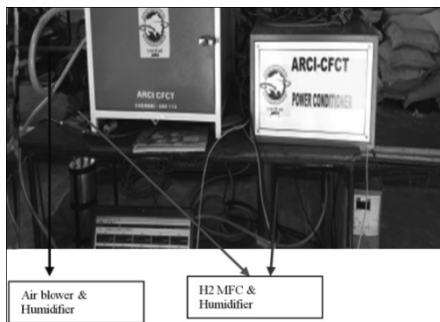


Fig. 1: PEMFC System

A separate manifold system was developed that was integrated with the electrochlorination plant and is given in Figure 2.



Fig. 2: The Manifold System

The power conditioners consisting of both dc-dc converter and dc-ac inverter are connected at the output level. Before

transporting to NLCIL, the stack was operated for its performance and fuel requirement and the data is shown in Figure 3.

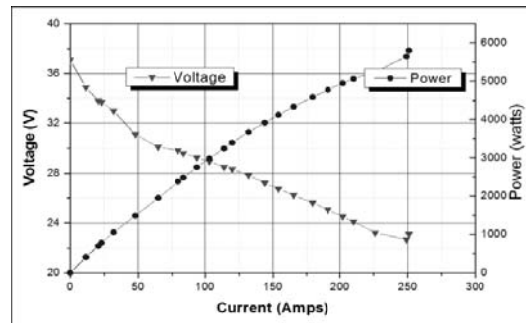


Fig. 3: Performance of Stack before Transportation

The system was demonstrated using the hydrogen provided by NLCIL, at the said site and the data was logged continuously using a data logger integrated with laptop. Every day the system was operated for a said period depending on the amount of hydrogen provided by NLCIL and was working satisfactorily. Initially, the stack was delivering a power of 1.8 kW using the hydrogen supplied by NLCIL. Individual cells were monitored continuously throughout the demonstration period.

The current voltage characteristics of the PEMFC system are shown in Figure 4.

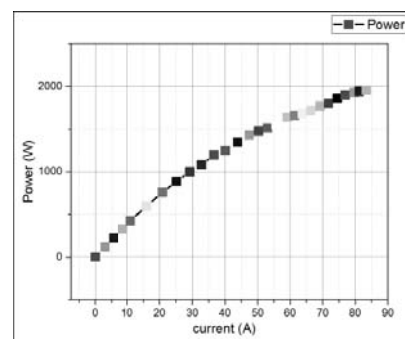
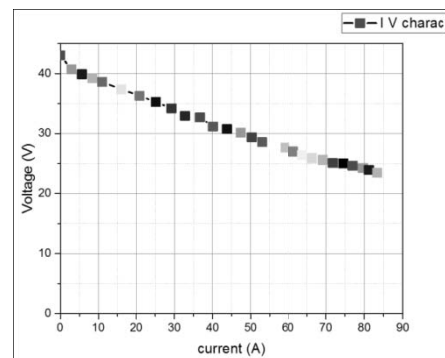
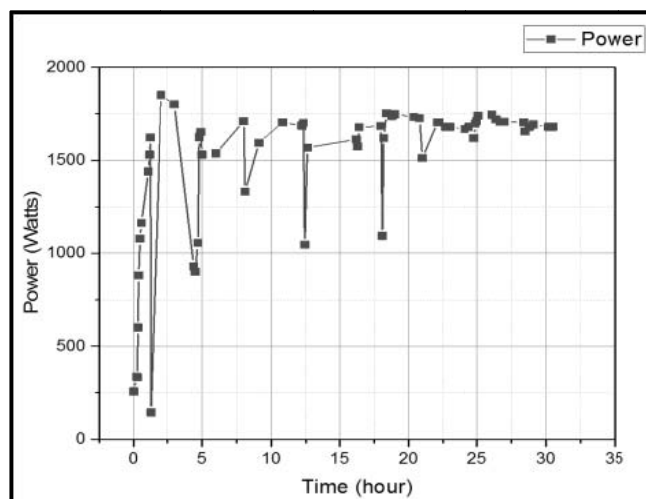


Fig. 4: Voltage and Power against Current of the PEMFC System



As one could see from Figure 4, that the system delivered an open circuit potential of 43 volts and delivering current of 85 A@23 V. The operating temperature was found to increase from RT to 50°C. Coolant water was optimized to maintain the stack at a convenient temperature of 50–55°C. The varying dc voltage of 43 to 23 V was conditioned for a constant dc voltage of 48 V to operate the dc loads and also inverted to ac of 230 V to use for ac applications.



The system was operated intermittently at the NLCIL site with the help of many cylinders of hydrogen compressed up to ~125 Kg/sq cm of pressure. Hydrogen flow was controlled and monitored using a mass flow controller. Air was supplied from a blower operating on 0–12 V power supply for air regulation. The stack was cooled by water provided by NLCIL, through internal manifold system and the

temperature was maintained between 50–54°C with the help of a thermocouple. During the period, the system generated power of 54 kWh (~1.8 kW for 30 hours) using hydrogen, which is supposed to deliver 60 kWh. This may be due to the high stoichiometry of 1.1. During the power generation, the generated DC power was fed to a power conditioner of both DC-AC inverters as well DC-DC converter. The following loads like 5 halogen lamps, AC display unit, LED panel, Industrial fan and all CFLamps.

Conclusions

It has been observed that PEMFC system worked at the industrial site with a current/voltage efficiency of 90%, system efficiency of 45% using the hydrogen provided by NLCIL. This can be implemented for street lighting in one sector in the NLCIL campus, as suggested by higher officials of NLCIL.

Acknowledgements

We would like to acknowledge both NLCIL and ARCI management for initiating this activity. A special mention to former ARCI Director and former Associate Director for their constant support and encouragement. We also thank ARCI Director, Associate Director for their continuous support. Special thanks to CFCT technical staffs for their dedication and without their help, this demonstration would not have been completed. We thank all the team members of CFCT, ARCI. Our sincere thanks to former NLCIL Director (Planning and Project) and present Director (Planning and Project) and General Manager (CARD and CEC) and all the NLCIL staff for supporting this activity.



The Intelligent Power Grid with Internet of Thing (IoT) Technology

Debasish Mondal¹

Abstract: An intelligent power grid or Smart Grid (SG) is a power system network that can intelligently integrate the behaviour and actions of all elements connected in it; generators, consumers and both in order to efficiently deliver sustainable, economic and secure electric supply. The Internet of Things (IoT) is an appropriate technology which can be utilized in power system network to make the power grid to be more “smart”. The IoT technology speeds up the sensing and information exchange among all the integrated elements of a power system network by which it is possible to monitor effectively the resilience of the power transmission grid, the stability and control of grid operation, reduction of economic loss and the prevention of damage due to natural disaster. This paper focuses on the path towards the application of IoT technology in smart grid architecture, grid resilience and the online condition monitoring and control of power transmission and grid operation.

Keywords: Flexible Alternating Current Transmission System (FACTS), Internet of Things (IoT), Phasor Measurement Unit (PMU), Power System Network, Smart Grid (SG).

Introduction

The Internet of Things (IoT) is a system of interrelated computing devices; mechanical, electrical or electronic machines, objects, animals or people that are provided with unique identifiers, ‘IP address’ and the ability to transfer data over a network without requiring direct human-to-human or human-to-computer interaction.

The goal of the IoT is to enable things to be connected anytime, anyplace, with anything and anyone ideally using any path/network and any service [1].

Almost every aspects and strategies of Smart Grid needs the support of IoT. An energy-efficient solution based on concept of Communicating Power Supplies (CPS) has been addressed in [2] to facilitate the information transfer and control the information between the device and building management system. In [3] the application of IoT is introduced in online monitoring of power system focusing on the construction and development of smart grid. A “vision of IoT” with China’s perspective has been depicted in [4], which describes the open and general IoT architecture and also discusses the opportunity and prospect of IoT. The nature and impact of IoT and how the IoT technology is driving energy innovation & solution in power industry has been reported in [5]. This report enables any organization to identify where the IoT can potentially create value in their industry and develop strategies to capture operational

benefit. The concept of smart grid and the IoT technology has also been presented in [6], where the urgency of applications of IoT and the IoT based construction of power grid are pointed out.

The Internet of Things technology for smart grid forms a high speed smart network among all kinds of information sensing equipments like; RFID device, Infrared sensors, the Global Positioning System (GPS), laser scanning, etc. [7]. The Phasor Measurement Units (PMU’s) becomes now the “health meter” for the grid in IoT, where the amount of information collected by the PMUs on the status of the power grid is found to be around 100 times denser than what is collected by the conventional units. Different examples are provided in [8] on how Texas Instruments (TI) has developed full system solutions by combining hardware and software to address some of the challenges in building a smarter and more connected power grid based on IoT.

This paper is presented the Smart Grid (SG) architecture based on IoT based technology and also analyses the fact of grid security and reliability through IoT. Finally, illustrated the way of online condition monitoring and control of power transmission grid through IoT.

Smart Grid Concept

The Smart Grid is a next-generation electric and communication network that can intelligently integrate the

¹RCC Institute of Information Technology, Beliaghata, Kolkata-700015, West Bengal, India. ✉ mondald12@yahoo.in

behaviour and actions of all users connected to it; generators, consumers and both in order to efficiently deliver sustainable, economic and secure electricity supplies for small to large-scale generation, transmission, distribution. It includes software and hardware applications for dynamic and optimum electric system operations, maintenance and controls at the supplier and consumer level. The conceptual model of a smart grid is shown in Figure 1 [9]-[10].

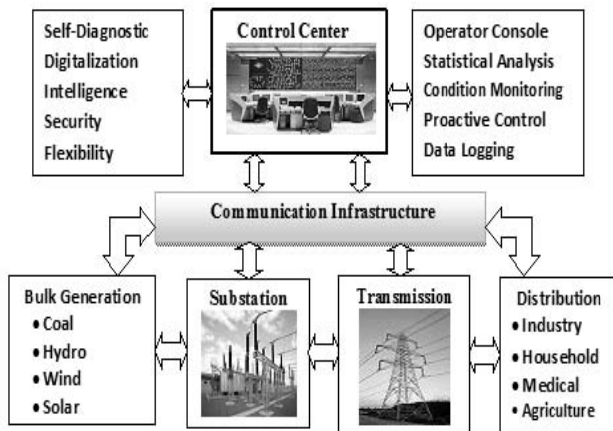


Fig. 1: A Conceptual Model of a Smart Grid

The concept of smart grid can be “market oriented” and the “grid oriented”. The main objective in market oriented grid concept is to increase the level of interaction between electricity suppliers and the consumers. Here, the concept of deregulation of electricity market is the prime matter. In grid oriented smart grid concept the main concern is the network or grid and the operations and control of grid. Aims of this concept are reducing investments costs in reinforcement of smart transmission network in the existing systems, control of outage, introduction of self-diagnostics features and condition monitoring of grid components.

Smart grid technologies usually refer to (i) the smart sensors or transducers that can sample power system dynamic variables at very fast rates and calculate their phase relationships by coordinating with a GPS time signal, (ii) the high bandwidth communications that can move voluminous measurement data to monitoring and control stations with high baud rate, and (iii) fast controllers like high speed circuit breakers and power electronic controls (FACTS) that can be operated by remote signals. These establish the possibility of many new integrated applications for monitoring and automatic control that can help the system operation and maintenance with intelligent way.

The present paper discusses the probable applications of these new technologies based on Internet of Things (IoT) that make possible the modifications of existing grid into more smarter transmission grid system.

IoT based Architecture of a Smart Grid

The Architecture of a Smart Grid based on IoT is broadly divided into three layers; perception or sensing layer, network or communication layer and application layer (Figure 2). These are relevant with information collections, information transmissions and information processing. In smart grid, these technologies can effectively be employed in order to provide important technical supports for the generation, transmission and distribution of electricity and other controlling & monitoring aspects [11].

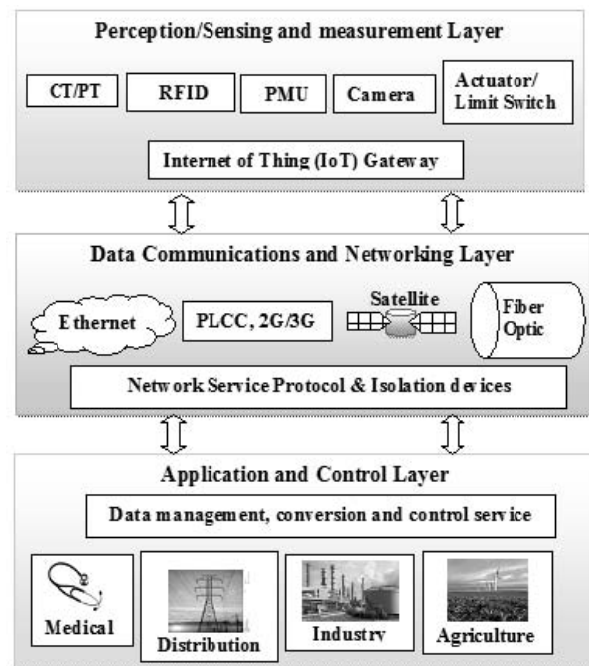


Fig. 2: The IoT based Architecture of a Smart Grid

Different sensors; Current Transformer (CT), Potential Transformer (PT), Phasor Measurement Unit (PMU), Radio-Frequency Identification (RFID) sensors, smart camera and others technical indicators which are directly coupled with physical parameters are mainly used to perceive data and gather information at the perception layer. The acquired data from the perception layer, reaches the level of application in smart grid via short distance (Zig-Bee, Bluetooth etc.), or wide area communication technology like IP based Internet, Fibre optic, Power Line Carrier (PLC), 2G/3G mobile communication network or satellite & cloud communication network etc.

The Application layer of IoT is the system’s application centre or control center of a smart grid. In this layer the applications of Internet of Things technology is involved with grid oriented smart grid infrastructure and all aspects of production and management through the use of intelligent computing, pattern recognition technology and other



technologies. The application layer contains local display units, final controlling elements, auto-contractors and circuit breakers and different type of consumers; home appliance, medical applications, agriculture sectors, industry usage, traffic and transportation control and public safety and security measures etc. In application layer through the integration of grid data analysis and processing, it is possible to achieve intelligent decision-making, control and services.

Power Grid Resilience through IoT Technology

The initial objective of grid modernization is to study its resilience, which ensures about the grid reliability and durability. Security and resiliency concerns have grown with increased risk to energy infrastructure from extreme weather, asymmetric physical threats and vulnerabilities, and with ever increasing cyber-sophistication. An IoT based infrastructure to achieve resilience for a power grid is represented in Figure 3. The grid reliability cannot be ascertained merely by keeping operating parameters within stability limit. Rather, resilience requires knowledge of the state of the grid that can come only from the ubiquitous deployment of a wide variety of networked sensors and control devices across the grid which can be communicated via standard protocols. Grid owners and operators need to prioritize the right projects that will protect critical assets from severe weather, cyber attacks, theft and terrorism; prevent disruption of

service for customers; restore service swiftly after an outage; and maintain/prepare for compliance with current and future regulatory standards.

In the question of resilience, the distribution grid will also be needed the flexibility and agility to accommodate all types of Distributed Energy Resources (DER); Li-ion storage and advanced renewable generation resources such as solar and wind, etc. However, solutions to this challenge may be emerging technology. Adding IoT technology to an inverter can enable intelligent automated local actions and standard-based monitoring and control of the device, making it a “smart inverter.” Smart-inverter standards limit risk by creating a reliable and accurate data stream on which personnel working on the transmission lines can count to reduce the safety hazards and based on which operators can rely to maintain grid reliability.

Condition Monitoring of Power Transmission Grid Applying IoT

In order to implement real-time online condition monitoring and control of power transmission, the IoT can play inevitable role (Figure 4). The monitoring of power transmission system can be achieved in two ways. One part is associated with the condition monitoring of the transmission lines which is particularly related to the disaster management. In overhead transmission lines, the IoT technology can be used not only to carry out the fault diagnostic, but also improve the perception of power transmission, including meteorological conditions, tower inclination etc. The IoT based sensors like conductor galloping and vibration sensor, meteorology sensor, icing and conductor temperature sensor are installed on the high voltage transmission lines; 220 kV, 500 kV or on the transmission tower. The communication between the IoT devices on the transmission lines and the master station is based on wireless networks, optical fibre or wireless broadband network.

The other part is related to the asset management, measurement and control of electrical parameters like voltage level, power consumptions and load conditions, phase and frequency to study the state and health of the grid. In asset management scheme the IoT uses the RFID coding system. With the help of RFID tags on the electric equipment, it is accurately possible to locate and supervise the health of electric equipments in the grid which enhances the power supply reliability and guarantee the stability of power grid. The IoT based ‘power monitor’ transmits data for power consumptions and load conditions from different load centres to a dedicated front end processor through wireless communication.

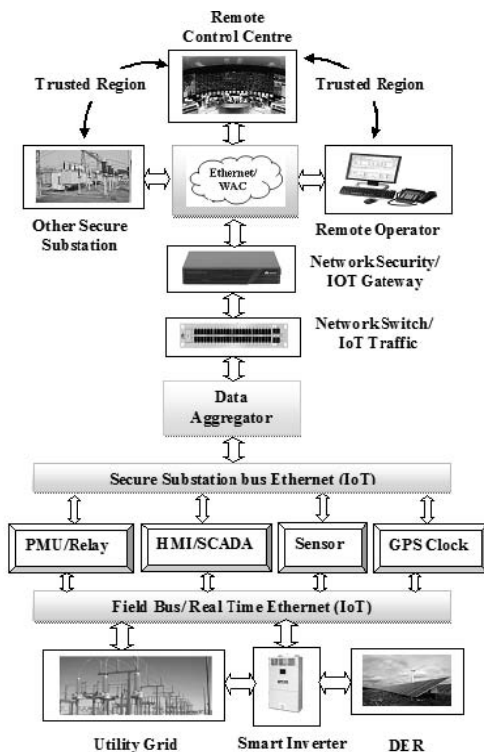


Fig. 3: IoT Based Infrastructure of Grid Resilience

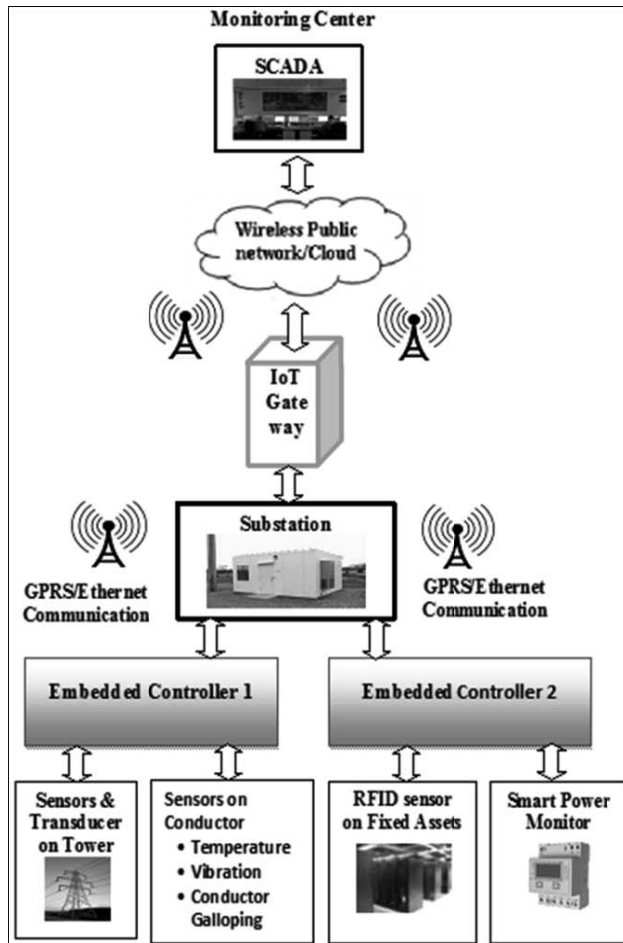


Fig. 4: Condition Monitoring of Power Transmission Line, Fixed Assets and Load Condition

The NXP LPC1768 microcontroller may be chosen for these applications [12] since it provides peripheral support for Ethernet which helps in implementing IoT part of the system. This embedded controller has library files built for Xively (cloud platform) which helps to monitor the values of sensors through Internet. It is a low power low cost device and it can fairly operate up to 100MHz operating frequency. It facilitates the Ethernet and USB to run at the same time without affecting the performance.

Due to the adoption of very complex system in smart grid, a high speed controlling devices like Flexible Alternating Current Transmission System (FACTS) with various advance control technologies can be a promising trait in IoT (Figure 5). Thyristor Controlled Series Compensator (TCSC), Static Synchronous Compensator (STACOM) and Unified Power Flow Controller (UPFC) are the important member of the FACTS family [13], which are proven to be very robust and effective selection in solving power system problems.

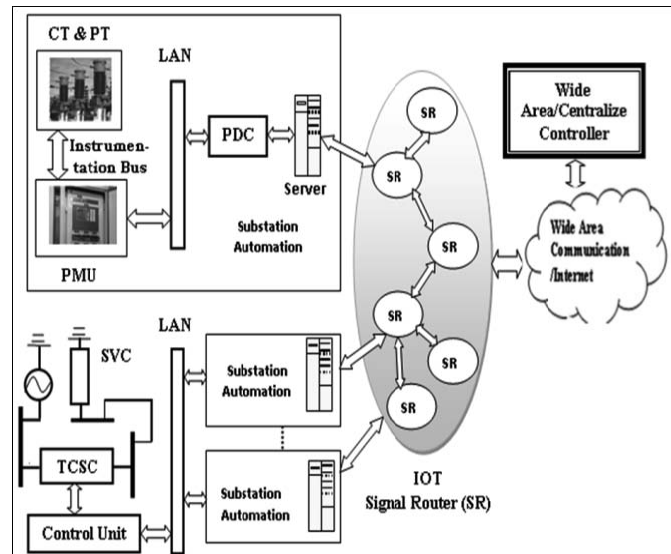


Fig. 5: IoT based Control of Power System Grid

The FACTS controllers are either connected in series or shunt with the transmission line, depending on their requirement in the power system. The FACTS controllers not only balance real and reactive power flow in the power system but also they can be used for solving various power system problems like power system steady state and transient stability, sub-synchronous resonance, dynamic voltage instability, congestion management, thermal ratings, etc.

The Phasor Measurement Units (PMU's) [14] becomes now the "health meter" for the grid in IoT, where the amount of information collected by the PMUs on the status of the power grid is found to be around 100 times denser than what is collected by the conventional units. The phasor measurement units provide synchronized positive sequence voltage and current measurements within a microsecond. This has been made possible by the availability of Global Positioning System (GPS) and the sampled data processing techniques developed through microprocessor. The custom built Digital Signal Processors (DSP) can perform this task through computation of Fast Fourier Transformation (FFT) of all harmonics up to the Nyquist limit. The computed string of phasors, one for each of the positive sequence measurements, is assembled in a Phasor Data Concentrator (PDC) and this data stream from PDC is then transmitted over a dedicated communication line through the modems.

In addition to measure positive sequence voltages and currents these systems also measure local frequency and rate of change of frequency and may be customized to measure harmonics, negative and zero sequence quantities as well as individual phase voltages and currents.



Conclusion

The development of IoT and its application in a Power System is a revolution to the power industry. This paper has dealt with the evolution and architecture of a Smart Power Grid System and its multiple aspects based on IoT technology. Although the enabling technologies described above make the IoT concept feasible, a large research effort is still required. But innovation is always a part of the electric utility heritage. Thus, focusing into this tradition it is essential to meet today's challenges in power transmission grid and create a more intelligent grid. The IoT offers exponential technologies that utility company can deploy and leverage to find new ways to explore and extract incremental value from the intelligent grid. However, the path forward is not always clear. The Information "value loop" provides a structured framework to help and understand how to create and capture value. Applying the realization of value loop from IoT technology to the electric utilities, it is possible to find the road ahead of intelligrid system and ultimately, the IoT will be instrumental in building a more connected, cost-effective and smarter smart grid.

References

- [1] Vermesan, O. and Friess, P., Internet of Things: Converging Technologies for Smart Environments and Integrated Ecosystems, River Publishers Series, Denmark, 2013.
- [2] Lanzisera, S., Weber, A.R., Liao, A., Pajak, D. and Meier, A.K., Communicating power supplies: Bringing the internet to the ubiquitous energy gateways of electronic devices. *IEEE Internet of Things Journal*, 1(2), 153–160 (2014).
- [3] Ou, Q., Zhen, Y., Li, X., Zhang, Y. and Zeng, L., Application of Internet of Things in Smart Grid Power Transmission. In: *2012 IEEE Third FTRA International Conference on Mobile, Ubiquitous, and Intelligent Computing*, Vancouver, Canada (2012), 96–100.
- [4] Chen, S., Xu, H., Liu, D., Hu, B. and Wang, H., A vision of IoT: Applications, Challenges, and Opportunities with China perspective. *IEEE Internet of Things Journal*, 1(4), 349–359 (2014).
- [5] Grant, C., McCue, J. and Young, R., The Power is on-How IoT technology is driving energy innovation. A report by the Deloitte center for Energy Solutions, Deloitte University Press, 1–20 (2015).
- [6] Hua, L., Junguo, Z. and Fantao, L., Internet of Things Technology and its Applications in Smart Grid. *TELKOMNIKA. Indonesian Journal of Electrical Engineering*, 2(12), 940–946 (2014).
- [7] Li Xun, G. Qing-wu and Hui, Q. The application of IoT in power systems, *Power System Protection and Control*. 38(22), 232–236 (2010).
- [8] Monnier, O., A smarter grid with the Internet of Things, *White paper, Worldwide Smart Grid Marketing Director Texas Instruments (TI)*, 1–10 (2013). www.ti.com/smartgrid.
- [9] Bose, A., Smart transmission grid applications and their supporting infrastructure, *IEEE Transactions on smart grid*, 1(1), 10–19 (2010).
- [10] Zhang, P., Li, F. and Bhatt, N., Next-Generation monitoring, analysis, and control for the future smart control center, *IEEE Transaction on Smart Grid.*, 1(2), 186–192 (2010).
- [11] Rao, W., Ding, J.Y. and Li, R., Application of Internet of Things Technology in Smart Grid, *Central China Electric Power*, 24(2), 1–5 (2011).
- [12] Sindhuja, P. and Balamurugan, M.S., Smart power monitoring and control system through internet of things using cloud data storage, *Indian Journal of Science and Technolog*, 8(19), 1–7 (2015).
- [13] Hingorani, N.G. and Gyugyi, L., Understanding FACTS: Concepts and Technology of Flexible AC Transmission System. IEEE Press. 2000.
- [14] Phadke, A.G. and Thorp, J.S., *Synchronized Phasor Measurements and Their Applications*. Springer: New York, 2008.



Towards Sustainability in Power

Ashok K. Jain¹ and Ranjit Sinha²

Abstract: *This work is an endeavour to substantially reduce the power consumption in domestic, entertainment and office environment in general.*

"If you can cool the person rather than the building where they work or live, that will save energy," said Yi Cui, an Associate Professor at Stanford University in the US on September 2, 2016.

The first idea presented is based on the observation that whole body achieves comfort level even with one part of the body being at that level, such as a Table fan at Head level or a Heater/Blower at foot level. For hot weather, a person needs to wear only a double walled cap hosting a small tubular duct outlet, receiving cool air from a small air conditioner. The air circulation through it would achieve the same comfort level as from total room air-conditioning at far lower energy consumption and costs. The second idea is similar. One occupies a small, perhaps less than 4.30 cu m of space while sleeping. Assuming a middle class couples have a bedroom to measure 40.50 cu m, an air-conditioner is used to cater to 47.61 cu m of space.

If duct of mosquito net size enclosure of 4.30 cu m is used while sleeping, only about 10% energy will be used, consequently saving in power. Experimental validations are also presented in the main work.

Keywords: Power Consumption, Energy, Carbon footprints, Environment.

Introduction

The surge in demand for energy is an indication of improving economy. As India grows into a global giant, the urgent need for clean, efficient and quality energy that does not add to Carbon footprints in production, transmission and usage, and yet meets the demand of all sectors, industrial and non-industrial, urban and rural, agriculture and domestic, office and entertainment, grows. And to meet this ever-growing demand, conventional wisdom dictates that more and more electricity generation plants be planned by the governments. This means huge capital cost and use of other scarce resources like coal and water. And perhaps, use oil and gas, much of it imported, and strengthen the transmission and distribution sectors. Every step means more expenditure. There is no denying that new power plants would be required, the systems must be strengthened, and energy usage increase assisted so that development goals are met. However, it will help, if one endeavours to reduce this heavy burden on our national resources and finances by innovating ways and means for reducing the consumption of power, at least in non-industrial domain without compromising quality or comfort. The first meaningful steps

have been taken. LED bulbs are available, some through the government and more in the open market. The prices are also declining and better and better LED bulbs are coming into the market. The issues of availability, affordability and accessibility are also being tackled head-on. Other initiatives are also being taken, some under implementation and some on the drawing-board. This work makes an endeavour in the direction of an adage, "Energy Saved is Energy Gained" The thrust of the authors is to promote the idea of energy savings with smart moves. Essentially it is a concept paper identifying some ideas for further development, trials and implementation.

Fundamental

It is a fact that if one sits at a table with a fan blowing onto his face, he achieves a comfort level that makes his entire body comfortable. It is a general practice. One can work on this fact for air-conditioning too. Similarly, keeping a heater/hot air blower at one's feet makes one comfortable in winter. Even a person with high fever gets relief by putting cold cloth strips on his forehead only. Hence the first idea stands.

¹Former Professor, Department of Electrical Engineering, Motilal Nehru National Institute of Technology Allahabad, India.

✉ akjferrocement@yahoo.com

²Tilothu Mahila Mandal, Bihar, India.



Idea No. 1

These observations lead us to the conclusion that blood flow in the body plays the role of the temperature equaliser in the body. If it is so, why control the weather of the whole room to make a few persons comfortable in the room? This led us to the following contraption.

With the continuous flow of cool air from the air-conditioning unit, the person would remain comfortable with just 0.03 cum of cool air compared to at least 30 cum of air to be cooled for the entire room. These Cool Caps (in Figure 1) can be an integral part of every chair in the room and whoever comes in and uses the Cool Caps will be comfortable. If the investment in Cool Caps appears to be threatening, consider the savings in capital expenses on the air-conditioning apparatus and the savings in energy bills.

{In this auditorium, there are about 500 people and so maximum 15 cum cool air is needed instead of 900 cum (15 m × 12 m × 5 m)}

One can easily appreciate the saving in power.

Extending the idea little further, just for 0.03 cum air, one can think of a solar powered air conditioning portable unit which can be conveniently carried on the back.

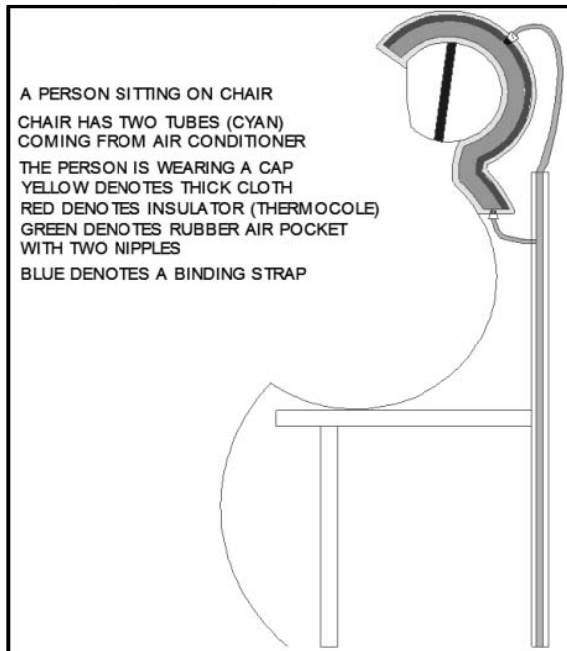


Fig. 1: Schematic Presentation of Cooling Cap

Idea No. 2

While sleeping, all needed to weather control a small space around the bed (like a mosquito net) and not the whole room. A set up on these lines is given in Figure 2.

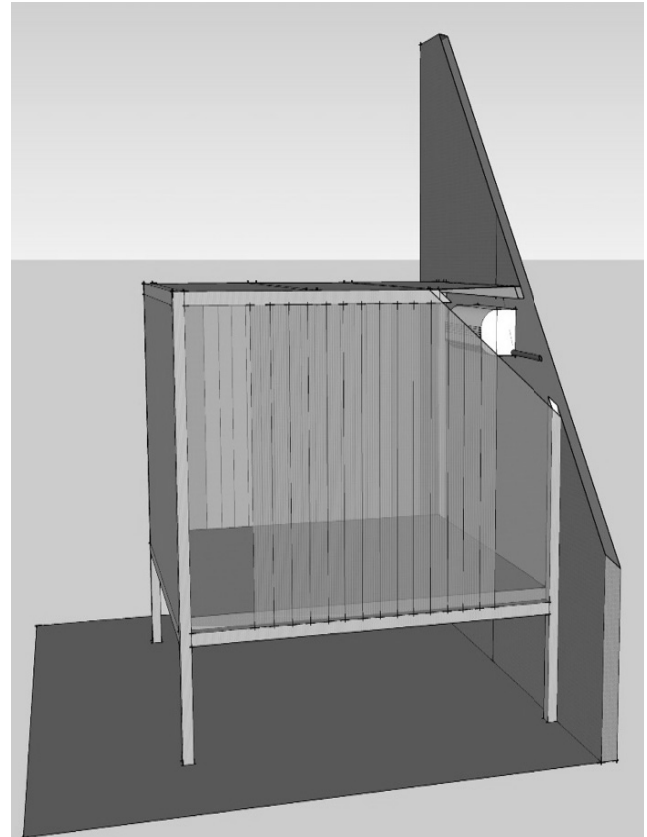


Fig. 2: Bed with Enclosure and Air Conditioner

Transparent or translucent plastic can be used to cover the pipe frame with plastic louvers on two sides for entry or exit to the bed. Louvers will also serve as air vents in the event of power failure. The total volume of air in this set up is only 4.30 cum as against room volume of about 40 cu m giving a consequent saving of power. One can either use a smaller air conditioner or use one outdoor unit of a split air conditioner to feed multiple beds. In addition, the volume of heated air going in the atmosphere will also get proportionately reduced.

Idea No. 3

These days almost 50% urban and about 5% rural households use some kind of a water purifier, which are electricity driven. The power consumption of these units is increasing day by day as new features are being added like R/O, U/V etc. The total average pure drinking water requirement is not more than 20 litres per family per day.

The Nano-particle based water purifiers can be used, as given in Figure 3. They are now available in the country which can give up to about 30 l pure water per day. These do not use any power, are cheaper, and have a life of about five years.

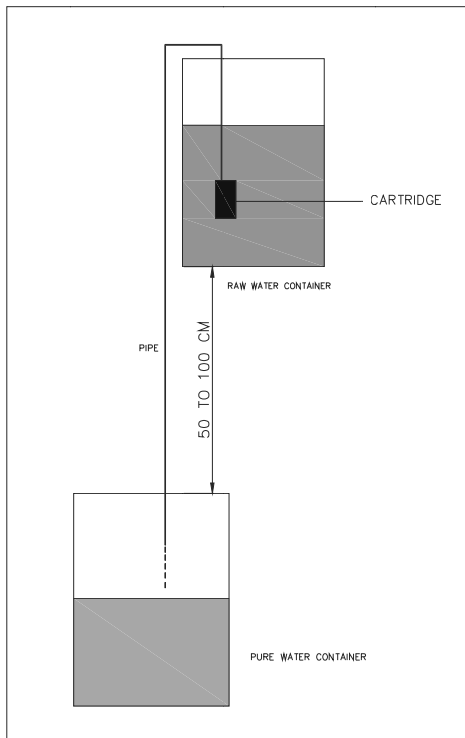


Fig. 3: Nano-Particle based Water Purification

Idea No. 4

While constructing a building, if one adopts the sandwich walls and roof system with two 25 mm thick ferrocement with 50-60 mm thick Expanded Poly-styrene (Thermocole) in between, the insulating properties of thermocole do provide a building with excellent thermal and acoustic properties. A sandwich construction in progress is given in Figure 4.

A two storied building made in Lucknow, Uttar Pradesh for a doctor couple, gave them an about 50% saving in weather control units whether hot or cold. A floor added in a three storied school building at Tilothu, Bihar showed a three degree drop in temperature inside the building with sandwich construction as compared to lower conventional constructions with one brick walls.

These advantages are in addition to about 40% saving in overall embedded energy in materials and 25% saving in labour component as compared to the conventional construction. It is also to be noted that overall load of this system of construction is very low and the fourth floor at Tilothu was not possible at all because of the excessive loading on the foundation.



Fig. 4: Sandwich Construction in Progress

Conclusion

Using these ideas, our power requirements in the domestic, office and entertainment domain can be reduced to a major extent.



Substation Automation: A Case Study

D.J. Patowary¹

Abstract: *The electrical power system has seen simultaneous development of few of its basic components—Intelligent Electronic Device (IEDs) like numerical relays (NR), intelligent meters, vacuum circuit breakers (VCB) etc. The advent of the IEDs has helped simplifying implementation of the substation automation (SA) system by way of offering an intelligent and interactive platform beyond the conventional SCADA systems. Some important capabilities of substation automation are:*

- *Increased performance and reliability of electrical protection.*
- *Capability to record alarms, events and disturbance which facilitates in power system fault analysis.*
- *Display of real time substation data.*
- *Remote monitoring and control.*
- *Increased integrity and safety of the electrical power network including advanced interlocking features.*
- *Advanced automation functions like intelligent load-shedding, tap changer, etc.*
- *Time synchronisation.*

Keywords: Substation Automation System, IEC61850 Communication Protocol, Intelligent Electronic Device, Retrofitting of Numerical Relay.

Introduction

Till the year 2000, communication protocol of the IEDs were different depending on manufacturers and protocol converters were used to communicate two different make of IEDs to integrate with substation automation system. Use of protocol converters resulted difficulty in communication which requires additional time, loss of data and also time synchronisation was difficult. In 2001, IEC 61850 communication protocol was introduced as an International standard with release of ten different standards. The new protocol has got acceptance from the Industry. This was considered to be one of the great things to happen in the field of IED communication which had the potential to be a game changer. The introduction of the Substation Configuration Language (SCL) of the IEC 61850 protocol has facilitated the interoperability between IEDs of different manufactures bringing great relief to the end users aspiring to implement Substation Automation System. The GOOSE functionality (Generic Object Oriented Substation Event) has made horizontal communication possible between the IEDs thereby reducing the control cabling. The client/server communication mode with 100 Mbps Fibre Optic (FO) communication has made it more efficient and faster.

In spite of acceptance of the new standard by the industry, the proprietary protocols were not discarded. The IED manufacturers were not ready to give up the proprietary protocol. In India, the IEC 61850 protocol was mostly used in the power distribution sectors while it was not marketed in the other industry sector in the initial stage.

It is during that time, an opportunity came to implement a substation automation system as part of a new project in one of the Indian Oil Refineries and it was decided to take the benefit of the IEC61850 communication protocol. In this article it is aimed to share the experience of implementing an SA System using the new communication protocol.

The salient features of the project were:

- A new 11 kV distribution switchgear.
- Retrofitting of Numerical relay in old 6.6 kV switch-gear.
- Creating facility for having a single substation automation system where all substations of the refinery will be integrated in future.
- Implementing an intelligent load shedding scheme.
- A substation automation system for control, monitoring and measurement functions.

¹Power and Utilities Department, Haldia Refinery, Indian Oil Corporation Limited, Haldia-721605, West Bengal, India. ✉ djp792@gmail.com

The first thing to be finalised in the new project was to use the IEC61850 communication protocol for all the hardware devices such as numerical relays, Ethernet switches, RTUs, etc. so that the interoperability benefit can be utilised in future. The decision to go for the new protocol was taken after detail product evaluation by ensuring interoperability test between the IED of different manufacturers- Siemens, ABB and Areva. In order to utilise the objective as mentioned above, detail planning was made as follows:

1. The new 11 kV switchboard to have numerical relays complying to IEC61850 communication protocol with dual redundant FO port. The relays to be utilised for providing feeder status (breaker, transformer), control (breaker ON/OFF) and measurement functions (Amps, volt, MW, MVAR, MVA).
2. Installation of RTUs complying with IEC 61850 protocol in all substations of the refinery (total 14 substations) provision for future integration.
3. Retrofitting an old 6.6 KV switchboard with numerical relays complying with IEC 61850 protocol.
4. All numerical relays to have dual redundant FO communication port.
5. Interconnecting all substation RTUs with dual redundant fibre optic network.
6. Implementing a customised load shedding programme having contingency based load shedding with frequency based load shedding as back up.
7. Use of numerical relays and RTUs as part of the load shedding scheme by utilising the benefit of GOOSE messaging; hard wired tripping from the RTUs in substations having old relays.
8. A substation automation system to integrate all functionalities – breaker control, feeder status, metering, and transformer tap changer and load shedding.
9. GPS based time synchronisation for the complete system.
10. To provide an intelligent and user friendly HMI for operator control.
11. To generate shift wise report.

The project was successfully commissioned in the year 2008 with full functionality of control, metering and protection functions and power load shedding scheme. It has gone several expansions with addition of more substations and also with numerical relays of other make. Few of the building blocks of the project are discussed as follows:

System Architecture

The vision of the project was to build a new substation and also integrate old substations under a new SA system. Hence the architecture was built with a combination of numerical relays and RTUs. The numerical relays to be used for

facilitating status, control and measurement functionality including alarm, event and disturbance recording for the new substation and other substation with retrofitting of numerical relays. The RTUs will be used to collect data and send trip command as potential free contact from the DO interface. A dedicated FO network to interconnect all the RTUs and numerical relays using industry grade Ethernet switches. Ethernet switches were installed in the new switchboard to connect the numerical relays. A part of the architecture is shown in Figure 1.

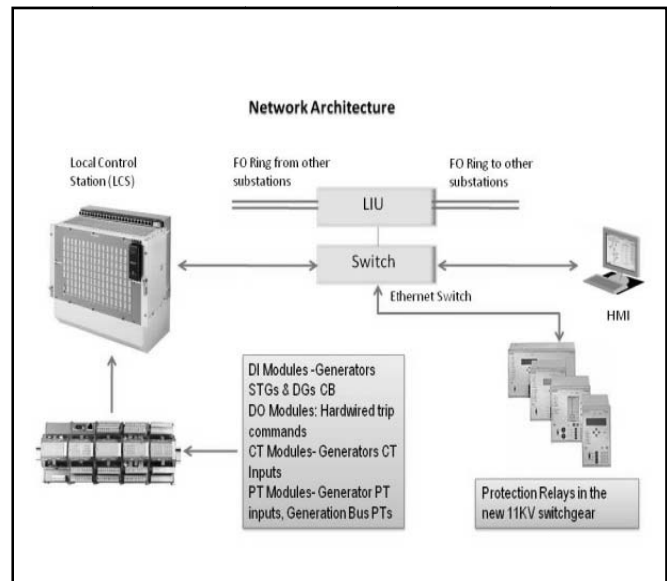


Fig. 1: Network Architecture

Network Monitoring

The GOOSE feature of the IEC 61850 protocol was utilised for horizontal communication for protection interlocks in the new switchboard and also to send Load shedding trip command. All operational (SCADA) and non-operational (alarm, event) data from the new switchboard and the retrofitted switchboard was available to the substation automation system through a rugged FO communication network. The most critical trip command for load shedding is also sent through the same communication network. These data are time critical and used for control and monitoring of the power system like breaker ON/OFF, transformer tap changing etc.

It was therefore critical to have a system of close monitoring of the communication network. It was achieved through dedicated software which indicates the status of communication in form of change of status in a dedicated network monitoring window and alarm. The complete network connecting the servers, RTUs, relays, LIUs and Ethernet switches were monitored (Figure 2).

HMI

Human Machine Interface (HMI) is the link between the operator and the machine. The HMI should therefore be very intuitively designed to ensure effective use of the intelligent hardware/devices for convenient and safe use of the power system. Considerable effort was put during the engineering stage to build the interface should be simple to understand & operated by the operator.

The single line diagram functions as the foundation to provide all relevant information to the operator. Real time data with regard to the status of the breaker or the status of various interlocks was made available as pop up screens. The real time status enables the operator to inform the maintenance engineer in case of any trouble. Sufficient checks and interlocks were provided to ensure safe operation of breaker or changes in the load shedding program. The real-time analogue values, breaker and interlock status, communication status and alarm/ event enable the operator to monitor the power system very efficiently and effectively. A glimpse of the HMI is shown in Figure 4.

Interoperability

After successful implementation of the initial project, opportunity came to realise the intended benefit in the initial

design phase when a new substation was to be integrated. The numerical relays were procured with IEC61850 protocol with due test certification from recognised international testing institutions for IEC61850 compliance. However, after connecting into the existing substation automation system, there were communication error and the new relays were not responding to commands and there was no status coming to the HMI. Prolonged consultation with the R&D group of both the vendor's and interoperability test at the manufacturers' R&D, the problem was not getting resolved. There were reservations to share the SCL files of the new relays. Ultimately, with firm ware update by the substation automation vendor, the new relays could be interfaced with the existing system. The whole process took approx. one and half years. This experience generated questions:

- Whether compliance certificate by verification institutes guarantees interoperability between different make of IEDs?

It will be therefore necessary to ensure interoperability test before procurement action and also asking to submit the Substation Configuration Language (SCL) files along with the IED as part of purchase order condition.



Fig. 4: A Glimpse of the HMI



Wish List

Considering the immense potential of the present day IEDs which is becoming more intelligent day by day and adding more and more functionality due to continuous R&D, the capability of the substation automation system must have increased manifold. Some requirements which can bring more value to power system automation and problems are discussed here.

Integration of Vacuum Interrupter Operating Cycle Diagram in NR

The operating cycle diagram as per IEC 62271-100 of a Siemens make VCB is shown in Figure 5 which shows relation between breaking current and interrupter life. The Siemens make numerical relays can record the breaking current as seen by the relay. Relays of other make may also have this feature. By incorporating the vacuum interrupter curve of different manufacturers in the relay library as a standard feature and making provision to record the fault current phase wise, an alarm or trip interlock can be generated to prevent the VCB to put into service once the interrupter reaches end of life. This can act as an important safety interlock to prevent damage to installations.

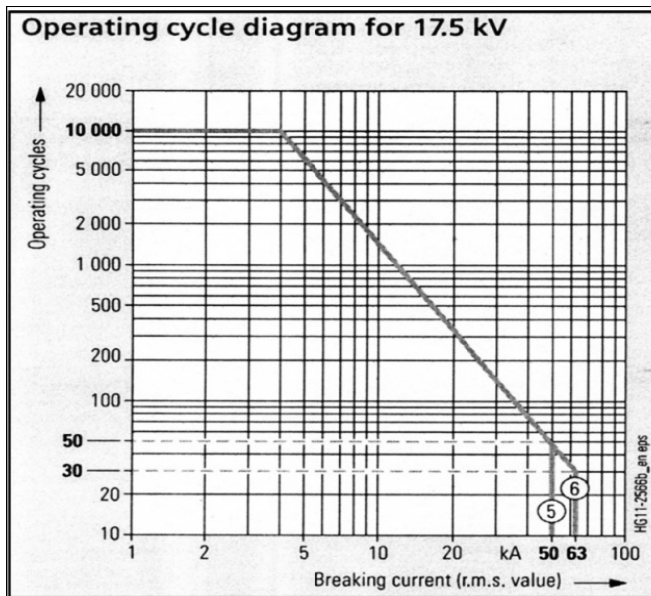


Fig. 5: Operating Cycle Diagram as per IEC 62271-100 of a Siemens make VCB

Standardisation of HMI

The manufacturers follow different approach for the HMI design. Preparing an efficient and effective HMI based on

various functionalities offered by the modern IEDs demands lot of man hour during the design stage. Some manufacturer may have tendency to complete the HMI design as soon as possible to save man hour. A common standard adopted by the industry for an intuitive HMI will benefit the end user.

Flash Memory

Some manufacturers (e.g. GE) provide Flash memory which is very helpful for field upgrades. This can be made a standard relay configuration in present day scenario to make the task of the field engineer safer and easier.

External Communication for Critical Alarm

The numerical relay continuously monitors the current and voltage profile and generates alarm/ events for minor changes (e.g. O/c start, E/F start) in the system parameter. These information can be very useful to the maintenance engineers if it is known at the right time. This can prevent many failures by doing preventive measures. This can be made possible by establishing mobile connectivity to send SMS based alarm to designated persons. Considering use of mobile connectivity in many facets of day to day life, this can be made as a standard feature by maintaining required security level.

Report Generation

Generation of shift wise energy report is an important activity. With installation of an intelligent substation automation system, the shift wise report generation should be easily available from the servers. Although the SA provides generation of daily reports, the quality of the reports is not in the expected line. Having third party software can generate customised report; but it should come as a standard tool as part of the SA system. The vendors' should give equal importance to this aspect.

Conclusion

The IEC61850 based substation automation system can bring many more benefit to the end user from the single reason that it ends dependency on proprietary protocol. However industry should come forward to make this open communication protocol realise its intended goal and bring benefit to the end user.

Acknowledgement

We thank the Senior Electrical Engineer of Indian Oil Corporation Ltd., Bongaigaon Refinery, Dhaligaon, Assam for providing necessary inputs for this article.



A Novel Non-Intrusive Load Monitoring Technique for Domestic Applications

Soumyajit Ghosh,^{*1} Arunava Chatterjee¹ and Debashis Chatterjee¹

Abstract: *The awareness of energy conservation has rapidly increased in recent years due to modern living standard of people and decrease in the use of fossil fuels. In this context, load monitoring is very effective for the end users to determine energy consumption and usage. Non-Intrusive Load Monitoring (NILM) is comparatively new technique to identify the power consumption of individual appliances from the aggregated household data in a single point of measurement. While many researchers have addressed the load identification using data driven steady state and transient state features, most of them focus on techniques using event based supervised learning method and some on optimization based methods. In this paper, a new simple idea of model based technique is demonstrated that can be easily implemented in domestic households with prior knowledge of current patterns.*

Keywords: Appliance Identification, Smart Metering, NILM, Smart Grid, Home Energy Management.

Introduction

Smart metering is the technologies provide exact solution for the implementation of energy management systems for residential purpose. The Government of India has already declared to install smart meter in several states for appropriate consumption of electric power [1]. Identification of loads is the major challenges in smart metering system and also it fulfills the various tasks in the control smart grid technology. Non-Intrusive Load Monitoring (NILM) is the latest technique for the purpose of load disaggregation. In this paper a new technique of a smart system (smart meter) can capable to disaggregate the whole energy consumption into individual consumers is presented. This way, the user will have a better understanding on how the energy is used and will be able to reduce his consumption Energy management for residential homes and/or offices requires both identification and prediction of the future usages or service requests of different appliances present in the buildings.

The issue of energy conservation has increased in recent years owing to decrease in conventional fuel reserves and increase in overall development. Overall devotion has been given to improve the energy efficiency, reliability, and functionality of household electric loads. Electricity is typically sold on a per-unit consumption basis. Concerns on climate change and global warming and reduction of greenhouse gas emission are the chief interest in the measures of energy efficiency. Today, most of the generated

electricity is consumed in commercial and domestic household appliances. Available literatures indicate that household electricity consumption can be reduced using better energy management systems. Smart grid accompanied with household automation network has the enough potential to become a significant way of managing energy for reducing residential energy consumption. To implement this, home appliances have to be modified. Traditional load monitoring method uses electricity meters at different point of the electrical installation to measure all possible load related variables. Various drawbacks are associated when applying this method such as the division of the load circuit, the cost of the electricity meters, the cost of installation, the space for installation the hardware. Traditional electrical and gas meters only measure total consumption and they provide no information regarding when the energy was consumed at each metered site. NILM has been major technique for monitoring the energy consumptions. In NILM technology smart meter play critical role for energy monitoring and transmit the information to the utilities. Smart meters provide a way of measuring this site-specific information, allowing price-setting company to announce different charges for consumption based on the time of uses and the season. Smart meters also give information about the measurements of surge voltages and harmonic distortion, allowing diagnosis of power quality problems. Electricity pricing usually peaks at certain predictable times of the day and the season. In particular, if generation is constrained, prices can rise if power from other jurisdictions or more costly generation is

¹Department of Electrical Engineering, Jadavpur University, Kolkata-700032, India. ✉* soumyajit.ju@gmail.com



brought online. The power companies will encourage consumers to adjust their consumption habits to be more responsive to market prices. The chief resources used in electricity generation are becoming fewer day by day, while the impact of renewable resources is still quite small. Now the time to implement the renewable energy technology and increases the energy efficiency is much more essential. In this concern the smart grid concept was implemented. The consumer must be able to understand how the energy is used so that they could find possibilities to increase the efficiency of energy.

The pioneer work was started by Hart [2] in MIT laboratory and this method is applicable for ON/OFF appliances and multi state appliances. In the same time, French researcher Sultanem [3] was also proposed almost same type of NILM technique but this method included the duration of the transient signal and harmonics. Lee *et al.*, proposed a technique that shows a correlation between the 5th and 7th harmonics and the real/reactive power being consumed by variable load appliances [4]. Recently emphasis has been put on research of the smart metering techniques because the smart meter has potential to implement NILM technique for betterment of home energy management system. Comprehensive NILM signature extraction for residential loads using the edge detection, event filtration and event clustering technique was developed by Dong *et al.* [5, 6]. The switching function based variable power estimating technique has significant improvement in NILM research [6, 7]. The waveform based estimator is used for the NILM technique for variable power loads [7]. The load identification technique is basically three types steady state features extraction [8, 9], transient state technique [9, 10] and other recent optimization based technique [11–14]. The basic NILM method was significantly improved by incorporation of harmonics to save the computational resources and improved performance. This method is applicable for ON/OFF load, multistate load and some extend to variable load appliances [11]. Neural network base signature extraction for appliances is based on continuous calculation of signal harmonics; basic idea is set of harmonics for all combination of appliances [12]. Current measurement is the one of major topic of NILM research. Instead of normal current transformers (CTs), coreless Hall Effect CTs have significant improvement in NILM accuracy [13]. A wavelet based NILM technique was recently developed in [15]. Event based clustering method was useful for residential load identification technique [16]. He *et al.* proposed a featured extraction technique using front end electronics topology. Appliances identification was done by knowledge based model driven network in [17]. A voltage-current (V-I) trajectory based method was also developed for load identification [18]. Today the most of focused loads are

variable power loads because tracking of these kind loads is very difficult. Also, load which consumes less power and same type of load identification when used simultaneously is harder to segregate.

In this paper, a novel non-intrusive load monitoring methodology is presented that can be effectively used for household load monitoring. The technique is based on determining the current signatures and simultaneously observing the transient waveforms of the system current and comparison between them to identify the load.

The System Studied and Proposed Technique

The system mainly considered is a household system with loads consisting of resistive appliances, motor-driven loads and electronic appliances. The resistive appliances can be further classified as mostly heating loads, toasters, incandescent lamps, etc. The motor driven loads are fans, food mixers, blenders, etc. Some of them can also be classified into predominantly inductive loads. Electronic appliances include chargers, personal computers, scanners, Fax equipments, etc. A typical system of household load with proposed sensing technique is shown in Figure 1.

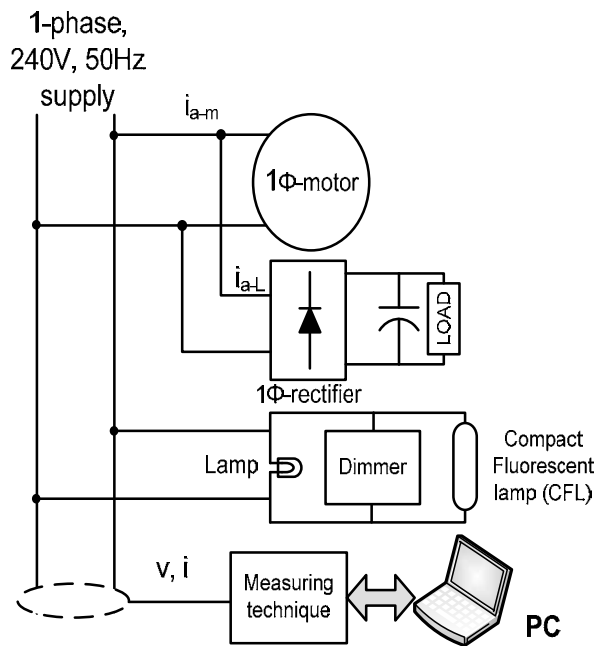


Fig. 1: Typical Household System Considered for Study

The measuring technique involves individually determining the current signatures of the different household loads installed and simultaneously observing the transient waveforms of the system current and comparing between the two to identify the load. Figure 2 gives the brief outline of the technique.

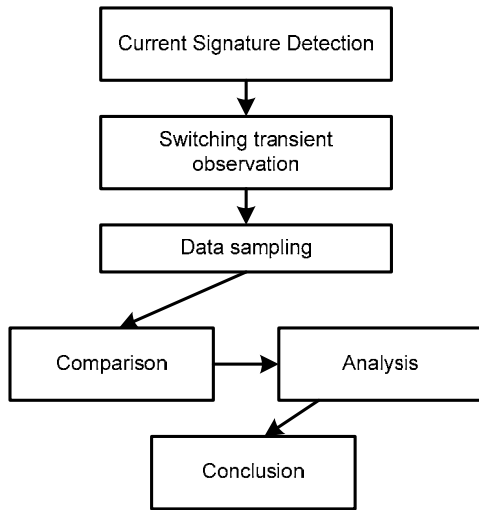


Fig. 2: Outline of the Proposed NILM Technique

Advantages of NILM

NILM helps in accurately identifying the load behavior in a particular power system and their condition monitoring. The load monitoring can also help determine the demand response in a household. Moreover, load forecasting and usage can be predicted other than identification and segregation of loads.

System Simulation and Results

A simulation study is carried out for the proposed technique using MATLAB/Simulink R2014b. The study involves separately studying the different loads and determining the effect on the individual source current signatures. Figure 3 below shows the individual load current signatures obtained.

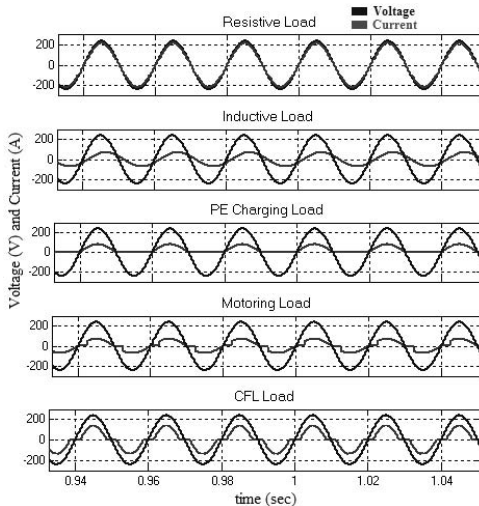


Fig. 3: Voltage and Current Waveforms for Different Household Load Types

It is observed from Figure 3 that different domestic loads have different current signatures and thus the current waveforms can be taken as effectively the criteria to distinguish between different loads. When all these loads are working together, the complex current waveform is different and during such operation, load segregation/identification becomes difficult.

Considering different loads considered in this paper to be operating at a time from the household supply, the complex waveform for the current and voltage is shown in Figure 4.

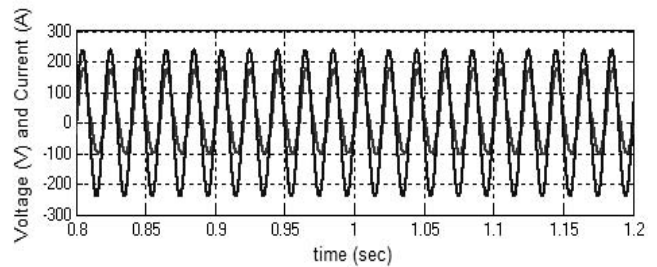


Fig. 4: Voltage and Current Waveform during Steady State for all the Loads Considered

The summation of different current harmonics leads to a complex current waveform as observed from Figure 4. During switching on and off of the different loads, the load waveforms are observed and noted. As observed in Figure 5, the different loads are switched on at time $t = 1$ s in order to distinguish between the transient current waveforms. The same is shown in the transient study in figure below.

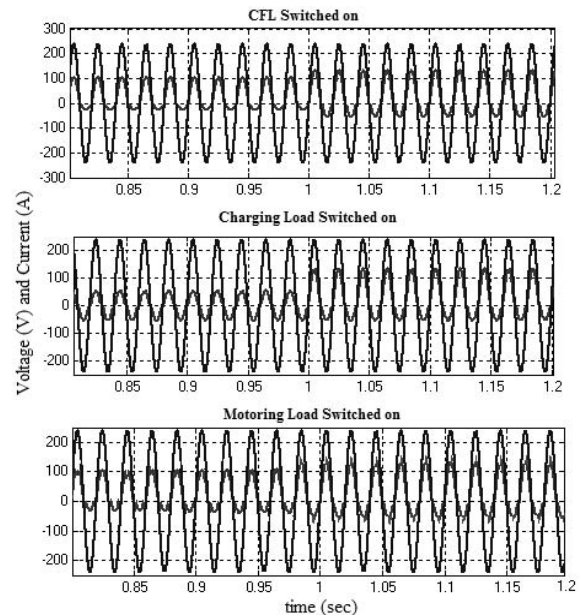


Fig. 5: Voltage and Current Waveforms during Load Switching Transients for Different Loads



As observed from Figure 5 during ‘switching on’ of the CFL load, the load current is increased with increase in peak current. Similarly, when a charging load is ‘switched on’, the positive peak is increased as shown in Figure 5. Thus in both these cases, the load can be clearly distinguished from the load current transient.

When motoring load with a speed control circuitry is ‘switched on’, the load current waveform is shown to be increased with a switched pattern as shown in Figure 5 last trace.

From the above patterns, thus it can be seen that with transient waveforms considered, the loads can be easily analyzed. Also when the resistive load is ‘switched on’ only the magnitude of the waveform is increased which is not shown here. These data can be fed to a personal computer (PC) for further analysis.

Remarks

The proposed technique uses simple observation based feature study and prior knowledge based approach to determine the domestic loads. However, it is emphasized here that for accurate determination, an optimization based approach can be adapted. Moreover, the determination is based on isolated household loads and is difficult to be applied with industrial loads or large scale loads.

Harmonic Analysis

A harmonic analysis of the waveforms have been performed to determine the underlying harmonic frequency currents for the waveforms shown. The results are tabulated below in Table 1.

Table 1: Harmonic Analysis of the Load Current Waveforms

For all loads considered in parallel				
THDi (%)	3rd (%)	5th (%)	7th (%)	
13.98	6.8	2.22	0.17	
With Charger switched on				
13.96	6.8	2.22	0.17	
With Motoring load switched on				
15.92	8.4	2.82	1.03	
With CFL load switched on				
14.17	7.4	2.13	0.32	

From the Table, it can be seen that there is not much difference in terms of the Total Harmonic Distortion (current) (THDi). Although the 3rd harmonics can be taken as a criteria for identification of the loads switched on, the

margin is very nominal. The proposed analysis technique thus can act as a criterion for study of the load behavior.

Conclusion

A simple NILM based load identification technique is presented in which the load is identified based on load current transient behavior. The detection is based on observation and analysis of the current waveform behavior. The detection technique is simple and robust. The effectiveness of the detection technique can be further increased using a proper algorithm with training capability. The training may be provided with the prior knowledge obtained from the proposed technique. A simulation study is presented which validates the proposed study.

Acknowledgment

The authors thank Visvesvaraya PhD Scheme, Government of India, for financially supporting the research work.

References

- [1] www.indiasmartgrid.org–Advanced Metering Infrastructure, Released at India Smart Grid Week, 17th March (2016), pp. 1–13, available online, accessed, 24 Oct. 2016.
- [2] Hart, G.W., Nonintrusive appliance load monitoring. *IEEE Proc.*, 80(12), 1870–1891 (1992).
- [3] Sultanem, F., Using appliance signature for monitoring residential loads at meter panel level. *IEEE Trans. Power Del.*, 6(4), 1380–1385 (1991).
- [4] Lee, K.D., Leeb, S.B., Norford, L.K., Armstrong, P.R., Holloway, J. and Shaw, S.R., Estimation of variable-speed-drive power consumption from harmonic content. *IEEE Trans. Energy Convers*, 20(3), 566–574 (2005).
- [5] Dong, M., Meira, P., Xu, W. and Freitas, W., An event window based load monitoring technique for smart meters. *IEEE Trans. Smart Grid*, 3(2), 787–796 (2012) .
- [6] Dong, M., Meira, P., Xu, W. and Chung, C., Non-intrusive signature extraction for major residential loads. *IEEE Trans. Smart Grid*, 4(3), 1421–1430 (2013).
- [7] Wichakool, W., Avestruz, A., Cox, R.W. and Leeb, S.B., Modeling and estimating current harmonics of variable electronic loads. *IEEE Trans. Power Electron*, 24(12), 2803–2811 (2009).
- [8] Wichakool, W., Advanced nonintrusive load monitoring system. Ph.D dissertation, *Dept. Elect. Engg. Comput. Sci., Massachusetts Inst. Technol.*, Cambridge, MA, USA, Feb. (2011).
- [9] Wichakool, W., Remscrim, Z., Orji, U.A. and Leeb, S.B., Smart metering of variable power loads. *IEEE Trans. Smart Grid* 6(1), 189–198 (2015).
- [10] Cole, A.I. and Albicki, A., Data extraction for effective non-intrusive identification of residential power loads. In: *IEEE Instrument and Measurement Technology Conference*, USA, May 18–21, (1998), pp. 812–815.



- [11] Liang, J., Ng, S., Kendall, G. and Cheng, J., Load signature study-part I: Basic concept signature, and methodology. *IEEE Trans Power Del.* 25(2), 551–560 (2010).
- [12] Leeb, S.B., Shaw, S.R. and Kirtley, J.L., Transient event detection in spectral envelope estimates for nonintrusive load monitoring. *IEEE Trans. Power Del.* 10(3), 1200–1210 (1995).
- [13] Laughman, C., Lee, K., Cox, R., Shaw, S., Leeb, S., Norford, L. and Armstrong, P., Power signature analysis. *IEEE Power Energy Mag.*, 1(2), 56–63 (2003).
- [14] Srinivasan, D., Ng, W.S. and Liew, A.C., Neural-network based signature recognition for harmonic source identification. *IEEE Trans Power Del.*, 21(1), 398–405 (2006).
- [15] Chang, H., Chen, K., Tsai, Y. and Lee, W., A new measurement method for power signatures of nonintrusive demand monitoring and load identification. *IEEE Trans. Ind. Appl.*, 48(2), 764–771 (2012).
- [16] Zeifman, M. and Roth, K., Nonintrusive appliance load monitoring: review and outlook. *IEEE Trans. Cons. Electron.*, 57(1), 76–84 (2011).
- [17] Gillis, J.M., Alshareef, S.M. and Morsi, W.G., Nonintrusive load monitoring using wavelet design and machine learning. *IEEE Trans. Smart Grid* 7(1), 320–328 (2016).
- [18] Wang, Z. and Zheng, G., Residential appliances identification and monitoring by a nonintrusive method. *IEEE Trans. Smart Grid* 3(1), 80–92 (2012).
- [19] He, D., Du, L., Yang, Y. and Habetler, T., Front-end electronic circuit topology analysis for model-driven classification and monitoring of appliance loads in smart buildings. *IEEE Trans. Smart Grid*, 3(4), 2286–2293 (2012).
- [20] Hassan, T., Javed, F. and Arshad, N., An empirical investigation of V-I trajectory based load signatures for non-intrusive load monitoring. *IEEE Trans. Smart Grid.*, 5(2), 870–878 (2014).



Economic Analysis and Technical Feasibility of Right to Electricity Act (REA) in India

Sreenath Sukumaran^{*1} and K. Sudhakar¹

Abstract: *The energy consumption and usage of a society reflects the standard of living condition in a country. This holds true with the developed countries such as USA (1843 W per capita), Japan (941), Germany (1160), Canada (2185). India, an emerging economy with 152 W per capita can be considered in the group of developed countries, only if access to reliable electricity is provided to its entire population irrespective of rural and urban variation. Though it is considered that the heart of India lies in villages, most of the rural population is still dreaming of better living conditions. According to census 2011, nearly 75 million households have no access to electricity. About 90% of them live in rural areas and are located out of national electricity grid because of its long distance from the grid, sparse population, remote location and geographical constraints. Out of the currently electrified villages, the reliability of electricity is to be improved by reducing the duration of blackouts. About 42% of rural households use kerosene for lighting while 93% of urban house hold use electricity for the same. In order to achieve sustainable growth across the country, income generation opportunities are to be created along with better lighting. government schemes such as Bharat Nirman, RGGVY and Panchayati Raj Amendment (11th schedule of the 73rd Amendment) did not succeed in achieving the ambitious 100% electrification. Rural load is characterized by dispersed population and low demand (resulting in low load densities).*

This in turn causes high capital costs of grid electrification. So national grid connection to all villages is not sustainable and there is a need to look for alternatives. At this point of time, a decentralized power system seems to be more viable from technical and financial point of view. The access to reliable electricity should be a right to all Indian household. It can be implemented on the lines of Right to Information (RTI) and Guaranteed Employment Act. This paper tries to formulate the Right of Electricity Act and showcase a methodology through which Right of Electricity Act can be implemented across the country along with its economic burden to government.

Keywords: Per Capita Power Consumption, House Hold, National Grid, Decentralized Power System.

Introduction

The world was very dynamic in the past 50 years. Electronic and electric gadgets have begun to influence day to day life. This in turn led to increase in the per capita energy.

So the parameter for development of a country can be the amount of energy consumed by its population. The developed countries like USA, Canada, France, UK are having high per capita consumption. India is having a low per capita energy consumption of 1010 units per year [1]. Her dream to become a world leader can be achieved only by providing more energy to all its people. The waves of digital revolution are lashing Indian shores. Indian population can no longer stay from the comfort and safety provided by digital equipments. Indian government is itself trying to digitalise its population. Ministry of power has been

undertaking many schemes to provide electricity to all Indian villages. Rural Electrification Corporation was established in 1969 to assist and financially support State Electricity Boards, State Government Departments and Rural Electric Cooperatives for rural electrification projects. A Subsidy of 90% towards capital expenditure is being provided, through Rural Electrification Corporation Limited (REC). Under Rajiv Gandhi Grameen Vidyutikaran Yojana (RGGVY), electricity distribution infrastructure is given a thrust so as to establish Rural Electricity Distribution Backbone (REDB) with at least a 33/11KV sub-station, a distribution transformer in a village. But at least 9000 villages are located in those places where grid extension can lead to ATC losses there by financial burden. Rural electrification scheme started with Kutir Jyoti Program (Launched in 1988–89) by providing single point connection to BPL Households with 100% grants. Later on few schemes were formulated which

¹Department of Energy, MANIT, Bhopal–462003, India.

✉* 152118211_sreenath@manit.ac.in; sukumaran.sreenath@gmail.com



are either discontinued or merged with new schemes. RGGVY (launched on Mar., 2005) aims in electrification of all Villages and Habitations by providing access to free electricity connection to BPL families.

Later on Deendayal Upadhyaya Gram Jyoti Yojana was launched in December 2014 by separating agricultural and non agricultural feeders, strengthening of sub-transmission and distribution system and by giving thrust on Renewable Energy (RE) sources and micro grid concept [2]. Though these schemes made a change in the life of some Indian people, still many villages are left of the national grid. Most of these un-electrified villages are identified by sparse and intermittent population, remotely location and communal problems.

According to Census of India, a village means a revenue area with a clear demarcated boundary and having an unique 6-digit census code (Census 2011). Within the revenue boundary of a village, a village may consist of multiple habitations (majra/tola). Habitations are parts of the village, each being a collection of households. Out of 6,40,930 villages, 6,22,478 villages (97.12%) have been electrified as on 02/10/2016. The remaining 18,452 villages were located in highly remote and inaccessible areas or areas plagued by insurgency and Left-wing extremism. The households residing in some of the electrified villages are suffering from black outs even for 12 hours a day. There can be a misconception that an electrified village means that all of its households are having accessibility to electricity. But as per the new definition given by Ministry of power, a village would be declared as electrified [3], if:

- Basic infrastructure such as Distribution.
- Transformer and Distribution lines are provided in the inhabited locality.
- Electricity is provided to public places like Schools, Panchayat Office, Health Centers, Dispensaries, Community centers, etc.
- The number of households electrified should be at least 10% of the total number of households in the village.

According to recent statistics by Indian government, electrification of all villages will be completed by March 2017. But the bitter truth is that only 873 Indian villages are providing electricity to all of its house hold [4]. So electrification of all households should be made the target rather than village electrification. The total number of households living in India is roughly 24,66,92,667. Out of which 16,78,26,730 house hold lives in rural areas while the remaining 7,88,65,937 households live in urban areas. According to census of India, 2011, the number of households using electricity as a source of lighting are 16,57,77,472 (67.2%) [5]. This indirectly reveals that these households have access to electricity. So the remaining 32.8% households are to be electrified as soon as possible.

It's time to focus on providing electricity to all households rather than village level. India, being the world's largest democracy, have been admired for the implementation of Right to Information Act (RTI) and Right to Employment Act. Thousands of people are beneficiaries of this mass approaching scheme. Similarly, on the lines of these acts, an Right to Electricity act can be successfully implemented in India. A simple definition of REA is providing calculated units of electricity to all households so as to meet their basic lighting needs. The objective of this paper is to formulate a definition for Right to Electricity Act and analyse its technical feasibility and economic burden.

Methodology

The core objective of Right to electricity act is to meet the necessary electrical energy need of the people in India. The basic need of electricity in any Indian household will be for lighting after sunshine hours, cooling during hot climate (fan), handheld device charging exclusively mobile phones. On this regard, the average daily electrical energy consumption of an Indian household is found out. BLDC fans are chosen because of its low energy consumption and it can work directly in DC power source. So the power consumed in a typical household may concluded as lighting points, BLDC fans and sockets for mobile/laptop/tablet charging.

All of these loads can function properly from a Solar PV power is the best option to meet the energy requirement of these homes because of its easy setup, rapid installation and versatile use. Since solar panel produces direct current, it has to be converted to AC for versatility. The AC current are again rectified and filtered to DC in house hold loads such as CFL, LED, mobile charger, TV. These conversion steps involve power loss and decrease in power quality. Along with these losses, PV systems have to incorporate charging and discharging losses in battery and resistive heating loss in conducting wires. So it is better to directly use the DC power produced by solar panel by connecting DC loads. It will not only reduces loss but also reduce cost of the system [6]. This is the extra advantage of using DC loads in these households. The solar system is designed according to the connected load and solar irradiation. This performance of the system is validated using PVgis software [7]. Indian government can provide DC solar system to all unelectrified household either at full subsidy or at interest free loans.

Results

Understanding the benefits of DC solar system, the loads in the household run in DC. Lights under the Act, government is supposed to meet the very basic load requirement of household. This will be a better stand so as to reduce financial burden. So the connected load of the house is



mainly for lighting and charging i.e. three 7 w LEDs and one 40 w charging socket. The cumulative daily load of such household is coming around 276 wh [8].The DC solar PV system designed for this load consists of:

- 80 watt polycrystalline solar panel
- 28 AH, 48 Vdc VRLA battery
- OGH controller for adequate protection for under voltage, over voltage.

The total cost of the system comes around 8,200 INR, though it is negotiable. Here 48 V dc is chosen for safety and low cable losses. These systems can be distributed to un-electrified household with full subsidy or partial subsidy from government. Considering giving full subsidy to 8.1 Cr un-electrified homes, the economic burden is around 66,420 Cr. The government can raise fund through sovereign bonds and UN support. The performance of the above system in an un-electrified household in Orissa is as shown in Figure 1.

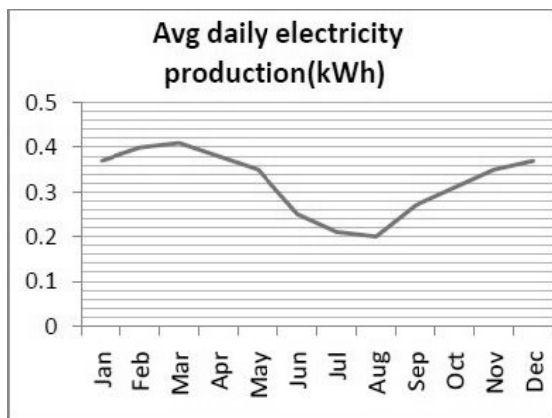


Fig. 1: Average Daily Electricity Production of the Given System (kwh)

IIT madras along with Cyngi has come up with inverter less solar DC system for homes with power consumption of 500wh and above. This system can power minimum three LED bulbs (equivalent to 11w CFL), two T5 tube light (4" LED), two BLDC fans, mobile charge and socket. The brain of the system is OGH controller, a patented device that connects to PV panel, battery, and supplies 48V DC to appliances and provides adequate protection for over voltage and over current. Losses in solar-DC system is as low as 7% (without battery loss) when compared to 25-45% losses in other solar systems [9]. As result of this, solar panel size also comes down (nearly a factor of 2) and battery size reduces by 20%. The following output lines are provided in the system are : Main DC Line – supplies 48V DC to DC appliances such as Fans, LED lights, Laptop/Mobile chargers, DC powered LCD/LED TVs, Emergency Line–supplies power to essential appliances of up to 100W in the event of ‘battery low’ conditions, Optional AC Power:

Additional augmentation when AC supply is available. System can be upgraded to accommodate more lights, fans, LCD TV. Off Grid Home (OGH) solar DC system consisting of 1 ceiling fan, a tube light, a bulb, a charger, 125wp solar panel, 1kWh battery costs 20,000INR. DC solar system of panel size 250 wp, 375 wp, 500 wp and up to 5 hours backup are also available. People in un-electrified household can choose from these systems according to their load demand. Government can promote them by giving interest free loans through public owned banks. Awareness creation about these products is also important.

Conclusion

The lifestyle of a society changes dramatically if they have access to electricity. In the present era of electronic gadgets, the life of people may not reach fullest without electricity. This means that time has come up to consider electricity among the basic need of life. The importance of implementing Right to Electricity Act lies here. All people of India should have access to electricity at least for lighting. If guaranteed amount of electricity is not provided within 15 days, the applicant household are entitled to an un-electrification allowance [10]. This is an initial draft of the act which can be put forward for discussion and clarification. Inverter less Solar DC system is best suitable option before government to fulfil the responsibility entitled by act. Though economic burden on government is high, the socio-cultural impact of this scheme should not be avoided. It will improve the health of people and reduce environmental pollution along with prolonged productivity per person. These benefits will indirectly help the government to reduce expenditure in other areas like health, power, urban planning etc.

Future Scope

The implementation of Right to Electricity Act is formulated by considering households individually. It is suggested to provide a standalone DC system to all household. Rather than this approach, a micro/mini grid can be developed for each village or hamlet. The power supply based on grid give more flexibility in electricity usage to its consumers [11]. The power source that fed the grid should be renewable energy source. The characteristics of village such as wind speed, solar irradiation, sunny days, amount of biomass available can be considered for the selection of type of renewable energy source [12]. For example, Rice husk power plants are more suitable in villages of Chhattisgarh while small hydro power plants are profitable in Jammu and Kashmir. The grid system also promotes cottage and small scale industries in those regions. These in turn generate employment in villages and will lead to reduction in rural to urban migration.



References

- [1] "List of countries by energy consumption per capita," Wikipedia. 19-Sep-2016.
- [2] Dr. Dinesh Arora, "Rural Electrification in India."
- [3] "GARV Dashboard." [Online]. Available: <http://www.garv.gov.in/dashboard>. [Accessed: 31-Oct-2016].
- [4] Bhattacharyya, S.C., "Energy access problem of the poor in India: Is rural electrification a remedy?," *Energy Policy*, Vol. 34, No. 18, pp. 3387–3397, Dec. 2006.
- [5] "Census of India: Source of lighting."
- [6] "OGH-Brochure.pdf."
- [7] Kumar, B. Shiva and Sudhakar, K., "Performance evaluation of 10 MW grid connected solar photovoltaic power plant in India," *Energy Rep.*, Vol. 1, pp. 184–192, Nov. 2015.
- [8] Shukla, A.K., Sudhakar, K. and Baredar, P., "Design, simulation and economic analysis of standalone roof top solar PV system in India," *Sol. Energy*, Vol. 136, pp. 437–449, Oct. 2016.
- [9] www.cygni.com.
- [10] Right to Information. <http://righttoinformation.gov.in> [Accessed: 31-Oct-2016].
- [11] Castellanos, J.G., Walker, M., Poggio, D., Pourkashanian, M. and Nimmo, W., "Modelling an off-grid integrated renewable energy system for rural electrification in India using photovoltaics and anaerobic digestion," *Renew. Energy*, Vol. 74, pp. 390–398, Feb. 2015.
- [12] Palit, D., Malhotra, R. and Mande, S., "Enhancing viability of biofuel-based decentralized power projects for rural electrification in India," *Environ. Dev. Sustain.*, pp. 1–21, Oct. 2015.



Increase Digital Data Transmission Speed and Storage Place on Reducing Total Bit Count of a Set of Binary Data Using Interlaced Binary Search

Aloke Sarkar^{1,2}

Abstract: The invention is defining an Encryption and Decryption Method (EDM) having a micro-architecture micro-programmed with Adaptive Delta Modulation (ADM) procedure that modulates the locus of the search path to search all quantized bytes with the Interlaced Binary Search (IBS) algorithm to store and transmit an equivalent binary code using lesser number of stream of serial bits than that of the source binary file. A binary file composed of 'nk' bytes (8nk bits) is grouped into 'n' groups of '8k' bits each. Each of these 'n' groups is termed as quantized bytes (Qb). The numbers corresponding to these n groups occupy into the binary search tree formed by the first 2^{8k} natural numbers ranging from 0 to $(2^{8k}-1)$. IBS algorithm searches this 'n' Qb in this binary search tree. The locus of the search path so generated is adaptive delta modulated to store and transmit. The IBS algorithm removes the limitations of binary search algorithm – inability to search simultaneously multiple items and the limit of the search efficiency by $\log_2 n$.

Keywords: Interlaced Binary Search, Data Encoder, Adaptive Delta Modulation, Quantizer, Successive analog Approximation.

Introduction

This paper is defining an Encryption and Decryption of binary data, using Interlaced Binary Search (IBS) algorithm that has two applications defined for till date – (1) Interlaced Analog to Digital Converter (IADC) [1–4] – parallel Input/Output (I/O) Analog to Digital Converter (A/D) (Figure 1) using one digital-to-analog converter, and (2) this compression of binary data (not published earlier). IBS removes deficiencies of Binary Search (BS). In one scan through a sorted list of 2^q items BS searches only one item using q trials. A scan (run) is the process of looking through all 2^q items of the list. BS searches n items in n scans. IBS search n items in one scan with combined efficiency of search being better than that of BS. Other than improvement over BS, IBS does not claim any improvement over any other search procedures.

Preliminary

A list of 2^q items are formed associated with key numbers ranging from 0 to (2^q-1) to form a binary search tree T. To search input item k (AK) out of n input items from 'to be Searched Items List' (SIL), the key associated with that item is to be searched for. BS sets 'LOWER BOUND' = LB = 0 'UPPER BOUND' = UB = (2^q-1) and 'MID POINT' = MP =

$AD = (LB+UB)/2$. MP sets three flags low (L), high (H) and finished (F) on comparing AK with AD (L = 1, H = 0 and F = 0 if $AK-\epsilon > AD$; L = 0, H = 1 and F = 0 if $AK+\epsilon < AD$; L = 0, H = 0 and F = 1 if $AK+\epsilon \geq AD \geq AK-\epsilon$

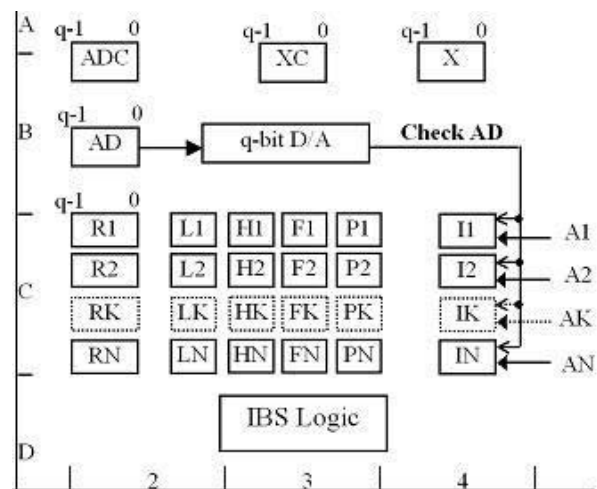


Fig. 1: IADC Schematic

where ϵ is input noise margin for an A/D, else $\epsilon = 0$). For L = 1 set LB = MP or for H = 1 set UB = MP and continue setting

¹Electronics & Communication Engg., Computer Engg. Associate Member of Institution of Engineers (India). ✉ alokesarkar@hotmail.com

²Senior Manager, Steel Authority of India Ltd., Rourkela Steel Plant, Rourkela, India.



and compare operation till $F = 1$ to complete search, output $RK = AD$. The 'span' from UB to LB is a search scope (parent). Resetting of LB/UB as per MP is narrowing down search scope that is generation of a child scope. For n items there is input time division multiplexing. To implement BS in hardware using q bit binary register (X and AD). $MP = (LB+UB)/2$ is implemented on shifting right X by 1 bit and setting $AD = (AD \text{ XOR } X)$. BS starts search on setting bit $(q-1)$ of X and shifts right till bit '0' is reached and again starts from bit $(q-1)$ of X to search another input. Initially AD is reset to '0'. At a test point for $H = 1$, reset current bit of AD with $AD = (AD \text{ XOR } X)$. BS instead of restarting on reaching bit 0 starts shift-left (multiply by 2) and also shift-right if required. At any point BS compares simultaneously all inputs with AD so generated.

BS uses some Boolean operations that are Shift-Left by 1 bit ($SL1$) to multiply by 2, Shift-Right by 1 bit ($SR1$) to divide by 2 (forms groups), XOR (exclusive-or), && (logical AND) and ++ (logical OR).

Interlaced Binary Search (IBS)

There are three phases. Phase-1 ($P1$) runs first independently to other two phases $P2$ and $P3$. At each test point the value of the node (AD) is compared with the values of items ($A_k: k = 1, 2, \dots, n$) and correspondingly a set of four binary flags are set/reset to value 1/0:

L_k : sets for $A_k > AD - \epsilon$ (limit $\epsilon \rightarrow 0$)

P_k : sets at COP for $A_k \leq AD - \epsilon$ or for $A_k < AD$, if $\epsilon = 0$.

H_k : sets for $A_k > AD + \epsilon$, for $\epsilon = 0$, $H_k = L_k$.

F_k : sets for $AD + \epsilon \geq A_k \geq AD - \epsilon$ (k 's search is completed,)

Phase I ($P1$): [X is a temporary variable. $XA []$ is a vector of 0 to $(q-1)$ elements. In comment section X and AD are 16-bit binary registers at start holds 0000_{16} .]

11: Set $X = 2^{q-1}$, $b = (q-1)$, $AD = 0$, $XA[] = 0$; [$X = (X \text{ XOR } 8000_{16})$].

12: Set $AD = AD + X$ and $XA[b] = 1$; [$AD = (AD \text{ XOR } X)$].

12.1: Check AD ; [compare test node with SIL , set L, H, F]

13: If (any $L_k = 0$), Then Set $AD = AD - X$ and $XA[b] = 0$;

[reset bit of AD as pointed by b , as if AD were a binary register ($AD = AD \text{ XOR } X$).]

13.1: If ((any $L_k = 0$) && ($X = 1$)), Then Check AD ; [This step is not trial point to calculate complexity.]

14: If $X \neq 1$, Then Set $X = X / 2$, $b = b - 1$ and go to step 12; [$P1$ Ends for $X = 1$. $X = (SR1 X)$.] [End of phase-1].

Phase II ($P2$): [A Change Over Point (COP) is generated if there is a jump from $P2$ to $P3$ and no P flag is set. ADC, XC, bc and XAC record AD, X, b , and XA respectively at COP .]

21: If $XA[b] = 0$, Then

1. Set $AD = AD + X$, $XA[b] = 1$; [$AD = (AD ++ X)$]

2. Check AD ; else jump to step-25.1

22: If (($ADC \geq AD$) && (all $P_k = 0$)), Then Set $X = XC$, $AD = ADC$, $b = bc$, $XA = XAC$ [Return to COP .]

22.1: Check AD ; [Executes on return to COP in step -22.]

23: If ((any $L_k = 0$) && (all $P_k = 0$)), Then

1. Set $XC = 2 * X$, $ADC = AD$, $bc = b + 1$, $XAC = XA$; [$XC = (SL1 X)$.]

2. If ($XC[bc] = 0$) Then Set $ADC = ADC + XC$, $XAC[bc] = 1$; [($ADC = ADC \text{ XOR } XC$)]

[Recording and generation of COP .]

24: If (any $L_k = 0$), Then jump to phase III.

25: If (all $H_k \neq 1$), Then go to step 26.

25.1: Else Set $X = 2 * X$, $b = b + 1$. [($X = SL1 X$)].

26: go to step 21 [End of phase-2.]

Phase III ($P3$): [Only during entry to $P3$, P_k flag(s) can be set if no other P_k is set.]

31.1: if (all $P_k = 0$), jump to step-22;

31.2: if ($b \neq 0$), Then Set $X = X / 2$, $b = b - 1$; [$X = (SR1 X)$]

else jump to step-21; [$P2, P3$ looping inside COP]

32: set $AD = AD - X$, $XA[b] = 0$. [$AD = (AD \text{ XOR } X)$.]

32.1: check AD ;

33: If((all $L_k = 1$) && (any $P_k = 1$)), Then Set $AD = AD + X$, $XA[b] = 1$. [($AD = AD \text{ XOR } X$).]

34: go to step 31. [End of phase-3.]

Theorem I: BS consumes $[5.2^{(q-2)} - 2.q + 2]$ trials to search out simultaneously all $2^{(q-1)}$ leaves of a complete binary search tree of depth q formed from first $(2^q - 1)$ natural numbers ranging from 1 to $(2^q - 1)$.

$$5.2^{(q-2)} - 2.q + 2 = L_{IBS} \text{ (say);}$$

Average run time per leaf = $5/2 - (q/2^{(q-2)}) + 2^{(2-q)} = O(5/2)$ for limit $q \rightarrow \infty$;

Total run time to search $2^q - 1$ leaves of complete binary search tree T of 2^q nodes with $BS = q.2^{q-1} = L_{BS}$ (say);

$$L_{BS} - L_{IBS} = q.2^{q-1} - 5.2^{q-2} + 2.q - 2 = (2^{(q-2)} + 1)(2.q - 5) + 3 = O(2^{(q-1)});$$

The efficiency (number of trials in comparison to binary search) of BS goes up as number of inputs goes up and also the deviation from mean of all items is low i.e. items are closely spaced in the binary search tree.

Worst Case of BS comes when there is requirement of simultaneous searching of 2 nodes with values 1 and $(2^{(q-1)} + 2^{(q-2)})$. Worst case run time is $(3q - 2)$.



Best Case of IBS $O(1)$. That is one trial per item search. Out of several possible best cases two possible best cases:

1. $n = 2 \cdot q - 1$. Each trial point of P1 and P2 will correspond to an item and there will be no generation of COP. This n items are: $2^{q-1}, 2^{q-2}, 2^{q-3}, \dots, 2^0, (2^0 + 2^1), (2^0 + 2^1 + 2^2), (2^0 + 2^1 + 2^2 + 2^3), \dots, (2^0 + 2^1 + \dots + 2^{q-1})$.

2. $n = (2q-1) + (q^2-3q+2)/2 = (q^2 + q)/2$. Let us associate generation of COP in above best case. We will take maximum possible COP generation. Each COP, C_z will search for z items with values $-(2^{z+1} + 2^{z-1} + 2^{z-2} + 2^{z-3} + \dots + 2^0), (2^{z+1} + 2^{z-2} + 2^{z-3} + 2^{z-4} + \dots + 2^0), (2^{z+1} + 2^{z-3} + 2^{z-4} + 2^{z-5} + \dots + 2^0), \dots, (2^{z+1} + 2^0)$. There will be $(q-2)$ COP ranging from C_1 to C_{q-2} .

Binary Data Encryption Using IBS

This is an algorithm for data encryption on convergence in analog and digital computations. It (recursion is possible) may be incorporated directly either in hardware or in software. The nk bytes of a binary file are grouped into sequentially numbered n groups of k bytes each (POS – position numbering) with the first n natural numbers starting from 0 to $(n-1)$. For storage or transmission, the positions' information in the binary search tree formed by the first 2^{8k} natural numbers starting from 0 to $(2^{8k} - 1)$ along with POS is passed using fewer bits. This asynchronous communication may be looked as a modulation scheme for processing discrete and quanta of analog signals – termed as quanta bytes (neither continuous nor defined by two states 1 or 0) – similar to adaptive delta modulation of analog signal.

Each byte $\{B_7, B_6, B_5, B_4, B_3, B_2, B_1, B_0\}$ (Figure 2) is converted into analog signal equivalent V_{xy} ($x = 0, 1, 2, \dots, (n-1)$ and $y = 0, 1, 2, \dots, (k-1)$) using (1). This V_{xy} analog signal equivalent is used to form V_q ($q = 0, 1, 2, \dots, (n-1)$) analog quanta – termed as Qb (Quantized byte) in the number system of base 2^8 as per (2). α and β are arbitrary conversion constants and may be adjusted to any values.

$$V_{xy} = \alpha [B_7 \times 2^7 + B_6 \times 2^6 + B_5 \times 2^5 + B_4 \times 2^4 + B_3 \times 2^3 + B_2 \times 2^2 + B_1 \times 2^1 + B_0 \times 2^0] \dots (1)$$

$$V_q = \beta [V_{q(k-1)} \times 2^{8(k-1)} + V_{q(k-2)} \times 2^{8(k-2)} + \dots + V_{q0}] \dots (2)$$

These n Qb^s match with some nodes of the binary search tree formed with the first 2^{8k} natural numbers starting from 0 to $(2^{8k} - 1)$. The IBS algorithm converts these Qb^s into equivalent

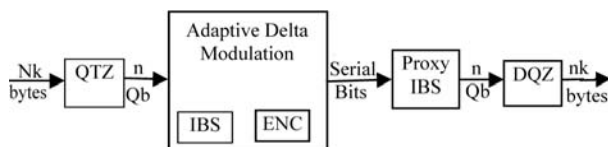


Fig. 2: Encryption of Binary Data Using IBS

serial bit stream. This resembles to adaptive delta modulation [5, 6] for digital signal processing. The serial bit stream can be used for storage and serial asynchronous transmission. A proxy interlaced binary search algorithm at the receiver accepts the serial bit stream for mimicking sender's IBS to generate Qb^s. A process termed as dequantization (DQZ) de-groups $8k$ bits of a recovered Qb into sequential k bytes. For this a Qb is a group defined by the set: $Qb = \{B_i; i = 0, 1, \dots, (k-1)\}$ where B_i stands for a byte.

Adaptive Delta Modulation Using IBS: Adaptive Delta Modulation (ADM) is a scheme of Differential Pulse Code Modulation (DPCM).

Adaptive Delta modulation of n Qbs':

1. Each of n Qbs is assigned with a number in the range 0 to $(n-1)$ to track the group sequence of nk bytes into n Qbs each of k bytes, e.g. 1st group is assigned with 0, 2nd group is assigned with 1 and so on. Call these numbers as POS and a POS needs $\log_2 n$ bits to represent a number.
2. In the process of IBS (through binary search tree of 2^{8k} nodes) when there is a match (i.e. for which flag F_k is set) the corresponding POS is to be transmitted instead of $8k$ bits.
3. During any phase of IBS, if value of AD matches with any one or more Qbs, transmitted bit sequence will be:
 M1 = 0: 1 Qb match and is followed with bits of corresponding POS.
 M1 = 1: more than 1 Qb match and is followed with bit M2.
 M2 = 0: less than 16 Qbs match and followed by a nibble – number of Qbs ; and the POSs of Qbs of successful match.
 M2 = 1: more than 15 Qbs match; a group of $\log_2 n$ bits to mark the number and the POSs of Qbs of successful match.
4. During phase-1 of IBS for no match case 2 bits are to be transmitted corresponding to one sequencing from step 12 through step 14 that are:
 P10 = 0 if step 13 sets $XA[b] = 0$.
 P10 = 1 if step 13 leaves $XA[b] = 1$.
 P11 = 0 for no successful match
 P11 = 1 for successful match and will be followed with the match as indicated above in paragraph #3.
5. During phase-2 of IBS for no match case 3 bits are to be transmitted corresponding to the sequencing from step 21 through step 26:
 P20 = 0 if step 24 does not allow jump.
 P20 = 1 if step 24 allows jump.
 P21 = 0 for no successful match



P21 = 1 for successful match and will be followed with the match as indicated above in paragraph #3.

P22 = 1 if step 23 records COP and P20 = 1 [generation of COP must be followed by jump to phase-3].

P22 = 1 if step 22 returns to COP [once a COP is generated, till its return another COP cannot be generated]. If preceded by P20 = 1, it will be implied that there is generation of another COP just after return from one COP.

P22 = 0 before return to COP as in step 22.

P22 = invalid after return from COP till generation of another COP. Validity starts after P20 = 1 followed by P22 = 1.

6. During phase-3 of IBS for no match case 2 bits are to be transmitted corresponding to one sequencing from step 31 through step 34 that are:

P30 = 0 if step 32 sets XA[b] = 0.

P30 = 1 if step 33 leaves XA[b] = 1.

P31 = 0 for no successful match [there will be P_k = 1]

P31 = 1 for successful match and will be followed with the match as indicated above in paragraph #3.

P32 [for returning from phase-3] = invalid if P31 = 0 [return from phase-3 is possible on either of two causes – (i) X = 1 i.e. b = 0, (ii) no P_k = 1 (no more phase-3 sequencing is required and return to COP)].

P32 = 0 if P31 = 1 and all P_k = 0 [return to phase-2].

P32 = 1 if P31 = 1 and any P_k = 1 [no return to phase-2].

7. To read the asynchronously transmitted serial bits the receiver will do:
- Running of an IBS through a binary search tree of 2^{8k} nodes.
 - Sequencing through the binary search tree is to be done as per information available through bits P10, P20, P22, P30, P31 and P32.
 - Identification of matching nodes through P11, P21, P31 and match bits defined in paragraph 3 above. Receiver on identification of Q_bs will extract constituting bytes through dequantization.

Compression Ratio (CR) = $(n/k).2^{-3} + (3.p/k).2^{-3}$ where p is trials per Q_b.

In IBS p is not fixed but variable. Proper choice of k is a factor to keep p low on keeping deviation among the values of Q_b low. To keep the deviation low there may be inclusion of error correcting bytes in the Q_b.

Conclusion

IBS is invented with the curiosity for the possibility of left shifting of the binary registers X and AD in the context of successive approximation A/D with input time division multiplexing. IADC will find application in real time analog process control. The data compression algorithm needs further standardization for use in practical data storage and transmission applications.

References

- [1] Alope, Sarkar “Hardware realization of high level language processor for analog process control”, All India Seminar on ‘Application of Evolutionary Strategies to Power, Signal Processing and Control’ (AES-2002), Rourkela, February 2002, pp. 122–124.
- [2] Alope, Sarkar “Analog to digital converter with software multiplexing”, ‘Emerging Trends in Mechatronics for Automation’, *Proceedings 18th National Convention of Mechanical Engineers*, Rourkela, Phoenix Publishing House Pvt. Ltd., November 2002, pp. 420–429.
- [3] Alope, Sarkar, “RXP: the hardware realization of high level interpreter” section X, 37th National Convention 2002 of Computer Society of India, Bangalore, Tata McGraw Hill, October 2002, pp. 325, section – hardware, Sl. No. 133, sub-heading—X. Ait Quantizer, p. 7.
- [4] Alope, Sarkar, “Hardware realization of level 5 virtual machine on Convergence in analog and digital computations”, *International Conference on Information Technology: Prospects & Challenges*, 2003, Nepal.
- [5] Herbert, Taub and Donald L., Schilling, “Principles of Communication Systems” Singapore, McGraw-Hill Book Company 1986.
- [6] Bruce, Carlson A., “Communication System” Singapore, McGraw-Hill Book Company 1986.



Expounding the Complications and Mitigations for Indian Military Force Related Communication Issues

Akarsh Goyal^{*1}, Nikhil Chaudhari¹, K. Naresh¹ and V. Balasubramanian¹

Abstract: Indian military is one of the largest and strongest in the world. It is a very important cog in the wheel for maintaining the welfare and prosperity in the nation. It is because of them that people are able to live at peace in their lush condos while they stand guard at our border 24×7 . Technology has been a great aid in their functioning. But inspite of so many advances in the science and research, everyday they have to face a myriad of problems. And a lot of these relate to remote communication facilities used by them. So in this paper, focus has been given on communication issues confronted by the army due to the enemies beyond the border line and during natural calamities. The threats due to both of these matters and the most innovative methods related to mobile computing to tackle them are listed here. Also at the end a new model is proposed which would be robust enough to handle these difficulties.

Keywords: Indian Military, Technology, Enemies, Natural Calamities, Security, Communication.

Introduction

India is a very vast and diverse country with people of all creeds, sects and castes living here. It is very difficult to maintain harmony and peace between so many people who could get incited by raising of a single sensitive issue. Also the country is surrounded by so many neighbours on all sides. Some of them have very cordial relations with India while some on the other hand are quite cold towards it.

Most of the nations look to increase their foothold in the subcontinent by acquiring more area of land from others. This is also done to support their increasing population. But the Indian military force proves to be a deterrent for them. They guard the borders at almost all times of the year even in very harsh conditions are there. Also a major part of the credit goes to them for quelling any internal disturbances within the nation which may be during riots, terrorist attacks or in areas where curfew is nature at their own base as well and also the enemy becoming more intelligent day by day the army needs to up its game. But the technology for logistics and communication used by the army proves to be a hindrance. Much of the equipment used for these purposes have now reached a stage of obsolescence. There is a need to upgrade the remote technologies used by them so as to give them an edge over the difficulties in their path.

So in this paper, the communication problems have been discussed that have been faced by the military due to enemies beyond the line and natural disasters. This paper

tried to provide possible solutions related to fields of mobile computing, wireless networks and sensor technology to mitigate them. In addition to it we provide a new holistic proposal which takes into consideration every scenario so as to tackle the issue.

Related Work

A lot of work has been done regarding the communication based security concerns, their solutions, network problems caused by disasters and their mitigations. A few of these elucidated here.

S. Alam [1] worked on wireless sensor network and explained the security threats related to the use of it. In 2004, Perrig *et al.* [2] displayed how major security steps could be implemented in wireless sensor networks and what are the research challenges associated with it. A survey on various aspects connected to ad hoc wireless networks has been performed in [3]. In [4] and [5] all the vulnerabilities, challenges, recent advances and future trends of wireless networks have been elicited. Grover *et al.* [6] have done a case study on jamming and anti-jamming techniques in communication systems. In this paper, jamming has been explained properly and method has been shown that when used effectively could tackle it. In [7] the disaster life cycle has been discussed and how operation research could be applied to it to gain useful insights. Kovács *et al.* identify the different challenges related to human logistics, mainly

¹School of Computer Science and Engineering, Vellore Institute of Technology University, Vellore-632014, Tamil Nadu, India.
✉ akarsh.goyal15@gmail.com

network systems, in [8] and disaster relief operations to mitigate it in [9]. Various disaster relief operations and resilience systems have been illustrated in [10] and [11] to provide support for a number of disaster organisations working to tackle the calamity problems. In 2015, Pradeep *et al.* [12] have explained the communication networks which could be put to great effect during emergency situations. In [13] a survey on wireless mesh networks has been done. Raniwala [14] have talked about the architecture of multi-channel wireless mesh networks and also have evaluated the performance of various distributed algorithms on the same.

New Proposal for Security against Enemy Beyond the Line Wireless Mesh Networks (WMNs) Integrated with New Security Systems

Here a new wireless mesh network system [13] with new management secured protocols is discussed that will prove very much beneficial for the army. This is because it could be deployed in highly sensitive areas and prove to be a good substitute in place of wireless sensor networks and ad hoc wireless networks which are normally used in military areas.

Architecture

A conventional architecture of a typical WMNS for which we propose a security and privacy protocol. The architecture is a very specific for the army that represents the majority of the real-world deployment scenarios for WMNs [13,14]. The structure of a hierarchical WMN consists of three layers as shown in Figure 1. At the top layers are the Internet Gateways (IGWs) that are connected to the wired Internet. The entities at the second level are called wireless Mesh Routers (MRs) that eliminate the need for wired infrastructure

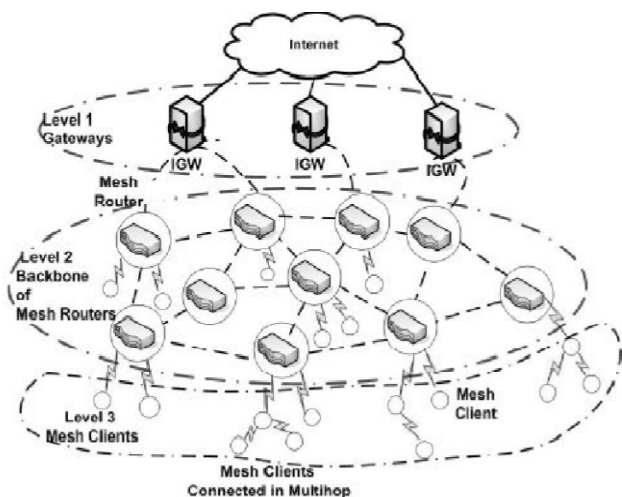


Fig. 1: The Three-Tier Architecture of a Wireless Mesh Network (WMN)

at every MR and forward their traffic in a multi-hop fashion towards the IGW. At the lowest level are the mesh clients (MCs) which are the wireless devices of the users. Internet connectivity and peer-to-peer communications inside the mesh are two critical applications for a WMN. Therefore the design of an efficient and low-overhead communication protocol which ensure security and privacy of the users is an essential requirement which poses significant research challenges.

The proposed security protocol serves the dual purpose of providing security in the access network (i.e., between the MCs and the MRs) and the backbone network (i.e., between the MRs and the IGWs). Hence they could be utilized properly by the army. The dual properties are described the following sub-sections.

Access Network Security

The access mechanism to this new WMN is assumed to be the same as that of a Local Area Network (LAN). This allows the users to access the services of the WMN exploiting the authentication and authorization mechanisms without installing any additional software. It is evident that such security solution provides protection to the wireless links between the MCs and the MRs. A separate security infrastructure is needed for the links in the backbone networks.

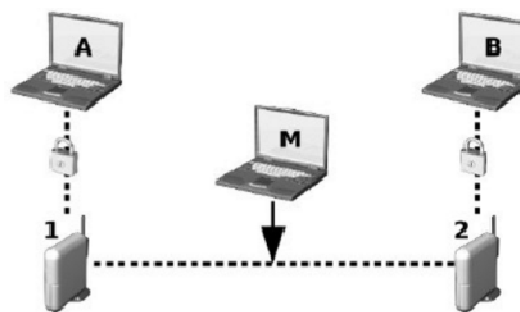


Fig. 2: Secure Information Exchange among the MCs A and B through the MRs 1 and 2

Figure 2 illustrates a scenario where users A and B are communicating in a secure way to MRs 1 and 2 respectively. If the wireless links are not protected, an intruder M will be able to eavesdrop on and possibly manipulate the information being exchanged over the network. This situation is prevented in the proposed security scheme which encrypts all the traffic transmitted on the wireless link using a stream cipher in the data link layer of the protocol stack.

Backbone Network Security

For providing security for the traffic in the backbone network, a two-step approach is adopted. When a new MR [13] joins the network, it first presents itself as an MC and

completes the association formalities. It subsequently upgrades its association by successfully authenticating to the AS. To make such authentication process efficient in a high mobility scenario, the key management and distribution processes have been designed in a way so as to minimize the effect of the authentication overhead on the network performance. The overview of the protocol is shown in Figure 3.

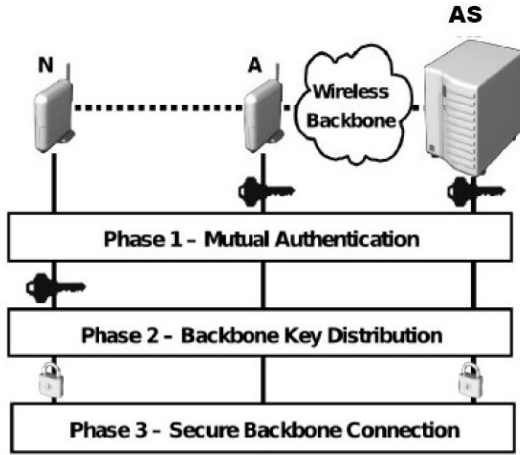


Fig. 3: Steps Performed by a New MR (N) Using Backbone Encrypted Traffic to Join the WMN

The Key Distribution Protocol

In this section, the details of the proposed key distribution and management protocol are presented. The protocol is essentially a server-initiated protocol and provides the clients (MRs and MCs), ie. the army, flexibility and autonomy during the key generation.

Server Initiated Key Management Protocol

In the proposed key management protocol delivers the keys to all the MRs from the AS in a reactive manner.

A newly joined MR, after its successful mutual authentication with a central server, sends its first request for a key list (and its time of generation) currently being used by other existing MRs in the wireless backbone. Let us denote the key list timestamp as TS_{KL} . Let us define a session as the maximum time interval for a validity of the key list currently being used by each node MR and MC). An MR, based on the time instance at which it joins the backbone, can find out the key (from the current list) being used by its peers (key ids) and the interval of validity of the key (T_i) using (1) and (2) as follows:

$$key_{idx} = \left\lfloor \frac{t_{now} - TS_{KL}}{timeout} \right\rfloor + 1 \quad \dots (1)$$

$$T_i = key_{idx} \times timeout - (t_{now} - TS_{KL}) \quad \dots (2)$$

In the proposed protocol, each WMN node requests the AS for the key list that will be used in the next session before the expiry of the current session. This is feature essential for nodes which are located multiple hops away from the AS, since, responses from the AS take a longer time to reach these nodes. So the army personnel stationed at the peak could interact with the base commanders.

In the proposed protocol, the correction factor is estimated based on the time to receive the response from the AS using (3), where t_s is the time instance when the first key request was sent, t_r is the time instance when the key response was received from the AS, and $timeout$ is the validity period of the key. Therefore, if a node fails to receive a response (i.e., the key list) from the AS [14] during the timeout, and takes a time t_{last} , it must send the next request to the AS before setting the last key.

$$c = \begin{cases} \left\lfloor \frac{t_{last} - timeout}{timeout} \right\rfloor & \text{if } t_{last} \geq timeout \\ 0 & \text{if } t_{last} < timeout \end{cases} \quad \dots (3)$$

$$t_{last} = t_r - t_s$$

The first request of the key list sent by the new node to the AS is forwarded by the peer to which it is connected as an MC through the wireless access network. However, the subsequent requests are sent directly over the wireless backbone.

For Mitigating Disasters

Many methods have been explained below which could be used for proper management and relief work during calamity situations faced by Indian army.

Wide Area Disseminator (WAD) Alarm Device

It will be based entirely on widely available mobile communications technologies such as Short Messages and CBM, aimed at rendering a cost effective and reliable mass alert system.

The system is compliant with CAP, which enables the authorized entity to distribute the same warning message to multiple media in one operation.

The block diagram of WAD Device is shown in Figure 4. It comprises of two basic elements – the Server and Clients. The server will reside in a secure facility and will be used by authorized persons to generate warning messages via SMS or CBM. The clients are the intended recipients of the above mentioned messages. Upon reception of the messages the clients will take necessary measures to inform the users. A responsible authority from the relief works would generate an alarm message from which would be received by mobile phones as well as alarm devices.



Once a warning message is received, the (WAD) alarm device responds by either emitting an audible alarm, by flashing a light, or by turning on a radio as directed by the message. The device will also include a call back function, which will allow users to call a dynamic hotline, in order to get more information. SMS-based alerting is used to activate selected alarms/individuals, while the CBM is used to activate all alarms.

The message types employed in the system are two-fold: warning messages, which carry the actual alerts, can either be sent as SMS or CBM. This allows the Alarm to benefit from the advantages of both type of messaging systems for each purpose.

Features of the Device

The overall capabilities of this Alarm Device are as follows:

1. It may be triggered by either SMS or a CBM.
2. Once triggered, the device will display the message on an LCD, emit an audible alarm, flash a light and/ or turn on an in-built radio in response to the trigger.
3. Responds only to warning message in a predetermined format and generated by a recognized source.
4. A hotline number can be sent with message, which the device can dial that number and make a call for more information/instructions.
5. The device is powered from the mains supply under normal operation, includes a backup for operation in the absence of mains power failure and is portable.

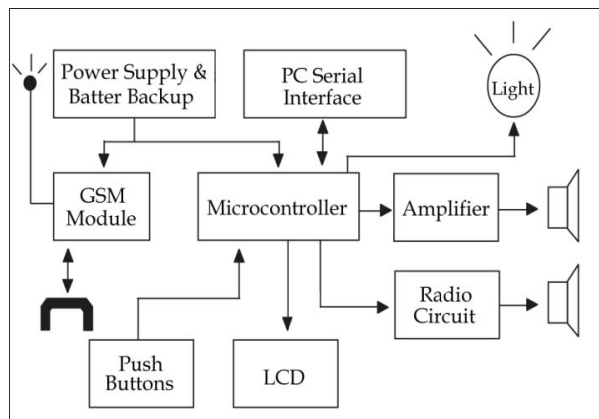


Fig. 4: Block Diagram of the WAD Alarm Device

The microcontroller and the GSM module [8] are the key components of the WAD alarm device. A suitable microcontroller was selected after taking various factors such as reliability, ruggedness, and ease of use. The microcontroller also houses a multitude of peripheral devices such as internal program flash memory, data memory, general purpose I/O, and USARTS.

Once in operation, the GSM module listens for any incoming SMS messages or CBMs. CBM-based warning messages will be broadcast on a predetermined dedicated logical broadcast channel. Upon the reception of a CBM or an SMS, a notification will be sent by the GSM module to the microcontroller. The microcontroller in turn will read and process the message. If the message is from an authorized source such as from military or government organisations (in case of SMS) and conforms to a given format, the WAD alarm device will be triggered. The alarm device is designed to power up from the main supply. The device is equipped with a back-up battery as a secondary power source. This battery is capable of powering the device for approximately seven hours. A battery was selected for this purpose after considering the size, cost, durability and maintenance.

The alarm device is designed to power up from the main supply. The device is equipped with a back-up battery as a secondary power source. This battery is capable of powering the device for approximately seven hours. A battery was selected for this purpose after considering the size, cost, durability and maintenance.

The functions of the five push button switches, call, ack, LCD, test and radio are given in Table 1.

Table 1: Functions of Push Buttons on the WAD

Button Name	Function
Radio	To turn ON/OFF Radio
Test	To start the test sequence
LCD	To turn ON LCD backlight
Ack	To send acknowledgement (This turns off Alarm and Light)
Call	To call for more information in the event of an emergency (This turns off Alarm and Light)

So this device could prove to be very beneficial in aiding the humongous amount of rescue work undertaken by the army.

Conclusion

The Indian Army shoulders the responsibility of protecting the citizens from various outer and internal encroachments. It goes about its task in a very concise manner. In the face of great adversities as well they display stoicism. But at the end of the day, they are also humans and they cannot always cover their backs. For accomplishing this thing, efficient technology should always be at their disposal. So to give our support to this, two problems, i.e., Security concerns due to enemies and calamities, in specific related to communication which forms an imperative part of the technology used by the Indian military were discussed in this paper. How these two issues could be very much threatening and the ways



which exist to mitigate them are mentioned elaborately here. Also, many new methods are proposed which are highly efficient and cost-effective for mass deployment for use by the army. If these systems are properly implemented, then they can prove to be very advantageous for the military and a deterrent in the path of the enemies of the country.

References

- [1] Alam, S. and De, D. (2014). Analysis of security threats in wireless sensor network. arXiv preprint arXiv:1406.0298.
- [2] Perrig, A., Stankovic, J. and Wagner, D. (2004). Security in wireless sensor networks. *Communications of the ACM*, 47(6), 53–57.
- [3] Singh, R.K., Joshi, R. and Singhal, M. (2013). Analysis of Security Threats and Vulnerabilities in Mobile Ad Hoc Network (MANET). *International Journal of Computer Applications*, 68(4).
- [4] Choi, M.K., Robles, R.J., Hong, C.H. and Kim, T.H. (2008). Wireless network security: Vulnerabilities, threats and countermeasures. *International Journal of Multimedia and Ubiquitous Engineering*, 3(3), 77–86.
- [5] Zou, Y., Zhu, J., Wang, X. and Hanzo, L. (2015). A Survey on Wireless Security: Technical Challenges, Recent Advances, and Future Trends.
- [6] Grover, K., Lim, A. and Yang, Q. (2014). Jamming and anti-jamming techniques in wireless networks: A survey. *International Journal of Ad Hoc and Ubiquitous Computing*, 17(4), 197–215.
- [7] Altay, N. and Green, W. G. (2006). OR/MS research in disaster operations management. *European journal of operational research*, 175(1), 475–493.
- [8] Kovács, G. and Spens, K. (2009). Identifying challenges in humanitarian logistics. *International Journal of Physical Distribution & Logistics Management*, 39(6), 506–528.
- [9] Kovács, G. and Spens, K.M. (2007). Humanitarian logistics in disaster relief operations. *International Journal of Physical Distribution & Logistics Management*, 37(2), 99–114.
- [10] Luis, E., Dolinskaya, I.S. and Smilowitz, K.R. (2012). Disaster relief routing: Integrating research and practice. *Socio-economic planning sciences*, 46(1), 88–97.
- [11] McDaniels, T., Chang, S., Cole, D., Mikawoz, J. and Longstaff, H. (2008). Fostering resilience to extreme events within infrastructure systems: Characterizing decision contexts for mitigation and adaptation. *Global Environmental Change*, 18(2), 310–318.
- [12] Pradeep, P.D. and Kumar, B.A. (2015). A Survey of Emergency Communication Network Architectures. *International Journal of u-and e-Service, Science and Technology*, 8(4), 61–68.
- [13] Akyildiz, I.F., Wang, X. and Wang, W. (2005). Wireless mesh networks: a survey. *Computer networks*, 47(4), 445–487.
- [14] Raniwala, A. and Chiueh, T.C. (2005, March). Architecture and algorithms for an IEEE 802.11-based multi-channel wireless mesh network. In *Proceedings IEEE 24th Annual Joint Conference of the IEEE Computer and Communications Societies* (Vol. 3, pp. 2223–2234). IEEE.



Study on 2.45 GHz Microwave Propagation in an ECR Plasma Enhanced Film Deposition System

Soumik Kumar Kundu¹, Samit Karmakar¹, Mili Sarkar¹ and G.S. Taki*¹

Abstract: In lower nanometer CMOS VLSI technology, high-K dielectrics are preferred to SiO₂ as a suitable gate insulator to substantially reduce tunneling current. The synthesis of nano-dimensional film of a suitable high-K dielectric material over the substrate involves highly sophisticated deposition processes. An Electron Cyclotron Resonance (ECR) high density plasma enhances the deposition rate at low temperature without causing damage to the substrate. An ECR plasma drastically improves the quality of deposited film working under very high vacuum environment. Such a deposition system has been designed and presently under development to synthesize high purity atomic dimensional films of metallic and non-metallic elements and compounds e.g., HfO₂, ZrO₂, Al₂O₃, Si₃N₄. A large amount of stored energy in a plasma enhances the CVD process providing better surface integration without altering the crystal structure of the substrate and synthesized film. The high density, low temperature plasma in ECR PE-CVD system breaks the precursor molecules to create desired more reactive radicals. A 2.45 GHz, 500W microwave system delivers power to a microwave cavity cum deposition chamber. A solenoid magnet assembly generates an iso-gauss surface of 875 Gauss over which the resonance of plasma electrons takes place. Besides other parameters, the efficient injection of microwave power plays a vital role in the deposition process. Here, an efficient simplified microwave injection system has been designed and presently under construction.

A magnetron injects microwave power through a rectangular waveguide WR340 with the help of a co-axial antenna. As the deposition takes place under vacuum, the microwave has to travel through a vacuum/air interface. So the design of the window is also a vital consideration including the material properties. We have planned to use 3 mm thick quartz window at the interface of chamber and wave guide. The microwave propagation and multiple-mode generations in the cylindrical cavity resonator have been studied with the help of COMSOL Multi-physics software. The interesting results achieved, have been presented in this paper in details.

Keywords: Electron Cyclotron Resonance, Multi-Mode, Coaxial Antenna, High-K Dielectric, Precursor.

Introduction

Advancement in device fabrication technology offers a large increment in the number of transistors per unit area in a Complementary MOS VLSI device. According to Moore's law "the complexity of a circuit normalized to cost increases by a factor of two every year" [1] Millions of transistors are now accommodated in a single chip with the help of the nano-fabrication technology. As the dimensions of the transistors decreases, several problems arise like short channel effect and tunneling effect. To overcome this problem, various dielectrics having higher dielectric constant are studied in place of SiO₂. To prepare nano-dimensional film of these dielectric materials needs a highly efficient deposition system. Thermal Chemical Vapor Deposition (CVD), Atomic Layer Deposition, Plasma Enhanced CVD

are usually used for these purposes. It has been planned to develop such a kind of efficient ECR plasma enhanced film deposition system [2, 3]. ECR Plasma Enhanced film deposition system is capable to develop uniform layer of High-K material [4, 5]. Here, we will use a 2.45 GHz, 500 W microwave system for creating confined high density plasma. The energetic electrons crack the precursor molecules to produce electrons, positively charged ions and radicals. A gradient mirror magnetic assembly generates a magnetic field of 875 Gauss over which resonance of plasma electrons take place. A SS 304 stainless steel vacuum chamber acts as the multimode cavity to generate ECR plasma and the film deposition takes place at the downstream of this chamber. To design a microwave injection system and the efficient propagation study of the microwave

¹Department of Electronics and Communication Engineering, Institute of Engineering and Management, Kolkata-700 091, India.
✉ gstaki@iemcal.com



inside the plasma chamber are the important aspects of our present work. For this study, we have used COMSOL Multi-Physics simulation software to study the electro-magnetic field propagation inside the ECR plasma chamber. The results of the study have been presented in this paper.

Microwave Propagation in ECR Plasma

Plasma is a charge neutral co-existence of electron, positive ions and neutral molecules. ECR Plasma is non-isotropic magnetically confined plasma. Due to the non-uniformity of the confined magnetic field complete charge neutrality cannot be achieved. So, a quasi-neutrality condition [6] always exists in ECR Plasma. But such plasma contains high density electrons, usually energized up to a very high level for producing high charge state ions. But in our present application, high energy electrons are not needed. The present need demands higher electron density with energy less than the ionization energy. It will basically produce neutral radicals and electrons. For generating high density electrons, microwave power density should be desirably high. Hence, an efficient injection of microwave power and its successful propagation inside the plasma is essential.

In ECR Plasma, electrons pick up energy from injected microwave power under cyclotron resonance condition. Ideally the particle frequency is equal to wave frequency.

Microwave may be written as:

$$\vec{E} = \vec{E}_0 \cos(\omega_0 t) \hat{e} = E_0 \cos(\omega_0 t) \hat{e}$$

ω_0 is the microwave frequency. In presence of a magnetic field (\vec{B}), electrons experience a force perpendicular to their direction of motion, which will make them rotate around the magnetic field lines with Cyclotron frequency (ω_c).

$$\omega_c = \frac{e\vec{B}}{m_e}$$

Where \vec{B} is the intensity of magnetic field, e and m_e are the charge and mass of electron respectively. If, $\omega_0 = \omega_c$ the electron will rotate in phase with the electric field and a global heating of electrons take place. The gain in electron energy is the net result of the Electron Cyclotron Resonance phenomenon.

Lorentz Force [6] is generated by suitable microwave injection and static magnetic assembly. Due to injected microwave, the orthogonal electric and magnetic field vectors propagate together inside the resonant cavity. Microwave is injected to the rectangular waveguide through a coaxial antenna feed. The wave excitation at coaxial antenna introduces Transverse Electromagnetic Mode (TEM) at the input and changes to Transverse Electric (TE) mode while it propagates through the rectangular waveguide

section. The mode transfer takes place at the transition of rectangular waveguide to cylindrical cavity interface. TE_{10} (dominant) mode becomes TE_{11} mode only if the diameter of the cavity is less than the wavelength λ at 2.45 GHz, otherwise it becomes multimode. In this study, we have designed a model accordingly.

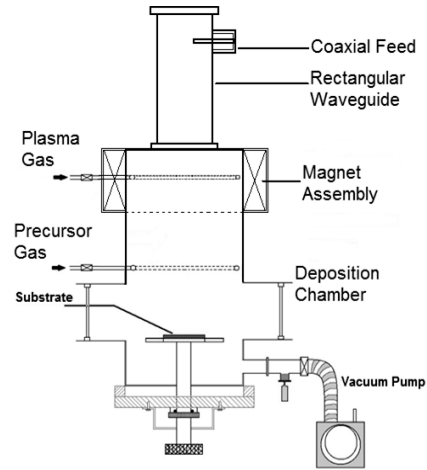


Fig. 1: Schematic Setup of Deposition System

Our system consists of four parts as mentioned:

1. Plasma cavity cum deposition chamber
2. Microwave power injection system
3. Magnetic assembly
4. High vacuum system.

150 mm diameter, 500 mm long stainless steel (SS 304) cylindrical cavity will be used for plasma generation and film deposition. High vacuum $\sim 5 \times 10^{-3}$ Torr will be achieved with the help of rotary vane pump. A 2.45 GHz 500 W magnetron is used to deliver power for plasma generation [7–9]. Figure 1 shows a schematic diagram of the PECVD system. The co-axial antenna of magnetron microwave generator injects power to the chamber through WR340 rectangular waveguide. The placement of the coaxial feed on the waveguide is the most critical part to match the impedance. Depending upon the wavelength (λ) at 2.45 GHz frequency the position of the coaxial antenna is extremely important to impart inductive or reactive impedance on the path of power injection. The placement of coaxial antenna at $\lambda/2$ eliminates the impedance mismatch and the majority of microwave power is injected successfully with a nominal amount of reflected power. A quartz microwave window has been designed to place at the interface between the cavity and waveguide. A 3 mm thick quartz window plate has been chosen due to its good microwave and also appreciably low out gassing rate in vacuum. A substrate holder is attached to the bottom flange with an O-ring rotary seal enabling us to easily adjust its vertical position.



Simulation of Microwave Injection

COMSOL Multi-Physics is a finite element analysis software which generates small meshes to cover whole surface or volume to which it calculates the field values at numerous number of points. This software allows us to simulate microwave propagation through the coaxial antenna to the waveguide and finally into the generated plasma in a cavity. Figure 2 shows the design of microwave injection line and resonant cavity over which simulation has been carried out.

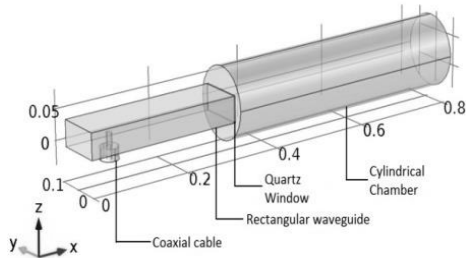


Fig. 2: Design of Microwave Injection Line and Resonant Cavity

A coaxial antenna is connected to a copper rectangular waveguide (WR340) at $\lambda/2=61.22$ mm from the shorter end as shown in Figure 2. The other end of the rectangular waveguide is connected to the plasma generation chamber through a 3-mm thick rectangular quartz window. Figure 3 shows the microwave propagation along with the electric and magnetic field directions on x-y plane. The direction of propagation is along x-axis. The diameter of the cylindrical chamber is taken as 120 mm for this design. The figure clearly shows that, propagation mode changes from TEM to TE_{11} mode. Figure 4 shows the multimode propagation for a higher cavity diameter of 150 mm. Figure 4(b) and 4(c) show the field contour inside waveguide and deposition chamber respectively illustrating efficient multimode generation and propagation.

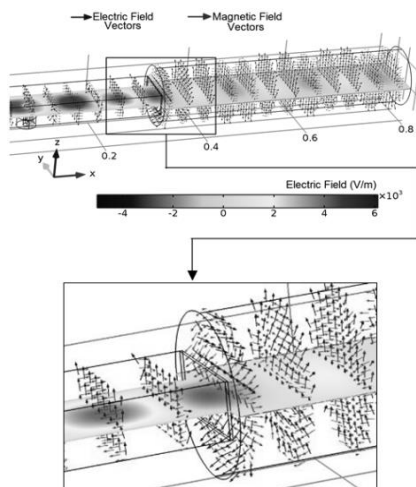


Fig. 3: Wave Propagation at 2.45 GHz in a 120 mm Diameter Chamber

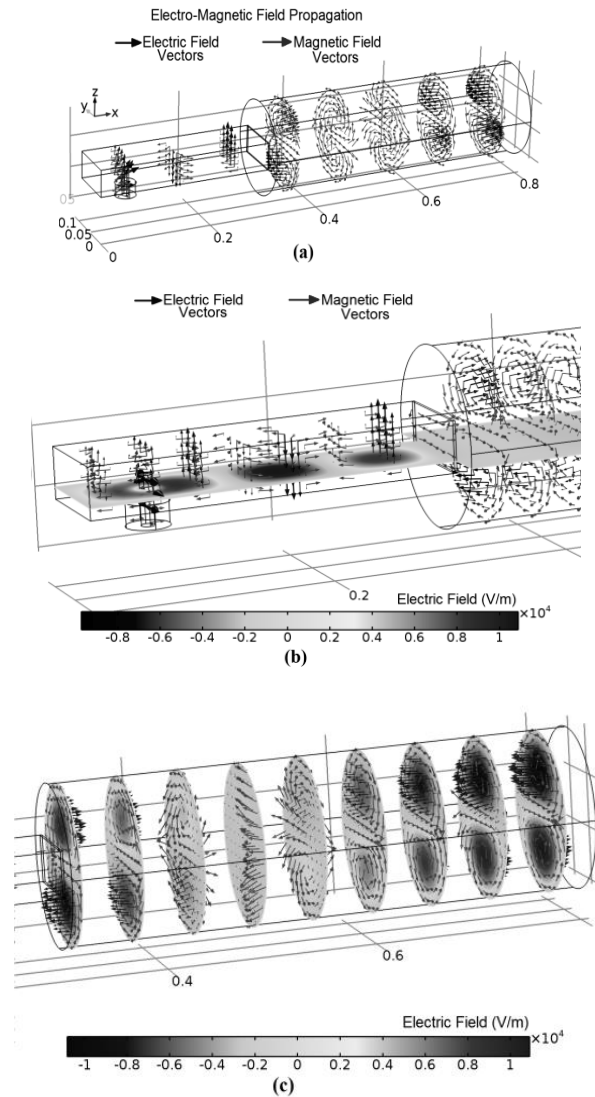


Fig. 4: (a) Distribution of Field Vectors at 2.45 GHz Cavity Diameter = 150 mm, (b) E-field Contour at X-Y Plane, (c) E-Field Contour at z-y Plane

Conclusion

A 2.45 GHz microwave injection and its efficient propagation through ECR Plasma have been studied here. The present study on the electro-magnetic field propagation over orthogonal plane surfaces provides substantial information about the ECR resonance zone. This study also describes the generation of various modes of Transverse Electric Field with varying chamber diameters. If the chamber diameter is less than λ , electric field propagated through the microwave window, transforms from TE_{10} (rectangular) to TE_{11} (circular) mode. But if the chamber diameter is greater than λ as shown in Figure 4, the simulation clearly shows multimode transmission instead of TE_{11} mode inside the



ECR Plasma. Our aim is to distribute the electric field evenly inside the cavity chamber for desirable plasma generation, which is satisfied by multimode propagation. The present simulation result helps to visualize and understand the most successful microwave injection and propagation inside ECR Plasma enhanced film deposition system.

References

- [1] Moore, G.E., Cramming more components onto integrated circuits, *Proceedings of the IEEE*, Vol. 38, No. 1, 1965.
- [2] Taki, G.S., Krishna, J.B.M., Gupta, Sayak Dutta; Karmakar, Samit; Kundu, Soumik Kumar, Reza, Samim Md., ECR Plasma Enhanced Film Deposition System, National Thematic Workshop on Recent Adv. In Mat. Sc. UGC-DAE-CSR Kolkata, 8–9 March, 2016.
- [3] Tarvainen, Olli, Thesis: Studies of Electron Cyclotron Resonance Ion Source Plasma Physics, 2005.
- [4] Kundu, Soumik Kumar; Karmakar, Samit, Reza, Md. Samim, Dutta, Arindam and, Taki, G.S., A Study on high-k gate stack for MOSFET, *International Conference and workshop on Comp. and Comm. (IEMCON)*, IEEE Conf. 15 to 17 Oct. 2015.
- [5] Nishikawa, K. and Wakatani, M., Book: Plasma Physics Basic Theory with Fusions and Applications, Springer, 2000.
- [6] Mitra, Monojit, Book: Microwave Engineering, Third Edition, 2006.
- [7] Taki, G.S. and Gupta, Sayak Dutta, Patent Application No. 1132/KOL/2015, Published on 04/12/2015.
- [8] Taki, G.S.; Gupta, Sayak Dutta, Patent Application No. 1029/KOL/2015, Published on 09/10/2015.
- [9] Taki, G.S., Patent Application No. 898/KOL/2015, Published on 11/09/2015.



Design and Development of Multi-Junction Solar Cell on Silicon

Anindya Ghosh^{*1}, Suchandra Mukherjee¹ and Payel Das²

Abstract: Unlike silicon, the III-V compound semiconductor materials provide the flexibility to realize multiple solar cells stacked on top of each other following same crystal lattice. The flexibility in band-gap selection provides an unprecedented degree of freedom in solar cell design through metamorphic or lattice-matched configurations based on III-V materials. The multiple solar cells stacked on top of one another in III-V multi-junction solar cells allow a much broader absorption of the incident solar spectrum compared to the conventional single-junction (1J) Si solar cells. The multiple III-V solar cells when connected in series and designed in such a way that they generate the same photo-current, allows linear addition of the voltages from the individual subcell resulting in higher conversion efficiencies. The four most readily available semiconductor substrates include Si, Ge, GaAs and InP. The ideal band-gap combination (1.85-1.90eV/1.42eV/1.0eV) for realizing high-efficiency triple-junction (3J) solar cell on GaAs substrate. The highest efficiency achieved from lattice-matched thin film 1J GaAs and 2J InGaP/GaAs solar cells are 28.8% and 30.8%, respectively at 1-sun. A record efficiency of 32.6% at 1000 suns has been demonstrated for the 2J InGaP/GaAs cell on GaAs substrate. Utilizing Ge (band-gap = 0.67eV) as the bottom subcell in a lattice-matched 3J solar cell configuration, cell efficiency in excess of 40% was demonstrated for the first time. To gain additional performance benefits, the InGaAs cell was grown the last in an inverted configuration and this approach is commonly known as inverted metamorphic or IMM approach. This IMM approach lead to an efficiency of 40.8% which utilized two metamorphic InGaAs subcells with band-gaps of 1.34 eV and 0.89 eV. Although all-Si structures have been proposed using amorphous silicon and silicon-based meta-materials to fabricate multi-junction cells, the most attractive and most flexible option remains growth of high quality III-V materials on Si.

Keywords: III-V Group Semiconductor, Si Solar Cell, Multi-Junction, CMOS, Photo Current.

Brief Summary

Unlike silicon, the III-V compound semiconductor materials provide the flexibility to realize multiple solar cells stacked on top of each other following same crystal lattice. The flexibility in band-gap selection provides an unprecedented degree of freedom in solar cell design through metamorphic or lattice-matched configurations based on III-V materials. The multiple solar cells stacked on top of one another in III-V multi-junction solar cells allow a much broader absorption of the incident solar spectrum compared to the conventional single-junction (1J) Si solar cells. The multiple III-V solar cells when connected in series and designed in such a way that they generate the same photo-current, allows linear addition of the voltages from the individual subcell resulting in higher conversion efficiencies. The four most readily available semiconductor substrates include Si, Ge, GaAs and InP. This places a constraint on the

band-gap and lattice-constant selection for optimal device design, wherein lattice-match structure are desired. The ideal band-gap combination (1.85–1.90 eV/1.42 eV/1.0 eV) for realizing high-efficiency triple-junction (3J) solar cell on GaAs substrate [1, 2]. The highest efficiency achieved from lattice-matched thin film 1J GaAs and 2J InGaP/GaAs solar cells are 28.8% and 30.8%, respectively at 1-sun [3]. A record efficiency of 32.6% at 1000 suns has been demonstrated for the 2J InGaP/GaAs cell on GaAs substrate [4]. However, experimental realization of high quality epitaxial 3J solar cells comprising of subcells with the ideal band-gap combinations has been quite challenging. Utilizing Ge (band-gap = 0.67eV) as the bottom subcell in a lattice-matched 3J solar cell configuration, cell efficiency in excess of 40% was demonstrated for the first time by King *et al.* [5]. In search for 1eV bottom subcell, the most commonly followed path initially was the integration of 1 eV

¹Department of Electronics and Communication Engineering, Swami Vivekananda Institute of Science & Technology, Kolkata-700145, West Bengal, India. ✉ anindya.ciem@gmail.com

²Department Electronics and Communication Engineering, Heritage Institute of Technology, Kolkata-700107, West Bengal, India.



metamorphic InGaAs solar cell in the 3J solar cell configuration with lattice-matched InGaP and GaAs as the top two subcells [6]. To gain additional performance benefits, the InGaAs cell was grown the last in an inverted configuration and this approach is commonly known as inverted metamorphic or IMM approach [6]. This IMM approach lead to an efficiency of 40.8% which utilized two metamorphic InGaAs subcells with band-gaps of 1.34 eV and 0.89 eV as the bottom two subcells in the 3J solar cell configuration.

Multi-junction cells remain the most successful high efficiency design concept, and the only one successfully commercialised. Nevertheless, these structures are still restricted to applications in space and under concentration, although generic terrestrial applications are tantalisingly close. The materials most suitable for multi-junction designs are the III-V materials families, that given their range of optical and material properties where incompatibilities, especially due to lattice constants, may be managed or even eliminated. The classic example is the growth of GaInP and GaInAs top and middle gap junctions on Ge substrates as bottom cell. This triple junction has achieved efficiencies [7] under concentration greater than 40% with both lattice matched and lattice mismatched approaches. The main disadvantages to widespread use of multi-junctions in renewable energy supply are materials and fabrication issues. The materials cost is partly due to the scarcity of some essential III-V materials such as In and Ga, but more importantly, it is due to the use of expensive substrates, since even Ge remains relatively costly in the competitive photovoltaic market.

However, Si suffers from a lack of semiconductors lattice matched to it, and from an indirect bandgap and low absorption coefficient. This is a disadvantage for most optoelectronic applications including multi-junction solar cell design. Although all-Si structures have been proposed, using amorphous silicon and silicon-based meta-materials to fabricate multi-junction cells [8], the most attractive and most flexible option remains growth of high quality III-V materials on Si.

Literature Survey

An early attempt to address this issue by Yang [9] simply grew a thick AlGaAs buffer layer on an active Si substrate, with a simple three-terminal design. This approach did not exceed efficiencies of 20%, and has not to date been developed further. Some years later, Taguchi *et al.* [10] adopted a not dissimilar structure with a high quality GaAs cell grown on a GaAs substrate and transferred to a Si substrate by liftoff. They chose a four-terminal design but again failed to demonstrate more than 19% efficiency. Geisz

and co-workers have since reported results on two-terminal designs. They have investigated both lattice matched attempts using nitrides [11] and lattice mismatched approaches using graded buffer techniques for strain relaxation minimising bulk defect densities [12]. The work of Lueck *et al.* [13] in the same year demonstrated similar techniques and achieved an efficiency of 17%. Work in this field continues with Putyato *et al.* [14] developing graded buffer approaches. While these methods have made progress, the efficiencies achieved remain subject to materials quality limitations due to the fundamental problem of high defect densities, despite the use of buffers to reduce them to acceptable levels.

This paper presents a quantitative study of silicon-based multi-junction solar cells for terrestrial applications developed by the Multispectral Solar Cells on Silicon (MULTISOLSI) project [15]. The study assumes a spectrum which corresponds to photovoltaic systems with no solar concentration. This is suitable for strategies prioritising a low system cost over cell efficiency and peak power. However, we are also aiming at relatively low cell cost with our silicon-based design, while nevertheless reaching high efficiencies.

The viability of III-V InGaP/GaAs solar cells on Si relies on the ability to grow high quality GaAs on Si with careful lattice engineering and substrate treatment. The polar on non-polar epitaxy, the thermal mismatch and the 4% lattice-mismatch makes the growth of GaAs on Si very challenging, rendering the metamorphic solar cell sensitive to defects including dislocation. These dislocations generated due to mismatch between GaAs and Si can propagate into the photoactive cell region and significantly impede the minority carrier lifetime and hence the overall cell performance [16–19].

The highest efficiency reported for single-junction (1J) GaAs on Si is 21.3% at 200 suns under AM 1.5D spectrum. While, the highest efficiency achieved for monolithic dual-junction 2J InGaP/GaAs solar cell on Si substrate is 18.6% at 1-sun under AM1.5G spectrum [20]. The corresponding highest efficiency achieved from lattice-matched thin film 2J InGaP/GaAs cells is 30.8% at 1-sun [3]. This record efficient lattice-matched thin film 2J solar cell was grown on GaAs substrate, which was then epitaxially released from the GaAs substrate using a wet-etching process. The lower efficiency of the 2J InGaP/GaAs solar cell on Si substrate [20] could be attributed to thick SiXGe1-X buffer layer, insufficient optimization of anti-reflective layers and most likely inadequate realization of the current-matching condition between the subcells, taking into account the impact of threading dislocations [20].



Proposed Plan of Work with Necessary Diagram

A detailed growth investigation has to be checked the development of III-V growth on Si using novel low cost three dimensional growth techniques. It involves Epitaxial Lateral Overgrowth (ELO) of lattice mismatched polar semiconductors on Si via growth of nano-seeds in apertures opened in thin SiO₂ layers.

We first examine the suitability of silicon for multi-junction cells from the commonly used ideal theoretical viewpoint of the radiative limit, but amended to maximise the radiative efficiency of multi-junction cells with non-ideal bandgaps and layer thicknesses. We then describe a quantitative analytical model capable of accurately modelling record multi-junction cells.

In order to design test structures for the novel growth method, we use an analytical model, which we sketch the main aspects here firstly for a single junction. With material parameters for the majority of semiconductors in the III-V family, including Si(Ge), it evaluates the External Quantum Efficiency (EQE) and photocurrent JPH as a function of bias by standard analytical solutions of transport and continuity equations in the depletion approximation for one-dimensional structures with abrupt interfaces. The point of interest in this model is the detailed accounting of loss mechanisms by explicit solution of non-radiative and radiative recombination losses in the different regions of the cell, and the inclusion of series and shunt resistances for each subcell.

The main focus is to investigate and optimize the performance of III-V InGaP/GaAs based dual-junction solar cells on Si substrate by taking into account the threading dislocations generated due to mismatch between GaAs and Si. The highest efficiency achieved till date utilizing the lattice-matched 2J InGaP/GaAs solar cells on GaAs substrate is 30.8% at 1-sun under AM1.5G spectrum. My goal is to investigate if one can theoretically model and optimize the performance of 2J InGaP/GaAs solar cell on Si substrate in close agreement with the performance of lattice-matched 2J InGaP/GaAs solar cells on GaAs substrate.

The modeling process for optimizing our III-V multi-junction solar cell designs was performed using a simulator, a general-purpose 2D/3D finite element analysis and modeling software for semiconductor devices.

Future Scope of Research

Investigating the use of Si for multi-junction cells, we have looked at non-ideal designs in the ideal radiative limit which include a Si subcell. These designs show that high efficiencies are achievable by balancing competing compromises of material restrictions and non-ideal optical properties.

In order to design real cells, we have developed a quantitative analytical model. We have validated this model by quantitatively reproducing state of the art light and dark current characteristics of record tandem and triple junction solar cells.

This leads to dark current fitting in terms of a single free parameter, which is the Shockley-Read-Hall non radiative lifetime in the space-charge region. With the exception of the reflectivity calculations which assume loss-free dual layer MgF/ZnS AR coats, the approach to modelling has been to use published experimental values for transport parameters, in order to maximise agreement with experimental data. The quantitative modelling of the record tandem and triple junction solar cells, together with the compatibility of transport parameters used with values in the literature give a high degree of confidence in this analytical modelling methodology. The minority carrier properties and SRH lifetimes used in the modelling are therefore reliable benchmarks for the material to be grown on Si by the growth methods developed within the MULTISOLSI project.

Applying this quantitative model to realistic solar cell designs combining Si and III-V materials, we first find that an appropriate tandem design of thinned GaAs on Si can deliver an efficiency of 29%, close to the 30% world record achieved with a GaAs substrate under a terrestrial spectrum with no concentration.

Furthermore, we find that more challenging growth of ternary materials deliver tandem efficiencies greater than 32%, and triple junction efficiencies greater than 36%.

These high efficiencies are remarkable in that they are achieved without solar concentration. They nevertheless reach efficiencies just a few percent below the maximum efficiencies achieved to date, at concentrations of 500 suns and above. This lack of concentrating optics invites the clear advantage of simple photovoltaic systems. More importantly, from the cell design point of view, it significantly relaxes the design criteria for tunnel junctions between subcells, due to the significantly reduced and less demanding current flow achievable with a terrestrial global spectrum.

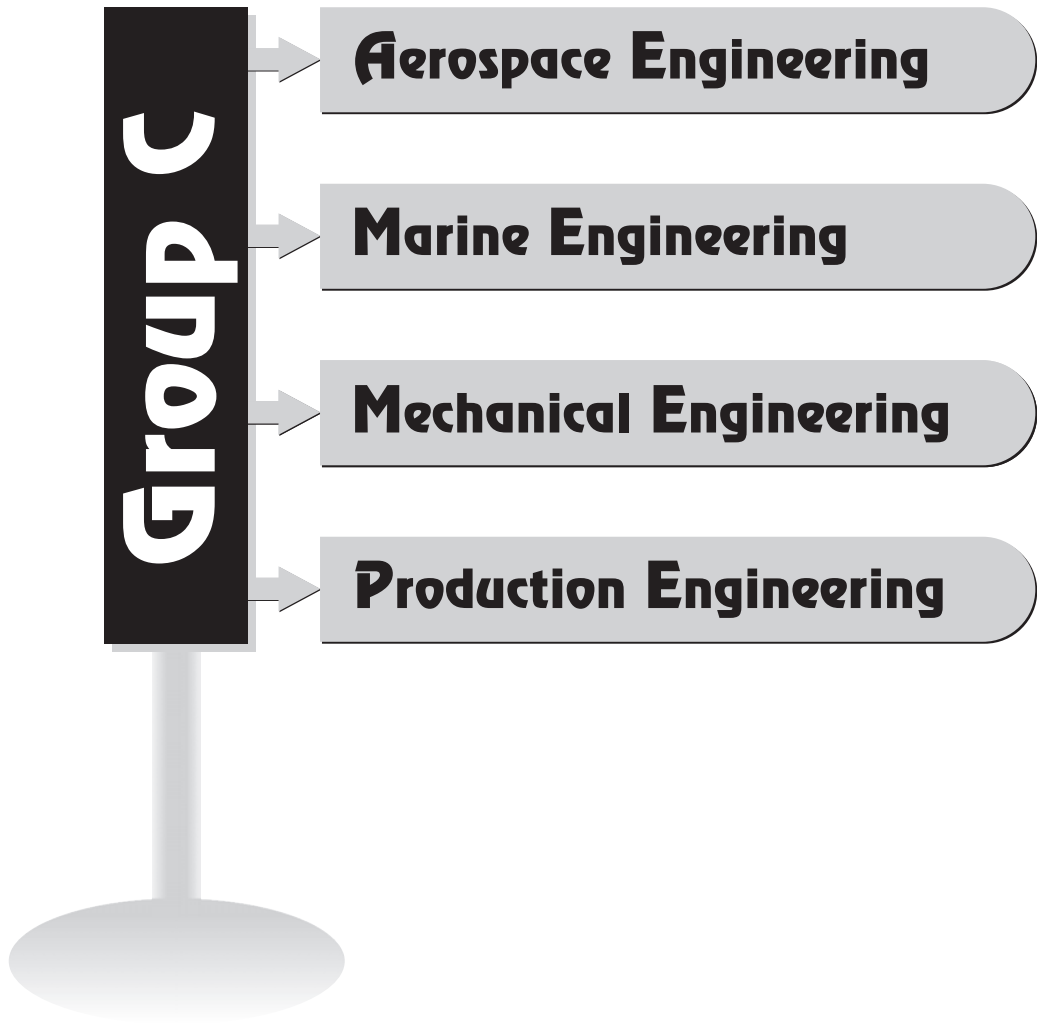
Conclusion

This work has been carried out within the MULTISOLSI project, which has demonstrated the growth of GaAs on Si without the formation of anti-phase domains, and without the generation of bulk defects. Work continues to develop a finer theoretical understanding of the three dimensional nature of the structures involved, of the corresponding tunnel junctions, and to optimize the growth and processing techniques required to fabricate these potentially ground-breaking designs.



References

- [1] King, R.R., *et al.*, Pathways to 40 percent-efficient concentrator photovoltaics, “*Proceedings of the 20th European Photovoltaic Solar Energy Conference*, Barcelona, Spain, 2005.
- [2] Wanlass, M., *et al.*, “Monolithic, ultra-thin GaInP/GaAs/GaInAs tandem solar cells,” *4th World Conference on Photovoltaic Energy Conversion*, 2006, pp. 729.
- [3] Green, M.A. *et al.*, “Solar cell efficiency tables (version 41),” *Progress in Photovoltaics: Research and Applications*, Vol. 21, 2013, pp. 1.
- [4] Garcia, *et al.*, “A 32.6% efficient lattice-matched dual-junction solar cell working at 1000 suns,” *Applied Physics Letters*, Vol. 94, 2009, pp. 053509.
- [5] King, R.R., *et al.*, “40% efficient metamorphic GaInP/GaInAs/Ge multijunction solar cells,” *Appl. Phys. Lett.*, Vol. 90, 2007, pp. 183516–1.
- [6] Geisz, J.F., *et al.*, “40.8% efficient inverted triple-junction solar cell with two independently metamorphic junctions,” *Appl. Phys. Lett.*, Vol. 93, 2008, pp. 123505–1.
- [7] Cotal, Hector; Fetzer, Chris; Boisvert, Joseph; Kinsey, Geoffrey; King, Richard; Hebert, Peter; Yoon, Hojun and Karam, Nasser, “III–V multijunction solar cells for concentrating photovoltaics”, *Energy Environ. Sci.*, 2009, 2, 174–192. DOI: 10.1039/B809257E.
- [8] Green, M.A., Cho, E.-C., Cho, Y., Huang, Y., Pink, E., Trupke, T., Lin, A., Fangsuwannarak, T., Puzzer, T., Conibeer, G. and Corkish, R. “All-silicon tandem cells based on ‘artificial’ semiconductor synthesised using silicon quantum dots in a dielectric matrix.” *Proc. 20th European Photovoltaic Solar Energy Conf.*(Barcelona, Spain). 2005.
- [9] Yang, Ming-ju; Soga, Tetsuo; Jimbo, Takashi and Umeno, Masayoshi, “High efficiency monolithic GaAs/Si tandem solar cells grown by MOCVD”, *First WCPEC*; Dec. 5–9, 1994; Hawaii, p. 1847–1850. DOI: 10.1109/WCPEC.1994.520725.
- [10] Taguchi, Hironori; Okada, Naoaki; Soga, Tetsuo; Jimbo, Takashi and Umeno, Masayoshi, “GaAs/Si tandem solar cell using epitaxial lift-off technique”, *3rd World Conference on Photovoltaic Energy Conversion* May 11–18, 2003 Osaka. Japan.
- [11] Geisz, J.F., Olson, J.M. and Friedman, D.J., “Toward a Monolithic Lattice-Matched III-V on Silicon Tandem Solar Cell”, *19th European PV Solar Energy Conference and Exhibit Paris*, France June 7–11, 2004.
- [12] Geisz, John F., Olson, J.M., Romero, M.J., Jiang, C.S. and Norman, A.G., “Lattice-mismatched GaAsP Solar Cells Grown on Silicon by OMVPE”, *4th World Conference on Photovoltaic Energy Conversion*, 2006, Hawaii DOI: 10.1109/WCPEC.2006.279570.
- [13] Lueck, M.R., Andre, C.L., Pitera, A.J., Lee, M.L., Fitzgerald, E.A. and Ringel, S.A., “Dual Junction GaInP/GaAs Solar Cells Grown on Metamorphic SiGe/Si Substrates With High Open Circuit Voltage”, *IEEE Electron Device Letters*, Vol. 27, No. 3, March 2006. DOI: 10.1109/LED.2006.870250.
- [14] Putyato, M.A., Semyagin, B.R., Emel’yanov, E.A., Pakhanov, N.A. and Preobrazhenskii, V.V., “Molecular-beam epitaxy of GaAs/Si(001) structures for high-performance tandem AIII-BV/Si-solar energy converters on an active silicon substrate”, *Russian Physics Journal*, Vol. 53, No. 9, 2011. DOI:10.1007/s11182-011-9509-3.
- [15] http://www.agence-nationale-recherche.fr/suivi-bilan/energie-durable/production-renouvelable-et-gestion-de-l-electricite/fiche-projet-progelec-2011/?tx_lwmsuivibilan_pi2%5BCODE%5D=ANR-11-RGE-0009
- [16] Lovejoy, M.L., *et al.*, “Minority hole mobility in GaAs,” in M.R. Brozel and G.E. Stillman (eds.), *Properties of Gallium Arsenide, Data Review Series No. 16*, London: INSPEC, 1996, pp. 123.
- [17] Lundstrom, M.S., “Minority carrier transport in III-V semiconductors,” in R.K. Willardson, A.C. Beer, and E.R. Weber (eds.), *Minority Carrier in III-V Semiconductors: Physics and Applications, Semiconductors and Semimetals*, vol. 39: Academic Press Inc., 1993, pp.193.
- [18] Andre, C.L., *et al.*, “Impact of dislocations on minority carrier electron and hole lifetimes in GaAs grown on metamorphic SiGe substrates,” *Appl. Phys. Lett.*, Vol. 84, 2004, pp. 3447.
- [19] Ghannam, M.Y., *et al.*, “Theoretical study of the impact of bulk and interface recombination on the performance of GaInP/GaAs/Ge triple junction tandem solar cells,” in *Proc. 3rd World Conf Photovoltaic Energy Convers.*, 2003, pp. 666.
- [20] Lueck, M.R., *et al.*, “Dual junction GaInP/GaAs solar cells grown on metamorphic SiGe/Si substrates with high open circuit voltage,” *IEEE Electron Device Letters*, Vol. 27, 2006, pp. 142.





Improving Competitiveness of Indian Shipbuilding: Intelligent Applications of Systems, Technologies and Economics

M.K. Ghosh Roy¹

Abstract: Indian Ship building industry stagnated for several decades after independence, while several emerging Asian countries like China, South Korea, Vietnam and even Philippines have developed internationally competitive shipbuilding industry. But the trend in the 21st century is positive as many shipyards in the private sectors are showing new vigour and exporting ships to international customers, while the public sector shipyards have delivered large and advanced naval ships to international class technology. The paper explores the possibility of improving the productivity of Indian shipbuilding to international standards through intelligent applications of advanced systems, modern technologies and favourable economic environment. It first reviews the current state of Indian shipyards and shipbuilding with its advantage of low labour cost. Next it recommends use of advanced systems for integrating steel fabrication with machinery fittings into simultaneous operation thereby compressing shipbuilding time drastically. Thereafter it prescribes introduction of high technology and appropriate machineries to further raise productivity. Finally, it emphasizes that the Government should bring in favourable economic incentives to help the economics of Indian shipbuilding industries in line with what other nations are assisting their ship buildings.

Keywords: Indus Valley, Congruent Shipbuilding, Batchline Shipbuilding.

Introduction

India, being virtually bounded on three sides by the Indian Ocean, seafaring came naturally to Indians. Indian seafaring dates back to the Indus Valley civilization about 3000 BC. A potsherd discovered at Mohenjo-Daro depicts a ship with masts (Figure 1). In the historical period, there were much maritime activities in the South-East Asia covering Cambodia, Sumatra, Java, Thailand, and Myanmar. Similarly seaborne trade prospered on the west coast carrying merchandise to East Africa, Red Sea and even continental Europe on Mediterranean Sea. After independence, India has naturally embarked upon developing shipbuilding, but the venture has apparently not yet succeeded. While newly emerging Asian countries like China, Vietnam, South Korea and even Philippines have developed internationally competitive shipbuilding industry, India has not reached the scale, sophistication and competitiveness of world stature. The reasons are manifold. But the trend in the 21st century is positive as many shipyards in the private sectors are showing new vigour and exporting ships to international customers, while the public sector shipyards have delivered large and advanced naval ships to international class technology. This paper presents an overview on Indian shipbuilding and how to improve its

competitiveness through induction of modern systems, technology and government-initiated favourable economic environment.

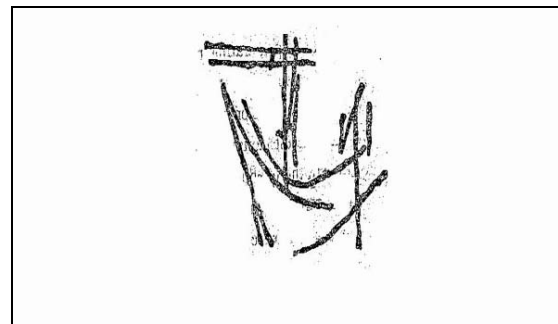


Fig. 1: A Sailing Ship-Mohenjo-Daro Potsherd

Current Status of Indian Shipbuilding Industry Today

The world seaborne trade is generally growing steadily at about 4% annually. Supporting the growing trade, the global shipbuilding deliveries are also growing (Figure 2). Hence it may be assumed that there will be demand for shipbuilding orders domestically and globally.

¹Former Senior Professor, Indian Institute of Technology Madras, Chennai, India. ✉ mkgghoshroy@gmail.com

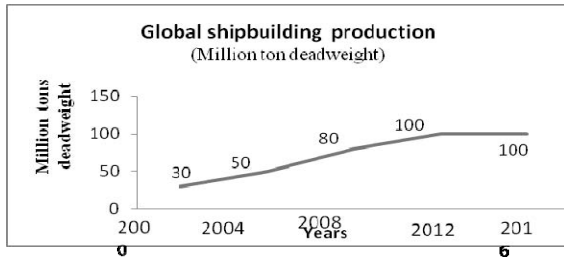


Fig. 2: Global Shipbuilding Production

The Indian shipbuilding industry which represented only about 0.1% of the global ship production in 2002 grew 10 folds accounting for 1%, amounting to a gross annual production value of USD 1.3 billion today (KPMG 2008). In physical output, India is believed to have 257 vessels on order in 2010 and occupying 6th rank in global shipbuilding capacity. In fact, India has emerged as an important destination for the construction of offshore vessels for the oil industry, which are highly specialized ships demanding high skill and is highly labour intensive to build. Presently India has a total of 32 shipyards (DI-IBD), prominent among them are:

Public Sector Shipyards

Garden Reach Shipbuilding, Cochin Shipyard, Hindustan Shipyard, Mazagon Docks, Goa Shipyard, Hooghly Dock.

Private Sector Shipyards

ABG Shipyard, Bharati Shipyard, Pipav Shipyard, Chowgule Shipyard, L & T Shipyard, Tembe Shipyard.

Labour Cost Advantage and New Shipbuilding Industries

Countries like China and to some extent Vietnam, Philippines and Taiwan have leveraged their inherent advantage of low cost manufacturing to enter into international Shipbuilding. In particular China's rise in shipbuilding is rather remarkable. Within a period of 5 years, China has



Fig. 3: Daily Cost of Shipbuilding Labour in Four Different Countries

risen to become the third largest shipbuilding nation after South Korea and Japan. India also enjoys low labour cost advantage as China (see Figure 3), which has helped India to grow shipbuilding in small and specialist offshore tugs and supply vessels, in which India has considerable skill advantage. But unlike China, India also generally suffers from low shipbuilding productivity.

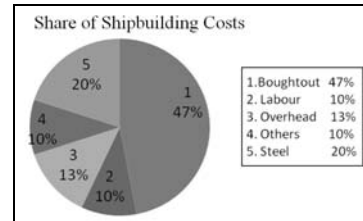


Fig. 4: Share of Shipbuilding Costs for Different Heads (USD/day)

Source: KPMG 2008, Data from Chinese sources.

Figure 4 shows the average constituent costs in building a ship from a Shanghai shipyard. It shows human capital costs consisting of direct labour and overhead of professional manpower and amounting to about 23%. This percentage cost is influenced by the labour cost advantage.

System Approach in Shipbuilding

Modern System Approach to Improve Indian Shipbuilding Productivity

India decidedly has a labour cost advantage, say vis-a-vis South Korea. In fact the Indian labour cost may only be one-fifth of Korean labour (see Figure 5). How it is then South Korea is a world leader in shipbuilding, with 70% of all ships built in South Korea being for export. This is possible because South Korea has quite high shipbuilding productivity so that the South Korean ships are cheaper, delivered faster with probably higher quality. To improve productivity of Indian shipbuilding, we need to study the break-up of shipbuilding processes in great depth. However, we are presenting here an outline discussion. Shipbuilding is an assembly industry consisting of two major streams.

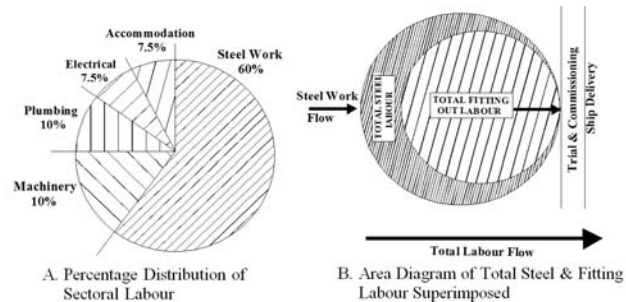


Fig. 5: Pie Diagram Shipbuilding Labour Distribution and Study

Source: MKGR.



1. A large steel fabrication work of the ship Hull, consisting about or more than 50% of the total labour cost;
2. An equally large and diversified fitting-out work of bought-out machineries and piping and other fitting-out constituting about or less than 50%.

About the steel work productivity we will deal separately in the next section. Then, let us see what the fitting out work comprise of:

1. Accommodation fitting out work
2. Machinery Fitting out
3. Piping Fitting out
4. Electrical Fitting out
5. Electronic Fitting out
6. Deck Machinery and Cargo Handling Fitting out
7. Painting, it being a large volume of work.

If the Hull steel work and the various other fitting work are represented in a Pie diagram, the comparative labour work ratios can be calculated of various sectors in Figure 5.

Congruent Shipbuilding

The different sectors of above shipbuilding operations occupy different time frames. To increase the productivity the operations should synchronize i.e. being carried out side by side at the same time, so that by the time the steel hull is ready, the fitting out work is also complete and a new ship is born. This process may also be named as Congruent Shipbuilding. By following these principles, the shipbuilding time might be brought down from 1 to 2 years to only a few months of the order of 4 to 6 months. Time compressed is cost or over-cost compressed, and the productivity increase by two folds or more. However, in India, a standard ship still takes 1 to 2 years to build and deliver.

Batch Line Shipbuilding

The principle of congruent shipbuilding of Figure 5 is implemented in the batch-line shipbuilding scheme in Figure 6. This batch line ship production scheme has been further compressed under cover ship factory kind of modern production technique.

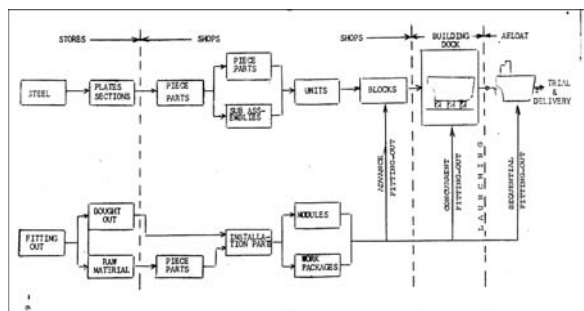


Fig. 6: Batch Line System of Ship Production

Technology for Shipbuilding

Induction of Technology to improve Indian Shipbuilding Steel Productivity.

Some of these technologies are directed to raise the quality and the productivity of steel fabrication.

Plate Preparation Shop

The first step in this direction is the establishment of steel plate preparation shop, where the steel plate is first shot-blasted and cleaned, and is immediately followed by spray painting. This ensures long life of the steel plate. In welded ship construction, plate edges need to be bevel-machined prior to V-groove welding. This edge preparation of plate is accomplished with an edge preparation milling machine.

Fast Fabrication

1. Even today the technical infrastructure including shop crange and fabrication work flow and layout are not always adequately upgraded and advanced, approaching the global standards of Japanese or South Korean shipyards.
2. There is need of high capacity digitized hydraulic Press for shaping plates quickly and accurately.
3. There shall be provided mechanically powered Jig and Fixtures which can move and rotate a large prefabricated steel unit so as to enable it to be welded in the downward position for all welding.
4. Additionally, it will help raise ship productivity, if one-side welding machines are provided so that large blocks of prefabricated steel blocks are not needed to be turned upside down to get it welded from both sides.

Machinery Fitting out Technologies: Application of 3D Printing Technologies

Conventionally, till the ship hull is fabricated, there is no platform on which the fittings can be built up. In the latest shipbuilding the problem is solved in two ways:

1. Even before the hull was completed, ship block (large ship part) was prefabricated on which the concerned fitting out parts which belonged to that part was erected. Thus fittings were progressed simultaneously with the progress of hull construction.
2. To assist the above progress, full scale mock up was built up from the two dimensional ship machinery fitting out drawings. This mock up technique was mostly adopted for the naval ships.
3. In more recent time, ship piping drawings were digitized in three dimensions and digitized data were fed as input to universal hydraulic pipe bending machine. The machine could give shape to full pipe with multiple bends from a single set of digital input.



Time has come to develop and employ 3D Printing technology to start the machinery fitting out much in advance; even before the ship hull construction has started. 3D Printing machine can build the machine unit and then all the piping models one by one. Individually each of them is a continuous unit and be replicated on the 3D Printer.

Design and Standardization for High Shipbuilding Productivity

Indian Techies are known all over the world for their design proficiency. Hence, design facilitating high production efficiency, a well-known strategy, should be pursued by the Indian shipyards with commendable benefits. Production-oriented design is effectively facilitated by practice of standardization of both Hull and Fitting out. Both efficient Production design and standardization can bring down cost and time of production substantially.

Economic Driver for Productivity

Favourable Economic Environment

If the economic environment is not favourable for the promotion of shipbuilding, it is apprehended that the competitive advantage of well-designed systems and modern technology will be neutralised. It is reported in the KPMG-FICCI study that the cost disadvantage of the current statutory burden and other old-fashioned trade practices may amount to as high as 30 per cent of the total manufacturing cost of ships. This is alarming and must not be allowed to ruin the nascent shipbuilding industry. It is known to all that the present statutory burden consists of multiple levies of Octoroi, CST, VAT and excise duty on shipyard and high corporate taxes compared to those of China and Vietnam. Added to the above overburden, the provision of various kinds of Bank guaranties and high Bank interests on sizable working capital requirements have been seriously weakening the competitiveness of Indian shipbuilding. Hopefully, the coming Goods and Service taxes (GST) will improve the situation considerably. The above FICCI Report recommends a comprehensive series of financial benefits, which are listed below:

- Direct subsidy against contract prices
- Provision of refund guaranties
- State funded or subsidized innovation, R&D to develop ship design, shipbuilding technology, or shipyard production expertise Project working capital finance on subsidized interest or interest-free loans, underwriting debt to reduce the commercial risk.

- Preferential tax schemes for shipowners or for shipyards.
- Exchange rate control for shipyards—this reduces one of the key risk factors.
- Incentives to ancillaries e.g. steel producers, main engine builders or equipment suppliers.

It is felt that at least some of these measures should be considered by the Government till the shipbuilding industry gains scale and volume compared to the international standard.

Modern Shipyards need High Investment

Encouraged by the recent growth momentum and improving national economic environment, Port Business companies, notably Adani Group and SKIL are believed to be in differing stages of developing shipyards. Shipping Lines too are eying at shipyards as lateral expansion. Apeejay Shipping, Mercator and Garware Offshore have entered market in alliance with leading players. Finally the heavy industry giant L & T and steel industry pioneer Tata Steel and also the other Steel Industry stalwart JSW exploring investments in shipbuilding. The overall investment prospects might exceed ₹ 20,000 crores within this decade or so.

Conclusion

High productivity is both a movement and engineering. It is both a technology and a culture. It requires as much of management input as technical application. Otherwise it is difficult to explain how the western shipbuilding nations like West Germany and England floundered in shipbuilding despite possessing technology, experience and long shipbuilding tradition in abundance, while high cost Japan still leads the world shipbuilding.

References

- [1] D & B Report (2008). Shipbuilding Overview.
- [2] DI-IBD Report (2013). Indian Shipbuilding Industry.
- [3] KPMG–FCCI Report (2008). Indian Shipbuilding Industry—poised for Take-off? Global Conference and Exposition on Shipbuilding.
- [4] Ghosh Roy, M.K. (1981). Productivity in Indian Shipyard.
- [5] Ghosh Roy, M.K. (1980). Modern Ship Production, Proceeding of Seminar Indian Shipbuilding 1980, Calcutta.
- [6] Ghosh Roy, M.K., A Survey of Shipbuilding and Shiprepair Industry, Chairman’s Address at the Seminar Indian Shipbuilding 1980, Calcutta.



Performance Analysis of a Solar Hydrogen Supported Hybrid Cold Storage

R.K. De¹ and A. Ganguly²

Abstract: In this paper, a scheme of a multi-commodity cold storage based on Lithium Bromide–water absorption system has been proposed. The cold storage is designed for storage of two commodities namely potato and olive for different months of a year for optimum utilization of the cold storage. A thermal model of the proposed cold storage system has been discussed and a computer program in MATLAB 8.0 has been developed based on the thermal model. The performance of the system has been analysed for representative days of different months of a climatic cycle for the storage of commodities under consideration. To make the system operational in rural areas where grid electricity may not be available on reliable basis round the clock, an outline for the power system based on solar photovoltaic thermal integrated with solar hydrogen hybrid system as backup has been proposed. The study reveals that the variation in the hourly daylong cooling load is found to be maximum during the month of March (about 29%) and minimum in the month of July (about 9%). Also, the cooling load of the cold storage is minimum in between July and September and maximum around October due to the significant effect of the product load.

Keywords: Cold Storage, Multi-Commodity, Photovoltaic, LiBr-Water Absorption.

Introduction

The loss of food grains is one of the greatest threats to food security worldwide, especially in the poor and developing nations. However; this is a global concern as roughly one-third of the edible parts of worldwide food production gets wasted, which amounts to about 1.3 billion tons of food wastage annually [1]. The post-harvest deterioration contributes towards a significant fraction of the total loss in food grains owing to poor storage facilities.

The issue of post harvest losses of food products is more significant in the developing countries like India, where agriculture represents a major part of the economy. The country has the distinction of producing almost all-tropical and exotic fruits and vegetables. However; due to the short shelf life of these crops and insufficient storage facility, as much as 30–35% of fruits and vegetables perish every year [2]. Over the past few years, the annual demand of a number of seasonal fruits, vegetables and flowers has increased rapidly. This emphasises upon the need for establishment of more number of cold storages in the nation. At present the country has 6156 number of cold storages [3] which are insufficient. The majority of them are dedicated for storage of a single commodity. This leads to insufficient utilization of the cold storage and thus there is loss in economy. So

development of large number of multi-commodity cold storage is the need of the hour as this sector is expected to grow at a compound annual growth rate of 16.09% by 2020 [3]. However, one of the major constraints in the establishment of cold storages in the rural areas is the availability of electricity on reliable basis. At present almost all the cold storages are powered through fossil fuel based energy sources which are responsible for environmental degradation. It may also be noted that the refrigeration devices alone consume about 15% of the worldwide electricity production [4]. So in this context, use of solar energy is a very promising option.

In the recent years, some research and development works have been reported in the field of cold storages, however cold storage systems supported by solar power are not commonly available [5]. In a very recent work, a conceptual design of a grid-interactive SPV/thermal-powered cold storage based on H₂O–LiBr absorption system for the storage of potatoes has been presented [1]. However, the cold storage was idle for about five months in a year which emphasises upon the need for development of multi-commodity cold storages.

A number of works have been reported on grid-interactive cold storage system supported with flat plate collectors.

¹Department of Mechanical Engineering, Indian Institute of Engineering Science and Technology, Shibpur, India.

²Department of Mechanical Engineering, OmDayal Group of Institutions, Uluberia, Howrah, India. ✉ aritra78@gmail.com



Some works are also found on combined SPV-PEM fuel cell systems for supplying electricity. However; no work is found at least in the open literature that proposes a standalone solar hydrogen system supported multi-commodity cold storage. This is the motivation behind the present work.

In this paper, a scheme of a multi-commodity cold storage based on LiBr-water absorption system has been proposed. The cold storage is designed for storage of potato and olive for different months of a year for optimum utilization of the cold storage. In India, potatoes are typically stored for a maximum span of seven months after the end of harvesting season in February [1] while; olives are stored for almost two months after the end of harvesting season in September [6]. The storage temperature of potato and olive are

4°C–12°C and 5°C–10°C [7] respectively. So in the present work, the cold storage temperature is assumed to be maintained at 8°C. It may be noted that, Potato is one of the most widely grown root-crops and consumed round the world, while; olive oil is widely used as cooking and salad oil. So both the products have considerable demand in the global market.

Scheme of the Proposed System

The schematic of the proposed system is shown in Figure 1. In the proposed system, water has been used as refrigerant while a solution of lithium bromide in water has been used as absorbent.

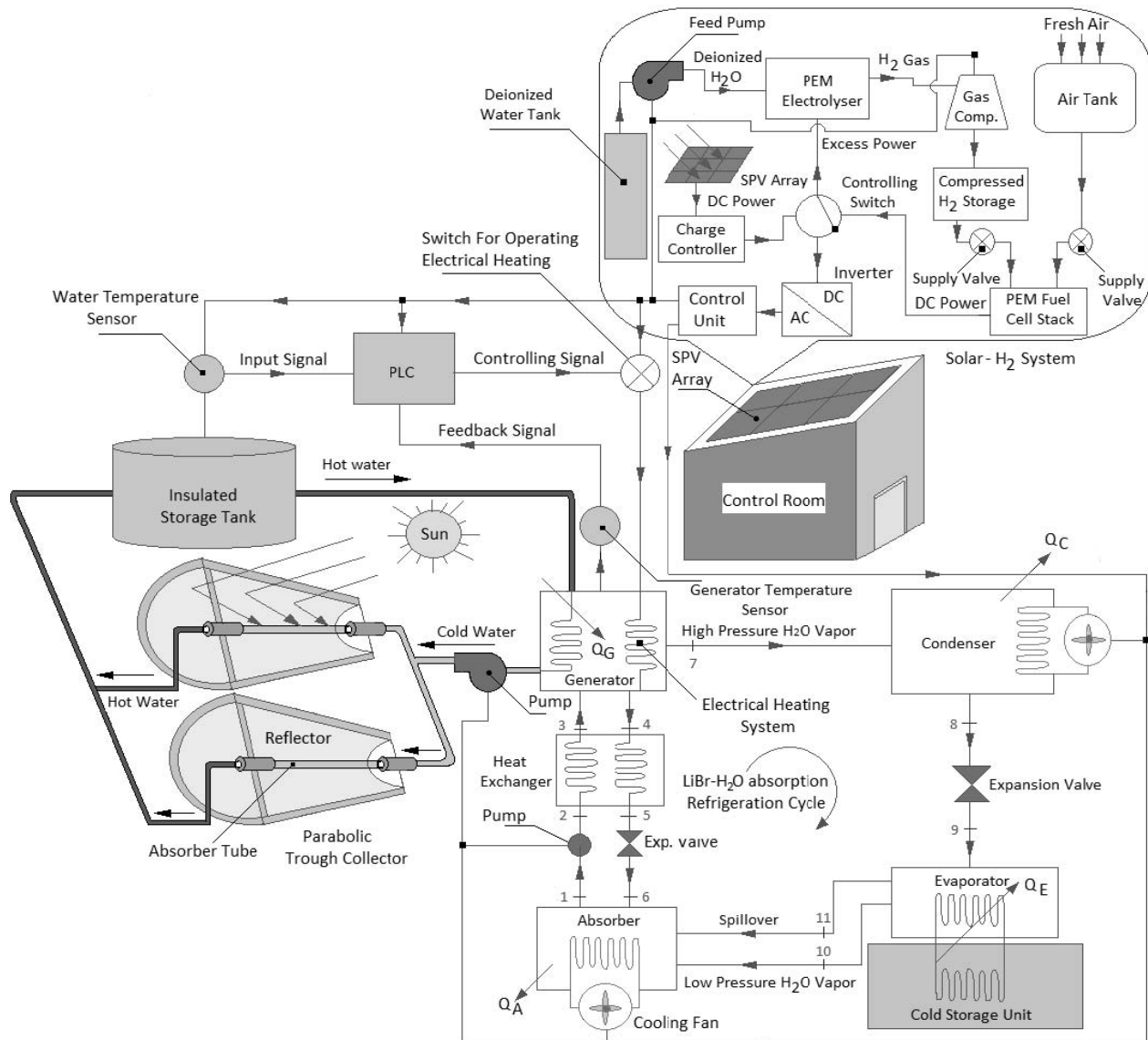


Fig. 1: Scheme of the Proposed Stand alone Multi-Commodity Cold Storage



The low pressure water vapour leaving the evaporator at state point 10 is readily absorbed in the absorber as it comes in contact with the weak solution of LiBr–H₂O. The absorber is cooled by using a cooling fan which releases the latent heat and maintain a constant temperature. The strong solution leaving the absorber at state point 1 is pumped to the generator where heat is supplied from an external source. The water vapour fraction goes off from the solution at high pressure at state point 7, while the remaining weak solution leaves the generator at state point 4 and returns back to the absorber through a pressure reducing valve. The water vapor at high pressure gets condensed to water in the condenser releasing the latent heat of condensation and a cooling fan is used. Thereafter, high pressure water expands through an expansion device from state point 8–9 to very low pressure and finally evaporates in the evaporator during the process 9–10 by taking the latent heat of evaporation from the cold storage unit. The mass flow rate of the refrigerant is adjusted such that the desired cold storage temperature is maintained. It is assumed that a small portion of the refrigerant leaves the evaporator as liquid spill–over at state point 11. An auxiliary heat exchanger has been provided to preheat the strong solution and to pre–cool the weak solution.

A parabolic trough collector based heating system has been used to track the solar energy for heating the water. The hot water, thus produced, is stored in an insulated storage tank and the same is re–circulated using a pump across the generator continuously to maintain a constant generator temperature of 90°C. An auxiliary electrical heating system has also been included for supplying heat to the working fluid in the generator if the hot water fails to meet the required temperature alone in the adverse weather conditions. For operating the electrical heating system an electronic control system consists of a Programmable Logic Controller (PLC), two temperature sensors and a controlling switch has been proposed (as shown in Figure 1).

To operate the cold storage in a stand–alone fashion, a solar photovoltaic array along with solar hydrogen based backup system has been used. An inverter has been used to convert the DC power generated by the solar photovoltaic array during the sunshine hours to AC power to meet the in–house requirements. After meeting the demand, the excess power is utilized to generate hydrogen gas in the electrolyser bank. The H₂ gas thus produced is compressed using a gas compressor which is supplied to the PEM fuel cell stack to produce electricity during the energy deficit hours on a sustainable basis.

Thermal Modeling

The thermal modeling of the cold storage includes the following:

Load Estimation of the Cold Storage

Total cooling load of the cold storage consist of several components such as: structural, ventilation, product, human occupancy and lighting load and can be given by:

$$\dot{Q}_{total} = \dot{Q}_{str} + \dot{Q}_{vent} + \dot{Q}_{prod} + \dot{Q}_{man} + \dot{Q}_{lighting} \quad \dots (1)$$

The structural load (\dot{Q}_{str}) can be estimated from the rate of heat gain through the building envelope which can be expressed as [1]:

$$\dot{Q}_{str} = \dot{Q}_{wall} + \dot{Q}_{roof} + \dot{Q}_{floor} + \dot{Q}_{door} \quad \dots (2)$$

The rate of heat gain through the exposed walls can be given by [1]:

$$\dot{Q}_{wall} = \frac{\Delta T}{R_{wall}} \quad \dots (3)$$

Where, ΔT is the effective temperature difference across the walls and R_{wall} represents combined thermal resistance and can be presented as [8]:

$$R_{wall} = \frac{1}{f_o} + \frac{1}{f_i} + \sum_{j=1}^n \frac{\Delta x}{k} \quad \dots (4)$$

The values heat transfer coefficients for outside and inside wall surfaces (f_o and f_i) and thermal conductivity of different materials (k) have been taken from literature [9].

The rate of heat gain through the roof and floor are estimated in a similar fashion.

The ventilation load due to infiltration of air can be expressed as:

$$\dot{Q}_{vent} = \dot{V}_{air} \rho_{air} C_p (T_{ambient} - T_{storage}) \quad \dots (5)$$

Where \dot{V}_{air} represents the volume flow rate of air which can be given by:

$$\dot{V}_{air} = \frac{[L \times B \times H] \times N}{24} \quad \dots (6)$$

Here, L B H are the dimension of the cold storage, while; N represents the number of air changes over 24 hours. The values are obtained from literature [1].

The product load comprises of load to bring the product to the storage temperature and load due to respiration (H_{resp}). It can be expressed as:

$$\dot{Q}_{prod} = \dot{m}_p c_p (T_{initial} - T_{store}) + H_{resp} \quad \dots (7)$$



Where \dot{m}_p denotes the time rate of loading of the product which can be given by:

$$\dot{m}_p = \frac{V_{eff} \rho_b}{\text{Loading Period}} \quad \dots (8)$$

Here ρ_b is the bulk density of the product and V_{eff} represents the effective storage volume. It is assumed that the potatoes and olives are stored at a uniform rate over the period of 50 days and 15 days respectively. The respiration load is the heat released by the product during breathing and the corresponding values are 0.018 mW/kg and 0.0645 mW/kg [7] for potato and olive respectively.

The human occupancy load due to metabolism may be given by [1]:

$$\dot{Q}_{man} = N_p \dot{Q}_{avg} \left[\frac{t}{24} \right] \quad \dots (9)$$

Here ' N_p ' represents the number of persons present in the cold storage for t hours in a day.

The heat added to the cold storage space by the electrical appliances ($\dot{Q}_{lighting}$) can be expressed as [9]:

$$\dot{Q}_{lighting} = 1.25 W_{total} \quad \dots (10) \quad \text{Where } W_{total} \text{ represents the total wattage of the electrical appliances.}$$

A safety factor of 10% is considered on the final value to encounter for the unpredicted leakages and inaccuracies [9]. Hence, the net cooling load or the evaporator load can be represented as:

$$\dot{Q}_E = 1.1 \dot{Q}_{total} \quad \dots (11)$$

Modeling of LiBr-Water Absorption Refrigeration System

Evaporator

The mass balance across the evaporator can be given by:

$$\dot{m}_9 = \dot{m}_{10} + \dot{m}_{11} \quad \dots (12)$$

The mass flow rate at state point 11 can be expressed as [10]:

$$\dot{m}_{11} = 0.025 \dot{m}_{10} \quad \dots (13)$$

The energy balance across the evaporator can be represented as:

$$\dot{Q}_E = \dot{m}_{10} h_{10} + \dot{m}_{11} h_{11} - \dot{m}_9 h_9 \quad \dots (14)$$

The enthalpy of refrigerant at state point 9 can be obtained as [10]:

$$h_9 = h_8 \quad \dots (15)$$

Absorber

The mass balance across the absorber can be given by [10]:

$$\dot{m}_1 = \dot{m}_{10} + \dot{m}_{11} + \dot{m}_6 \quad \dots (16)$$

and

$$x_1 \dot{m}_1 = x_6 \dot{m}_6 \quad \dots (17)$$

Where, x_1 and x_6 are the mass fractions of the solutions. The enthalpy of solution at state point 6 can be estimated from throttling model:

$$h_6 = h_5 \quad \dots (18)$$

The energy balance on the solution heat exchanger can be given by [10]:

$$\dot{m}_2 h_2 + \dot{m}_4 h_4 = \dot{m}_3 h_3 + \dot{m}_5 h_5 \quad \dots (19)$$

The enthalpy at state point 2 is determined from an isentropic pump model and can be given by:

$$\dot{W}_p = \frac{\dot{m}_1}{\eta_p} \int_{P_1}^{P_2} v dp = \dot{m}_1 (h_2 - h_1) \quad \dots (20)$$

Where, η_p denotes the efficiency of the pump. Finally, the energy balance across the absorber can be represented as:

$$\dot{Q}_A = \dot{m}_{10} h_{10} + \dot{m}_{11} h_{11} + \dot{m}_6 h_6 - \dot{m}_1 h_1 \quad \dots (21)$$

Generator

The generator load can be obtained from the energy balance:

$$\dot{Q}_G = \dot{m}_4 h_4 + \dot{m}_7 h_7 - \dot{m}_3 h_3 \quad \dots (22)$$

Condenser

The heat transfer in the condenser can be expressed as:

$$\dot{Q}_C = \dot{m}_7 (h_7 - h_8) \quad \dots (23)$$

Enthalpy at all the state points of absorption refrigeration system are estimated from curve fit [10].

Fan Power Estimation

The power consumed by the cooling fan can be estimated as [11]:

$$\dot{W}_F = \frac{\dot{V}_{air} \Delta P_{fan}}{\eta_{fan}} \quad \dots (24)$$

In Eq. (24), \dot{V}_{air} represents the volume flow rate of air across the fan and ΔP_{fan} denotes the pressure drop across the fan which can be expressed as [11]:

$$\Delta P_{fan} = 1.760 u_{max}^{1.6312} n \quad \dots (25)$$



The maximum cooling air velocity (u_{max}) is assumed to be 2.5 m/s [11] while; n represents the number of rows.

Finally, the COP of the system can be given by [1]:

$$COP = \frac{\dot{Q}_E}{\dot{Q}_G + \dot{W}_P + \dot{W}_F} \quad \dots (26)$$

Results and Discussions

A computer program in MATLAB 8.0 has been developed based on the thermal model discussed in the previous section. The program takes hourly values of climate data for the chosen location (Kolkata) [12] along with some other data related to the product to be stored and some design parameters of the proposed refrigeration system as inputs and estimates the cooling load, generator load, absorber load and the load on the condenser on an hourly basis. The program also calculates the hourly power consumed by the solution pump, cooling fan and the system COP. The performance of the proposed system has been analyzed for representative days in different months for the storage of potato and olive.

Figures 2 and 3 represents hourly variation of cooling load for potato and olive respectively for different months of their growing season. It is observed that the cooling load for both the products follows a trend similar to that of ambient temperature with time of the day. This is due to the fact that the product load, structural load and ventilation load being major contributors of the total cooling load vary directly with the ambient temperature and thus the total cooling load follows a similar trend. The cooling load is found to be minimum around 5:00 hours for all the months while; it is maximum in between 12:00 to 14:00 depending upon the respective months. The variation in the hourly values of cooling load (between maximum to minimum) is found to be about 9% (July) to 29% (March) owing to the higher fluctuation in ambient temperature in March.

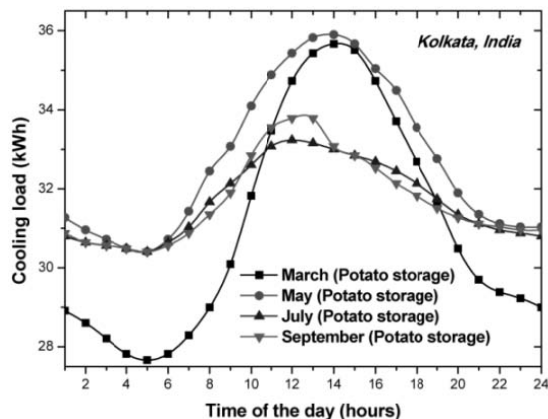


Fig. 2: Hourly Variation of Cooling Load for Potato

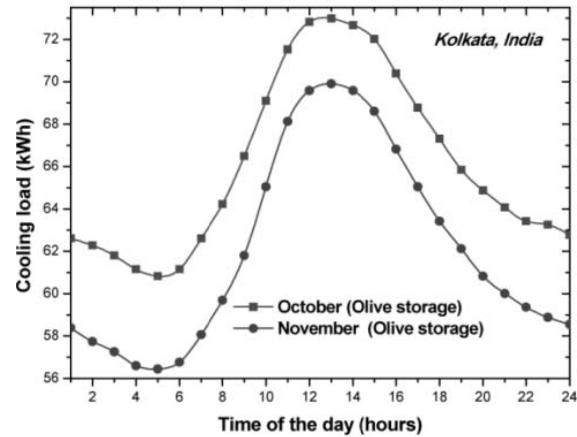


Fig. 3: Hourly Variation of Cooling Load for Olive

Figure 4 represents the daily average variation of cold storage loads for different months. It is observed that the daily average cooling load is minimum in between the month of July and September and it reaches at its peak around October with an increase of 120% owing to much higher product load for olive compared to potato. From the figure, it can also be noted that the generator and condenser load are following a trend similar to that of cooling load due to the proportional variation of them with cooling load.

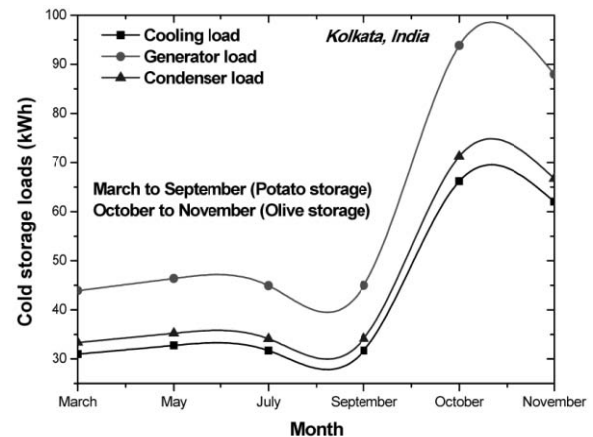


Fig. 4: Daily Average Variation of Cold Storage Loads for Different Months

Figure 5 represents the daily average variation of COP for different months of the proposed cold storage. It can be noted from the figure that the value of COP is minimum in between the month of July and September while; it is maximum around the month of October. The percentage change in the value of COP is very less throughout, however; this variation is quite satisfactory with the result obtained from literature [1]. The possible reason for this trend is due to the fact that variation of COP is a strong function of cooling load and it follows a similar trend with that.

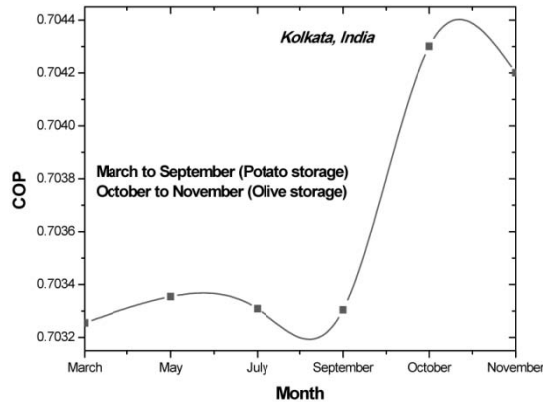


Fig. 5: Daily Average Variation of COP for Different Months

Conclusion

In this work, a scheme of a standalone, grid independent solar hydrogen system supported multi-commodity cold storage based on LiBr-water absorption system has been proposed for the storage of potato and olive for different months of a year and the performance of the proposed system has been analysed.

The following points have been revealed from the present study:

- The cooling load of the proposed cold storage is found to be minimum in between July and September while; it is maximum around October due to the significant effect of product load.
- The variation in hourly cooling load for a day is found to be maximum in the month of March (about 29%) while; the same is minimum in July (about 9%).
- It is found that any change in the cooling load results in a proportional variation in generator load and the load on condenser.
- The study presents an outline of a solar hydrogen supported standalone multi-commodity cold storage for operation in rural areas.

References

- [1] Basu, D.N. and Ganguly, A., Solar thermal-photovoltaic powered potato cold storage-Conceptual design and performance analyses. *Applied Energy*, **165**, 308-317 (2016).
- [2] Fruits and Vegetables Sector: An Overview, <http://www.dsir.gov.in/reports/ittp_tedo/agro/AF_Farm_Fruits_Vegetables_Intro.pdf> [accessed 27.08.2016].
- [3] Cold storage market in India 2015-2020 <<http://www.novonous.com/publications/cold-storage-market-india-2015-2020>> [accessed 27.08.2016].
- [4] Perier-Muzet, M., Bedecarrats, J.P., Stouffs, P. and Castaing-Lasvignottes, J., Design and dynamic behaviour of a cold storage system combined with a solar powered thermo-acoustic refrigerator. *Appl Therm Eng.*, **68**(1-2), 115-24 (2014).
- [5] Garg, H.P. and Prakash, J., *Solar energy: fundamentals and applications*. (Tata McGraw-Hill, New Delhi, 2013), p. 284.
- [6] Bhowmick, N., *Some lesser known minor fruit crops of northern parts of West Bengal, International Symposium on Pomegranate and Minor-including Mediterranean-Fruits* (2011) <http://www.actahort.org/books/890/890_4.htm> [accessed 27.08.2016]
- [7] ASHRAE Refrigeration Handbook (SI) (2002) <www.demec.ufpr.br> [accessed 6.06.15].
- [8] Chourasia, M.K. and Goswami, T.K., Efficient design, operation, maintenance and management of cold storage. *J Biol. Sci.*, 1(1), 70-93 (2009).
- [9] Arora, C.P., *Refrigeration and air conditioning*. 3rd ed., (McGraw-Hill Education, New Delhi India, 2012).
- [10] Florides, G.A., Kalogirou, S.A., Tassou, S.A. and Wrobel, L.C., Design and construction of a LiBr-water absorption machine, *Energy Conversion and Management*, **44**, 2483-2508 (2003).
- [11] Lin, P., Wang, R.Z. and Xia, Z.Z., Numerical investigation of a two-stage air-cooled absorption refrigeration system for solar cooling: cycle analysis and absorption cooling performances, *Renewable Energy*, **36**(5), 1401-1412 (2011).
- [12] RMC-weather information 2009 (Regional Meteorological Centre, Kolkata, India 2009).



Trimming Combustion by CO/CO₂ Measurement

Shaji Jose¹ and P. Sathees Chandra²

Abstract: The importance of proper combustion in the boiler is a topic that has been under discussion ever since the introduction of process control for the safe and efficient control of furnace. Combustion or burning is a high temperature exothermic chemical reaction between a fuel and an oxidant. Usually atmospheric oxygen acts as oxidant that reacts with various types of fuels to form a mixture of gaseous products termed as flue gas. The flame and heat produced in the process make the combustion self sustaining. Providing excess air is the usual methodology adopted by the operating engineers to ensure complete combustion and to minimize the harm that can come by way of incomplete combustion i.e., production of harmful/toxic gases in the in the flue mixture and sudden combustion in some localized area in the boiler and the consequent explosion that it can lead to. Though this is a safer method this cannot be adopted as a thumb rule as this reduces the boiler efficiency. Measurement of O₂ in the flue gases is done to have an eye on this. But recent researches have revealed that knowing the amount of CO/CO₂ present in the flue gases helps us to have a better idea of the burning of the fuel in the furnace. Measurement of CO/CO₂ is gaining momentum since these gases can be present in the flue gas only due to combustion. The developments in the field of analytical instrumentation have made it possible for us to measure the amount of CO & CO₂ present in the flue gases more accurately. Our work is aimed to throw more light in this area of optimizing the boiler combustion by the measurement of CO & CO₂ present in the flue gases and utilizing it to fine tune the control of excess air.

Keywords: Process Control, Boiler Efficiency, Optimization, Control of Excess Air.

Combustion

Chemistry of Combustion

Simple combustion involves the reaction of oxygen in the air with carbon and hydrogen in the fuel, to form carbon dioxide and water and produce heat. Under ideal conditions, the only gases in the exhaust flue are CO₂, water vapour and nitrogen from the combustion air. When O₂ appears in the flue exhaust, it usually means that more air (20.9% of which is O₂) was supplied than was needed for complete combustion to occur. Some O₂ is left over. In other words, the measurement of O₂ gas in the flue indicates that extra combustion air, or *Excess Air*, was supplied to the combustion reaction. When too little air is supplied to the burner, there is not enough oxygen to completely form CO₂ with all the carbon in the fuel. Instead, some oxygen combines with carbon to form carbon monoxide (CO). CO is a highly toxic gas associated with incomplete combustion and efforts must be made to minimize its formation. This effort goes hand-in-hand with improving fuel efficiency and reducing soot generation.

As a rule, the most efficient and cost-effective use of fuel takes place when the CO₂ concentration in the exhaust is

maximized. Theoretically, this occurs when there is just enough O₂ in the supplied air to react with all the carbon in the fuel supplied. This quantity of supplied air is often referred to as the *theoretical air*.

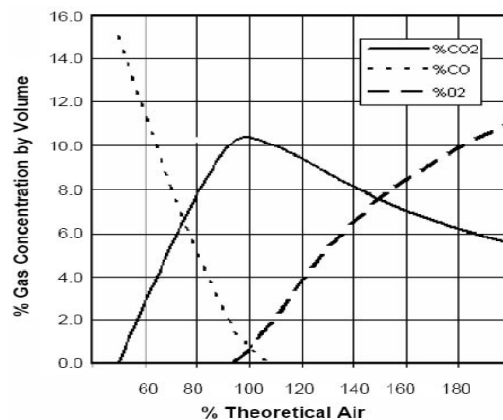


Fig. 1: Flue Gas Concentrations against Theoretical Combustion Air, %

The theoretical air required for the combustion reaction depends on fuel composition and the rate at which the fuel is

¹Chief Manager (Mechanical), Thermal Section-2, Neyveli Lignite Corporation Ltd., Tamilnadu, India. ✉shajejose@gmail.com

¹Chief Manager (C&I), Thermal Section-1, Neyveli Lignite Corporation Ltd., Tamilnadu, India. ✉satperooly@gmail.com



used (e.g. tons/hr, m³/sec etc.). In real-world combustion, factors such as the condition of the burner and the burner design also influence the amount of air that is needed. The theoretical air is rarely enough.

The general relationship between the O₂ supplied and the concentration of CO₂ and CO in the exhaust is illustrated in Figure 1. As the air level is increased and approaches 100% of the theoretical air, the concentration of CO molecules decreases rapidly as they pick up additional oxygen atoms and form CO₂. Still more combustion air and CO₂ reaches a maximum value. After that, air begins to dilute the exhaust gases, causing the CO₂ concentration to drop. The maximum value of CO₂ is dependent on the type of fuel used.

Combustion Analysis

Combustion analysis is part of a process intended to improve fuel economy, reduce undesirable exhaust emissions and improve the safety of fuel burning equipment. Combustion analysis begins with the measurement of flue gas concentrations and gas temperature, and may include the measurement of draft pressure and soot level. To measure gas concentration, a probe is inserted into the exhaust flue and a gas sample drawn out. Exhaust gas temperature is measured using a thermocouple positioned to measure the highest exhaust gas temperature. Soot is measured from a gas sample drawn off the exhaust flue. Draft is the differential pressure between the inside and outside of the exhaust flue. Once these measurements are made, the data is interpreted using calculated combustion parameters such as combustion efficiency and excess air.

Combustion Efficiency Calculation

Combustion efficiency is expressed as a percent and determined by subtracting individual stack heat losses, as percents of the fuel's heating value, from the total heating value of the fuel (100%). Dry gas loss and latent heat loss due to H₂ in the fuel are typically the largest sources of stack loss. Others can be included, such as heat loss from moisture in the air and fuel and losses from the formation of CO rather than CO₂. This basic form for calculating efficiency is described in the ASME Power test code 4.1 and is applicable for losses other than flue losses when determining total system efficiency by the Heat-Loss method.

% Net Combustion Efficiency

$$= 100 - \left(\frac{\text{Flue heat losses/kg fuel}}{\text{Fuel heating value/kg fuel}} \right) \times 100$$

Flue heat losses = $L_g + L_h + L_m + L_{co}$

where,

L_g = heat loss due to dry gas

L_h = heat loss due to moisture from burning hydrogen

L_m = heat loss due to moisture in fuel

L_{co} = heat loss from the formation of CO.

Heat Loss Due from the Formation of Carbon Monoxide (L_{co})

Carbon in the fuel reacts with oxygen to form CO first, then CO₂, generate a total of 33,800 KJ of heat per Kg of carbon. If the reaction stops at CO because of insufficient O₂ or poor mixing of fuel and air only 10,100 KJ is released and 23,700 KJ of energy is lost, which is quite a big loss and is to be minimised.

$$L_{CO} = \left(\frac{\% \text{ CO}}{\% \text{ CO}_2 + \% \text{ CO}} \right) \times 23,700 \times C_b$$

where C_b = fractional carbon content.

Excess Air

Insufficient combustion air causes a reduction in fuel efficiency, creates highly toxic carbon monoxide gas and produces soot. To ensure there is enough oxygen to completely react with the fuel, extra combustion air is usually supplied. This extra air, called "Excess Air", is expressed as the percent air above the amount theoretically needed for complete combustion. In real-world combustion, the excess air required for gaseous fuels is typically about 15%. Significantly more may be needed for liquid and solid fuels. A good estimate of excess air can be determined using the following formula. This calculation uses the oxygen concentration measured in the exhaust. If the CO concentration is very high, it may also be included in the excess air calculation,

$$\% \text{ Excess Air} = \left(\frac{\% \text{ O}_2 \text{ measured}}{20.9 - \% \text{ O}_2 \text{ measured}} \right) \times 100$$

Although required, higher excess air comes with a price—it wastes fuel. There are a number of reasons why this occurs but, stated simply, supply air cools the combustion system by absorbing heat and transporting it out the exhaust flue. The more air, the more the cooling. Consider, too, that nitrogen, which makes up about eighty percent of the air, plays no role chemically to produce heat. It does, however, add significantly to the weight of gas that absorbs heat energy. Figure 2 illustrates how increasing excess reduces combustion efficiency.

Using too much excess air is one of the principal causes of poor fuel economy. For this reason, optimizing excess air usage can be one of the simplest ways to achieve significant fuel savings. Adding additional excess air is often done to reduce the CO concentration. Too much excess air can actually have the reverse effect of increasing CO. This



results when fuel and air no longer mix properly in the burner, reducing the time of contact between oxygen and fuel and inhibiting a complete reaction.

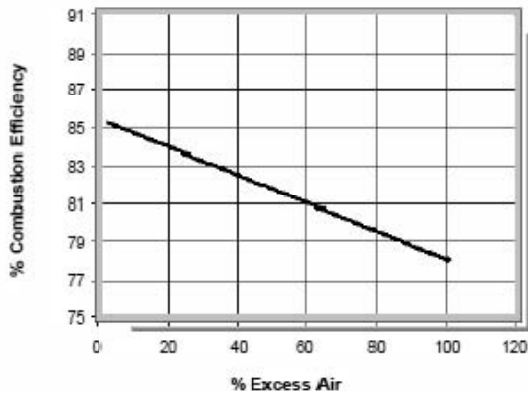


Fig. 2: Combustion Efficiency against Excess Air (fuel oil), %

Study of Flue Gas

Emission Rate Calculations using Dry Gas Factors

The emission rate calculation presented below uses the dry gas factor F_d . Dry factors are incorporated into the values are shown in Table 1. The table values (E_r), convert the measured concentrations of emission gases CO, NO_x, and SO₂ from ppm to kg/KJ of fuel.

$$E = E_g \times E_r \times \left(\frac{20.9}{20.9 - O_2 \text{ measured}} \right)$$

where, E = Emission rate, kg/ KJ of fuel
 E_g = Gas concentration, ppm
 E_r = Emission rate conversion from the table below
 O_2 measured = Oxygen concentration in the flue gas.

Calculating the Carbon Dioxide Concentration

Carbon dioxide (CO₂) forms when carbon in the fuel combines with O₂ in the combustion air. When there is just enough O₂ supplied to react with the carbon in the fuel, the CO₂ concentration in the stack exhaust is at its highest level. This is generally at or close to the ideal operating condition for the heat generating equipment.

The maximum possible CO₂ exhaust concentration depends ultimately on the carbon content of the fuel being burned. This number, the CO₂ maximum, appears often in combustion calculations, such as the one below for determining the percent of CO₂ in the exhaust.

% CO₂ by Volume

$$= CO_2 \text{ (maximum)} \times \left(\frac{20.9 - O_2 \text{ measured}}{20.9} \right)$$

Analysis & Tuning-up

Gas analysers are essential tools to monitor the emission gases and to maintain high efficiency. The total efficiency is an ideal combination of combustion efficiency, minimum environmental pollution and a safe working atmosphere.

Combustion analyzers can determine the amount of excess air in combustion by measuring the contents of flue gases. It is recommended that such an investment for boiler systems with annual fuel costs above ₹ 30 Lakhs is worthy & cost effective. Equipment that measures oxygen is more precise than carbon dioxide measuring devices. The other crucial measurement is CO measured in ppm (parts per million).

Information from the combustion analysis equipment is used to calibrate the settings on the air and fuel supply systems for the combustion process. In modern boilers, excess air should achieve approximately 10% (2.2% oxygen). This will vary from boiler/burner to boiler/burner and from application to application.

Using an Electronic Combustion Analyzer

- After the checking the combustion analyzer calibration, connect the gas sampling probe to the instrument.
- Insert the gas sampling probe into the flue.
- Be sure the gas sampling pump is ON and all temperature probes are attached. The electronic analyzer is now ready for use to tune the system to optimize combustion efficiency and to monitor any emission gases for which the appropriate sensor is installed.
- Combustion analysis should be performed on a warmed up unit at firing rates typical of normal operation.
- The burner control system to be put in manual mode and test several firing rates for combustion efficiency and emission gas concentrations.
- Observe the values on the combustion analyzer. If the percentage of O₂ in the stack is at the lower end of the expected minimum values (as specified by equipment manufacturer) and the CO emissions are low with no smoke being generated, the burner is probably tuned at or near optimum efficiency at this firing rate.

Table 1: Emission Rate Conversion Table

E_r	Nat.gas	Propane	Oil #1	Oil #2	Coal	Wood	Bagasse	Coke
SO ₂	0.003242	0.003242	0.003421	0.003421	0.003667	0.003421	0.003578	0.003734
No _x	0.002325	0.002325	0.002460	0.002460	0.002638	0.002460	0.002236	0.002638
CO	0.001409	0.001409	0.001498	0.001498	0.001610	0.001498	0.001498	0.001610



- It is good to have a CO reading of less than 250 ppm in the flue gas (although some analysts say that a reading less than 400 ppm is sufficient).
- Observe the O₂ level on the combustion analyzer at these settings.
- Compare the measured value of oxygen at this burner setting to the minimum value of excess oxygen recommended by the local authority.
- When an adjustment has been completed, verify the new adjustment has not had an adverse effect on the other firing rates that have already been adjusted.

Controls in Thermal Power Plants

Boiler Master

This is basically a pressure controller which regulates the Throttle pressure to a fixed set point and provides the demand signal to the Fuel Master.

Fuel Master

This provides the fuel flow input to the boiler by (i) Summing up the feeder speed signals and by multiplying it with the bed thickness of the fuel and also its bulk density index to form the total coal flow signals or by (ii) Gravimetric measurement system which lets us know the actual weight of the coal/fuel flow into the boiler.

Air Master

This decides the total airflow for the boiler (sum of Secondary air, Tertiary air or Hot air, Hopper air, Oil airflow etc.) as a function of the total Fuel flow. For any required change in load, firstly the change is implemented in the Airflow and only after getting the feedback for the altered in airflow, the change is applied to the fuel flow. This is very significant especially when, we have to increase the fuel flow. An Air Master Controller is shown in Figure 3.

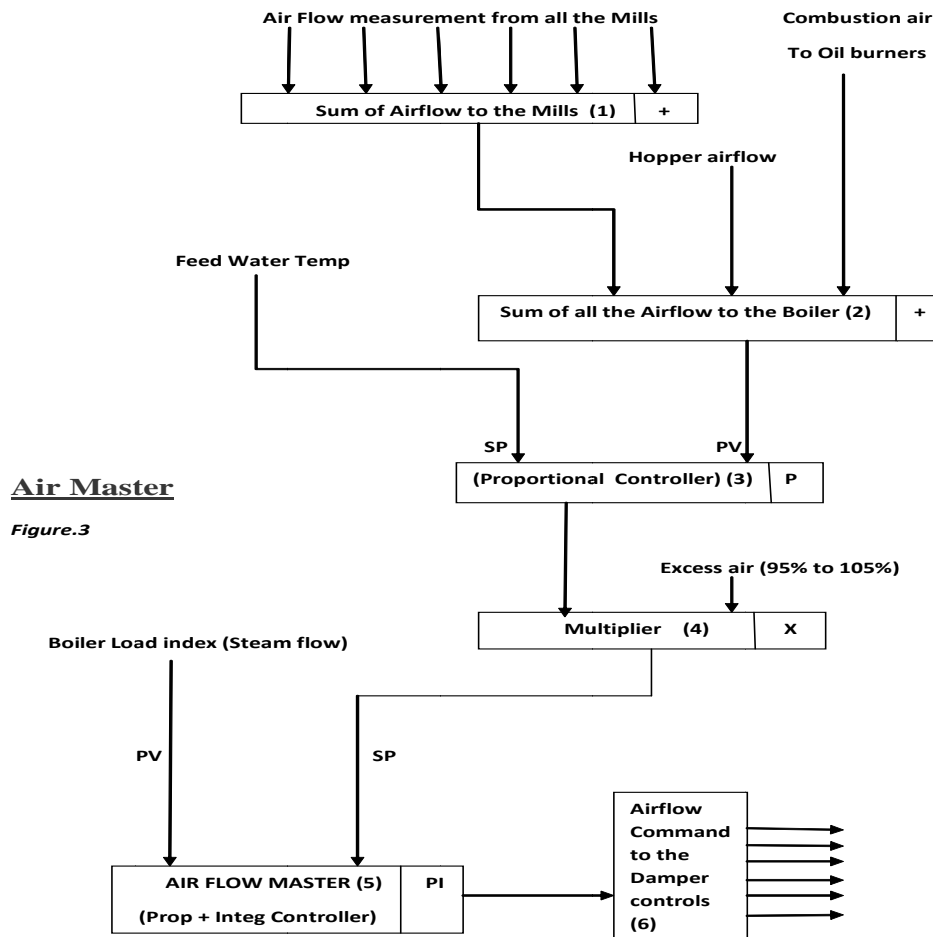


Fig. 3: Air Master Controller

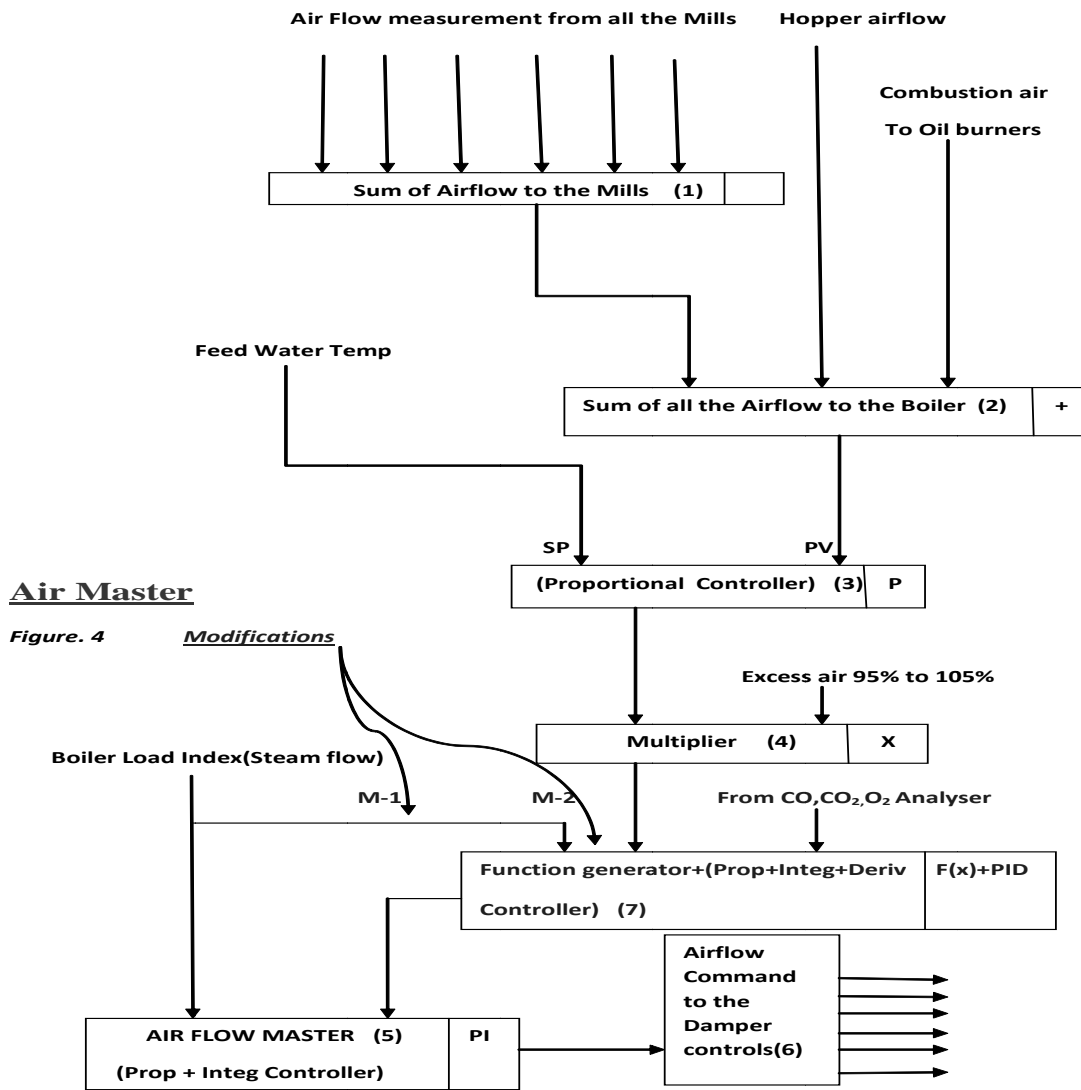


Fig. 4: Air Master Controller (Modified)

The total air flow is calculated as the sum of Secondary air , Hot air or Tertiary air, Hopper air by the Summation block (1) and the Combustion air of oil burners (if they are in service) by the Summation block (2). It is given a correction by the Feed water temperature at the Proportional Controller (3). This value is multiplied by a factor between 95% and 105% (set manually) in the Multiplier block (4) by which it can decide the amount of excess air that can be admitted to the boiler. This is then compared with the Boiler Load index (live Steam flow) before it goes as the Set point for the Airflow Master–Proportional Integral Controller (5).

The output of this Controller goes as the command signal to the Air damper controls (6) which controls all the Secondary air, Hot air or Tertiary air and the Hopper air dampers-and

regulates the air flow to the boiler. This is the normal circuit. The modification in the Master Controller is indicated in Figure 4 by M-1 and M-2.

Here,

M-1: Steam flow is taken into consideration. A new “Function generator + PID Controller” (7) is introduced into the circuit. The amount of excess air needed is a function of Boiler load and this is built in the Function generator.

M-2: The output of the Flue gas analyser (amount of CO, CO₂ & O₂ present) goes to Controller (7) and which is a PID Controller (7) now. The output of Controller (7) goes to Air Master Controller (5).



Salient Points

- The amount of excess air needed is a function of Boiler load (%excess air is lower @ higher loads and higher @lower loads) is taken care of by the Function generator F(x)-(M-1)
- Variation in the flue gas chemistry is given immediate attention, as it is an input going directly to the Airflow Master and Derivative (D) is also added to the normal Proportional Integral (PI) Controller (7) for quick action. Its weightage to be decided during the tuning of the Controller-(M-2)
- Combustion analysers which can measure CO, CO₂ & O₂ with a single probe are available in the market. They are available at various temperature ratings from 200°C to 1000°C.
- Up to 4 probes can be connected to as single processing/ computing unit and this proves to be economical.
- Two/four probes kept @ the Economiser outlet should give more accurate reading because; the exit gases will be thoroughly mixed and homogeneous here. A feed-

back from here directly to Air Master (refer 3.3.2 M-2) will lessen the time required to get close to the minimum “excess-air flow”.

Conclusion

These measures should greatly help to reduce the excess air by around 0.5% to 1.50%. It may take much time and many attempts to tune the Controllers to get the required Boiler performance. But it is worth it.

Bigger the Boiler, greater will be the savings.

References

- [1] Swagelok Energy advisors Inc. Steam Systems Best Practises Document No. 4 (1–2).
- [2] TSI Inc. Combustion analysis Basics (7–30).
- [3] India Boiler dot com. Improving performance (87–92).
- [4] Hartmann & Braun. Contronic Control Systems.
- [5] Testo India Pvt. Ltd. Gas analysers.



Experimental Investigation on a 660 MW Supercritical Boiler with MOIS Technology

Anuj Tomar^{*1} and Vinod Kumar¹

Abstract: Experimental studies were carried out on a 660 MW supercritical boiler that was ignited by the technology of mini-oil ignition. The variation of steam temperature and pressure, wall temperature of heat exchange surfaces and combustion status were monitored. Test results demonstrated that the pulverized coal is able to be combusted fully and stably in the less-oil ignition combustor, and the wall temperature of the combustor remains less than 300°C. It was also shown that the wall temperature of heat exchange surfaces is also not overheated, which expands uniformly, and the rising rate of the steam temperature and pressure satisfies the requirement of operation design. In addition, compared to the cases using conventional ignition techniques, the economical benefit by employing the technology of mini-oil ignition is pronounced.

Keywords: Supercritical Boilers, Micro Oil Gun Ignition Technology, Economic Feasibility.

Introduction

Oil-saving ignition technology has been extensively studied due to the large consumption of oil during boiler start-up and pulverized coal combustion stabilization with the conventional coal burning method. In a conventional pulverized coal combustion boiler, oil which is delivered by the Oil-Gun (OG) is primarily used to pre-heat the furnace. When the radiation from the flame and heat exchange surfaces can give the coal particle sufficient energy, then coal is fed by primary air and burned with secondary air, so stable combustion is sustained in the boiler. Meanwhile, during burning of low-quality coal or at the reduction of boilers capacity, it is also necessary to introduce additional thermal energy such as oil into the system to support stable combustion. Therefore, many of the liquid fuel are consumed in these above processes.

In order to achieve certain savings of liquid fuel, a great number of efforts have been made to investigate and develop the technology of oil-saving ignition, i.e. plasma-aided ignition technology, high-temperature air ignition technology, laser-heated ignition technology and induction-heating ignition technology. Note that all the four above-mentioned technologies are free from utilization of oil in assisting the ignition. However, some shortcomings for oil-free technologies, when facing the engineering applications, are found, such as too high operating costs, frequent

maintenance during operation and lack of system stability. Recently, a Mini-Oil Ignition Technology (MOIS) has been proposed, which have the advantages of low operating costs, high oil-saving rates, maintenance-free and good performance in stability.

Present Scenario

- India depends on Gulf countries for 70% of its oil needs.
- At 23% of total energy supply, Petroleum is India's second largest source, half the market share of coal. Boosted by fallen crude prices, India is expected to overtake Japan to become the world's 3rd largest oil consumer, at about 4.1 million b/d. India is now where China was a decade ago, and oil consumption is strongly linked to economic growth.
- Stringent environment norms.
- Weakening of INR vis-à-vis foreign currencies.
- Tariff-based bidding in Indian power sector.
- High cost involved for secondary fuel.
- Pollution issues and other disadvantages (like fire prone etc.) of using the oil.

Supercritical Boilers

“Supercritical” is a thermodynamic expression describing the state of a substance where there is no clear distinction

¹Sasan Power Ltd. Singrauli, Madhya Pradesh, India. ✉ *anuj.tomar@relianceada.com



between the liquid and the gaseous phase (i.e. they are a homogenous fluid). Water reaches this state at a pressure above 225 Kg/cm². The comparative statement between supercritical and sub critical boilers are shown in Figure 1.

The critical pressure and temperature for water are

- Pressure = 225.56 Kg/cm²
- Temperature = 374.15°C

Comparison	Subcritical (Drum+Forced Circulation)	Supercritical (Once-Through)
Main Steam Press	16MPa (Typical)	24MPa (Typical)
System Schematics		
Pressure Parts Material	Base	Higher, due to the Higher Steam Condition
Plant Heat Rate	Base	Better, amount of spray does not impact plant heat rate.
Load Change Rate	Base	Better, due to the Quicker Response Than Drum Type
Environmental Impact	Base	Better, due to the Better Plant Eff.

Fig. 1: Sub-Critical and Super Critical Boiler Comparison

Micro Oil Ignition Technology

Mini oil ignition system is the perfect combination of micro oil ignition and combustion technology at very low load operation, it can greatly reduce the combustion support oil in a thermal power plant, it also reduce the cost of power generation. MOIS have the advantages of low operating costs, high oil-saving rates, maintenance-free and good performance in stability. Schematic diagram of firing system is shown in Figure 2.

Mini oil ignition system is set up pulverized coal concentrating device in a specially designed micro oil burner. The system uses ring concentration technology to increase the coal concentration of pulverized coal, and form dense or dilute coal. With pulverized coal air flow conveying, dense coal is heated in the first combustion chamber by micro oil gun (because it use trace amounts of fuel combustion to produce a high temp flame). The pulverized coal breaks out volatile matter and quickly flame. The burning coal mix and ignite dense phase pulverized coal in the secondary combustion chamber. In this way the micro oil ignition system works to burn all coal. The Mini-oil

Ignition technology is the application of Enhanced Oil Firing Technology which uses small quantity of fuel oil, high compressed air for atomization and gasification of oil releasing sufficient high heat flame (1600~1800 deg C). The pulverized coal passes through specially designed coal burner, the high heat oil flame and absorbs the heat (staged Combustion), releases volatile matter and quickly burns. The wall temperature of the oil combustor will increased rapidly and due to its heat absorbing and storing property of the material, rapid gasification of oil takes place and accelerates oil firing and produce high temperature oil flame.

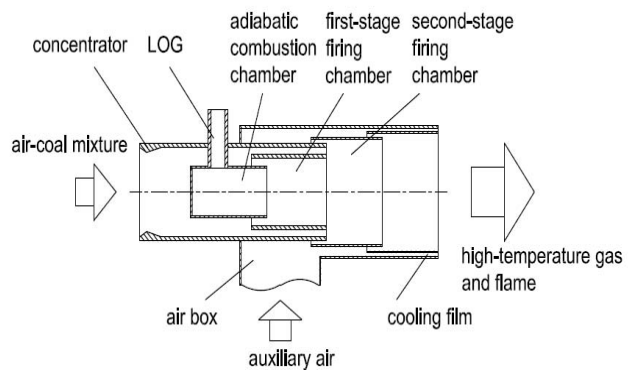


Fig. 2: Schematic Diagram of the LOB



Fig. 3: Oil Burner Internal View

When the ignition state is normal, the micro oil burners can be used as the main original burner. With film cooling technology, micro oil ignition system could prevent primary air pipe and burner (Figure 3) to burn out.

Micro oil gun is installed at each corner coal layer of Mill-A. When PA temp reaches around 100–150 deg C mill can be taken in service.

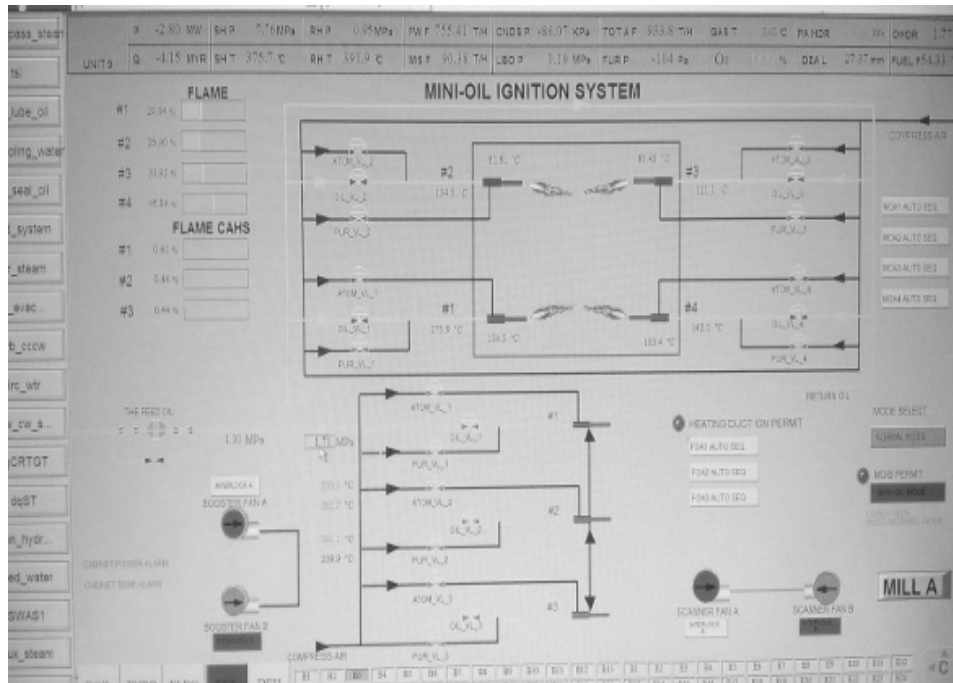


Fig. 4: MOIS Graphics

At present said technology is implemented by APL in India. Normal Oil gun capacity is 2-4 KL /hrs where micro oil gun capacity is only 0.3 KL to 0.4 KL/hrs.

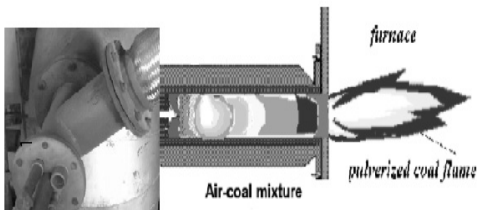


Fig. 5: MOIS Flame

This technology can be used with following options:

1. Micro oil gun with normal oil guns:
2. We can use the micro oil gun in

Coal burners at one elevation or we may go for two coal elevations.

DE	Normal Oil guns
C	Normal coal burners
BC	Normal Oil guns
B	Normal coal burners
AB	Normal oil guns
A	Micro oil gun burner

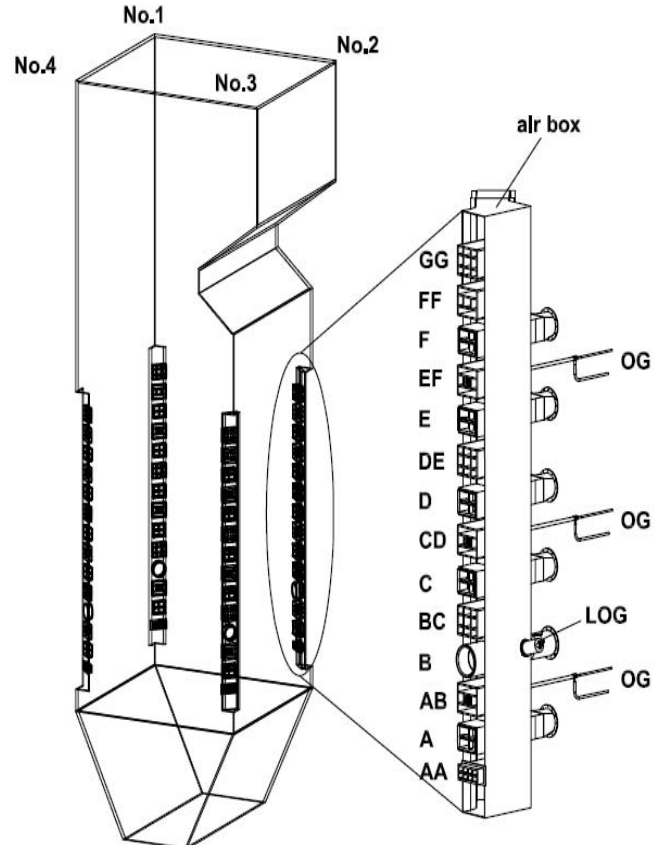


Fig. 6: Boiler Wind Box and Elevations



Mini Oil Ignition System Components

MOIS (Figures 4 and 5)) is made up of oil burning chamber, pulverized coal concentration device, first level coal combustion chamber and second level coal combustion chamber.

- Replacement of existing coal burner to newly designed coal burner. (at selected location)
- Replacement of existing coal burner elbow with newly designed elbow with arrangement to install the Mini Oil Gun.
- Combustion Support air from cold PA header for mini oil guns.
- Flame fan for cooling of flame cameras installed inside wind box. (Figure 6)
- PA Heating Guns (3 Nos) installed in Hot PA Header.
- Booster fans for combustion support air from cold PA header for PA heating guns.
- Service Air for LDO Atomization.
- LDO supply and return line.
- Instruments and control supply.
- Cables, cabinet and DCS.
- Software (Logics and alarms).

The burner nozzle is shown in Figure 7 and coal pipe bend with mini oil gun pipe in Figure 8.

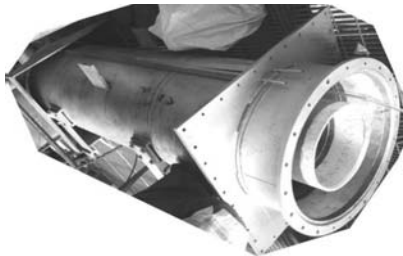


Fig. 7: Burner Nozzle



Fig. 8: Coal Pipe Bend with Mini Oil Gun Pipe

Typical Startup Procedure

Here take a 660 MW unit as an example:

Prepare for unit startup—Start PA fan—Warm the mill air by using Micro oil gun/steam heater in PA duct—Start boiler

micro oil gun—Start first mill—Start coal feeder—Ensure combustion inside furnace—Start second mill—Start third mill—Minimum stable load without oil support—Stop Micro oil gun—Start other mills—Full Load

- Open the SADC of the Mill-A coal burner to ensure coal burner cooling and control the temperature < 500°C
- Start PA Heating system by starting the PA duct mini oil guns one by one.
- Mill-A outlet temperature @ 60 to 70°C start Mill-A, start coal feeder—A and observe the coal flame appearance from the flame camera. (Coal flame should be established within 180 sec).
- Control the PA inlet temperature to Mill-A with coal air damper and number of guns in service.
- Estimation of initial coal feed rate:

$$\frac{2500 \times 10500 \times 4}{4200 \times 1000} = 25 \text{ tph}$$

The actual flame inside the boiler is shown in Figure 9 and a MOIS local panel is shown in Figure 10.

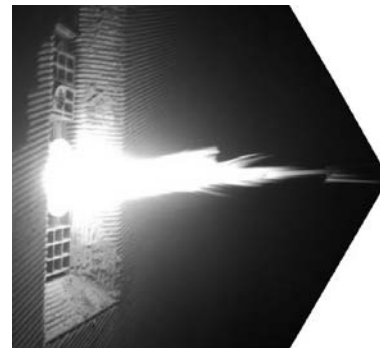


Fig. 9: Actual Flame Photo (inside boiler)



Fig. 10: MOIS Local Panel



Economic Benefits

Installing Micro oil gun ignition system, the following saving can be achieved based on APL experience:

No	Description	With Normal Oil Gun Ignition	After Micro Oil Gun System Implementation
1.	Unit cold startup	120 Kl	25–30 Kl
2.	Warm startup	85 Kl	18–21 Kl
3.	Hot start up	65 Kl	15–16 Kl

*As per above table we can save approx 95 KL HSD in Cold start up, 67 KL in warm start up and 50–60 KL in Hot start up:

$$\text{Cost of 95 KL HSD @ ₹ 56000/Kl} = 95 \times 56000 = ₹ 5320000/-$$

$$\text{Cost of 67 KL HSD @ ₹ 56000/Kl} = 67 \times 56000 = ₹ 3752000/-$$

$$\text{Cost of 50 KL HSD @ ₹ 56000/Kl} = 50 \times 56000 = ₹ 2800000.$$

Cost of installation of MOIS is approx- ₹ 4 crore in one unit, So we can pay back of installation cost of micro oil gun system after 8 cold start up or 10–11 warm start up or 14–15 hot start up's.

Estimated Value for installation of Micro oil gun system in three Units.

Application Feasibility

- Implementation and application need shutdown of unit and modification and replacement in coal pipe and bends.

- Case Study Implemented at 2 locations in India.
- Our Oil gun capacity is 2 KL /hrs. where micro oil gun capacity is only 0.3 KL to 0.4 KL/hrs.

Venders

- The Yantai Longyuan Power Technology Co. CHINA.
- SEC China.
- XCC China.

Conclusion

- Minimum 5–6 month required for manufacturing, supply, shipment process and erection at site.
- Present cost of installation of MOIS is approx - Rs. 4 Cr in one unit.
- In present scenario, MOIS installation can be done in any unit during overhaul.
- MOIS is already implemented at various large size boilers in China and other foreign countries. It has a good future in Indian power industry.

References

[1] Experimental investigation on a 600 MWe supercritical boiler with the technology of less-oil ignition by Mr. Sun, Chi, Zhu and Wang.

[2] Nie, X., Zhou, Z.J., Lu, M., *et al.* "Experimental study on pulverized coal flow ignition and flameout in high temperature air," Proceedings of the CSEE, 2008.

[3] All the figures (1–10) are of installation done in India.



Design and Kinematic Simulations of 3-PRS Spatial Parallel Mechanism

R. Sai Kiran Kumar^{*1} and J. Srinivas¹

Abstract: *The present work focuses on kinematics studies and design of a 3-PRS parallel mechanism and its control. Towards the development of a hybrid milling machine with 5-axis where the spindle is fixed to a portal frame, while the work piece is manipulated by x-y platform, a 3-PRS mechanism is designed. Forward and inverse kinematics and dynamics are studied and workspace, Jacobian analysis are conducted to know the workable operating region of the mechanism. In this mechanism each prismatic joint is driven by a separate stepper motor as per the requirements for the trajectory tracking. The virtual simulations are carried out in multibody simulations tool ADAMS and the control programs are developed in MATLAB/Simulink. For achieving greater precision, the revolute joints are replaced by compliant links with narrow sections and the force control requirements at the moving platform are achieved by a suitable control means.*

Keywords: Parallel Manipulator, Constrained Motion, Kinematic Characteristics, Trajectory Tracking.

Introduction

Parallel mechanisms are studied widely over the past one decade due to their several advantages such as high speed and large payload capacity. In their architecture, the moving platform is actuated by a set of legs connected to the base platform.

Parallel mechanisms have become popular in several mechatronics and automation applications due to their high stiffness, large payload ability and good precision. Parallel mechanisms have two platforms connected by expandable legs. Metrological, medical and communication fields require new mechanisms capable of achieving ultra-precision accuracy.

Mechatronics applications in such parallel mechanisms could lead to more realistic products such as welding and machining platforms. Several parallel mechanisms have been studied extensively by numerous scientists. The basic parallel mechanism is a 6 DOF Stewart and Gough platform. Due to its complexity in kinematics and dynamics solutions various configurations have been proposed in literature. There are other types of parallel mechanisms having only 3 DOF and can be used effectively in several applications. One of the famous 3 DOF mechanism is 3-PRS which has been studied for a long time since the year 2000. The axis-symmetric arrangement of 3-PRS causes a kind of precision solutions during its operation.

Literature Review

The 3-PRS parallel manipulator has different methods on arrangement of actuators with adjustable angle layout. The variation of kinematics in terms of workspace and dexterity with different actuator arrangements along with forward, inverse and velocity kinematics problems are often problems of interest here [1]. Parasitic motion occurring in the constrained DOF of a 3-PRS parallel mechanism is key issues affecting its applications. The 3-PRS is classified into seven subcategories based on geometrical arrangements of limbs. Then parasitic motion of each subcategory is discussed in detail in [2]. Under the assumption of small displacements, the solid body kinematics of the 3-PRS has been studied. Analysis of forward and inverse kinematics and calculating the rotations that the revolute and spherical flexure joints must perform were discussed. After defining some design requirements, the necessary displacements to fulfill, a design process based on calculations has been established in [3]. The change in the reachable workspace of a 3-PRS parallel manipulator with variable actuator layout angle was studied. Workspace of a parallel manipulator is the important aspect to reflect its working capacity and it is necessary to analyze the shape and volume of the workspace for enhancing the applications of parallel manipulator [4].

The Analytic Hierarchy Process (AHP), being an uncomplicated Fuzzy logic technique but an authoritative decision-

¹Department of Mechanical Engineering, NIT, Rourkela-769008, India. ✉srim07@yahoo.co.in



making tool that has been applied to solve different manufacturing problems. The AHP has functioned to calculate the weight criteria to find work volume of parallel manipulator [5]. Commonly used stiffness performance indices, the minimum and maximum Eigen values of the stiffness matrix are used to evaluate the stiffness of the 3-PRS mechanism in [6]. The 3 Degrees of Freedom (DOF) parallel mechanism with combined mobility is an important category of the lower-mobility parallel mechanism. In 3-PRS, P denotes prismatic pair, R as revolute and S as spherical joint. It has one translational and two rotational DOFs as described in [7]. The direct kinematics solution for a novel 3-PRS parallel mechanism using a geometric method based on three coupled trigonometric equations was proposed. Using Bezout's elimination method, solution to direct kinematics problem was obtained as shown in Ref [8]. The mobility analysis of the 3-PRS parallel manipulator can be implemented successfully by adopting a recent theory of DOF for complex spatial mechanisms [9]. In general, from the kinematic analysis, the workspace orientation of the 3-PRS parallel manipulator is analyzed and the 3D view of the workspace is drawn from inverse solution. The design and the practical applications of the parallel manipulator was studied by Chena *et al.*[10]. Optimizing the geometrical parameters for specific workspace is another important area of research. Zhang and Fang [11] carried-out the constrained optimization analysis of 3-PRS manipulator to find the geometrical parameter of manipulator. Abbasnejad *et al.*[12] presented forward kinematic problem of the 3-PRS parallel manipulator using Homotopy Continuation Method (HCM). Shi *et al.* [13] employed 3-PRS parallel mechanism as a welding tool head to form a five axis welding machine tool to perform friction stir welding. For orientation capability, the kinematic features have to be analyzed. Here also, they obtained a set of optimized geometrical parameters to develop a prototype machine for friction stir welding.

Kinematics of Manipulator

Figure 1 shows the 3-PRS mechanism with 3 prismatic actuators moving in the horizontal base plane. The base platform is described by equilateral triangle $A_1A_2A_3$ with circumcircle of radius equal to a and mobile platform is another equilateral triangle $B_1B_2B_3$ of circum circle radius of b . Both the platforms are connected by revolute (R)-spherical (S) legs.

The revolute joints in each leg are mounted on prismatic actuators. The input motion is given by the translations (s_i) of the prismatic actuators, while the output of the mechanism is given as translation and rotations of the mobile platform center. There are certain constrains which lead to the mobility of the mechanism equal to 3 instead of 6. Thus, the linkage is fully actuated special mechanism.

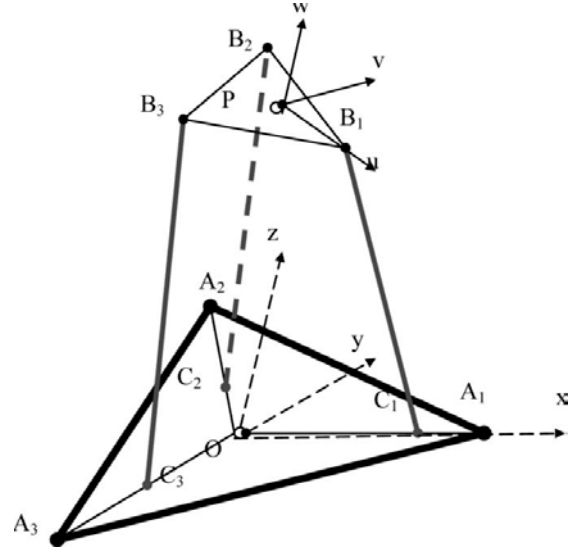


Fig. 1: Structure of 3-PRS Mechanism
($a = OA_1 = OA_2 = OA_3$ and $b = PB_1 = PB_2 = PB_3$)

Kinematic Equations

The position of the moving platform center is described by 3 translations p_x, p_y, p_z and 3 rotations ψ, θ and ϕ respectively about X, Y and Z axis of fixed mobile frame. From geometry therefore,

$$OP = \{p_x \ p_y \ p_z\}^T \quad \dots (1)$$

On the other hand the initial positions of the prismatic actuators are described by OA_1, OA_2 and OA_3 which can be expressed in terms of the base platform of size a . likewise, the position of the points B_1, B_2 and B_3 with respective mobile platform P are expressed as PB_1, PB_2 and PB_3 which can be written in terms of mobile platform of side b . finally the position of the points B with respective of fixed platform center O is given by,

$$OB_i = OP + [R]PB_i, \ i = 1, 2, 3 \quad \dots (2)$$

Here, [R] is rotation matrix transforming the vector from moving frame to fixed frame and is expressed in terms of platform rotations ψ, θ and ϕ . The resulting expressions for the position vectors OB_1, OB_2 and OB_3 are given as follows,

$$OB_1 = \{p_x + u_x b, \ p_y + u_y b, \ p_z + u_z b\} \quad \dots (3)$$

$$OB_2 = \left\{ p_x \frac{u_x b}{2} + \frac{\sqrt{3} v_x b}{2}, \ p_y \frac{u_y b}{2} + \frac{\sqrt{3} v_y b}{2}, \ p_z - \frac{u_z b}{2} + \frac{\sqrt{3} v_z b}{2} \right\} \quad \dots (4)$$

$$OB_3 = \left\{ p_x \frac{u_x b}{2} - \frac{\sqrt{3} v_x b}{2}, \ p_y \frac{u_y b}{2} - \frac{\sqrt{3} v_y b}{2}, \ p_z - \frac{u_z b}{2} - \frac{\sqrt{3} v_z b}{2} \right\} \quad \dots (5)$$

As the leg length $C_i B_i$ is constant ($= 1$), and the revolute joints set the spherical joints to move in a fixed plane, the following constrains are imposed on the mechanism.



$$OB_1y = 0; \quad \dots (6)$$

$$OB_2y = -\sqrt{3} OB_2x; \quad \dots (7)$$

$$OB_3y = \sqrt{3} OB_3x; \quad \dots (8)$$

Substitute in OB_i expressions following conditions are obtained,

$$p_y = -b \cos \psi \sin \phi; \quad \dots (9)$$

$$p_x = \frac{b}{2} (\cos \theta \cos \phi - \cos \phi \cos \psi + \sin \psi \sin \theta \sin \phi) \quad \dots (10)$$

$$\phi = \text{atan}\left(\frac{\sin \psi \sin \theta}{\cos \psi + \cos \theta}\right); \quad \dots (11)$$

Inverse kinematics of 3-PRS linkage obtains the actuated joint variables s_1 , s_2 and s_3 from a given position and orientation of the mobile platform center P. From Fig.1, it is possible to write,

$$A_i B_i = s_i(OA_i) + L(C_i B_i) \quad \dots (12)$$

Where $C_i B_i$ refers to the unit vector along each of the 3 legs.

Rearranging and squaring the components a quadratic equation is obtained, whose roots are given by,

$$s_i = A_i B_i(OA_i) \pm \sqrt{(A_i B_i \cdot OA_i)^2 - A_i B_i \cdot A_i B_i + L^2} \quad \dots (13)$$

The first unit vector OA_i is expressed as follows,

$$OA_1 = \{-\cos \alpha \ 0 \ -\sin \alpha\}^T \quad \dots (14)$$

$$OA_2 = \left\{\frac{1}{2} \cos \alpha - \frac{\sqrt{3}}{2} \cos \alpha \ -\sin \alpha\right\}^T \quad \dots (15)$$

$$OA_3 = \left\{\frac{1}{2} \cos \alpha \ \frac{\sqrt{3}}{2} \cos \alpha \ -\sin \alpha\right\}^T \quad \dots (16)$$

The vectors q_1 , q_2 , and q_3 are represented along $A_1 B_1$, $A_2 B_2$ and $A_3 B_3$ as,

$$q_1 = [a - s_1 \cos \alpha - L \cos \alpha_1 \ 0 \ -s_1 \sin \alpha - L \sin \alpha_1]^T \quad \dots (17)$$

$$q_2 = [-(a - s_2 \cos \alpha - L \cos \alpha_2) / 2 \ \sqrt{3}(a - s_2 \cos \alpha - L \cos \alpha_2) / 2 \ -s_2 \sin \alpha - L \sin \alpha_2]^T \quad \dots (18)$$

$$q_3 = [-(a - s_3 \cos \alpha - L \cos \alpha_3) / 2 \ -\sqrt{3}(a - s_3 \cos \alpha - L \cos \alpha_3) / 2 \ -s_3 \sin \alpha - L \sin \alpha_3]^T \quad \dots (19)$$

Forward Kinematics

The forward position kinematics obtains position and orientation of the moving platform by a given set of actuated inputs. So, the input for forward kinematics is the vector of 3 actuated joint variables S_1 , S_2 and S_3 and the output is the vector of Cartesian variables which describe position and orientation of moving platform.

Considering the geometric distance between two S joints B_i and B_j is equal to a constant, it can be written as,

$$\| \overline{B_i B_j} \| = \sqrt{3} b, (i \neq j) \quad \dots (20)$$

The following equations can be derived as forward kinematics,

$$[q_i - q_{i+1}]^T [q_i - q_{i+1}] - 3b^2 = 0, i = 1, 2, 3. \quad \dots (21)$$

Workspace

The reachable workspace of the manipulator is the space generated by the point P with at least one orientation. For a given pose of the point P if $s_{\min} \leq s_i \leq s_{\max}$, then the pose belongs to reachable workspace. In order to analyze the workspace with respect to independent motions the parasitic motions P_x , P_y and ϕ are important. In the present work the platform orientation is first computed using given p_x , p_y and p_z by constraint equations. Then the coordinates of point B_1 , B_2 and B_3 are obtained. Further the unit vectors $A_i B_i$ are estimated with the knowledge of leg angles α_1 , α_2 and α_3 . Finally inverse kinematic equations with negative root are selected find s_1 , s_2 and s_3 . The process is repeated for a combination of p_x , p_y and p_z . The set of p_x , p_y and p_z satisfying $s_{\min} \leq s_i \leq s_{\max}$ are stored as array of workspace points. This procedure is slightly different from that of a standard 6 DOF manipulator.

Jacobian Analysis

The vector loop for the i^{th} link can be written as,

$$OP + OB_i = OA_i + s_i \frac{OA_i}{|OA_i|} + L I_i \quad \dots (22)$$

where I_i is the unit vector along $C_i B_i$, s_i represents the linear displacement of the i^{th} actuator, and $\frac{OA_i}{|OA_i|}$ is the corresponding unit vector along OA_i , $i = 1, 2, 3$.

On differentiating both sides with respect to time,

$$v_p + \omega_p \times OB_i = v_i \frac{OA_i}{|OA_i|} + L \omega_i \times I_i \quad \dots (23)$$

where “ \times ” represents the cross product between vectors, v_p and ω_p denotes the three-dimensional linear and angular velocity of the moving platform respectively, v_i is the velocity of the i^{th} linear actuator, and ω_i represents the three-dimensional angular velocity of link $C_i B_i$.

Let $\dot{X} = \{v_p \ \omega_p\}^T$ and $\dot{d} = \{s_1 \ s_2 \ s_3\}^T$ be the vectors of the moving platform velocities and the actuated joint rates, respectively. Matrix form can be represent as,

$$J_x \dot{X} = J_q \dot{d} \quad \dots (24)$$

$$\text{Where } J_x = \begin{bmatrix} I_1^T & (OB_1 \times I_1)^T \\ I_2^T & (OB_2 \times I_2)^T \\ I_3^T & (OB_3 \times I_3)^T \end{bmatrix} \quad \dots (25)$$



$$J_q = \begin{bmatrix} I_1 \cdot \frac{OA_1}{|OA_1|} & 0 & 0 \\ 0 & I_2 \cdot \frac{OA_2}{|OA_2|} & 0 \\ 0 & 0 & I_3 \cdot \frac{OA_3}{|OA_3|} \end{bmatrix} \dots (26)$$

Therefore,

$$\underline{\dot{d}} = J_q^{-1} \cdot J_x \dot{X} = [J] \dot{X} \dots (27)$$

So, this represents a inverse velocity solution of the manipulator. The \dot{X} has 6 elements of which only 3 are independent and hence a constrained Jacobian matrix has to

be formulated so that $\dot{d} = [J] \begin{pmatrix} \dot{p}_z \\ \dot{\psi} \\ \dot{\theta} \end{pmatrix}$.

Results and Discussions

In order to illustrate the kinematic characteristics following dimensions of the linkage are considered:

Base platform radius $a = 400\text{mm}$, mobile platform radius $b = 200\text{ mm}$, leg lengths $L = 550\text{ mm}$, included angle $\alpha = 30$ degrees. Also the mobile platform independent variables $p_z \in [400, 700]\text{ mm}$, $\psi \in [-90, 90]$ degrees, $\theta \in [-90, 90]$ degrees are considered. The inverse kinematic analysis is conducted to find actuator variables s_1, s_2 and s_3 . The 3 dimensional workspace of the proposed 3-PRS parallel manipulator is shown in Figure 2.

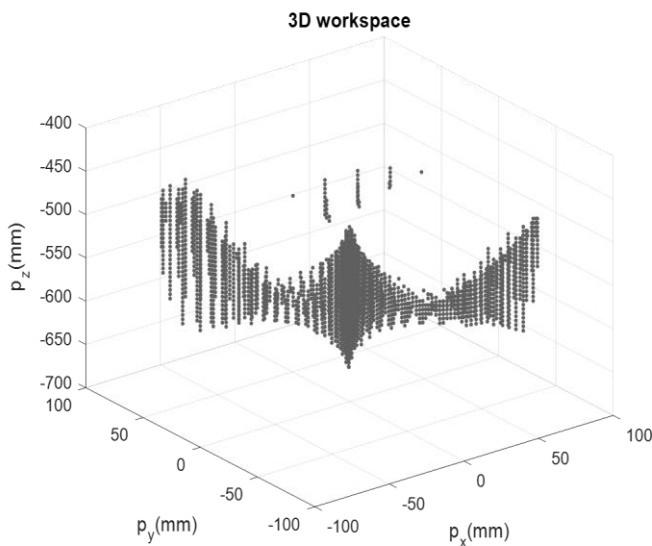


Fig. 2: 3D Workspace

The 2 dimensional workspace of the 3-PRS parallel manipulator is shown in the Figures 3–8 on changing the included angle α from 0 to 105°.

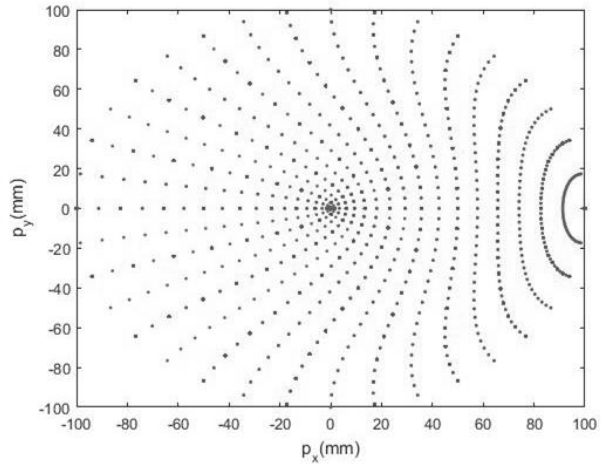


Fig. 3: 2D Workspace at $\alpha = 0^\circ$

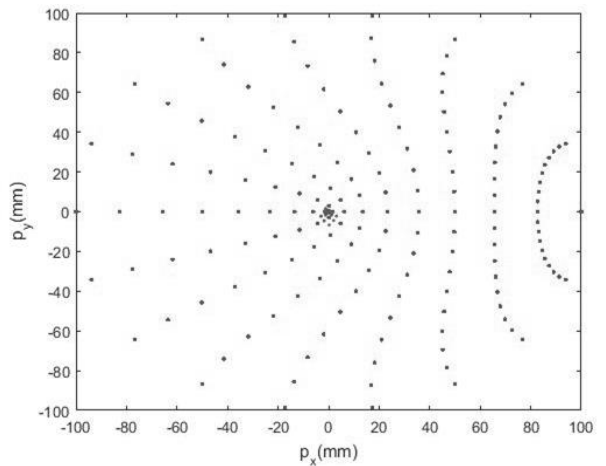


Fig. 4: 2D Workspace at $\alpha = 30^\circ$

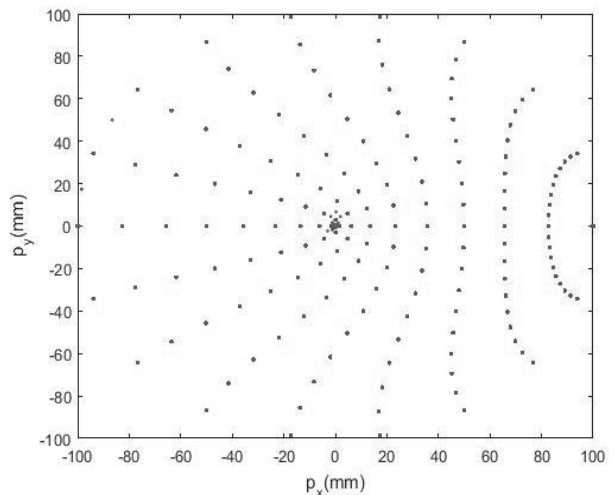


Fig. 5: 2D Workspace at $\alpha = 45^\circ$

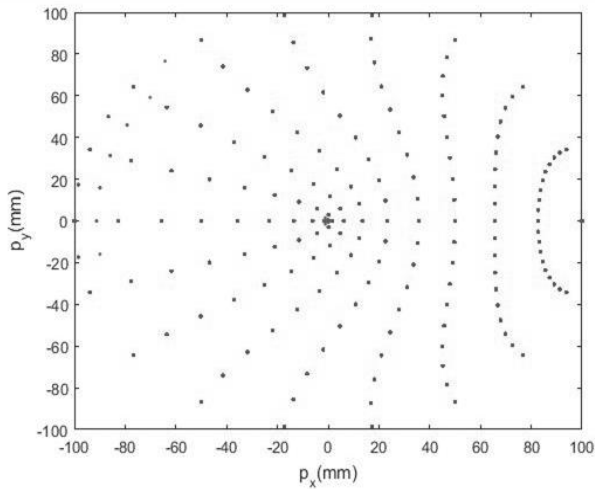


Fig. 6: 2D Workspace at $\alpha = 60^\circ$

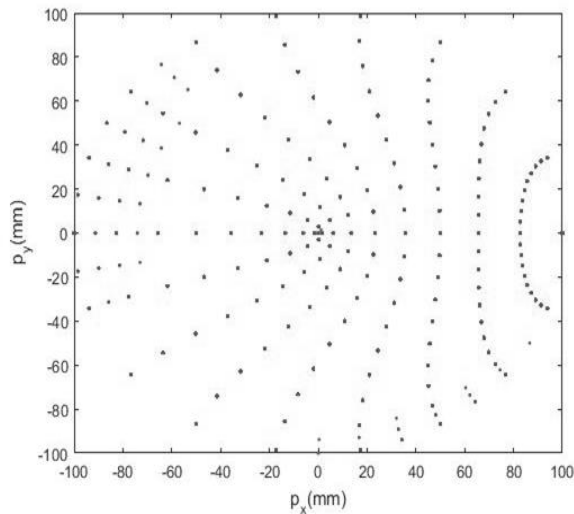


Fig. 7: 2D Workspace at $\alpha = 90^\circ$

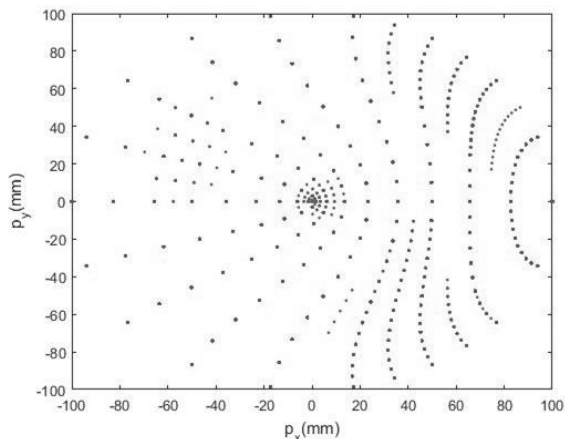


Fig. 8: 2D Workspace at $\alpha = 105^\circ$

The center of this work region moves towards right as the included angle α increases. The proposed model is drawn in solid works as 3D assembly model and is shown in Figure 9.

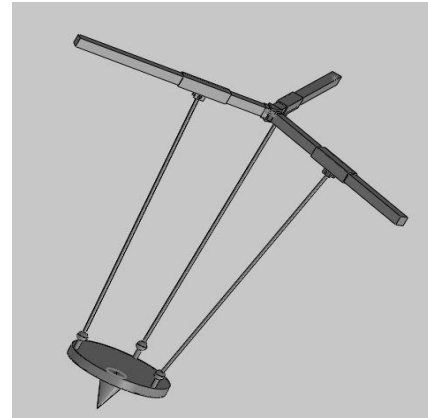


Fig. 9: Solid Model

Conclusion

The inverse kinematic equations were solved in MATLAB. The optimized set of solutions is used to draw the workspace of the 3-PRS parallel manipulator. On using the geometrical parameters a solid model is drawn in solidworks. As a next step analysis of the solid model as to be carried out in ADAMS software. The work is under progress.

References

- [1] Li, Y. and Xu, Q., Kinematic analysis of a 3-PRS parallel manipulator, *Robotics and computer-Integrated Manufacturing*, 23, 395–408 (2007).
- [2] Li, Q., Chen, Z., Chen, Q., Wu, C. and Hu, X., Parasitic motion comparison of 3-PRS parallel mechanism with different limb arrangements, *Robotics and computer-Integrated Manufacturing*, 27, 389–396 (2011).
- [3] Ruiz, A., Campa, F.J., Roldan-Paraponiaris, C., Altuzarra, O. and Pinto, C., Experimental validation of the kinematic design of 3-PRS compliant parallel mechanisms, *Mechatronics*, 39, 77–88 (2016).
- [4] Li, Y. and Xu, Q., Kinematics and dexterity analysis for a novel 3-DOF translational parallel manipulator. In: Proceeding of IEEE international conference on robotics and automation, *Barcelona, Spain* (2005), .p. 2955–60.
- [5] Mahapatro, M. and Selvakumar, A., Weight criteria detection to find work volume of 3-PRS parallel manipulator using fuzzy logic, *Procedia engineering*, 97, 1929–1934 (2014).
- [6] Han, X., Wang, Y. and Shi, J., Stiffness modeling of 3-PRS mechanism, *World Academy of science, Engineering and technology*, 6, 12–23 (2012).
- [7] Liu, X.J., Wu, C., Wang, J.S. and Bonev, I., Attitude description method of PPS type parallel robotic mechanisms, *Chinese Journal of Mechanical Engineering*, 44(10), 19–23 (2008).



- [8] Tsai, M.S., Shiau, T.N., Tsai, Y.J. and Chang, T.H., Direct kinematic analysis of a 3-PRS parallel mechanism, *Mechanism and Machine Theory*, 38, 71–83 (2003).
- [9] Zhao, J.S., Zhou, K. and Feng, Z.J., A theory of degrees of freedom for mechanisms. *Mech Mach Theory*. 39(6), 621–43 (2004).
- [10] Chena, W., Zhao, L. and Mo, X., The orientation workspace of a 3-PRS parallel manipulator, In *Proc. IEEE conference on consumer electronics and communication*, 875–78 (2011).
- [11] Zhang, X. and Fang, H., Optimization of a 3-PRS parallel manipulator based on interval analysis, In Proceedings of the *10th World Congress on Intelligent Control and Automation*, Beijing, China (2012), .p. 2452–56.
- [12] Abbasnejad, G., Zarkandi, S. and Imani, M., Forward kinematics analysis of a 3-PRS parallel manipulator, World Academy of Science, Engineering and Technology International Journal of Mechanical, Aerospace, Industrial, Mechatronics and Manufacturing Engineering, 4, 73–79 (2010).
- [13] Shi, J., Wang, Y., Zhang, G. and Ding, H., Optimal design of 3-DOF PKM module for friction stir welding, *Int J Adv Manuf Technol*, 66, 1879–1889 (2013).



Relation between SIF and Crack Geometry

Prerna Rai¹ and Shalendra Kumar²

Abstract: Engineering materials inherently contain flaws or discontinuities of various categories (geometries) at different locations which, depending upon the loading pattern or fatigue cycles, may lead to failure of the component due to formation and propagation of cracks. The driving force for a crack to expand is not the strain or stress but the Stress Intensity Factor (SIF), universally represented as K . The stress intensity factor embodies both the stress and the crack size and uniquely describes the crack tip stress field independent of global geometry. This study deals with parametric study on Stress Intensity Factor, which are functions of crack geometry and stress. SIF gives the stress field at the tip of the flaw/crack independent of the global geometry. It is computed using Displacement Co-relation Technique. 2-D and 3-D models for different conditions have been created and have been analyzed using the program ANSYS. The SIF was computed for different crack front angle and results thus found in the process has been plotted to predict relation between various parameters like crack location, cylinder's radius to thickness ratio (R/t), crack minor axis to cylinder thickness ratio (a/t) and the crack geometry ratio (a/c). The study carried out in this investigation lead to significant knowledge, which has resulted in establishing relations between SIF and various parameters of crack geometry.

Keywords: Fracture Mechanics, Stress Intensity Factor, Crack Modeling, ANSYS.

Introduction

The driving force for a crack to expand is not the strain or stress but the stress intensity factor, universally known as K . This is not as the stress concentration factor, K_t or as the strain hardening exponents k or k' . The stress intensity factor embodies both the stress and the crack size and uniquely describes the crack tip stress field independent of global geometry.

The SIF is a measure of the strength of the stress singularity at a crack tip, and is useful from a mechanics perspective as it characterizes the displacement, stress and strain in and around the crack tip. Additionally, the stress intensity concept is important in terms of crack extension as critical values of the SIF govern crack initiation.

It is important that the stress-intensity factor is not dependent on the coordinates, r and θ , hence they control the intensity of the stress fields but not the distribution for each mode. It has been observed that the stress-intensity factors must contain the magnitude of loading forces linearly for linear-elastic bodies and must also depend upon the configuration of the body including the crack size [1]. Consequently, stress-intensity factors may be physically interpreted as parameters which reflect the re-distribution of stress in a body due to the introduction of a crack, and in particular they indicate the type (mode) and magnitude of force

transmission through the crack tip region. The relationship between K , applied stress (σ) and crack size (a) is:

$$K_I = \sigma \sqrt{\pi a} \beta \quad \dots (1)$$

The compliance function, β describes the geometry of the structure, component or specimen in which the crack exists. It takes a very complex mathematical description in some cases [2–3].

The parameter (K) gives the possibility to analyze the possible crack growth or the possible catastrophic failure if a given load is applied to the structure. The stress intensity factor can be computed using stress and strain analysis or parameters that measure the energy released by crack growth [4–5]. The estimation of stress intensity factors can be done either by analytical or numerical techniques. Normally, the analytical ones are more complex to compute; however they have some advantages, because an analytical solution can be applied for a range of crack lengths. The numerical techniques require the computation of stress or strain field for each crack length and therefore for each value of SIF.

FEM Using ANSYS

For complex structures, it is difficult to perform an analysis taking into account all boundary effects near the crack tip, so the numerical calculation of SIF has some advantages for these structures [6]. The evolution of computers (hardware

^{1,2} Department of Mechanical Engineering, NIT Jamshedpur, India.
✉ ¹prernarai26@gmail.com; ²shalkumar.me@nitjsr.ac.in



and software) permits the use of more complex numerical techniques and to obtain solutions with smaller computation time. Hence, the numerical techniques for estimating stress intensity factors are nowadays more popular than the analytical techniques. If a relation between some of its factors can be established or implied, then the complex solutions can be avoided in most of the situations.

The finite element method has been used extensively in solving problems involving homogeneous materials. The finite element method has been largely used to analyze various mechanical problems. It has been widely employed for the solution of problems in linear elastic fracture problems. Modeling and simulation of the different geometry with the help of commercially available structural analysis software ANSYS was done for SIF calculation.

Stresses and displacements at the vicinity of the crack tip reveals that the cracked structure possess a singular stress field i.e. the stress gradient at the vicinity of crack tip is extremely high. Thus to accurately simulate the stress singularity a very fine mesh is required in the region near to the crack tip.

The finite element program for three-dimensional problems has been used to perform the computations [7]. The recommended element type for the three-dimensional model is SOLID 95. The first row of elements around the crack front should be singular elements.

Modeling of Crack in ANSYS

Top down modeling and bottom up both methods is used to create a 3D cracked structure. MESH200 and SOLID95 are used as element types for meshing. A semi-circular area is created at a key point perpendicular to the plane on which keypoints are created. This area is created to form the tubular volume around crack front. Area created at the first key point is dragged along the lines to form a tubular volume around crack front. Model has two symmetry planes. Planes along longitudinal and circumferential directions are symmetry planes as shown in Figure 1.

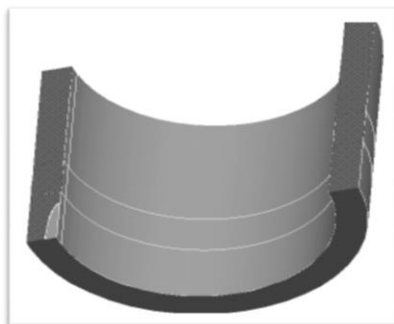


Fig. 1: Symmetry Areas around the Crack and Cylinder

Cylinder is generated including the crack. Cylinder is divided into sub volumes. This volume is meshed by different element sizes. The smallest volume around crack is the finest mesh. The volume around this small volume is less fine. Finally, rest of the cylinder has coarse mesh. Meshed area is swept along the crack front to form a tubular volume. For different a/c, a/t and R/t values, geometry of the crack and cylinder change. In some cases volumes need special effort for meshing. Different element sizes are needed with these cases.

Internal pressure is applied to the inner, outer and embedded axial cracks. Internal pressure is applied as 10 MPa in all cases. Edges of the cylinder are stress free. While axial tension loading is applied to the inner, outer and embedded circumferential cracks. Axial stress applied is 10 MPa in all circumferential cases. Crack is located in the symmetry plane. Then stress intensity factors are calculated by using displacement correlation technique.

$$K_I = \frac{\sqrt{2\pi} \times E}{4(1-\nu^2)} \cdot \left[\frac{R_3^{\frac{3}{2}} u_{b2} - R_2^{\frac{3}{2}} u_{b3}}{\sqrt{R_2} \sqrt{R_3} (R_3 - R_2)} \right] \dots (2)$$

Cylinders

Crack front angle (ϕ) at 0 is the deepest point and angle 90 is the surface point. Inner pressure of 10MPa is applied to the structure. Results are obtained for cylindrical structures having different R/t, a/t & a/c values. R is 50 mm for all cases but a, c and t changes. Results are obtained for the following values;

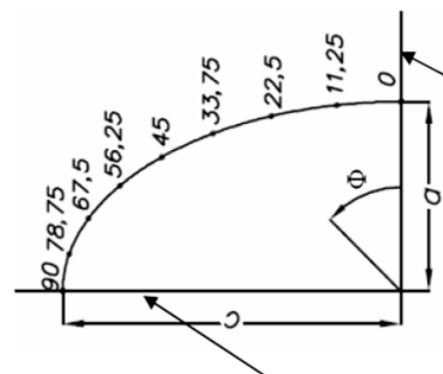


Fig. 2: Crack Front Angle (ϕ) Depiction

The models under consideration are: (1) finite axial internal surface cracked cylinder (2) finite axial external surface cracked cylinder (3) finite axial embedded cracked cylinder (4) Inner circumferential cracked cylinder (5) Outer circumferential cracked cylinder (6) embedded circumferential cracked cylinder. The crack front angle is depicted in Figure 2 and the circumferential cracks are depicted in Figure 3.



Table 1: SIF Data for Circumferential Embedded Elliptical Crack in a Cylinder

R/t	a/t	a/c	a	$\phi = 0$	$\phi = 22.5$	$\phi = 45$	$\phi = 67.5$	$\phi = 90$	$\phi = 112.5$	$\phi = 135$	$\phi = 157.5$	$\phi = 180$
5	0.2	0.2	2	1.01	0.96	0.84	0.64	0.44	0.64	0.84	0.97	1.02
5	0.2	0.4	2	0.91	0.87	0.78	0.65	0.56	0.65	0.78	0.87	0.91
5	0.2	0.8	2	0.72	0.71	0.68	0.65	0.64	0.65	0.68	0.71	0.72
5	0.3	0.4	3	0.97	0.92	0.82	0.68	0.59	0.68	0.83	0.94	0.99
5	0.4	0.2	4	1.39	1.23	1.06	0.83	0.59	0.93	1.11	1.35	1.56
10	0.2	0.2	1	1.01	0.96	0.84	0.64	0.44	0.64	0.84	0.96	1.02
10	0.3	0.2	1.5	1.12	1.05	0.89	0.67	0.46	0.67	0.91	1.07	1.14
20	0.2	0.2	0.5	1.01	0.96	0.84	0.64	0.44	0.64	0.84	0.96	1.02
20	0.3	0.2	0.8	1.12	1.05	0.89	0.66	0.45	0.67	0.9	1.06	1.13

R/t = 5, 10 and 20
a/t = 0.2, 0.4 and 0.6
a/c = 0.2, 0.4 and 0.8

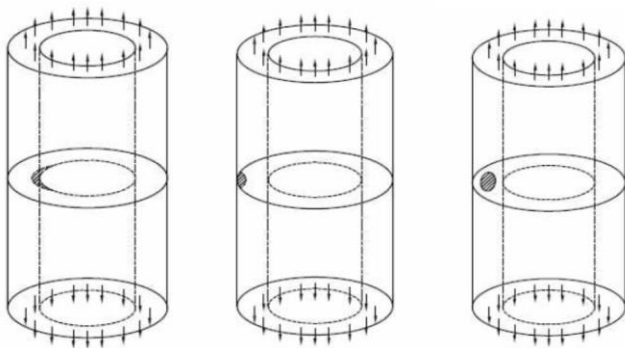


Fig. 3: Circumferential Cracks

Plates

Pressure of 20 MPa is applied for 3 plate cases of uniform thickness 10 mm. Results are obtained at crack tip for following values of a/t and a/c ratio in semi elliptical surface crack.

a/t = 0.2, 0.4, 0.6 and 0.8

a/c = 0.1, 0.2, 0.4, 0.6 and 1

Since in infinite crack, the crack runs throughout the breadth of plate only variation in a/t is possible. Following value of a/t are considered: 0.1, 0.2, 0.3, 0.4, 0.5, 0.6, 0.7, 0.8 and 0.9.

For embedded crack following value of a/t, a/c and e are considered:

a/t = 0.01, 0.1, 0.2 and 0.3

a/c = 1.0, 0.5 and 0.25

e = 0, 1.5 and 3.

Results and Discussion

The data generated as stated were tabulated and interpreted on the underlying principle of solid mechanics.

In finite axial external crack, SIF is maximum at the crack tip (crack front angle 0) and increase in a/c ratio decreases the SIF value i.e. SIF is inversely proportional to a/c value.

The value and variation (range for diff a/c) in SIF increases with increase in a/t ratio. Also, as R/t ratio increases the value of SIF increases proportionately. The value of SIF under same condition of load and geometry is slightly greater for internal surface crack as compared to External surface crack but this difference does not exist when value of R/t increases. Other findings are same as that in Internal Surface crack.

In finite axial embedded crack the variation in SIF along the crack decreases with increase in a/c ratio and there exists a symmetry along the crack such that though magnitude varies with parameters but distribution of SIF remains constant.

The SIF values for finite axial internal surface crack and external surface crack in a cylinder are shown in Table 2 and Table 3 respectively.

The value of SIF for circumferential cracks is far less than SIF for axial cracks (Figure 4). Also the variation in SIF at different crack front angles is small as compared to axial cracks. The variation between SIF and Crack angle reveals that there is negligible difference in SIF for inner and outer circumferential cracks. The predominant effect which is shown by R/t in axial cracks does not exist in circumferential cracks. The values obtained for circumferential embedded elliptical crack shows that as a/c increases, the variation in SIF decreases. Comparing the data from circumferential embedded crack complements our earlier conclusion that variation in R/t has less effect in circumferential cracks. The value of SIF in embedded for axial cracks is less as compared to other cracks but the same relation does not hold good for circumferential cracks.



Table 2: SIF Values for Finite Axial Internal Surface Crack in a Cylinder

R/t	a/t	a/c	a	$\varphi = 0$	$\varphi = 11.25$	$\varphi = 22.5$	$\varphi = 33.75$	$\varphi = 45$	$\varphi = 56.25$	$\varphi = 67.5$	$\varphi = 78.75$	$\varphi = 90$
5	0.2	0.2	2	6.41	6.3	6.25	5.99	5.59	5.07	4.41	3.67	3.44
5	0.2	0.4	2	5.58	5.5	5.49	5.3	5.03	4.7	4.35	4.1	4.11
5	0.2	0.8	2	4.34	4.3	4.35	4.31	4.27	4.24	4.25	4.36	4.31
5	0.4	0.2	4	7.25	7.16	7.11	6.79	6.32	5.73	5.02	4.24	3.96
5	0.6	0.2	6	8.82	8.78	8.59	8.26	7.53	6.77	5.95	5.12	4.95
10	0.2	0.2	1	11.92	11.8	11.7	11.16	10.4	9.4	8.15	6.76	6.21
10	0.4	0.2	2	13.89	13.61	13.46	12.8	11.9	10.75	9.36	7.79	7.38
20	0.2	0.2	0.5	22.9	22.71	22.46	21.41	19.89	17.92	15.48	12.88	11.72
20	0.4	0.2	1	26.87	26.59	26.28	24.96	23.14	20.83	18.06	15.04	13.94

Table 3: SIF Values for Finite Axial External Surface Crack in a Cylinder

R/t	a/t	a/c	a	$\varphi = 0$	$\varphi = 11.25$	$\varphi = 22.5$	$\varphi = 33.75$	$\varphi = 45$	$\varphi = 56.25$	$\varphi = 67.5$	$\varphi = 78.75$	$\varphi = 90$
5	0.2	0.2	2	4.76	4.67	4.61	4.37	4.03	3.61	3.09	2.53	2.35
5	0.2	0.4	2	4.12	4.06	4.03	3.87	3.64	3.37	3.09	2.88	2.86
5	0.2	0.8	2	3.16	3.13	3.15	3.11	3.07	3.03	3.02	3.00	3.03
5	0.4	0.4	4	4.78	4.69	4.65	4.46	4.19	3.88	3.56	3.34	3.21
5	0.6	0.2	6	8.18	8.05	7.82	7.19	6.38	5.52	4.59	3.72	3.38
10	0.2	0.2	1	10.32	10.20	10.08	9.58	8.87	7.96	6.84	5.63	5.15
10	0.4	0.2	2	12.88	12.69	12.39	11.64	10.66	9.49	8.09	6.65	6.21
20	0.2	0.2	0.5	21.36	21.17	20.86	19.82	18.29	16.18	12.83	10.55	7.96
20	0.4	0.2	1	26.25	25.90	25.51	24.07	22.14	19.76	16.98	14.02	12.93

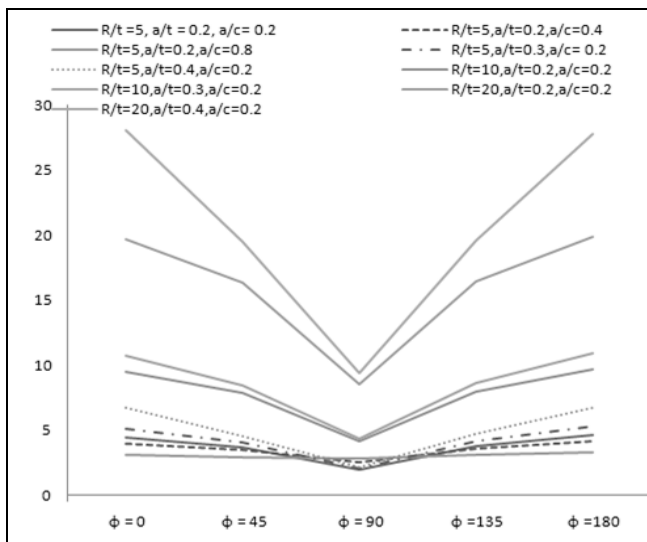


Fig. 4: Variation of SIF for Crack Geometry of Finite Axial Embedded Crack in Cylinder

In plates, SIF is maximum at certain value of a/c i.e. for a definite elliptical crack the value of SIF has found as maximum. Also, when plotted against a/t ratio shows that,

there is in general, an increase in SIF value with increase in a/t ratio except for circular crack. The value of SIF increases tremendously once a threshold value or certain thickness in plate is covered by the crack. The value of SIF for embedded cracks is low compared to others cracks in plates with same value of pressure applied to it. The eccentricity of crack has little effect on value of SIF. Further, the circular cracks show a deviation in SIF patterns as shown by elliptical cracks (Figure 5).

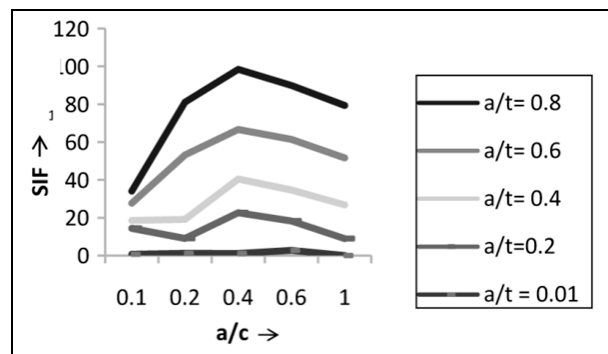


Fig. 5: Variation of SIF with a/c at Diff a/t Ratio in Semi Elliptical Surface Crack of a Plate



Conclusion

The SIF value that was obtained for different geometry at various points of the crack emerges with some conclusive findings which are listed as:

- Stress intensity factor increases linearly as load increases at constant length/width ratio.
- Stress intensity factor is independent of Length/width ratio.
- Stress intensity factor decreases with increase in angle ϕ as well as a/c ratio.
- SIF increases with increase in R/t ratio.
- The difference in KI for varying a/c increases with increase in R/t except for circumferential cracks in cylinder.
- Difference in KI for varying a/c increases with increase in a/t ratio.
- Embedded crack has lower SIF value than that of surface cracks except for circumferential cracks in cylinder where there is hardly any change.
- Value of SIF for circumferential cracks is less than that of axial cracks in cylinder.
- Distribution pattern of SIF is same in embedded cracks though the parameters effecting its value changes.

References

- [1] Paris, Paul C. and Sih, George C., "Stress Analysis of Crack", Department of Mechanics, Lehigh University, June, 1964.
- [2] Castro, P.M.S.T. De and Pastrama, S.D.; "The compounding method for calculating stress intensity factors: description and applications", U.P.B. Sci. Bull., Series D, Vol. 64, No. 4, 2002.
- [3] Cartwright, D.J. and Rooke, D.P. "Approximate stress intensity factors compounded from known solutions", *Engineering Fracture Mechanics*, 6(3), pp. 563–571, 1974.
- [4] Kumar, Prashant; "Elements of fracture mechanics", Tata McGraw Hill Publication, Third reprint, pp. 9–95, 2011.
- [5] R.J. Sanford, "Principles of Fracture Mechanics", 1st Edition, Pearson Education, 2003.
- [6] Smith, S.A. and Raju, I.S., "Evaluation of Stress-Intensity Factors Using General Finite-Element Models", *Fatigue and Fracture Mechanics: 29th Volume*, ASTM STP 1321, T.L. Panontin and S.D. Sheppard, Eds., American Society for Testing and Materials, 1998.
- [7] Release 11.0 Documentation and tutorials for ANSYS.
- [8] Lockwood and Allison Marie, "Development of Probability Model for Fatigue Crack Growth Using Response Surface Method", University of Tennessee Honors Thesis Projects (2002).
- [9] Molent, L., Jones, R., Barter, S. and Pitt, S., "Recent developments in fatigue crack growth assessment", *Int. J. Fatigue*, 28, pp. 1759–1768, 2006.
- [10] Hediaand, H.S. and Aldousari, S.M., "Three-Dimensional Finite Element Model for Evaluation of the Stress Intensity Factors for Different Fracture Modes of Homogeneous Bimaterial", *Eng. Sci.*, Vol. 18, No. 1, pp. 73–87, 2007.
- [11] Jia, J.H., Z.Q. Zhang and C. Zhang. "Numerical Simulation of Stress Intensity Factor for Socket Weld Toe Cracks in Small Branch Pipes." *Procedia Engineering*, 130 (2015): 150–157.
- [12] Peng, Yang, *et al.* "Modified stress intensity factor equations for semi-elliptical surface cracks in finite thickness and width plates." *Procedia Engineering* 14 (2011): 2601–2608.
- [13] <http://www.matthewpais.com/crack-growth>



Design and Fabrication of Industrial Robot for the Automotive Industry

E. Bhaskaran¹

Abstract: The Industrial Robot named “MECHRO” designed to pick and place objects of maximum one kg and used in the Automotive and Electronics Industry. Its main function is to pick the objects, lift it, move to a distance, orient it and then place the objects. This robot is provided with four degrees of freedom out of which one is the linear movement of the gripper and remaining three are rotary motions. The type of configuration used is the “SCARA CONFIGURATION” which is a combination of cylindrical configuration and revolute configuration operating in horizontal plane. The drive system incorporated is “The electrical drive system”. This is accomplished by making use of stepper motors one for each axis. The distinct parts of “Mechro” are the upper arm, lower arm, the gripper and base. The arms are made of Aluminum and its houses the drive system consisting of motors, sprockets, chains and gears. The gripper is also made of Aluminum. Mild steel screw shaft at the end of the lower arm provides the linear movement of the gripper. The Base of ‘Robot’ is made of a heavy material whose main function is to support whole unit in stable condition during operation. Stepper motors have been chosen to avoid feedback, reduce cost, and make the control system less complicated. The stepper motors were controlled through a computer. This facilities the programmer to write the control programme in any convenient language. On completion of Fabrication the experimental robot was assembled and tested for working. The motors were run and tested for the specified speed. The Gripper assembly was tested and the following results were inferred. The Gripper opening and closing was found to be 0–35 mm. The roll of the Gripper was 360°. For every revolution of the gripper the M-12 screw advanced by 1.7 mm (pitch) giving the vertical linear movement of the gripper. Next the rotations at the axes were examined and the rotation of the elbow axis was found to be equal to 255° and at the shoulder axis 360° rotation was obtained. The gripper was found to grip a load of 1 kg. The robot is command to move 20 inches and the actual move is measured and found to be 19.99 inches. The error is ± 0.01 inch and can be represented as an accuracy error of 0.05% less than the commanded distance.

Keywords: Automotive Industrial Robot; SCARA Configuration; Four Degree of Freedom.

Introduction

Robot may be defined as a computer-controlled re-programmable mechanical manipulator with several degrees of freedom capable of being programmed to carry out one or more industrial tasks [1].

Technical Survey

Chronology of development related to robotics technology, including significant robot applications are available from 1700 onwards till today [2].

It is for all the above said reasons; Researcher has selected this topic “INDUSTRIAL ROBOT” for research work to focus towards the Design, Fabrication and control of the Experimental Robot.

SCARA Coordinated Robots

The term SCARA robot (Selective Compliance Assembly Robot Arm) also has two revolute joints and one prismatic joint to position the wrist. However a SCARA robot the axes of all three joints are vertical. The first revolute joint swings the arm back and forth about a base axis that can also be thought of as a vertical shoulder axis. The second revolute joint swings the forearm back and forth about a vertical elbow axis. Thus the two revolute joints control motion in a horizontal plane. The vertical component of the motion is provided by the third joint, a prismatic joint which slides the wrist up and down. The shape of a horizontal cross section of the work envelope of SCARA robot can be quite complex, depending upon the limits on the ranges of travel for the first two axes [3]. In SCARA manipulator, a jointed arm and

¹Department of Industries and Commerce, Government of Tamil Nadu, India. ✉ e.bhaskaran19@gmail.com



cylindrical configurations are combined resulting in revolute motions confined to horizontal plane. This configuration provides substantial rigidity for the robot in the vertical direction, but has compliance in the horizontal plane. This makes it ideal for many assembly tasks [4]. Advantages are extremely good manoeuvrability and access within its programmable area. SCARA robot is fast operation; high accuracy; relatively high payload capacity.

Classification based on power system employed is Robot Power Systems; Electric Motors; Hydraulic Systems and Pneumatic Systems. Classification based on application on which the robots are employed is welding robots; Spray Painting Robot; Assembly Robot and Handling Robots. A SCARA robot is very suitable for assembly operations and is therefore extensively used in several industries for this purpose [5].

Objective of the Study

The objective of the study is to do the Experimental Robot which was designed for the SCARA configuration for the following reasons like it is a combination of revolute and cylindrical configuration; it provides a larger work volume and this is more suitable for assembly type operations. Assembly tasks predominantly require movement in the horizontal plane coupled with simple vertical movement for picking, placing and insertion operations.

Description of “Mechro”

This Robot is experimental Robot named ‘MECHRO’ designed to pick and place objects within its reach. Its main function is to pick the objects, lift it, move to a distance, orient it and then place the objects. This robot is provided with four degrees of freedom out of which one is the linear movement of the gripper and remaining three are rotary motions. The type of configuration used is the “SCARA CONFIGURATION” which is a combination of cylindrical configuration and revolute configuration operating in horizontal plane. The drive system incorporated is “The electrical drive system”. This is accomplished by making use of stepper motors one for each axis. The distinct parts of “Mechro” are the upper arm, lower arm, the gripper and base. The arms are made of Aluminium and its houses the drive system consisting of motors, sprockets, chains and gears. The gripper is also made of Aluminium. Mild steel screw shaft at the end of the lower arm provides the linear movement of the gripper. The Base of ‘Robot’ is made of a heavy material whose main function is to support whole unit in stable condition during operation. Stepper motors have been chosen to avoid feedback, reduce cost, and make the control system less complicated. The stepper motors were controlled through a computer. This facilities

the programmer to write the control programme in any convenient language.

Design of ‘Mechro’

The Experimental Robot “Mechro” was provided with four degrees of freedom. 1. Rotation of the upper arm about the shoulder axis, 2. Rotation of the fore arm about the elbow axis. 3. Vertical linear movement of the gripper. 4. Roll of the gripper about a vertical axis is the four degrees of freedom.

The upper and lower arms are made of a pair of parallel Aluminium plates connected with support rods as it was decided to design an open construction, so that all the mechanisms will be clearly visible. This will enable future students to study them and make further improvements to increase the efficiency. The various elements to be designed are: 1) The Gripper, 2) Fore arm, 3) Upper arm and 4) Base.

The Gripper

In almost all the robots, a major proportion of the load carrying capacity of the robot arm is taken by the gripper’s self-weight. In the present design, care is taken to minimize the weight of the gripper and hence a kinematic system was designed. Gripper was designed for a capacity of 1 kg and for an opening range of 0–25 mm.

To grip this load each jaw should generate a force ‘F’ equal to $1/4\mu$ kgf.

= Coefficient of friction of gripping face. Lining the gripping face with rubber = 0.3

$$F = 0.833 \text{ kgf.}$$

Gripper Link

Using basic kinematic principles of the Links were dimensioned to achieve a maximum opening of 25 mm as shown in Figure 2 and Figure 3.

Force required at the draw link of the finger = $1 \times 7.4/3 = 2.46 \text{ kg.}$

Force required along the draw link ‘x’ = $2.46/\cos 50^\circ = 3.83 \text{ kg.}$

Axial force required at the nut ‘L’ = $3.83/\cos 40^\circ = 4.99 \text{ kg.}$

Load on the nut for two fingers = $2 \times 4.99 = 10 \text{ kg.}$

Gripper Actuation

An M-bolt with brass nut was used to actuate the gripper.

The torque required to turn the gripper actuation screw,

$$T = W.r. [\tan (\alpha + \phi)]$$



W - load on the nut = 10 kg.
 r - radius at which the force is acting = 4 mm.
 α - helix angle = 3.08° for M-8
 ϕ - Friction angle for a combination of mild steel and brass = 29.68°

Torque required for actuating the gripper $T = w.r [\tan (\alpha + \phi)] = 2.57 \text{ kg.cm.}$

Taking into consideration the torque required to overcome inertia and other losses due to friction, the net torque required for this actuation = 3 kg cm.

Gripper Linear Movement

The linear vertical movement of the gripper to lift the objects was obtained by using a M-12 screw with a brass nut.

Total load on the vertical screw shaft 'W' = Weight of gripper assembly + weight of motor for gripper actuation = 2.5 kg.

Torque required to rotate the nut for raising or lowering the gripper assembly,

$$T = W.r. [\tan (\alpha + \phi)] = 1.08 \text{ kg cm.}$$

r - radius of the screw = 6 mm
 α - helix angle of M-12 = 6.2
 ϕ - Friction angle for a combination of mild steel and brass = 29.68°

Torque required to rotate the nut = $W.r. [\tan (\alpha + \phi)] = 1.08 \text{ kg cm.}$

Torque to be overcome due to collar friction = $\mu W (R + r)/2$

μ - coefficient of friction = 0.3
 w - load on the nut = 2.5 kg
 R - Outer radius of the collar = 24/2 mm
 r - Internal radius of the collar = 12/2 mm

Torque to be overcome = $0.3 \times 2.5 (24 + 12)/2 = 1.35 \text{ kg.cm.}$

Total torque required for the gripper movement vertically = $1.08 + 1.35 = 2.43 \text{ kg cm.}$

To provide a roll to the gripper we are providing a key way in the Screw Shaft and corresponding key in a brass collar.

Design of Arm Plates

The arm was assumed to be a cantilever with two parallel plates.

Lower Arm

Load at the end of the lower arm = weight of the gripper assembly + weight of motor + self-weight of M-12 Screw + weight of sprockets, collars = 3.5 kg.

Maximum Bending moment of each plate 'M' = 41.5 kg cm.

The required minimum thickness of the plate was found using the relation.

$$M/Z = f_s$$

f_s - Allowable shear stress for Al = 525 kg/cm²

A factor of safety of 1.6 was taken.

$$f_s = \frac{M}{Z}$$

$$Z = bd^2/6 \quad b = 60 \text{ mm}$$

$$41.5/6/6 \times d^2 = 525/1.6, \quad d = 3.5 \text{ mm}$$

Since this Robot is an experimental open structured robot in order to accommodate the bearings, gears and chain sprockets a plate width of 60 mm was selected.

Upper Arm

Considering the loads on the upper arm, the maximum Bending moment on each plate of the arm 'M' = 82 kg cm. The Thickness of plate was taken as, 4 mm. Available standard sizes in the market are 5 mm and so 5 mm thick plates were used.

Shaft Design

Shoulder Shaft

Loads acting on the shaft are:

$$\text{Maximum moment} = 7 \times 20 + 1.3 \times 10 + 6.5 \times 20 = 283 \text{ kg cm.}$$

The shaft diameter was obtained using the relation,

$$\frac{\pi}{16} \times f_s \times d^3 = M \frac{\pi}{16} \times \frac{520}{2} \times d^3 = \sqrt{1^2 + 98^2}$$

$$d = 1.3$$

The diameter of the shaft = 1.3 cm.

Elbow Shaft

Maximum moment 'M' = 104 kg.cm

The torque on the shaft 'T' = 2 kg cm.

The shaft diameter was found using the relation,

$$\frac{\pi}{16} \times f_s \times d^3 = \sqrt{M^2 + T^2}$$

$$\frac{\pi}{16} \times 525 \times d^3 = \sqrt{104^2 + 2^2}$$

The diameter's' = 1 cm.

Since there is radial as well as axial load on the bearings, it should be of a deep groove type. But, as the smallest deep



groove ball bearing available is 15 mm inner diameter, both the shafts are designed to suit the bearings.

Table 1: Torque and Gear Reduction of Axes

Axes	Torque (kg cm)	Gear Reduction
Gripper rolling	4	1:2
Gripper linear movement	4	1:2.9
Elbow	4	1:2
Shoulder	4	1:8

Source: Experimental Data.

Gears: Gear Specifications are given in Table 1.

Gear I

Module ‘m’ = 1.25 mm
 Centre distance ‘a’ = 70 mm
 Total number of teeth ‘z’ = 112
 Face Width = 10 mm.

Gear II

Module = 1.25 mm
 Face Width = 10 mm
 Centre distance = 90 mm
 Total number of teeth = 144.

Checking Face Width for Load

$$\sigma_b = \frac{i+1 [Mt]}{a.m.b.y}$$

i - reduction ratio = 2
 y - Lewis Form Factor

$\sigma_b = 71 \text{ kg/cm}^2$ which is less than 360 kg/cm^2 for Nylon.

Base: The researcher has designed a trapezoidal base weighing 12 kg to counter balance the whole unit and to give stability.

Control Systems

Computers play an important role in control systems. The main objective of using computer in control is to replace as much of the conventional hardware with software and to simply existing hardware.

Micro Computer

The microcomputer used is PC.

Hardware Details

1. System unit
2. Disk drives

3. Display
4. Keyboard
5. Other peripherals.

System Unit

This is the Heart and Brain of the PC as shown in Figure 1.

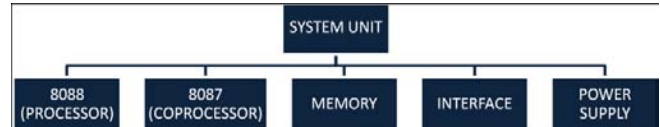


Fig. 1: Representation of PC System Unit

The microprocessor 8088 can be efficiently used to give a sequence of pulses to rotate the stepper motors either clockwise or counter clockwise direction. So, the micro-processor generates two inputs (i) the pulses which cause phase excitation (ii) a direction signal which determines the sequence of excited phases and therefore the direction of rotation of stepper motor. By mechanical design, we made these rotations to move the various parts of the robot to pick and place the object. However to get proper speed we have to introduce delay between any two pulses. During this delay the microprocessor simply wastes time doing no useful work.

Micro Computer Interfacing

Any microprocessor based system design involves interfacing of the processor with one or more peripheral devices for the purpose of communication with the environment one such single device is PPI 8255.

In this system, IBMPC/XT AT are used. Compatible digital/output add on card. This has 4 numbers of 8255 residing on it. 8255 is a flexible interface chip for parallel input/output devices such as displays and other equipment.

Each 8255 IC consists of three parts of 8 bit PA, PB and PC port. The PC port may also be used as two half ports of 4 bits, PC upper (PC 4–7) and PC lower (PC 0–3). Each of these ports and half ports can be configured as an input as an output port by a software control.

Data is transferred between Micro processor and PPI on (D0–D1) data lines. RD and WR signals are used for indicating to the 8255 whether a read or write operation is being performed. Before doing this the 8255 chip must be selected using CS (Chip Select) input.

Power amplification is necessary to excite the motor coils from the digital logic level signals. So, an interface circuit is needed between the motor and 1/2 microcomputer port. This can be provided by a Darlington pair which has high current gain.



A, B, C, D 4 line of output port of 8255 (PA0-PA3)

Red, Orange, Blue, Green Leads of Stepper Motor for Phase 1 and Phase 2 winding.

White Supply (from the power supply circuit).

Power Supply

This unit needs a voltage +12V dc to actuate the stepper motor. Therefore the 240 ac supply is first stepped down to (0–15V) by a transformer and then passed through a bridge rectifier, where we get rectified D.C. voltage. Furthermore it is filtered and +12 dc is obtained which is now fed to the stepper motor. Since this is an open loop system, there is always a possibility of error in it. This can be improved by having feedback. Improvisation can be done by having vision, and tactile sensors.

Further Developments that can be Made in the Robot

This experimental robot which is of SCARA configuration is mainly intended for assembly operations. Especially in Automotive and Electronics Industries where the parts to be handled are minute and delicate handling becomes easier. For any future developments our robot is flexible to take up the modifications. Welding: By inserting a welding head it can perform operations like spot welding, fusion welding. By replacing the welding head by a cutting torch it is also possible to achieve flame cutting under robot control path control is required for the purpose. The gripper can also be replaced by a magnetic gripper. The single gripper can be replaced by multi grippers and it is used where the task is short in relation to the end effector change time. This design incorporates a number of grippers, tools or sensors within a single end effector. They are provided on a rotatable turret which can be indexed to bring any individual element into position.

Testing

On completion of Fabrication the experimental robot was assembled and tested for working. The motors were run and tested for the specified speed. The Gripper assembly was tested and the following results were inferred. The Gripper opening and closing was found to be 0–35 mm.

The roll of the Gripper was 360°. For every revolution of the gripper the M-12 screw advanced by 1.7 mm (pitch) giving the vertical linear movement of the gripper. Next the rotations at the axes were examined and the rotation of the elbow axis was found to be equal to 255° and at the shoulder axis 360° rotation was obtained. The gripper was found to grip a load of 1 kg as shown in Figures 2, 3 and 4 where the robot is carrying a calculator.

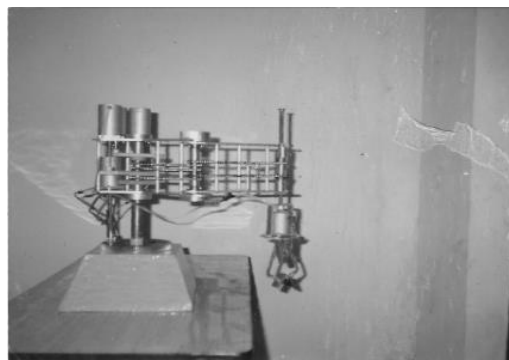


Fig. 2: Front View of the Mechro

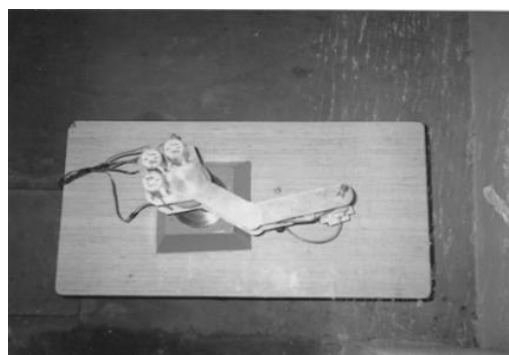


Fig. 3: Top View of the Mechro



Fig. 4: Mechro Holding a Calculator

Conclusion

Accuracy is the difference between the measured value and the command value of a specified position in the robot's work space. Position accuracy is measurable by making a series of measurements of the difference between the actual position and desired position of the manipulator. Assume the robot is command to move 20 inches and the actual move is



measured and found to be 19.99 inches. The error is ± 0.01 inch and can be represented as an accuracy error of 0.05% less than the commanded distance. Repeatability is a measure of the spread of positions in a series of attempts to position the manipulator at a fixed location. Good repeatability is the ability to repeat the same position several times within a specified tolerance. Repeatability is a more important consideration than accuracy. Both short-term and long-term repeatability exist. Long-term repeatability is of concern for robot applications requiring the same identical task to be performed over several months. Over a long time period, the effect of component wear and aging on repeatability must be considered. For many applications where the robot is frequently reprogrammed for new tasks, only short-term repeatability is important. To conclude the designed and fabricated robot was tested and found that the payload capacity is maximum of 1 kg for example as per Fig. 14 the MECHRO is carrying a calculator. Hence this robot will carry a payload of maximum 1 kg for the light automotive components up to maximum of 1 kg and for electronic component assembly industry up to 1kg unless like the commercially SCARA robot available in the market e.g., KUKA, EPSON, DENSO, TOSHIBA, MTAB INDIA etc.

The novelty of this robot is low cost where the stepper motor is used for the applications of high accuracy and repeatability with slower speed. The robot is designed with a trapezoidal base weighing 12 kg to counter balance the whole unit and to give stability. The payload to weight ratio and power to payload ratio is high like other robots. This robot withstands vibration ensuring structural buckling and payload stability is also high. The motion of two jaws is only linear and will open upto 35 mm.

References

- [1] Jones, Barry Leatham (1987). Elements of Industrial Robotics, Pitman Publishing, London, p. 3.
- [2] Groover, Mikell P.; Weiss, Mitchell; Nagel, Roger N. and Odrey, Nicholas G. (1986). Industrial Robotics, Technology, Programming and Applications, Mc Graw Hill International Editions, New York, pp. 10–11.
- [3] Schilling, Robert J. (2007). Fundamentals of Robotics, Prentice Hall of India Private Limited, New Delhi, p. 6.
- [4] Srinivas, J., Dukkupati, R.V. and Ramji, K. (2009). Robotics, Control and Programming, Narosa Publishing House, New Delhi, p. 24.
- [5] Saha, S.K. (2008). Introduction to Robotics, Tata Mc Graw Hill Education Private Limited, New Delhi, p. 28.



The Use of a Multilevel Arrangement for Photovoltaic Power Generation

Antariksha Sarkar¹ and Bidyut Kumar Bhattacharyya²

Abstract: Existing solar power generation systems, especially of the photovoltaic type, have limited efficiency owing to their stationary implementation. A simple observation of the most efficient natural solar harvesters, i.e. plants and trees, indicates a more optimized structural layout for capture of photon packets. They also exhibit heliotropism/ phototropism (solar-tracking). An amalgamation of these features into a solar-array support structure have been pursued to various degrees in the past to obtain varying degrees of success. A novel structural design has been proposed in this study to maximize solar power generation while optimizing efficiency and reliability. Simplicity of structural erection and cost effectiveness are other important parameters of this study.

Keywords: Solar Energy, Photovoltaic, Solar Thermal Energy (STE), Tracking, Concentrated Solar Power (CSP).

Introduction

Human beings have been using solar energy since the dawn of civilization. Almost all the different forms of energy available on earth ranging from geothermal energy to fossil fuels can be attributed to being converted from solar energy. Rapidly deteriorating global climatic conditions necessitate the use of cleaner energy sources. Unprecedented development in human trade and commerce resulted in several uneconomical practices in the past century. Although mechanization and automation has brought much comfort to our lives, it has come at the cost of social irresponsibility. This has consequently resulted in a great economic and social rift, both of which can be traced to widely varying standards of living and energy usage.

Renewed research interest in various applications of solar energy towards the beginning of the twentieth century has expanded the horizons of use of solar energy [1]. Newer approaches to harvesting solar energy include the use of silicon based electronics (photovoltaic), concentrating solar heat and thermal absorption systems. Alternatively, vapor absorption type refrigeration systems have been designed [2] wherein solar heat is used as the heat source for evaporative media at the absorption side. Sufficient technology has been available since the middle of the twentieth century to energize residential homes entirely through solar energy, complete with heating, cooling and electricity [3]. Yet, costs have remained prohibitively high and this has been the

primary deterrent for implementation of alternative locally generated energy unto the present day. Integration of alternative energy sources for application in residential complex also requires considerable forethought and advanced (sometimes uncommon) methods of construction. This again comes at added expenses. Besides, the limited availability of alternative energy (varying by climate or geography) and low conversion factors result in minimal amounts of available energy which is suitable only for very small families with moderate energy requirements. Notwithstanding these limitations, however, most governments have recently opted to provide reward programs to citizens who choose to become energy independent through local generation. These programs will help offset the initial high investments and may become profitable if the reward programs are extended over long periods. Thus a clear motivation can be established in the development of alternative energy systems that have higher conversion factors and demand less initial investments per unit of energy.

Design and Construction

Among the systems that have already been commercially adopted, photovoltaic energy production is the most prevalent commercial form [4] and therefore added concentration should be laid on the enhancement of the design and deployment of solar cells. Three research areas

¹Department of Mechanical Engineering, NIT, Agartala, Tripura-799055, India.

✉ antariksha106@gmail.com

²Professor, Department of Electrical Engineering, NIT, Agartala, Tripura-799055, India.



can be earmarked for primary focus in this field, the first being the receptivity of the solar cells, in other words, the efficiency of conversion of photons to electricity. The second objective is to ensure optimal incidence of the solar radiation on solar cells at all times of the day, which can be achieved through tracking. The third objective, which is important from the perspective of the economy, is the reduction in deployment area since solar photovoltaic farms need to occupy very large spaces, more so where the energy potential is low (which decreases with proximity of location to the poles). Keeping these important design considerations in mind, a novel design approach was considered instead of pursuing a line of investigation based on existing design standards. The integration of existing commercially available elements into the design would be considered an obvious benefit as it would negate the requirement for special manufacturing techniques. In this article, the proposed prototype obtained after several iterations of design study has the following key components:

1. A central trunk (Figure1) that acts as the backbone of the multi-level system and provides single degree of freedom (Figure1) in the vertical (z) rotary axis to facilitate azimuthal tracking (following sun from east to west).
2. Rigid extensions called branches (Figure1) from the central trunk of varying lengths placed at strategic angles in the horizontal plane to eliminate shadows from upper levels.
3. Support stands above the branches (Figure 1) to hold the photovoltaic panels (Figure 1) and provide single degree of freedom in the horizontal (x) rotary axis for individual zenith tracking (since incidence angles vary slightly from lower to upper members of the tree).
4. Guided translation along the branches (Figure 2) for individual stand supports to eliminate shadows created by external objects.

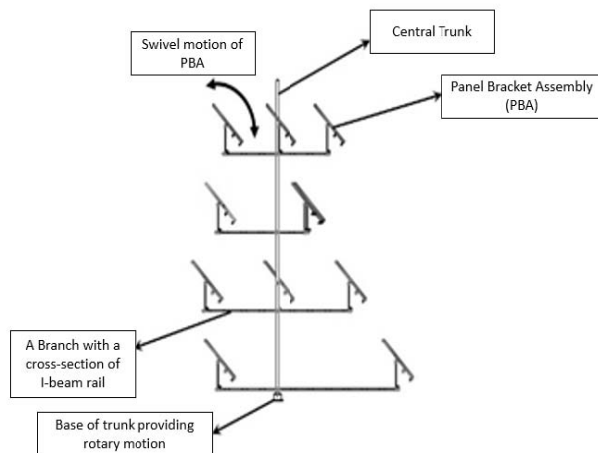


Fig. 1: Side View Showing Components of the Solar Tree

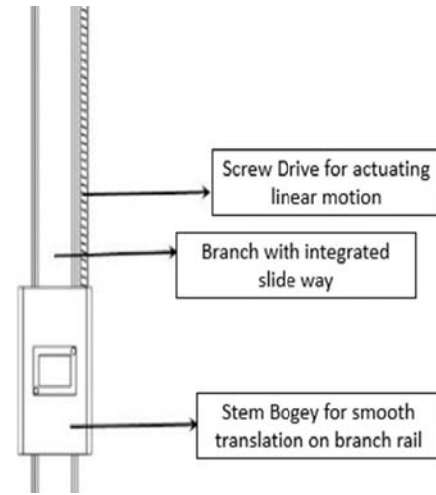


Fig. 2: Diagram for Translation along Branch

A more detailed discussion of the design should be undertaken at this point to elucidate finer points of the design. The central load supporting vertical structure, the trunk, is capable of rotating from east to west, thereby providing the capability of azimuthal solar tracking. The base of the trunk is a thrust bearing which carries the load of the tree structure as well as provide rotary motion to the trunk via a gear/belt drive. The controlling drive motor is supervised by the central control network. In a farm deployment with multiple installations, all trunks are to be rotated by equal angles from their initial position depending on the shift of solar position.

The branches are extended members that pan out from the central trunk and are distributed at equal radial intervals to form circular symmetry in such a way that they cover minimal area when viewed from the top plane. This ensures that more tree structures can be deployed when land space is limited. Branches are further divided into layers. A four layer structure is chosen for optimal weight to power generation ratio. Each layer consists of three branches spaced 120° apart. The layers themselves are radially shifted from the adjacent layer by 30° , so the total angular displacement from top to bottom layers is 120° and this design ensures complete non-overlap and thereby guarantees zero shadow formation for an individual tree. This arrangement has the added advantage of being dynamically balanced due to equally displaced end loads. In case of multiple number of trees being deployed on a single large farm, the trees have to be spaced in a diamond pattern to eliminate the formation of shadows and structural interference. Such an arrangement will augment land usage and minimize (vertical) space wastage. Additionally, if this installation is deployed in city streets near buildings where they may be overshadowed by external factors, a linear motion guide motor arrangement is to be provided on a per-branch basis so that the panel support structure (the stem)

may translate to a brightly illuminated position away from the shadows. Each branch holds a panel bracket assembly supported by a stand called the stem. Each panel bracket may hold multiple solar panels, the number of panels restricted to the total weight supported by each branch. The panel bracket assembly has a hinge at its back and is hinged to the stem (Figure 3). The hinge allows rotary motion via gears (Figure 3) which makes zenith tracking possible. Since each branch is at a different height, the tilt angles on zenith trackers at the upper levels of the structure are compensated marginally, thus making it possible to track the vertical shift of the sun with all the panels correctly. Viewed from the reference point of the sun, the entire tree structure would look like a flat surface at all times during the solar day (Figure 4), and this is the reason for maximum generation output. Due to the inherent tendency of the system towards phototropism, it may also be effectively deployed for solar-thermal applications. However, due to the flat nature of the incidence surface, it cannot be applied to concentrator systems.

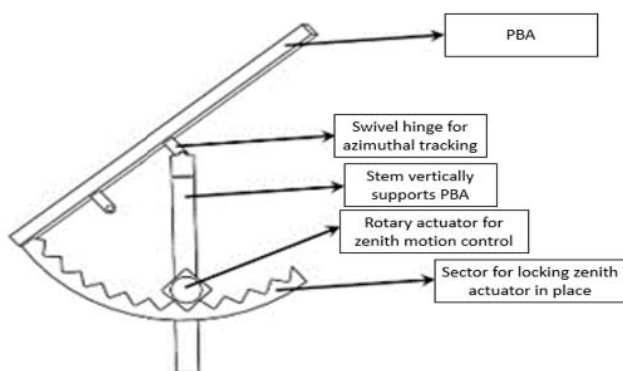


Fig. 3: Detailed Diagram Showing Layout of Components for Zenith Tracking

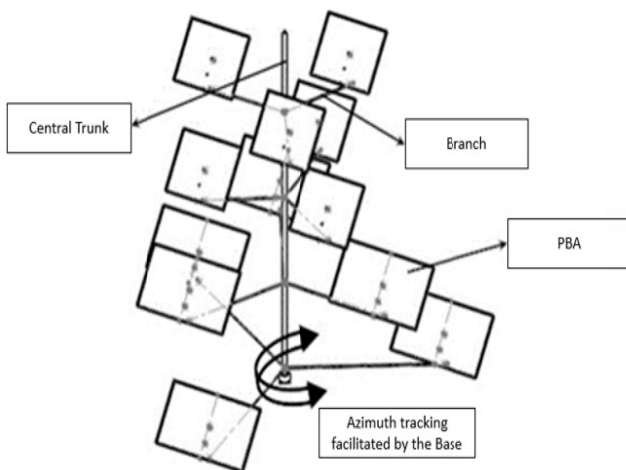


Fig. 4: The Complete Multi-Level Solar Tree Structure (Note the single actuator for azimuthal tracking)

The primary control unit may be programmed temporally, since the rotation speed of the earth is uniform. Analyzing historical weather data, it is possible to surmise the correct azimuth and zenith angles of the sun. Nevertheless, a more optimal method for tracking the sun during partially cloudy weather could be achieved with a bank of photo resistive sensors to provide real-time feedback for actual brightness. Instead of deploying separate control leaders to separate trees, a unified approach could be taken, wherein, a central control supervisor would provide necessary actuation data to all the structures, thereby enhancing reliability by reducing elements of failure, and subsequently reduce the costs of deployment.

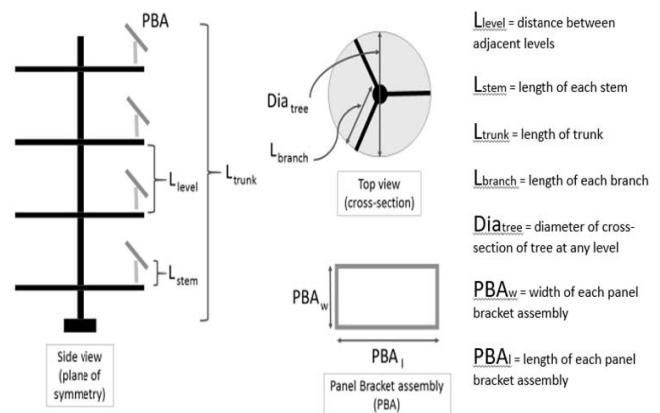


Fig. 5: Conceptual Tree Layout Showing Critical Dimensions

The significant variables to be considered for the design are illustrated (Figure 5) along with the conceptual diagram of the structure. Proportionate scaling of these variables will result customized dimensioning for individual applications.

Economic Ramifications

Although a thorough study on the cost-effectiveness of the design needs to be done from a commercial perspective, initial design review has ensued in very encouraging results. Independent studies have found that implementation of solar tracking enhances the efficiency of each panel by about 25% to 40% depending on geographical location [5]. One must bear in mind that each panel needs to be separately controlled in conventional trackers, thereby consuming more energy for the entire tracking-equipped power station. The aggregation of multiple panel systems into one structure will result in higher efficiencies due to reduced power consumption by the system. In the proposed design study, the total space utilized compared to an equivalent fixed structure was 41.67% only, effectively meaning that the use of the proposed structure would result in 58.33% better land utilization and cut the cost of land required by the same amount. Alternatively, deployment of such superstructures



would result in progressively better economic performances with the magnitude of the scale of deployment.

Future Scope

Implementation of flexible photovoltaic material (organic and lightweight) to the branches and trunk (stems remain under the permanent shadow of panel bracket assemblies) can add considerably to the total output of the system while successfully mimicking photosynthesis of green stems of plants. Prohibitive costs of these systems has rendered testing and experimentation of such advanced photonics beyond the scope of this project. At present, flexible photovoltaic arrays recuperate far less energy per unit area compared to rigid arrays, nevertheless steady improvements in electrical design means that once they match or surpass the generation capabilities of rigid arrays, the entire tree structure can be deployed with these innovative receptors. Doing so will come with the added benefit of a greater degree of flexibility by positioning individual receptors more easily to replicate the behavior of phototropic leaves while consuming significantly less energy per motion actuation.

Conclusion

In this study, an enhanced structural design was proposed for implementation on photovoltaic power generation systems.

The primary benefits obtained by the application of this design is reduction of space per unit of generated power and enhanced generation capabilities per panel. Additionally, due to the compactness and high output capabilities, these structures can now be deployed individually for local generation, i.e. inside traffic circles or by roadsides. Implementation of such structures is a way of achieving energy independence in remote areas near the equatorial region, where these systems will be most effective.

References

- [1] Green, M.A., Solar cells: Operating principles, technology, and system applications, 1982.
- [2] Kim, D. and Ferreira, C.L., Solar refrigeration options—A state-of-the-art review. *International Journal of refrigeration*, 2008, 31(1): pp. 3–15.
- [3] MIT, History, Solar1. SOLAR 7 1939 [cited 2016 September 19]; Available from: <http://web.mit.edu/solardecathlon/solar1.html>.
- [4] Dincer, F., The analysis on photovoltaic electricity generation status, potential and policies of the leading countries in solar energy. *Renewable and Sustainable Energy Reviews*, 2011, 15(1): p. 713–720.
- [5] Rizk, J. and Chaiko, Y. Solar tracking system: more efficient use of solar panels. in *Proceedings of World Academy of Science, Engineering and Technology*, 2008. Citeseer.



Surface Roughness and Tool Wear Optimization in Hard Turning Using Taguchi Based Utility Concept during Comparative Assessment of Inserts

K. Venkata Subbaiah¹, Ch. Suresh¹ and Ch. Raju²

Abstract: The present experimental analysis aims to compare the conventional cutting inserts with wiper cutting inserts during the hard turning of AISI 4340 steel and estimating the optimum machining parameters using Taguchi based utility concept. Type of insert, hardness, cutting speed, feed, and depth of cut are taken as process parameters. Taguchi's L18 orthogonal array was used to conduct the experimental tests. Parametric analysis carried in order to know the influence of each process parameter on the three important Surface Roughness and tool wear. Taguchi based utility concept used to optimize the process parameters for individual response and multi-response outputs. Finally ANOVA concept is employed on multi SN ratio to find out the relative significance of machining parameter in terms of their percentage contribution.

Keywords: Hard Turning, AISI 4340 Steel, Surface Roughness, Tool Wear, Wiper Ceramic Insert, Utility Concept.

Introduction

Present manufacturing industries ultimate aim is to produce high quality products at low cost to stand in highly competitive manufacturing industries. Hard turning is becoming the prime option for steels to turn at hard state (45-65) as it has several benefits over conventional turning methods of machining and grinding. It reduces the machining time about 60% of conventional hard turning time, even at a lower depth of cuts and feed rates [1].

Surface roughness characteristics are important to the functionality of machined components; hence due to the understanding the surface generation mechanisms the manufacturing industries are able to improve the durability of their machined components. Tool wear is also prime machining parameter as it directly related to manufacturing cost and surface to be generated. As a result, a large number of investigations have been conducted to determine the effect of parameters such as feed rate, tool nose radius, cutting speed, and depth of cut on machining parameter. Kopac *et al.* [2] state that, an increase in cutting speed results smoother surface with ceramic inserts. Noordin *et al.* [3] find the feed was the most significant factor for surface roughness, while hard turning of AISI 1045 steel bars with coated carbide. Thamizhmanii *et al.* [4] confirm that the depth of cut is the important parameter and cutting speed had less influence on

surface roughness. Boucha *et al.* [5] conduct an experimental study with the CBN tool in the view of tool wear and cutting forces at various levels work piece hardness and cutting speeds. Ohtani and Yokagawa [6] stated that the main wear mechanism of CBN and ceramic tools is due to abrasion.

Optimization of process parameters is an essential criterion during the manufacturing to acquire high quality. Generally, the Taguchi method is the best option for optimize process parameters to achieve high quality [7, 8]. However, an application of Taguchi is limited to the optimization of a single performance characteristic [9]. In the present investigation, a multi characteristics optimization model based on Taguchi based utility concept has been used for multi response optimisation.

Experimental Setup

Work Piece Material

The work piece material was AISI 4340 steel as round bars of 30 mm diameter and an axial length of 150 mm. The synthesis of material is 0.38% C, 0.228% Si, 0.609% Mn, 0.95% Cr, 1.5% Ni, 0.22% S, 0.226% Mo and 0.026% P. AISI 4340 harden steel has numerous applications in automobile industry such as parts like axles, gears, camshafts, driving pinion, link parts, etc. The work piece

¹Department of Mechanical Engineering, Andhra University, Visakhapatnam-530003, India.

²Department of Mechanical Engineering, Govt. Polytechnic, Narsipatnam, Andhra Pradesh-530003, India. ✉ chraju99@gmail.com



shown in Figure 1 of AISI 4340 steel was firstly hardened took after by oil quenched to attain a hardness of 50 HRC [10, 11]. A rough turning pass was directed at first to eliminate the run out of the work piece, after that diameter obtained for experimentation is roughly 25 mm.



Fig. 1: Workpieces at Different Hardness



Fig. 3: Mitutoyo Surface Tester

Experimental and Measurement Apparatus

The hard turning of the work piece in dry turning conditions was directed on A high-speed precision CNC Lathe (shown in fig 2), Jobber XL Make, Model NH 22 having following specifications: Maximum Power: 7.5 HP, Spindle speed: 5000 RPM. The cutting insert used is wiper ceramic inserts mixed ceramic designation of GC6050 WH. The nose radius is constant 0.8 mm supplied by the manufacturer. The cutting inserts were clamped on the tool holder (make: Sandvik coromat, model: PCLN L 2525 M12). The surface roughness of the turned examples was measured with Mitutoyo make surface roughness analyzer shown in figure 3, with a cut-off length of 0.8 mm over three sampling lengths. The average value of surface roughness was utilized to measure the roughness accomplished on machined surfaces. The width of tool flank wear (V_b) was measured by using a Nikon optical microscope which is connected to a digital camera and computer.

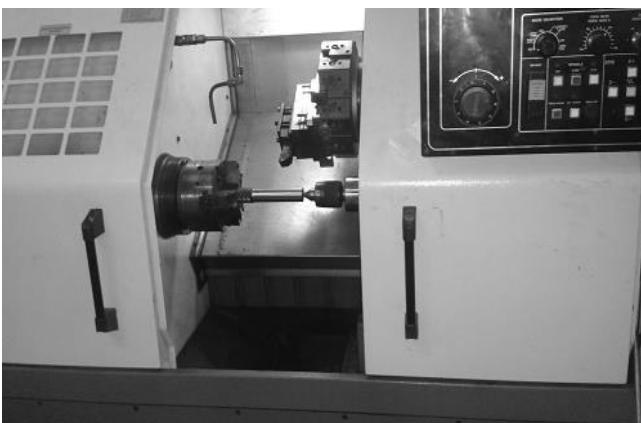


Fig. 2: CNC Jobber XL Lathe

Methodology

Taguchi Method

The Taguchi method is a commonly adopted approach for optimizing design parameters by the application of statistical and engineering concepts. An OA is a small set from all possibilities which helps to determine least no. of experiments. To obtain optimum process parameters setting, Taguchi proposed a statistical measure of performance called signal to noise ratio. In addition to S/N ratio, ANOVA is used to indicate the influence of process parameters on performance measures. Taguchi's L18 Orthogonal Array (OA) is chosen as the experimental design in the present research as mixed levels were presented in the selected process parameters. Table 1 presents the selected levels of cutting speed, feed, and depth of cut levels were preferred within the intervals prescribed by cutting tool's manufacturer. Table 2 presents the L18 OA corresponding responses of R_a and V_b .

Table 1: Process Parameters and Ranges

Parameter	Levels		
	1	2	3
Insert (I)	con	wiper	-
Hardness (H)	45	50	55
Cutting Speed (V_c)	140	180	220
Feed (f)	0.1	0.2	0.3
Depth of cut (A_p)	0.1	0.2	0.3



Table 2: Experimental Results

Sl. No.	I	H (HRC)	V _c m/min	F _s mm/rev	A _p mm	R _a μm	V _b μm
1	CON	45	140	0.1	0.1	1.06	35
2	CON	45	180	0.2	0.2	1.07	55
3	CON	45	220	0.3	0.3	1.38	85
4	CON	50	140	0.1	0.2	1.26	40
5	CON	50	180	0.2	0.3	1.44	70
6	CON	50	220	0.3	0.1	1.59	60
7	CON	55	140	0.2	0.1	1.43	65
8	CON	55	180	0.3	0.2	1.58	58
9	CON	55	220	0.1	0.3	1.38	90
10	WIPER	45	140	0.3	0.3	0.54	50
11	WIPER	45	180	0.1	0.1	0.54	34
12	WIPER	45	220	0.2	0.2	0.51	60
13	WIPER	50	140	0.2	0.3	0.57	50
14	WIPER	50	180	0.3	0.1	0.61	44
15	WIPER	50	220	0.1	0.2	0.30	40
16	WIPER	55	140	0.3	0.2	0.67	50
17	WIPER	55	180	0.1	0.3	0.62	70
18	WIPER	55	220	0.2	0.1	0.69	75

Utility Concept

Quality is the important attribute, which is used to evaluate product by customers. This quality is controlled and improved for their products more acceptable by customers. In other view based on number of dissimilar objective customers evaluated a product performance. A composite index is achieved by combination of various evaluated attributes for improving the rational decision making. This composite index is known as utility of a product. The summation of utilities of each objective indicates the overall utility of a product.

According to the utility theory X_i is the measure of effectiveness of an attribute (or quality characteristics) i and there are n attributes evaluating the outcome space, then the joint utility function can be expressed as:

$$U(X_1, X_2, \dots, X_n) = f(U_1(X_1), U_2(X_2), \dots, U_n(X_n)) \quad \dots (1)$$

Here, $U_i(X_i)$ is the utility of the i^{th} attribute. The overall utility function is the sum of individual utilities if the attributes are independent, and is given as follows:

$$U(X_1, X_2, \dots, X_n) = \sum_{i=1}^n U_i(X_i) \quad \dots (2)$$

The overall utility function after assigning weights to the attributes can be expressed as:

$$U(X_1, X_2, \dots, X_n) = \sum_{i=1}^n W_i U_i(X_i) \quad \dots (3)$$

where, $\sum_{i=1}^n W_i = 1$ and W_i is the weight assigned to the attribute i . The sum of the weights for all attributes must be equal to 1. The overall utility function is of the “larger-the-best” type characteristics. When utility function is maximized, the objective functions are considered to be optimized.

Results and Discussion

Analysis of Variance for Single Responses

ANOVA results from Tables 3 & 4 used to establishing the significance of the process parameters on response parameters. Statistical significance of any process parameter on the response is considered only when its P-value is lower than 0.05 [21]. All this analysis is carried at 95% confidence level ($\alpha = 0.05$).

It is seen in Table 3 that the process parameters Insert, H, and F are significant sources on average Ra, as their P-value is less than 0.05. Type of insert is the most significant factor on Ra as its F-value is 210. From Figure 2, Main effects plot of data means reveals that wiper insert produces fine surface finish compared to the conventional inserts. It is also confirmed from the Table 3 and Figure 4, both H and F shows only moderate influence on Ra. However, cutting speed and depth of cut does not show any statistical significance on Ra as their F-values are 0.44 and 1.16, the same is also confirmed from the Figure 6 as they produce almost horizontal lines on main effect plots of Ra.

Table 3: Analysis of Variance for Ra

Source	DF	Seq SS	F	P	%C
INSERT	1	2.82665	210.59	0	87.40
H	2	0.13582	5.06	0.038	4.20
Vc	2	0.01173	0.44	0.661	0.36
F	2	0.1218	4.54	0.048	3.77
Ap	2	0.03121	1.16	0.36	0.97
Error	8	0.10738			3.32
Total	17	3.23458			

ANOVA results for the V_b presented in Table 4 shows H, V_c and A_p are the most significant factors on V_b , as their P-value is less than 0.05 and their F-values are 22, 26 and 37 respectively. Figure 5 shows main effects plot of data means for V_b , it is observed that wiper insert shows good performance over conventional ones and higher feed rates reported with higher levels of H, V_c and A_p . However, feed



rate does not show any significance on V_b , however, lower V_b values are reported at higher levels of feed rates.

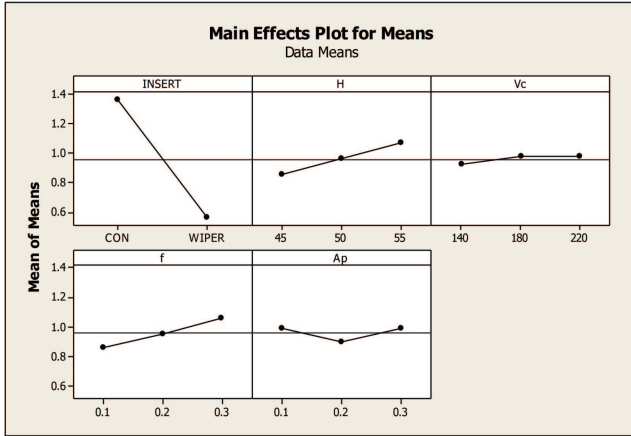


Fig. 4: Main Effects Plot of Data Means for R_a

Table 4: Analysis of Variance for V_b

Source	DF	Seq SS	F	P	%C
INSERT	1	401.39	17.22	0.003	8.87
H	2	1053.44	22.6	0.001	23.27
Vc	2	1240.11	26.61	0	27.39
F	2	365.78	7.85	0.013	8.08
Ap	2	1280.44	27.47	0	28.28
Error	8	186.44			4.12
Total	17	4527.61			

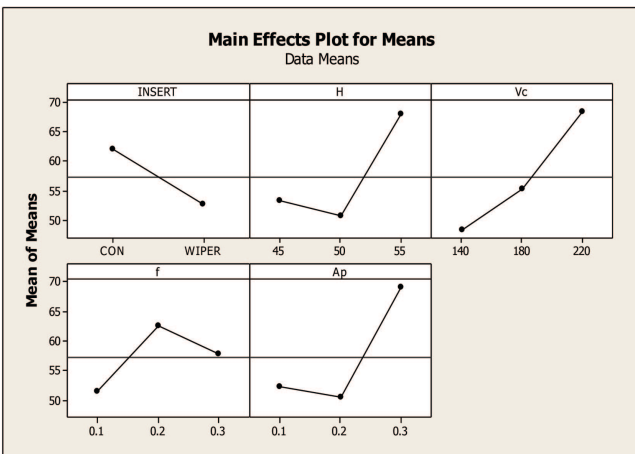


Fig. 5: Main Effects Plot of Data Means for V_b

Multi Response Optimization

The objective of the present work is to minimize surface roughness and tool wear in hard turning process optimization. In this paper, the following algorithm is suggested based on Taguchi's technique and utility concept.

1. Use the Taguchi matrix experimental design and analysis to find out the optimal value of each of the selected process responses.
2. Construct a preference scale for each response based on their optimal value and minimum acceptable level (Eqs. 4 & 5).

$$\dots (4)$$

$$\dots (5)$$

3. Assign weights (W_i) based on the experience and customer preference, keeping in view that the total sum of weights is equal to 1 such that the (Eq. 6).

$$\dots (6)$$

4. Find overall utility values for different experimental trial conditions considering all the responses involved in multi-response optimization (Eq. 7). Table 6 shows the overall utility values.

$$U = \sum_{i=1}^n W_i P_i$$

5. Use the values determined in step 4 as raw responses of different trial conditions of the experimental matrix. If trials are repeated, find S/N ratios (HB type), as the utility is a higher-the-better type characteristic.
6. Analyze the results as per the standard procedure suggested by Taguchi.
7. Find the optimal settings of process parameters for mean and S/N utility based on the analysis performed in step 6.
8. Predict optimal values of different response characteristics for the optimal parametric setting that maximizes the overall utility as determined in step 7.
9. Conduct confirmation experiments to verify the optimal results.

The utility values obtained as per the above equations are reported in Table 5 and it indicate the overall utility for minimum surface roughness and tool wear and highest overall utility value is obtained at I2, H2, V_{C3} , F1, Ap2 levels. Figure 6 shows the multi response main effects plot for SN ratio (surface roughness and tool wear). The values for process parameters that results in optimized value of R_a (optimized) and V_b (optimized) using utility concept are at INSERT = Wiper, H = 45 HRC, $V_c = 220$ m/min, $f = 0.1$ mm/rev, $A_p = 0.2$ mm.



Table 5: Utility Data Based on Response Characteristics

S. No.	USR	UTW	U overall
1	2.19	8.73	2.73
2	2.14	4.55	1.67
3	0.76	0.53	0.32
4	1.24	7.49	2.18
5	0.55	2.32	0.72
6	0.00	3.75	0.94
7	0.58	3.01	0.90
8	0.02	4.06	1.02
9	0.75	0.00	0.19
10	5.83	5.43	2.81
11	5.79	9.00	3.70
12	6.10	3.75	2.46
13	5.50	5.43	2.73
14	5.20	6.61	2.95
15	9.06	7.49	4.14
16	4.63	5.43	2.52
17	5.05	2.32	1.84
18	4.48	1.68	1.54

ANOVA results for the overall utility presented in Table 6 shows all process parameters are significant factors as their P-value is less than 0.05. Type of insert used for the hard turning is the most influencing parameter for this model and its F-value is 85. The contribution of type of insert is 50% on the overall utility model and hardened is also shows its contribution for this multi response parameter.

Table 6: Analysis of Variance for Utility

Source	DF	Seq SS	F	P	%C
INSERT	1	10.9329	85.16	0	49.77
H	2	3.5743	13.92	0.002	16.27
V _c	2	1.5355	5.98	0.026	6.99
F	2	2.2596	8.8	0.01	10.29
A _p	2	2.6381	10.27	0.006	12.01
Error	8	1.0271			4.68
Total	17	21.9675			

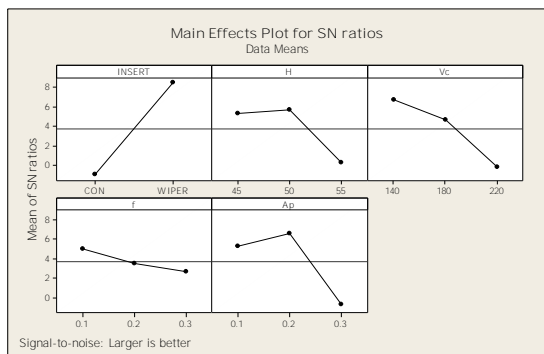


Fig. 6: Main Effects Plot of SN Ratios for Utility

Conclusion

- Type of insert is the most significant factor on surface roughness (R_a) and hardness and feed show moderate influence only.

- Depth of cut is the most significant factor on tool wear (V_b) and hardness and feed show moderate influence only.
- ANOVA results of overall utility, for multi-response optimization, Type of insert, is most significant controlled factor followed by Hardness.
- Hard turning with wiper inserts provides lower values surface roughness which is comparable with the grinding, i.e. R_a = 0.30 μm.
- Main effect plots confirms that wiper inserts shows their overall superiority over conventional one in both surface roughness and tool wear.
- The present work may be extended to study the influence of wiper inserts and hardness on other responses like tool wear, tool life and cutting forces, etc. under different cutting environments.

References

- [1] Huddle, D., “New Hard Turning Tools and Techniques Offer a Cost-effective Alternative to Grinding”, Tooling and Production Magazine (2001).
- [2] Kopac, J., Bahor, M. and Sokovic, M., “Optimal Machining Parameters for Achieving the Desired Surface Roughness in Fine Turning of Cold Pre-Formed Steel Work pieces”, *International Journal of Machine Tools and Manufacture*, 42 (2002), 707–716.
- [3] Noordin, M.Y., Venkatesh, V.C., Sharif, S., Elting, S. and Abdullah, A., “Application of Response Surface Methodology in Describing the Performance of Coated Carbide Tools When Turning AISI 1045 Steel”, *Journal of Materials Processing Technology*, 145 (2004), 46–58.
- [4] Thamizhmanii, S., Saparudin, S. and Hasan, S., “Analyses of Surface Roughness by Turning Process Using Taguchi Method”, *Journal of Achievements in Materials and Manufacturing Engineering*, 20(1), (2006), 503–506.
- [5] Boucha, K., Yaltese, M.A., Mabrouki, T. and Rigal, J.F., Statistical analysis of surface roughness and cutting forces using Response Surface Methodology in hard turning of AISI 52100 steel with CBN tool, *Int. J. Refract. Met. Hard Mater.* 28 (2010), 349–361.
- [6] Ohtani, T. and Yokogawa, H., The effects of workpiece hardness on tool wear characteristics, *Bull. Jpn. Soc. Precis. Eng.*, 22(3), (1988) 229–231.
- [7] Ross, P.J., Taguchi techniques for quality engineering, McGraw-Hill, New York (1996).
- [8] Taguchi, G., Introduction to quality engineering, Asian productivity organization, Tokyo. (1990).
- [9] Lin, J.L., Wang, K.S., Yan, B.H. and Tarng, Y.S., *J. Mater. Proc. Tech.*, 102, 48 (2000).
- [10] Luo, S.Y., Liao, Y.S., Tsai, Y.Y., Wear characteristics in turning high hardness alloy steel by ceramic and CBN tools, *J. Mater. Process. Technol.*, 88 (1999), 114–121.
- [11] Lee, W.S. and Su, T.T., Mechanical properties and micro-structural features of AISI 4340 high-strength alloy steel under quenched and tempered conditions, *J. Mater. Process. Technol.*, 87 (1999), 198–206.



Multi Response Optimization of the Performance Characteristics in Stir Casting Process for Fabrication of Red Mud Based Aluminium Metal Matrix Composite

Amit Sharma^{*1}, R.M. Belokar² and Sanjeev Kumar³

Abstract: The aim of this paper is to experimentally investigate the stir casting process parameters for producing good quality casting. Taguchi's orthogonal array is used for experimental design. Stir casting process is used for fabricating the MMC under the influence of inert gas. Three process parameters i.e. reinforcement percentage, grain size and blade angle are varied to study their effect on the response variable i.e. tensile strength and micro hardness. The experimental results are evaluated by using the hybrid GRA coupled PCA methodology and the optimum conditions are found by using the Taguchi method. ANOVA is applied to evaluate the contribution of design factors on the response variables and the results reveal that the tensile strength and micro hardness are strongly influenced by the reinforcement percentage followed by the grain size and blade angle. Micro structural characterization of the MMC is carried out to verify the effect of the process parameters on the quality characteristics of the developed MMC. EDS, XRD test results confirms the presence of red mud particles in the developed MMC. Optimal settings provided by the hybrid optimization methodology resulted in improving the quality of the MMC.

Keywords: GRA, PCA, Taguchi, Al2024, Red Mud.

Introduction

Aluminium metal matrix composites are extensively used in defence, aerospace and automotive industry owing to their enhanced properties in terms of high strength to weight ratio, hardness, stiffness and ductility [1]. The properties of the composite can be tailored made depending on the reinforcement used [2]. The most commonly used reinforcement materials are SiC, Al₂O₃, and B₄C [3–5]. Several researchers have investigated the effect of different type of reinforcements on the mechanical properties of the composite and it has been observed that the mechanical properties of the composite increases with the increase in reinforcement percentage [6–8]. There are several techniques available for the production of aluminium MMC out of which stir casting is the most economical one [9–10].

Taguchi method is vastly used by researcher all around the world for optimization problems. Ficici *et al.* used Taguchi method to optimize the weight loss of brake pad in automotive brake system. Author reported that volume fraction and pressure were the two main controlling

parameters that have a very strong effect on the wear of brake pad. The optimal condition was found to be volume fraction (20%), pressure (0.5 bar), sliding distance (2 km) and sliding speed (7 m/s). Confirmatory test was conducted using the optimal settings and a good agreement was found between the predicted and actual weight loss [11]. Vankanti *et al.* used Taguchi method to optimize the process parameters in drilling of glass fiber reinforced polymer (GFRP) composite. The optimum condition for thrust was found to be speed (500 rpm), feed rate (0.04 mm/rev), point angle (90°) and chisel edge width (0.8 mm) whereas for torque it was found to be speed (500 rpm), feed rate (0.06 mm/rev), point angle (95°) and chisel edge width (1.6 mm) [12]. Geetha *et al.* carried out optimization of tensile characteristics of Al356 alloy reinforced with red mud composite. Temperature was found to be the most significant factor followed by weight percentage and ageing time. Validation of the optimal condition was carried out with confirmatory test [13]. Lin *et al.* used Taguchi method for optimization of the machining parameters in magnetic force assisted EDM. Author concluded that S/N ratios

^{1,2} Production and Industrial Engineering Department, PEC University of Technology, Chandigarh, India. ✉*amiter84@gmail.com

³ Mechanical Engineering Department, PEC University of Technology, Chandigarh, India.



correlated with MRR and SR for the optimal combination levels are 9.76 and 12.48 dB higher than the initial experimental conditions and emphasized that the method was successful in optimizing the machining parameters for both MRR and SR [14].

Taguchi method is helpful in optimizing single response but there are several cases in which more than one response are to be optimized simultaneously. Grey theory has been effectively used in optimizing multiple responses. Several researchers have used this powerful theory for the analysis of multi response optimization problem. Nooral *et al.* used grey relational analysis for simultaneously optimizing the machining parameter of drilling Al/SiC MMC. Author concluded that the use of grey relational analysis improved the performance of the responses in drilling process [15]. Ramesh *et al.* used grey relational analysis for the optimization of surface roughness and tool wear in turning of magnesium alloy AZ91D. Author concluded that the analysis was found effective in minimizing the surface roughness and tool flank wear [16]. Narender *et al.* carried out optimization of EDM parameters on machining Al/10%SiCp composite using grey relational analysis. Author concluded that the analysis resulted in improving the performance of the process and was successful in optimizing the multiple responses [17]. Varun *et al.* carried out simultaneous optimization of WEDM responses using grey relational analysis while machining EN 353. Author concluded that GRA was helpful in optimizing the multiple responses and the optimal parameter combination were found to be T_{on} (110 μ s), T_{off} (55 μ s), IP (11 A), SV (10 V) [18]. Jangra *et al.* used GRA for optimization of multi machining characteristics in WEDM of WC/5.3%Co composite and the analysis was useful in predicting the optimal conditions. The computed grey grade value corresponding to the optimal setting was found to be 0.6561 which was greater than the highest grade value among the total experiments performed which ultimately resulted in better machining characteristics [19].

The main drawback of GRA is the establishment of weighing values of the different quality characteristics. This problem can be rectified by using principal component analysis (PCA). By using this process we can evaluate the weighing values of multiple quality characteristics in a systematic way and the same can be used to find the respective grey relational grades. Adalarasan *et al.* used PCA to find the optimal process parameters in friction welding of Al/SiC/Al₂O₃ composite. Author concluded that the analysis significantly improved the S/N ratio and the quality characteristics. The joint formed with the optimal settings predicted by the methodology showed symmetric flash, good matrix reinforcement bonding and minimal voids in fractured surface with improved mechanical properties [20]. Puhan

et al. used PCA with fuzzy inference system for determining the optimal settings in non-conventional machining of AlSiC_p MMC. Author concluded that the optimal settings were found out to be discharge current (1 A), pulse-on-time (200 μ s), duty cycle (85%), flushing pressure (3.92 bar), SiC (15%) and mesh size (300) which resulted in optimizing the responses MRR, TWR, surface roughness and circularity [21]. Rao *et al.* used PCA for simultaneous optimization of correlated multiple responses of wire electric discharge machining process for machining SiC_p reinforced ZC63 metal matrix composite. Author concluded that the optimum process parameters were found to be particulate size (25 μ m), SiC_p (10%), pulse-on-time (6 μ s), pulse-off-time (25 μ s) and wire tension (1 gm) and the methodology was effective in producing the best results [22].

In this study Al2024/red mud MMC has been fabricated using stir casting process and the results are analysed using the hybrid GRA coupled PCA methodology for simultaneously optimizing the stir casting process parameters. Taguchi S/N ratio is used to evaluate the S/N ratio of the response values using “larger the better” criterion. Data is normalised using the grey analysis which is further processed and grey relational coefficients for the individual responses are calculated. PCA is used to find the weighing component of individual response and using these weights grey relational grades are calculated. Taguchi method is applied on the grey relational grades which act as a single response to the multi response optimization problem and the optimal values levels of the process parameters are determined. ANOVA is applied on the grey relational grade to find the effect of individual process parameter on the response values. In the end, confirmatory experiments are performed to validate the effectiveness of the GRA coupled PCA methodology.

Experimental Work

Fabrication of Al/2024 MMC using Stir Casting Setup

The MMC was manufactured using two-step stir casting technique. Al-2024 aluminium alloy is used as the matrix and red mud is used as the reinforcement. The density of red mud (3.2 gm/cm³) is closer to that of aluminium (2.78 gm/cm³). The reinforcement used for the investigation has Fe₂O₃, TiO₂, SiO₂ and other elements in small quantity. The aluminium alloy was fed into the specially designed and developed muffle furnace and was melted at 700°C. An interrupted flow of inert gas (argon) was used from the side arm of the muffle furnace to prevent the melt from coming in direct contact with atmospheric gases, thereby avoiding oxidation at high temperature. The temperature of the furnace was lowered to 640 \pm 5°C to bring the melt into semi solid state and then the preheated red mud particles were added into the melt. Stirring was done at 700 rpm with particular stirrer blades constantly with an electric stirrer.



Small amount of magnesium was added to enhance the wettability. Temperature of the melt was again raised to 700°C and stirring was further continued for five minutes. The mixture was then poured to a cylindrical mould and the melt was allowed to solidify for half an hour. The same procedure was followed to prepare other samples of different wt % of red mud ranging from 5% to 15% with grain sizes ranging from 90 μ to 250 μ respectively along with different type of stirrer blades. Tables 1 and 2 represent the composition of Al2024 and red mud respectively.

Table 1: Aluminium Alloy 2024 Composition

Conc.	Cu	Mg	Si	Fe	Mn	Zn	Ti	Cr	Al
%	4.29	1.29	0.07	0.2	0.54	0.03	0.06	0.01	Rem.

Table 2: Red Mud Composition

Conc.	Al ₂ O ₃	Fe ₂ O ₃	SiO ₂	TiO ₂	Na ₂ O	CaO	LOI
%	17–19	35–36	7–9	14–16	5–6	3–5	10–12

Plan of Investigation

The processing parameters considered for this study are given in Table 3. Experimental trials are conducted using Orthogonal Array (OA) having three design factors which are varied at three levels. Degrees of Freedom (DOF) needed for designing the experiment is six. So, L₉ OA is selected according to the degree of freedom and is used for designing the experiment. The experiments are performed according to the L₉ OA shown in Table 4 and the response values of the individual trial are displayed in Table 5.

Table 3: Process Parameters and Their Corresponding Levels

Factors	Designation	Levels (coded)		
		-1	0	1
Reinforcement (%)	A	5	10	15
Grain Size (Microns)	B	90	150	250
Blade Angle (Degree)	C	90	120	180

Table 4: L₉ Orthogonal Array

Run	Reinforcement (%)	Grain Size (Microns)	Blade Angle (Degree)
1	1	0	1
2	1	1	-1
3	1	-1	0
4	0	1	0
5	0	-1	1
6	-1	0	0
7	-1	1	1
8	0	0	-1
9	-1	-1	-1

Optimization Steps

Step 1: Find S/N Ratio

Taguchi method is one of the most widely used statistical tools in the design and analysis of the experiment. It is used to optimize the design parameters in a very effective manner so as to produce low cost and high quality product [23]. In the present investigation, larger the better criterion is considered for deriving the S/N ratios. The S/N ratios are calculated for the considered response using the formulas given below:

(a) Larger the better

$$SN_{LB} = -10 \log \left(\frac{1}{n} \sum_{i=1}^n \frac{1}{y_i^2} \right) \quad \dots (1)$$

Where *n* is the number of replications & *y_i* is the observed response value (*i* = 1, 2, 3,....., *n*)

(b) Smaller the better

$$SN_{SB} = -10 \log \left(\frac{1}{n} \sum_{i=1}^n y_i^2 \right) \quad \dots (2)$$

(c) Nominal the better

$$SN_{NB} = -10 \log \left(\frac{\bar{y}^2}{S^2} \right) \quad \dots (3)$$

Where, $\bar{y} = \frac{1}{n} \sum_{i=1}^n y_i$,

$$S = \sqrt{\frac{\sum_{i=1}^n (y_i - \bar{y})^2}{n-1}}$$

Step 2: Calculate the Normalized Values of the Respective Responses from the S/N Ratio

Grey relational analysis (GRA) is a technique that measures the correlation degree between the factors and is characterized by small data requirements and multifactor analysis [24]. It involves data pre-processing depending upon the criterion to be used. Normalization is a process of transforming the input data to acceptable values for further processing. It is very important to normalize the original data before performing any further analysis of the using the GRA process. The normalization is done using the equations given below:

(a) Larger the better

$$x_i^*(k) = \frac{y_i^0(k) - \min y_i^0(k)}{\max y_i^0(k) - \min y_i^0(k)} \quad \dots (4)$$

(b) Smaller the better

$$x_i^*(k) = \frac{\max y_i^0(k) - y_i^0(k)}{\max y_i^0(k) - \min y_i^0(k)} \quad \dots (5)$$



(c) Nominal the better

$$x_i^*(k) = 1 - \frac{|y_i^0(k) - y^0|}{\max y_i^0(k) - y^0} \quad \dots (6)$$

Where $x_i^*(k)$ is the normalized values found using the larger the better criterion, $\max y_i^0(k)$ is the highest value of $y_i^0(k)$, $\min y_i^0(k)$ is the lowest value of $y_i^0(k)$ and y^0 is the desired value.

Step 3: Derive the Grey Relational Co-efficient

Further, a grey relational coefficient is derived from the normalized values of tensile strength and hardness using the equation given below:

$$\xi_i(k) = \frac{\Delta_{min} + \zeta \Delta_{max}}{\Delta_{0i}(k) + \zeta \Delta_{max}} \quad \dots (7)$$

Where, $\xi_i(k)$ is the grey relational coefficient, $i = 1, 2, 3, 4, 5, \dots, n$ & $k = 1, 2, 3, 4, 5, \dots, m$, n and m are the number of trials and responses respectively.

$\Delta_{0i}(k)$ = is the deviation sequence,

$$\Delta_{0i}(k) = \|x_0^*(k) - x_i^*(k)\|$$

$$\Delta_{min} = \min_{j \in i} \min_k \|x_0^*(k) - x_j^*(k)\| \quad \dots (8)$$

$$\Delta_{max} = \max_{j \in i} \max_k \|x_0^*(k) - x_j^*(k)\| \quad \dots (9)$$

$x_0^*(k)$ represents the reference sequence and $x_i^*(k)$ represents the comparability sequence. ζ represent the identification coefficient, where $\zeta \in [0, 1]$.

Step 4: Find the Weighing Component of the Quality Characteristics Using PCA

PCA is a multivariate statistical approach introduced by Pearson and further developed by Hotelling [25]. PCA can convert the multiple correlated responses data into several uncorrelated quality indices [26]. In order to make all the responses with different dimensions at diverse ranges of the system unique, PCA is usually used in the data pre-processing. The steps of calculating the weighing component are given below.

(a) Array the measured multiple responses during the process,

$$A = \begin{bmatrix} y_{11} & y_{12} & y_{13} & \dots & y_{1k} \\ y_{21} & y_{22} & y_{23} & \dots & y_{2k} \\ y_{31} & y_{32} & y_{33} & \dots & y_{3k} \\ \vdots & \vdots & \vdots & \ddots & \vdots \\ y_{i1} & y_{i2} & y_{i3} & \dots & y_{ik} \end{bmatrix} \quad \dots (10)$$

Where, i and k represents the number of experimental runs and number of response respectively.

(b) Calculate the variance-covariance matrix M from the normalized data.

$$M = \begin{bmatrix} N_{11} & N_{12} & N_{13} & \dots & N_{1k} \\ N_{21} & N_{22} & N_{23} & \dots & N_{2k} \\ N_{31} & N_{32} & N_{33} & \dots & N_{3k} \\ \vdots & \vdots & \vdots & \ddots & \vdots \\ N_{i1} & N_{i2} & N_{i3} & \dots & N_{ik} \end{bmatrix} \quad \dots (11)$$

$$N_{k,l} = \frac{Cov[x_i(k), x_i(l)]}{\sqrt{Var[x_i(k)] \times Var[x_i(l)]}} \quad \dots (12)$$

Where $l = 1, 2, 3, \dots, k$ and $Cov[x_i(k), x_i(l)]$ is the covariance of sequence $x_i(k)$ and $x_i(l)$.

(c) Calculate the eigen values and eigen vectors from the correlation coefficient array and denoted by λ_j and V_j respectively

$$(R - \lambda_j I_m) V_{ij} = 0 \quad \dots (13)$$

Where λ_j eigenvalues, $\sum_{j=1}^n \lambda_j = n$, $j = 1, 2, 3, \dots, n$

$V_{ij} = [a_{j1} a_{j2} \dots a_{jn}]^T$ eigenvectors corresponding to the eigen value λ_j ,

The eigen vector V_j represents the weighting factor of k number of quality characteristics of the j^{th} principal component and is used for calculating the grey relational grade value.

Step 5: Generate the Grey Relational Grade (GRG)

GRG value is found by using the equation given below where γ is the grey relational grade value of the respective trial. Considering the weights the GRG can be found as,

$$\gamma_i = \sum_{k=1}^n w_k \xi_i(k) \quad \dots (14)$$

Where, $\sum_{k=1}^n w_k = 1$, the total sum of the weights should always be equal to 1. In this w_k represents the weight value of individual factor which was evaluated using the principal component analysis.

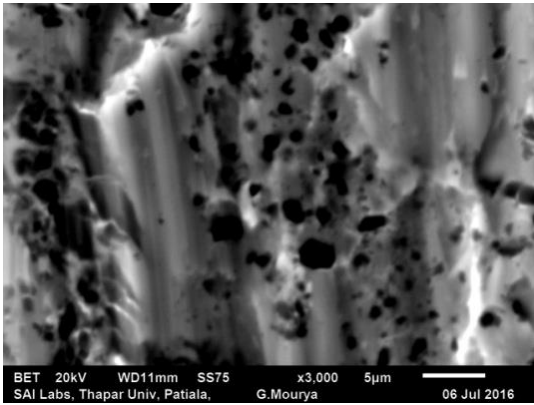
Results and Discussion

Microstructure Characterization

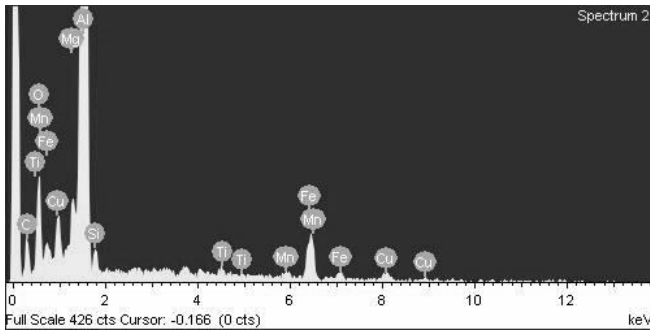
The developed MMC was characterized using SEM, EDS and XRD. Figure 1(a) shows SEM micrograph of the composite in BET mode. From the figure it is clear that the uniform distribution and good wettability of the red mud particles is achieved in the matrix material. This might have happened due to the formation of vortex at high speed of the stirrer [27]. From the analysis of the response values which are given in Table 5 it is observed that with the increase in reinforcement the tensile strength and microhardness of the MMC increases which also indicate good bonding between the matrix and the reinforcement particles [28]. From the figure it is also observed that the MMC is having minimal



porosity which shows that the process can be effectively used for the fabrication of the composite. EDS (Figure 1–b) and XRD (Figure 2) results reveal the presence of the elements like Fe, Ti, TiO₂, Si, SiO₂ in the developed MMC which confirms the presence of red mud particles in the MMC.



(a)



(b)

Fig. 1: (a) SEM Micrograph and (b) EDS Analysis of the Developed Al2024/red Mud MMC

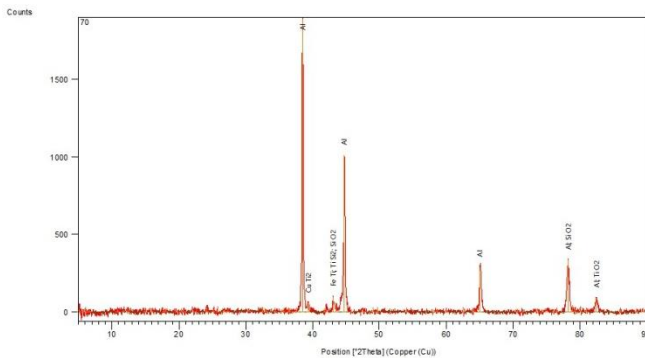


Fig. 2: XRD Results of the Al2024/red Mud MMC

Optimization Procedure

In this paper, tensile strength and micro hardness are considered as the quality characteristics that are to be

optimized simultaneously and the process parameters considered for the fabrication of Al2024/red mud MMC are reinforcement percentage, grain size and stirrer blade angle. Taguchi’s S/N ratio employing “larger-the-better” (Eq. 1) criterion is used for finding out the values of the respective responses. Table 5 represents the average values and S/N ratio of tensile strength and micro hardness respectively.

Table 5: Average Values and S/N Ratio of Each Run

Run	Average Values		S/N Ratio	
	Tensile Strength (MPa)	Microhardness (VHN)	Tensile Strength (MPa)	Microhardness (VHN)
1	163.47	75.4	44.27	37.55
2	166.09	75.7	44.41	37.58
3	165.33	82.9	44.37	38.37
4	135.73	70.6	42.65	36.98
5	162.1	72.4	44.2	37.19
6	141.39	74.1	43.01	37.4
7	124.73	73.8	41.92	37.36
8	157.7	66.9	43.96	36.51
9	152.51	72.4	43.67	37.19

After finding out the S/N ratio of the respective responses the next step is to calculate the normalised values for further processing of the data. Normalised values are calculated using the eq. (4) and the results are tabulated in Table 6.

Table 6: Normalised Values after Data Pre-processing

Run	Normalised Values	
	Tensile Strength	Microhardness
1	0.744	0.559
2	1.000	0.575
3	0.775	1.000
4	0.231	0.253
5	0.722	0.366
6	0.345	0.478
7	0.000	0.457
8	0.646	0.000
9	0.554	0.366

Further the grey relational coefficient values of the respective responses are calculated using eq. (7). Prior to finding the grey relational coefficient we have to find the deviation sequence of the individual quality characteristics which is given below:

$$\Delta_{01}(1) = |x_0^*(1) - x_1^*(1)| = |1.00 - 0.744| = 0.2563$$



$$\Delta_{01}(2) = |x_0^*(2) - x_1^*(2)| = |1.00 - 0.559| = 0.4409$$

Table 7 represents the deviation sequence values of the individual quality characteristics. From Table 7 the values of Δ_{min} and Δ_{max} are expressed as below,

$$\Delta_{min} = \Delta_{02}(1) = \Delta_{03}(2) = 0.00$$

$$\Delta_{max} = \Delta_{07}(1) = \Delta_{08}(2) = 1.00$$

The value of the identification coefficient (ζ) is taken as 0.5 representing equal weightage to both the quality characteristics. By substituting all the values in eq. (7), grey relational coefficient values are calculated and the results are shown in Table 8.

Table 7: Deviation Sequence of Quality Characteristics

Run	Deviation Sequence	
	Tensile Strength	Micro Hardness
1	0.2563	0.4409
2	0.0000	0.4247
3	0.2247	0.0000
4	0.7690	0.7473
5	0.2785	0.6344
6	0.6551	0.5215
7	1.0000	0.5430
8	0.3544	1.0000
9	0.4462	0.6344

Table 8: Grey Relational Coefficient Values of Quality Characteristics

Run	Grey Relational Coefficient	
	Tensile Strength	Micro Hardness
1	0.6611	0.5314
2	1.0000	0.5407
3	0.6900	1.0000
4	0.3940	0.4009
5	0.6423	0.4408
6	0.4329	0.4895
7	0.3333	0.4794
8	0.5852	0.3333
9	0.5284	0.4408

Next step is to calculate the grey relational grade, but for calculating the GRG values we have to calculate the weighing values of each quality characteristics with respective to their importance relative to the analysis. Principal component analysis (PCA) is employed for finding the individual weightage of the quality characteristics. Table 8 represent the grey relational coefficient values which are

used for finding out the correlation coefficient matrix along with the corresponding eigen values. Table 9 represent the eigen analysis of the correlation matrix along with the eigen vectors corresponding to each eigen values. The square of the primary principal component (PC1) represent the contribution of the respective quality characteristics and is shown in Table 10.

Table 9: Eigen Analysis of the Correlation Matrix

Eigen Value	1.3176	0.6824
Variable	PC1	PC2
Tensile Strength	0.707	-0.707
Microhardness	0.707	0.707
Proportion	0.659	0.341
Cumulative	0.659	1

Table 10: Contribution of Each Quality Characteristics

Quality Characteristics	Contribution
Tensile Strength	0.499849
Microhardness	0.499849

Moreover the proportion variance explained by PC1 is 65% and is used for the calculation of grey relational grade. The results of the grey relational grade are shown in table along with the individual ranking.

Higher grey relational grade value represents higher performance of the multiple quality characteristics. Thus from Table 11 we can observe that the process parameter combination represented in experimental run 3 has the highest GRG value (0.8447) and is the best combination out of the nine experimental runs.

Table 11: Grey Relational Grade along with Individual Ranking

Run	Grey Relational Grade	Ranking
1	0.5961	3
2	0.7701	2
3	0.8447	1
4	0.3973	9
5	0.5414	4
6	0.4610	6
7	0.4062	8
8	0.4591	7
9	0.4844	5

Next step is to find the optimal settings of the process parameters for getting the highest grey relational grade. Taguchi method is employed to find the optimal process parameter setting and ANOVA is employed to study the



effect of each process parameter on the multiple quality characteristics. GRG values are used as the response for carrying out the analysis using the Taguchi method. Average GRG values of the individual process parameters are shown in Table 12. Figure 3 represents the main effect plot of the SN ratio and from figure we can see that the best parameter setting for obtaining the highest GRG is found out to be A3, B1 and C1.

Table 12: Response Table for Grey Relational Grade

Level	Reinforcement	Grain Size	Blade Angle
1	0.4506	0.6235	0.5712
2	0.4659	0.5054	0.5677
3	0.737	0.5246	0.5146
Delta	0.2864	0.1181	0.0567
Rank	1	2	3

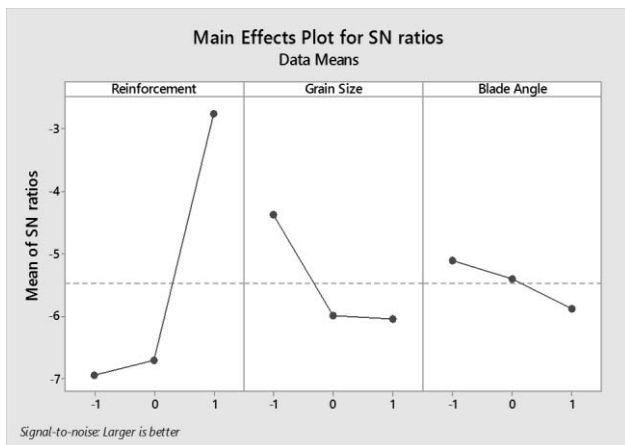


Fig. 3: Effect of Individual Process Parameters on the Quality Characteristics

The plots for mean S/N ratio of grey grade are presented in Figure 3. In the plot, if the point is near the mean line (represented as dotted line) it shows that it has little effect on the considered response whereas the point which has the highest inclination from the average line corresponds to the most significant effect on the quality characteristics. From Figure 3 it can be derived that reinforcement percentage has the highest inclination from the mean which represent that the reinforcement percentage has the maximum influence on the multiple quality characteristics and the best results are obtained at level 3 of the reinforcement percentage. Optimum level for grain size and blade angle was found to be level 1.

Analysis of variance (ANOVA) is a very powerful method that is used to predict the effect of the design factors on the considered performance variable. With ANOVA we can analyse the effect of each factor in terms of percentage

contribution and evaluate what effect the parameter has on the considered response. The effect of the process parameters i.e. reinforcement percentage, grain size and blade angle on the response variable i.e tensile strength and microhardness, are evaluated at 95% confidence interval. The analysis of variance test results with respective degree of freedom (DOF), sum of square (S), Variance (V) and percentage contribution (P) are shown in Table 13.

Table 13: ANOVA Table for the Grey Relational Grade

Analysis of Variance for Means				
Source	DOF	S	V	P
Reinforcement	2	0.1557	0.0779	77.11
Grain Size	2	0.0241	0.0121	11.94
Blade Angle	2	0.0060	0.0030	2.99
Residual Error	2	0.0161	0.0080	7.96
Total	8	0.2019		

From the table we can see that reinforcement percentage has the major influence on the multiple quality characteristics and is clearly seen with the highest percentage contribution of 77.11%. The analysis further reveals that reinforcement percentage was followed by grain size which was having an effect of 11.94% on the multiple performance characteristics followed by blade angle which was having minor effect on the multiple responses with a value of 2.99%.

Confirmation Experiments

The confirmatory experiments are conducted using the optimum levels of each processing parameters to verify the improvement in the multiple performance characteristics for the fabrication of Al2024/Red Mud MMC recommended by the hybrid methodology. The values obtained by the confirmatory experiments are shown in table 14 which shows that the hybrid methodology can be successfully used for optimizing the multi response problems.

Table 14: Verification Test Results

	Optimal Settings		Difference/Gain
	Predicted	Actual	
Level of factors	A3, B1, C1	A3, B1, C1	
Tensile Strength	189.24	191.85	2.61
Microhardness	80.32	80.7	0.38

Conclusion

In this paper a hybrid optimization technique along with Taguchi method is proposed to find out the optimal settings of stir casting process parameters in order to simultaneously



optimize multiple quality characteristics. Taguchi's orthogonal array is used to design the experiment and from the analysis of the results it is concluded that tensile strength and micro hardness increases with the increase in reinforcement percentage whereas it decreases with the increasing values of grain size and blade angle. From the statistical analysis it is observed that the process parameters such as reinforcement percentage and grain size had a major effect on the mechanical properties whereas blade angle was having minor effect on the grey relational grade. Treating GRG as a single response it was analyzed using Taguchi's method. Optimal settings were established from the response graph and the optimal settings were found to be A3, B1 and C1 i.e. reinforcement percentage (15%), grain size (90 microns) and blade angle (90°). Confirmatory experiments were conducted at optimal settings and the values of tensile strength and microhardness were found to be 191.85 MPa and 80.7 VHN respectively. Microstructural analysis was carried out which confirms the presence of red mud particles in the MMC. This study exhibit that the hybrid optimization technique can be successfully used to optimize multiple quality characteristics.

References

- [1] Tee, K.L., Lu, L. and Lai, M.O., "Synthesis of in situ Al-TiB₂ composites using stir cast route", *Composite Structure*, 47, pp. 589–593 (1999).
- [2] Abdel-Azim, A.N., Kassem, M.A., El-Baradie, Z.M. and Waly, M., "Structure and properties of short alumina fibre reinforced AlSi18CuNi produced by stir casting", *Materials Letters*, 56, pp. 963–969 (2002).
- [3] Suresha, S. and Sridhara, B.K., "Friction characteristics of aluminium silicon carbide graphite hybrid composites", *Materials and Design*, 34, pp. 576–583 (2012).
- [4] Kumar, A., Lal, S. and Kumar, S., "Fabrication and characterization of A359/Al₂O₃ metal matrix composite using electromagnetic stir casting", *Journal of material Res. Tech.*, 2(3), pp. 250–254 (2013).
- [5] Kalaiselvan, K., Murugan, N. and Parameswaran, S., "Production and characterization of AA6061-B₄C stir cast composite", *Materials and Design*, 32, pp. 4004–4009 (2011).
- [6] Kok, M., "Production and mechanical properties of Al₂O₃ particle reinforced 2024 aluminium alloy composites", *Journal of Materials Processing Technology*, 161, pp. 381–387 (2005).
- [7] Singla, D.M., Dwivedi, D., Singh, L. and Chawla, V., "Development of aluminium based silicon carbide particulate metal matrix composite", *Journal of Minerals and materials characterization & engineering*, 8(6), pp. 455–467 (2009).
- [8] Sozhamannan, G.G., Prabu, S.B. and Venkatgalapathy, V.S.K., "Effect of processing parameters on metal matrix composite: Stir casting process", *Journal of surface engineered materials and advanced technology*, pp. 11–15 (2012).
- [9] Seo, Y.H. and Kang, C.G., "Effects of hot extrusion through a curved die on the mechanical properties of Al-SiC composites fabricated by melt stirring", *Composites Science and Technology*, 59, pp. 643–654 (1999).
- [10] Hashim, J., Looney, L. and Hashmi, M.S.J., "Metal matrix composites" Production by the stir casting method", *Journal of material processing technology*, 92, pp. 1–7 (1999).
- [11] Ficici, F., Durat, M. and Kapsiz, M., "Optimization of tribological parameters for a brake pad using Taguchi design method", *Journal of the Brazilian Society of Mechanical Sciences and Engineering*, vol. 36, pp. 653–659 (2014).
- [12] Vankanti, V.K. and Ganta, V., "Optimization of process parameters in drilling of GFRP composite using Taguchi method", *Journal of Materials Research and Technology*, 3(1), pp. 35–41 (2014).
- [13] Geetha, B. and Ganesan, K., "Optimization of Tensile Characteristics of Al356 alloy reinforced with volume fraction of Red Mud Metal Matrix Composite", *Procedia Engineering*, 97, pp. 614–624 (2014).
- [14] Lin, Y.C., Chen, Y.F., Wang, D.A. and Lee, H.S., "Optimization of machining parameters in magnetic force assisted EDM based on Taguchi method", *Journal of Materials Processing Technology*, 209, pp. 3374–3383 (2009).
- [15] Haq, N.A., Marimuthu, P. and Jeyapaul, R., "Multi response optimization of machining parameters of drilling Al/SiC metal matrix composite using grey relational analysis in the Taguchi method", *The International Journal of Advanced Manufacturing Technology*, 37, pp. 250–255 (2008).
- [16] Ramesh, S., Viswanathan, R. and Ambika, S., "Measurement and optimization of surface roughness and tool wear via grey relational analysis, TOPSIS and RSA techniques", *ELSEVIER*, 78, pp. 63–72 (2016).
- [17] Singh, P.N., Raghukandan, K. and Pai, B.C., "Optimization by Grey relational analysis of EDM parameters on machining Al/10%SiCp composites", 155–156, pp. 1658–1661 (2004).
- [18] Varun, A. and Venkaiah, N., "Simultaneous optimization of WEDM responses using grey relational analysis coupled with genetic algorithm while machining EN53", *The International Journal of Advanced Manufacturing Technology*, 76, pp. 675–690 (2015).
- [19] Jangra, K., Grover, S. and Aggarwal, A., "Optimization of multi machining characteristics in WEDM of WC-5.3%Co composite using integrated approach of Taguchi, GRA and entropy method", *Frontiers of Mechanical Engineering*, 7(3), pp. 288–299 (2012).
- [20] Adalarasan, R. and Sundaram, A.S., "Parameter design in friction welding of Al/SiC/Al₂O₃ composite using grey theory based principal component analysis (GT-PCA)", *Journal of the Brazilian Society of Mechanical Sciences and Engineering*, 37, pp. 1515–1528 (2015).
- [21] Puhan, D., Mahapatra, S.S., Sahu, J. and Das, L., "A hybrid approach for multi-response optimization of non-conventional machining on AlSiC_p MMC", *Measurement*, 46, pp. 3581–3592 (2013).
- [22] Rao, T.B. and Krishna, A.G., "Simultaneous optimization of multiple performance characteristics in WEDM for machining ZC63/SiC_p MMC", *Advances in Manufacturing*, 1, pp. 265–275 (2013).



- [23] Taguchi, G. and Konishi, S., “Taguchi methods, orthogonal arrays and linear graphs”, *Tools for quality engineering, American supplier institute, Egypt*, pp. 35–38 (1987).
- [24] Deng, J.L., “Introduction to Grey system”, *J. Grey system*, 1(1), pp.1–24 (1989).
- [25] Pearson, K., “On lines and planes of closest fit to systems of points in space”, *Philos. Mag.*, 62:559–572 (1901).
- [26] Hotelling, H., “Analysis of a complex of statistical variables into principal components”, *J Educe Psychol*, 24:417, 441 (1933).
- [27] Naher, S., Brabazon, D. and Looney, L., “Development and assessment of a new quick quench stir caster design for the production of metal matrix composites”, *Journal of material processing technology*, 16, pp. 430–439 (2004).
- [28] Chawla, N. and Shen, Y.L., “Mechanical behaviour of particle reinforced metal matrix composites”, *Advanced engineering materials*, 3(6) (2001).



Reduction in GHG Emission in Iron Ore Sintering Process

Subhra Dhara^{*1}, S.K. Jha¹ and A. Arora¹

Abstract: Sintering is the most prevalent process for agglomerating iron ore fines. The process starts with homogeneously mixing various ore fines along with flux and other metallurgical waste fines. Then the mixture is added with 8–10% of water and subjected to controlled rotation in a rotating drum, so as to form granules (mean size > 3 mm). Water is added as binder in this granulation process. Afterwards, granules are ignited (at temperature > 1300°C), so that fines are incipiently fused to form a lumpy porous mass (sinter) suitable to be charged in Blast Furnaces. Coke breeze is conventionally being used as heat source for this fusion reaction, however its role is much broader. It supplies the heat required for evaporation of granulation water and acts as reducing agent for partial reduction of Fe₂O₃ to FeO. Generally, 70–75 kg of coke breeze is consumed to produce 1 ton of good quality sinter in industrial practices; which in turn emits 215 kg of CO₂ (GHG) to environment. Granulation is the single most critical step in raw mix preparation; amount and properties of granulation water effects granulation index and subsequently sintering process and final product. So, any effort that can reduce specific balling water consumed without sacrificing its binding properties can effectively reduce coke required for water evaporation and overall coke breeze consumption and subsequently GHG emission. Hence for sustainability of industrial sintering operation, it is strongly envisaged to minimize specific coke breeze consumption. Water surface tension is a unique property, which exerts a strong cohesive force on adjacent fine particles, acts positively to form capillary bridges in between granulated fines and increases granulation efficiency. On the contrary, it is the same water surface tension that restricts water to disperse well among layers of fines, as quickly as required during granulation. A water molecule is typically dipolar, with dipole moment as high as 1.85 D. Literature study reveals that, water molecules get preferentially oriented when subjected to external magnetic field, which causes reduction in Hydrogen bond angle from 104.45° and subsequent reduction in surface tension. RDCIS has developed a novel method to optimally reduce surface tension of granulation water by 16.92%, by passing it through a controlled magnetic field. This reduction is optimal, to achieve uniform dispersion of granulation water even upto the bottommost fines layer within the short granulation time without any adverse effect on strength of capillary bridges and granulation efficiency. This system was successfully implemented in an industrial sintering plant of SAIL. As a result, granulation water could evenly be dispersed within the fines layer and 8% reduction in specific granulation water could be recorded; along with 9% increase in granulation index. Reduction in specific granulation water effectively reduced the coke breeze required for water evaporation and hence a reduction in specific coke breeze consumption by 2.24 kg per ton of sinter produced could be achieved. This lead to reduction in CO₂ emission by 6.93 kg per ton of sinter produced, which is equal to reduced GHG emission by 33000 ton/annum from a single sinter plant.

Keywords: Granulation, Coke Breeze Consumption, Magnetic Treatment, Water Surface Tension, Capillary Force.

Introduction

Sintering is a process of agglomerating iron ore fines. These fines are generated during iron mining operation, which can't be charged directly into BFs due to size constraint. Hence, they are mixed with lime stone and dolomite fines, coke breeze, various metallurgical wastes e.g. mill scale, flue dust, BOF slag etc. and fused incipiently to form lumpy porous iron bearing mass called sinter. Due to

environmental restrictions and significant technological advantages over iron ore lumps, sinter plants have become very common in every modern Integrated Steel Plants.

Sintering is a four step process namely dry mixing, balling, ignition and cooling. Firstly, iron ore fines (< 10 mm), coke breeze (< 3 mm), flux fines (< 3 mm) and other fine metallurgical wastes (e.g. mill scale, flue dust, lime dust) are blended as per pre-calculated ratio and mixed

¹R&D Centre for Iron & Steel, Steel Authority of India Limited, Ranchi, India. ✉*subhra@sail-rdcis.com



homogeneously in primary mixing drums. Then the mixture is subjected to rotation in wet condition (**Granulation Process**), inside balling drums. Here raw mix is converted into green sinter granules of size preferably more than 3 mm. The green mix is then fed on moving sinter pallets through gravity segregation principle. Pallet top layer is subjected to direct flame heating inside an ignition furnace. The coke breeze present in top layer is ignited, supplying thermal energy for partial melting of ore and flux decomposition. Simultaneously, bottom-ward suction (Dwight-Lyod type) is created through the moving pallet. This suction causes hot waste gases of combustion to pass through green mix layers beneath the igniting top layer. Convective heat transfer causes drying of these layers followed by coke breeze ignition and incipient fusion (sintering). Speed of pallet movement is so adjusted with under-grate suction, that the whole bed of green mix is sintered till the end of sinter machine length. Then the sintered bed is crushed to form sinter pieces. Afterwards the products (still in hot condition) are screened in hot screen for separating out undersize fractions (< 8 mm). Oversize sinter is cooled on coolers (straight line or circular) through air up-draft method. Cooler speed is adjusted according to the air draft rate, so that sinter products are cooled to temperature less than 80°C . Cooled sinter product is again screened in cold screen for separating out undersize (< 5 mm generally) while the oversize is consumed in Blast Furnaces as iron bearing burden. Under size sinter is recycled as return sinter in sintering process cycle.

Overview of the Granulation Process

Granulation is the process in which primary fine particles enlarge their size by forming granules. Whereas the raw feed is characterized by widely different chemical composition and size distribution (from 10 to < 0.063 mm), granules have several favourable mechanical features e.g.:

1. Uniform sizes
2. Determined shapes
3. Better strength
4. Homogenized composition and properties.

The optimal size distribution of granules after granulation is summarized as about: 50% particles with > 10 mm, about 30% particles with 5–8 mm, about 10% particles with 8–10 mm and 10% other particles [1]. As a result, void space in sinter mix bed and the pre-ignition permeability is greatly increased. Resultant to this, air-filtration velocity through bed increases manifold with subsequent increase in sinter machine productivity. Moreover, the fines in the granules, which react and melt readily at lower temperatures, are situated at outer layers, while coarser particles, which are more reducible and resistant to hot degradation, form the core [2]. Thus thermo-chemical stages during sintering e.g.

decomposing and partial fusion, reduction and crystal re-orientation can occur at faster rates.

Granulation Mechanism

Granule structure is quite composite comprising core seed and primary layer of fines which cements larger particles present in the secondary layer. Venkatramana *et al.* [3] divides feed to the balling drums into three components: coarse (seeds or nuclei), intermediates and fines (layering material). Though the size range, precise roll or even the existence of an intermediate size fraction with distinct agglomeration behaviour have not been clearly established, some postulate that intermediates in the size range of 0.2–0.7 mm, 0.5–2 mm or 0.5–1 mm play essentially no role in granulation. In contradiction, it is assumed that, there is an intermediate 0.5–1 mm class of particles that can switch roles as either seeds or adhering fines, depending on moisture and material properties. Lister *et al.* [4] considers there is no existence of intermediate particle range. There is smooth transition from completely adhering to completely nuclei particles as particle size increases. In the intermediate size ranges, for one particular size fraction, some particles act as nuclei while other particles of same size are adhering. Distribution of particles between adhering and nuclei is a function of moisture content.

Granule growth regime is broadly classified into (i) wetting and nucleation (ii) consolidation and growth (iii) breakage and attrition [2]. The auto-layering mechanism [4] i.e. coating of fines present in the feed onto the coarse size fractions which act as seeds or nuclei, act as reason for granule growth. The auto-layering process is explained by many postulates. In the k-postulate, the rate of pickup of fine particles is proportional to surface area of rolling granule and a layer is formed whose thickness is the same irrespective of the nuclei size. Whereas in the more general p-postulate, the rate of layering is proportional to volume of rolling granule, and consequently, the granule size is proportional to the seed size. Mixed postulate explains as layering occurs initially by a coating of fixed thickness, which is followed by proportionate growth of granules.

Effect of Granulation Water on Granulation Process

For ore particle to be associated with one another in the course of granulation, a certain amount of moisture must be present on the surface of the particles to function as bridge. More the water content added into the mixture, better is the granulation (till the optimum amount). The total layer thickness increases with water content of the granulating charge, with subsequent increase in mean granule size [2].



The packed bed permeability increases when the moisture content is increased and exhibited a maximum value at a certain moisture level. Xuewei *et al.* [5–7] indicated that permeability of sintering bed increases with increasing water content added during granulation; first a maximum permeability reaches at suitable water content, then the permeability decrease with increasing water content; i.e. the relationship between permeability of burden and the water content added in the mixture is similar to a parabolic curve. However this maximum value was different for each raw material samples.

Moreover, when a certain amount of moisture has been added to the ore particles, the moisture on the surface of the ore is thought to be affected by the moisture absorption capacity (water saturation volume) of the ore [8]. Also water dispersion rate i.e. rate at which water penetrates through bed of fine raw mix is an important factor. With typical layers of mixed fines and minimum void space, it needs longer residence time of whole granulating charge to get sufficient water bridge for granulation. But as in the case in industrial operation, feed materials at bottom layers are poorly bonded by weak water bridges, due to low water dispersion and high feed rate.

Water: An Introduction

According to Hawley’s condensed chemical dictionary, water is defined as a colourless, odourless, tasteless liquid, with different allotropic forms e.g. ice (solid) and steam (vapour). Molecular arrangement reveals that (Figure 1) each Hydrogen nucleus is bound to the central Oxygen atom by covalent bond [9]; however structurally a tetrahedral geometry in which the angle between electron pairs (and therefore the H-O-H bond angle) is 109.5°. But because the two non-bonding pairs remain closer to the oxygen atom, these exert a stronger repulsion against the two covalent bonding pairs, effectively pushing the two hydrogen atoms closer together. This results in a distorted tetrahedral arrangement in which the H-O-H angle is 104.5°.

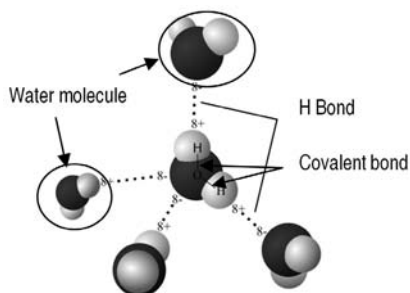


Fig. 1: Water Molecule Structure

The water molecule is electrically neutral, but the positive and negative charges are not distributed uniformly. Negative

charge is concentrated at the Oxygen end, which constitutes an electric dipole of considerably high dipole moment as 1.85 D. This partially positive Hydrogen atom in one water molecule is electrostatically attracted to the partially negative Oxygen of a neighbouring molecule which is called Hydrogen bond, a weak but unique bond existing in water.

Effect of Magnetic Field on Water Surface Tension

Studies [10, 11] reveal that, randomly arranged water molecules are arranged in uniform direction when subjected to magnetic field. This mode of arrangement causes decrease in covalent bond angle to less than 104.5°, leading to subsequent decrease in consolidation degree between water molecules. Concept diagram of this effect can be seen from Figure 2. This change in water molecular structure reduces surface tension of water.

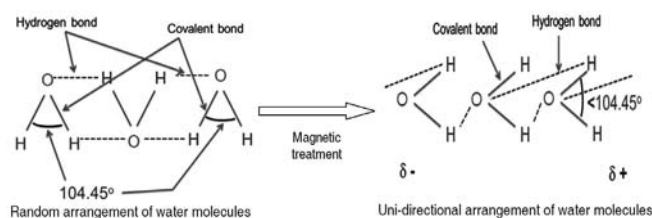


Fig. 2: Effect of Magnetic Treatment on Water Molecular Arrangement

Magnetic Treatment on Water Surface Tension: Lab Experiment

Lab scale trials were conducted to measure effect of magnetic treatment on water surface tension. Magnetic water conditioners were installed on water supply lines, and samples have been collected before and after magnetic water conditioners. The surface tension of respective water samples were measured using capillary method. The reduction in surface tension in percentage terms is reported in Figure 3.

Application of Magnetic Treated Water in Industrial Sintering Process

The activation of water treatment using magnetic field depends on three following conditions⁽⁷⁾:

- Magnetic flux density
- Duration of exposing water to magnetized field (velocity of water current)
- Amount of exposing water to the magnetic field
- Temperature of water
- Purity of water.

Accordingly, six nos. of magnetic water conditioners of calculated magnetic strength were installed around water

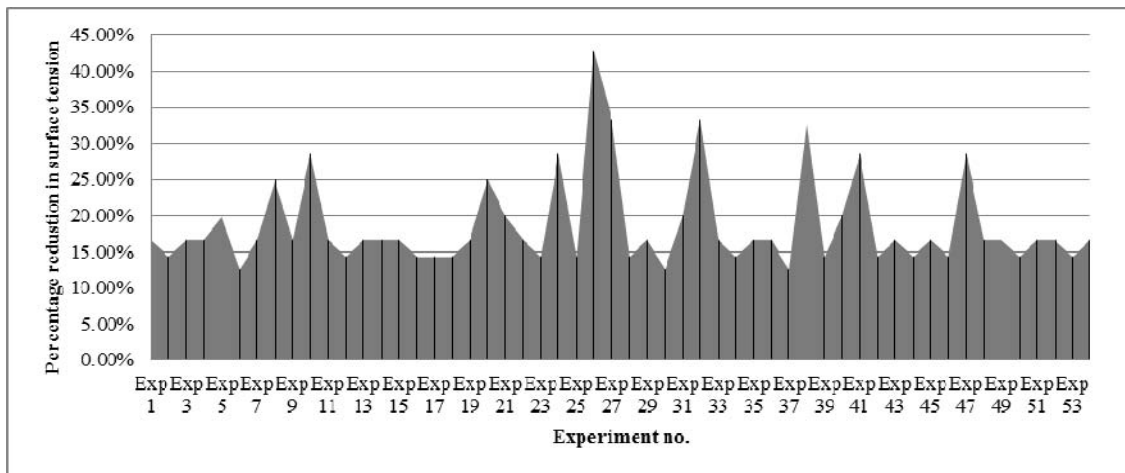


Fig. 3: Surface Tension Reduction after Magnetic Treatment

Results and Discussion

Series of trials, data collection and analysis were conducted to compare performance of sintering plant performance with and without magnetic treated water.

Improvement in Granulation Degree

Granulation degree is the ratio of +3 mm in sinter raw mix after and before balling drums. Samples from conveyor belt before each drum has been collected and granulometry analysis with 3 mm screen carried out. Similarly samples have been collected from discharge end of same drum and analyzed for granulometry. Care has been taken to collect the sample from outlet just 3 min after input sample collection to match with normal traverse time from charging to discharge end of baling drum. Absolute weight and percentage of +3 mm calculated and recorded which is compared for normal water and that with magnetic treated water (Figure 4).

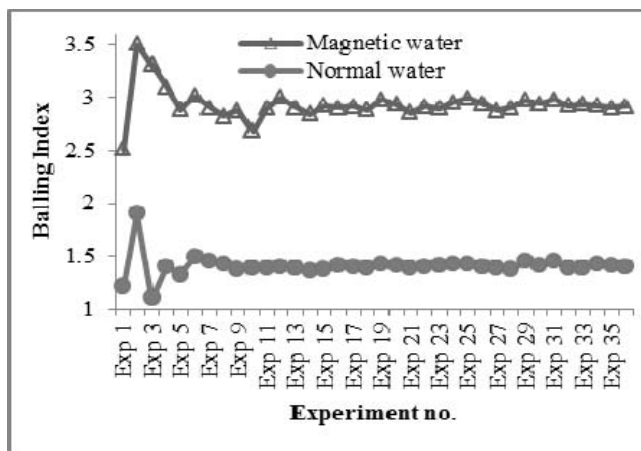


Fig. 4: Effect on Balling Index after Magnetic Treated Water Addition

Reduction in surface tension increases dispersion of water among fine raw mix inside balling drum. Hence each layer has sufficient water to form strong water bridges around; without compromising on fed rate or residence time. So granules formed are stronger in terms of compression, with subsequent reduction in breakage due to abrasion. 9% increase in granulation degree could thus be realized.

Reduction in Specific Coke Breeze Consumption

Better dispersion of balling water among fine charge actually increased efficiency of water to act as binder. Hence specific water content required for balling could be reduced by 8%. (Figure 5).

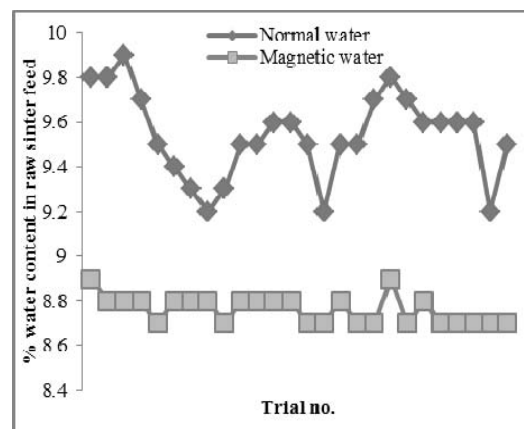


Fig. 5: Percentage Water Content in Raw Sinter Feed

This reduced water content subsequently decreased the water load on sintering process, specifically on drying and re-condensation stages. This means lower content of water to be vaporized in drying zone and reduced specific water in moisture re-condensation zone. This has saved coke breeze,



consumed for sintering process. Figure 6 shows trend of trial data on specific coke breeze consumption, 2.24 kg/ton on average.

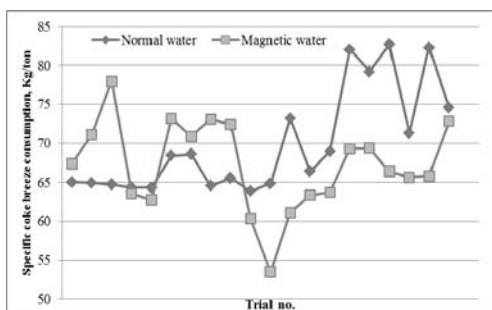


Fig. 6: Specific Coke Breeze Consumption in Sintering

Conclusion

Granulation is important in many respects for iron ore sintering process. By granulation, fine particles of diversified chemistry and property are homogenized with subsequent increase in their mean size, suitable for charging on moving sinter pallets. Researches have analyzed the granulation process and various factors controlling the same. Feed characteristics and role of water, process variables of balling operation are established to effect the process.

Water surface tension is a necessary evil in sintering process. On one hand, it helps in granulation by forming water bridges among fine particles; on the other side it restricts rate of water dispersion among fines during industrial scale continuous operation.

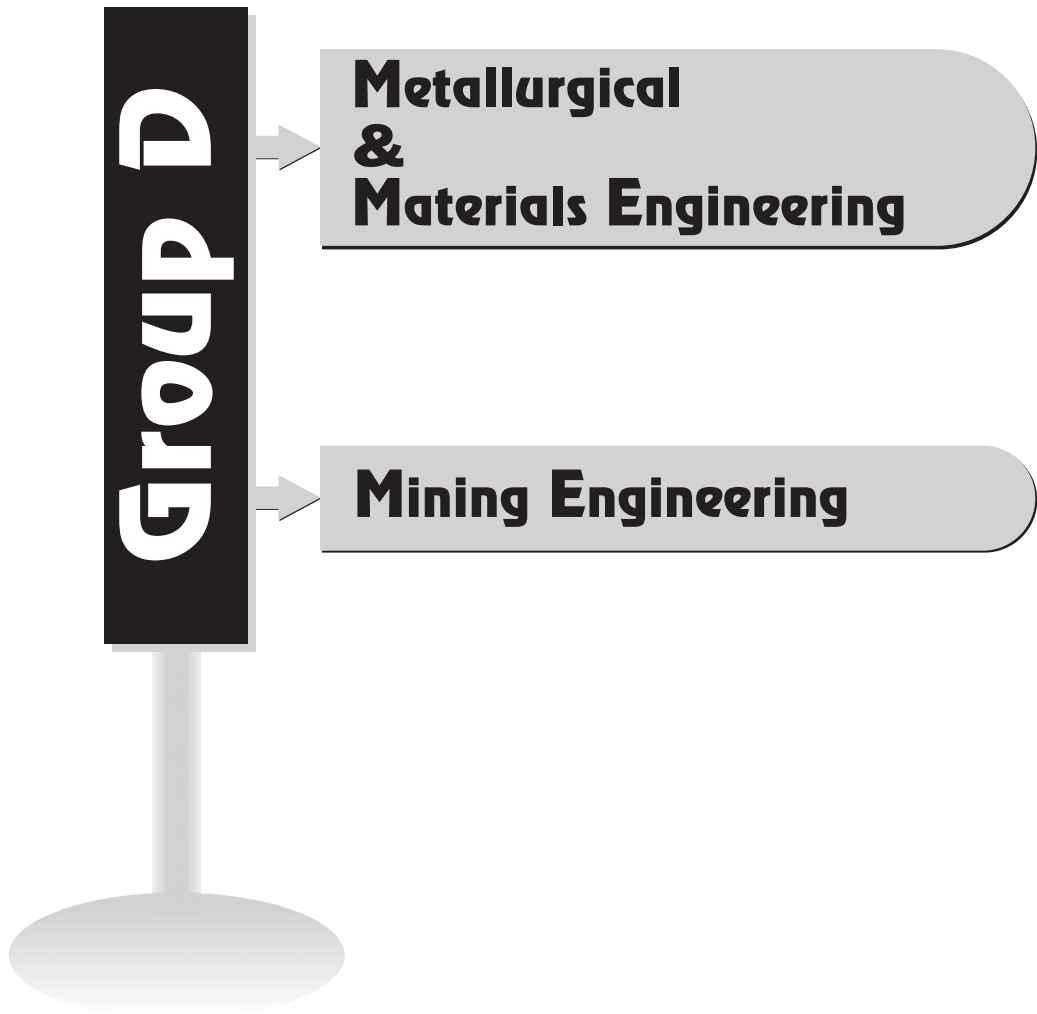
Hydrogen bond is a typical property of water molecules, causing surface tension to exist and water dispersion rate is inversely proportional to surface tension. Magnetic field is explained to arrange random water molecules in uni-direction, causing water molecule to condense and resultant reduction in surface tension.

Lab study revealed 16.92% reduction in water surface tension because of magnetic treatment. Accordingly, magnetic water conditioners were designed and installed in sinter machines of Bokaro Steel Plant. The results of the magnetic water addition are summarized as below:

- Granulation degree improved by 9%
- Water content in sinter feed could be reduced by 8%
- Reduction in specific coke breeze consumption by 2.24 kg per ton of sinter produced achieved.
- This led to reduction in CO₂ emission by 6.93 kg per ton of sinter produced, which is equal to reduced GHG emission by 33000 ton/annum from a single sinter plant.

References

- [1] Lv, Xuewei., Bai, Chenguang., Qiu, Guibao., Zhang, Shengfu and Hu, Meilong: "Moisture capacity: definition, measurement and application in determining the optimal water content in granulation" *ISIJ International* Vol. 50 (2010), No. 5, pp. 695–701.
- [2] Venkataramana, R., Kapur, P.C. and Gupta, S.S., "Modelling of granulation by a two-stage auto-layering mechanism in continuous industrial drums" *Chemical Engineering Science*, Vol. 57 (2002), pp. 1685–1693.
- [3] Venkataramana, R., Gupta, S.S., Kapur, P.C. and Ramachandran, N., "Modelling of iron ore sinter fed granulation" *Tata search* 1997, pp. 91–97.
- [4] Lister, J.D., Waters, A.G. and Nicol, S.K.: "A model for predicting the size distribution of product from a granulating drum" *Transactions ISIJ* 1986, Vol. 26, pp. 1036–1044.
- [5] Khosa, Jasbir and Manuel, James, "Predicting granulation behavior of iron ores based on size distribution and composition" *ISIJ International*, Vol. 47 (2007), No. 7, pp. 965–972.
- [6] Lv, Xuewei, Bai, Chenguang, Qiu, Guibao, Zhang, Shengfu and Hu, Meilong, "Moisture capacity: definition, measurement and application in determining the optimal water content in granulation" *ISIJ International*, Vol. 50 (2010), No. 5, pp. 695–701.
- [7] Yoshinaga, M., Sato, S. and Kawaguchi, T., *Australia Japan Extractive Metallurgy Symposium*, Sydney (1980), pp. 145.
- [8] Matsumura, Toshihide, Maki, Takeshi, Amano, Shinji, Sakamoto, Mitsuru and Iwasaki, Nobuyukki : "Effect of moisture absorption behavior on optimal granulation moisture value of sinter raw material" *ISIJ International*, Vol. 49 (2009), No. 5, pp. 618–624.
- [9] <http://en.wikipedia.org/wiki/Water>
- [10] Ahmed, S.A., "Effect of magnetic water on engineering properties of concrete", College of Engineering, Water Resource Department, University of Mosul, Iraq.
- [11] Martynenko, V.A. *et al.*, "Effect of sintering with water subjected to magnetic field", No. 5, *Metallurgist* 1967.





Investigation of Tribological Performance of Hybrid Aluminium Metal Matrix Composites

R.S.S. Raju^{*1}, M.K. Panigrahi², R.I. Ganguly² and G.S. Rao³

Abstract: The present investigation is carried out to develop new generation hybrid aluminum metal matrix composites with Coconut Shell Ash (CSA), Al_2O_3 , graphite mixture as reinforcement for analyzing the tribological effects of different parameters such as load, sliding distance and sliding velocity. Al-CSA, Al- Al_2O_3 , Al-CSA-Gr, and Al- Al_2O_3 -Gr composites are prepared with percentage of volume of 15% and graphite with 3% by stir casting route. XRD analysis of shell material has revealed the presence of hard phases of SiC, Al_2O_3 , and Fe_2O_3 . The worn out surfaces are examined under Scanning Electron Microscope (SEM) and elemental analysis is carried out by EDS analysis. The works predominantly deal with physical, mechanical, and wear properties of as-prepared hybrid MMCs. The conducted mechanical test of the entire hybrid MMCs indicated better strength and wear resistance than the base material i.e., Aluminium alloy. Al-CSA composite has revealed better mechanical properties like tensile, hardness than others composites. Moreover, Al-CSA-Gr exhibits better tribological performance than the other composites.

Keywords: AMC, CSA, Wear Rate, COF.

Introduction

Metal Matrix Composites (MMCs) bring significant profit since attainable properties are prominent for the components concerned and employed to meet diversified demands of many industries. Moreover, aluminium alloy has been finding wide application in various industries due to its high strength – weight ratio, high specific stiffness, and high thermal conductivity with a low coefficient of thermal expansion and high wear resistance. Precisely, Aluminium Metal Matrix Composites (AMC) are effectively implemented in few industrial applications like aerospace, automotive, defence, and electronic packing [1,2]. From literature, it can be observed that physical, mechanical and tribological properties were improved by the addition of hard ceramic intermetallic compound into the Al matrix. Moreover, the materials like hard and soft reinforcements such as SiC, Al_2O_3 , TiC, SiC- Al_2O_3 , B_4C -Gr, Al_2O_3 -Gr, SiC-Gr, and Graphite (Gr) have been used as artificial reinforcement for preparation of composite. However, various agro wastes like fly ash [3,4], red mud [5] and colliery shale [6], rice husk [7], shell char [8,9], and bagasse [10] are used as reinforcements in Al-Si, Al-Cu, Al-Mg and Al-Zn are used as matrix in the fabrication of AMCs. However, there is a

critical issue in preparation of the composite with respect to fabrication and processing [11]. Generally, AMC is fabricated by liquid metallurgy (i.e., stir or compo casting and infiltration), squeeze casting and powder metallurgy route. For the mass and low cost production, liquid metallurgy route is most preferred than the other one.

Aku *et al.*[8]evaluated microstructure, hardness and density of coconut shell ash composites having 3-15% weight volume. They found that by increasing the vol. % of reinforcement, density decreases and hardness values increases. Shen *et al.* [12] reported on the correlation between hardness and tensile strength of composite, based on the effect of particle size, volume fraction and aging behaviour of prepared with Al-Cu-Mg alloy reinforced with SiC. Seo and Kang[13] prepared a composite with SiC as reinforcement with various volume fraction (0.05 to 0.20 of size 13-22 μm) which injected into an Al6061 molten alloy by stir casting route. Afterward, the composites are extruded at 500°C at a constant velocity of 2mm/min. The extruded composites are examined with extrusion force, particle distribution, microstructure, and mechanical behavior, which compared with monolithic alloy. Mahendra *et al.* [14] Prepared aluminum (2024) composites reinforced with SiC,

¹Department of Mechanical Engineering, Gandhi Institute of Engineering and Technology, Gunupur, Odisha, India. ✉ sivaraju80@gmail.com.

²Department of Metallurgical Engineering, Gandhi Institute of Engineering and Technology, Gunupur, Odisha, India.

³Department of Mechanical Engineering, RVR&JC College of Engineering, Guntur, Andhra Pradesh, India.



fly ash and hybrid of SiC-fly ash at various volume fractions (0, 5, and 10%) by stir casting route. Moreover, the authors reported on mechanical properties i.e. density, tensile strength, hardness, % of elongation and yield strength of all the composites. Certainly, hybrid composite exhibits better mechanical properties than the other. Aibodion and Hassan [15] studied the effect of mechanical and microstructural properties on Al-Si-Fe reinforced with Silicon carbide of 5–25% of volume. The authors concluded that increase of reinforcement increases hardness, tensile strength, and porosity whereas decrease density and impact strength. The composite has improved mechanical properties due to the addition and uniform distribution of reinforcement (SiC) in the ductile matrix. Kumar *et al.* [16] prepared two composites i.e. aluminum 6061 and 7075 as base matrix along with reinforcement by SiC and Al₂O₃ respectively via liquid metallurgy technique. The composites were examined of mechanical, physical, metallography and tribological performance. They revealed that density, hardness and tensile strength of composite enhanced with reinforcements. Kok and Ozdin [17] investigated the wear mechanisms of the 2024 aluminum alloy composites reinforced with Al₂O₃. They reported that wear resistance of the composites was greater than the base alloy, and increased with increasing reinforced particles size, also decreased with increase of sliding distance, load and the abrasive particle size.

In the present work, Coconut Shell Ash (CSA), alumina and graphite particles are used as reinforcement materials for the preparation of aluminum metal matrix composite i.e., Al-15% CSA, Al-15% Al₂O₃, Al-15% CSA-3% Gr, and Al-15% Al₂O₃-3% Gr by stir-casting route. The present work aims study structure by XRD, EDS, density, and mechanical properties such as tensile, hardness (Brinell), abrasion resistance at a variable parameter i.e. load, and sliding distance and sliding speed remain constant. Moreover, coefficient of friction and wear rate are response for as-prepared composites.

Materials and Methods

Materials

In the present work, Al 1100 grade aluminum (HINDALCO, BBSR) is used as the matrix, whereas CSA (procured from the local market), Al₂O₃, Gr is used as reinforcement for the preparation of composites. Al₂O₃ and graphite are supplied by National Aluminium Company limited (NALCO).

Preparation of Al-based Composite

The composites i.e., Al-CSA, Al-Al₂O₃, Al-CSA-Gr, and Al-Al₂O₃-Gr are prepared by using stir casting technique at a constant volume percentage CSA (15%), Al₂O₃ (15%) and graphite (3%).

For the preparation of Al-CSA composite, CSA is used as reinforcement. Initially, coconut shells are crushed in a jaw crusher in order to get small flakes followed by grounding in a hammer mill to produce a coarser form of CSA powder. The obtained powder is packed in a graphite crucible and fired in an electric resistance furnace at the temperature of 1100°C and cooled at furnace temperature to form micro-sized CSA powder. Finally, the CSA powder is sieved in a rotary sieve shaker with the size of ≤ 240 BSS mesh (63 microns). Similarly, the collected Al₂O₃ and graphite are sieved to ≤ 240 BSS mesh and are used as reinforcement.

The stir casting technique is employed for the preparation of Al-MMCs. In this process, the aluminium matrix is pre-heated at 450°C and melting temperature is raised up to 670°C to keep the matrix alloy in a semi-solid state. Also, the as-prepared particles are pre-heated in an electric arc furnace up to 3 hours for 1100°C (CSA), 500°C (Al₂O₃) respectively. The pre-heated-particles are dispersed in a hybrid. Thereafter, the molten metal along with reinforcements is stirred with the help of a motor driven stirrer in the presence of argon gas at a speed of 600 rpm up to 9 minutes. Then, the molten metal is superheated above the liquid temperature at 690°C and poured into a preheated (300°C) cast iron mold of the size of 100 × 20 × 40 mm³. Finally, the composites such as Al-15% CSA, Al-15% Al₂O₃, Al-15% CSA-3% Gr, and Al-15% Al₂O₃- 3% Gr are obtained.

Characterization Techniques

The as-prepared Al-alloys were characterized for their structural, morphological and mechanical properties. X-ray diffraction pattern for the Al-alloys was recorded using an X-ray diffractometer (Phillips PW-1729) using CuK α radiation of wavelength $\lambda = 0.1541$ nm in the scan range $2\theta = 10-60^\circ$. Morphology of the sample was investigated using scanning electron microscope (SEM with EDXA, JEOL JSM-5600LV) which also has been used for compositional analysis of the prepared Al-alloys. Microstructural examinations (ASTM E-7-95) of samples have been carried out using standard metallography technique (ASTM E-7). The entire composite is performed with Brinell hardness tester with a load of 250 kg and 5 mm ball indenter. The tensile properties of the composites have been tested with Hounsfield tensometer (model: ETM-ER3/ 772/12) at a velocity of 1 mm/sec with a maximum load of 20 KN following the ASTM standard E8. Pin on the disc wear testing machine (Model: TR-201 LE-PHM 400) is used for conducting the wear test (ASTM-G99) experiments on composites.

Results and Discussion

Characterization of CSA

XRD Spectrum of coconut shell ash, Al-Al₂O₃, Al-CSA, Al-Al₂O₃-Gr, and Al-CSA-Gr is shown in Figure 1a. Broaden peak is observed from XRD pattern of aluminium



composites at (2 theta), whereas two prominent peaks are observed. The composites are also indicated two peaks with a variation of intensity along with small broaden. This signifies that crystalline phases have existed. Figure 1b, presence of chemical components SiO₂, Al₂O₃, Fe₂O₃ is major constituents in CSA whereas MgO, CaO and K₂O are minor. The EDS peaks indicate the presence of carbon, apparently in the form of graphite. The formation of in-situ mixing of components such as SiO₂, Al₂O₃, and graphite which results improves physical-mechanical properties by thermal treatment. Al₂O₃ and SiO₂ are well-known reinforcing additives for improving wear resistance and strength for Al-MMCs. CaO is reacting with alumina and silica to form aluminates and calcium silicates, which have good adhesive properties and improves load bearing capability [18]. Manganisa (MgO) is a refractory material, which possesses to withstand high temperature, low thermal conductivity, and better thermal shocking resistance [19].

Mechanical Properties of Al-MMCs

The mechanical and physical properties of composites are shown in Figure 2. The hardness of composites i.e. Al-CSA,

Al-Al₂O₃, Al-CSA –Gr, Al-Al₂O₃ – Gr increased due to the hardness of reinforced particle such as CSA, Al₂O₃ in addition to the uniform distribution of reinforcement in composite. Similarly, graphite is less dense substance than aluminum and alumina. Moreover, the graphite percentage increases with increase of porosity and decrease of density shown in Figure 2. The tensile strength increases with intending to volume fraction of CSA, Al₂O₃ particles, even as the elongation decreases with increase in the addition of reinforcement particles. Hardness and % of elongation are inversely proportional character, with an increase in reinforcement as observed in Figure 2, which is due to strain hardening of the composite. The strength of composite has been increasing due to the addition of hard ceramic reinforced particulates. The interfacial among matrix with reinforcement strengthens mechanism of grain size. Reinforcement particles are harder due to the presence of reinforced CSA, Al₂O₃, which increases load bearing capability, and constraints dislocation movement of the matrix reduces interspacing, particle movement has been critical [20–21].

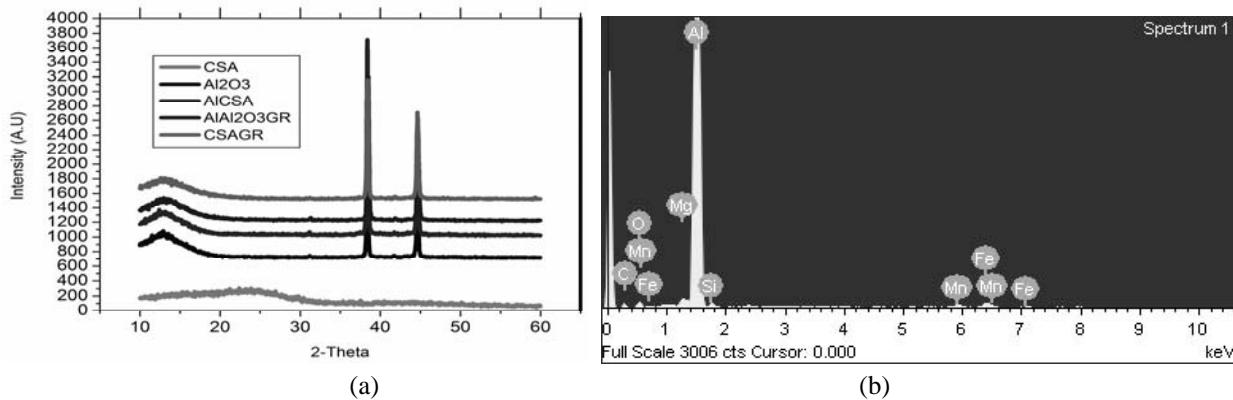


Fig. 1: XRD of Al-Composites with EDS of Coconut Shell

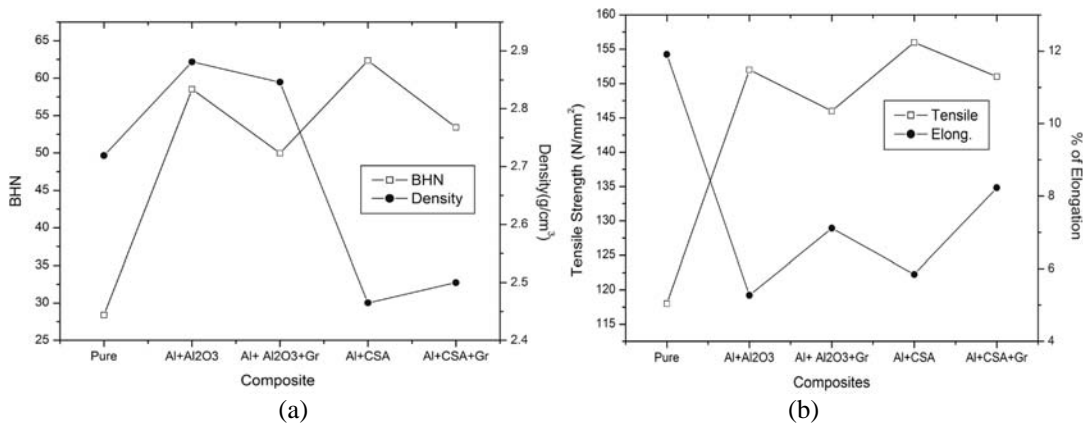


Fig. 2: Properties of Composites



Tribological Study of Composites

Figures 3 & 4 represent the effect of load on condition of a constant sliding distance 2000m and sliding velocity 1.5 m/s). Figure 3, the coefficient of friction is directly proportional to load for all the materials. Pure matrix exhibit least coefficient of friction followed Al-CSA-Gr and Al-Al₂O₃-Gr composites. The coefficient of friction is lower in base matrix due to soft nature. The composite exhibits higher value than the base matrix. Due to the addition of reinforcement, the frictional force has been increased. It conversely increases due to the contact of harder face particles (CSA, Al₂O₃) to counter surface. Moreover, the aluminum (matrix) debris is transferred into the counter surface, resulting in increase in coefficient of friction with respect to load. This can be attributed to the plastic deformation in composite, which increases with increase in applied load. Moreover, due to adhesion, at an early period, the movement between the pin and counter face is difficult. This leads to utilization of more energy to overcome friction between pin and disc, which increases coefficient of friction and plastic deformation.

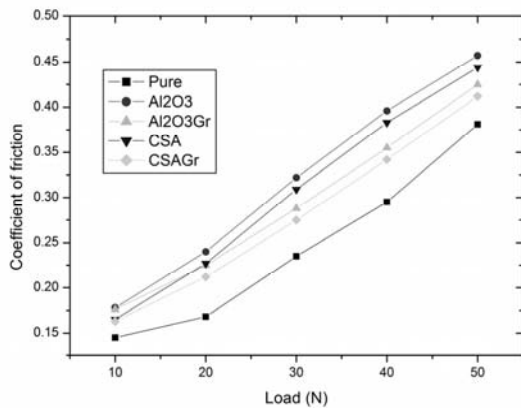


Fig. 3: Coefficient of Friction of Al-composites

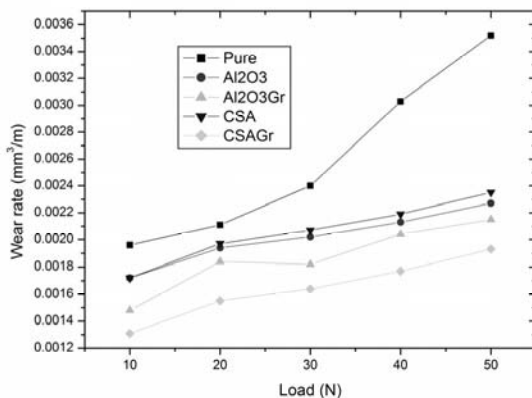


Fig. 4: Wear Rate of Al-Composites

Figure 4 represent wear rate of composites at a constant condition of speed and sliding distance with varying load. It clear that the load increases with increase of wear rate in composites due to thermal softening and high frictional forces. In wear mechanism, the major role in composite as a uniform distribution of particles and interfacial bonding with the matrix. It clearly shows that, the composites with graphite exhibits better wear rate than others since graphite acts as a self-lubricant, foremost to reduction of wear rate. Similarly, the hard phase reinforced particle (CSA, Al₂O₃) are distributed properly and strongly bound with matrix. Finally, Al-CSA-Gr exhibited better wear rate than the other, because of reinforcement (CSA) constitute of various elements and those having own advantages. Al₂O₃, SiO₂, and MgO are capable of bearing of temperature. CaO is a good binder. Similarly, Gr and Fe₂O₃ are forming an oxide layer at the counter face in higher load and sliding distance, which prevent the matrix from plastic deformation.

Conclusions

The AMC composites are successfully prepared by stir casting route using Al1100 as matrix whereas, CSA, Al₂O₃, and Gr are reinforcements. Various elements presents in CSA are examined by EDS, whereas, different phases are observed in XRD pattern. Mechanical and physical properties of all composites are resolute and compared with base alloy. The results exhibit Al-CSA performed better mechanical properties than the other. Moreover, the density of composite are reduced with increase of reinforcements i.e. CSA and Gr. Similarly, the density of composite is increased with addition of Al₂O₃. Al-CSA revealed better hardness and tensile strength than the others. Due to the supplementary of Gr, density and hardness are decreased with improving elongation of composite. Al-CSA-Gr displayed better elongation and low density with better wear resistance than the other. All composite wear resistance has been tested under uniform conditions (i.e. track diameter, sliding velocity and sliding distance) of varying loads from 10 to 50N. All the composites enhanced wear resistance than the base alloy. Graphite composites have superior wear resistance than the other, and also act as a self-lubricant. Al-CSA-Gr composite is exhibiting less wear and weight loss than the others since graphite form a thin film and reinforced particles are harder in nature.

References

- [1] Totten, M.D.S. George E., Totten, G.E. and MacKenzie, D.S., Handbook of Aluminum; Volume 1: Physical Metallurgy and Processes, 2003. doi:10.1201/9780203912607.
- [2] Hatch, J.E., Aluminum Properties and Physical Metallurgy, in: ASM (Ed.), ASM Int., Ohio, US, 1984: pp. 1–24. doi:10.1361/appm1984p001.



- [3] Govindarao, R., Ganguly, R.I., Dash, R.R., Rao, P. Surya Prakash, Reddy, G.S. and Singh, S.K., Development of a Novel Aluminium Based Metal Matrix Composite using Insitu Ternary Mixture (Al_2O_3 - SiC-C) Prepared by Thermal Treatment of Fly-ash, *Trans. Indian Inst. Met.* 68 (2015) 951–958. doi:10.1007/s12666-015-0532-x.
- [4] Rohatgi, P.K., Daoud, A., Schultz, B.F. and Puri, T., Microstructure and mechanical behavior of die casting AZ91D-Fly ash cenosphere composites, *Compos. Part A.* 40 (2009) 883–896. doi:10.1016/j.compositesa.2009.04.014.
- [5] Prasad, N., Sutar, H., Mishra, S.C., Sahoo, S.K., Acharya, S.K., Dry Sliding Wear Behavior of Aluminium Matrix Composite Using Red Mud an Industrial Waste, *Int. Res. J. Pure Appl. Chem.*, 3 (2013), 59–74.
- [6] Siva, S.B. Venkata, Ganguly, R.I., Rao, G. Srinivasa and Sahoo, K.L., Quantitative studies on wear behavior of Al-(Al_2O_3 -SiC-C) composite prepared with in situ ceramic composite developed from colliery waste, *J. Eng. Tribol.* 229 (2015) 823–834. doi:10.1177/1350650115570696.
- [7] Alaneme, K.K., Akintunde, I.B., Olubambi, P.A. and Adewale, T.M., Fabrication characteristics and mechanical behaviour of rice husk ash–Alumina reinforced Al-Mg-Si alloy matrix hybrid composites, *J. Mater. Res. Technol.* 2 (2013) 60–67. doi:10.1016/j.jmrt.2013.03.012.
- [8] Aku, S.Y., Yawas, D.S. and Apasi, A., Evaluation of Cast Al-Si-Fe alloy/Coconut Shell Ash Particulate Composites, *Gazi Univ. J. Sci.* 26 (2013) 449–457.
- [9] Murali, T.P., Surappa, M.K. and Rohatgi, P.K., Preparation and properties of Al-alloy coconut shell char particulate composites, *Metall. Trans. B.*, 13 (1982), 485–494. doi:10.1007/BF02667765.
- [10] Aigbodion, V.S., Hassan, S.B., Dauda, E.T. and Mohammed, R.A., Experimental Study of Ageing Behaviour of Al-Cu-Mg/Bagasse Ash Particulate Composites, *Tribol. Ind.*, 33 (2011), 28–35.
- [11] Surappa, M.K., Aluminium matrix composites: Challenges and opportunities, *Sadhana.* 28 (2003) 319–334.
- [12] Shen, Y.L., Williams, J.J., Piotrowski, G., Chawla, N. and Guo, Y.L., Correlation between tensile and indentation behavior of particle-reinforced metal matrix composites: An experimental and numerical study, *Acta Mater.* 49 (2001) 3219–3229. doi:10.1016/S1359-6454(01)00226-9.
- [13] SEO, Y.H. and Kang, C.G., Effects of hot extrusion through a curved die on the mechanical properties of SiCp/Al composites fabricated by melt-stirring, *Compos. Sci. Technol.* 59 (1999), 643–654. <http://cat.inist.fr/?aModele=afficheN&cpsidt=1910144> (accessed August 1, 2016).
- [14] Boopathi, M., Arulshri, K.P. and Iyandurai, N., Evaluation of Mechanical Properties of Aluminium Alloy 2024 Reinforced With Silicon Carbide and Fly Ash Hybrid Metal Matrix Composites, *Am. J. Appl. Sci.*, 10 (2013), 219–229. doi:10.3844/ajassp.2013.219.229.
- [15] Aigbodion, V.S. and Hassan, S.B., Effects of silicon carbide reinforcement on microstructure and properties of cast Al–Si–Fe/SiC particulate composites, *Mater. Sci. Eng. A.* 447 (2007) 355–360. doi:10.1016/j.msea.2006.11.030.
- [16] Kumar, G.B.V., Rao, C.S.P., Selvaraj, N. and Bhagyashekar, M.S., Studies on Al6061-SiC and Al7075-Al 2O_3 Metal Matrix Composites, *J. Miner. Mater. Charact. Eng.* 9 (2010) 43–55. doi:10.4236/jmmce.2010.91004.
- [17] Kök, M., Özdin, K., Wear resistance of aluminium alloy and its composites reinforced by Al_2O_3 particles, *J. Mater. Process. Technol.*, 183 (2007), 301–309. doi:10.1016/j.jmatprotec.2006.10.021.
- [18] Kenny, M., Oates, T., Kenny, M. and Oates, T., Lime and Limestone, in: *Ullmann's Encycl. Ind. Chem.*, Wiley-VCH Verlag GmbH & Co. KGaA, Weinheim, Germany, 2007. doi:10.1002/14356007.a15_317.pub2.
- [19] Baghchesara, M.A., Abdizadeh, H. and Baharvandi, H.R., Effects of MgO Nano Particles on Microstructural and Mechanical Properties of Aluminum Matrix Composite Prepared via Powder Metallurgy Route, *Int. J. Mod. Phys. Conf. Ser.* 5 (2012) 607–614. doi:10.1142/S201019451200253X.
- [20] Alpas, A.T. and Zhang, J., Effect of microstructure (particulate size and volume fraction) and counterface material on the sliding wear resistance of particulate-reinforced aluminum matrix composites, *Metall. Mater. Trans. A.* 25 (1994), 969–983. doi:10.1007/BF02652272.
- [21] Chawla, N. and Shen, Y., Mechanical Behavior of Particle Reinforced Metal Matrix Composites, *Adv. Eng. Mater.* 3 (2001) 357–370. doi:1438-1656/01/0606-0357 \$ 17.50+.50/0.



Advanced High Strength Steel for Structural Applications

B. Chaudhuri¹ and A.K. Samanta²

Abstract: High strength steel (yield strength >350 MPa), though popular in developed countries, is comparatively new product in India. Main reasons are the loss of elongation and weldability of high strength steel compared to normal mild steel. When combined with appropriate manufacturing techniques, advanced high-strength steels offer opportunities for reduced product weight, enhanced crash performance, manufacturing process consolidation and cost reduction.

The paper analyzes the reasons for not using high strength steel for structural purposes widely. The aim of the paper is to provide guidance to design and fabricate structure with high strength steel. The properties that need to be considered by designers when specifying steel construction products are Strength, Toughness, Ductility, Weldability and Durability. The use of high tensile steel can reduce the volume of steel needed but the steel needs to be tough at operating temperatures and it should also exhibit sufficient ductility to withstand any ductile crack propagation. Therefore, higher strength steels require improved toughness and ductility, which can be achieved only with low carbon clean steel and by maximizing grain refinement. The implementation of the Thermo-Mechanical Rolling process (TMR) is an efficient way to achieve this. The paper analyzes the various ways by which high strength steel will help in sustainable development of structure with economy.

Keywords: High Strength Low Alloy Steel, Thermo-Mechanical Controlled Processes (TMCP), Weldability, Durability.

Introduction

Steel is extensively used for structural purpose because of its high strength to weight ratio in comparison with any other materials such as concrete. In fact, in many cases, steel is the only material that can be used such as rail. Steel used for general purpose has been specified in IS: 2062–2011. Chemical composition and mechanical properties of the steel specified in given in Table 1 and Table 2. High Strength Steel, as indicated by name, offers higher level of strength, normally more than 350 MPa yield stress. Higher level of strength is desirable because it make structure lighter. However, there is some hindrances. The structures are made through welding as an important joining method. Carbon equivalent of the steel having more that 350 MPa yield stress is 0.50% or above which makes the welding of steel difficult. That is why structural steel having less than 350 MPa yield stress is generally available and is used in India. Fatigue is another criterion. The hindrances have been removed by the production of high strength low alloy (HSLA) steel.

HSLA steels differ from other steels in the way that they are not made to meet a specific chemical composition but rather

to specific mechanical properties. The carbon content ranges between 0.05–0.25% to retain formability and weldability. These steels are weldable. In some cases, MIG, TIG, FCAW or similar advanced welding processes may be required. Their yield strengths can be anywhere between 250–800 MPa [1] or more. Because of their higher strength and toughness, HSLA steels usually require 25% to 30% more power to form, as compared to carbon steels. Copper, silicon, nickel, chromium and phosphorus are added to increase corrosion resistance. Zirconium, calcium, and rare earth elements are added for sulfide-inclusion shape control which increases formability. These are needed because most HSLA steels have directionally sensitive properties.

Formability and impact strength can vary significantly when tested longitudinally and transversely to the grain. Bends that are parallel to the longitudinal grain are more likely to crack around the outer edge because it experiences tensile loads. This directional characteristic is substantially reduced in HSLA steels that have been treated for sulfide shape control. Properties of few HSLA steel are given in Table 3.

¹ Professor & Director (Project), SDET-Brainware Group of Institution, Kolkata, India.

² Manager (Mechanical), Institute For Steel Development & Growth, Kolkata, India. ✉ asim_samanta@hotmail.com



Table 1: Chemical Composition of Structural Steel (IS: 2062–2011)

Grade/ Designation	Quality	Ladle Analysis, % Max					CE, % Max	Mode of Deoxidation
		C	Mn	S	P	Si		
E 250	A	0.23	1.50	0.045	0.045	0.40	0.42	Semi Killed/Killed
	BR/BO	0.22	1.50	0.045	0.045	0.40	0.41	Semi Killed/Killed
	C	0.20	1.50	0.040	0.040	0.40	0.39	Killed
E 275	A	0.23	1.50	0.045	0.045	0.40	0.43	Semi Killed/Killed
	BR/BO	0.22	1.50	0.045	0.045	0.40	0.42	Semi Killed/Killed
	C	0.20	1.50	0.040	0.040	0.40	0.41	Killed
E 300	A/BR/BO	0.20	1.50	0.045	0.045	0.45	0.44	Semi Killed/Killed
	C	0.20	1.50	0.040	0.040	0.40	0.44	Killed
E 350	A/BR/BO	0.20	1.55	0.045	0.045	0.45	0.47	Semi Killed/Killed
	C	0.20	1.50	0.040	0.040	0.45	0.45	Killed
E 410	A/BR/BO	0.20	1.60	0.045	0.045	0.45	0.50	Semi Killed/Killed
	C	0.20	1.60	0.040	0.040	0.45	0.50	Killed
E 450	A/BR	0.22	1.65	0.045	0.045	0.45	0.52	Semi Killed/Killed
E 550	A/	0.22	1.65	0.020	0.025	0.50	0.54	Semi Killed/Killed
E 600	BR	0.22	1.70	0.020	0.025	0.50	0.54	Semi Killed/Killed
E 650	A/BR	0.22	1.70	0.015	0.025	0.50	0.55	Semi Killed/Killed

Table 2: Properties of Structural Steel (IS: 2062–2011)

Grade/ Designation	Quality	UTS, Min, MPa	Yield Stress Min MPa			Elongation % Min.	Bend Diameter		Charpy Impact Test	
			<20	20–40	>40		< 25	>25	Temp, °C	Min, J
E 250	A	410	250	240	230	23	2t	3t	–	–
	BR	410	250	240	230	23	2t	3t	RT	27
	BO	410	250	240	230	23	2t	3t	0	27
	C	410	250	240	230	23	2t	3t	–20	27
E 275	A	430	275	265	255	22	2t	3t	–	–
	BR	430	275	265	255	22	2t	3t	RT	27
	BO	430	275	265	255	22	2t	3t	0	27
	C	430	275	265	255	22	2t	3t	–20	27
E 300	A	440	300	290	280	22	2t	–	–	–
	BR	440	300	290	280	22	2t	–	RT	27
	BO	440	300	290	280	22	2t	–	0	27
	C	440	300	290	280	22	2t	–	–20	27
E 350	A	490	350	330	320	22	2t	–	–	–
	BR	490	350	330	320	22	2t	–	RT	27
	BO	490	350	330	320	22	2t	–	0	27
	C	490	350	330	320	22	2t	–	–20	27
E 410	A	540	410	390	380	20	2t	–	–	25
	BR	540	410	390	380	20	2t	–	RT	25
	BO	540	410	390	380	20	2t	–	0	25
	C	540	410	390	380	20	2t	–	–20	25
E 450	A	570	450	430	420	20	2.5t	–	–	–
	BR	570	450	430	420	20	2.5t	–	RT	20
E 550	A	650	550	530	520	12	3t	–	–	–
	BR	650	550	530	520	12	3t	–	RT	15
E 600	A	730	600	580	570	12	3.5t	–	–	–
	BR	730	600	580	570	12	3.5t	–	RT	15
E 650	A	780	650	630	620	12	4t	–	–	–
	BR	780	650	630	620	12	4t	–	RT	15



Table 3: Properties of HSLA Steels

Standard	Grade	Ladle Analysis, % Max					UTS, Min, MPa	Y S, Min, MPa
		C	Mn	S	P	Si		
ASTM A 514	B	0.21	1.00	0.035	0.035	0.35	760	690
	H	0.21	1.00	0.035	0.035	0.35	760	690
	F	0.20	1.00	0.035	0.035	0.35	760	690
	Q	0.21	1.30	0.035	0.035	0.35	690	621
ASTM A 656	80	0.18	1.65	0.035	0.025	0.60	620	550
ASTM A 572	50	0.23	1.35	0.050	0.040	0.40	450	345
EN 10149	S 460 MC	0.12	1.60	0.020	0.025	0.50	520	460
EN 10149	S 700 MC	0.12	2.10	0.015	0.025	0.60	750	700

Manufacturing of High Strength Steel

Many of the well understood metallurgical principles can be utilised to satisfy the overall mechanical property requirements for high strength structural steels, namely [2]:

- reduced carbon content to improve weldability and toughness.
- decreased grain size (ferrite and/or bainite) to give increased strength and increased toughness.
- decreased impurity content (S, P, O) to increase toughness in particular and through thickness homogeneity.
- increased alloying with Ni, Cr, Mo to give solid solution and transformation strengthening, especially at the higher strength levels.

Hot metal, after pretreatment [3] is refined in an oxygen blowing converter. Then the molten steel is treated using a vacuum degasser to achieve lower carbon content. The decarburising step is followed by addition of microalloying elements, with the aim of formation of carbides of microalloying elements for precipitation hardening [4].

Molten steel that has had its chemical composition thus adjusted is continuously cast into slabs, which in turn, passes through subsequent processes such as hot rolling, cold rolling and turned into final products. The vertical mould continuous caster, in which the mould and support rolls are arranged vertically, is used for better quality because it promotes the separation (by flotation) of non-metallic inclusions poured into the mould.

The main purpose of HSLA steel processing is to produce fine and homogenous ferrite grains as well as high volume fraction of carbide/nitride precipitate during or after austenite-ferrite transformation.

Thermo-Mechanical Controlled Processing (TMCP) is adopted during rolling [5]. In controlled rolling operation, specific amount of deformation is given at specific temperature range. The basic essence of controlled rolling operation is grain refinement through repeated crystallisation, during which appropriate microstructure and mechanical properties are imparted. The steels are reheated to 1050–1250°C and soaked enough for sufficient dissolution of carbonitride precipitates. Rolling passes in the roughing stand has to be designed to reduce the austenite grain size by successive recrystallisation. Thereafter, further reduction is achieved in finishing stands at suitable temperature (about 800–500°C).

To compensate for the loss of carbon and to increase tensile strength, small additions of alloying elements such as niobium (<0.10%), titanium (<0.030%) and vanadium (<0.15%) are made, perhaps also with small amounts of molybdenum, chromium, copper and nitrogen. These elements are strong carbide and nitride formers, producing a fine dispersion of stable precipitates that inhibit grain growth during hot rolling and assist in nucleating fine grained ferrite during cooling. These elements also provide some increase in strength by precipitation hardening. The effect of alloying element is given in Table 4.

Table 4: Effect of Alloying Elements on High Strength Steel

Element	Percentage added	Effect on Properties
Copper	0.2–1.5	Improves atmospheric corrosion resistance
Nickel	At least half of the copper content	Benefits surface quality
Niobium	0.02	Increased tensile strength and yield point
Nitrogen	0.003–0.012	Contributes to strength and can improve weldability
Vanadium	Up to 0.12	Increases strength without reducing weldability



Welding of HSLA Steels

IS: 2062–2011 specifies steel up to 650 MPa Yield Stress. If high strength steel is produced by increasing of carbon then carbon equivalent becomes more ($>0.50\%$) which turns the steel to be more difficult for welding and less resistant to fatigue.

But HSLA steels show generally improved weldability compared to conventional structural steels. For example, S460 grade steel has CE of 0.40 which is lower than that of S355 grade steel [6]. Despite the improved weldability, there are some fabrication problems. Firstly, hydrogen induced cold cracking.

The low carbon content, hence low carbon equivalent, sometimes less than 0.30 CE, means that these steels have a low sensitivity to hydrogen cold cracking but it may be noted that the standard carbon equivalent formula is not valid for all of these steels and cannot always be relied upon when calculating preheat temperatures.

The HSLA steels can be welded with lower preheats than would be permitted for conventional carbon-manganese steels, despite their higher strength. The highest risk of cold cracking in these types of steels is therefore in the weld metal, rather than in HAZ. There are several reasons for this.

- (a) The high strength of the parent metal means higher residual stresses during welding.
- (b) To match the tensile strength and toughness of the parent steel, the filler metals need to be more highly alloyed and therefore will have a higher CE.
- (c) The weld metal transforms from austenite to ferrite at a lower temperature than the parent steel (it is generally the other way round in a conventional carbon-manganese steel) meaning that any hydrogen in the HAZ is rejected into the still austenitic weld metal which has a high solubility for hydrogen.

A preheat based on the weld metal composition is therefore advisable and low hydrogen techniques must be used.

Secondly, even though steels generally have very low levels of sulphur, the steels containing less than 0.05% C may suffer from solidification cracking in the root pass of butt joints, particularly if the root bead is deposited at a high welding speed. The reason for this is that high dilution of the filler metal produces a weld metal low in carbon. This low carbon content in its turn leads to excessive grain growth of the austenite during welding and these large grains increase the risk of centre line solidification cracking in the root bead. This problem appears to be most prevalent in pipe butt joints welded using cellulosic electrodes, probably due to it being possible to use a fast, vertical-down welding technique.

Thirdly, toughness and strength in the HAZ can be an issue. The steel manufacturer takes great care to control rolling temperatures and cooling rates to provide the desired properties. The component is then welded, producing a heat affected zone that has experienced an uncontrolled cycle of heat treatment. The microstructure in the HAZ will vary with respect to the composition of the steel and the welding process heat input. A high heat input will promote grain growth and this will have an adverse effect on both strength and toughness. As a rule of thumb, heat input should be restricted to around 2.5 kJ/mm maximum and the interpass temperature maintained at 250°C maximum, although some of the steels containing titanium and boron can tolerate heat inputs as high as 4.5 kJ/mm without undue loss of strength. For a definitive statement on heat input control the advice of the steel manufacturer should be sought.

These steels must under no circumstances be normalised or tempered although post weld heat treatment (PWHT) is often a requirement when the component thickness is greater than 30 mm. Care needs to be taken, if PWHT is applied, that the soak temperature does not exceed 600°C; a temperature range of 550°C to 600°C is often specified. The reason for this is that many of the TMCP steels are accelerated cooled to a temperature of around 620°C; heat treating at or close to this temperature will result in a substantial reduction in tensile strength due to over-tempering. The same restriction applies to any hot working activity-plate must not be hot rolled and the temperature of local heating for correction of distortion must not be allowed to exceed 600°C. It should be noted that PWHT is not recommended in case of Q & T high strength steels.

HSLA steel (especially AST A656 Grade 80) can be easily welded using suitable shop or field practices by all the usual low-hydrogen welding processes; Shielded Metal-Arc (SMAW) with AWS-E9018 electrode, Submerged-Arc (SAW) with flux/wire combination of matching strength, Gas Metal Arc (GMAW) with ER90 wire, and Flux Cored (FCAW) with E90T wire. In all the cases, except submerged arc welding [7], a precautionary preheat of 250°F (120°C) is recommended to remove any surface moisture for thicknesses up to 20 mm.

Use of High Strength Steel

The development and use of High Strength Low Alloy (HSLA) steels has been driven by the need to reduce costs, the higher strength compared with conventional carbon-manganese steel enabling thinner and lighter structures to be erected. The majority of these steels are to be found in structural applications, offshore structures, buildings, ship-



building etc. Tensile strengths of up to 690 MPa are achievable whilst still maintaining good weldability and high notch toughness. In practical design, however, other factors also have to be considered for a successful application of these steels, e.g., formability, weldability, stiffness, buckling, safety, crash resistance and fatigue.

In addition to the above, HSLA steels have been found to be used in various industries which include oil and gas pipeline (with lower impact transition temperature value, also suitable in arctic region), heavy-duty highway and off-road vehicles (having increased load bearing capacities and better environmental friendliness), construction and farm machinery, industrial equipment, storage tanks, mine and railroad cars, barges and dredges, lawn mowers etc. High strength steels can increase static strength, crash resistance, and energy absorption. Cold-rolled and hot-dip galvanized steel grades are today used successfully in the automotive industry for increased safety and weight reduction in applications like door impact beams, bumper reinforcements and seat construction [8].

An interesting advantage of HSLA steels is seen in the construction of tall television transmitter masts. The extra strength of the steel has helped the sections making up the mast can be thinner and more stable because they offer less resistance to the wind. HSLA steel makes it more durable and gives it a longer useful life span. It is therefore selected for use in street lighting poles, oil storage tanks and earth moving equipments.

Use of High Strength Steel in Construction

The general principles of design of structures on the limit state at which they would become unfit for their intended use. Previously, an acceptable margin of strength was ensured by limiting the calculated stresses under working load to some proportion of the material strength, say $2/3^{\text{rd}}$ of yield stress. It is now appreciated that in many parts of a steel structure, yield stress is reached locally without distress. Due to the reserves of ductility in the steel, the member possesses margins of strength much greater than that supposed by 'elastic' design.

Failure due to inadequate strength is only one of a relevant ultimate limit states for structural steelwork. Others are instability due to sway, overturning or buckling, fatigue and brittle fracture. Serviceability checks are also carried out in relation to excessive deflection, vibration and corrosion.

The selection of the grade of steel to be used in a structure depends not only on economics but also on the stress system imposed on the member. The effect of tensile, compressive and bending stresses on the load carrying capacity of hot rolled sections is discussed below.

Tension Members!

The tension member transmitting a direct pull between two points in a structure is the simplest and most effective structural element. In theory, it may be thin and of small cross section but in practice its efficiency may be impaired by the end connections required to join it to other members in the frame. Some of the main uses are as tension chords and internal ties in trusses and lattice girders, bracing members and hangers in suspended buildings. Open and closed single rolled sections such as angles or channels are typical of light trusses or are used as compound sections when the loads are heavier. Larger H sections are used to support heavy loads such as in a truss bridge or as heavy lattice girders in industrial buildings. Splices are needed to join long tension members that have been broken into shorter sections for ease of fabrication and erection.

The most economical and efficient use of HSLA steels is in members stressed in tension and where dead load is the predominant load.

Beams

The main function of beams is to transfer load by bending action. In a typical multi-storey building they would comprise the horizontal members which span between adjacent columns. Secondary beams might also be used to transmit the floor loading to the main beam. For the most usual forms of structural framing, it is normally sufficient to consider only bending effects. In such cases the applied load will increase until the full plastic moment is reached at the most highly stressed cross section resulting in the formation of a plastic hinge. It is assumed that this can take place without premature buckling of the compression flange toes or the web.

Using hybrid steel girders (i.e. welded girders with combination of steel grades, usually HSS in the flanges and ordinary steel grades in the web) instead of homogeneous steel girders offers a more economical solution in compression.

Columns

The principal function of the column is to transfer compressive loads but it may also be required to carry bending moments depending upon its location in the structure. Under a nominally axial load, the response of the member depends on a number of factors, the most important being its length and cross sectional area, the stress/strain characteristics of the steel, the conditions of its support and the method of manufacture. Ideally, stocky columns deform by squashing under load when the yield stress is reached.



If the material experiences strain hardening at high strains, the condition of first yield is not affected but the collapse load may be increased. This will be more significant at low slenderness ratios for which the deformation is predominantly plastic. A number of the higher strength steels show no yield point but exhibit work hardening; this would also have a beneficial effect at low slenderness ratios. These suggest that the benefits of using higher strength steel arise for slenderness ratios below approximately 60.

An example of higher strength for column is given here. For a four storey office building, the column is initially designed with HEA 240 steel with a minimum yield stress of 240 N/mm². The column distance was 7.2 m in each direction with an imposed floor loading of 2 kN/m². The buckling length was taken to be 70% of the column height. By substituting steels with yield stresses of 355 and 460 N/mm², it was possible to reduce the basic section size to HEA 200 and HEA 180 respectively. The corresponding weight savings were 26% and 38%. A maximum reduction of 40% in the space occupied by the columns was calculated using the steel with a yield stress of 460 N/mm². An increase in floor loading to 3.5 kN/m² simulated the design of a multi-storey car park using the same column sizes and distances. In this case replacing mild steel with the 460 grade resulted in a weight saving of up to 40% and a reduction in the space occupied by each column of up to 33%.

In compression, High Strength Steel are most effective in heavily loaded, stocky columns or in stiffened compression elements where buckling is not the controlling criterion [9].

Fatigue

When fatigue is the decisive factor in the design, the higher yield strength does not seem to offer additional economic advantages, because the static design stresses are limited and the higher grade cannot be effectively utilized [10]. However, in case, fatigue problems are only localized (e.g. in a number of joints/connections), improvements at fatigue sensitive locations can be achieved by altering the design at the specific location (e.g. use cast joints instead of direct welded connections in truss, use locally thicker steel plates etc.) and/or by post weld treatments. Therefore, economic benefits from the hybrid construction (combination of high strength and mild steel grades) can still be gained from the overall structure steel dead weight reduction.

Conclusion

Application of high strength steels offer great potential for the use of high strength steels when strength is the governing criterion. The advantages of using HSS are generally a result of reduced weight and dimensions. Design stresses can be increased and section thickness may be reduced, resulting in significant weight savings. Reduced section thickness can also save on welding costs as well as on fabrication, erection and transportation costs. Simplified structural components and construction techniques are often possible, particularly for large structures and foundation costs may also be reduced due to lower dead weight.

Moreover, using high strength steel (HSS) not only enhances economy in the first place but also contributes in saving resources.

References

- [1] Kim, Do-Hwan; Lee, Seung-Eun and Kim, Jin-Ho, "HSA800 – High Strength Steel for Buildings", *CTBUH 9th World Congress Proceedings*, p. 817, 2012, Shanghai.
- [2] Billingham, J., Sharp, J.V., Spurrier, J. and Kilgallon, P.J., "Review of the Performance of High Strength Steels Used Offshore", *School of Industrial and Manufacturing Science, Cranfield University, Cranfield, Bedfordshire*, 2003.
- [3] Khanna, Rachit and Jha, Shambhu Kumar, "High Strength Low Alloy Steels–Indian Scenario".
- [4] Watanabe, Yoshiyuki; Ishibashi, Kiyoshi; Yoshi, Kenichi; Inoue, Hajime and Yoshida, Yuzuru, "Development of 590 N/mm² Steel with Good Weldability for Building Structures", *NIPPON Steel Technical Report*, No. 90, July 2004.
- [5] Skobir, Danijela A., "High Strength Low Alloy (HSLA) Steels", *Institute of Metals and Technology*, Ljubljana, Slovenia.
- [6] Schroter, F., "Trends of Using High Strength Steel for Heavy Steel Structure", AG der Dillinger Huttenwerke, Dillingen, Germany.
- [7] "A 656 Grade 80 Steel Plate"–SSAB Brochure.
- [8] Jan-Olof Sperle and Kennet Olsson, "High Strength and Ultra High Strength Steel for Weight Reduction in Structural and Safety Related Applications", SSAB Tunnpå AB, Borlänge, Sweden.
- [9] Gogou, Eleni, "Use of High Strength Steel Grades for Economical Bridge Design", Department of Civil Engineering and Geosciences, Delft University of Technology, Iv-Infra, Amsterdam, April 2012.
- [10] Latham, D.J. and Lapwood, D.G., "Increased Use of Higher Strength Steel in Structures", *Technical Steel Research Report, Commission of the European Communities*, 1991.



Effect of Ceria (CeO_2) and Yttria (Y_2O_3) Coating on High Temperature Corrosion Resistance of 2.25 Cr-1 Mo Steel in $\text{SO}_2 + \text{O}_2$ Atmosphere

D. Ghosh¹, S. Das² and S.K. Mitra³

Abstract: This work is primarily aimed to study the effect of Ceria (CeO_2) and Yttria (Y_2O_3) superficial coating on the high temperature corrosion behavior of 2.25 Cr-1 Mo steel in $\text{SO}_2 + \text{O}_2$ (ratio 2:1) environment. The isothermal corrosion study of uncoated as well as Ceria and Yttria coated specimens are carried out in $\text{SO}_2 + \text{O}_2$ environment at 973 K for 150 hours. The post corroded specimens are characterized in SEM, EDS and XRD. The results show significant improvement of corrosion resistance of coated specimen in comparison to the uncoated one. All the specimens show parabolic rate growth kinetics which indicates that corrosion is governed by outward cation and inward anion migration. The thermal cycling behavior (upto three cycles) of the uncoated and coated specimens are also examined in the same environment for 100 hours. The results show that Ceria and Yttria coated specimen shows significant improvement of the corrosion resistance compared to uncoated specimens under thermal cycles. The parabolic rate constant (k_p) of Ceria and Yttria coated specimen decreases as thermal cycling increases. The detail mechanism of corrosion is explained in this paper.

Keywords: 2.25 Cr-1 Mo Steel, Corrosion, Ceria, Yttria, Thermal Cycling.

Introduction

Low alloy Cr-Mo steel such as 2.25 Cr-1 Mo steel are widely used for construction of super-heater and re-heater tubes of thermal power plant boilers, petrochemical and refinery industries. High temperature corrosion is a key issue for different engineering components in different aggressive environments. The drastic material degradation of the component leads to premature failure of the component and affect the reliability, availability and safety of the component [1–4]. These components are operated at high temperature and are subjected to thermal fluctuations under normal operating conditions and hence, need protection from high-temperature corrosion resistance. Numerous investigation regarding the beneficial effect of rare-earth elements or their oxides either in the form of alloy additions or oxide dispersions in the alloys have received special attention for more than two decades for improving high temperature oxidation resistance as well as exhibiting improved scale adherence to the metal/alloy substrates [5–12]. The aim of most of these studies is to judge the high temperature corrosion behavior under isothermal and cyclic environment. However, many metallic components in different industries are invariably subjected to sulfidizing environments under

the actual service conditions which frequently lead to the failures of protective Cr_2O_3 layers and thus allow more aggressive attack of the metallic components.

High temperature corrosion of structural alloys in sulfur bearing environments is many orders of magnitude higher than in oxidizing environments. The corrosion is drastic at high temperature in sulfur bearing environments and often lead to the severe metal loss from the external surface and finally results in premature retirement of the components. The addition of reactive elements, such as Cerium and Yttrium, is of interest because of their beneficial effects on oxide scale properties, including resistance to spallation [8–17]. Addition of these elements is possible either by alloying or by incorporation into a surface layer (for instance, by ion implantation or by coating).

The present study is an attempt to investigate the high temperature corrosion behaviour of uncoated and CeO_2 and Y_2O_3 coated low alloy steel (2.25 Cr-1 Mo) under isothermal conditions. The estimation of the corrosion rate and the study of reactions kinetics are necessary supplements in this investigation along with post corroded scale characterization.

¹ Scientist, NDT & Metallurgy group, CSIR – Central Mechanical Research Institute CMERI, Durgapur, India. ✉ dbslo12000@gmail.com

² Junior Research Fellow, NDT & Metallurgy Group, CMERI, Durgapur–713209, India.

³ Professor, Metallurgical and Materials Engineering Dept, NIT, Durgapur, India.



Materials and Methods

The initial material is normalized (1223 K/30 min/air cooled) and tempered (1003 K/60 min/air cooled) 2.25 Cr-1 Mo steel plate of 6.0 mm thickness. The chemical compositions of the steel is estimated and is shown in Table 1. The specimen coupons of dimensions 30 mm × 20 mm × 2 mm are prepared from the initial material for the experimental studies. The specimen coupons were further subjected to mechanical polishing upto 1000 grit Sic emery paper. The specimen was subsequently rinsed in distilled water followed by drying in acetone.

Table 1: Chemical Analysis (Weight Percent) of 2.25 Cr-1 Mo Steel

C	Mn	Si	S	P	Cr	Mo	Fe
0.11	0.51	0.19	0.008	0.012	2.07	0.95	Balance

The CeO₂ (3 μm) and Y₂O₃ (5 μm) powders are taken for the superficial coating. The CeO₂ and Y₂O₃ powder are separately mixed thoroughly with ethanol to prepare a slurry for superficial coating. The polished samples are dipped in the slurry for 10 minutes to have a uniform coating over the substrate. The deposited substrate are further dried in oven at 473 K for 120 minutes to obtain good adherent coatings. The slurry is prepared for the different concentrations of the powder to achieve different depositions rate over the substrate. Finally, three deposition rate (0.15 mg/cm², 0.30 mg/cm² and 0.50 mg/cm²) by changing the concentration of CeO₂ powder are obtained the slurry. In the same way, superficial coating of two different deposit (0.15 mg/cm² and 0.25 mg/cm²) of Y₂O₃ were also prepared.

The coated samples are mounted in cross section and the samples are further examined in Scanning Electron Microscope (Model-Hitachi S-3000 N, Make-Hitachi limited, Japan). The cross-sectional view of the Ceria (CeO₂) and Ytria (Y₂O₃) coated sample is shown in Figure 1.

Experimental Procedure

Isothermal corrosion study was carried out in mixed gas SO₂/O₂ (2:1) environment at 973 K for 150 hours in a Vertical tubular furnace attached with digital weighing balance. The SO₂ and O₂ cylinders with calibrated flow meter were connected with the furnace for preparation of the corrosive environment. The calibrated flow meter was used for controlling the gas flow of SO₂ and O₂. All the gases were supplied by M/S British Oxygen Limited (BOC) with 99.99% purity. The SO₂ and O₂ mixture (2:1 ratio by volume) was prepared by controlling the desired flow through the gas flow meter. The mixed gases were dried with P₂O₅ before entering into high temperature furnace. The total flow rate maintained was approximately 80 ml/minute in all the cases. The partial pressure of oxygen (P_{O₂}) and sulfur (P_{S₂}) in

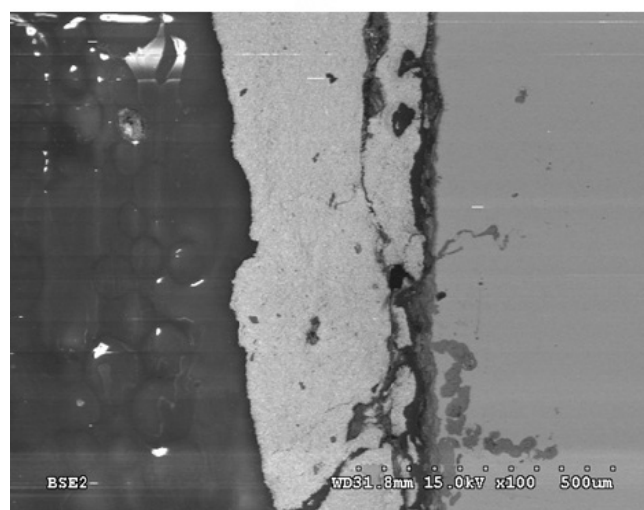
equilibrium with SO₂ was estimated and found to be P_{O₂} = 1.5 × 10⁻¹¹ atm and P_{S₂} = 0.75 × 10⁻¹¹ atm respectively.

Since, the equilibrium of the reaction SO₂ + ½O₂ = SO₃ is slowly established, a Platinum (Pt) catalyst was used to ensure the rapid equilibration. The catalyst was made from the Pt-mesh in the form of a small bucket, in which the specimen was placed inside the horizontal tube furnace.

Post corroded specimens were characterized using Scanning Electron microscopy (SEM), Energy dispersive spectroscopy (Model-Thermo EDS, Make Thermonoran, USA) and X-ray diffraction system (XRD) [Model-TestPro make-PANalytical, Netherlands).



(a)



(b)

Fig. 1: Cross Sectional View of (a) CeO₂ Coated (50 mg/cm²) and (b) Y₂O₃ Coated (0.25 mg/cm²) Specimen



Results and Discussion

SEM Study of the Coated Specimen

Figure 2 shows the SEM micrograph of the top surface of CeO₂ coated (0.30 mg/cm²) and Y₂O₃ coated (0.15 mg/cm²) specimens. The figure shows globular type of deposit in case of CeO₂ coated specimen Figure (2a), which is adherent over the substrate while, Figure (2b) shows, irregular shaped adherent deposits over the substrate.

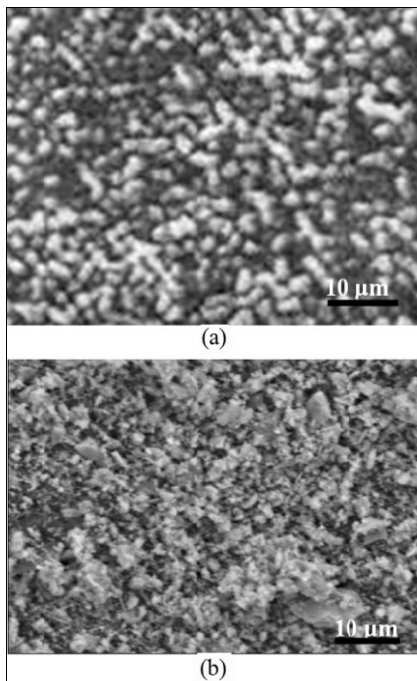


Fig. 2: SEM Micrograph of Top Surface of (a) CeO₂ Coated (0.30 mg/cm²) and (b) Y₂O₃ Coated (0.15 mg/cm²) Specimen

Kinetic Behavior

The kinetic data of the mass gain per unit area as a function of time for the uncoated CeO₂ and Y₂O₃ coated steel are presented in Figure 3. The CeO₂ coating (0.30 mg/cm² depositions rate) gives a significant improvement in corrosion resistance in SO₂ + O₂ environments in comparison to the uncoated specimen as suggested in Figure 3(a). The figure also reveals that the highest corrosion resistance is achieved in case of CeO₂ coating of optimum depositions rate (0.30 mg/cm²). Neither too low (0.15 mg/cm²) or too high (0.50 mg/cm²) coating depositions rate, shows the best corrosion resistance.

The kinetic behavior of the uncoated and Y₂O₃ coated specimens is shown in Figure 3(b). The figure reveals significant improvement of the corrosion rate in case of coated specimen. The figure also suggests the best corrosion resistance at optimum depositions rate (i.e. 0.15 mg/cm²).

The figure also suggests that most of the coated and uncoated specimen follows approximately parabolic rate kinetics as per the following equations,

$$\left(\frac{\Delta W}{A}\right)^2 = K_p t \quad \dots (1)$$

where, $\Delta W/A$ = weight gain per unit area (mg/cm²);
 K_p = parabolic rate constant (mg²cm⁻⁴s⁻¹)
 t = time in seconds.

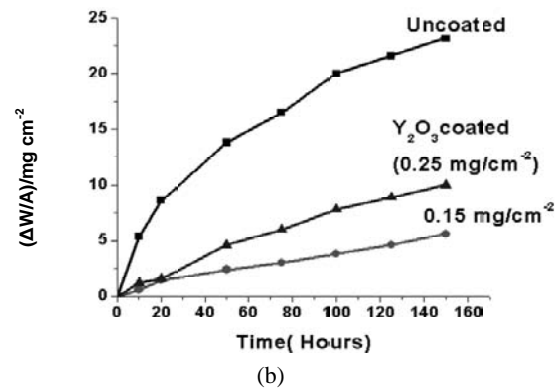
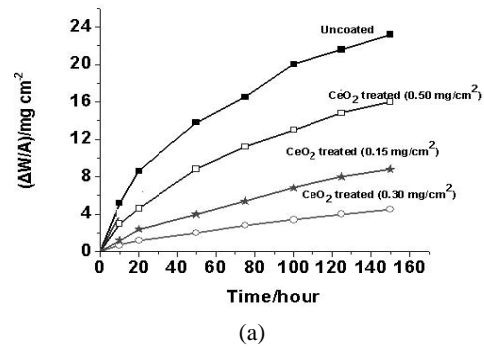


Fig. 3: Weight Gain vs Time Plot of (a) Uncoated and CeO₂ Coated and (b) Uncoated and Y₂O₃ Coated 2.25 Cr-1 Mo Steel in SO₂ + O₂ (2:1) Environment at 973 K for 150 Hours

Characterizations of Post Corroded Specimens

Figure 4 reveals the SEM morphology of the outer surfaces of the post corroded CeO₂ coated (0.30 mg/cm²), Ytria coated (0.15 mg/cm²) and uncoated specimen. The figure shows the segregation of cerium oxide particle along the grain boundaries Figure 4(a). These particles at the grain boundaries during corrosion form the complex compound, which inhibit the migrations of outward diffusions of cations and improve the corrosion resistance. On the other hand Figure 4(b) suggests also the segregations of yttrium oxide particles along certain directions. The scale morphology of the outer scale of the post corroded uncoated specimen shows the extensive scale cracking and spallations of the scale from the substrate Figure 4(c). This indicates that the



scales formed of the uncoated specimen is unprotective, which is subjected to scale cracking and spallation. The XRD analysis of the outer surface of the post corroded specimen CeO_2 and Y_2O_3 are shown in Figure 5. The post corroded CeO_2 coated specimen detects the presence of Fe_2O_3 , CeO_2 , $(\text{Fe, Cr})_2\text{O}_3$ and CeFeO_3 as shown in Figure 5(a), while the presence of Fe_2O_3 , FeY_2O_4 , Y_2O_3 , FeS phases are confirmed Figure 5(b) in case of Y_2O_3 coated specimen.

The Ceria (CeO_2) and Ytria (Y_2O_3) coating on the alloy surface, results in an improvement in the corrosion resistance which can be attributed to the presence of particles of the CeO_2 and Y_2O_3 over the substrate. These oxide particles may act as the nucleation sites for oxide growth and have formed complex compound like CeFeO_3 and FeY_2O_4 . These compounds act as pegs at the initial grain boundaries, as a result of which the scale is being keyed down to the alloy surface and thereby improves the scale adhesion. These will create effective barrier for the outward cationic transport and improve the corrosion resistance to a great extent. Further, the reduction in corrosion rate arising from the changed mechanism of scale growth (from outward scale growth to inward scale growth) definitely cut down the possibility of vacancy coalescence at the inner surface and there by facilitating better scale adhesion.

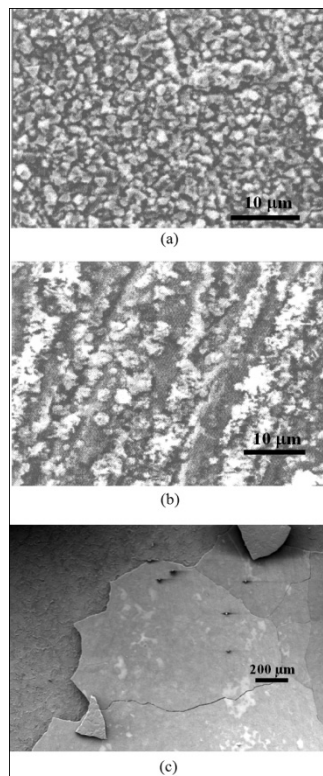


Fig. 4: SEM Micrograph of Post Corroded (a) CeO_2 Coated, (b) Y_2O_3 Coated and (c) Uncoated Specimen

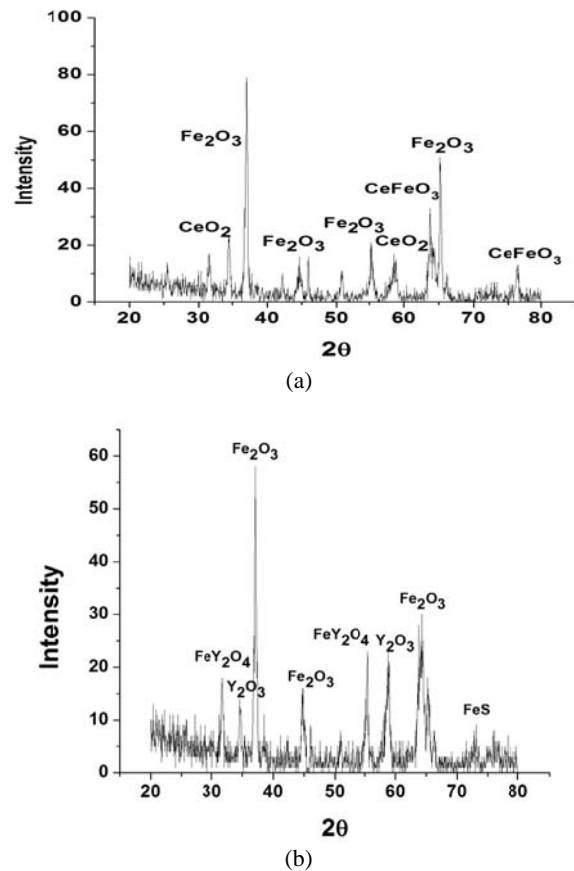


Fig. 5: XRD Analysis of Outer Surface of Post Corroded (a) CeO_2 and (b) Y_2O_3 Specimen

Behavior of the Coated and Uncoated Specimen under Thermal Cycling Conditions

The same coated and uncoated specimens were exposed for thermal cycling studies in mixed gas $\text{SO}_2 + \text{O}_2$ environment at 973 K for 100 hours. The specimens were exposed in the furnace and then re exposed after cooling to study the behavior in thermal cyclic conditions. The test was continued up to three cycles. The parabolic rate constants are calculated from the kinetic data in different thermal cycles and are represented in Table 2 and Figure 6. The results show the higher parabolic rate constant of uncoated specimen compared to CeO_2 and Y_2O_3 coated specimen in 1st cycle. The post corroded scale of uncoated specimen is found cracked and spalled completely after 1st cycle, while parabolic constant of CeO_2 and Y_2O_3 specimen is lowered as thermal cycle proceeds up to 3rd cycle (Figure 6). The improvement of the corrosion resistance of CeO_2 and Y_2O_3 coated specimen during thermal cycle can be attributed to the formation of complex compound CeFeO_3 and FeY_2O_4 , which acts as act as graded seal to accommodate the thermal stresses during thermal cycling.



Table 2: Parabolic Rate Constant (K_p) of Uncoated and Coated Specimen for Different Thermal Cycles

Identification	K_p ($mg^2cm^{-4}s^{-1}$)	K_p ($mg^2cm^{-4}s^{-1}$)	K_p ($mg^2cm^{-4}s^{-1}$)
	First Cycle	Second Cycle	Third Cycle
Uncoated specimen	11.10×10^{-4}	Scale spallation	–
CeO ₂ coated (0.30 mg/cm ²)	0.36×10^{-4}	0.30×10^{-4}	0.25×10^{-4}
Y ₂ O ₃ coated (0.15 mg/cm ²)	0.42×10^{-4}	0.3×10^{-4}	0.28×10^{-4}

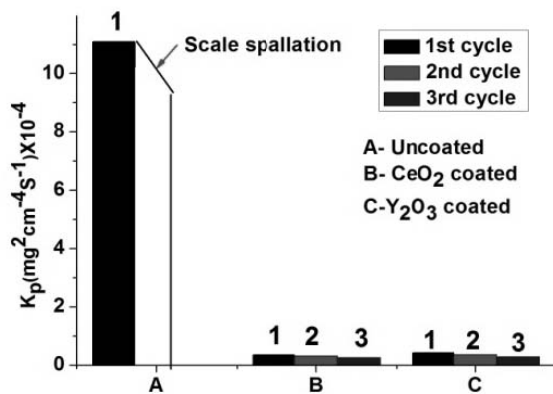


Fig. 6: Parabolic Rate Constant (K_p) of Uncoated, CeO₂ Coated and Y₂O₃ Coated Specimen in Different Thermal Cycles

Conclusion

The following conclusions can be drawn on the basis of results and discussion:

1. The application of CeO₂ and Y₂O₃ superficial coating over the substrate of 2.25 Cr-1 Mo steel, significantly improves the corrosion resistance in SO₂ + O₂ (ratio 2:1) gaseous environment at 973 K.
2. The kinetic behavior of both uncoated and coated specimen in isothermal corrosion studies follows approximately the parabolic growth rate, which indicates that corrosion process is governed by the diffusional growth like outward cation and inward anion migration.
3. The improvement of the corrosion resistance for CeO₂ and Y₂O₃ coating in isothermal corrosion study can be attributed to CeO₂ and Y₂O₃ particles, which may act as the nucleation sites, preferably over the grain boundaries for oxide growth. These reactive oxides also formed complex compound CeFeO₃ and FeY₂O₄ which act as barrier for the outward transport of cation and inward transport of anion and improve the corrosion resistance to a significant extent.
4. The corrosion resistance of CeO₂ and Y₂O₃ coated specimen is also significantly improved in comparison

to the thermal cyclic conditions in SO₂ + O₂ environment. The complex compound like CeFeO₃ and Y₂O₃ formation during coating, act as graded seal to accommodate the thermal stresses. So the corrosion resistance of the coated specimen is significantly improved during various thermal cycling due to the excellent scale adherence of the coating with the substrate. These compounds also act as pegs at the initial grain boundaries, as a result of which scale is being keyed down to the alloy surface and improves the corrosion resistance.

5. Finally, application of CeO₂ and Y₂O₃ superficial coating can be used for effective corrosion protection at high temperature in different critical components of thermal power plant boiler and petrochemical and refinery industries in SO₂ + O₂ environment.

Acknowledgement

The authors acknowledged the financial support from the Network Project: NWP 0027 of Council of Scientific and Industrial Research, New Delhi to carry out the research work. The authors gratefully acknowledge personnel from NDT & Metallurgy group, CRF for their continuous effort in the characterization part of paper. Lastly, the authors are also indebted to CSIR-CMERI for their support to write this paper.

References

- [1] Viswanathan, R. Damage Mechanism and Life Assessment of high temperature components, ASM International, Ohio, 1989.
- [2] Ghosh, D. and Mitra, S.K., High Temperature Material and Processes., Vol. 31, pp.727–731, 2012.
- [3] Ghosh, D., Roy, H. and Shukla, A.K., High Temperature Material and Processes., Vol. 28, pp. 109–114, 2010.
- [4] Ghosh, D. and Mitra, S.K., High Temperature Material and Processes., Vol. 1, pp. 81–85, 2011.
- [5] Whittle, D.P., Stringer, J., Phil. Trans. R. Soc. London., Vol. 295, pp. 309–329, 1980.
- [6] Stroosnijder, M.F., Guttman, V., Fransen, T. and Wit, J.H.W. de, Oxidation of Metals, Vol. 33, p. 371, 1990.
- [7] Moon, D.P. and Bannett, M.J., Mater. Sci. forum, Vol., 43, pp. 269, 1989.
- [8] Papaicovou, P., Hussey, R.J., Mitchell, D.F. and Graham, M.J., Oxidation of Metals. Vol. 33, pp. 19, 1990.
- [9] Ramanathan, L.V., *Proceedings of the 11th ICMC* (Vol. 4) Florence, Italy. April 2–6, pp. 177, 1990.
- [10] Mitra, S.K., Auddya, A. and Bose, S.K. React solids Vol. 6. 301, 1989.
- [11] Bennet, M.J. and Moon, D.P. “The role of active elements in the oxidation behavior high temperature Metals”,



- Commission of European communities E Lang. ed, pp. 111, 1989.
- [12] Whittle, D.P. and Stringer, J., Phil. Trans. R. Soc. London., Vol. 295 pp 309–329, 1980.
- [13] Moon, D.P., Material Science and Engineering, Vol. 5, 754, 1989.
- [14] Ghosh, D. and Mitra, S.K., J. Inst. Eng. Ser. D., Vol. 93, 59–93, 2012.
- [15] Hasanneja, H. and Shahrabi, T., Surface Engineering., Vol. 28, pp. 418–423, 2012.
- [16] Ghosh, D., Shukla, A.K. and Mitra, S.K., Effect of Ceria Coating on Corrosion Behavior of Low Alloy Steel, Surface Engineering (DOI 10.1179/1743294413Y.0000000167).
- [17] Ghosh, D., Shukla, A.K. and Mitra, S.K., Influence of CeO₂ superficial coating on the high temperature corrosion behavior of 2.25 Cr-1 Mo steel in SO₂ + O₂ atmosphere, Protection of metals and physical chemistry of surfaces (Article in press).



Engineering Practices for Failure Analysis of Boiler Tube Failures in Power Plants: A Case Study

Pranab Ray¹, Debashis Sarkar² and B. Chaudhuri³

Abstract: Failure of boiler water/steam wall tubes in a thermal power station is a very common phenomenon. A systematic study of the failures may lead to minimization of the failure occurrences preventing disruption of power generation and associated monetary losses. In this context, it may be mentioned that a systematic approach to failure analysis requires the use of various tools of analysis available in the hands of an analyst. Based on the preliminary observation which also include comprehensive plant data collection, an analyst has to decide types of test that will be of relevance. Other than conventional NDT techniques, oxide scale thickness gauging, sometimes even radiography, chemical analysis, mechanical properties assessment, metallographic evaluations, etc. are resorted to. With the availability of state of art testing equipment such as scanning electron metallography, jobs of analysts have become simpler. However, as finding the root cause of failure is very critical, analyst's capability in understanding in diverse fields is of paramount importance.

As a case study, in the present paper example of failure analysis of a medium reheater (MRH) leakage in a 300 MW fluidized bed boiler has been considered. During the working life of less than 2 years, the unit has faced this type of MRH tube rupture several times. All failures had occurred in same coil at same branch of tubes and at same location. As mentioned above, after collection of plant data and preliminary visual observation, the analyst decided the tests to be conducted and after conducting these tests, inferences have been drawn subsequently. Wall thinning, due to excessive coal-ash corrosion, and overheating, due to scale buildup on the tube were measured, and estimations of the average corrosion and scale growth rates were made. Finally it was concluded that the root cause of the failure is very high rate of localized fire side erosion of the Medium Reheater Tubes.

Keywords: Failure Analysis, Reheater Tubes, Leakage, Corrosion, Overheating.

Introduction

In power plants boiler tube failures are inevitable. Whatever the fuel being fired, all high pressure boilers are bound to have tube failures at some point or other. Boiler tube failure has a very adverse effect on the functioning of the power plants both in terms of availability of power as well as cost. There are many different types of boiler tube failure mechanisms, which can be sorted into six general categories:

- Stress rupture (short-term overheating, high temperature creep, dissimilar metal welds).
- Water-side corrosion (caustic corrosion, hydrogen damage, pitting, stress corrosion cracking).
- Fire-side corrosion (low temperature, water wall, ash).

- Erosion (fly ash, falling slag, soot blower, coal particle).
- Fatigue (vibration, thermal expansion).
- Lack of quality control (damage during chemical cleaning, poor water chemistry control, material defects, welding defects).

These six groups can further be sub-divided in to twenty primary type defects. They are as follows:

1. Short term overheating failure
2. Long term overheating failure also known as creep
3. Dissimilar metal weld failure
4. Fatigue caused by vibration
5. Thermal fatigue due to temperature fluctuation
6. Corrosion fatigue
7. Caustic corrosion inside the tubes

¹TMC Institute of Learning, Kolkata, India. ✉ tmcil@tmcgroupindia.com

²Test Metal Corporation, Kolkata, India.

³Ex-Professor, Jadavpur University, India.



8. Hydrogen damage in water wall internal surface
9. Tube internal pitting
10. Fly ash erosion
11. Falling slag erosion
12. Soot blower erosion
13. Coal particle erosion
14. Low temperature flue gas corrosion
15. Fireside water wall corrosion
16. Coal ash corrosion
17. Oil ash corrosion
18. Damage during maintenance cleaning

19. Chemical excursion damage
20. Material defects and welding defects.

The tube failures during initial period of operation are different from the ones which occur during normal operation. During initial period of operation types of tube failures seen are short term overheating due to blockage in fluid path by some foreign material, weld failure, material defects, and sometimes fatigue failures. In the case of failures during normal operation any of the twenty different types of failures mentioned above may occur. Figure 1 shows a few photos of various types of tube failures.

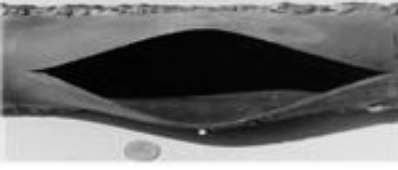
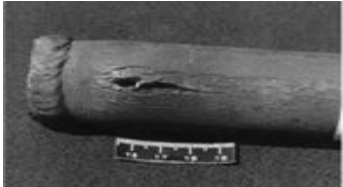
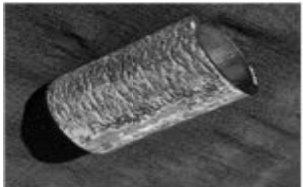
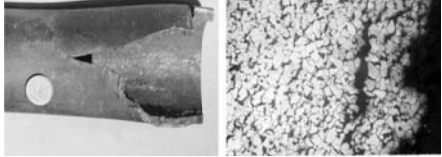
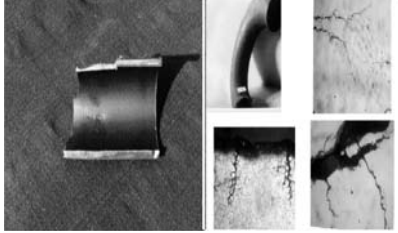
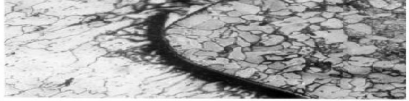
		
<p>Short Term Overheating Leads to stress rupture of the tube. Causes of short term overheating are formation of debris and scale on the steam/water tube, high heat transfer rate or improper firing and low water/steam level due to poor circulation.</p>	<p>Long Term Overheating Long term overheating failure occurs due to selection of incorrect material, scale formation inside the tube, water side deposits.</p>	<p>Fatigue Failure Thermal Fatigue failure arises due to improper flexibility, attachment weld corrosion, cold bend restriction to the thermal expansion, improper heat treatment and contouring of welds.</p>
		
<p>High Temperature Creep It leads to stress rupture of boiler tubes. Causes for such failures are partial choking of tube, general blockage, incorrect material, material transition and higher stress due to weld attachment.</p>	<p>Caustic Corrosion It arises due feed water system corrosion deposits, condenser tube leakage, higher concentration of NaOH in boiler water and temperature increase due to internal deposits.</p>	<p>Failure Due to Hydrogen Corrosion This type of damage results from low pH corrosion reaction which results in the production of atomic hydrogen which in turn results in formation of cracks at the grain boundaries longitudinal bars occurs with thick tip.</p>
		
<p>Failed Tube Due to Stress Corrosion Such cracks are generally observed in super-heater, re-heater region having concentration of chlorides, sulphates or hydroxide and stresses in fabrication service etc. like bends, attachment weld.</p>	<p>Failures Due to Dissimilar Metal Welds It causes rupture of boiler tubes as shown. This type of failure mainly occurs due to use of dissimilar metal rods for welding the tube. The prime location of dissimilar metal weld failures are super-heater, re-heater dissimilar weld joints.</p>	<p>Failures Due to Fly Ash Erosion Ash having abrasive action erodes the outer surface of tubes in Economizer, LTSH, Re-heater regions. The major causes of fly ash erosions are temperature of flue gas, high ash content in coal high flue gas velocity and high impingement angle of ash particle.</p>

Fig. 1: Boiler Tube Failures and Their Patterns Due to Various Reasons of Failures



Failure Mechanisms

The service environment of fossil-fired boilers along with human errors during engineering, fabrication, construction, operation, and maintenance will always result in occasional Boiler Tube Failures (BTF). The frequency of these failures depends on the corrective actions taken to prevent or reduce boiler tube damage. Repeated BTF result in frequent forced outages, and ultimately in costly extended outages for major tubing replacement.

Primary factors influencing repeat tube failures are:

- not following state-of-the-art operation maintenance or engineering practices
- lack of proper boiler tube failure root cause analysis
- wrong choice of corrective/preventive action
- lack of definitive boiler tube failure reporting and monitoring.

Capabilities of Analysts

However, as finding the root cause of failure is very critical, analyst's capability in understanding in diverse fields is of paramount importance. These capabilities may include expertise in many diverse disciplines, such as Analytical Metallurgy, Chemical cleaning and preservation, Chemical Engineering, Chemistry, Combustion, Corrosion, Dynamics and flow-induced vibration, Fluid Mechanics and Heat transfer, Fuels and fuels analysis, Materials performance and mechanical testing, Measurements, Mechanical design, Nondestructive methods of diagnostics, Pollution control, Quality control, Stress analysis, finite element analysis, water chemistry, Welding or other manufacturing technologies, etc.

Sampling and Sample Preparation

Prior to removing a failed tube, the tube is marked and photo-documented (gas flow direction, fluid flow direction, row number, elevation, boiler section, etc.). The visual condition of nearby tubes and the proximity of the damaged tubing to attachments, soot-blowers, etc. should also be documented.

Samples should be of reasonable length and cuts should be made well away of any visible damage. Dry cuts should be made with an electric or air powered reciprocating saw or grinder with a thin cut-off wheel to obtain high quality uts. Tube ends should be sealed with tape to prevent contamination or loss of deposits or scale. The tube samples should be carefully packed to prevent damage during shipment.

The following information should be provided with the tube sample(s):

- Boiler operating pressure, temperature, steaming rate, and unit MW;
- Drawing of boiler showing the location of each tube sample;
- Specified tube material, dimensions, etc.;
- Operating hours since commercial operation date or tube replacement;
- Tube failure history of the boiler;
- Boiler maintenance records (i.e., replacements or modifications) for the boiler section of concern;
- Boiler water chemistry (typical chemistry and frequency, extent, and duration of excursions);
- Layup procedures (short-term, long-term);
- Any additional pertinent information on the unit.

Activities to be Undertaken

- Visual inspection
- Determination of chemical composition and morphology of deposits
- Deposit Weight Density (DWD) determination
- Scale thickness measurement
- Pit depth measurements
- Wall loss determination
- Metallurgical analysis
- Material composition and microstructure
- Determination of failure mechanism
- Root cause analysis
- Recommend corrective actions
- Determination of time for tube replacement.

Case Study

During the working life of less than 2 years in a 300 MW fluidized bed boiler in a thermal power plant, the unit had faced Medium Recharge Heater (MRH) tube rupture several times. All failures had occurred in same coil, at same branch of tubes and at same location (app. 9 M below the roof, facing LHS water wall tubes). The present failure investigation had to be undertaken because the tube portion failed again and was replaced after similar rupture failure on another tube of the same coil. On each failure, nearby MRH tubes and facing water wall tubes got affected and needed localized insertion of new tube piece. Basic important data of the plant are furnished in Table 1.



Table 1: Plant Design and Operational Data

Sl. No.	Description	Remarks
1.	Type of boiler	Fluidised bed
2.	Date of Commissioning	20.07.2008
3.	Installed Capacity	300 MW
4.	Failure occurred on	26.04.2010
5.	Design Steam Inlet Temp. of MRH coil	329.6°C
6.	Design Steam Outlet Temp. of MRH coil	540°C
7.	Design Flue Temp.	972°C
8.	MRH tube design dimension	60 mm OD × 4 mm thick
9.	Water wall tube design dimension	63.5 mm OD × 7.5 mm thick
10.	MRH tube material spec. (ruptured portion)	12 Cr1 Mo VG
11.	Water wall tube material spec.	SA 210, Grade-C

Portion of the tube no. 12, 14 & 16, MRH coil no. 1 containing affected portion, identified as MRH 12, MRH 14 & MRH16 respectively in this paper.

Portion of two affected LHS water wall tubes containing affected portion, identified as WWT in this paper.

Portion of LHS water wall tube no. 5 affected during failure containing affected portion, identified as WW 5 in this paper.

Sequence of Activities for Conducting Failure Analysis

To carry out the investigation, following test schedule was followed:

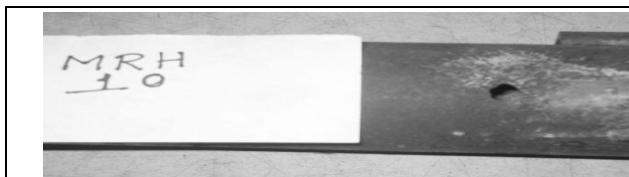
- Visual Inspection
- Ultrasonic Thickness Gauging
- Oxide Scale Gauging
- Tensile Testing
- Chemical Analysis
- Hardness Testing
- Scanning Electron Microscopy
- Metallographic Evaluation.

Samples Received

Portion of the tube no. 10, MRH coil no. 1 containing rupture point, identified as MRH 10 in this paper.

Visual Inspection

In the Figure 2 glimpses of the visual observations on samples received in the present case study have been elaborated.



Sample No. MRH—10 - Outer & inner surface shows uniform scale deposit, mixture of black and brown colour. The neighboring surface of leakage shows inverse bulging effect. Thinning observed on the leakage spot.



Sample No. MRH—12 - Both the outer & inner surface shows uniform scale deposit, mixture of black & brown color. The neighboring surface of leakage shows minor bulging effect. Thinning observed on the leakage spot.



Sample No. MRH—14 - Both the outer and inner surface shows uniform scale deposit, mixture of black and brown color. The neighboring surface of leakage shows minor bulging effect.

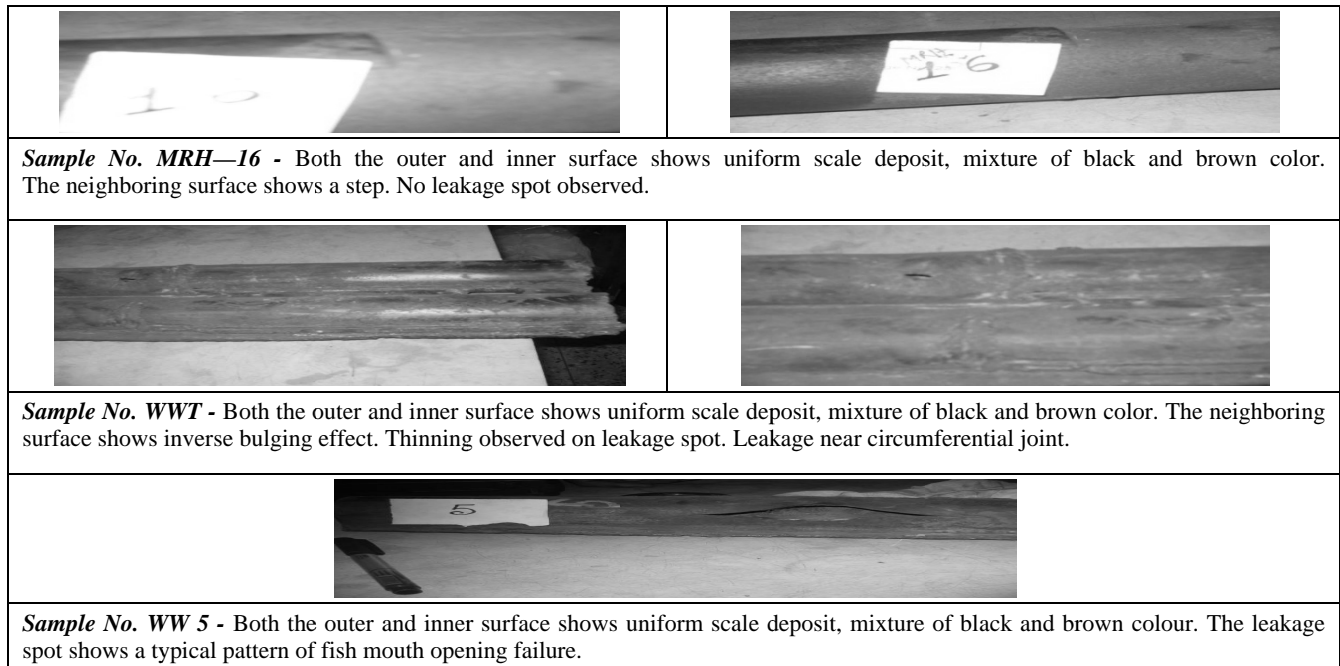


Fig. 2: Glimpses of the Visual Observations on Samples Received

Ultrasonic Thickness Measurement Test

Ultrasonic Thickness Measurement was carried out on several locations along the length of the samples and circumferentially on four spots at each longitudinal location

assuming leakage spot at 6’o clock position. Outer diameter was also measured at possible locations. In Table 2(a), results of Ultrasonic thickness measurement have been compiled.

Table 2(a): Results of Ultrasonic Thickness Measurement

Sample No.	Design Data	Spot No	Observed Thickness (mm)				Observed OD (mm)	Remarks	
			6”O clock	9”O clock	12”O clock	3”O clock			
MRH 10	Thickness 4 mm Diameter 60 mm	1	3.9	4.1	3.9	4.8	60.00	Beside leakage spot Along leakage spot Beside leakage spot	
		2	4.0	4.1	3.8	4.8			
		3	3.8	4.5	3.1	4.7			59.5
		4	–	–	3.8	–			
		5	3.9	4.7	3.9	4.8			
		6	3.9	4.8	3.9	4.3			60.0
MRH 12	Thickness 4 mm Diameter 60 mm	1	4.8	3.9	4.0	4.0	60.0	Beside leakage spot Beside leakage spot	
		2	3.9	4.5	4.0	3.1			
		3	4.0	3.7	3.5	3.4			60.0
		4	3.8	4.4	3.9	3.8			58.9
		5	4.1	3.9	4.6	4.0			60.0
MRH 14	Thickness 4 mm Diameter 60 mm	1	4.1	4.2	4.0	4.1	60.00	Beside leakage spot	
		2	4.7	4.1	4.0	4.2			
		3	–	3.9	3.8	3.6			
		4	4.7	–	3.5	–			



Sample No.	Design Data	Spot No	Observed Thickness (mm)				Observed OD (mm)	Remarks
			6" O clock	9" O clock	12" O clock	3" O clock		
		5	–	4.7	3.7	4.1	59.15	Along leakage spot
		6	4.6	–	4.2	–		Beside leakage spot
		7	4.7	4.7	4.2	4.2	60.0	
MRH 16	Thickness 4 mm Diameter 60 mm	1	4.0	4.6	4.2	4.5	60.0	Beside step marking Beside step marking
		2	4.1	4.6	4.2	4.5		
		3	4.1	4.0	3.7	4.0	60.0	
		4	4.1	4.0	4.2	4.2	59.0	
		5	4.3	4.1	4.4	4.2	60.0	
WWT	Thickness 7.5 mm Diameter 63.5 mm	Minimum – 6.8 mm Maximum – 8.2 mm					62.0 to 63.0	
WW 5	Thickness 7.5 mm Diameter 63.5 mm	1	6.8		7.7			Beside leakage spot Along leakage spot Beside leakage spot
		2	6.9		7.7			
		3	5.3		7.6			
		4	5.4		7.8			
		5	7.7		7.7			

Oxide Scale Thickness Measurement

Steam side oxide scale thickness was measured on MRH tube samples. The results are tabulated in Table 2(b). Considering the damage of oxide layers during failure, the maximum values observed are taken into consideration.

Table 2(b): Oxide Scale Thickness Measurement

Sample No.	Maximum Oxide Scale Thickness Measured (mm)
MRH 10	0.11
MRH 12	0.09
MRH 14	0.10
MRH 16	0.12

Other Test Results

Results of tensile tests, chemical analyses and hardness measurement have been shown in Table 2(c), 2(d), and 2(e).

Table 2(e): Tensile Test Report

Location	Sample No.	Yield Strength (Mpa)	Ultimate Tensile Strength (Mpa)	% Elongation
Medium Reheater Tubes	MRH10	374	523	21.2
	MRH12	402	542	22.3
	MRH14	361	535	20.6
	MRH16	472	584	17.20
	As specified in code 12 Cr-1 Mo VG	255 (min)	470–640	21 (min)
Water Wall Tubes	WW5	358	511	28.8
	As specified in code SA 210 Gr.C	275 (min)	485 (min)	30 (min)

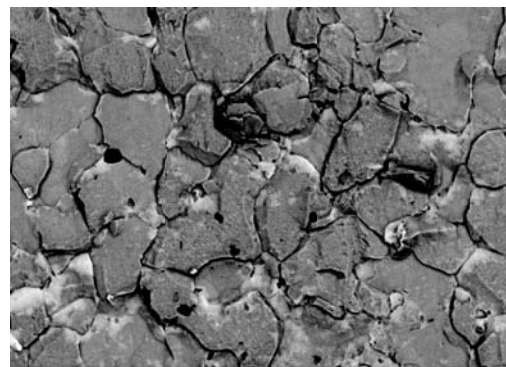


Table 2(d): Chemical Analysis Test Report

Sample No.	Wt. %							
	C	Mn	Si	S	P	Cr	Mo	V
On Medium Reheater Tubes								
MRH 10	0.14	0.46	0.25	0.027	0.029	0.93	0.30	0.25
MRH 12	0.16	0.54	0.26	0.028	0.031	0.97	0.31	0.20
MRH 14	0.14	0.51	0.25	0.027	0.028	1.10	0.26	0.33
MRH 16	0.13	0.50	0.25	0.029	0.029	1.10	0.26	0.29
Specified in code 12 Cr-1 Mo VG	0.08–0.15	0.40–0.70	0.17–0.37	0.030 (max)	0.030 (max)	0.9–1.2	0.25–0.35	0.15–0.30
On Water wall Tubes								
WW5	0.22	0.62	0.26	0.027	0.029			
Specified in code SA 210 Gr.C	0.27 (max)	0.93 (max)	0.10 (min)	0.035 (max)	0.035 (max)			

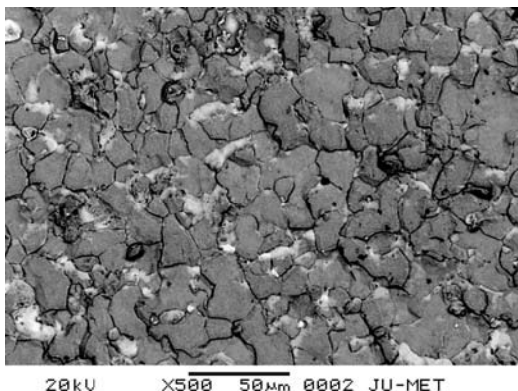
Table 2(e): Hardness Test Report

Sample No.	Observed Hardness (RB)			
	A	B	C	D
MRH 10	84	82	84	85
MRH 12	82	84	85	85
MRH 14	78	80	83	82
MRH 16	85	84	80	82
WW 5	82	84	85	82
WWT	80	81	78	82



Scanning Electron Micrography

One sample from tube no. MRH–10 was observed under scanning electron microscope at Department of Metallurgical and Material Engineering, Jadavpur University, Kolkata. The microstructure shows a healthy ferritic matrix. No significant creep damage has been noticed. No significant difference in microstructure along the cross section of the sample is observed. Representative micro-photographs are given below.



Optical Microscopy

Metallographs of various samples from optical microscopy are shown in Figure 3.

Summary of Findings

- Some tubes show inverse bulging at failed spot, some tubes show bulging also.
- Sign of fish mouth opening has been observed on MRH 12 & 14.
- Typical fish mouth opening has been observed on WW 5.
- Significant localised thinning has been observed on all the tubes.
- Tendency on lowering of diameter (about 1mm) has been observed on all the tubes, even at the locations just beside the bulged portion.
- Minor oxide scaling is observed on all the MRH tubes.
- Chemical analysis confirms that MRH tube material belongs to 12 Cr-1 Mo VG and Water wall tube material belongs to SA 210 Gr.C.



	<p style="text-align: center;"><i>Sample No. MRH 10</i></p> <p>Microstructure shows predominantly ferritic matrix with pearlite. No significant creep decay is observed. Pearlite decomposition has just initiated. No significant change in microstructure along the cross section is observed. No significant effect of corrosion is observed on internal as well as external surface.</p>
	<p style="text-align: center;"><i>Sample No. – MRH 12</i></p> <p>Microstructure shows predominantly ferritic matrix with thick pearlite regions in between. No significant creep decay is observed. No significant change in microstructure along the cross section is observed. No significant effect of corrosion is observed on internal as well as external.</p>
	<p style="text-align: center;"><i>Sample No. – MRH 14</i></p> <p>Microstructure shows predominantly ferritic matrix with pearlite. No significant creep decay is observed. Pearlite decomposition has just initiated. No significant change in microstructure along the cross section is observed. No significant effect of corrosion is observed on internal as well as external surface.</p>
	<p style="text-align: center;"><i>Sample No. – MRH 16</i></p> <p>Microstructure shows predominantly ferritic matrix with pearlite. No significant creep decay is observed. Pearlite decomposition has just initiated. No significant change in microstructure along the cross section is observed. No significant effect of corrosion is observed on internal as well as external surface.</p>
	<p style="text-align: center;"><i>Sample No. – WWT</i></p> <p>Microstructure shows predominantly ferritic matrix with thick pearlite regions in between. No significant creep decay is observed. No significant change in microstructure along the cross section is observed. No significant effect of corrosion is observed on internal as well as external surface.</p>
	<p style="text-align: center;"><i>Sample No. – WW 5</i></p> <p>Microstructure shows predominantly ferritic matrix with thick pearlite regions in between. No significant creep decay is observed. No significant change in microstructure along the cross section is observed. No significant effect of corrosion is observed on internal as well as external surface.</p>

Fig. 3: Metallographs

- Physical test results conform to the specification of the respective tubes. Elongation of tube no. MRH 10, 12 & 14 is just around the minimum values mentioned in the specification. Elongation of tube no. MRH 16 & WW 5 falls below the specified limit.
- Hardness values of MRH tubes lie in between 78 to 85 HRB. No specific values on hardness have been mentioned in grade 12 Cr-1 Mo VG. ASTM recommends maximum 85 HRB for standard ferritic alloy steel seamless tubes for high temperature use. The result



shows that the hardness values of all the MRH tubes reach the upper line of the specified value.

- Hardness values of Water Wall tubes lie in between 82 to 85 HRB. SA 210 Gr.C suggests maximum 89 HRB. The hardness values of the failed water wall tubes also approach to the upper line of specified limit.
- No significant creep damage has been observed on the MRH and water wall tubes. Presence of bainite has been observed. In electron microscopy also, no significant deviation have been observed.

Discussions and Conclusions

The failure in tube number MRH 10 has occurred from a portion which was replaced just before less than one month. The history of such failures indicates that the failure is very much localised i.e. confined in a particular location of the furnace.

It is also confirmed by the plant personnel that initially the leakage occurred in a MRH tube followed by damage of nearby MRH and waterwall tubes by high pressure steam/water jetting from leakage point. Among the samples under investigation, only MRH 10 contains the source leakage point on failure, others are the affected tubes on same occurrence, except tube no. WW 5. WW 5 is the affected tube of such similar failure occurred..

Test results, in summary, could not reveal any significant deviation except some hardening effect i.e. decrement of ductility, increment of hardness, etc. This minor hardening effect may also occur as a result of quenching by steam/water jetting after leakage. The presence of bainites in micro-structure also may come as a result of such quenching.

This type of jetting after failure washes out the tube surfaces faced. This result localized thinning, inverse bulging, steps on outer surface, leakage with or without minor bulging, etc. based on direction, temperature, pressure, etc. of the steam jet leakage. This is very common after boiler tube leakage. But, for obvious reason, these indications are not found on tube containing source leakage.

In this investigation, the tube containing original leakage point, tube Number MRH 10, also shows similar indications like localized thinning, inverse bulging etc, a typical effect of external erosion. It indicates that some external erosion mechanisms were also on action on outer surface of tube no. MRH 10 before failure. This portion of the tube was replaced with at least 4.8 mm thickness (the thickness observed on the healthier portion of the same tube piece). The external erosion mechanisms are seen to be very severe which brings down the thickness of the tube piece from 4.8 mm to 3.1 mm within a time span of about one month only. These mechanisms are also found very much localized. Fire side erosion on the furnace tubes occurred due to following reasons:

- Fly ash erosion
- Falling slag erosion
- Coal particle erosion
- Soot blower erosion
- Coolant erosion from nozzles fitted with any control instruments for cooling of sensors.

Among the above mechanisms, the first three cannot be very much localized. Localised faster fire side erosion takes place normally due to last two reasons. Furnace design, positioning of soot blowers and self cooled sensors should be reviewed for proper identification of reason of such higher rate of external erosion.

Fish mouth opening during failure is a typical example of long term overheating failure predominantly assisted by creep. Among all the failed samples of earlier similar failures, the sample WW 5 was selected for investigation due to the unlikely presence of a typical fish mouth opening. Investigation could not reveal any creep decay. The tube was not under operation for long time because it failed only after 20 months of commissioning. The mechanisms of fish mouth failure occurrence follows steps like softening due to creep decay, bulging under internal pressure, thinning due to bulging and finally rupture along the longitudinal axis of bulged portion. The similar situation may occur if a ductile tube is brought under operation with thickness less than its minimum designed calculated thickness. The failure in water wall tube WW 5 with fish mouth opening can thus be concluded that localized thinning occurred in this tube during failure occurred previously, the tube could not be noticed and brought into operation, bulging occurred in this tube piece before the day under consideration, failure occurred on MRH tube on the day under consideration, the steam/water jet hit the bulged location of WW 5 and finally failed with fish mouth opening under dual effect of external jetting and internal pressure.

Finally, it was concluded that the root cause of the failure is higher rate of localized fire side erosion of the Medium Reheater Tubes.

Recommendations

- Reviewing of furnace design, positioning of soot blowers and self cooled sensors for proper identification of reason of such higher rate of external erosion.
- After identification, complete removal of any option of such further external erosion.
- Thorough Ultrasonic Thickness measurement of Medium reheater tubes and waterwall tubes, replacement of the thinned tube portions.
- After taking above steps, comprehensive visual inspection and thickness measurement after 16,000 hours of running.



Synthesis and Characterization of Perovskite BaSnO₃ by Variable Methods: A Comparative Study

Asima Adak (Maity)¹, Soumya Mukherjee^{*2,3},
Mahua Ghosh Chaudhuri² and Siddhartha Mukherjee²

Abstract: Perovskite Barium Stannate (BaSnO₃) has shown many interesting properties like electrical, catalytic, semiconducting, capacitive and thus have been the most versatile ceramic oxides. Transitional metal doping at B site, leads to modification of semiconducting, electrical, catalytic, piezoelectric properties. Such versatile materials are observed to be synthesized by different techniques such as solid state ceramic method, ball milling, hydrothermal, planetary mill activation, Sol-gel and so on. Synthesized samples are mainly characterized by XRD for phase identification and purity of the material, SEM images give morphological formation, TEM studies give structural information, optical and bonding characteristics identified by FTIR analysis. The piezoelectric, dielectric, optical properties, electrical conductivity of the undoped and doped perovskite are reported in line of applications. In the present article the authors tried to briefly describe the properties of the material in nanometer scale with respect to morphological formation.

Keywords: Perovskite, XRD, SEM, TEM, Dielectric.

Introduction

Till now researchers have worked on various perovskite grade materials to study their properties and possible applications. Perovskite dielectric material BaSnO₃ exhibits various properties like electrical, thermal, photocatalytic, photovoltaic, semiconducting type and so on. Lanthanum doped perovskite Barium stannate also exhibit sensing and thermoelectric properties at high temperature [1]. Perovskite type oxide uses Al₂O₃ mainly as a tool to construct gas sensor for detecting inflammable or toxic gases such as CO, NO, C₂H₅OH [2]. Gas sensor fabricated by the material is found to work mainly based on the comparison of electrical resistance of semiconductor oxide in air and in the presence of detected gas (CO, H₂, etc.) [2]. Lanthanum doped BaSnO₃ system is observed to be used for humidity sensor material [3]. Humidity sensors are applied for quality control of production processes and products as electronic devices, precision instruments, textile and foodstuffs. It is also found in domestic application such as smart control of living environment in a building [3]. Some characteristics of humidity sensor such as high sensitivity, chemical and thermal stability, high reproducibility, no hysteresis, low cost and long life are observed to make it fit for versatile

applications [2, 3]. In Non-linear dielectric material, dielectric constant can be controlled by adjusting field strength. The result of such observations leads to development of some devices like dielectric amplifier, parametric device, microwave frequency multiplier, switching circuit snubber and the microwave ferroelectric phase shifter used in phased array antenna [4]. The ferroelectric barium stannate titanate shows abnormal C-curve and clockwise reversible hysteresis loop in temperature range 10–40°C [4]. Previous research articles indicate Barium Stannate Titanate (BTS) as a binary solid solution system that is combined with ferroelectric barium titanate and non ferroelectric barium stannate [5]. Both the material have perovskite type structure with ABO₃ formula where B sites of this structure is shifted by either titanium or tin ions which leads to applications like capacitor, bolometer, actuator and microwave phase shifter since the curie temperature, dielectric maxima can be shifted by changing the tin content and also it has high permittivity [5]. BTS is calcined at high temperature around 1500 K, hence the optimized technique to prepare BTS is either ball milling or solid state reaction [5]. With increase in temperature from room temperature, low frequency dielectric relaxation is observed in BTS ceramics [6]. BTS has high dielectric permittivity which is dependent on the tin content in a wide

¹ Department of Electronics & Communication Engineering, Heritage Institute of Technology, Kolkata–700107, India.

² Department of Metallurgical & Material Engineering, Jadavpur University, Kolkata–700032, India.

³ Amity School of Engineering and Technology, Amity University Kolkata Campus, Kolkata–700156, India.

✉ *smmukherjee3@gmail.com



temperature range [7]. Barium stannate titanates (BTS) is a functionally graded materials (FGM) which should satisfy the following requirement like presence of electrical (dielectric, ferroelectric, piezoelectric), magnetic multifunctional properties, structural performance such as mechanical and thermal expansion [7]. Barium stannate exhibits dielectric property, electrical conduction behavior by doping with nickel (Ni), niobium (Nb) [8, 9]. Also electrical resistivity decreases with increasing the concentration of niobium [9]. BaSnO_3 perovskite material behaves as a n type semiconductor with a band gap of 3.4 eV [8–10] while the porous BaSnO_3 hollow structure shows photovoltaic effect in visible region [10]. In the present article authors discuss the different process by which undoped and doped barium stannate is easily prepared by solid state ceramic sintering, ball milling process. Initially crystallization temperature and thermal behavior are easily determined by TG/DTA analysis. Phase identification, crystal structure are mainly characterized by XRD, while microscopic characterization evaluated by SEM, FESEM and TEM reveals structural and surface morphology of the perovskites. Properties like dielectric, electrical, ferroelectric and piezoelectric are compared for undoped and doped systems.

Experimental Process, Results and Discussion

Experimental Process

Undoped BaSnO_3 and La, Cr, Ni, Ti, Y, Dy, Nb & Sr doped BaSnO_3 were prepared by solid state ceramic method, ball milling and mechanically mixing by Agate mortar. A required appropriate amount of stoichiometric precursors were added, calcinations were carried out for different dopants in the same process. Knowledge based on the previous works on the synthesis routes of nanocrystalline BaSnO_3 like solid state ceramic, ball milling, mechanically mixing by Agate mortar, Modified auto-igniting combustion, Chemical precipitation, Hydrothermal, Precursor, Reverse micelle, Cold isostatic pressing and Sol-gel route aids in to form the advantages or disadvantages of those processing routes. Among all the solid state ceramic method, ball milling is observed to be very simple method and cost effective. Sol-gel method has some advantages like homogeneity, purity, size control, low temperature and others. A simple chemical route of BaSnO_3 synthesis method which claims at the same time the use of very few and low cost chemical reagents, namely $\text{Ba}(\text{OH})_2$ and $\text{K}_2\text{SnO}_3 \cdot 3\text{H}_2\text{O}$, accompanied by short calcination times, simplicity, mass-production and high level of repeatability. All these synthesis characteristics are important for a successful industrialization implementation of the method [11, 12]. The method presented here, is a three-step method which can be described in Figure 1.

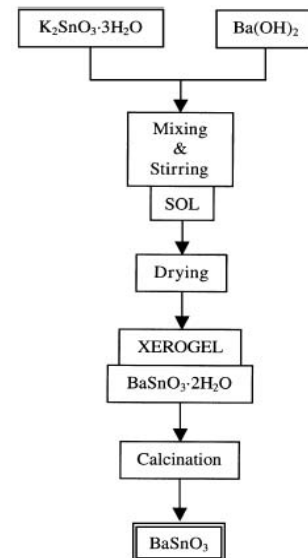


Fig. 1: Scheme of the BaSnO_3 Synthesis Method Presented. Three Synthesis Steps can be Well Defined [11]

XRD Analysis

The crystallization behaviours of the samples are investigated with XRD and the results shows that doped and undoped barium stannate has single phase perovskite structure [13]. The crystalline size was calculated with full width half maximum (FWHM) using the Scherrer formula along the major planes of (011) reflection [14]. Based on the Rietveld analysis the structural parameters of BaSnO_3 are found to be cubic perovskite structure and its corresponding lattice parameters. The XRD of the sample annealed at 1200°C is shown in the Figure 2.

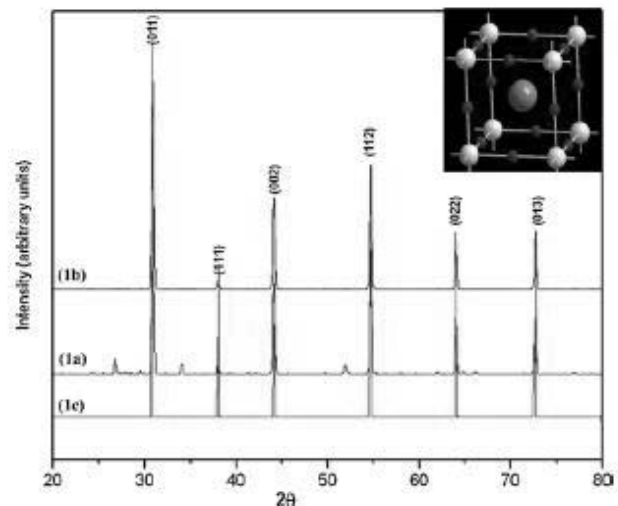


Fig. 2: XRD Patterns of (a) As-Prepared BaSnO_3 (b) BaSnO_3 Annealed at 1200°C and (c) Powder Pattern Obtained from Rietveld Analysis [14]



SEM Analysis

SEM micrographs of undoped and doped samples show uniform fine grained microstructure. The average grain size for doped and undoped lies in the range 2–4 μm with a few finer grains [1, 8, 9]. It has been seen that grain size decreases with increasing dopant composition [1, 8]. Figure 3 shows the SEM micrograph of the perovskite-type BaSnO_3 formed by the hydrothermal treatment at 573 K for 120 s under saturated vapor pressure. It shows that the particles have a well faceted cubic morphology having an average size of approximately 7 μm [15].

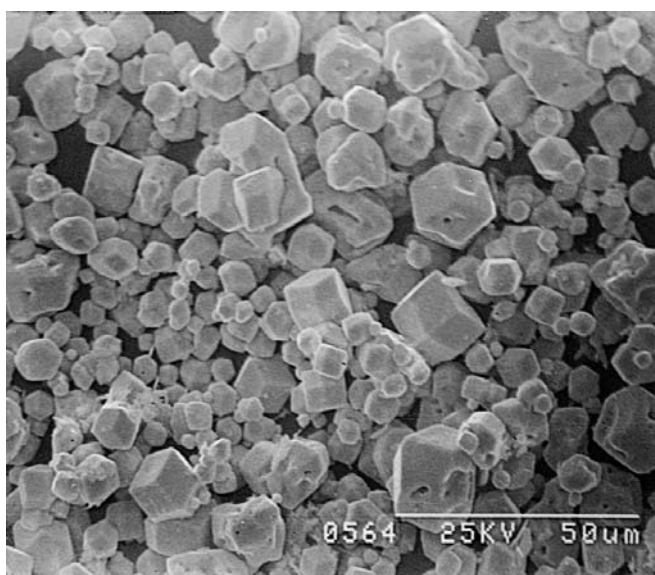


Fig. 3: The SEM Micrograph of Perovskite-Type BaSnO_3 Prepared by Hydrothermal Treatment at 573 K for 120 s under Saturated Vapor Pressure [15]

TEM Analysis

High resolution structural, morphological characterisations of the powder calcined at 1100°C in static air have been performed by using TEM and SAED techniques. BaSnO_3 quasi-spherical nanoparticles of mean size of about 200 nm noted are shown in Figure 4. However, among these quasi-spherical nanoparticles, researchers have also observed few BaCO_3 particles that adopt a stick-like morphology (Figure 4). Stick-like or needlelike particles are quite bigger than spherical nanoparticles, having lengths up to 3 μm and widths in the range 200–500 nm. SAED pattern indexation has shown that the main part of diffracted spots information belongs to the BaSnO_3 crystalline structure (1–5 rings) while the indexation of the spots (spots A–D) shows the presence of BaCO_3 in that samples. The presence in the SAED pattern is shown in Figure 4 along with two diffuse spots dividing the (002) interplanar distance as well as the diffuse line in the (0 0 2) direction [12].

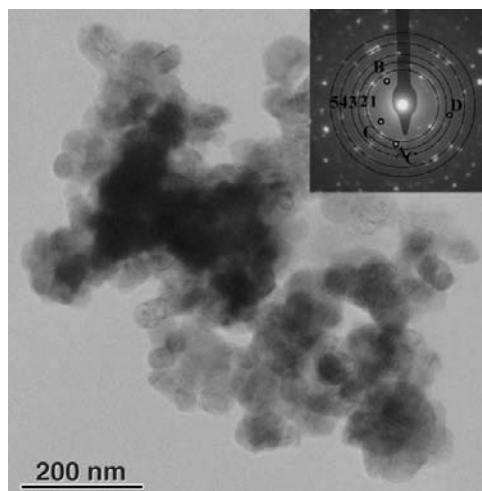


Fig. 4: TEM Bright Field Micrograph of the BaSnO_3 Quasi-Spherical Nanoparticles and SAED Pattern Obtained from a Wide Region Containing both Spherical and Stick-Like Nanoparticles [12]

FTIR Analysis

Figure 5 shows a typical IR spectra of as-prepared nanocrystalline BaSnO_3 powder. The IR active mode appears as a very strong absorption band at 629 cm^{-1} in the spectrum. The Raman active mode has become active in the IR spectrum and is observed as a doublet at 568 and 579 cm^{-1} . The splitting of the degenerate modes and the appearance of inactive modes in the spectra suggest a lowering of symmetry due to distortion. The intense sharp peak at 1060 cm^{-1} in the IR spectrum is due to the presence of BaCO_3 in the combustion method product. The IR spectrum also shows the presence of BaCO_3 in the sample. The absorption bands at 856, 1050 and 1450 cm^{-1} are the characteristic bands of BaCO_3 [14, 16].

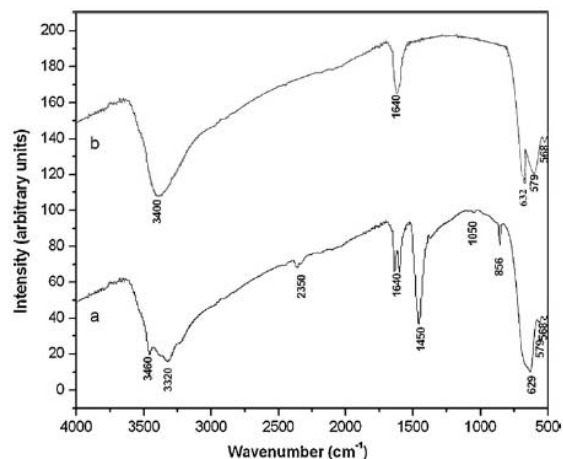


Fig. 5: FTIR Spectra of BaSnO_3 Nanoparticles (a) As-Prepared (b) Heated at 1200°C [14, 16]



Properties

Optical Property

The optical properties of ABO_3 are improved when they are doped with different rare earth ions such as Sm, Tm, Tb, Er, Eu, Dy [17]. A strong room-temperature near-IR luminescence can be observed for the terbium (Tb) doped BaSnO_3 material. Photoluminescence (PL) and radioluminescence (RL) emissions in the near-IR region can also be observed. Rare earth doped BaSnO_3 play an important role as multi-functional candidates in the fabrication of optoelectronic devices [18]. 5% Fe doped barium stannate thin films exhibit maximum crystallinity and transparency over 85% in the visible region [19].

Piezoelectric and Electrostrictive Properties

The effect of heavy dose gamma ray irradiation on the ferroelectric and piezoelectric properties of the synthesized titanium doped BaSnO_3 i.e. barium stannate titanate ceramics has been observed. It has been found that on irradiation the ferroelectric property decreases with decreasing values of remanent polarization P_r and coercive electric field E_c in hysteresis loop. The piezoelectric properties including piezoelectric coefficient d_{33} , electrostrictive strain and electromechanical coupling coefficient (K_p) also decrease following the same trend of P_r and E_c . Grain size also decreases and grain patterns become irregular after irradiation [20, 21]. Generally this clockwise reversible hysteresis loop are observed in barium stannate titanate ceramics in the temperature range 10–40°C [22].

Pyroelectric Property

Pyroelectric effects of ferroelectric materials i.e. doped BaSnO_3 are manifested in a change in polarization as a function of temperature, which results in a reduction of the bound charge required for compensation of the reduced dipole moment on increasing temperature and vice versa on decreasing temperature [21].

Electrical Conductivity Property

The maximum conductivity of nanocrystalline BaSnO_3 is found to be $3.63 \times 10^{-3} \text{ S cm}^{-1}$ at 650°C. The total conductivity is found to increase with increase in temperature [23]. The properties of substitutionally doped, $\text{BaSn}_{1-x}\text{Sb}_x\text{O}_3$ samples are investigated. The electrical conductivity increases drastically for samples $\text{BaSn}_{1-x}\text{Sb}_x\text{O}_3$ with $x \leq 0.05$, exhibits a transition from an insulating to a metallic state. For higher doping levels, $0.05 < x < 0.15$, the conductivity saturates at 4 S cm^{-1} [22]. Besides yttrium doped BaSnO_3 i.e. $\text{Ba}_2\text{SnYO}_{5.5}$ provides high protonic conductivity [24].

The yttrium doped barium stannate, i.e. $\text{YBa}_2\text{SnO}_{5.5}$ also finds applications as substrates for high temperature superconducting materials, in microwave integrated circuits and transmission lines because of their compatible dielectric properties, lattice matching, thermal expansion coefficients and chemical non-reactivity with the superconductors at the processing temperature [25].

The silicon doped barium stannate i.e. $\text{BaSn}_{1-x}\text{Si}_x\text{O}_3$ samples show NTCR (Negative Temperature Coefficient of Resistance) behavior and a better electrical conduction at elevated temperature than undoped BaSnO_3 ceramic bodies [26]. The conductivity of barium stannate increases sharply (by four orders of magnitude) at a particular relative humidity (RH), temperature and frequency (i.e. for RH 10%, temperature 31 °C and frequency 1 kHz) if it is doped with lanthanum and the dopant (La) concentration varies from 0 to 10 mol% [10].

It has been found that electrical resistivity for niobium doped barium stannate $\text{BaSn}_{1-x}\text{Nb}_x\text{O}_3$ decreases with increasing x for $x \leq 0.01$. It again increases with Nb variations for $x > 0.01$ [12].

Magnetic Property

The undoped BaSnO_3 is diamagnetic; upon doping Mn, the diamagnetic character of BaSnO_3 diminishes and the ferromagnetic character evolves gradually with increasing Mn-content [27]. These Fe-doped BaSnO_3 systems exhibit ferromagnetism at room temperature with an average magnetic moment of 0.047, 0.038 and 0.025 $\mu\text{B}/\text{Fe}$ and Curie temperature of 510, 462 and 446 K, respectively [28]. Room temperature ferromagnetism is exhibited by 5 and 10% Fe doped barium stannate powder and film [19].

Dielectric Property

Doped BaSnO_3 are ferroelectric ceramics which are characterized by (i) high dielectric constant (200–10,000) compared to ordinary insulating materials (5–100), (ii) relatively low dielectric loss tangent (0.1%–7%), (iii) high DC resistivity, (iv) moderate dielectric breakdown strength (100–120 kV/cm) and (v) nonlinear electrical, electro-mechanical and electro-optic behaviour. In $\text{BaTi}_{1-x}\text{Sn}_x\text{O}_3$ ceramics, it is possible to control the room temperature values of dielectric, electromechanical and elastic coefficients in a fairly wide range. With increasing Sn content, the Curie temperature T_c of the paraelectric–ferroelectric phase transition decreases considerably [29–31]. The reversible dielectric nonlinearities of several barium stannate titanate ceramics are investigated both in ferroelectric and paraelectric phases [32]. It has been observed that the value of peak dielectric constant (ϵ_{max}), Curie temperature is strongly dependent on frequency and dopant concentration [29].



Applications

Capacitive Application

BaSnO₃ has been used to prepare capacitors owing to its characteristic dielectric properties [3]. Since capacitance is proportional to dielectric constant, capacitance increases with the increase in dielectric property. It has been used to prepare thermally stable capacitors and to fabricate ceramic boundary layer capacitors when combined with BaTiO₃ [4, 33].

In order to produce capacitor components based on BaSnO₃, dense (almost pore free) material bodies are required because pores would act as sink to the electrical charge carriers and would be the source of poor grain to grain connectivity and significant dielectric loss. The addition of additive BaGeO₃ can significantly reduce the sintering temperature obtaining dense ceramic bodies due to an improvement of the densification behavior [34]. Generally the single capacitive sensor chip are fabricated with multiple capacitive sensors [35].

Ethanol and Gas Sensing Applications

Ethanol-sensing and gas sensing characteristics of barium stannate prepared by chemical precipitation synthesis route are interesting. The concentration for all test gases is 1000 ppm. The response of the sensor to ethanol is reported in journals. The material exhibits very low response to petrol, LPG, H₂ and CO. Among these gases, the maximum response is 3.4 for petrol at 290°C. However, its response to ethanol is very high. At 290°C, the response to 1000 ppm ethanol is 31.7. It may be observed that the sensor exhibits the highest response around 290. The responses decrease with increasing temperature above 290°C [2]. For CO gas sensor the mechanism of CO sensitivity is supposed to be a surface reaction process. Thus to get a high gas sensitivity, the CO elementary sensor is realized as a thin film. The sensitivities of the BaSnO₃ thin films to CO are measured as a function of the temperature and the oxygen concentration [36]. It is observed that the BaSnO₃ thin films are insensitive to CO₂ and NH₃ [37].

Humidity Sensing Application

Barium stannate has a sensing properties required to act as a humidity sensing materials. This property was seen while BaSnO₃ was synthesized by cold isostatic pressing route [7]. The relative humidity inside a chamber was regulated by mixing two streams of dry and wet nitrogen gas with BaSnO₃ sample. Lanthanum doped barium stannate exhibits superior response to the change in humidity [4]. Combination of BaTiO₃ with BaSnO₃ (BTS), results in development of better relative humidity sensor based material system [33]. The

influence of the Ni ions which partly substitute the Ba ions in the barium stannate (Ba_{1-x}Ni_xSnO₃, where x = 0; 0.1; 0.2; 0.5), on the sensitivity to humidity shows that the sensitivity to humidity within 22% RH (Relative Humidity) and 75% RH for the substitution with x = 0 and 0.1, and 22% RH–98% RH for the substitution with x = 0.5. The response time is two times shorter than that of the sample without nickel substitution [38].

Conclusion

From the above studies we can now draw the following major conclusion of nano-barium barium stannate materials: Nanocrystalline BaSnO₃ is a very important functional material possessing many interesting properties. The fine-grained BaSnO₃ powders can be prepared at relatively low temperatures. The results of XRD, DTA, TGA, FTIR spectroscopy, High resolution microscopy analysis gives the lot of informations about the characteristics of nanocrystalline BaSnO₃. The materials noted to possess good electrical, dielectric, piezoelectric, ferroelectric and optical properties when BaSnO₃ is doped with titanium, antimony, yttrium, etc. Nanocrystalline BaSnO₃ has been used to prepare thermally stable capacitors and it can make better capacitor when combined with BaTiO₃. BaSnO₃ sensors are multifunctional because they can sense various gases, ethanol, humidity, temperature. BaSnO₃ sensors exhibit very low response to petrol, LPG, H₂ and CO. However, its response to ethanol is very remarkable. Milling technique can be used as one of the simple synthesis route because the high-energy ball milling process is a promising method due to its simple processing practice compared with the conventional solid-state reaction and wet-chemistry based processes. Different metals can be used as doping material which can enhance the properties of pure BaSnO₃. Gas sensing property can be improved based on reaction chemistry.

Acknowledgment

The authors are greatly indebted to Department of Metallurgical and Materials Engineering, Jadavpur university, Kolkata, India, for giving the opportunity to take up this interesting project work.

References

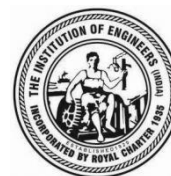
- [1] Upadhyay, Shail; Parkash, Om and Kumar, Devendra, "Solubility of lanthanum, nickel and chromium in barium stannate", *Materials Letters*, Vol. 49, pp. 251–255, 2001.
- [2] Kocemba, I., M. Wróbel-Jędrzejewska, Szychowska, A., Rynkowski, J. and Głowka, M., "The properties of barium stannate and aluminum oxide-based gas sensor The role of Al₂O₃ in this system, *Sensors and Actuators B*", Vol. 121, pp. 401–405, 2007.



- [3] Upadhyay, Shail and Kavitha, P., "Lanthanum doped barium stannate for humidity sensor", *Materials Letters*, Vol. 61, pp. 1912–1915, 2007.
- [4] Wei, Xiaoyong; Feng, Yujun; Hang, Lianmao; Xia, Song; Jin, Li and Yao, Xi, "Abnormal C–V curve and clockwise hysteresis loop in ferroelectric barium stannate titanate ceramics", *Materials Science and Engineering B*, Vol. 120, pp. 64–67, 2005.
- [5] Wei, Xiaoyong and Yao, Xi, "Preparation, structure and dielectric property of barium stannate titanate ceramics", *Materials Science and Engineering B*, Vol. 137, pp. 184–188, 2007.
- [6] Wei, Xiaoyong; Feng, Yujun; Wan, Xing and Yao, Xi, "Evolution of dielectric relaxation of barium stannate titanate ceramics", *Ceramics International*, Vol. 30, pp. 1397–1400, 2004.
- [7] Markovic, Smilja; Jovalekic, C. edimir; Veselinovic, Ljiljana; Mentus, Slavko and Uskokovic, Dragan, "Electrical properties of barium titanate stannate functionally graded materials", *Journal of the European Ceramic Society*, Vol. 30, pp. 1427–1435, 2010.
- [8] Upadhyay, Shail; Parkash, Om and Kumar, Devendra, "Synthesis, structure and electrical behaviour of nickel-doped barium stannate", *Journal of Alloys and Compounds*, Vol. 432, pp. 258–264, 2007.
- [9] Singh, Prabhakar; Sebastian, C. Peter; Kumar, Devendra and Parkash, Om, "Correlation of microstructure and electrical conduction behaviour with defect structure of niobium doped barium stannate", *Journal of Alloys and Compounds*, Vol. 437, pp. 34–38, 2007.
- [10] Li, Bi-hui; Tang, Yi-wen; Luo, Li-juan; Xiao, Ting; Li, Dawei; Hu, Xiao-yan and Yuan, Min, "Fabrication of porous BaSnO₃ hollow architectures using BaCO₃@SnO₂ core-shell nanorods as precursors", *Applied Surface Science*, Vol. 257, pp. 197–202, 2010.
- [11] Cerdà, J., Arbiol, J., Diaz, R., Dezanneau, G. and Morante, J.R., "Synthesis of perovskite-type BaSnO₃ particles obtained by a new simple wet chemical route based on a sol-gel process", *Materials Letters*, Vol. 56, pp. 131–136, 2002.
- [12] Cerda, J., Arbiol, J., Dezanneau, G., Díaz, R. and Morante, J.R., "Perovskite-type BaSnO₃ powders for high temperature gas sensor applications", *Sensors and Actuators B*, Vol. 84, pp. 21–25, 2002.
- [13] Wei, Xiaoyong and Yao, Xi, "Preparation, structure and dielectric property of barium stannate titanate ceramics", *Materials Science and Engineering B*, Vol. 137, pp. 184–188, 2007.
- [14] Deepa, A.S., Vidya, S., Manu, P.C., Solomon, S., John, A. and Thomas, J.K., "Structural and optical characterization of BaSnO₃ nanopowder synthesized through a novel combustion technique", *Journal of Alloys and Compounds*, Vol. 509, pp. 1830–1835, 2011.
- [15] Udawatte, C.P. and Yoshimura, M., "Preparation of well-crystallized BaSnO powders under 3 hydrothermal conditions", *Materials Letters*, Vol. 47, pp. 7–10, 2001.
- [16] Lu, W. and Schmidt, H., "Synthesis of Tin Oxide Hydrate (SnO₂·xH₂O) Gel and its Effects on the Hydrothermal Preparation of BaSnO₃ Powders", *Advanced Powder Technology*, Vol. 19, pp. 1–12, 2008.
- [17] Lu, Z., Chen, L., Tang, Y. and Li, Y., "Preparation and luminescence properties of Eu³⁺-doped MSnO₃ (M = Ca, Sr and Ba) perovskite materials", *Journal of Alloys and Compounds*, Vol. 387, pp. 1–2, 2005.
- [18] Ayvacıklı, M., Canimoglu, A., Karabulut, Y., Kotan, Z., Herval, L.K.S., de Godoy, M.P.F., Gobato, Y.G., Henini, M. and Can, N., "Radioluminescence and photoluminescence characterization of Eu and Tb doped barium stannate phosphor ceramics", *Journal of Alloys and Compounds*, Vol. 590, pp. 417–423, 2014.
- [19] James, K.K.; Aravind, Arun and Jayaraj, M.K., "Structural, optical and magnetic properties of Fe-doped bariumstannate thin films grown by PLD", *Applied Surface Science*, Vol. 282, pp. 121–125, 2013.
- [20] Nath, A.K., Medhi, "Effect of gamma ray irradiation on the ferroelectric and piezoelectric properties of barium stannate titanate ceramics", *Radiation Physics and Chemistry*, Vol. 91, pp. 44–49, 2013.
- [21] Singh, K.C., Nath, A.K., Laishram, R. and Thakur, O.P. "Structural, electrical and piezoelectric properties of nanocrystalline tin-substituted barium titanate ceramics", *Journal of Alloys and Compounds*, Vol. 509, pp. 2597–2601, 2011.
- [22] Wei, X., Feng, Y., Hang, L., Xia, S., Jin, L. and Yao, X., "Abnormal C–V curve and clockwise hysteresis loop in ferroelectric barium stannate titanate ceramics", *Materials Science and Engineering B*, Vol. 120, pp. 64–67, 2005.
- [23] Bradha, M., Vijayaraghavan, T. and Ashok, A., "Synthesis and total conductivity studies in BaSnO₃", *Materials Letters*, Vol. 125, pp. 187–190, 2014.
- [24] Wang, Y., Chesnaud, A., Bevilion, E., Dezanneau, G. and Yang, J., "Synthesis and electrical properties of nano-structured Ba₂SnYO_{5.5} proton conductor", *Ceramics International*, Vol. 37, pp. 3351–3355, 2011.
- [25] Vidya, S., Rejith, P.P., John, A., Solomon, S., Deepa, A.S. and Thomas, J.K., "Electrical, optical and vibrational characteristics of nano structured yttrium barium stannous oxide synthesized through a modified combustion method", *Materials Research Bulletin*, Vol. 46(), pp. 1723–1728, 2011.
- [26] Köferstein, R., Jäger, L., Zenkner, M., Müller, T. and Ebbinghaus, S.G., "The influence of the additive BaGeO₃ on BaSnO₃ ceramics", *Journal of the European Ceramic Society*, Vol. 30, pp. 1419–1425, 2010.
- [27] Balamurugan, K., Kumar, N.H., Ramachandran, B., Rao, M.S.R., Chelvane, J.A., Santhosh, P.N., "Magnetic and optical properties of Mn-doped BaSnO₃", *Solid State Communications*, Vol. 149, No. (21–22), pp. 884–887, 2009.
- [28] Geske, L., Lorenz, V., Müller, T., Jäger, L., Beige, H., Abicht, H.-P. and Mueller, V., "Dielectric and electromechanical characterization of fine-grain BaTi_{0.95}Sn_{0.05}O₃ ceramics sintered from glycolate-precursor powder", *Journal of the European Ceramic Society*, Vol. 25, No. (12), pp. 2537–2542, 2005.
- [29] Nath, A.K., Singh, K.C., Laishram, R. and Thakur, O.P., "Ferroelectric, piezoelectric and electrostrictive properties of



- Ba(Ti_{1-x}Sn_x)O₃ ceramics obtained from nanocrystalline powder”, *Materials Science and Engineering B*, Vol. 172, pp. 151–155, 2010.
- [30] Zenkner, M., Jger, L., Köferstein, R. and Abicht, H.-P., “Synthesis and characterization of nanoscaled Ba(Ti_{1-x}-ySn_xGey)O₃ powders and corresponding ceramics”, *Solid State Sciences*, Vol. 10, pp. 1556–1562, 2008.
- [31] Wei, X., Feng, Y., Hang, L. and Yao, X., “Dielectric properties of barium stannate titanate ceramics under bias field”, *Ceramics International*, Vol. 30, pp. 1401–1404, 2004.
- [32] Azad, A.-M. and Hon, N.C., “Characterization of BaSnO₃-based ceramics: Part 1. Synthesis, processing and microstructural development”, *Journal of Alloys and Compounds*, Vol. 270, pp. 95–106, 1998.
- [33] McCorkle, D.L., Warmack, R.J., Patel, S.V., Mlsna, T., Hunter, S.R. and Ferrell, T.L., “Ethanol vapor detection in aqueous environments using micro-capacitors and dielectric polymers”, *Sensors and Actuators B*, Vol. 107, pp. 892–903, 2005.
- [34] Lampe, U., Gerblinger, J. and Meixner, H., “Carbon-monoxide sensors based on thin films of BaSnO₃”, *Sensors and Actuators B Chemical*, Vol. 25, No. (1–3), pp. 657–660, 1995.
- [35] Cerdà, J., Arbiol, J., Dezanneau, G., Díaz, R. and Morante, J.R., “Perovskite-Type BaSnO₃ powders for high temperature gas sensor applications”, *Sensors and Actuators B*, Vol. 84, pp. 21–25, 2002.
- [36] Doroftei, C., Popa, P.D. and Iacomi, F., ” Study of the influence of nickel ions substitutes in barium stannates used as humidity resistive sensors” *Sensors and Actuators A, Physical*, Vol. 173, No. 1, pp. 24–29, 2012.
- [37] Manorama, S.V., Reddy, C.V.G. and Rao, V.J., “X-ray photoelectron spectroscopic studies of noble metal-incorporated BaSnO₃ based gas sensors”, *Applied Surface Science*, Vol. 174, pp. 93–105, 2001.
- [38] Doroftei, C., Popa, P.D. and Iacomi, F., “Study of the influence of nickel ions substitutes in barium stannates used as humidity resistive sensors,” *Sensors and Actuators A, Physical*, Vol. 173, No. 1, pp. 24–29, 2012.



Mechano-Chemical Synthesis of Nanocrystalline Hydroxyapatite from Egg Shells and Phosphoric Acid

Anindya Pal¹, Shubhadeep Maity², Sumit Chabri³, Supriya Bera²,
Amit Roy Chowdhury⁴, Mitun Das⁵ and Arijit Sinha^{*1}

Abstract: The aim of the present study is synthesis of hydroxyapatite from egg shell. Nano-crystalline hydroxyapatite (HAp) ceramics were successfully fabricated by a mechanochemical method using egg shells and phosphoric acid. The CaO and H₃PO₄ acid at different wt.% ratios i.e. 1:0.75, 1:1.1, 1:1.25, 1:1.5 and 1:1.75, were ball milled and then heat treated at 1000°C for 3 hr to complete reactions. The synthesized powders were characterized using X-ray diffraction, FTIR spectroscopy, scanning electron microscope and high resolution transmission electron microscopy.

Keywords: Mechanochemical Synthesis, X-ray Diffraction, Egg Shell, Hydroxyapatite, Biocompatibility.

Introduction

Hydroxyapatite (HAp), (Ca₁₀) (PO₄)₆(OH)₂ is the main component of human bone and teeth. HAp is among the few bioactive materials, which will support bone in-growth and osseointegration when used in orthopaedic and dental applications. HAp can be successfully synthesized from various biogenic materials, viz., coral, seashell, eggshell, body fluids by solid state reactions, chemical precipitation, hydrothermal reactions, sol-gel methods and mechanochemical methods using different calcium and phosphorus-containing starting materials. HAp can be successfully produced from recycled eggshells along with phosphoric acid. The phases so obtained depend on the ratio of calcined eggshells to phosphoric acid, the calcinations temperature and the mechanochemical activation method i.e., high energy ball milling (HEBM) [1]. Research carried out so far suggests that these natural resources can be a good source of biological HAp or the promising alternative of Ca and P precursor for the production of phase-pure and thermally stable HAp. Furthermore, HAp synthesized from the natural raw materials or natural waste can be more beneficial as it often contains useful ions, which are useful for fast bone regeneration process [2]. Among different biogenic materials, sea shells were found to be an attractive material

as it contains 95–99% CaCO₃ with trace amount of rear oxides (SiO₂, MgO, Al₂O₃, SrO, P₂O₅, Na₂O, and SO₃), nanoscale arrangement of crystals and high compressive strength than common mineral crystal [3–5, 7]. Vecchio *et al.* demonstrated conversion of different egg shells to hydroxyapatite structure through hydrothermal reaction at relatively low temperature [3]. The partially converted shell with dense HAp layer on shell structure showed fracture strength similar to the compact human bone [3, 4]. Lemos *et al.* synthesized nano hydroxyapatite powder from egg shells via hydrothermal transformation [5]. Several other researchers also studied synthesis of HAp powder from egg shell using ball milling and wet chemical synthesis route [6–9]. The ball milling (mechanochemical) followed by heat treatment route produces more complete conversion of initial powder, resulting in the formation of HAp with trace amount of β-TCP (β-Tricalcium phosphate) [6, 7]. However, none of these mechanochemically synthesized powders were evaluated for bioactivity study.

In present investigation, eggshells were collected and washed properly with detergent followed by calcinations at 1000°C for 3 hours. The structural and morphological analyses were done using X-Ray diffraction technique and scanning electron microscope. During the first 30 minutes

¹Dr. M.N. Dastur School of Materials Science and Engineering, Indian Institute of Engineering Science and Technology, Shibpur, Howrah–711103, India. ✉*arijit@matse.iiests.ac.in

²Department of Metallurgical and Materials Engineering. NIT, Durgapur–713209, India.

³Department of Metallurgy and Materials Engineering, Indian Institute of Engineering Science and Technology, Shibpur, Howrah–711103, India.

⁴Department of Aerospace Engineering and Applied Mechanics, Indian Institute of Engineering Science and Technology, Shibpur, Howrah–711103, India.

⁵Bioceramics and Coating Division, CSIR-Central Glass and Ceramic Research Institute, 196 Raja S.C. Mullick Road, Kolkata–700032, India.



most of the organic materials were burnt out, and then the eggshell were converted to CaO as visualize from the XRD. The calcined shells were crushed and subjected to HEBM in Fritsch Pulverisette P6 planetary mill with phosphoric acid in different weight ratios for 20 hours at 300 rpm. The ball milled powder were further heat treated at 1000°C for 3 hours. The ball milled and heat treated powders were further subjected to structural and morphological analyses. The presence of HAp was not observed after ball milling, whereas HAp and other calcium phosphate phases appeared after heat treatment of the ball milled powders.

Materials and Methods

Powder preparation In the present study, egg shell was used as a source of calcium for mechanochemical synthesis of HAp. The collected egg shell was washed with detergent, dried and then crushed into small pieces which were further calcined at 1000°C for 3 hours. Most of the organic materials were burnt out during the first 30 minutes. The calcined egg shell powders were mixed with H₃PO₄ acid in CaO:H₃PO₄ wt% ratio of 1:0.75, 1:1.0, 1:1.25, 1:1.5 and 1:1.75, respectively. The mixtures were ball milled for 20 hours at a speed of 300 rpm to achieve homogenous mixtures. The ball mill (Fritsch Pulverisette P6 planetary mill) was equipped with tungsten carbide balls and vial. After milling, powders were dried and followed by heat treated at 1000°C for 3 hours. Table 1 shows the nomenclature of the samples and processing conditions. The schematic of processing steps can be seen in Figure 1.

The morphologies of the calcined egg shell, synthesized powders, and heat treated powders were examined using scanning electron microscope (HITACHI, S-3400 N). The quantitative analysis of ball milled powder was examined by HRTEM equipped with a Si detector operated at an acceleration voltage of 20 kV using the associated software of Energy-Dispersive X-ray spectroscopy (EDX).

Table 1: The Nomenclature of the Samples

Sample	Seashell Powder: H ₃ PO ₄ acid	Processing Condition
HAp1	1:0.75	Seashell and H ₃ PO ₄ composities ball mill for 20 hrs, followed by sintering at 1000°C for 3 hrs.
HAp2	1:1.0	
Hap3	1:1.25	
Hap4	1:1.5	
Hap5	1:1.75	

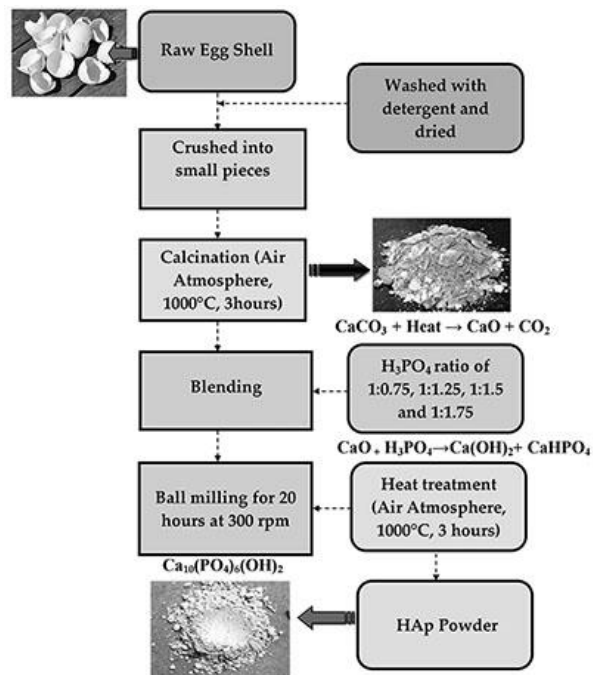
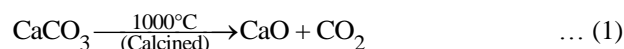


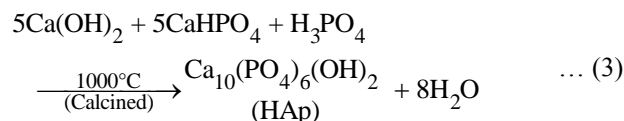
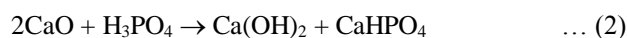
Fig. 1: Process Flowchart of HAp Synthesized by the Mechanochemical Method

Results and Discussion

Powder synthesis and XRD analysis In the present study, egg shell was used as a source of calcium for mechanochemical synthesis of HAp. During calcination, the organic materials of raw egg shell burnt out and completely converted into CaO as per following reaction:



The trace amount of Ca(OH)₂ in the calcined powder is may be due to moisture absorption from the atmosphere (Figure 2). However, in the present study the calcined powder has been considered as pure CaO and mixed H₃PO₄ acid at CaO:H₃PO₄ wt% ratio of 1:0.75, 1:1.1, 1:1.25, 1:1.5 and 1:1.75, respectively. The XRD of ball milled powder (CaO:H₃PO₄ wt% ratio 1:1.5). After milling, powders were dried and followed by heat treatment at 1000°C for 3 hours in the air. The following reactions occurred and the reactant phases were analyzed through XRD. The CaO:H₃PO₄ wt% ratio in the precursor powder mixture influenced the reactant phases.



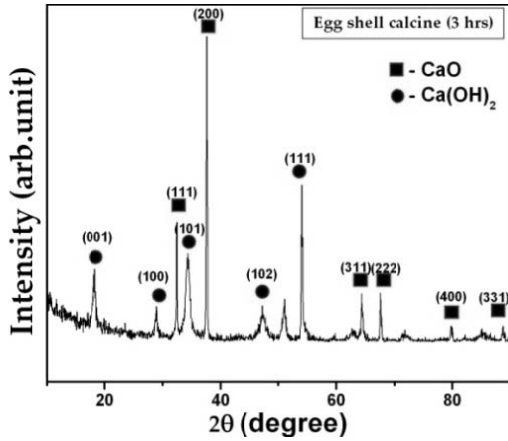


Fig. 2: XRD Patterns of the Calcine Eggshell for 3 Hours at 1000°C

The XRD patterns of heat treated powders are presented in Figure 3. The XRD pattern shown in Figure 3 reveals the intense peak ($2\theta = 25.92^\circ, 31.22^\circ, 32.62^\circ, 39.97^\circ, 47.27^\circ, 51.77^\circ, 49.82^\circ$) corresponding to (002, 211, 300, 310, 222, 410, 320) reflection of HAp (JCPDS file No: 076-0694) along with the adjacent peaks corresponding to (100) reflections of the β -TCP. With increase in CaO: H_3PO_4 wt.% ratio, HAp phase increase whereas CaO and β -TCP reduced in the heat treated powders.

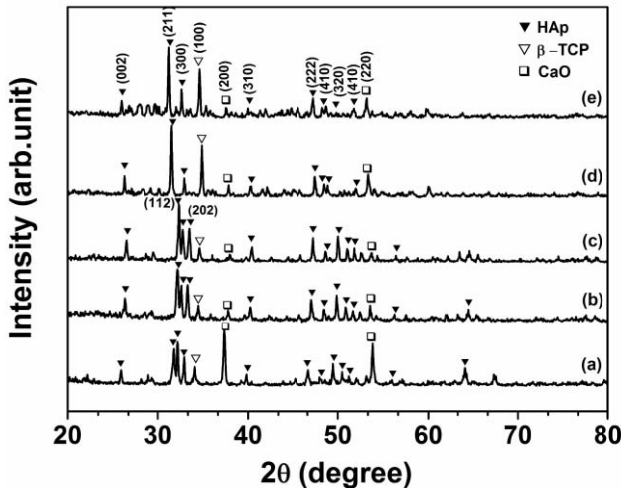


Fig. 3: XRD Patterns of 20 Hours Ball Milled Powders, Heat Treated at 1000°C for 3 Hours Synthesized from the Mixing Ratio of (a) 1:0.75, (b) 1:1.1, (c) 1:1.25, (d) 1:1.5 and (e) 1:1.75

FTIR Analysis

Figure 4 show the FTIR spectra of heat treated powder (CaO: H_3PO_4 wt.% ratio of 1:1.5). The FTIR spectrum is dominated by νOH at 3568 cm^{-1} , detected as a hydroxyl group. The stretching (ν_3) and bending (ν_4) modes of PO_4^{3-} ion were detected at around 1042, 602 and 570 cm^{-1} respectively. The symmetrical stretching modes (ν_1 and ν_2) of

PO_4^{3-} ion were also found at around 466 cm^{-1} respectively. The bands at 3418 and 1597 cm^{-1} correspond to adsorbed H_2O . Crystallized HAp with some carbonate substitution is formed only after heat treatment at 1000°C . The stretching vibrations, ascribed to CO_3^{2-} at around 1412 and 1090 cm^{-1} were present. It has been reported that this kind of apatite is more similar to biological apatite and could be more suitable for bone replacement materials [10].

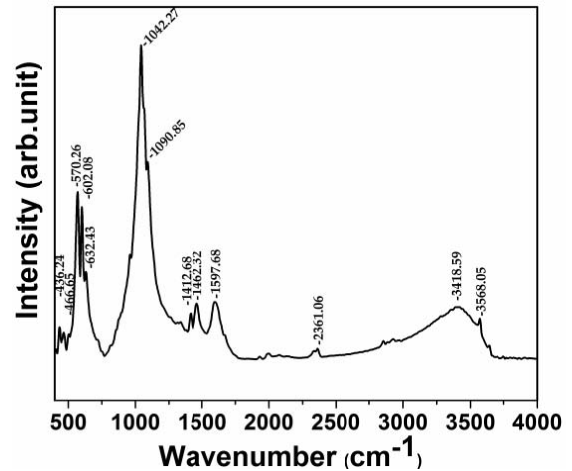


Fig. 4: FTIR Spectra of HAp Precursor and Powders Milled for 1 hour and then Sintered in air at 1000°C for 3 hours

Powder Morphology

Figure 5 show the FE-SEM images of the HAp sample synthesized from phosphoric acid and egg shell powders heat treated for 3 hours at 1000°C . The powder gets agglomerated becomes polygonal structure due to high temperature heat treatment. Figure 6 shows the EDX spectra of the HAp powder after heat treatment at 1000°C for 3 hours. The compositional analysis from EDX showed the presence of calcium, phosphorus and oxygen and Ca/P in the synthesized powder were close to 1.6.

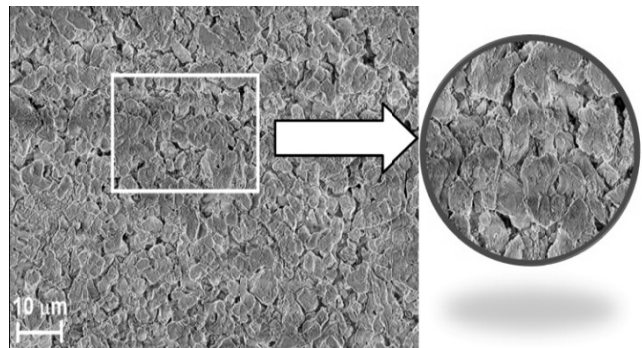


Fig. 5: FE-SEM Images of the Sample Synthesized from Phosphoric Acid and Egg Shell Powders Heat Treated for 3 Hours at 1000°C and Enlarge View of the Same at Higher Magnification

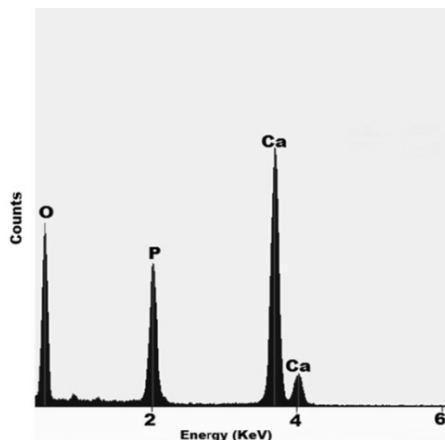


Fig. 6: EDX of the Sintered Powder

Conclusions

Nano-sized HAp powders have been synthesized successfully from a recycled egg shell and phosphoric acid by a mechanochemical method. This process is cost-effective and relatively simple technique for converting waste egg shells into valuable HAp. HAp powder of high crystallinity was developed after ball milling and subsequent heat treatment at 1000°C. The initial CaO: H₃PO₄ ratio is important to obtain the desired phase with crystallinity. The hydroxyapatite powder synthesized from CaO:H₃PO₄ wt. ratio of 1:1.5, produced HAp powder.

Acknowledgments

Author acknowledges the financial support from the Centre for Excellence in Microstructurally Designed Advanced Materials, TEQIP II, Indian Institute of Engineering Science and Technology, Shibpur.

References

- [1] Wua, S., Hsua, H., Hsua, S., Chang, Y. and Ho, W., Effects of heat treatment on the synthesis of hydroxyapatite from eggshell powders. *Ceramics International* 41, 10718–10724 (2015).
- [2] Ripamontia, U., Crooksa, J., Khoalia, L. and Roden, L., The induction of bone formation by coral-derived calcium carbonate/hydroxyapatite constructs. *Biomater.* 30, 1428–1439 (2009).
- [3] Vecchioa, K.S., Zhangb, X., J.B. Massiec, Wangc, M. and Kim, C.W., Conversion of bulk seashells to biocompatible hydroxyapatite for bone implants. *Acta Biomater.* 3, 910 (2007).
- [4] Zhang, X. and Vecchio, K.S., Creation of dense hydroxyapatite (synthetic bone) by hydrothermal conversion of seashells. *Mat. Sci. and Engg. C* 26, 1445–1450 (2006).
- [5] Lemos, A.F., Rocha, J.H.G., Quaresma, S.S.F., Kannan, S., Oktar, F.N., Agathopoulos, S. and Ferreira, J.M.F., Hydroxyapatite nano-powders produced hydrothermally from nacreous material. *J. of the European Ceramic Society* 26, 3639–3646 (2006).
- [6] Gergely, G., Wéber, F., Lukács, I., Illés, L., Tóth, A.L., Horváth, Z.E., Mihály, J. and Balázs, C., Nano-hydroxyapatite preparation from biogenic raw materials. *Cent. Eur. J. Chem.* 8, 375–381 (2010).
- [7] Wu, S.C., Hsu, H.C., Wu, Y.N. and Ho, W.F., Hydroxyapatite synthesized from oyster shell powders by ball milling and heat treatment. *Mater. Char.* 62, 1180–1187 (2011).
- [8] Santhosh, S. and Prabu, S.B., Thermal stability of nano hydroxyapatite synthesized from sea shells through wet chemical synthesis. *Mat. Lett.* 97, 121–124 (2013).
- [9] Rujitanapanich, S., Kumpapan, P. and Wanjanoi, P., Synthesis of Hydroxyapatite from Oyster Shell via Precipitation. *Energy Procedia* 56, 112–117 (2014).
- [10] Fathi, M.H. and Zahrani, E.M., Mechanical alloying synthesis and bioactivity evaluation of nano crystalline fluoridated hydroxyapatite. *J. of Crystal Growth* 311, 1392–1403 (2009).



Sustainable Rural Development through Responsible Mining of Natural Resources of Kotah Stone in Rajasthan

S.C. Agarwal¹

Abstract: Minerals resources normally occur in remote locations in and around villages in rural area. Exploitation of natural mineral resources enhances socio-economic development of rural areas. Beside generating employment to rural mass, it also helps in sustainable development of the area by generating required financial resources shared by Lessee with local government. The state of Rajasthan has been blessed with vast deposit of dimensional limestone commercially marketed as Kotah Stone. The vast deposit of Kotah Stone covers over hundred villages spreading over 55 sq km of Ramganjmandi and Chechat tehsil in Kota district. Another large area in Jhalawar district. Mining industry is providing employment to over 2 lac workers of which 80% are inhabitants from local villages, both male and female. Mining for Kotah Stone has been going on since 1945 but all manual till 1992. Manual mining faced many challenges such as low productivity, high generation of waste, poor mineral conservation and poor earning and created economical, environmental and social crises. It was on threshold of closure of mining operations.

To address these challenges, an innovative mining technology was established by the author in 1992. The innovated technology improved productivity four times, waste generation reduced to a third, ensured high standard of safety, improved overall economics appreciably. The innovative mining technique proved to be a responsible and good mining practice. Responsible practices are defined as practices that are widely recognised by interested stakeholders as being the most effective way to achieve agreed goals, given the current state of knowledge. The responsible innovative mining technology of Kotah Stone has proved to be blessing for mine workers and their family by multiplying their earnings through increased productivity, improved working conditions. It resulted in enhanced welfare, prosperity of workers and their families. Prosperity keeps the worker and his family happy. The state of Rajasthan, in past has witnessed a number of draughts but fortunately villagers employed, directly or indirectly with Kotah Stone mining have escaped these miseries. Kotah Stone industry has proved to be back bone for sustainable development of a number of villages falling in lease area and are developing as smart village.

Keywords: Sustainable, Responsible Practice, Kotah Stone.

Introduction

Nearly everything manufactured or constructed—from buildings, roads, computers and trains—contains material mined from the Earth. Mining is a complex and intensive process that can have major environmental and social impacts. However, in most cases the most negative social and environmental impacts can be avoided if companies operate according to best and responsible practice standards.

Responsible Mining Defined by IRMA, Innovative Responsible Mining Assurance-Draft-16 as:

“The goal should be to maximise the contribution to the Social well-being of villages and their habitants. In a way it ensures an equitable distribution of its costs and benefits to

all stakeholders and without reducing the potential of future generation”. The overall objective for Responsible Mining is that industrial mining should:

- respect the human rights and aspirations of affected communities;
- provide safe, healthy and respectful workplaces;
- avoid or minimise harm to the environment; and,
- leave positive legacies.

Kotah Stone

Geology and Mining for Kotah Stone

The state of Rajasthan has been gifted by nature with abundant reserves of Kotah Stone. Kotah Stone is basically flaggy, naturally splittable, low grade limestone, confined in

¹ President, Associated Stone Industries (Kotah) Ltd. India.
✉ scagarwal42@yahoo.com



a zone of 15M. It is overlaid by OB. It is extracted in form of slabs/tiles of required dimension. Over last six decades it has been used as an excellent flooring stone, yet most economical, world over.

Conventional Mining

Mining for Kotah Stone has been going on in state of Raj since 1945. It has been all manual including waste handling. It is all about peeling the layers of Kotah Stone one by one by crowbar and then splitting along foliation and finally sizing the irregular piece into dimensional size by chisel and hammer to yield a single and compact slab/tile ready for use. Figure 1 shows typical conventional manual mining of Kotah Stone.



Fig. 1: Conventional Manual Mining of Kotah Stone

Some 220 splits in varying thickness of 12 mm to 50 mm have been mined. Any layer with thickness lower than 12 mm and more than 50 mm in thickness have not been mined but thrown as waste. Employment was large and the overall productivity was about 39 sq ft/per man shift. The mineral recovery was about 35–40%.

Impact of Past Mining on Social, Economical, Safety and Environmental Status:

- In past Kotah Stone mining was all manual and it was more of a handicraft.
- Though it provided a large employment to both males and females, even to those who migrated from adjoining states, but it was very wasteful both on human effort as well on natural resources.
- Productivity was very low, hence the poor earning in spite of both husband and wife working. To supplement income at times even children were engaged. Each family had to borrow money for discharging social responsibilities. Non-payment of advances/loan lead to many criminal activities and even lead to labour bonding.

- Education among children was very low, living conditions were poor, one could hardly see a pucca dwelling for mine workers.
- Poor health standards, poor health care facilities, bad drinking habits causing lungs diseases.
- Lack of appropriate mining technology had been major cause of poor safety standards, large number of accidents including fatal and serious body injury as well excessive human suffering. Major part of human efforts had been wasted in non-productive jobs causing excessive fatigue and mental stress, inflicting excessive injuries to eye, leg, foot, arm, fingers and spinal chord.

Best Practice and Responsible Mining for Kotah Stone

To address economic and environmental issues arising from manual mining, an innovative mining technique was evolved. The concept was to first cut the layers in-situ to size required before separating the blocks. All sides cut blocks were then splitted by same techniques to yield all sides cut slabs/tiles. To do so, portable diamond cutter were designed fitted with steel blades tipped with diamond cutting bits. The cutter is electrically operated on portable track. Water is used at pressure to cool the cutting tool and also flush out the cutting slurry. The new technique is shown in Figure 2.

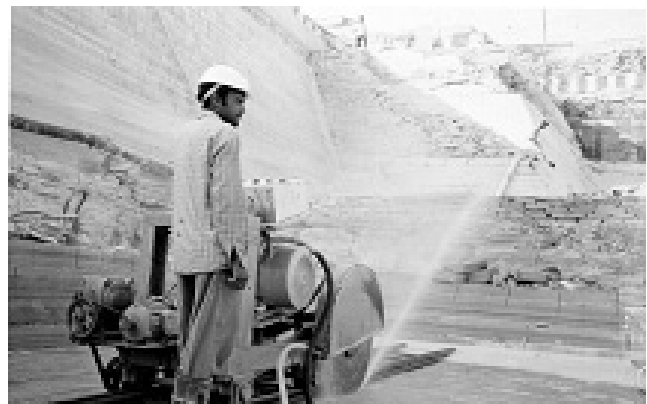


Fig. 2: Innovative Mining of Kotah Stone



Social Impact of Responsible Mining with Best Practice

The innovative mining technique proved to be responsible and the best mining practice till today. It is always expected that best mining practice be responsible to society and remove their miseries, upgrade their living standard and provide a clean, green, safe and peaceful environment.

After implementation of best practice of Kotah Stone mining productivity increased four times to 120 sqft/man shift and mineral recovery doubled to 90% resulting in increased earning of workmen.

Community and Stakeholders Engagement

The main stakeholders include local habitants, owners of land falling in lease area, village panchayat, local administration and state administration responsible for village development, providing basic amenities and mine operator. It was very essential to take all stakeholders into confidences and meeting their expectations from mineral excavation. Their involvement is equally important for the success of mining project. As far as mine operators are concerned they are drawing benefits of this revolutionary technology to not just improve their profits but also bring down costs, increase efficiencies, improve safety standards at workplace and reduce waste.

Obtaining Community Support and Delivering Benefits

Community support can only be obtained by delivering them benefits through employment, medical care, children education, social security through PF, gratuity, skill development and rehabilitation of those displaced from mining area.

Kotah Stone mining work force constitutes more than 80% local habitants. An image showing the local inhabitants at work in Kotah Stone quarry is shown in Figure 3.

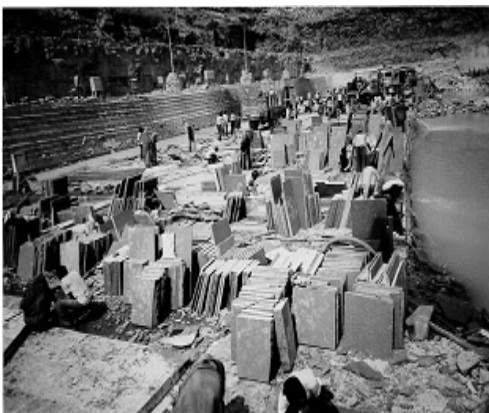


Fig. 3: Employment of Locals in Kotah Stone Quarry

They are all in all categories, unskilled, semi-skilled and partly skilled category. After the implementation of best mining practice, more skilled and highly skilled workers were required. Continuous and regular training of existing workers in training centre as well on job paid rich dividend. There has been dramatic change in skill development as is evident from following statistics:

Skill Development (Social benefit) from Best Practice:

	US.	SS.	S
Manual	56%	40%	4%
Innovative	28%	54%	18%

With the changing social attitude towards female child education, women participation in labour force has reduced to less than 20% from 40% prior to adopting responsible mining practices.

Impact on Environment and Responsibility

Regional environment in and around mining area does effect the society and its residents; may it be quality of water they drink, quality of air that they breath general hygiene that they live in, green, safe and peaceful environment.

Water Quality

The Kotah Stone quarries get filled up with rain water (Figure 4). This water, on lab test found to be potable and safe for drinking. However, for the purpose of drinking, the abandoned pits are fenced and secured from animals to avoid water pollution.

Active mining pits get polluted from cutting slurry and water is used for cooling cutting tools. Hence there is no pumping of such water for drinking.



Fig. 4: Quarries Filled Up with Rain Water

Water Quantity

This best practice in Kotah Stone mining has brought lot of relief to availability of water by deferring the de-watering of quarries from earlier 3 months to now 9 months. Water from quarries is now available even in peak summer for agriculture, washing, bathing and cleaning.



Air Quality

In any open pit mining operation generation of air particulates is unavoidable but with due precautions it can be regulated to harmless limits. Dust creates many respiratory problems specially if it is silicious. Silicosis is a dangerous respiratory disease, commonly prevalent in Indian sandstone mines. Although Kotah Stone contains high silica but fortunately it is intrinsically held and liberate only at-90 microns. No mining process in Kotah Stone grinds stone to such fine level.

After adopting best mining practice in Kotah Stone mining, generation of air particulates has been substantially reduced, collected, suppressed from being airborne at the source of generation. Wet cutting of Kotah Stone at quarry floor has suppressed dust totally. Dust during drilling has been reduced again due to wet drilling, proper care of equipment, drilling bits etc. Regular water spray on haul roads has taken care of dust due vehicular movement.

With increase in production, vehicular movement has also multiplied both in waste handling as well in production movement. Mandatory maintenance of vehicles, out dating 10 yrs vehicle from circuit, regulating carrying load to permitted capacity and maintaining safe gradient to avoid excessive throttling have been the measures adopted to minimise air pollution.

Greenhouse Gas Emissions

Initially, because poor quality and continuity of electric power from state grid at 440 Volt, the best practice for extraction of Kotah Stone started powering the cutting machines with diesel generator. Beside of continuously increasing fuel cost and theft it had added to greenhouse emission. To address these two major problems, environment and increasing cost, electric power supply from state grid at 33 V and stepped down at 440 V at place of use was planned and found best option. This system eliminated all air pollution at site beside reducing cost of power.

Mine Waste Management

Kotah Stone mines generated two types of waste, one solid waste from OB and waste at quarry floor during sizing of slabs and tile and slurry waste from in-situ cutting of Kotah Stone layers at quarry floor. The generation of production waste at quarry floor has reduced to one sixth after introducing best practice of mining. But for natural dip of deposit, the OB increased from 0 at out crop in 1945, 12 mtr in 1988, to as much as 60 mtr as of now. This waste consists of non-splittable thick layers of low-grade of limestone containing 34% CaO, 23% SiO₂ which could not be used in cement manufacturing.

After intensive R & D work in CSIR Labs, technology has been established to manufacture normal portland cement out of Kotah Stone quarry waste. The process involves first enriching low grade waste, through wet beneficiation, to a grade of CaO-44% and SiO₂-13%. The beneficiated material made a good raw-mix for clinkerisation.

On grinding the clinker 53 grade OPC cement has been obtained. The schematic of an integrated cement plant is shown in Figure 5.

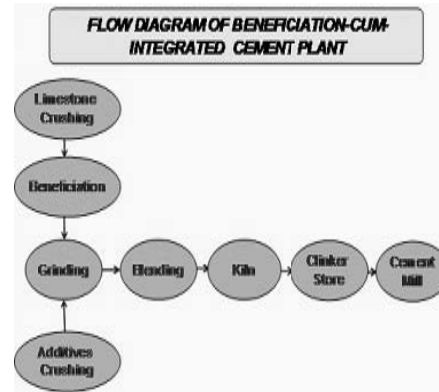


Fig. 5: Flow Diagram of Integrated Cement Plant

It is estimated that 2.5 MT of Kotah Stone quarry waste will be recycled to produce 1 MTPA Clinker. Kotah Stone deposit when completely exhausted will provide regular employment to these mine workers. It is well recognised that manufacturing can make disproportionate contribution in terms of job creation, innovation, and social prosperity. It will be true initiative towards “Make in India”.

Such plant based on recycling waste, will also reclaim waste land to ground level, useful for either agriculture or habitation. It is estimated that 1 MTPA clinker plant over 40 yrs life, will reclaim some 240 hectare land to original level.

As of now such waste dump at few places are capped with black cotton soil available from top layer of OB followed by dense plantation [Figures 6 & 7].



Fig. 6: Dumps with Soil Capping



Fig. 7: Dumps with Dense Plantation

Impact on Health and Safety Standards

Occupational health impacts related to the mining industry may include physical injuries; musculoskeletal disorders; noise-induced hearing loss; hand-arm vibration syndrome; skin cancer; dermatitis; heat exhaustion; hypothermia; eye disorders respiratory disorders; decreased mental health and well-being.

Now responsible mining practice provided a clean, green and cool working environment. This has definitely long-term effect on the health of mine worker and he rarely falls prey to such dreaded diseases. A healthy man is safe man, less prone to accident and highly productive.

It is the responsibility of employers to ensure that working environment is safe and healthy, and the duty of workers to take care of their own safety as well as the safety of anyone who might be affected by their actions. The most important risk related to Kotah Stone quarries include, fatal accidents physical injuries requiring treatment, work related diseases like hearing impairment due to long-term exposure to noise.

HIV/AIDS, Tuberculosis (TB) and Malaria-57

In past, due to low productivity, large employment and poor earning had been the main causes of non hygienic living condition in Kotah Stone mining area and diseases like HIV AIDS, TB, Malaria were not uncommon. Alcoholism and malnutrition had been main cause of these diseases.

It is because of increased productivity, migration of workers from adjoining states has zeroed down. Regular health check-up is now organised by mine operators. Malaria has been practically eradicated. Regular health awareness camps against HIV and AIDS are sponsored by mine operators and organised by State Government.

Pollution from Noise

Like other mining project, extraction of Kotah Stone and processing process generates noise of varying level and

nature. The development of innovated mechanised process and use of mechanical equipment have increased the noise problem both during extraction as well inprocessing. For last few decades, human concern about protection against noise environment has grown rapidly as it has been recognised that the rise in noise level beyond certain level can't be allowed indefinitely. Prolonged exposure of human being beyond acceptable limits leads to hearing loss and other adverse changes in physiological, psychological and behavioural consequences. In a detailed survey it has been observed that:

- Average level of noise level at and in surrounding of a pit with 6 diamond Cutter = 76.2 dB(A)
- Average level of noise at drilling site varies from 92.4 dB to 79.5 dB(A) as per different activities.
- Average level of noise at loading level by 35 T dumpers and hydraulic excavator varies between 90.1 to 93.4 dB(A).
- Average level of noise during operation of hydraulic excavator. Varies between 72.7 to 90.6 dB(A) as per different activities.
- Average level of noise during dozer operation is of the order of 101 dB(A).
- Average level of noise during operation of generator varied from 97.9 dB in side and 78.4 dB outside of generator room.
- At the processing level, average noise level varied from 92.7 to 107.9 dB(A).

From the above observations it is evident that noise level at all levels is higher than permissible norms of 90 dB(A) at work place both in mines and the processing plants.

Noise Control Measures

Provision and use of earplugs and ear head sets by workman made mandatory at workplace both at mine and processing plant level. Regular check up of bearings and other maintenance of machinery was made regular feature.

Safety

The responsible innovated mining technology proved to be clean, much safer, environment-friendly. This process has eliminated many hazardous manual process resulting sharp reduction in accidents, human fatigue and stress, as summarised below:

- The frequency of accidents and number of persons injured annually has reduced to one sixth.
- Man days lost per lac sq ft of production has reduced from 36.6 to as low as 13 only.
- Man days lost per lac man days employed has reduced from 1150 to 900 by adopting appropriate technology.



- Man days lost per accident with conventional mining varied from 15.8 to 20.5 but with mechanised system it has otherwise increased to 27.3 to 35.5. It is because with use of machines, severity of injury has increased. This calls for improving the skill of operators and general training on machines is organised regularly.

Improved Welfare Condition

The responsible innovated mining technology proved to be blessing for mine workers and their family in multiplying their earnings because of increased productivity. Prosperity keeps the worker and his family happy. A happy worker is a safe worker, undoubtedly.

Child Labour and Bonded Labour

With conventional manual mining employment was very large and earning was low. Worker had to bargain for heavy advances at employment time and during the employment also which many a times he was unable to pay off. This led to processing bonding conditions.

However after implementing best practice of quarrying Kotah Stone, the earnings multiplied three times which is sufficient to fulfil his all personal/social needs. Yet for additional need he draws advance from his PF a/c rather than begging from employer/contractor.

Conclusion

Invariably mining adversely effect the social and environmental issues that can be avoided if companies operate according to best and responsible practice standards.

The goal of responsible mining should be to maximise the contribution to the Social well-being of the current generation in a way that ensures an equitable distribution of its costs and benefits, without reducing the potential for future generations to meet their own.

It is very essential to involve and take all stakeholders into confidences and meeting their expectations from mineral excavation and obtain community support through employment, medical care, children education, social security, skill development and rehabilitation of those displaced from mining area.

To address social economic and environmental issues arising from manual mining of Kotah Stone, an innovative mining technique was evolved which proved to be best and responsible mining practice till today to achieve agreed goals, given the current state of knowledge.

It was in true spirit what Guru Madhwan said that responsible engineering in Kotah Stone mining has dramatically enhanced living standards, boosted economies of rural area and serve the society”.

Kotah Stone mine operators are drawing benefits of this revolutionary technology to not just improve their profits but also bring down costs, increase efficiencies, improve safety standards at workplace and reduce waste.

What “Walter Isaacson” had said it was Engineering challenge for turning problems into opportunities.

“Gordon England”, former US Secretary Navy and Defence rightly said: It is understanding how and why the engineering mindset is supremely important for everything from technology to human progress.



Initiatives for Mine Reclamation in Central Coalfields Limited to Save Environment

Rajeev Singh¹ and Alok Kumar Singh²

Abstract: In national economy, coal will remain the prime energy resource. It will continue to contribute significantly towards fulfilling the need of power required for growth of nation. Central Coalfields Limited (CCL) is committed to achieve the production targets. CCL is well aware of the effects of mining on the environment. Mines are site specific and for mining coal, land is the most important resource. CCL is committed to ensure restoration of environment and eco-system, ecological balance disturbed due to mining activities. Mines are being monitored for land reclamation by Remote Sensing techniques. Mine Closure Plans are also important feature in planning and working of the mines.

Keywords: CIL, CCL, Coal, Mine, Reclamation.

Introduction

Coal is the prime energy resource and has a key role in the growing economy of India. The economic development of any country largely depends upon its industrial progress. A set of nation-building initiatives has been taken by the Government of India to transform India into a global design and manufacturing hub and because of these initiatives, growth rate of the nation has stabilized. The World Bank in June, 2016 retained a growth rate of 7.6% for India in 2016–17, which it said could accelerate to 7.7% in 2017–18 and 7.8% in 2018–19. To achieve this, there is huge demand for power in India. Power is essential and most important factor for industrial and business set up.

The overall power generation in the country has increased during 2015–16 compared to 2014–15 at an overall growth rate of 5.64% and a growth rate of 7.46% has been recorded in thermal category. Coal is the backbone of power generation in India. The current per capita commercial primary energy consumption in India is about 535 kgoe/year, which is well below that of developed countries. Driven by the rising population, expanding economy and a quest for improved quality of life, energy usage in India is expected to rise. Demand for coal will go up every year with the growth and development of our industries.

Coal India Limited (CIL) is the largest coal producing company in the world and Central Coalfields Limited (CCL) is its fastest growing subsidiary. India has set an ambitious target of 1 billion tonnes coal production by Coal India

Limited by FY 2020 and will need huge investments in coal mining and its allied sectors like power, steel, cement, infrastructure for logistics, and coal washeries for achieving this goal. CCL has recorded an increase of coal production from 47.08 MT in FY 2010 to 61.32 MT in FY 2016. The ambitious target assigned to CCL for extraction of coal in FY 2020 is 133.5 MT. The Coal India Limited subsidiary has commissioned six Greenfield Projects in last three years (2013–14 to 2015–16) with the combined capacity of 40 MT which will be expanded to 100 MT.

To ensure that the growth of nation does not suffer for want of availability of coal, CCL has to grow from 61.32 MT to 133.5 MT in a short span of four years. Under present leadership, CCL is confident to cope up with tremendous pressure successfully and achieve the target.

Impact of Coal Mining Upon Environment

In the context of the non-diminishing influence of coal, CCL is committed to save and preserve environment and also to ensure restoration of environment and ecological balance disturbed due to mining activities. The mining industry has degraded the environmental parameters during the mining operations which sometimes persist for several years even after the stoppage of work in the mines. CCL is well aware of the effects of opencast mining on environment. Hence, it gives due importance to pollution control, reclaiming land and maintaining ecological balance. The company has given this mission high priority. The vision of Company includes

¹ Chief Manager (Mining), Contract Management Cell, Central Coalfields Limited, Ranchi, India. ✉ rsingh4.mining@centralcoalfields.in

² Senior Manager (Mining), CMD Secretariat, Central Coalfields Limited, Ranchi, India. ✉ aksingh007@gmail.com



attaining environmentally and socially sustainable growth in an eco-friendly manner. Environmental sustainability programmes are important to control and mitigate the negative impacts on environment.

Nowadays, environmental concerns are addressed before the actual mining starts at the planning stage itself. An environmental management plan is prepared for the mine which is approved by Ministry of Environment, Forest and Climate Change, Government of India, if lease area of mine is more than 150 ha, otherwise by State Level Environment Impact Assessment Authority (SEIAA). The mine starts construction and operational activities only after getting environmental clearance and consent from regulatory authorities. The conditions specified in the clearance are to be complied with and are regularly monitored by the regulators. The conditions are elaborate and specify many aspects showing concern for environment.

In the letter of environmental clearance of Ashoka Opencast Expansion Coal Mine Project (6.5 MTPA to 10 MTPA), the following specific conditions have been given:

Quote

Clause A. (iii) Topsoil should be stacked properly with proper slope at earmarked site(s) and should not be kept active and shall be used for reclamation and development of green belt.

(iv) OB should be stacked at earmarked one external OB dump site within ML area and shall be a maximum height of 60m only and consist of three benches of 20 m each.

(vii) Mineral transportation from mine to CHP from CHP to railway siding by road. The road shall be metal topped. Green belt shall be developed on both sides of the road.

(xi) The total area that shall be brought under afforestation at the time of mine closure shall not be less than 918.076 ha which includes reclaimed external OB dump and backfilled area (516.63 ha), along with ML boundary, safety zone (5.043 ha) and undisturbed area, along roads and infrastructure, green belt (401.44 ha) and in township outside the lease by planting native species in consultation with the local DFO/Agricultural Department. The density of the trees should be around 2500 plants per ha.

Unquote

In CCL, the mines have increasingly been developed into highly mechanized, opencast mines. Land is the most important natural resource, which embodies soil, water, flora, fauna and total eco system. All human activities are based on land. In view of the quantum of coal to be produced by CCL, there is huge involvement of land. Large patches of

land are being used by CCL with efforts being made for minimal degradation of environment. The purpose of this paper is to highlight the work done by CCL to save environment and to reclaim the land degraded during mining activities.

Reclamation of Land

In CCL, steps are being taken to mitigate the negative impacts of coal mining by land reclamation and biodiversity conservation. Reclamation of land is done in steps- back-filling, technical reclamation and biological reclamation. Purpose of reclamation of land is to restore it to an acceptable form and to make it usable and productive for agricultural or forestry purposes, etc. In mines, overburden, including top soil, is removed and dumped at pre-assigned places, both Inpit as well as at external places. With mega projects coming up, the quantum of overburden is increasing. CCL is particular about management of overburden dumping.

Large quantities of ash are generated by thermal power stations. Mines in B & K area and Rajrappa Area have accommodated fly ash generated by M/s DVC & M/s. Hindalco, Muri respectively. Further, bottom ash is being utilized for the purpose of hydraulic stowing in different underground mines of Kathara area.

Technical reclamation involves back filling of excavated area with over burden in systematic manner. In some of the mines the overburden removed for extraction of coal is completely backfilled in the decoaled area and suitably reclaimed. Top soil is spread over reclaimed land. The technically reclaimed ground is further reclaimed biologically and the area converted into a mixed species forest. In the area under reclamation, improvement in the moisture content, pH and overall nutrient contents of soil has been observed. The topsoil is an important ingredient of the overburden, as most of the biological activity takes place here. It is given due importance during its removal and during its conservation and reuse. Tree plantation helps in preserving the environment and is very crucial in the process of biological reclamation of land. The total plantation done in CCL since 1992 is more than 75 lakhs, covering about 4740 ha in all the mining areas of CCL. Afforestation of 3.25 acres is done for every 1 acre of forest land used for mining.

The success in land reclamation of mines spoils and afforestation has been very significant in mines like Ashok, Piparwar, etc. The mined out areas or the de-coaled area is refilled with overburden at places where no mining is required in future. OB fills and dumps are not very conducive to growth of plants, since these sites do not contain adequate plant nutrients. Top soil is kept separately for spreading over backfilled area.



During last ten years the plantation done is more than 37 lakhs indicating improvement in bio-diversity and environment. It has also helped in sequestration of carbon in terrestrial eco system. Bio-reclamation of degraded mined areas has been done of more than 4680 ha (since 1992) of different types of land. An Eco park has been developed at Piparwar OCP over reclaimed land. Such parks will be developed gradually in other areas also.

Monitoring of Reclamation

The quality and extent of reclamation is corroborated by the satellite imagery of the area, monitored by CMPDI through remote sensing on a regular basis. The large producing mines are being monitored for land reclamation by Remote Sensing techniques through CMPDI on annual basis. Objective of the land restoration/reclamation monitoring is to assess the area of backfilled, plantation, social forestry, active mining area, water bodies and distribution of wasteland, agricultural land and forest in the leasehold area of the project. This will help in assessing the progressive status of mined land reclamation and to take up remedial measures, if any, required for environmental protection.

Land reclamation monitoring of all opencast coal mining projects also comply the statutory requirements of Ministry of Environment and Forest. Such monitoring not only facilitate in taking timely mitigation neasures against environmental degradation, but also enable CCL to utilize the reclaimed land for larger socio-economic benefits in a planned way. Five large open cast projects of CCL-Ashok OCP, Piparwar OCP, KDH OCP, Parej East OCP and Rajrappa OCP are monitored every year.

Projectwise Land Reclamation Status in Opencast Projects of CCL based on Satellite Data of the year 2015

% Calculated in terms of Total Excavated Area

(Area in Km²)

Sl. No.	Project Name	Leasehold		Biological Reclamation (Plantation)		Technical Reclamation (Under Backfilling)		Area under Active Mining		Total Excavated Area		Total Area under Reclamation	
		i		ii		iii		iv		ii+iii+iv		ii+iii	
		2014	2015	2014	2015	2014	2015	2014	2015	2014	2015	2014	2015
1.	Piparwar	11.20	11.20	4.97 62.59	4.71 61.25	1.05 13.22	1.22 15.86	1.92 24.18	1.76 22.89	7.94	7.69	6.02 75.82	5.93 77.11
2.	Rajrappa	19.82	19.82	7.30 70.67	6.89 67.81	1.88 18.20	2.17 21.36	1.15 11.13	1.10 10.83	10.33	10.16	9.18 88.87	9.06 89.17
3.	Ashok	6.75	6.75	1.30 41.14	1.30 36.21	0.96 30.38	1.23 34.26	0.90 28.48	1.06 29.53	3.16	3.59	2.26 71.52	2.53 70.47
4.	KDH	4.50	4.50	1.47 44.68	1.47 42.36	1.26 38.30	1.49 42.94	0.56 17.02	0.51 14.70	3.29	3.47	2.73 82.98	2.96 85.30
5.	Parej East	6.20	6.20	0.66 34.92	0.70 36.46	0.85 44.97	0.89 46.35	0.38 20.11	0.33 17.19	1.89	1.92	1.51 79.89	1.59 82.81
	Total	48.47	48.47	15.70 59.00	15.07 56.17	6.00 22.55	7.00 26.09	4.91 18.45	4.76 17.74	26.61	26.83	21.70 81.55	22.07 82.26



Migratory Birds in the Reclaimed Voids



Projectwise Land Reclamation Status in Opencast Projects of CCL based on Satellite Data of the year 2015

% Calculated in terms of Total Excavated Area

(Area in ha)

Sl. No.	Project Name	Leasehold		Biological Reclamation (Plantation)		Technical Reclamation (Under Backfilling)		Area under Active Mining		Total Excavated Area		Total Area under Reclamation	
		i		ii		iii		iv		ii+iii+iv		ii+iii	
		2012	2015	2012	2015	2012	2015	2012	2015	2012	2015	2012	2015
1.	Tetariakhar	205	205.59	3.46 12.31	1.46 2.21	3.4 12.10	36.29 55.02	21.25 75.60	28.21 42.77	28.11	65.96	6.86 24.40	37.75 57.23
2.	Dakra	252.52	252.52	44.82 37.79	38.71 27.77	47.05 39.67	82.79 59.39	26.74 22.54	17.91 12.85	118.61	139.41	91.87 77.46	121.5 87.15
3.	Magadh*	1571	1704	0 0.00	0 0.00	0 0.00	20.35 54.53	0 0.00	16.97 45.47	0.00	37.32	0 0.00	20.35 54.53
4.	Amrapali*	1520	1300	0 0.00	0 0.00	0 0.00	59.3 33.10	0 0.00	119.86 66.90	0.00	179.16	0 0.00	59.3 33.10
5.	Giddi - A*	494	494.2	103.04 35.21	122.43 39.27	106.4 36.36	106.51 34.16	83.22 28.44	82.83 26.57	292.66	311.77	209.44 71.56	228.94 73.43
6.	Pundi*	852	1357.2	35.24 26.68	38.24 27.97	53.28 40.35	57.55 42.09	43.54 32.97	40.94 29.94	132.06	136.73	88.52 67.03	95.79 70.06
7.	Kedla*	901	1157.43	11.37 5.35	28.51 13.10	127.75 60.08	145.3 66.78	73.51 34.57	43.77 20.12	212.63	217.58	139.12 65.43	173.81 79.88
8.	Jarangdih*	494.52	179.05	184.57 73.01	27.19 30.04	34.85 13.79	38.02 42.01	33.38 13.20	25.30 27.95	252.80	90.51	219.42 86.80	65.21 72.05
9.	Kathara*	792.81	792.52	198.08 42.90	228.88 45.16	135.82 29.41	183.39 36.18	127.86 27.69	94.58 18.66	461.76	506.85	333.90 72.31	412.27 81.34
10.	Konar*	308.69	729.40	0.00 0.00	51.27 38.41	0.00 0.00	20.62 15.45	0.00 0.00	61.58 46.14	0.00	133.47	0.00 0.00	71.89 53.86
11.	Karo*	1204.00	575.00	64.40 48.36	42.08 29.94	30.77 23.11	56.38 40.11	38.00 28.53	42.10 29.95	133.17	140.56	95.17 71.47	98.46 70.05
12.	Karma*	298.96	298.96	6.85 12.89	10.57 19.33	27.86 52.43	20.55 37.59	18.43 34.68	23.55 43.08	53.14	54.67	34.71 65.32	31.12 56.92
	Total	8894.50	9045.87	651.83 38.69	589.34 29.26	567.18 33.66	827.05 41.07	465.93 27.65	597.60 29.67	1684.94	2013.99	1219.01 72.35	1416.39 70.33

* Leasehold is modified in 2015 w.r.t. 2012.



In addition the following projects were monitored once in every three years. New Gidi 'C' OC, Religara OC, Sirka OC, Giddi-A OC, Bhurkunda OC/Sangam OC, Urimari Expn. OC, North Urimari OC, Konar OC, Kargali OC, Bokaro OC, Khasmahal OC, Karo OC, Selected Dhorri OC, Tarmi OC, Amlo OC, Dhorri OC, Pichri OC, Jharkhand OC, Tapin OC, Kedla OC, Govindpur Ph-II OC, Jarangdih OC, Kathara OC, Topa RO OC, Karma OC, Ara OC, Pundi OC, Pindra OC, Saruber/Chainpur OC, Magadh OC, Amarapali OC, Rohini OC, Purnadih OC, Dakra OC, Tetariakhar OC.

Out of the total mine leasehold area of 48.47 km² of the five opencast projects viz. Ashok, Piparwar, KD Hesalong, Parej East and Rajrappa considered for monitoring during year 2015–16; total excavated area is only 26.83 km² (55.35% of lease area) of which 15.07 km² area (56.17%) has been planted, 7.00 km² area (26.09%) has come under backfilling and 4.76 km² area (17.74%) is under active mining. It is seen from the analysis that 82.26% area of these opencast projects have come under reclamation and balance 17.74% area is under active mining. Area of biological reclamation (plantation) has reached 15.07 km² as a result of measures taken by CCL, towards environmental protection.

Eco-restoration at Sangam OCP of Barka Sayal Area: An experimental project to scientifically reclaim old mined out areas using grass, bamboo and other species has been under taken in association with Dr C.R. Babu, member EAV, MoEF.



A Memorandum of Understanding (MoU) has been recently signed between Coal India Limited (CIL) and Indian Council of Forestry Research and Education (ICFRE) for effectively monitoring of environment related issues in the coal mining projects.

Mine Closure

Mine closure planning is required to restore the disturbed area after extraction of planned quantity of coal, to the

acceptable level of local community and regulatory authority. Mining activities leave long lasting impacts on the landscape, ecology and on local inhabitants. These activities disturb the delicate environmental and social equilibrium that exists in its area of influence. Hence, it becomes imperative on part of the mine operator to restore the equilibrium in the mine affected area that existed in the pre-mining period. Thus, any mining venture must have adequate closure plan, aimed at rehabilitation of disturbed area, which should be acceptable to local community as well as regulatory authority.

Mine closure encompasses rehabilitation process designed to restore physical, chemical and biological quality disturbed by the mining activities. Mine closure is not just something that happens at the end of a mine's life rather mine closure is an ongoing series of decisions and activities beginning in the pre-mining stage of mine and ending with a sustainable site that can be returned to the community.

Thus, a Mine Closure Plan needs to define the responsibilities of the different agencies like the mine management, other regulatory bodies, Central and State Governments after mine closure.

When the environmental clearance is granted, detail deliberation of mine closure plan is made therein. It mentions both Progressive Mine Closure Plan and Final Mine Closure Plan. Progressive Mine Closure Plan includes various land use activities to be done continuously and sequentially during the entire period of the mining operations. The Final Mine Closure Plan would start towards the end of mine life and may continue even after the reserves are exhausted and/or mining is discontinued till the mining area is restored to an acceptable level to create a self sustained ecosystem. In all the areas of CCL, steps are taken to comply with all the directives given in the environmental clearance.

In the letter dated 27.10.2008, vide which environmental clearance was accorded to Magadh Opencast Expansion Project (12 MTPA to 20 MTPA), mention has been made of Progressive Mine Closure Plan and Final Mine Closure Plan. The letter states,

Quote

"2. A. (xii) A Progressive Mine Closure Plan shall be implemented by reclamation of 558 ha of quarry area by backfilling and afforestation by planting native plant species in consultation with the local DFO/Agricultural Department. The density of the trees shall be around 2500 plants per ha. Quarry area of 268 ha which is too steep for backfilling shall be bio-reclaimed by plantation using geotextile material in critical patches. About 320 ha of decoaled area/void which is being converted into a water reservoir shall be gently sloped



and the upper benches of the reservoir shall be terraced and stabilized with plantation.”

(xx) A Final Mine Closure Plan alongwith details of Corpus Fund shall be submitted to the Ministry of Environment & Forests 5 years in advance of final mine closure for approval.”

Unquote

The details are self evident. The closure of mines evolves environmental, technical, social aspect and financial assurance for implementing the post closure activities as per guidelines of Ministry of Coal.

Accumulated water in abandoned mines is to be used for supply of drinking water to neighbouring villages. CCL intends to sign an MoU with State Government to achieve the common goal of providing water from suitable mines for use by villagers for their various needs. About 25 Billion Gallon of water is available in 88 number of mine voids in CCL. Accumulated water in abandoned mines is beneficial to the nearby land and recharges water level. It also prevents illegal mining in the area. The underlying coal seams in the area can be taken in future after dewatering of the abandoned mine.

Conclusion

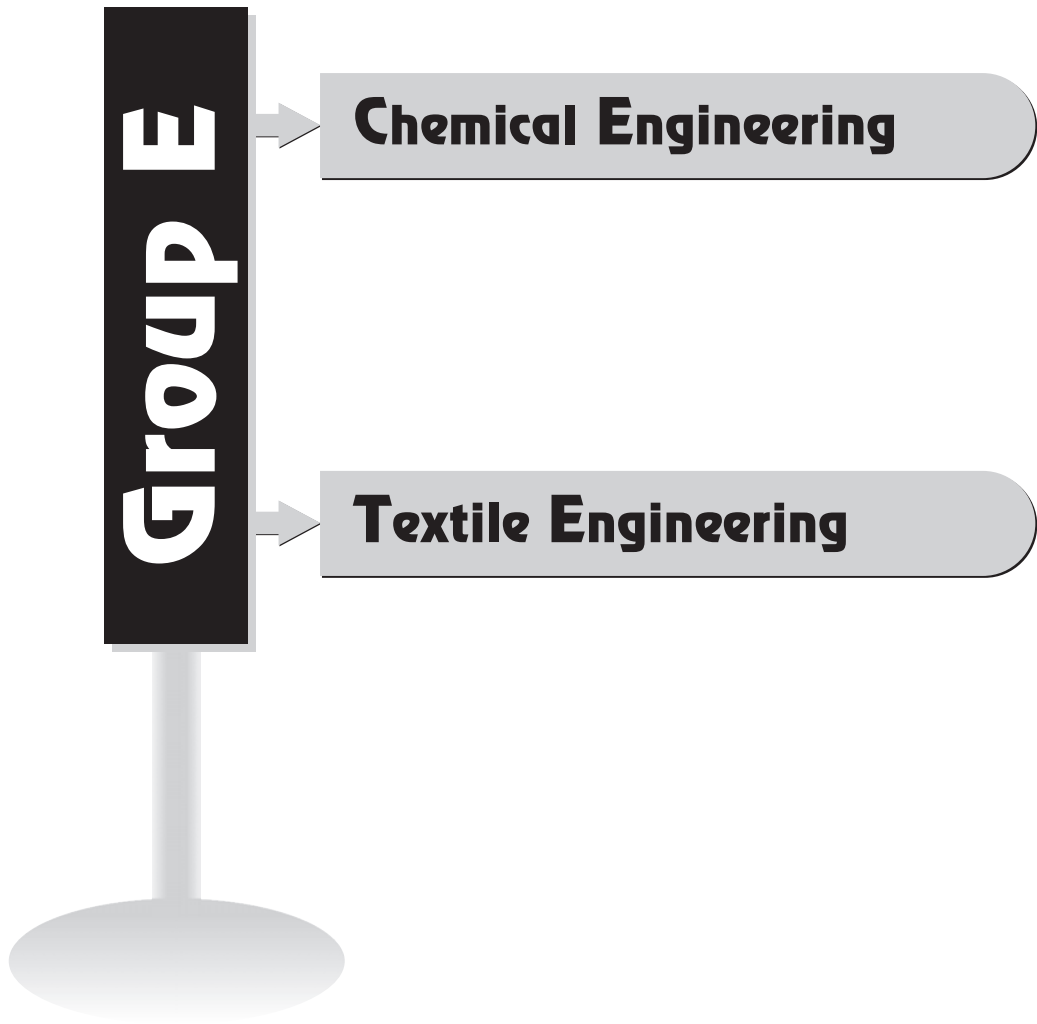
Mine reclamation and restoration is now an integral part of coal mining. All opencast must deploy state of the art technology, like surface miners, tube conveyors, silo loading, rail transport for reducing pollution. The railway sidings should be within the leasehold of the mines as has been planned in CCL.

CCL is going for “Green Energy Hub” comprising mine, washeries, and reject based power plants. Eco-parks have been planned. Transfer of coal over large distances should be discouraged by setting up Pit Head Power Plants. It is better to transfer “Coal by Wire” than by Rail.

The present work is expected to signpost a way toward the efforts put in by CCL in the implementation of state-of-the-art mine reclamation strategy, using satellite imagery and other means.

References

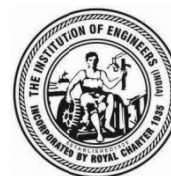
- [1] Annual Report 2015–16 of Central Coalfields Limited.
- [2] Land Restoration/Reclamation Monitoring of more than 5 million cum. (Coal + OB) Capacity Opencast Coal Mines Based on Satellite Data of the Year 2015–CMPDIL.
- [3] Land Restoration/Reclamation Monitoring of less than 5 million cum. (Coal + OB) Capacity Opencast Coal Mines Based on Satellite Data of the Year 2015–CMPDIL.



Group E

Chemical Engineering

Textile Engineering



Transesterification of Mixture of Edible and Non-Edible Vegetable Oils using Heterogeneous Catalyst Developed from Marble Slurry

Jharna Gupta¹, Madhu Agarwal*¹ and A.K. Dalai²

Abstract: In the present study, production of biodiesel from mixture of edible and non-edible oils using Hydroxyapatite (HAp) catalyst derived from Marble Slurry (MS) was investigated. The combination of oils has been optimized to get suitable mixture for production of biodiesel. The developed catalysts were characterized with X-Ray Diffraction (XRD) and Fourier Transform Infrared Spectroscopy (FTIR). Experimental result showed that biodiesel yield has been increased from 91% to 94% with reaction parameters such as reaction temperature 65°C, reaction time 3 hr, methanol to oil molar ratio 12:1 and catalyst concentration 4wt%. The solid base catalyst from marble slurry i.e. HAp exhibits excellent catalytic activity and stability for the transesterification reaction, which suggested that this catalyst could be potentially used as a solid base catalyst for biodiesel production from mixture of edible and non-edible oils.

Keywords: Biodiesel, Mixture of Oils, Marble Slurry, Transesterification.

Introduction

Renewable energy sources have become more attractive recently due to its environmental benefits, high energy demands and the high cost of crude oil [1]. In this regard, biodiesel can be an alternative fuel source for energy production. The main advantages of biodiesel as an alternative fuel are its renewability, biodegradability, nontoxic nature, and blending capacity with other energy sources [2]. Biodiesel is also known as Fatty Acid Methyl Ester (FAME) obtained by the transesterification reaction of methanol and vegetable oil in the presence of catalyst [3]. Transesterification reaction can be catalyzed by homogeneous and heterogeneous catalyst. Commonly used homogeneous catalysts are NaOH, KOH and CH₃ONa which have high catalytic activity, but it is also difficult to separate, purify and reuse them after the reaction [4]. Till now various heterogeneous alkali catalysts such as Zeolite [5, 6], alkali earth metal oxides [7, 8], KF/γAl₂O₃ [9, 10] and sodium aluminate etc. [11] have been developed for biodiesel production. However at the present time, only few heterogeneous catalysts are being used in the industry due to high cost associated with catalyst synthesis.

The best way to reduce the cost of heterogeneous catalyst for biodiesel production is to use waste as catalytic materials. Various types of wastes have been investigated as catalyst

such as Marble Slurry [12] (MS), Dolomites [13] and waste shells such as waste egg shell [14, 15], oyster shell [16], and scallop shell [17], bivalve clam shells [18] and bones [19]. Among them, CaO is one of widely-used catalysts due to its highly availability in nature, low cost and high activity.

From survey it is found that higher amount of catalyst and a longer reaction time are necessary for high biodiesel yield in case of heterogeneous catalyst. So to solve these problems, highly active basic solid catalyst also has been investigated from these wastes such as snail shell [20] reported a yield of 87.28% after 5–8 hr reaction time using 2wt% catalyst, waste dolomite [21] reported 91.87% biodiesel yield after 3 hr reaction time by using 3wt% catalyst and waste marble¹² reported yield of 88% by 3wt% catalyst for 3 hr.

Among these wastes, MS is a natural calcium carbonate source found in several areas of world such as India USA, Belgium, France, Spain, Sweden, Italy, Egypt, Portugal, Brazil and Greece. In marble processing plant, during the cutting process 20–30% of the marble block turns into dust. This type of waste is often disposed near residential areas. Stocking of these wastes is impossible; hence marble wastes constitute an environmental Pollutant [22]. In India, Rajasthan State Pollution Control Board (RSPCB) proposed a project of two plants at Udaipur to recycle synthesis. It is also depends on different reaction parameters such as catalyst

¹ Department of Chemical Engineering, MNIT Jaipur, India. ✉* magarwal.chem@mmit.ac.in²

² Department of Chemical Engineering, University of Saskatchewan, Canada.



loading, methanol to oil ratio, temperature and time. So the biodiesel production by MS and its derivative i.e. HAp as catalyst with different reaction parameters is of particular interest in our study.

In the present research work, we have investigated the use of Calcined Marble Slurry (CMS) and its derivative i.e. Hydroxyapatite (HAp) as heterogeneous base catalyst. This developed catalyst was used for biodiesel production. Fuel properties of biodiesel were compared with ASTM D6751 specifications.

Experimental Section

Materials

Natural MS was obtained from Jaipur, Rajasthan, India. Mixture of oil was purchased from the local market. Anhydrous methanol of analytical grade, and Potassium dihydrogen orthophosphate [KH_2PO_4] from Merck limited, Mumbai India was used in this study.

Characterization of Oil

The quality of oil is expressed in terms of the physicochemical properties such as density, acid value, kinematic viscosity, saponification value and flash point, fire point etc. These properties of oil (without further treatment) were determined as per ASTM D6751 Standard which has shown in Table 1.

Table 1: Properties of Mixture of Oils

Properties	Measured Value
Color	Burnt brown
Acid value (mg of KOH/gm of oil)	15.68
FFA (%)	7.84
Density (gm/ml)	0.85
Kinematic viscosity at 40°C (Cst)	33.0
Saponification value (mg of KOH/gm of oil)	196.3
Molecular weight (gm/mol)	931.6
Ester value (mg of KOH/gm of oil)	180.7
% glycerin	9.9

Catalyst Preparation

The MS sample was collected from marble shop of Jaipur, Rajasthan. MS was washed with deionized water three to four times for removing dust and impurities, and then dried at 120°C for 10 h. After drying, MS was calcined at temperature of 800°C for 3 hr in muffle furnace. The Calcined material was then cooled down to room temperature in a desiccator and then used as heterogeneous base catalyst for biodiesel production.

The synthesized basic heterogeneous catalyst form MS powder i.e. HAp was prepared by wet method. Twenty grams of dried MS powder was mixed in 800 ml of 1 M Potassium dihydrogen orthophosphate [KH_2PO_4]. The solution in the Pyrex glass was heated by microwave for 20 minutes. These processes result in HAp powder. HAp powder was cleaned with distilled water and was dried by microwave for 15 minutes followed by 5 h calcination at 850°C. Untreated MS and resulted catalyst into powder form as shown in Figure 1.

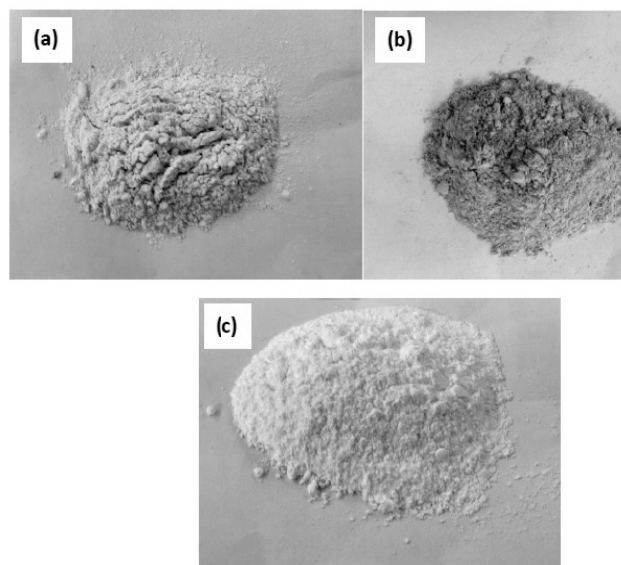


Fig. 1: (a) Marble Slurry (MS) (b) Calcined Marble Slurry (CMS) (c) Hydroxyapatite (HAp)

Catalyst Characterization

In order to determine the crystalline nature of calcined marble slurry and HAp, X-Ray Diffraction (XRD) patterns for each catalyst samples were analyzed using XRD (X-Pert pro powder analytical instrument). The FTIR spectra were recorded on FTIR spectrometer (Perkin Elmer spectra two) in the range of 400–4000 cm^{-1} . The KBr pellet method was used for the sample preparation.

Transesterification Reaction Procedure

The transesterification reaction was carried out using MS derived heterogeneous catalyst. The 100 ml of oil mixture was preheated and added into the flask containing methanol to oil molar ratio (1:12 mol) and catalyst concentration (4wt%) under vigorous stirring. The transesterification reaction was carried out at constant temperature of 65°C with a reaction time (3 hours). After the reaction, the reaction mixture was allowed to cool down and transferred to the separating funnel for separation of phases as shown in Figure 2. The solid base catalyst was removed from the



reaction mixture via centrifugation at 5000 rpm for 20 min. Glycerol was then separated using a separating funnel, and the excessive amount of methanol from FAME was evaporated under reduced pressure in a rotary evaporator. Then FAME was stored for characterization use.

The percentage of biodiesel yield was defined as follows:

$$\text{Biodiesel yield (\%)} = \frac{(\text{volume of biodiesel (ml)})}{(\text{volume of oil (ml)})} \times 100 \quad \dots (1)$$

Result and Discussion

Catalyst Characterization

XRD Analysis

To investigate the structure and crystallinity of the catalyst, the X-Ray. Diffraction analysis was done as shown in Figure 2. Figure 2 shows the XRD result of MS, CMS and HAp powder. The crystalline of all the samples were probed by XRD. In Figure 2(a), the parent material showed major diffraction peaks at 29.38°, 30.92° and 41.06° which is characteristic of CaCO₃ MS and after calcination as shown in Figure 2(b), the reflection arising from MS were lost, coincident with the appearance of new crystalline phase that can be assigned to highly crystalline CaO (33.92°, 37.11°, and 42.65°) as described in literature [23, 24]. In Figure 2(c) XRD patterns of HAp shows the two highest peaks at 31.02° and 50.61° which is characteristics of HAp and closed to HAp standard compared with literature [25, 26]. These result indicated that the MS had been successfully synthesized into HAp. Analysis of these peaks at XRD patterns of HAp showed level of purity reaches 100%.

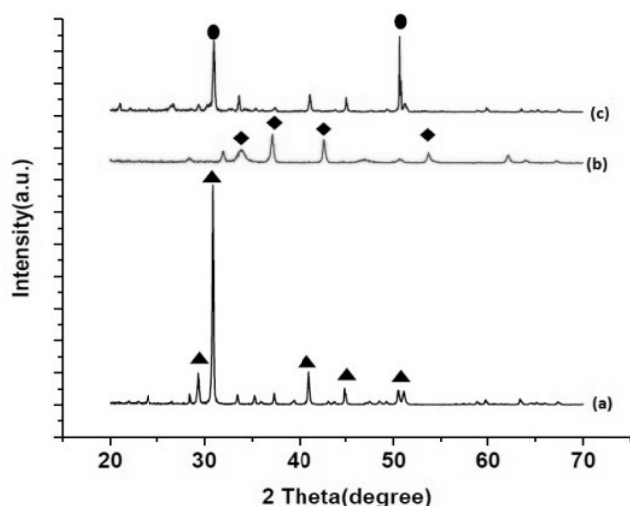


Fig. 2: XRD Curve for (a) Marble Slurry (MS) (b) Calcined Marble Slurry (CMS) (c) Hydroxyapatite (HAP) (Symbols: ▲=CaCO₃, ◆= CaO, ●=HAp)

FTIR Analysis

FTIR analysis of MS (uncalcined and calcined) and HAp powder was performed as shown in Figure 3. Two well defined infrared bands around 878 and 1435 cm⁻¹ are characteristic of the C-O stretching and bending modes of CaCO₃ as shown in Figure 3(a) [27]. The intensity of these bands decreases and alter during calcinations at 800°C due to thermal decomposition of CaCO₃ and formation of CaO and Ca(OH)₂. One sharp band appears 3642 cm⁻¹ due to the formation of basic OH groups attached to the calcium atoms as shown in Figure 3(b) [27]. Hydroxyl stretch is observed at 3643 cm⁻¹ in the spectra of HAp as shown in Figure 3(c). There were also bands at 103.04 cm⁻¹ and 1420 cm⁻¹, which were assigned to the phosphate group and the carbonate group (CO₃²⁻) [25, 26].

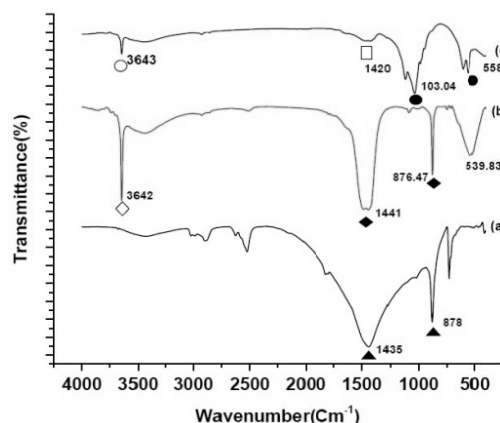


Fig. 3: FTIR Curve for (a) Marble slurry (MS) (b) Calcined Marble Slurry (CMS) (c) Hydroxyapatite (HAP) (Symbols: ▲= CaCO₃, ◆= CaO, ◇= Ca(OH)₂, ●= PO₄³⁻, □= CO₃²⁻, ○= OH⁻)

Biodiesel Characterization

Properties of Biodiesel produced from oil were analyzed. These properties of biodiesel were compared as per ASTM D6751 Standard²⁷ which has shown in Table 2.

Table 2: Properties of Biodiesel

Properties	Unit	Biodiesel from CMS	Biodiesel from HAp	ASTM Standard
Density	(gm/ml)	0.878	0.889	0.860–0.900
Kinematic viscosity	at 40°C (Cst)	4.982	5.721	1.9–6.0
Acid value	(mg of KOH/gm of oil)	0.43	0.49	0.50
Cloud point	°C	6	9	-3 to 12
Pour point	°C	-3	3	-15 to 10
Flash point	°C	160	155	130–170

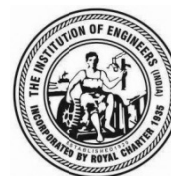


Conclusion

The calcined marble slurry and HAp used as a catalyst for biodiesel production from transesterification reaction by using mixture of oil. The prepared basic solid catalysts were characterized by XRD, FTIR, SEM and TGA. The characterization results show that the HAp catalyst exhibits stronger basicity than that of CMS. Among both catalysts tested, HAp shows high catalytic activity with good biodiesel yield i.e. above 94% in the biodiesel production from mixture of oil at the reaction conditions such as reaction time of 3h, methanol to oil molar ratio of 12:1, reaction temperature of 65°C and catalyst loading of 4wt%. The HAp catalyst from MS exhibits excellent catalytic activity and stability in the transesterification reaction.

References

- [1] Chouhan, A.P. Singh and Sarma, A.K. "Modern heterogeneous catalysts for biodiesel production: a comprehensive review." *Renewable and Sustainable Energy Reviews* 15.9 (2011): 4378–4399.
- [2] Jairam, Suguna, *et al.* "KI-impregnated oyster shell as a solid catalyst for soybean oil transesterification." *Bioresource technology* 104 (2012): 329–335.
- [3] Agarwal, Madhu, *et al.* "Study of catalytic behavior of KOH as homogeneous and heterogeneous catalyst for biodiesel production." *Journal of the Taiwan Institute of Chemical Engineers* 43.1 (2012): 89–94.
- [4] Jharna Gupta and Madhu Agarwal. "Biodiesel Production by Heterogeneous Catalyst: A Review." *ISST journal of Applied Chemistry* 6.1 (2015): 53–60.
- [5] Purova, Ralitsa, *et al.* "Pillared HMCM-36 zeolite catalyst for biodiesel production by esterification of palmitic acid." *Journal of Molecular Catalysis A: Chemical* 406 (2015): 159–167.
- [6] Volli, Vikranth and Purkait, M.K., "Selective preparation of zeolite X and A from flyash and its use as catalyst for biodiesel production." *Journal of hazardous materials*, 297 (2015): 101–111.
- [7] Lee, H.V. and Taufiq-Yap, Y.H., "Optimization study of binary metal oxides catalyzed transesterification system for biodiesel production." *Process Safety and Environmental Protection*, 94 (2015): 430–440.
- [8] Lee, H.V. and Taufiq-Yap, Y.H., "Optimization study of binary metal oxides catalyzed transesterification system for biodiesel production." *Process Safety and Environmental Protection*, 94 (2015): 430–440.
- [9] Gao, Lijing, *et al.* "Biodiesel production from palm oil over monolithic KF/ γ -Al₂O₃/honeycomb ceramic catalyst." *Applied Energy*, 146 (2015): 196–201.
- [10] Shahraki, Hassan, Entezari, Mohamad Hassan and Goharshadi, E.K. "Sono-synthesis of biodiesel from soybean oil by KF/ γ -Al₂O₃ as a nano-solid-basecatalyst." *Ultrasonics sonochemistry*, 23 (2015): 266–274.
- [11] Wan, Tao, *et al.* "Application of sodium aluminate as a heterogeneous base catalyst for biodiesel production from soybean oil." *Energy & Fuels*, 23.2 (2009): 1089–1092.
- [12] Balakrishnan, K., Olutoye, M.A. and Hameed, B.H. "Synthesis of methyl esters from waste cooking oil using construction waste material as solid base catalyst." *Bioresource technology*, 128 (2013): 788–791.
- [13] Correia, Leandro Marques, *et al.* "Characterization and application of dolomite as catalytic precursor for canola and sunflower oils for biodiesel production." *Chemical Engineering Journal*, 269 (2015): 35–43.
- [14] Niju, Subramaniapillai, Meera, K.M., Begum, S. and Anantharaman, Narayanan. "Modification of egg shell and its application in biodiesel production." *Journal of Saudi Chemical Society*, 18.5 (2014): 702–706.
- [15] Zeng, Danlin, *et al.* "Preparation and characterization of a strong solid base from waste eggshell for biodiesel production." *Journal of Environmental Chemical Engineering*, 3.1 (2015): 560–564.
- [16] Jairam, Suguna, *et al.* "KI-impregnated oyster shell as a solid catalyst for soybean oil transesterification." *Bioresource technology*, 104 (2012): 329–335.
- [17] Sirisomboonchai, Suchada, *et al.* "Biodiesel production from waste cooking oil using calcined scallop shell as catalyst." *Energy Conversion and Management*, 95 (2015): 242–247.
- [18] Niju, S., Meera, K.M., Begum, Sheriffa and Anantharaman, N. "Enhancement of biodiesel synthesis over highly active CaO derived from natural white bivalve clam shell." *Arabian Journal of Chemistry* (2014).
- [19] Farooq, Muhammad and Ramli, Anita, "Biodiesel production from low FFA waste cooking oil using heterogeneous catalyst derived from chicken bones." *Renewable Energy* 76 (2015): 362–368.
- [20] Birla, Ashish, *et al.* "Kinetics studies of synthesis of biodiesel from waste frying oil using a heterogeneous catalyst derived from snail shell." *Bioresource technology* 106 (2012): 95–100.
- [21] Ilgen, Oguzhan. "Dolomite as a heterogeneous catalyst for transesterification of canola oil." *Fuel Processing Technology* 92.3 (2011): 452–455.
- [22] Gencel, Osman, *et al.* "Properties of concrete paving blocks made with waste marble." *Journal of Cleaner Production*, 21.1 (2012): 62–70.
- [23] Zeng, Danlin, *et al.* "Preparation and characterization of a strong solid base from waste eggshell for biodiesel production." *Journal of Environmental Chemical Engineering*, 3.1 (2015): 560–564.
- [24] Wei, Ziku, Chunli Xu, and Baoxin Li. "Application of waste eggshell as low-cost solid catalyst for biodiesel production." *Bioresource technology*, 100.11 (2009): 2883–2885.
- [25] Chen, Guanyi, *et al.* "Biodiesel production from palm oil using active and stable K doped hydroxyapatite catalysts." *Energy Conversion and Management*, 98 (2015): 463–469.
- [26] Pujiyanto, Eko; Laksono, Pringgo Widyo and Triyono, Joko. "Synthesis and characterization of hydroxyapatite powder from natural gypsum rock." *Advanced Materials Research*, Vol. 893, 2014.
- [27] Suryaputra, Wijaya, *et al.* "Waste capiz (*Amusium cristatum*) shell as a new heterogeneous catalyst for biodiesel production." *Renewable energy*, 50 (2013): 795–799.



Physicochemical Studies of $\text{TiO}_2/\text{Fe}_2\text{O}_3/\text{ZnO}$ Heterostructure Assemblies for Electrochemical Water Splitting/Dye Degradation Applications

Dilip Kumar Behara^{*1}, M. Sudha Maheswari¹ and T. Jalajakshi¹

Abstract: Growing energy demands depends considerably on renewable and pollution-free energy sources, which seems to be essential ingredients for long-term socioeconomic stability. Semiconductor materials play an important role in extracting needful energy from existing renewable energy forms. Contemporary research focuses on the development of different semiconductor materials and their combination in a coagent manner such as “heterostructure assemblies” that utilizes the synergic interaction between materials combined. Since, the formed “heterojunction” between material interfaces will promote the interfacial charge carriers separation, transport events at molecular level, and thereby improve the kinetics and reaction rate compared to individual counter parts. Herein, we report heterostructure assembly of stable, non-toxic semiconductor materials: TiO_2 , Fe_2O_3 and ZnO for electrochemical water splitting and dye degradation applications. All the three materials chosen from either Type-I or Type-II heterostructure assembly with each other and facilitate the charge carrier movements from one material to other for better utilization of electric flux at the interfaces. Preliminary studies suggest that ternary heterostructure electrode $\text{TiO}_2/\text{ZnO}/\text{Fe}_2\text{O}_3/\text{Ti}$ shows better electrical activity towards electrochemical crystal violet dye degradation in comparison to binary heterostructure (TiO_2/ZnO , $\text{TiO}_2/\text{Fe}_2\text{O}_3$) and individual materials (TiO_2 , ZnO , Fe_2O_3) substantiating the importance of synchronized charge transport across material interfaces. The same electrode assembly is tested for electrochemical water splitting reaction and the work is under progress. The outcomes of present study will help to design more pronounced heterostructure assemblies for better performance towards electrochemical water splitting and other complex dye degradation studies.

Keywords: Heterostructure, Water Splitting, Crystal Violet Dye, Synchronized Charge Transport.

Introduction

The society is very much aware about the undesirable impacts of various industrial effluents on the environment. Since, a large quantity of dyes was produced as effluents from various textile industries which are highly toxic and carcinogenic to living organisms on earth. Therefore it is necessary to treat the effluents and make them toxic-free [1]. Textile effluents typically have strong colour due to unfixed stature (dyes) and therefore it is inevitable to remove these dyes before they let in to water bodies. There are various wastewater treatment techniques such as biological, chemical and physicochemical methods, etc. All these methods have certain constraints that cause insufficient effectiveness when applied individually. For example, (1) the chemical or physicochemical methods will often cause secondary pollution or require post-treatment, (2) biological approaches suffer with microbial inhibition problem leading to very low treatment efficiencies [2, 3].

Over the past 10 years, electrochemical techniques found to be substantial interest for wastewater remediation due to significant characteristics such as versatility, environmental compatibility and potential cost effectiveness in comparison to conventional methods. Further, electrochemical techniques offer promising approaches for the prevention of pollution problems in the process industry as they does not yield any sludge [4]. Additionally, electrochemical techniques are compatible with the environment owing to special features such as simple equipment, easy operation, and lower operating temperature. The applied potential in electrochemical approaches induces redox reactions upon the electrode surface resulting in the transformation and destruction of the dye molecules almost completely into CO_2 and H_2O [5]. Semiconductor nanostructure materials having superior physicochemical properties are being employed for potential applications in electrochemical research problems such as dye degradation, water splitting, etc. Although, several

¹Department of Chemical Engineering, Jawaharlal Nehru Technological University Anantapur (JNTUA), College of Engineering, Anantapur, India.
✉ dileepbh.chemengg@jntua.ac.in



semiconductor materials have significant potential in electrochemical applications but TiO_2 , ZnO are mostly preferred mostly due to its nontoxicity, water insolubility, hydrophilicity, cheap availability, and highly stable towards corrosion [6, 7]. Recently, Fe_2O_3 is chosen as an alternative material to TiO_2 and ZnO for dye degradation studies because it possesses superior characteristics such as high physical and chemical stability, nontoxicity, environmental compatibility, low cost, oxidative power, magnetic activity, resistance to corrosion [8]. Therefore, it is advantageous to combine Fe_2O_3 with TiO_2 , ZnO materials to extract the desirable properties. The formed heterostructure assembly will enhance the performance than individual counter parts due to synergistic interaction between material interphases [9].

Herein, we report synthesis and fabrication of $\text{TiO}_2/\text{ZnO}/\text{Fe}_2\text{O}_3$ composite heterostructure to enhance the performance of crystal violet dye degradation upon external electrochemical potential application. In order to capitalize the support interaction on catalyst assembly prepared, Titanium (Ti) substrate is chosen for fabrication, which is of reasonable cost and high conductivity [10]. The fabricated ternary electrode on Ti substrate ($\text{TiO}_2/\text{ZnO}/\text{Fe}_2\text{O}_3/\text{Ti}$) shows enhanced performance over other fabricated electrodes (TiO_2 , ZnO , TiO_2/ZnO , $\text{TiO}_2/\text{Fe}_2\text{O}_3$, and $\text{TiO}_2/\text{ZnO}/\text{Fe}_2\text{O}_3$) substantiating the importance of synchronized charge transport across material interfaces [11]. The experiments with fabricated electrode towards electrochemical water splitting are under progress. The outcomes of present study will help to design more pronounced heterostructure assemblies for better performance towards electrochemical water splitting and complex dye degradation studies.

Experimental Section

Materials and Methods

Zinc acetate di-hydrate [$\text{Zn}(\text{O}_2\text{CCH}_3)_2(\text{H}_2\text{O})_2$], Ethanol ($\text{C}_2\text{H}_5\text{OH}$), Triethanolamine ($\text{C}_6\text{H}_{15}\text{NO}_3$), Titanium isopropoxide [$\text{Ti}\{\text{OCH}(\text{CH}_3)_2\}_4$], Iron(III) nitrate nonahydrate ($\text{Fe}(\text{NO}_3)_3 \cdot 9\text{H}_2\text{O}$), Ammonia (NH_3), Sodium sulphate (Na_2SO_4), and Isopropyl alcohol ($\text{C}_3\text{H}_8\text{O}$) purchased from Sigma Aldrich Chemicals (India) Ltd. Nafion (10%) liquid solution is purchased Dupont Chemicals, USA. Crystal violet dye was purchased from Sigma-Aldrich is used as model dye in present study. All the reagents were analytically pure and used as received without further purification. The deionized water was used throughout the experiments.

Synthesis of TiO_2 Nanoparticles

9 ml of TTIP was added drop wise into a homogeneous mixture of ethanol (150 ml) and 3.75 ml of deionized water. The reaction mixture was kept under agitation for 4 h at 85°C under magnetic stirring. After that, the sample was dried at

60°C for 30 min and calcined in muffle furnace for 3 h at 400°C to yield the anatase TiO_2 phase [9, 11–13].

Synthesis of ZnO Nanoparticles

ZnO nanoparticles were prepared by sol-gel method. 30 ml of Triethanolamine (TEA), 20 ml deionized water were mixed and 2 ml of ethanol was added drop wise and stirred for 2–3 h. Then, 5.39 g of Zinc acetate di-hydrate was taken in 50 ml of deionized water and stirred for 20 min and 0.5 ml ethanol was added into the solution during stirring. Centrifugation followed by drying of particles was done at 95°C in hot air oven for 8h and finally calcined for 3 h at 900°C [14].

Synthesis of Fe_2O_3 Nanoparticles

Fe_2O_3 nanoparticles were prepared by sol-gel method. 4 g of $\text{Fe}(\text{NO}_3)_3 \cdot 9\text{H}_2\text{O}$ in 100 ml deionized water was stirred for 30 min. Also, 1.5g of gelatin was stirred in 100 ml deionized water for 30 min at 60°C . Now, gelatin solution was slowly added to iron nitrate solution and stirred for 1 h. The gel formed was dried for 6 h in hot air oven at 60°C and calcined for 1 h at 600°C [15].

Synthesis of TiO_2/ZnO Nanocomposite

TiO_2/ZnO nanocomposite was synthesized by sol-gel method. TTIP was taken in 1:1 ratio of isopropanol and water. Then, Zinc acetate was added in the ratio of Ti: Zn = 5:1 along with 0.5N of acetic acid. This mixture was stirred for overnight. Centrifugation followed by calcination at 400°C for 4 h yields composite nanoparticles [16].

Synthesis of $\text{TiO}_2/\text{ZnO}/\text{Fe}_2\text{O}_3$ Nanocomposite

The synthesis procedure of the composites was shown schematically in the Figure 1. 5.18 ml of TTIP, 1.52 g of ($\text{Fe}(\text{NO}_3)_3 \cdot 9\text{H}_2\text{O}$) were mixed with 60 ml of ethanol and stirred for 2 h. 10 mg of ZnO nanoparticles were added during stirring. After that, 36 ml of deionized water was added and stirring is continued for another 24 h. During stirring, the solution is maintained at a pH of 10 by adding 8 ml of ammonia. Then resulting mixture was kept in dark for overnight. Then, centrifugation was done. Finally, resulting particles were dried and calcined for 6 h at 400°C [17].

Electrode Fabrication

40 mg of nanoparticles (TiO_2 , ZnO , Fe_2O_3 , TiO_2/ZnO , $\text{TiO}_2/\text{Fe}_2\text{O}_3$, and $\text{TiO}_2/\text{ZnO}/\text{Fe}_2\text{O}_3$) were weighed and mixed with 2 ml of isopropanol small amount of Nafion (20 μl). Then, it was sonicated for 1 h. The slurry was applied on Ti plate (effective electrode area $\sim 1\text{ cm}^2$) and dried at 60°C on hot plate.

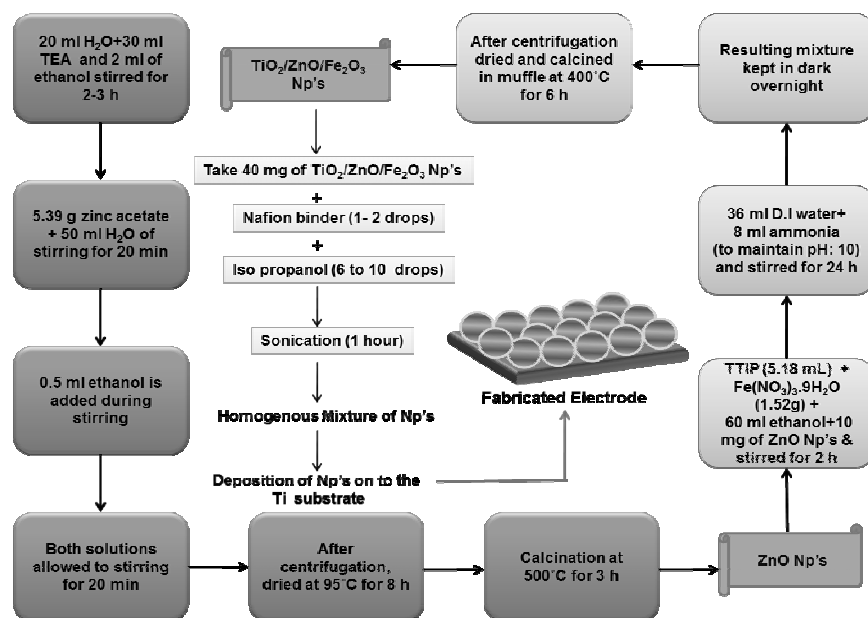


Fig. 1: Synthesis and Fabrication of $\text{TiO}_2/\text{ZnO}/\text{Fe}_2\text{O}_3$ Nanocomposite Electrode on Ti Substrate

Electrochemical Measurements

Voltammetric measurements were carried out at room temperature using Potentiostat (K-lyte 1.0). The cell used for cyclic voltammetric experiments was three-electrode type. Bare Ti, Ti/TiO_2 , Ti/ZnO , $\text{Ti}/\text{Fe}_2\text{O}_3$, $\text{Ti}/\text{TiO}_2/\text{ZnO}$, $\text{Ti}/\text{TiO}_2/\text{Fe}_2\text{O}_3$ and $\text{Ti}/\text{TiO}_2/\text{ZnO}/\text{Fe}_2\text{O}_3$ were used as working electrode (effective electrode area $\sim 1\text{cm}^2$), while Ag/AgCl and Pt mesh were used as reference and counter electrodes respectively. $0.1\text{M Na}_2\text{SO}_4$ solution was chosen as supporting electrolyte. Cyclic voltammetric studies were performed at different applied voltages of 0.6V , 1.2V , 1.2V , 1.3V , 1.2V and 1.0V for Bare Ti, Ti/TiO_2 , Ti/ZnO , $\text{Ti}/\text{Fe}_2\text{O}_3$, $\text{Ti}/\text{TiO}_2/\text{ZnO}$ and $\text{Ti}/\text{TiO}_2/\text{Fe}_2\text{O}_3$ respectively at a scan rate of 0.05V/s . Dye concentration of 10mg/L was selected for all experiments. UV-V is spectrophotometer was used to measure the decolorization efficiency at different intervals and is calculated by the following formula [5],

$$\% \text{ decolorization} = (A_0 - A)/A_0 \times 100 \quad \dots (1)$$

where A_0 and A are the absorbance (at the maximum wavelength, λ_{max}) of dye solution before and after electrochemical treatment.

Results and Discussions

Characterization of Nanoparticles

In order to understand the crystalline nature of synthesized materials, X-Ray Diffractogram (XRD) pattern has been taken (Figure 2). The diffractogram pattern taken were

indexed properly for all crystalline peaks and compared with JCPDS data file. Figure 2(a) shows the major peaks at 2θ values of 25.5° , 40.0° , 48.0° , 54.2° , 62.4° corresponds to the planes of (101), (004), (102), (110), and (211) tetragonal anatase TiO_2 (JCPDS Card No. 21-1272) [18]. The crystallite size of TiO_2 nanoparticles was estimated to be 15.93nm from Debye Scherrer formula.

The peaks at (100), (002), (101), (102), (110), (103), and (112) corresponds to the standard hexagonal wurtzite ZnO (JCPDS card no. 36-1451) as shown in Figure 2(b) [19]. The crystallite size of these ZnO nanoparticles was estimated as 19.84nm . Furthermore, major peaks at 2θ values of 26.1° , 32.5° , 35.4° , 49.2° , 62.2° could be assigned to $\alpha\text{-Fe}_2\text{O}_3$ (012), (104), (110), (024) and (214) crystal planes (JCPDS card No. 03-0800) as shown in Figure 2(c) [18]. The crystallite size of these Fe_2O_3 nanoparticles was estimated to be 26.577nm . Therefore, the diffractogram pattern confirms highly crystalline nature of synthesized materials as anatase TiO_2 , ZnO and $\alpha\text{-Fe}_2\text{O}_3$ respectively. In order to study the surface morphology and topography of synthesized single materials (TiO_2 , ZnO , Fe_2O_3) and heterostructure assemblies ($\text{TiO}_2/\text{ZnO}/\text{Fe}_2\text{O}_3$), Scanning Electron Microscopy (SEM) studies were done as shown in Figure 3. SEM image of TiO_2 nanoparticles is depicted in Figure 3(a) that clearly shows the spherical shape of the TiO_2 particles. But, $\alpha\text{-Fe}_2\text{O}_3$ nanoparticles were formed as aggregated particles and aggregates did not possess any definite shape as shown in the Figure 3(b). The SEM image of ZnO has clearly revealed hexagonal shape as shown in Figure 3(c). Figure 3(d) show the SEM image of $\text{TiO}_2/\text{ZnO}/\text{Fe}_2\text{O}_3$ nanocomposite/

heterostructure. Coupling between the three nanoparticles is observed but, aggregated surface of Fe₂O₃ particles surrounded with TiO₂ and ZnO particles. However, the shapes of the TiO₂ and ZnO nanoparticles are formed as observed in the individual TiO₂, ZnO particles.

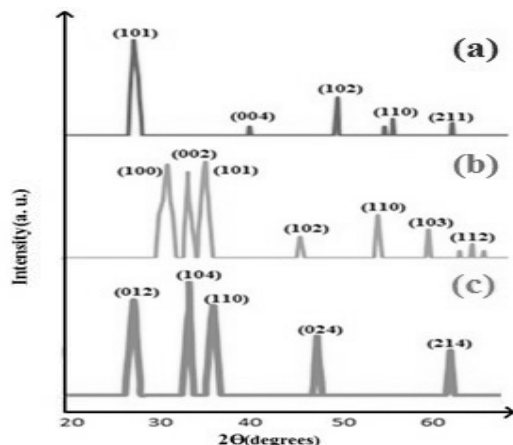


Fig. 2: XRD Pattern of (a) TiO₂, (b) ZnO and (c) α-Fe₂O₃ Nanoparticles

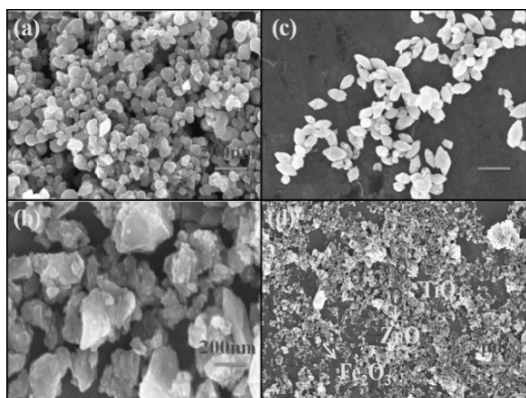


Fig. 3: FE-SEM Images of (a) TiO₂ Nanoparticles, (b) Fe₂O₃ Nanoparticles, (c) ZnO Nanoparticles, and (d) TiO₂/ZnO/Fe₂O₃ Nanocomposite

In order to determine functional groups present in the synthesized material, FTIR analysis was done (Figure 4). The broad peak at 3456.42 cm⁻¹ corresponds to the OH stretching vibration in pure ZnO, whereas the peak at 612.49 cm⁻¹ clearly indicates Zn-O stretching and the peaks at 1557.95 cm⁻¹ and 1071.4 cm⁻¹ were attributed to the C-O stretching vibration [19]. The broad band observed at 3421 cm⁻¹ was assigned to the asymmetrical and symmetrical stretching vibrations of hydroxyl group (-OH) of TiO₂, the band at 1636.35 cm⁻¹ corresponds to deformative vibration of Ti-OH stretching modes and the band at 827.05 cm⁻¹ corresponds to the Ti-O bending mode of TiO₂ [20]. The peak at 583.54 cm⁻¹ represents to Fe-O stretching mode, the

broad band observed at 3279.81 cm⁻¹ corresponds to stretching vibrations of (-OH) and peak at 1558.17 cm⁻¹ attributed to the C-O stretching vibrations of α-Fe₂O₃ [21]. Similarly, TiO₂/Fe₂O₃ and TiO₂/ZnO nanocomposites confirm the presence of bonds of individual TiO₂, Fe₂O₃ and ZnO nanoparticles.

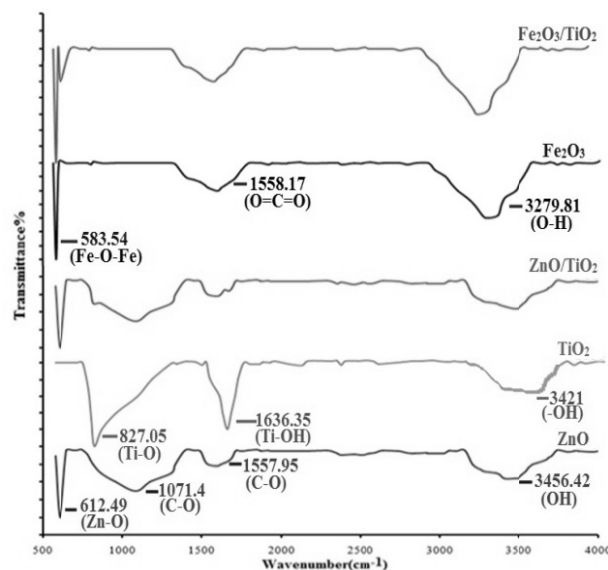
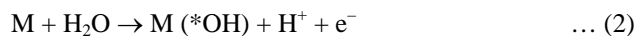


Fig. 4: FTIR Spectra of TiO₂, ZnO, Fe₂O₃, TiO₂/ZnO and TiO₂/Fe₂O₃ Nanoparticles

Electrochemical Measurements

In order to estimate the performance of fabricated electrodes, electrochemical measurements were done. During electrochemical treatment, the initial reaction corresponds to the oxidation of water molecules leading to the formation of physisorbed hydroxyl radical (M (*OH)) [5],



where, M is the electro-catalyst.

Higher oxide or superoxide (MO) may be formed if higher oxidation states are available for a metal oxide anode,



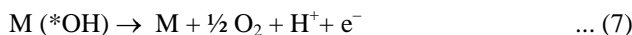
The redox couple MO/M acts as a mediator in the oxidation of organics. It competes with the side reaction of oxygen evolution via chemical decomposition of the higher oxide species,



A weaker oxidant like ozone also can be generated from water discharge at the anode,



Reaction of direct oxidation of M (*OH) to O₂ competes with reaction of its dimerization to hydrogen peroxide by reaction,



The first common step during electrochemical treatment is the discharge of water molecules to hydroxyl radicals as shown in the equation (2) [22]. The produced hydroxyl radicals were responsible for the cleavage of chromophore group in the crystal violet dye that is responsible for the colour of the dye. During cyclic voltammery, the voltages applied for the electro-catalysts (bare Ti, Ti/TiO₂, Ti/ZnO, Ti/Fe₂O₃, Ti/TiO₂/ZnO, Ti/TiO₂/Fe₂O₃ and Ti/TiO₂/ZnO/Fe₂O₃) are 0.6V, 1.2V, 1.2V, 1.3V, 1.2V, 1.0V and 1.2V respectively. These are the potentials where the oxidation peak hump begins. As the rate of degradation depend on the *OH radicals, the electrocatalyst is in a way to promote the *OH radicals towards instant involvement in dye degradation reactions due to the short lifetime of the *OH radicals [23].

This suggests the fast electron transport is essential for effective operation of semiconductor material interfaces. The present study describes heterostructure assemblies which either form type-I or type-II heterojunction thereby providing effective electron path for transport of charged species. Further, the assembly of heterostructures provide high accommodation for dye molecules and oxidizing agents due to large surface area of the nanocomposites. Therefore, ternary heterostructure assembly (TiO₂/ZnO/Fe₂O₃@Ti) performs better than binary (TiO₂/ZnO@Ti, TiO₂/Fe₂O₃@Ti) or individual material phases (bare Ti, Ti/TiO₂, Ti/ZnO, Ti/Fe₂O₃) in degradation of crystal violet dye.

Dye Degradation Studies

According to UV-Vis spectra, nearly complete decolourization of the crystal violet dye ($\lambda_{max} = 578 \text{ nm}$) was achieved for all electro-catalysts in present study. The percentage of decolourization observed for composites Ti/TiO₂/ZnO, Ti/TiO₂/Fe₂O₃ and Ti/TiO₂/ZnO/Fe₂O₃ are 24.0, 35.1, 39 within 2 h respectively (Figure 5b).

Similarly, the percentage of decolourization observed for bare Ti, Ti/TiO₂, Ti/ZnO, and Ti/Fe₂O₃ are 11.5, 10.0, 17 and 18 within 2 h respectively. The increased percentage of decolourization in composites is due to the immediate degradation reactions are occurring through the release of higher *OH radicals, but in the remaining anodes, at the start of degradation treatment the formation of *OH radicals is less.

Thus, lower degradation rate is observed in case of individual materials in comparison to binary or ternary composites. However, nearly complete decolourization is achieved with all electro-catalysts, but with varying degradation rates as shown in the Figure 5(a).

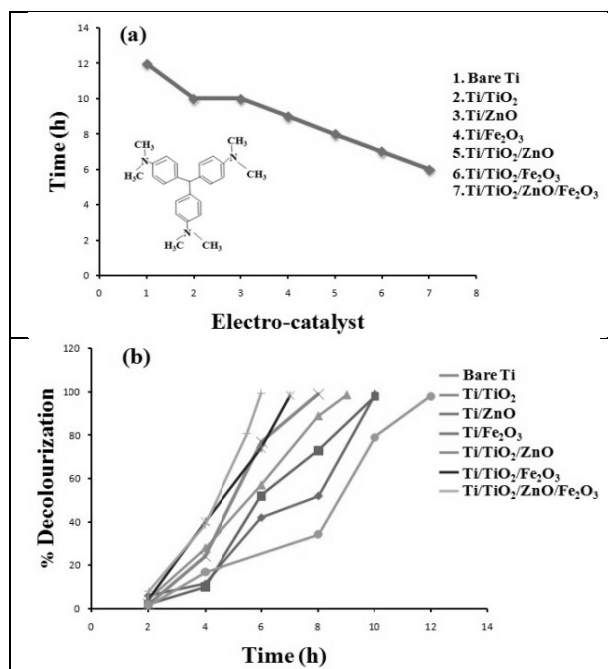


Fig. 5: (a) Time(h) v/s Electro-Catalyst, (b) % Decolourization v/s Time (h)

Conclusions

Present study describes the importance of synchronized charge transport across TiO₂/ZnO/Fe₂O₃ heterostructure assembly fabricated on Ti substrate towards electrochemical crystal violet dye degradation and water splitting reaction. The ternary electrocatalyst assembly (TiO₂/ZnO/Fe₂O₃@Ti) has shown enhanced performance over binary (TiO₂/ZnO@Ti, TiO₂/Fe₂O₃@Ti) and single material (bare Ti, Ti/TiO₂, Ti/ZnO, Ti/Fe₂O₃) substantiating the importance of synchronized charge transport. The outcomes of present study will help to design more pronounced heterostructure assemblies for better performance towards electrochemical water splitting and complex dye degradation studies.

Acknowledgements

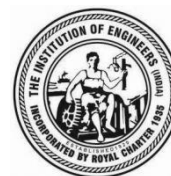
The authors are thankful to Head of Chemical Engineering department, JNTUA College of Engineering, Anantapur for providing the facilities to carry out the experiments. Further, the authors acknowledge the contribution of IIT Kanpur, RIPER, OTRI-JNTUA for providing various characterization tools in analysis/interpretation of various synthesized samples.

References

- [1] Pradhan, Gajendra Kumar and Parida, K.M., Fabrication of iron-cerium mixed oxide: an effective photocatalyst for dye degradation, International Journal of Engineering, Science and Technology, 2, 9, 53–65 (2010).



- [2] Yang, Huimin; Liang, Jintao; Zhang, Li and Liang, Zhenhai, Electrochemical Oxidation Degradation of Methyl Orange Wastewater by Nb/PbO₂ Electrode, *Int. J. Electrochem. Sci.*, 11, 1121–1134 (2016).
- [3] Desai, Sudhanva M., Charyulu, N.C.L.N., Behara, Dilip Kumar and Satyanarayana, Suggala V., “Statistical optimization of adsorption variables for biosorption of chromium (VI) using carrot based adsorbents-equilibrium and kinetic studies”, *Journal of Environmental Research and Development*, 10, 3, 392–406, (2016).
- [4] Bensalaha, N., Alfaro, M.A. Quiroz and Martínez-Huitle, C.A., Electrochemical treatment of synthetic wastewaters containing Alphazurine A dye, *Chemical Engineering Journal*, 149, 348–352 (2009).
- [5] Jović, Milica; Stanković, Dalibor; Manojlović, Dragan; Anđelković, Ivan; Milić, Anđelija; Dojčinović, Biljana and Roglić, Goran, Study of the Electrochemical Oxidation of Reactive Textile Dyes Using Platinum Electrode, *Int. J. Electrochem. Sci.*, 8 168–183 (2013).
- [6] Kumar, S. Girish and Devi, L. Gomathi, Review on Modified TiO₂ Photocatalysis under UV/Visible Light: Selected Results and Related Mechanisms on Interfacial Charge Carrier Transfer Dynamics, *J. Phys. Chem. A*, 115, 13211–13241 (2011).
- [7] Maheswari M., Sudha, Jalajakshi, T. and Behara, Dilip Kumar, The strategic role of TiO₂ based photocatalysts in dye degradation studies: A short Review”, *International Journal of Advance Research in Science and Engineering* (ISSN 2319-8354), 05, 01 (2016).
- [8] Socha, A., Sochocka, E., Podsiadly, R. and Sokolowska, J., Electrochemical removal of synthetic textile dyes from aqueous solutions using Ti/Pt anode: role of dye structure, *Color. Technol.*, 122, 207–212, (2006)
- [9] Behara, Dilip Kumar; Upadhyay, Arun Prakash; Sharma, Gyan Prakash; Kiran, B.V. Sai Krishna; Sri Sivakumar and Pala, Raj Ganesh S., “Heterostructures based on TiO₂ and Silicon for Solar Hydrogen generation”, *Advanced Functional Materials*, (219–281), © 2015, Scrivener Publishing LLC, Ashutosh Tiwari and Lokman Uzun (eds.), online (ISBN No: 9781118998977).
- [10] Upadhyay, Arun Prakash; Behara, Dilip Kumar; Sharma, Gyan Prakash; Bajpai, Anshuman; Sharac, Nicholas; Ragan, Regina; Pala, Raj Ganesh S. and Sri Sivakumar, Generic Process for Highly Stable Metallic Nanoparticle Semiconductor Heterostructures via Click Chemistry for Electro/Photocatalytic Applications, *ACS Appl. Mater. Interfaces*, 5, 9554–9562 (2013).
- [11] Behara, Dilip Kumar; Sharma, Gyan Prakash; Upadhyay, Arun Prakash; Prakash, Maurya Gyan; Pala, Raj Ganesh S. and Sivakumar, Sri, Synchronization of charge carrier separation by tailoring the interface of Si-Au-TiO₂ heterostructures via click chemistry for PEC water splitting, *Chemical Engineering Science*, 154, 150–169 (2016).
- [12] Behara, Dilip Kumar; Ummireddi, Ashok Kumar; Aragona, Vidyasagar; Gupta, Prashant Kumar; Pala, Raj Ganesh S. and Sivakumar, Sri, Coupled optical absorption, charge carrier separation, and surface electrochemistry in surface disordered/hydrogenated TiO₂ for enhanced PEC water splitting reaction, *Phys. Chem. Chem. Phys.*, 18, 8364 (2016).
- [13] Upadhyay, Arun Prakash; Behara, Dilip Kumar; Sharma, Gyan Prakash; Prakash, Maurya Gyan; Pala, Raj Ganesh S. and Sivakumar, Sri, Fabricating appropriate Band-Edge-Staggered Hetero Semiconductors with Optically Activated Au Nanoparticles via Click Chemistry for Photoelectrochemical Water Splitting, *ACS Sustainable Chem. Eng.*, 4 (9), 4511–4520 (2016).
- [14] Thesis: Ghosh, Surya Prakash, synthesis and characterization of zinc oxide nanoparticles by sol-gel process, National Institute of Technology, Rourkela, Rourkela-769008, Orissa, India (2012).
- [15] Bageri, Samira; Chandrappa, K.G. and Sharifah Bee Abd Hamid, Res., Generation of Hematite Nanoparticles via Sol-Gel Method, *J. Chem. Sci.*, 3(7), 62–68 (2013).
- [16] Is Fatimah, Novitasari, Preparation of TiO₂-ZnO and its activity test in sonophotocatalytic degradation of phenol, *Mater. Sci. Eng.*, 107, 01 (2003).
- [17] Palanisamy, B., Babu, C.M., Sundaravel, B., Anandan, S. and Murugesan, V., Sol-Gel synthesis of mesoporous mixed Fe₂O₃/TiO₂ photocatalyst: Application for degradation of 4-Chlorophenol *Journal of Hazardous Materials*, 252–253, 233–242 (2013).
- [18] Patra, Astam K., Dutta, Arghya and Bhaumik, Asim, Highly Ordered Mesoporous TiO₂-Fe₂O₃ Mixed Oxide synthesized by Sol-Gel Pathway: An Efficient and Reusable Heterocatalyst for Dehalogenation reaction, *ACS Appl. Mater. Interfaces*, 4, 5022–5028 (2012).
- [19] Sharma, Rajni; Alam, Firoz; Sharma, A.K.; Dutta, V. and Dhawan, S.K., ZnO Anchored Graphene Hydrophobic Nanocomposite-based bulk Heterojunction Solar cells showing enhanced short-circuit current, *J. Mater. Chem.*, C, 2, 8142–8151 (2014).
- [20] Amalraj, Augustine and Pius, Anitha, Photocatalytic Degradation of Alizarin red S and Bismarck Brown R using TiO₂ photocatalyst, *J. Chem Applied Biochem.*, 1 (1): 105 (2014).
- [21] Sahoo, S.K., Agarwal, K.; Singh, A.K., Polke, B.G. and Raha, K.C., Characterization of γ - and α -Fe₂O₃ nano powders synthesized by emulsion precipitation-calcination route and rheological behavior of α -Fe₂O₃, *International Journal of Engineering, Science and Technology*, 2, 8, 118–126 (2010).
- [22] Moura, Dayanne Chianca de; Quiroz, Marco Antonio; Silva, Djalma Ribeiro da; Salazar, Ricardo and Martínez-Huitle, Carlos Alberto, Electrochemical degradation of Acid Blue 113 dye using TiO₂-nanotubes decorated with PbO₂ as anode, *Environmental Nanotechnology, Monitoring & Management*, 5, 13–20 (2016).
- [23] Gligorovski, Sasho; Strekowski, Rafal; Barbati, Stephane and Vione, Davide, *Environmental Implications of Hydroxyl Radicals (OH)*, *Chem. Rev.*, 115 (24), 13051–13092 (2015).



Biodiesel Synthesis from Soybean Oil in a Tubular Reactor: Numerical Study

D. Madhurima Reddy¹ and Nanda Kishore^{*1}

Abstract: Biodiesel is considered as a sustainable alternative to diesel fuel, as it can be utilized instead of petroleum diesel. In the lieu of petroleum reserves getting diminished, biodiesel satisfies global energy requirement and lessens the environmental impact. Biodiesel is synthesized from the transesterification reaction taking place between, methanol and triglycerides under the presence of catalyst. Vegetable oils, waste cooking oils and animal fats are the few sources of triglyceride. In this work, the transesterification reaction between waste vegetable oils (soybean oil) and methanol is modeled and simulated in a tubular reactor of height 353 mm and width 21.8 mm. The convection–diffusion–reaction species transport model present in computational fluid dynamics based software ANSYS Fluent v.16.2 is used to model the reaction. The effects of molar ratio of methanol to triglyceride and temperature on the biodiesel yield are studied in this work. The results show that as the molar ratio and temperature increase, the biodiesel yield also increase. The data obtained from the literature, shows the model is in good agreement with the literature counterparts.

Keywords: Biodiesel Synthesis, Transesterification Reaction, Waste Soybean Oil, Tubular Reactor, Molar Ratio, Mass Transfer Controlled.

Introduction

Economic development of any country depends on the Energy. Energy is the basic requirement for any sector of the economy. But a question arises here, that for how long these energy producing fuels will last? Dependency of humans on petroleum or diesel as transportation fuel or to run every sector of the economy has increased so much over time that, it has created many environmental concerns [1]. These fuels come at high cost and with a global impact. It is well known to us, that global warming has become the most potential threat to the earth nowadays. Concerns from both political and environmental groups about the use of fossil based energy carriers are driving our society in search of new alternatives. Biomass is such source of energy which can be used to give clean and green biofuels. It is highly abundant and carbon–neutral renewable energy resource. Biofuels can take the form of any state of matter. Bio-char in solid state, ethanol and biodiesel in liquid state and biogas in gaseous state are produced from biomass [2]. As a coin has two sides to it, biodiesel also has its own advantages and disadvantages. Biodiesel has an ability to reduce the impact on climate change by reducing carbon monoxide, hydrocarbons, sulfur and pollutant particulates [3]. Its

renewability, non-toxicity, biodegradable nature, inherent lubricity and superior flash point are some more advantages biodiesel has. But some of its disadvantages include expensive than petroleum diesel, high cost of feedstock, not suitable for use in low temperature, low volumetric energy content, increases NO_x emissions, etc.

The literature contains hundreds of references of biodiesel production from a wide variety of oilseeds. The dominant feedstocks are soybean in the U.S. [4–7], rapeseed oil [8] in Europe and palm oil [9, 10] in South-East Asia. Other vegetable oils having potential interest as biodiesel feedstocks include corn, sunflower [11, 12], camelina, cottonseed, mustard, safflower, coconut, jatropha [13] and castor beans. Animal fats (mainly beef tallow) [14] and used cooking oil have very good market for biodiesel production. Production of biodiesel from algae [15, 16] is also of great interest.

Biodiesel is commonly produced by transesterification of vegetable oil, waste vegetable oils and animal fats. Transesterification reaction is between an oil or fat and alcohol to form esters and glycerol. This reaction can take place with or without the catalyst. Vegetable oils and animal fats contain triglycerides which is the main reactant for transesterification reaction. The reaction involves Triglyceride (TG) reacting

¹ Department of Chemical Engineering, IIT Guwahati, Assam–781039, India.
✉*nkishore@iitg.ernet.in; mail2nkishore@gmail.com



with Alcohol (A) in the presence of catalyst to form Fatty Acid Alkyl Ester (FAAE) and Glycerol (G) [17]. Since most used alcohol is methanol, the biodiesel then produce from the reaction is called Fatty Acid Methyl Ester (FAME). Techniques employed for production of biodiesel depends on type of catalysts and often used techniques are base catalysis, acid catalysis, enzymatic conversion, solid catalyst, non-catalytic conversions, BIOX process and supercritical processes. These conversions are often carried out in batch reactor, semi-continuous flow reactors, continuous flow reactors, ultrasonic reactors, supercritical reactors, micro-wave reactors, tubular reactors, etc.

Further the chemical composition of biodiesel is dependent upon the feedstock from which it is produced, as vegetable oils and animal fats of differing origin have dissimilar fatty acid compositions [18]. Vegetable oils are more viscous than diesel fuel, therefore they reduce fuel atomization and increase the penetration, which in turn cause engine choking and thickening of oils. Therefore, to reduce the viscosity, different methods like dilution, micro-emulsification, pyrolysis and transesterification are used [1].

Finally, the transesterification reaction involving vegetable oils to produce biodiesel has been given a lot of importance by numerous researchers which received large amounts of citations in the scientific and patent literature [5, 19, 20] on the basis of experimental works; however, a limited literature is available on the numerical simulation of the transesterification of triglycerides, due to the multi-physics involved in such reactive flow. Therefore, this work is aimed numerically investigate the modeling and simulations of biodiesel synthesis process in tubular reactors under varying conditions of the molar ratio of methanol to vegetable oils, temperature, and different biomasses using a Computational Fluid Dynamics (CFD) based solver.

Literature Review

Since the literature on the production of biodiesel originating different biomasses, different production techniques and different types of reactors used for the production is voluminous, only experimental and numerical studies pertaining to transesterification of vegetable oils under various conditions are presented herein. For instance, Freedman *et al.* [5] studied the transesterification kinetics of soybean oil and reported the effects of molar ratio, time and temperature on ester formation from butanol and soybean oil. Nouredini and Zhu [7] also studied the kinetics of transesterification of soybean oil. They reported the effect of mixing intensity and temperature on the rate of reaction, while molar ratio and concentration of catalyst were held constant. They proposed a reaction mechanism consisting of an initial mass transfer-controlled region followed by kinetically controlled region. They also reported rate constants and activation energies at

different mixing intensities. Klofutar *et al.* [21] investigated the batch transesterification reaction of rapeseed and waste sunflower oils with methanol in the presence of potassium hydroxide as a catalyst. They studied the effect of temperature on the reaction rate while molar ratio was held constant. They quantitatively monitored the transesterification reaction with the help of size-exclusion chromatography and ^1H NMR spectroscopy. They reported the reaction rate constants and activation energies for both waste sunflower oil and rapeseed oil, by solving the set of differential equations characterizing the stepwise reactions involved in transesterification reaction using fourth order R-K method.

Recently, Wen and Petera [22] reported CFD numerical simulation of biodiesel synthesis in a spinning disc reactor in 2015. CFD software ANSYS FLUENT v.13.0 was used to simulate biodiesel synthesis from canola oil and methanol in presence of NaOH in spinning double disc reactor. The reactor consists of two flat discs of 50 mm, located coaxially and parallel to each other with a gap of 0.2 mm between the discs. The mass transfer formulation was used to accomplish the simulation of this model. The research work included the study of hydrodynamics of properties of spinning disc reactor. The effect of rotational speed of upper disc on the conversion of triglyceride is reported. Rotational speed above 1000 rpm caused shorter residence time and on other hand also improved production efficiency. Richard *et al.* [23] made an attempt to model the reaction kinetics of transesterification reaction of sunflower oil with ethanol in micro-reactors at 65°C by inducing better control for heat and mass transfer and were successful. The model was simulated at different ethanol to oil molar ratios. A single set of kinetic parameter was used to determine kinetic constants and mass transfer coefficients. Chokchai *et al.* [24] used conventional process for producing biodiesel. The research work focuses on feasibility study of using reactive distillation to produce biodiesel from palm oil. They assumed using reactive distillation can reduce the amount of excess alcohol in the feed stream bringing its stoichiometric ratio close to that of oil. ASPEN plus 2006 has been used to simulate this process. The results show that a 4:1 molar ratio of methanol to oil and the reboiler temperature at 150°C produces 97.36 wt% methyl ester in 5.6 minutes, that is 5 times fast than reaction time taken in conventional process. The excess alcohol at the input was reduced by 66%. But need of the hour is to optimize the transesterification reaction to meet the growing demand of biodiesel. Assessing the performance of innovative reactors is difficult due to the liquid-liquid reaction mixture that is affected by mass transfer, reaction kinetics and component solubility. Boer and Bahri [25] presented a CFD model of a tubular reactor developed in ANSYS CFX that can be used to predict onset of mixing via turbulent flow. According to the authors, this advancement in the modeling of two phase transesterification reaction makes



possible to accurately model any liquid–liquid flow in tubular reactors or pipes. Hydrothermal liquefaction of biomass is one of methods to produce biofuels, which include biodiesels and bio–oils. Syed [26] performed hydrothermal liquefaction of biomass in a continuous flow tubular reactor. The work includes the CFD simulation of the process in ANSYS FLUENT. The model geometry and mesh of micro reactor are developed in ANSYS GAMBIT. The continuous media is supercritical water which works as catalyst. The authors examined the velocity and temperature distributions and reaction kinetics and the reactions in ANSYS FLUENT are not authentic because the solution did not converge. The authors have proposed that more investigations have to be done on reaction pathways involving supercritical water as catalyst. In this paper, the numerical modeling of alkali-catalyzed Waste Cooking Oil (WCO) transesterification in a stirred tank reactor is presented. Based on the Reynolds Average Navier-Stokes equation, Nabeel *et al.* [27] developed a 3-D model to simulate the transesterification of WCO in a stirred tank reactor using a commercial numerical solver. Two models were compared for the reaction. One of the models included the rate constant (finite rate model) on one hand and the other (eddy dissipation model) helped account for turbulence. Thermodynamic properties of the reaction components were incorporated as user defined function for the mixing models in ANSYS FLUENT. FAME yield were predicted in terms of species concentration and compared fairly well with experimental condition for 1 and 2-L spinning tank reactor, where yield from the numerical model varied by about 18 and 23% for 1 and 2-L spinning tank reactor respectively. Highlighting the advantages of small scale production, Boer and Bahr [28] proposed this paper which developed CFD model in ANSYS CFX that encapsulates the liquid-liquid flow phenomena observed in the reaction medium. The paper includes an analysis of the reaction mixture focusing on necessary simplifying assumptions, experimental flow visualization results and an investigation of different simulation settings. Many micro devices have been tested in order to enhance the interaction between vegetable oil and alcohol to raise the conversion into biodiesel. Santana *et al.* [29] studied numerically the use of a Spiral-micro mixer for mixing and reaction of *Jatropha curcas* oil and ethanol for the production of biodiesel. The simulated micro devices had 200 μm in height and width. The mixing of the fluid was analyzed with Reynolds numbers ranging from 0.67 to 100 and reaction studies were carried out for the same Reynolds numbers and a residence time ranging from 0.2 to 1000 s. The Spiral-micro mixer showed the highest mixing between the oil and ethanol. The highest conversion of vegetable oil in biodiesel was obtained with the T-micro mixer (average of 51.8%) and for the Spiral-micro mixer (average of 50%) for Reynolds number studied. They proposed that an increment in residence time

increased conversion, and the maximum conversion achieved was 98.48% and 99.99% for T-micro mixer and Spiral-micro mixer, respectively. The efficiency of mixing and reaction process can be increased and high conversion ratios obtained using this type of micro mixer. Scott *et al.* [30] modeled continuous reactor system using transesterification of soybean or rapeseed oil with methanol in presence of homogeneous catalyst. The authors studied the reactor performances in terms of biodiesel yields for plug flow and continuous stirred reactors and mixing behaviors of inter-stage phase separation using ASPEN Plus. The results shows that reverse reactions can prevail when inter-stage separation is not efficient enough at removing the glycerin co-product. The authors stated that methanol to oil ratio can improve any reacting system performance. Janajreh and Al Shrah [31] numerically simulated the multiple step transesterification of waste oil in tubular reactor in three dimensional way. This work explains the fact that transesterification reaction of triglyceride and alcohol is mass transfer limited. They modeled the reaction in tubular reactor to understand the distribution of species and to use it as a design tool to develop the reactor design. They reported that to avoid stratification and promote mass transfer, reactants should be homogenized and they need to be injected at a high velocity so that they get premixed. They estimated the total residence time to be on the order of 20 seconds.

Hydrolysis of oils and fats into free fatty acids is a commercial win for chemical industries. Sometimes the conventional way of producing biodiesel can be expensive due to non-availability of feedstock, or low free fatty acids in oils. An alternative to that is hydrolysis of oils to fatty acids followed by esterification to biodiesel [32]. W.-C. Wang *et al.* [33] modeled 3D continuous counter current hydrolysis of canola oil in transient state. They used ANSYS CFX v.11.0 to model the kinetics of hydrolysis reactions. Distilled water and canola oil were used as feedstock. A 316SS reactor of 150 cm and 8.9 cm ID was used to perform the hydrolysis reactions. Both the feedstock are injected through tubes from top the reactor. Canola oil was introduced from 120 cm below the top of the reactor and distilled water was introduced from 25 cm below the top of the reactor. This is done to enhance the mixing of two liquids by considering the density differences in water and oil. The geometry and mesh are created using ANSYS Workbench v.12. The CFD simulation was carried out for 600 time steps, where each time step represented 30 s of the physical reaction time. The total time of the reaction was 300 minutes. They monitored the concentrations of TG, DG, MG, and FFA across the simulation time. They concluded that the simulation results were in good agreement with experimental data, as the flow properties and reaction kinetics were accurate. Machado *et al.* [34] also used the hydrolysis–esterification method to produce biodiesel. In this work, two steps involving two



reactors are included. The hydrolysis step is carried out in packed bed reactor, and esterification step is carried out in reactive distillation column. Reactive distillation combines both physical separation and chemical reaction. They also reported advantages of using reactive distillation column and are increased productivity and selectivity, reduced energy usage, no need of solvents, and most importantly addressing the advantages of process intensification. Their work presents computer simulation of continuous multi-stage process for biodiesel production from soybean oil and ethanol using hydro-esterification process. They calculated material flows, analyzed energy balance and process economics. They reported that at a molar feed ratio of water to soybean oil of 5.7:1 and a minimum input flow of soybean oil of 30 mol/min leads to high conversions. The sensitivity analysis results show the conversions can be reached above 99%, if the operating conditions are optimized.

On the basis of aforementioned literature, the objective of the present work is set as to numerically model and simulate the biodiesel synthesis process in tubular reactors for varying molar ratios of methanol to vegetable oils, biomass source and temperature. For this purpose, CFD modeling and simulation procedure is applied to biodiesel production process so that to understand the chemical and physical processes in a better way. ANSYS Fluent v.16.2 is adopted to model the tubular reactor used for the transesterification reaction for biodiesel production.

Problem Statement and Mathematical Formulation

Consider a tubular reactor of height and diameter 353 mm and 21.8 mm, respectively, with sizes of inlet and outlet tubes being 5 mm each as shown in Figure 1. In the present work, the transesterification reaction takes place between waste soybean oil (triglyceride) and methanol. The reactants are premixed and pumped at a velocity of 1.6 m/s. The reaction mixture is considered to be in single phase. The reaction is assumed to proceed as soon as the reactant components are introduced into the reactor with the help of a pump. The concentration of base catalyst (NaOH solution) is

1 wt%, and the diffusivity value for the reacting mixture is assumed to be constant and equal to $7 \times 10^{-9} \text{ m}^2\text{s}^{-1}$ [22]. The species physiochemical properties and molecular weights are given Table 1. The kinetics required for the modeling and simulation of this process are adopted from experimental work due to Nouredini and Zhu [7] and are given in Table 2. The governing equations for this process are as follows:

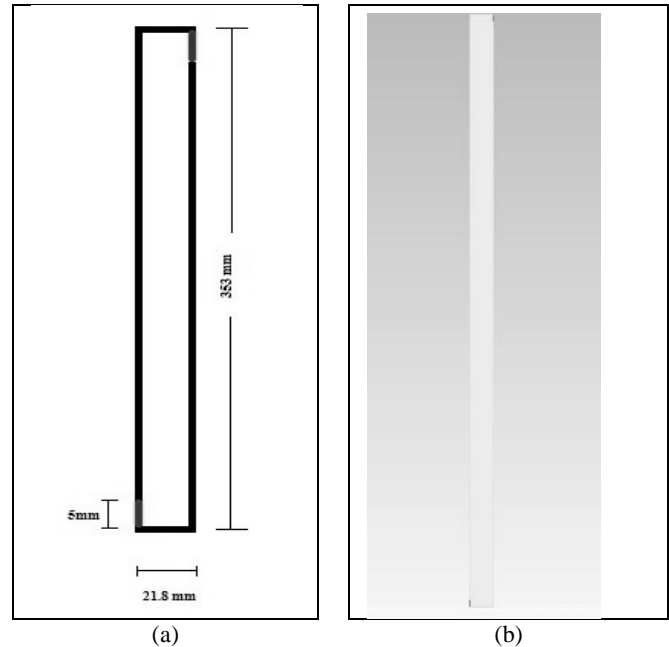


Fig. 1: (a) Schematic Representation of the Tubular Reactor and (b) Corresponding Mesh View

Continuity equation:

$$\frac{\partial \rho}{\partial t} + \nabla \cdot \rho U = 0 \quad \dots (1)$$

where ρ is the density of the fluid phase and U is the mean velocity vector of that phase. There are no source terms in the continuity equation or interphase transfer terms as mass is not created or transferred in the domain.

Table 1: Summary of Physiochemical Properties of Various Species involved in this Study

Species	Chemical Formula	Molecular Weight	Density, kg/m ³	Specific Heat, Cp, J/kg-K	Viscosity, kg/m-s
Methanol	CH ₄ O	32	791.8	1470	3.96×10^{-4}
Triglyceride	C ₅₄ H ₁₀₄ O ₆	885	883.3	2200	1.61×10^{-2}
Glycerol	C ₃ H ₈ O ₃	92	1261	2386	1.412
Biodiesel	C ₁₈ H ₃₆ O ₂	296	870	1187	1.12×10^{-3}

Table 2: Chemical Kinetics for Each Reaction involved in the Present Process [7]

Parameter	TG → DG	DG → TG	DG → MG	MG → DG	MG → GL	GL → MG
Rate constant, k _i (m ³ /mol-sec)	8.333×10^{-7}	1.833×10^{-6}	3.583×10^{-6}	2.047×10^{-5}	4.033×10^{-6}	1.167×10^{-7}
Activation energy, A _i (J/ kgmol)	5.5×10^7	4.16×10^7	8.31×10^7	6.13×10^7	2.69×10^7	4.013×10^7
Pre-exponential factor, k _o	3.925×10^7	5.78×10^5	5.91×10^{22}	9.88×10^9	5355	21533



Momentum equation:

$$\frac{\partial \rho U}{\partial t} + (\nabla \cdot \rho U U) = -\nabla p + \nabla \cdot \tau + \rho g \quad \dots (2)$$

Energy equation:

$$\rho C_p \frac{DT}{Dt} = \nabla \cdot \lambda_e \nabla T - \nabla \cdot \sum_i \rho h_i(T) D_e \nabla m_i - \rho \sum_i \frac{Dm_i}{Dt} h_i(T) \quad \dots (3)$$

Species transport equation:

$$\begin{aligned} \frac{\partial}{\partial t} (\rho m_i) + \frac{\partial}{\partial x_i} (\rho u_i m_i) \\ = \frac{\partial}{\partial x_i} \left(\rho D_{i,m} + \frac{\mu_i}{Sc_t} \right) \frac{\partial m_i}{\partial x_i} + R_i + S_i \end{aligned} \quad \dots (4)$$

where $D_{i,m}$ is the diffusion coefficient of the m_i specie, and Sc_i is the turbulent Schmidt number.

Species mass fraction:

$$\frac{\partial}{\partial t} (\rho Y_i) + \nabla \cdot (\rho v Y_i) = -\nabla \cdot J_i + R_i + S_i \quad \dots (5)$$

$\nabla \cdot J_i$ is the diffusion flux of species i , that arises due to concentration gradients the diffusion flux of species is given by,

$$J_i = -\rho D_{i,m} \nabla Y_i \quad \dots (6)$$

where R_i is the reaction source term account for species reaction. The chemical reaction rate is given by the Finite rate/Eddy dissipation model as below,

$$R_i = M_{w,i} \cdot \sum_{r=1}^{N_R} R'_{i,r} \quad \dots (7)$$

$k-\epsilon$ turbulence model:

It is a two equation model which gives the general description of turbulence by means of two transport equations. The first transported variable determines the energy in the turbulence and is called turbulent kinetic energy (k). The second transported variable is the turbulent dissipation (ϵ) which determines the rate of dissipation of the turbulent kinetic energy.

$$\begin{aligned} \frac{\partial}{\partial t} (\rho k) + \frac{\partial}{\partial x_i} (\rho k u_i) = \frac{\partial}{\partial x_j} \left[\left(\mu + \frac{\mu_t}{\sigma_k} \right) \frac{\partial k}{\partial x_j} \right] \\ + G_k + G_b - \rho \epsilon - Y_M + S_k \end{aligned} \quad \dots (8)$$

$$\begin{aligned} \frac{\partial}{\partial t} (\rho \epsilon) + \frac{\partial}{\partial x_i} (\rho \epsilon u_i) = \frac{\partial}{\partial x_j} \left[\left(\mu + \frac{\mu_t}{\sigma_\epsilon} \right) \frac{\partial \epsilon}{\partial x_j} \right] \\ + C_{1\epsilon} (G_k + C_{3\epsilon} G_b) - C_{2\epsilon p} \frac{\epsilon^2}{k} + S_\epsilon \end{aligned} \quad \dots (9)$$

where, G_k , G_b represents generation of turbulent kinetic energy due to mean velocity gradients and buoyancy. μ_t represents the eddy/turbulent viscosity. Y_M is the fluctuation dilation, and S_k , S_ϵ are the source terms.

Numerical Methodology

Aforementioned governing conservation equations of mass, momentum, energy, species transport and kinetics of biodiesel synthesis along with appropriate boundary conditions are simultaneously solved using a computational fluid dynamics based solver, ANSYS 14.5 in conjunction with mesh generating solver GAMBIT 2.4. In order to generate the mesh in the entire tubular reactor, first individual faces such as bottom face, top face, left wall face, right wall face, inlet and outlet faces with specified dimensions as shown in Figure 1(a) are designed. Then all these faces joined together to form a complete reactor, subsequently number of mesh intervals along each face are provided and then finally quadrilateral mesh is generated in the entire reactor domain as shown in Figure 1(b). The total numbers of cell, face and node present in the mesh developed for the geometry shown in Figure 1(a) are 310164, 628758 and 155457, respectively. Further the type of boundary has also been assigned along each face of the reactor and the default interior of the reactor is fit as continuum fluid medium as all chemical components involved in this process are in liquid form. Thus generated mesh is exported to ANSYS Fluent 14.5 and the same has been checked for mesh accuracy. Since all chemical components involved in this study are in liquid form, the multiphase model of the solver is not selected in this study. The standard k- ϵ viscous model is chosen along with species transport and turbulence-chemistry interaction models are selected. After selection of models, the materials and their properties are selected either from the dropdown menu of the solver or provided according to property details of components given in Table 1. Since the reaction components are premixed, the mixture properties of the species are specified in the mixture category which includes specifying the reaction kinetic data that is provided in Table 2. Then the boundary conditions are supplied in accordance with the combination of independent variables for a given simulation. Finally, after supplying all aforementioned information in the software, the final solutions procedure is initiated using a Semi-Implicit Model for Pressure-Linked Equations (SIMPLE) solver. The final converged solutions are saved and proceed for post processing for evaluation of the results.

Validation

The transesterification of soybean vegetables oils in tubular reactor has been simulated by Isa metal [31] using the experimental kinetics reported by Nouredini and Zhu [7]. Thus in this work validation has been carried out with results of Isam *et al.* [31] at 50°C, methanol to TG molar ratio of 6:1, and inlet velocity of 1.6m/s; and presented in Table 3. From this table it can be deduced that the mass fractions of all species involved in the reaction are in good agreement with the reported values of Isam *et al.* [31]. The present



conversion is 61.05% whereas that of Isam *et al.* [31] is 62.9%. This validation sets up the reliability and accuracy of the present solution methodology to extend for obtaining the simulation results on biodiesel from soybean vegetable oil under mass controlled conditions.

Table 3: Comparison of Mass Fractions of Reaction Species of Present Work with those of Isam *et al.* [31]

Species	Inlet Mass Fractions	Present Work	Isam <i>et al.</i> [31]
TG	0.143	0.0557	0.053
Methanol	0.857	0.0932	0.0833
DG		0.0001	0.0002
MG		0.0453	0.06
Glycerol		0.0010	0.00132
Biodiesel		0.6105	0.629
Conversion		61.05%	62.9%

Results and Discussion

Figure 2 shows the effect of molar ratio on the yield of biodiesel at different temperatures. It can be seen from this figure that for all values of the temperature, the yield of biodiesel increases with the increasing molar ratio. At small temperature of $T = 50^{\circ}\text{C}$, the biodiesel versus molar ratio attains a kind of stability after molar ratio of 8; however, for other two values of the temperatures, the biodiesel versus molar ratio curve almost linearly increases with the temperature.

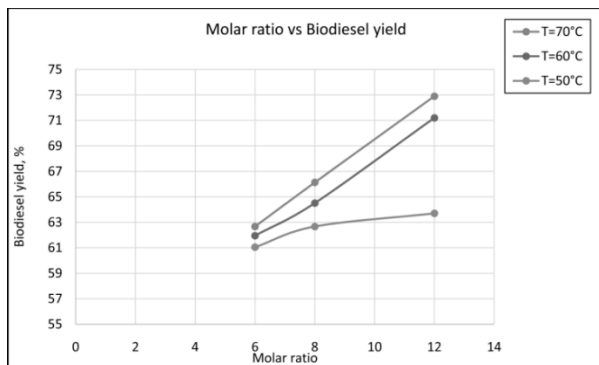


Fig. 2: Molar Ratio vs. Biodiesel Yield for Transesterification Reaction for Waste Soybean Oil

Figure 3 shows the effect of the temperature on the biodiesel yield for different molar ratios. It can be seen from this figure that for all values of the molar ratio, the biodiesel yield increases with increasing temperatures. At molar ratio 12:1, the biodiesel versus temperature curve tend to become stable after $T = 60^{\circ}\text{C}$, but for other two values of molar ratio, almost linearly increasing trend of biodiesel yield versus temperature is found.

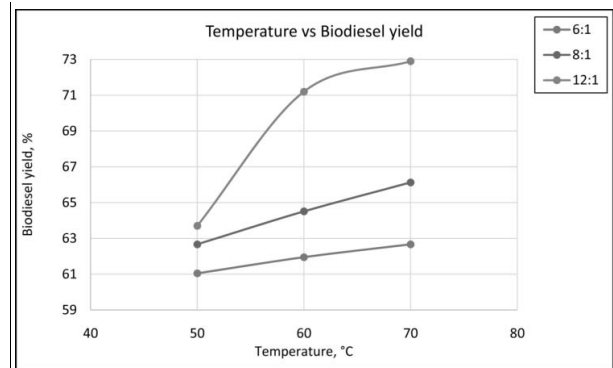


Fig. 3: Temperature vs. Biodiesel Yield for Transesterification Reaction for Waste Soybean Oil

Figure 4 shows the effect of molar ratio on the biodiesel yield due to the mass transfer controlled transesterification of waste soybean oil at different temperatures. From this figure it can be observed that for all values of the temperature, the biodiesel yield due to mass transfer controlled transesterification increase with molar ratio. Furthermore, unlike the case of normal transesterification reaction, in the case of mass controlled transesterification the biodiesel yield has increased substantially and a kind of stability of curve is attained for molar ratio > 8 regardless the values of the temperature.

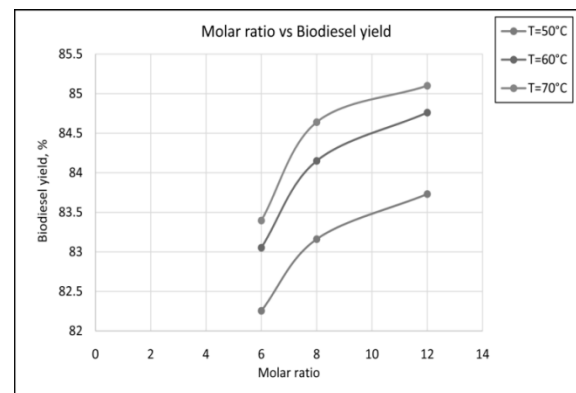


Fig. 4: Molar Ratio vs. Biodiesel Yield for the Mass Transfer Controlled Transesterification Reaction for Waste Soybean Oil

Figure 5 shows the effect of temperature on the yield of biodiesel due to mass transfer controlled transesterification of waste soybean oil for different molar ratio values. From this figure, it can be observed that regardless the values of the molar ratio, the biodiesel yield due to mass transfer controlled transesterification reaction increases with the temperature and the corresponding curves attain a kind of stable behavior when temperature goes beyond 60°C . Furthermore, compared to normal transesterification, the yield of biodiesel due to mass transfer controlled transesterification is substantially large for all combinations of the molar ratio and temperature.

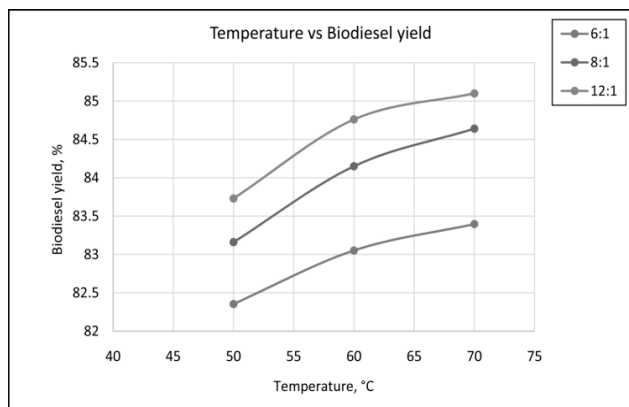


Fig. 5: Temperature vs Biodiesel Yield for Mass Transfer Controlled Transesterification Reaction for Waste Soybean Oil

Conclusions

With the increase in global human population and environmental concerns, the need for renewable energy is also increasing. Biodiesel has become more attractive recently because of its environmental benefits. The synthesis of biodiesel has therefore become more challenging. Transesterification reaction is currently the most appropriate and convenient method. The same has been simulated as part of this thesis work. The meshing software GAMBIT v.2.4 and CFD software ANSYS Fluent v.16.2 was successfully used for modelling and simulating the biodiesel synthesis process in a tubular reactor:

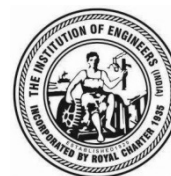
- The transesterification reaction was modelled using waste soybean oil and methanol. Kinetic data from the literature has been used to study the chemical reaction.
- The results were validated with literature values which showed that the conversion obtained from the simulation is acceptable.
- Transesterification reaction can also be mass transfer limited. To study the effect of mass transfer on the biodiesel yield, the diffusion coefficients were employed. The results show that the yield of biodiesel has increased when the reaction is mass transfer limited for all combinations of the temperature and molar ratio.

References

- [1] Sarin, Amit, Biodiesel: Production and properties. *Royal Society of Chemistry* (2012).
- [2] Thanh, Le Tu, *et al.* "Catalytic technologies for biodiesel fuel production and utilization of glycerol: A Review." *Catalysts*, 2, 191–222 (2012).
- [3] Portha, J.F., Allain, F., Coupard, V., Dandeu, A., Girot, E., Schaer, E. and Falk, L., Simulation and kinetic study of transesterification of triolein to biodiesel using modular reactors. *Chemical Engineering Journal*, 207, 285–298 (2012).
- [4] Diasakou, M., Louloui, A. and Papayannakos, N., "Kinetics of the non-catalytic transesterification of soybean oil." *Fuel* 77.12 (1998): 1297–1302.
- [5] Freedman, Bernard; Butterfield, Royden O. and Pryde, Everett H. "Transesterification kinetics of soybean oil 1." *Journal of the American Oil Chemists' Society*, 63.10 (1986): 1375–1380.
- [6] He, Huayang, *et al.* "Transesterification kinetics of soybean oil for production of biodiesel in supercritical methanol." *Journal of the American Oil Chemists' Society*, 84.4 (2007): 399–404.
- [7] Nouredini, Hossein and Zhu, D. "Kinetics of transesterification of soybean oil." *Journal of the American Oil Chemists' Society* 74.11 (1997): 1457–1463.
- [8] Cao, Peigang, André Y. Tremblay and Dubé, Marc A., "Kinetics of canola oil transesterification in a membrane reactor." *Industrial and Engineering Chemistry Research*, 48.5 (2009): 2533–2541.
- [9] Al-Zuhair, Sulaiman, Fan Wei Ling and Jun, Lim Song. "Proposed kinetic mechanism of the production of biodiesel from palm oil using lipase." *Process Biochemistry*, 42.6 (2007): 951–960.
- [10] Darnoko, D. and Cheryan, Munir, "Kinetics of palm oil transesterification in a batch reactor." *Journal of the American Oil Chemists' Society* 77.12 (2000): 1263–1267
- [11] Bambase, Manolito E., *et al.* "Kinetics of hydroxide catalyzed methanolysis of crude sunflower oil for the production of fuel grade methyl esters." *Journal of Chemical Technology and Biotechnology* 82.3 (2007): 273–280.
- [12] Berrios, M., *et al.* "A kinetic study of the esterification of free fatty acids (FFA) in sunflower oil." *Fuel* 86.15 (2007): 2383–2388.
- [13] Koh, May Ying and Tinia Idaty Mohd Ghazi. "A review of biodiesel production from *Jatropha curcas* L. oil." *Renewable and Sustainable Energy Reviews* 15.5 (2011): 2240–2251.
- [14] Ma, Fangrui, Clements, L.D. and Hanna, M.A. "The effects of catalyst, free fatty acids, and water on transesterification of beef tallow." *Transactions of the ASAE*, 41.5 (1998): 1261.
- [15] Shay, E. Griffin. "Diesel fuel from vegetable oils: status and opportunities." *Biomass and Bioenergy*, 4.4 (1993): 227–242.
- [16] Nagle, Nick and Lemke, Pete. "Production of methyl ester fuel from microalgae." *Applied Biochemistry and Biotechnology* 24.1 (1990): 355–361.
- [17] Dunford, Nurhan Turgut. *Biodiesel production techniques*. Oklahoma Cooperative Extension Service, Division of Agricultural Sciences and Natural Resources, 2007.
- [18] Moser, Bryan R. "Biodiesel production, properties, and feedstocks." *Biofuels*. Springer New York, 2011. 285–347.
- [19] Freedman, B.E.H.P., Pryde, E.H. and Mounts, T.L. "Variables affecting the yields of fatty esters from transesterified vegetable oils." *Journal of the American Oil Chemists Society* 61.10 (1984): 1638–1643.
- [20] Ali, Yusuf. "Beef tallow as a biodiesel fuel." (1995).
- [21] Klofutar, Boštjan, *et al.* "The transesterification of rapeseed and waste sunflower oils: mass-transfer and kinetics in a laboratory batch reactor and in an industrial-scale reactor/



- separator setup.” *Bioresource technology* 101.10 (2010): 3333–3344.
- [22] Wen, Zhuqing and Petera, Jerzy. “CFD Numerical Simulation of Biodiesel Synthesis in a Spinning Disc Reactor.” *Chemical and Process Engineering*, 36.1 (2015): 21–37.
- [23] Richard, Romain; Thiebaud-Roux, Sophie and Prat, Laurent. “Modelling the kinetics of transesterification reaction of sunflower oil with ethanol in microreactors.” *Chemical Engineering Science* 87 (2013): 258–269.
- [24] Mueanmas, Chokchai; Prasertsit, Kulchanat and Tongurai, Chakrit. “Transesterification of triolein with methanol in reactive distillation column: simulation studies.” *International Journal of Chemical Reactor Engineering* 8.1 (2010).
- [25] de Boer, Karne and Bahri, Parisa A. “Development and validation of a two phase CFD model for tubular biodiesel reactors.” *Computers and Chemical Engineering* 82 (2015): 129–143.
- [26] Syed, Alizeb Hussain, “CFD modeling for direct liquefaction of biomass in hydrothermal media” (2013).
- [27] Adeyemi, Nabeel A., *et al.* “CFD Modeling of Waste Cooking Oil Transesterification in a Stirred Tank Reactor.” *World Applied Sciences Journal*, 21 (2013): 151–158.
- [28] De Boer, Karne and Bahri, Parisa A. “Investigation of liquid-liquid two phase flow in biodiesel production.” *Seventh international conference on CFD in the minerals and process industries Melbourne, Australia*, 2009.
- [29] Santana, Harrson S., *et al.* “Numerical Study of Mixing and Reaction for Biodiesel Production in Spiral Microchannel.” *Chemical Engineering Transactions*, 43 (2015).
- [30] Stiefel, Scott and Gustavo, Dassori. “Simulation of biodiesel production through transesterification of vegetable oils.” *Industrial & Engineering Chemistry Research*, 48.3 (2008): 1068–1071.
- [31] Janajreh, Isam and Shrah, Mohammed Al. “Numerical Simulation of Multiple Step Transesterification of Waste Oil in Tubular Reactor.” *Journal of Infrastructure Systems* (2013): A4014007.
- [32] Satyarthi, J.K., Srinivas, D. and Ratnasamy, P. “Hydrolysis of vegetable oils and fats to fatty acids over solid acid catalysts.” *Applied Catalysis A: General* 391.1 (2011): 427–435.
- [33] Wang, Wei-Cheng; Natelson, Robert H.; Stikeleather, Larry F. and Roberts, William L. “CFD simulation of transient stage of continuous counter current hydrolysis of canola oil.” *Computers & Chemical Engineering* 43 (2012): 108–119.
- [34] Machado, G.D., Souza, T.L. de, Aranda, D.A.G., Pessoa, F.L.P., Castier, M., Cabral, V.F. and Cardozo-Filho, L., “Computer simulation of biodiesel production by hydro-esterification.” *Chemical Engineering and Processing: Process Intensification* (2015).



Synthesis, Characterization, Stability Evaluation and Release Kinetics of Trehalose-Encapsulated Bioactive-Nanocapsules

Surashree Sen Gupta^{*1} and Mahua Ghosh¹

Abstract: Nanocapsules containing Secoisolariciresinol Diglucoside (SDG) encapsulated with trehalose was prepared by the water-in-oil-in-water emulsion technique. They had an encapsulation efficiency of $(83.4 \pm 2.82)\%$. The size-reduction was achieved by high pressure homogenization and particle-size was (208.6 ± 2.68) nm. The morphology of the dried nanocapsules was observed to be uniform and smooth in texture. Diffraction patterns confirmed the purity of the trehalose encapsulant. Differential Scanning Calorimetry (DSC) studies detected uniformity of the outer shell structure of nanocapsules. Release was sustained in nature and continued up to 10 hours. Shelf-life studies revealed that after 30 days on being exposed to a relative humidity of 97% SDG retention was 98.2%.

Keywords: Nanocapsules, SDG, Trehalose, Emulsion, Sustained Release.

Introduction

Bioactive products like flaxseed lignans show several health promoting effects including anti-carcinogenic, oestrogenic, antioxidative effects [1–3]. The most potent flaxseed lignan is Secoisolariciresinol Diglucoside (SDG). However due to its extended structure, efficient absorption and utilization of the lignan poses a predicament. A feasible solution to this problem is the nanoencapsulation of SDG which will ensure the targeted delivery and appropriate storage of the bioactive compound by suitable means as nanoencapsulation entails the confinement of vital ingredients in a minuscule level. A range of different encapsulating methods and materials have been described [4–6]. By application of various encapsulating materials and suitable methods, the nanocapsules that are produced demonstrate specific attributes in terms of particle size, stability, method of core release and so on. Hence it is imperative that the encapsulation method for every bioactive compound should be designed specifically based on its functionality and the surrounding matrix in which it will be released. Furthermore the safety and biodegradability of the nanocarrier is also essential as the final product is intended for consumption purposes. Hence keeping all these facts in mind trehalose has been chosen as the suitable encapsulant [7] while freeze-drying method was selected as the process of encapsulation [8]. As a coating material trehalose demonstrated certain properties like temperature resistance and rheological uniformity.

Hence in the present work nanocapsules have been prepared for SDG using trehalose as the encapsulant. The prepared nanocapsules were characterized from all aspects including shelf-life and release behavior. The study showcased immense prospect of these nanocapsules for application in the food and beverage industries.

Materials and Methods

Materials

Flaxseeds were obtained from Directorate of Agriculture, Govt. of West Bengal, India. SDG was isolated from flaxseed by following the method of Al-Jumaily *et al.* [9]. Flaxseed oil was purchased from local market. D (+) Trehalose was procured from Sigma-Aldrich Co., St. Louis, USA. All other reagents were of analytical grade and procured from Merck India Ltd., Mumbai, India.

Encapsulation of SDG

A double emulsion was synthesized for encapsulating water-soluble SDG. About 1g of SDG was mixed with water which will form the inner core phase. This was heated to 60°C. Double the amount of flaxseed oil, as the amount of water taken, was mixed with span 60 and lecithin in the ratio of 70:30 and heated to 60°C. Gradually the aqueous phase containing SDG was dispersed into the oil phase under agitation with a magnetic stirrer and then blended together

¹Department of Chemical Technology, University College of Science and Technology, University of Calcutta, Kolkata-700009, India.
✉*surashree_sg@yahoo.co.in



using a high-speed blender at 60°C for 30 minutes at 5000 rpm. After complete addition of the aqueous phase, the system was cooled to bring down to room temperature. The prepared W/O emulsion was mixed with measured quantity of lecithin. 20% (w/w) of the emulsion was homogenized with 80% (w/w) of aqueous solution containing Tween 20 emulsifier and trehalose as the encapsulant. The encapsulant was used in an equal proportion as the amount of W/O emulsion (W/O emulsion: trehalose = 1:1). Tween 20 and lecithin emulsifiers were used in the proportion of 70:30. The outer aqueous layer consisted of an aqueous phosphate buffer of pH 7, with 100 mM NaCl. The W/O phase was blended with the aqueous solutions using homogenizer at 8000 rpm with 6 re-circulations using homogenizer to get pre-emulsions. The resultant emulsions were further homogenized with high speed stirrer at 30,000 rpm for 15 minute. Size-reduction was achieved by high pressure homogenization technique (NanoDebee [8799], B.E.E. International Inc., Easton, MA 02375, USA) with a hydraulic pressure of 3000 psi and a homogenization pressure of 40,000 psi and 5 cycles at 5°C.

Particle-Size Determination and Powder Production

The particle size distribution and mean droplet diameter of the emulsions were measured using dynamic light scattering technique (Nano-ZS, Malvern Instruments, Worcestershire, UK). Mean particle diameters were reported as Z-average diameters. Samples were diluted prior to the measurements to avoid multiple scattering effects, using a dilution factor of 1:10 sample-to-deionised water. Data reported was a mean of 3 consecutive readings.

The emulsions were initially frozen with liquid nitrogen (-196°C) and then stored overnight at -70°C. Next day the frozen emulsions were lyophilized. An Eyela Freeze Dryer (Type - FD-5N, Ser. No. 10160657, AC100V, and 50/60 Hz 500 W, Tokyo Rikakikai Co. Ltd., Japan) was used for freeze drying which was operated at -20°C and a chamber pressure of 13.3 Pa. The dried emulsions were crushed with mortar and pestle to get uniform powder-like products.

Efficiency of Encapsulation

Content of SDG in nanocapsules were analyzed by hydrolyzing the capsules. Approximately 10 mg nanospheres were hydrolyzed in 10 ml of 1(N) HCl solution and agitated in an orbital shaker maintained at room temperature for 12 hour at 200 rpm. After 12 hour, the oil was extracted with hexane. Hexane and ethanol were used to separate the other components. SDG comes in the ethanol phase which was then evaporated to dryness and the amount of SDG collected was noted quantitatively and confirmed spectrophotometrically. The processes were repeated three times.

Encapsulation efficiency = [(actual loading of bioactive product)/(theoretical loading of bioactive product)] × 100

Morphology

The surface morphology of the dried nanocapsules was observed using scanning electron microscopy [Carl Zeiss EVO18 (Special Edition) Germany]. Prior to observation, samples were mounted on metal grids, using double-sided adhesive tapes and coated by gold under vacuum.

Crystallinity

Nanocapsules were analyzed for crystallinity by X-Ray Diffraction (XRD) technique. Diffractometer (XPRT-PRO from Panalytical Diffractometer) was used Cu α ($\lambda = 1.5406$) as X-ray source. K $_{\alpha 1\alpha 2\beta}$ radiation from copper was used at 40 kV and 30 mA. K $_{\alpha 2}$ /K $_{\alpha 1}$ ratio was 0.50000. Scanning velocity was 1°/minute from 2° to 80°. Experiments were performed at 25°C.

Oxidative Stability

Pressurized DSC experiments were carried out for the nanocapsules to assess their oxidative stability using a TGA/DSC1 thermal analyzer from Mettler, Toledo, Switzerland, using software STAR^c System. Typically, 1 mg of sample was placed in an aluminum pan hermetically sealed with a pinhole lid and oxidized in the presence of dry air (Gateway Airgas, St. Louis, Mo, USA), which was pressurized in the module at a constant pressure of 200 psi. A 5°C minute⁻¹ heating rate from 20 to 120°C was used during each experiment. The oxidation onset was calculated from a plot of heat flow (W/g) versus temperature for each experiment. The sample was run in triplicate, and average values rounded to the nearest whole degree are reported.

Release of SDG

The nanocapsules were placed in glass bottles containing 30 mL dissolution media consisting of Phosphate Buffered Saline (PBS) with pH 7.4 which corresponds to the pH of small intestine. It was incubated in a shaking bath at 37°C and 100 rpm. At time intervals of 0, 1, 2, 3, 4, 5, 6, 7, 8, 9 and 10 hr 10 mL samples were withdrawn and filtered. 10 mL of fresh PBS was added to the mixture and the filtered residues were also added back to the dissolution media. The 10 mL filtrate was thereby processed. The filtrate was taken in a separating funnel and was extracted with hexane. The hexane layer was discarded and the ethanol layer was taken and absorbance was measured at 280 nm. The concentration of SDG was calculated according to equation (1),

$$C = A/\epsilon L \quad \dots (1)$$



Where C = concentration of SDG

A = absorbance of the SDG at maximum wave length (λ_{\max})

ϵ = molar extinction coefficient of SDG (SDG = $3208 \text{ Lmol}^{-1}\text{cm}^{-1}$ at 280 nm [10])

L = distance (1 cm)

Release Kinetics

The *in vitro* lipid release patterns were fitted to various release kinetic models like Hixson–Crowell cube root law [11] and Korsmeyer–Peppas model [12].

Shelf-life of the Nanocapsules

Evacuated, sealed desiccators filled with calcium chloride at 30°C and a beaker with saturated solution of potassium sulphate ($a_w = 0.97$) was kept overnight. 1 g of the nanocapsules was kept in a beaker inside the desiccators for 30 days. After 0, 5, 10, 15, 20, 25 and 30 days samples were removed and analyzed for moisture content and amount of SDG retention.

Moisture content: Weighed amount of capsules on a watch glass were placed in oven at 110°C for 6 hr. Gravimetric difference in weight before and after drying gives the moisture content.

SDG retention: Weighed amount of capsules were hydrolyzed with 1(N) HCl (20 mL) for 12 hour at 300 rpm. After 12 hour the samples were treated in a similar manner as above (for release study) and concentration were evaluated according to equation (1).

Statistical Analysis

Statistical analysis was performed using one-way Analysis of Variance (ANOVA). For statistical studies OriginLab software (OriginLab Corporation, Northampton, UK) was used. Values were expressed as Mean \pm SEM.

Results and Discussion

Particle Size and Efficiency of Encapsulation

The particle-size of the SDG nanoemulsion was evaluated to be (208.6 ± 2.68) nm. The generally accepted droplet-size for nanoemulsions is between 20 to 500 nm [13]. Hence in the present work an acceptable water-in-oil-in-water nanoemulsion was successfully prepared. The smaller the droplet size of emulsions better is its stability and shelf-life [13]. Hence in this case as a droplet size of 208.6 nm was achieved the nanoemulsion was free from any kind of coalescence or agglomeration behavior of the emulsion droplets.

An encapsulation efficiency of $(84.4 \pm 2.82)\%$ was achieved. The core composition plays a vital role in determining the

stability of a nanocapsule. It is important that a high SDG loading is achieved while retaining the basic nanocapsules characteristics [14]. A loss of about 16% occurred probably during the processing step. Modulating the core material composition while adjusting the processing steps are necessary to further enhance encapsulation efficiency.

Morphology

The surface morphology of the nanocapsules is observed in Figure 1. The surfaces of the nanocapsules were dry, opaque and homogeneous in nature. A dense packing along with a distinct boundary demarcation was observed for the molecules.

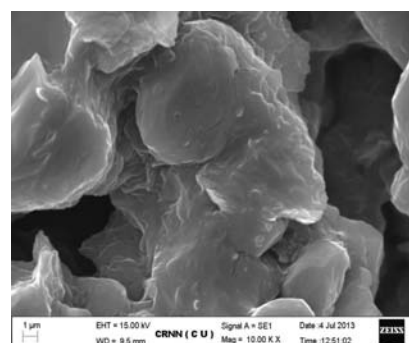


Fig. 1: SEM Micrograph of SDG Nanocapsules

Crystallinity Study

The XRD crystallograph is shown in Figure 2. XRD diffraction patterns help to understand the exact crystalline/amorphous nature of an encapsulant [15]. It is essential in this context as a clear idea regarding the purity of the shell can be interpreted from the data. Large Bragg peaks are observed in Figure 2, which is characteristic of trehalose. Hence it is affirmed that there is no crack or leakage in the nanocapsule structure as pure, unscathed trehalose structure has been detected from the crystallographic analysis.

Oxidative Stability

From Figure 3 it is evident that there are no cracks on the outermost shell of the nanocapsules. Hence the core materials were not released [16]. This observation is in parity with the XRD studies. The crystalline nature of the encapsulant is the primary factor which controls the thermal stability of the nanocapsules between 20 to 120°C . Trehalose could also withstand the entire process of nanocapsule synthesis involving the variable temperature processing, without affecting the property of the nanocapsules leading to their deterioration. Furthermore the formation of the nanoemulsion, involving choice of emulsifiers and lipid, was also quite efficient which imparted sufficient stability to the entire nanostructure.

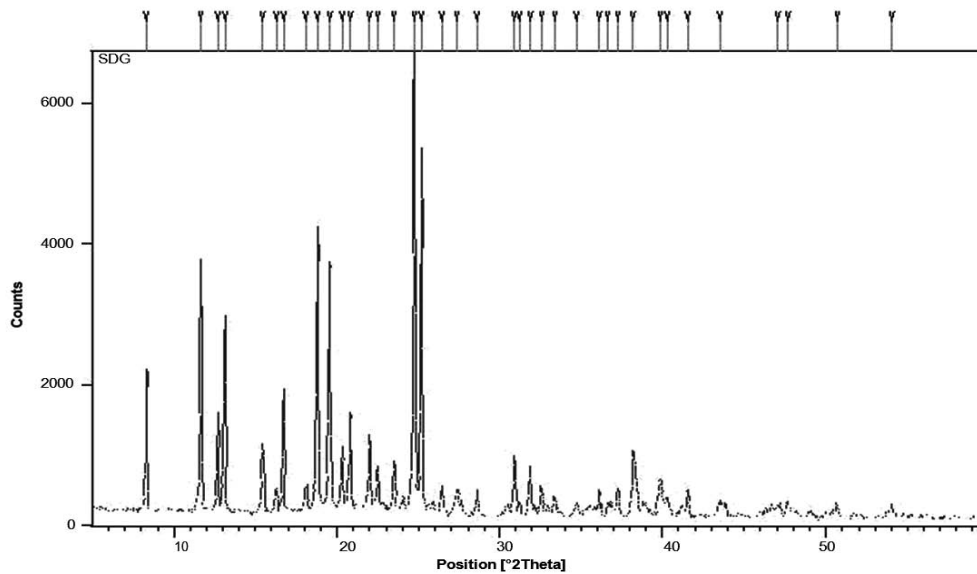


Fig. 2: XRD Crystallograph of SDG Nanocapsules

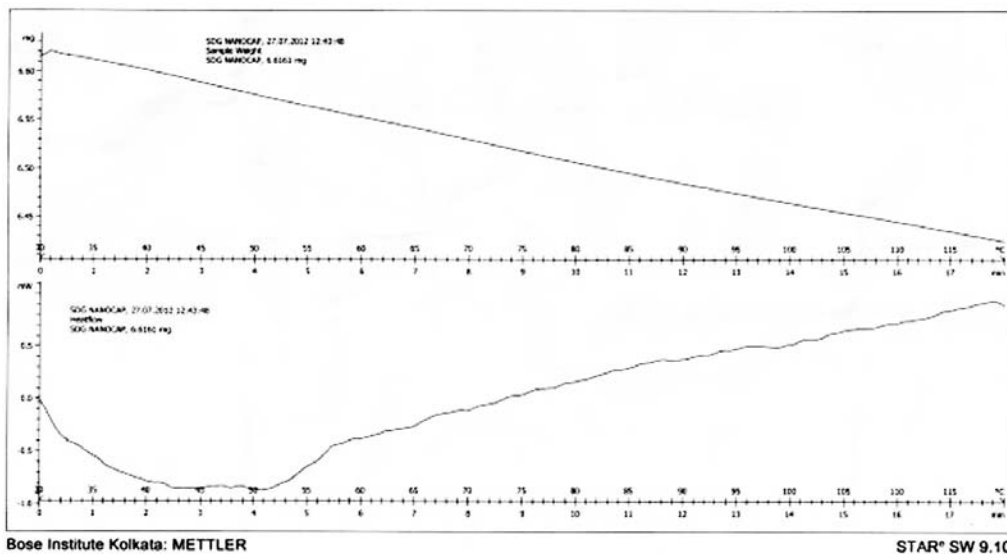


Fig. 3: DSC Graph of SDG Nanocapsules

Release of SDG

Figure 4 gives a clear picture of the release profile of SDG. After 1 hour about $(0.53 \pm 0.02) \times 10^{-3}$ mol/L, after 2 hour $(1.03 \pm 0.11) \times 10^{-3}$ mol/L, after 3 hour $(1.17 \pm 0.08) \times 10^{-3}$ mol/L, after 4 hour $(1.23 \pm 0.07) \times 10^{-3}$ mol/L SDG was detected. However after 5 hour the amount of SDG detected was gradually found to lower to $(1.22 \pm 0.05) \times 10^{-3}$ mol/L, $(1.17 \pm 0.12) \times 10^{-3}$ mol/L after 6 hour $(1.12 \pm 0.06) \times 10^{-3}$ mol/L after 7 hour, $(1.07 \pm 0.09) \times 10^{-3}$ mol/L after 8 hour

$(1.05 \pm 0.10) \times 10^{-3}$ mol/L after 9 hour, and finally $(1.04 \pm 0.08) \times 10^{-3}$ mol/L after 10 hour.

The sustained release was due to trehalose forming a compact structure and displaying slow decay. In addition, the presence of an intermediate layer of flaxseed oil also contributed towards insinuating the controlled release of SDG. Beyond 5 hours, the proportion of SDG gradually lowered because the amount of SDG released into the medium was less than the amount withdrawn. The pH-dependent release profile actually portrayed the behaviour of the nanocapsules in human small intestine.

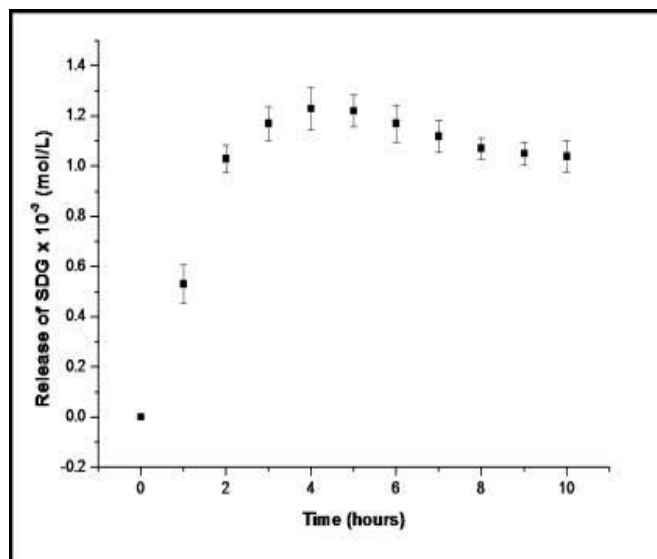


Fig. 4: Release of SDG from the Nanocapsules

Release Kinetics

The release profile of SDG from nanocapsules was plotted as cube root of lipid (%) remaining in matrix against time (Hixson-crowell cube root law) and the log cumulative lipid release (%) against log time (Korsmeyer model) (Figure 5). The release of SDG from nanocapsules was fitted in different models. It was observed that the best fit was for Korsmeyer-Peppas model, $R^2 = 0.426$ (Figure 5b) and the worst fit was for Hixson-Crowell cube root law, $R^2 = 0.147$ (Figure 5a). The value of the release exponent (n) is obtained from the Korsmeyer-Peppas model which in this case was found to be 0.228 which is less than the standard value of 0.5 (When $n = 0.5$, lipid is released from the nanocapsules with Quasi-Fickian diffusion mechanism; when $n > 0.5$, then non-Fickian or zero order release exists; when $n < 0.5$, then Fickian diffusion for spherical capsules) [12]. Here it is observed that Fickian diffusional release occurs due to the molecular diffusion process from spherical nanocapsules.

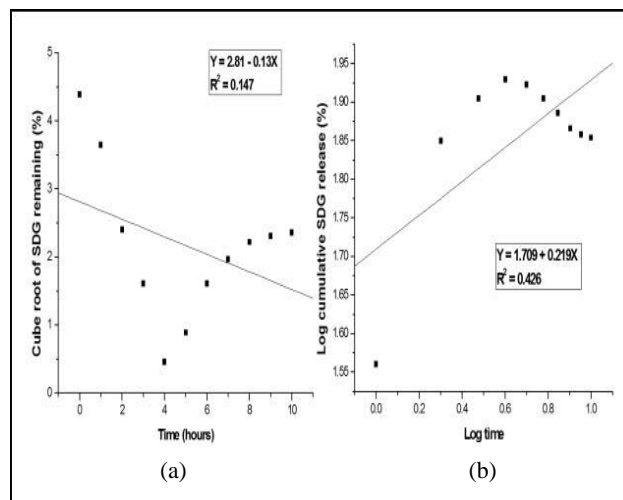


Fig. 5: Release Kinetics of SDG Nanocapsules

Shelf-Life Study

A high retention of SDG was observed for the nanocapsules upto 30 days at a water activity of 0.97 (Table 1). Humidity is a critical factor for the long time preservation of nanocapsules containing bioactive component. It plays an important role in hampering the physical and chemical stability of any emulsion based encapsulation system. Trehalose displayed an extremely moisture-resistant nature which prevented any sort of deformation of the nanocapsules. Hence much change in SDG retention was not observed during the prolonged preservation of nanocapsules upto 30 days.

Conclusion

Trehalose-encapsulated SDG nanocapsules, were successfully synthesized by multiple emulsion technique. The emulsifier system selected for the manufacture of the emulsion proved to be effective in the sustained release of SDG from the nanocapsules. An excellent shelf-life was also observed for the nanocapsules.

Table 1: Shelf-Life Study of SDG Nanocapsules

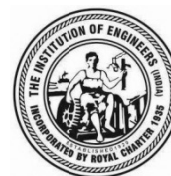
Time → (days)	SDG (%) ^a							Moisture Content (%) ^b						
	0	5	10	15	20	25	30	0	5	10	15	20	25	30
SDG nanocapsule	99.2	99.2	98.9	98.8	98.5	98.2	98.2	18.5	15.6	12.5	8.40	1.43	0.49	0.3
	±	±	±	±	±	±	±	±	±	±	±	±	±	±
	1.22	1.98	2.46	3.78	1.96	2.67	2.92	1.39	1.33	1.33	1.31	0.32	0.37	0.18

^{a,b}Values are expressed as mean ± S.E.M, n = 3.



References

- [1] Adlercreutz, H. and Mazur, W., Phyto-oestrogens and Western disease. *Ann. Med.* 29, 95–120 (1997).
- [2] Penumathsa, S.V., Koneru, S., Zhan, L., John, S., Menon, V.P., Prasad, K. and Maulik, N., Secoisolariciresinol diglucoside induces neovascularization-mediated cardio-protection against ischemia-reperfusion injury in hypercholesterolemic myocardium. *J. Mol. Cell Cardiol.* 44(1), 170–179 (2007).
- [3] Zhang, W., Wang, X., Liu, Y., Tian, H., Flickinger, B., Empie, M.W. and Sun, S.Z., Dietary flaxseed lignan extract lowers plasma cholesterol and glucose concentrations in hypercholesterolaemic subjects. *Br. J.Nutr.* 99(6), 1301–1309 (2008).
- [4] Funhoff, A.M., Monge, S., Teeuwen, R. and Koning, G.A., N.M.E. Schuurmans-Nieuwenbroek, D.J.A. Crommelin *et al.*, PEG shielded polymeric double-layered micelles for gene delivery. *J. Control Release* 102, 711–724 (2005).
- [5] Galindo-Rodriguez, S., Allemann, E., Fessi, H. and Doelker, E., Physicochemical parameters associated with nanoparticle formation in the salting-out, emulsification–diffusion and nanoprecipitation methods. *Pharm. Res.* 21, 1428–1439 (2004).
- [6] Garipey, E.R., Leclairb, G., Hildgen, P., Gupta, A. and Leroux, J.C., Thermosensitive chitosan-based hydrogel containing liposomes for the delivery of hydrophilic molecules. *J. Control Release*, 82, 373– 383 (2002).
- [7] Cerimedo, S.M.A., Cerdeiro, M., Candal, J.R. and Herrera, L.M., Microencapsulation of a low-trans fat in trehalose as affected by emulsifier type. *Journal of the American Oil Chemists’ Society*, 85(9), 797– 807 (2008).
- [8] Desobry, S.A., Netto, F.M. and Labuza, T.P., Comparison of spray-drying, drum-drying and freeze-drying for b-carotene encapsulation and preservation. *Journal of Food Science*, 62(6), 1158–1162 (1997).
- [9] Al-Jumaily, E.F., Al-Shimarya, A.O.A. and Shubbr, E.K. Extraction and Purification of lignan compound from flax seed *Linum usitatissimum*. *Asian Journal of Plant Science and Research*, 2(3), 306–312 (2012).
- [10] Farah, H., *Antioxidant properties of flaxseed lignans using in vitro model systems*. A Doctoral Thesis submitted to the College of Pharmacy and Nutrition of the University of Saskatchewan, Saskatoon, Saskatchewan, Canada (2006).
- [11] Hixson, A.W. and Crowell, J.H., Dependence of reaction velocity upon surface and agitation (I) theoretical consideration. *Ind. Engg. Chem.*, 23, 923–931 (1931).
- [12] Korsmeyer, R.W., Gurny, R., Doelker, E., Buri, P. and Peppas, N.A., Mechanisms of solute release from porous hydrophilic polymers. *Int. J. Pharm.* 15, 25–35 (1983).
- [13] Sharma, N., Bansal, M., Visht, S., Sharma, P.K. and Kulkarni, G.T., Nanoemulsion: A new concept of delivery system. *Chron. Young Sci.*, 1, 2–6 (2010).
- [14] Delmas, T., Fraichard, A., Bayle, P.-A., Texier, I., Bardet, M., Baudry, J., Bibette, J. and Couffin, A.-C., Encapsulation and Release Behavior from Lipid Nanoparticles: Model Study with Nile Red Fluorophore. *Journal of Colloid Science and Biotechnology*, 1, 16–25 (2012).
- [15] Gupta, S. Sen and Ghosh, M., Comparative study of the properties and release kinetics of two different types of nanocapsules based on polysaccharide encapsulants. *Nutrition and Food Science International Journal*, 1(2), 001–007 (2016).
- [16] Gupta, S. Sen and Ghosh, M., Synthesis, characterization, stability evaluation and release kinetics of fiber-encapsulated carotene nano-capsules. *GRASAS Y ACEITES* 66 (4), e104 (2015).



Bio-Nanotube and Regenerative Medicine: A New Look to Molecular Engineering Design

N.K. Brahma¹

Abstract: Nanotechnology and regenerative medicine are to be considered as smart appropriate technology in social and medical engineering for the welfare of human well being in future. The trends of engineering design are rapidly changing due to population explosion, pollution and biodiversity. The classical engineering concepts of Civil, Mechanical, Polymer, Electrical, Electronics and Telecommunication, Chemical, Environment, Architecture, Computer and Agriculture, with similar importance are moving towards smart (i.e., to reduce time, space and energy) design, slowly shifting from classical design to molecular design. Nanotechnology, Genetic Engineering and Imaging supported to design/develop new material (polymer), usable to environment, medical and engineering applications. Carbon Nanotube (CNT) is one example. However CNT has side effect in case of medical applications and in drug delivery. To replace CNT immobilized with different drugs, antibacterial, anticancer target specific, silver (Ag), gold (Au), platinum (Pt) nanomaterials are used in chemotherapy. To reduce side effects of host-vs-graft activities and immune suppression, Bio-Nanotube (BNT) is designed and is applied in animal model.

The author in this paper will discuss the application of BNT as for chemotherapy and vaccine development for new look of molecular design.

Keywords: BNT, CNT, Regenerative Medicine, Vaccine, Totipotent.

Introduction

A Bio-Nanotube (BNT), was conceptualized in Figure 1. BNT was isolated from Genetically Engineered (GE) *Escherichia coli* K-12 Yale strain and was used for antidiarrheal vaccine on Balb/C mice. Immune response was identified on BNT (Fimbriae/pili) of GE *E. coli* bacteria, without observing any side effect of cellular damage on mice, when inoculated. Regenerative medicine is the consideration of regeneration of damaged and amputated tissue

and bones, applicable in case of cancer and accident. BNT involved in repairing and immune response of cells and tissues in Balb/C, 8 weeks old male mice and was designed in GE bacteria as shown in Figure 2 [1, 2] and to replace Carbon Nanotube (CNT), Figure 3, steps were used. Totipotent tissue, scaffolding tissue growth has been similarly conceptualized, inoculated *in vivo* into mice. A double mantel CNT structure is reproduced in Figure 4.

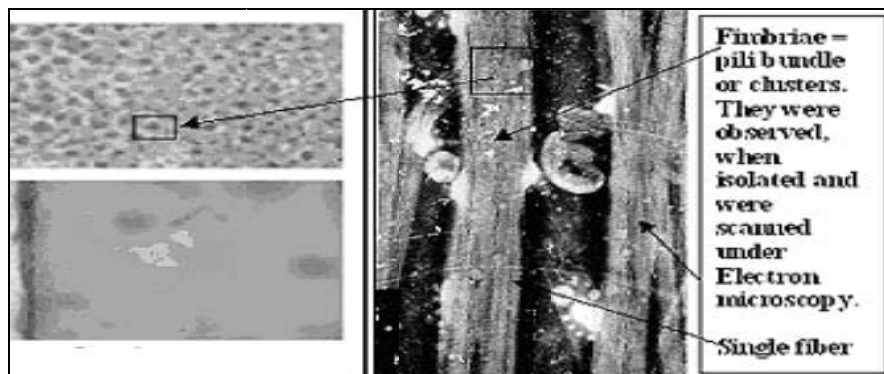


Fig. 1: Clustering Scanning Electron Microscopy (SEM) View of BNT (Fimbriae/pili), Appeared as Dots on Membrane

¹ Institute of Genetic Engineering, Badu, Kolkata-700128, India. ✉ profbrahma@gmail.com; nkbrahma@rediffmail.com

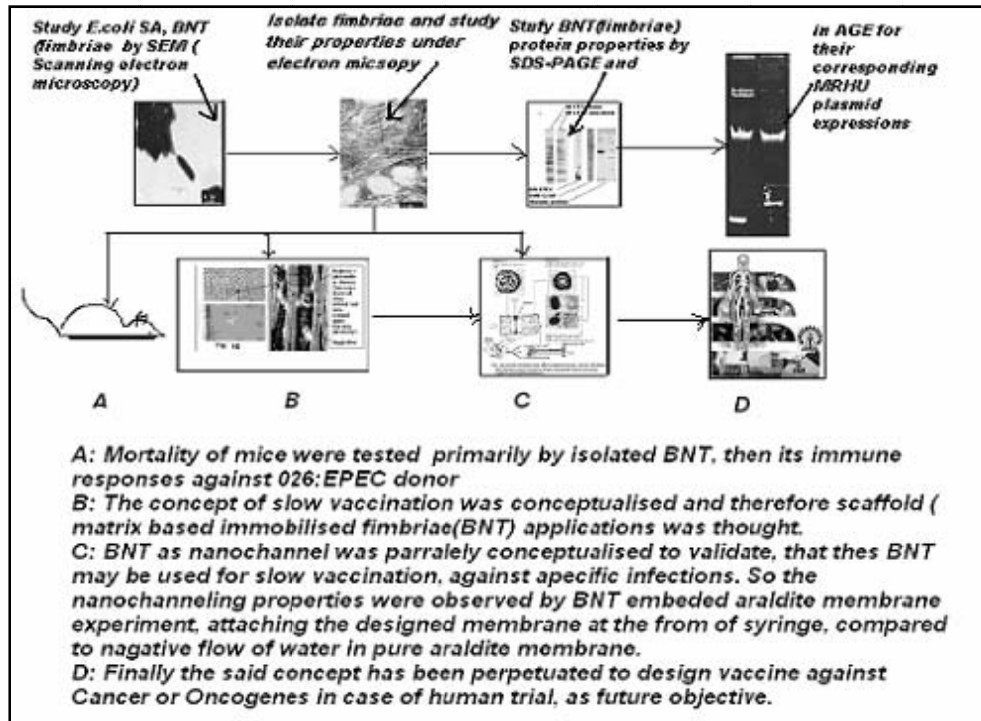


Fig. 2: Steps for Vaccination and Regeneration

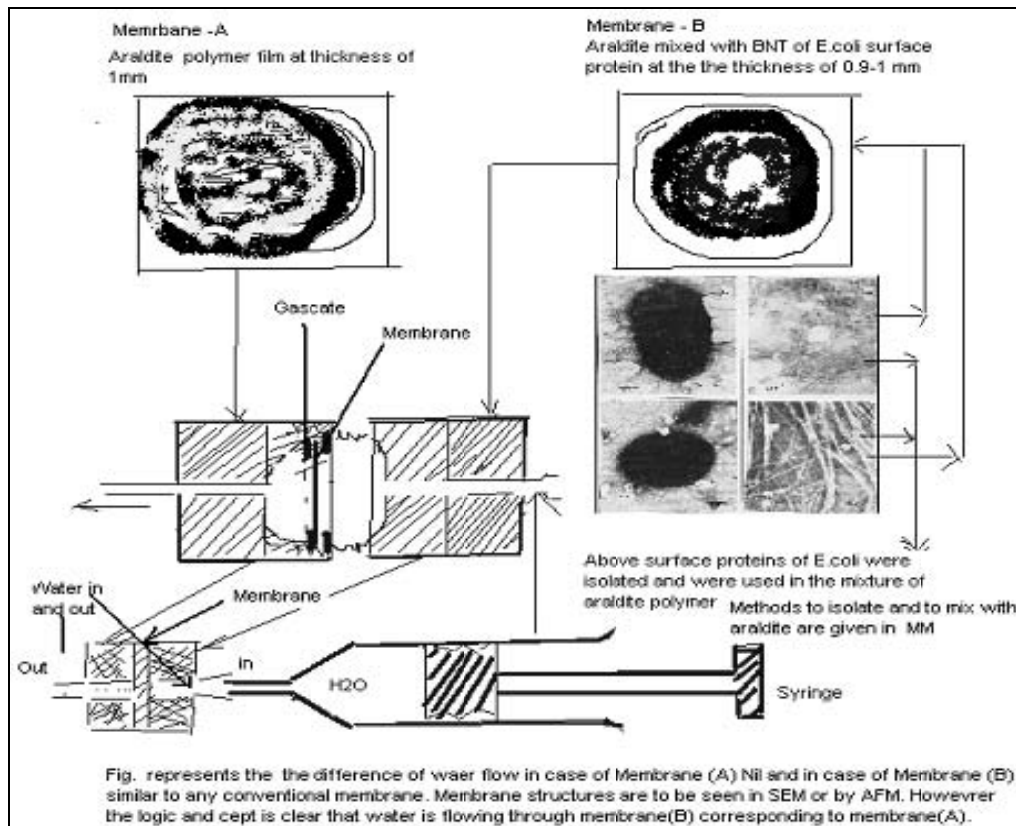


Fig. 3: Syringe and Membrane based BNT Delivery Process

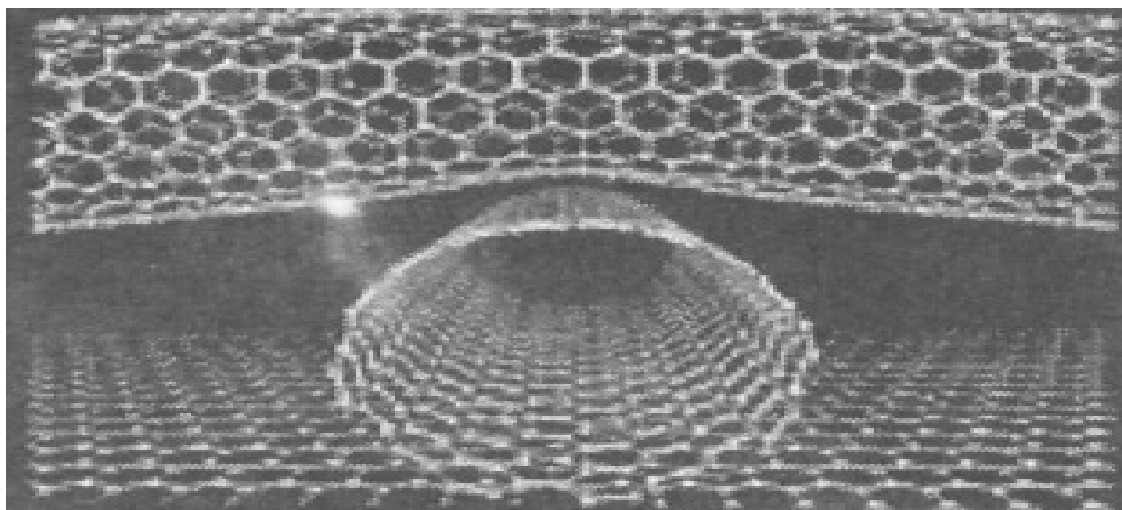


Fig. 4: Double Chambered CNT

Steps Involved in Designing Molecular Engineering of BNT for Animal Model

E. coli K-12 was collected from the source HCL-Pune. It was preserved in slant and in other appropriate vials.

Cells were also preserved in glycerin based eppendorf tube in deep freeze of -45°C to -75°C and or as dry cell in sealed glass. The strain was then inoculated to nutrient broth and was grown in 2 lt cultures. In case of rapid Deoxyribo Nucleic Acid (DNA) isolation, the culture of cell was kept in one eppendorf tube at 1 ml volume. The cells were then centrifuged. Pellets were then washed by sterile distilled water and then by Tris-HCL at pH 7.8. The cells were then lysed by lytic buffer. The lytic buffer contains alkaline pH of 12.34, containing SDS (sodium Dodecyl Sulphate), EDTA, Tris and lysozyme pH was adjusted by NaOH and HCL through digital pH meter at room temperature of 25°C . The risk starts when the cell lyses and naked DNA comes out from the cell. Starting from isolation of DNA, measures to prevent contamination should be taken very carefully in microbiological laboratory. In case of pathogenic microbes, the risk of contamination is high in laboratory. But in case of isolated DNA, the risk factor is increased thousand times with respect to cell engineering and manipulation and the same has the impact to environment also, if the methodology fails to synthesis DNA, Ribonucleic Acid (RNA), protein, (i.e., the products applicable to regenerative medicine and environment) [1–7].

A New Look of Molecular Engineering

GE and Molecular Engineering (ME) need proper measurement like any classical engineering design. For example the growth of microbes required time-vs-population growth measurement, including to look other biological factors like

properties of DNA, represented by plasmid, chromosome, which support to carry biological information. ME concepts as developed by microanalysis, like micropipetting, cutting of DNA by restriction enzyme to design new plasmid molecules, which may express the desired protein in *E. coli* K-12, Yale strain, after giving proper pH, temperature, nutrient and selective media support to protect from infection and maintain sterility to isolate desired target specific protein molecules (i.e., not to allow hybrid DNA, transconjugant proteins to express prototroph protein). To hold constitutive auxotrophic phenol-genotypes and for desired protein expressions, selection of transconjugant for ME design is important, which will not allow any entry of foreign DNA. Chemical Engineers understand fermentation and product yield but fail to realize the potential power of microbes from different sources, which can corrupt the system by infecting bioreactors of capacity 1000 lt, causing damage to billion dollars project. To supply the fermented product to Down Stream Process (DSP), which involves the maximum cost (75%) in pharmaceutical industries and obey all basic processes of chemical mechanical unit operation, separation technologies (i.e. centrifugation, filtration, drying, etc.) and preparation of drugs (either in the form of solid powder and/or as liquid/gel encapsulated in the form of capsule). Up to the Up Stream Process (USP), all steps must be carried out maintaining absolute sterility to pure form of DNA expressing replication, transcription and translation to generate desired protein like insulin, growth hormones, anti-diarrheal vaccine.

Bacterio-Genetical DNA Application in Production of Diarrhea Vaccine

The engineers and the scientists have to realize the importance of the bacterio-genetical studies, to control all



necessities of human well-being in future, starting from medicine, food and pollution control. The strength of microbes is not to be underestimated and has already been mentioned by Louise Pasteur about 100 years ago. It seems, to day, that microbial population can grow like any dimensions of galaxy, if they are being allowed growing continuously and can cover the whole surface of the earth within few months and days. The microbes ferment or oxidize any amount of substrate in few minutes or days, if the environment supports them to grow. One example is the dead animals get fouled, transformed to a liquid mass or skeleton, spreading obnoxious smells to the environment, due to bacterial contamination.

So the utility of microbes can be divided in two parts. The first is for using microbes for the benefits of mankind, aseptically and the second is to protect mankind from infectious diseases or pest derived from microbes. The utility of microbial tools actually remains under the control of scientists and engineers, to use them as alternative to nuclear power. The knowledge to deal microbes aseptically using classical microbiology to GE and ME applicable to medicine, environment and engineering design classical bacteriogenetics to molecular DNA, DNA cloning and large production of industrially important microbes and finally to study GE and ME. Another important aspect would be that after the classification of DNA, RNA and protein, researcher and engineer should think first how to use these microbes aseptically for maximum benefits. To describe this, author has chosen the basic diarrhea infection of human and domestic animals. A case study has been chosen, which would be described in following steps:

- Different pathogenic bacterial strains were collected and their pheno-genotypical characters at the laboratory scale were studied at different cross over *E. coli* K-12 nal[®], sm[®] recipient (F⁻) strain studies.
- The pathogenic and toxigenic activities of these pathogenic microbes were also studied occasionally on Balb/C mice.
- The experiments were carried out to investigate and isolate important bacterial strains possessing Colonization Factor Antigen (CFA) and virulence properties.
- Plasmid DNA was isolated in agarose gel electrophoresis method and their molecular weights profiles were studied [3–5].
- For different bacterial pathogenic and toxigenic activities, some specific diarrhea causing bacteria were collected.

These bacteria caused severe diarrhea to domestic animal and human. To prove, that foreign specific DNA, as isolated from *E. coli* or from distant species of enterobacteriaceae, may be plasmids born, if they are confirming pathogenic and toxigenic natures. In addition to that it is also recognized,

that the R-plasmids are frequently observed among these pathogenic and toxigenic *E. coli*, belonging to Enterotoxigenic *E. coli* (ETEC) and Enteropathogenic *E. coli* (EPEC) and several other UTI or urinary tract infecting groups.

To carry out such bacterio-genetical assays, the next attempt was to study the plasmid profiles of pathogenic *E. coli* or any industrially important microbes (bacteria). As soon as it is completed, one has to study the transferable conjugative natures of plasmids into *E. coli* K-12 C600 Yale strain by simple conjugation, i.e., the transferability of bacterial donor plasmids *in vivo* into *E. coli* K-12 to study the plasmid gene expression. By this process conjugative (transferable) and non-conjugative (non-transferable) plasmids were separated. Hybrid conjugants were selected by means of counter-selective assays. To verify the process, that a counter-selective *E. coli* K-12 carries donor plasmid, autoradiographic analysis was carried out and DNA plasmid profile were analyzed. In case, autoradiography tests are not possible, then plasmid profile tests by (RE) must be carried out.

Auxotrophic *E. coli* K-12 is a well known bacteria strain, whose genetic properties are thoroughly studied all over the world. It is used to study bacteriogenetics, rDNA technology, biochemistry, biotechnology and biochemical engineering. In this study, plasmid transformations of two selective donors of positive MRHU (+) plasmid 08: ETEC and 026: EPEC, were selected. These strains caused severe diarrhea and are born with MRHU (+) factor. The earlier studies of conjugation, showed that the recipients of *E. coli* K-12 occasionally received donor MRHU (+) plasmid, but were transformed to prototroph during transconjugant MRHU (+) plasmid expression. After counter-selection, hybrid auxotrophic *E. coli* K-12 were transformed into phototrophic recombinants/transconjugants, which damaged the genetic study of hybrid transconjugants/recombinants. The reason to study MRHU (+) diarrhea causing activities of donor at selective genetic markers were impossible.

Global Chemotherapeutic Demands

Depending upon the particular fields of chemotherapy, the application of GE and BNT concepts are optimized and can differ with respect to their priorities. Usually these objectives include a number of different criteria. The general objectives of bioprocess optimization can be process stabilization, quality assurance and cost management [7, 8]. Special objectives of bioprocess optimization can be used for instance in product biotechnology for high product yield, i.e. high productivity low substrate consumption, high product quality, efficient control of metabolic activity and unit operations, efficient downstream processing efficient process scheduling, low overall costs of the entire process, high process reliability and reproducibility. For instance in environmental biotechnology, cost-effective pollution process reliability and

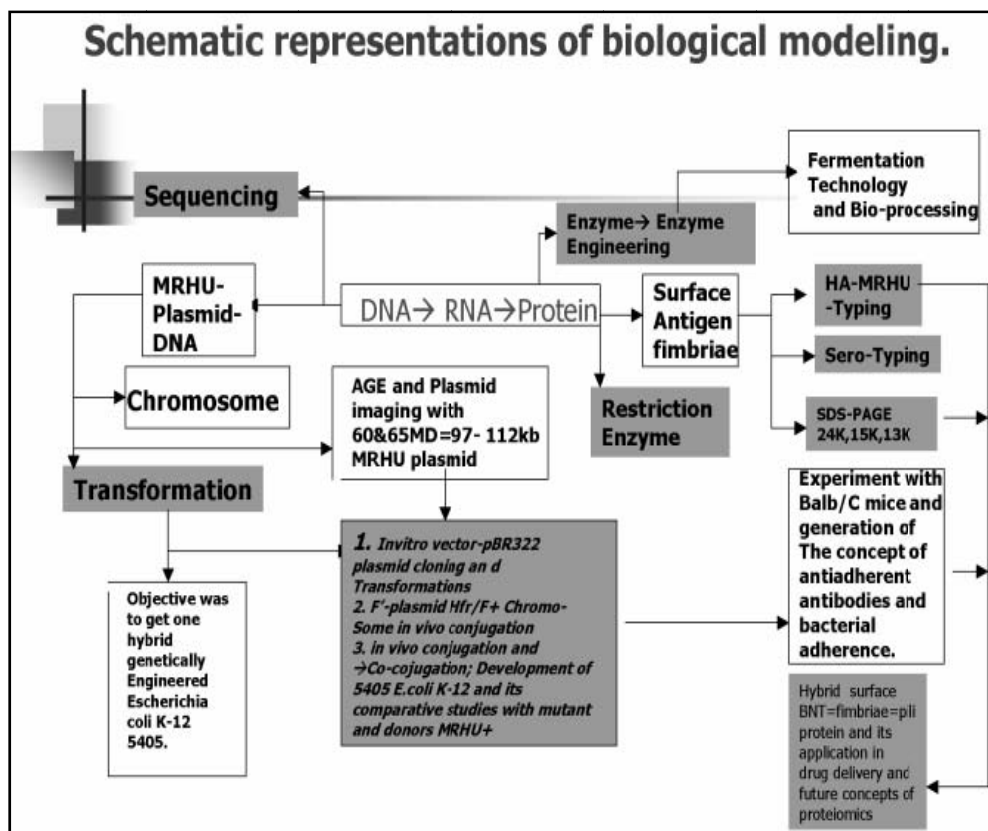


Fig. 5: Steps/Algorithm as Used to Design Genetically Engineered and to Select BNT like Nanotube

reproducibility. For instance in environmental biotechnology, cost-effective pollution control, compliance with legal requirements, minimization of energy costs, efficient biological, chemical and physical unit operations are easier to implement. An efficient operation is depending on changing loads, low overall costs of the entire process, high process reliability and reproducibility, for instance in food biotechnology, high product quality, product safety, efficient control of metabolic activity, efficient unit operations, efficient process scheduling, low overall costs of the entire process, high process reliability and reproducibility are essential [8–11]. In medicine, patient well-being; reliable, quick and cost-effective diagnosis; reliable, adequate and efficient diagnosis and therapy, individual and patient friendly diagnosis and therapy, minimization of treatment costs are essential and the same is possible through ME, GE and paradigm shift of engineering design.

Conclusion

BNT ME conceptually describes its uses and applications in designing ME and regenerative medicine. ME is represented by classical, thermo dynamical mathematical, experimental search methods and obey the following steps:

- Select a system,
- Select variables,
- Perform experiments and test product,
- Submit data for statistical and regression analysis,
- Specifications for feasibility program,
- Select constraints for grid search,
- Evaluate grid search, defined by appropriate equations.

It does not require continuity or differentiable mathematical function. For pharmaceutical product optimization, two major steps were used: (a) feasibility search, as used to locate set of response constraints that are just within the limit of possibility and (b) grid search. Experimental range is divided into grid of specific sizes. ME outcome can be related to quite different criteria, such as maximum product yield in pharmaceutical industry, high quality in food production, maximum remediation performance in environmental biotechnology, in a wider context, well-being of patient through medicine. Many bioprocesses still have the potential to be improved considerably with respect to these criteria. In order to achieve substantial improvements in ME designs, a systematic approach to bioprocess optimization is required. Using Biocontrol's intelligent technologies, the



systematic approach of biocontrol can be achieved. The expertise of biotechnology and information technology provides the right combination to put this optimization potential successfully into practice. Biocontrol approach covers theoretical and experimental aspects of bioprocess analysis and optimization in order to implement novel optimization strategies.

References

- [1] Brahma, N.K., Enterobacterial MRHA plasmid and its possible Genetic Transformation with *Escherichia coli* K-12 at auxotrophic Phenotypes. *Indian J. Microbial*, 38 (4); 43–50 (1999).
- [2] Brahma, N.K., Genetically Engineered Hybrid 5405 E.coli K-12 fimbriae in vaccination with Balb/c mice against 026: serotype EPEC diarrhea. *Ind. Chem. Engg.*, 39; (1) 17.
- [3] Martin, R.B., Fisher, M.E., Minchin, R.F. and Teo, K.L., *Mathematical Biosciences*, 99(2), 205–230 (1990).
- [4] Brahma, N.K. (TBMIAO). www.Saboi.Org. Vol. 21(1); 20–28 (2007).
- [5] Brahma, N.K., ITCSE, (Introduction to Chemical Science and Engineering) Lambert Pub, USA, Germany, IEI Library (2010).
- [6] Feng, S.S. and Chien, S., Chemotherapeutic engineering: Application and further development of chemical engineering principles for chemotherapy of cancer and other diseases. *Chemical Engineering Science*, 58(18), 4087–4114 (2003).
- [7] Liang, Y., Leung, K.-S. and Mok, T.S.K., A novel evolutionary drug scheduling model in cancer chemotherapy. *IEEE Transactions on Information Technology in Biomedicine*, 10(2), 237–245 (2006).
- [8] Parker, R.S. and Doyle, F.J., Control-relevant modeling in drug delivery. *Advanced Drug Delivery Reviews*, 48, 211–228 (2001).
- [9] Zitzler, E., Evolutionary algorithms for multi-objective optimization: Methods and applications. *Swiss Federal Institute of Technology, Zurich* (1999).
- [10] Patil, P.D. and Gude, V. Gnaneswar, *et al.*, Optimization of direct conversion of wet algae to Biodiesel Under Super critical Methanol condition, *Biosource technology*, 102:118–122 (2011).
- [11] Rashid, U. and Fidunder, S., Tiago Vicente PhD Seminar, Animal Cell Technology Lab, *Adv. Biochemical Engg. Biotech*, 53:17–59 (1999).



Bio-Engineering Approach to Control River Bank Erosion

T. Sanyal¹

Abstract: River bank erosion is a natural hazard that manifests more commonly in regions with unstable soil stratification. Causes behind river bank erosion are several, the most common being large water level fluctuation of river. Fluvial drag and vortices at bank toe are other common causes. Design principle for bank protection against erosion is based on i) prevention of migration of bank soil, ii) facilitating dissipation of pore water intruded into the bank soil without disturbing the bank configuration and iii) inducing accretion of silt on the eroded bank. Besides providing direct protection of the affected bank, sometimes structural interventions may be necessary in conjunction. The conventional practice of placing granular inverted filter over eroded banks, apart from environmental limitations, is fraught with constructional impreciseness leading to recurrence of failure. As a result bio-engineering measures are now being increasingly favored even in developed countries to control river bank erosion. Bio-engineering approach is engineered utilization of appropriate natural resources keeping in view site-specific technical needs. Jute Geotextiles (JGT), a kind of technical textile, in conjunction with appropriate vegetation can cater to the technical requirements as effectively as inverted granular filter. Vetiver grass in rivers carrying sweet water and mangroves in brackish water zones are effective as soil-binder, silt-inducer and flow-attenuator. JGT incidentally has been used successfully in more than fifty eroded river banks all over the country. It is felt that given the environmental adversities looming large, bio-engineering approach for control of river bank erosion strongly deserves encouragement by the Government and engineers.

Keywords: Bio-Engineering, Jute Geotextile, Transmissivity, Vetiver, Mangroves.

Introduction

Erosion of banks of rivers and waterways is a frequently occurring phenomenon especially in regimes with unsettled soil stratification. There are several reasons for river bank erosion of which the combined effect of rise of water level in rivers during the monsoon and drawdown thereafter is the most common. Velocity of flow hugging a bank, eddies at the bank toe, severe wind-induced waves are other common causes of river bank erosion. The conventional approach to control river bank erosion is to place inverted granular filter over the affected bank after correcting the bank slope to a stable profile. With development of geotextiles the function of filter required to stabilize the eroded bank can be far better managed. The current trend is to adopt bio-engineering measures which utilize natural resources to protect the eroded/erosion-prone river banks. This is in essence utilization of engineered natural resources to control soil-related distresses as in the case of river bank erosion. The paper discusses in brief the basic technology and the natural implements that can be engineered to control river bank erosion.

Causes of River Bank Erosion

As indicated the most common cause of river bank erosion is sharp water level fluctuation. Water above the ambient level during the rains intrudes into the bank soil and the intruded pore water tries to force its way back into the river when the level goes down, toppling the bank soil in the process. Extent of intrusion of water into bank soil depends principally on hydraulic conductivity of bank soil while magnitude of erosion of bank is a factor of its 'erodibility'. At ambient level of water in rivers banks seldom erode as pore water pressure within bank soil is counter-balanced by water pressure of river. River erosion takes place when hydraulic gradient is formed due to recession of water level. The other reason of bank erosion is the frictional drag exerted by the flow hugging it. River bank may succumb to such fluvial erosive forces ('erosivity') exerted on bank. The third common cause is formation of eddies at the bank toe which eat up bank soil progressively from bottom.

Strong wind-induced waves may also cause bank erosion. Waves generated by large vessels may also erode river banks occasionally.

¹ Former Chief Hydraulic Engineer, Calcutta Port Trust, Kolkata & Former Chief Consultant, National Jute Board, Govt. of India.
✉ sanyaltapobrata@gmail.com



Remedial Principle

The basic principle to control river bank erosion caused as a result of water level fluctuation is i) to check migration of soil particles from the affected bank and ii) to facilitate dissipation of pore water pressure generated within bank soil. Understandably what is needed is a filter over the affected bank that can fulfill both the requirements concurrently. Granular inverted filter is conventionally recommended for the purpose. To control erosion caused by fluvial frictional drag, usually repulsion of flow away from the bank by construction of spurs etc is advocated. Eddies at bank toe may be controlled by building submerged spurs. The conventional practice of placing granular inverted filter over eroded banks, apart from environmental limitations and high cost, is fraught with constructional impreciseness leading to recurrence of failure. As a result bio-engineering measures are now being increasingly favored even in developed countries to control river bank erosion.

Bio-Engineering Technique

Simply expressed, bio-engineering approach is engineered application of appropriate natural resources keeping in view the remedial principle as indicated and site-conditions. The two remedial functions are carried out by geotextiles, preferably natural geotextiles while function of soil-binding is done by appropriate vegetation. Each part of a plant performs distinct functions. Roots increase hydraulic conductivity of soil and reinforce them by performing functions of anchorage, absorption, conduction and storage. Stems help in interception of soil particles on move. Leaves aid storage and enhances aesthetic appeal. Pore water pressure in the underground is eased off due to transpiration through roots. Vegetation with deep roots and high survivability rate should be chosen considering the climatic and geotechnical conditions. Vegetation strengthens the top soil improves integrity of the soil body.

Role of Geotextile in River Bank Erosion Control

Filtration, the critical requirement for designing a protective cover over the eroded bank, as indicated implies two-fold functions viz a) checking migration of bank soil particles and b) easing of confined pore water within the bank soil. A filter over the affected bank is needed till vegetation is sufficiently mature to perform its expected functions. Filtration function is best performed by specially made fabric known as geotextile—a kind of technical textile having its pores so designed as would not allow the most of bank soil particles to pass through and. at the same time facilitate passage of pore water across (‘permeability’) and along (‘transmissivity’) it. Understandably the functions are contrasting. Optimizing the pore size of geotextiles holds the key as smaller the pore size, the better will be particle-restraint and the lower will be

its permeability. Prior judicious empirical compromise of pore size is thus called for. Geotextile should be tailor-made to cater to this requirement, besides possessing adequate tensile strength to withstand installation and other imposed stresses. Synthetic (polymeric) geotextiles are commonly used in the overseas for its durability, dimensional uniformity and affordable price. But it suffers from environmental limitations as polyamides, polyethylene etc that go in its making are not eco-concordant. It is for this reason natural geotextiles, especially Jute Geotextiles (JGT) is being increasingly favored for its eco-compatibility, spinnability and high initial modulus as an integral component of bio-engineering technique. JGT in addition supports growth of vegetation and biodegrade after leaving nutrients as residue hastening growth of vegetation for soil-binding.

Design Elements

Design of JGT should thus focus on two factors i.e. AOS (Apparent Opening Size) of woven JGT and co-efficient of permeability of JGT with relation to average grain size distribution of bank soil and hydraulic conductivity of bank soil respectively. Empirical relations have been developed for man-made geotextiles, which have the advantage of yarn uniformity and dimensional stability. Considering features of jute fibers it is suggested that AOS of JGT should be allowed sufficient tolerance (say 15%) considering its lack of dimensional uniformity and for ‘hairiness’ of its yarns. Tensile strength of 20 kN/m of woven JGT is usually adequate for most river bank applications. Besides AOS of JGT, it is necessary to design the granular armor layer over JGT laid on the prepared bank slope to lend stability to the bank against uplift forces. It requires to be ensured that displacement of armor layer should be minimal and JGT should not turn into a plane of sliding. Vegetation will sprout through the interspaces of armor rock. It is important to point out that the selected woven JGT must be durable enough to last till the bank soil stabilizes to an acceptable degree. Bank erosion caused due to complex hydraulic milieu may take longer time for stabilization necessitating extended effective life of JGT. Bank soil may stabilize sufficiently if filtration is effective for at least two seasons usually. JGT remains unaffected for six months without treatment usually. Protective coating over it is therefore needed to enhance the fabric durability for at least three years. Such eco-friendly water-repellent protective coating is claimed to have been developed by IIT, Kharagpur and also by Indian Jute Industries’ Research Association, Kolkata. When bank soil propelled by pore water pressure tries to ease out of pores of the geotextile, larger particles form an arch-like configuration over JGT pores and restrain smaller particles from migrating. The process results in altered disposition of soil particles in bank soil and lends a state of compactness and



also effects of filter ('filter cake'). In reversing flow conditions, filter cake formation in bank soil is usually partial when the cycle time is too short to form a graded soil filter. In rapidly reversing flow conditions even partial filter cake formation in bank soil may not be attainable. In such conditions, granular filter is used in conjunction with JGT. Light weight JGT is adequate for unidirectional flow conditions, whereas thick GT should be suitable for rapidly reversing flow conditions. Research institutes in the west have developed separate empirical design criteria for synthetic geotextiles for river bank protection against erosion. On the basis of experience gained in more than fifty field applications with JGT for control of river bank erosion in India, the following empirical criteria are recommended for ensuring soil retention.

- If d_{40} is ≤ 0.06 mm, then O_{90} should be less than d_{90} , $10d_{50}$ and $300 \mu\text{m}$ separately
- If d_{40} is > 0.06 mm, then O_{90} should be less than $1.5 d_{10} U^{1/2}$, d_{50} and $500 \mu\text{m}$ separately (Sanyal 2016)

To fulfill permeability requirements the basis principle is that as long as the permeability of the geotextile (k_g) is greater than the permeability of the soil (k_s), the flow of water will not be impeded at the soil/geotextile interface. For practical applications, the following indicators may be adopted for JGT as recommended in Geotextiles & Geomembranes Manual (Ingold: 1994).

- If d_{40} is ≤ 0.06 mm, then $300 \mu\text{m} < O_{90} < 1500 \mu\text{m}$ and $5\text{mm} < t_{\text{JGT}} < 15$ mm
- If d_{40} is > 0.06 mm, then $500 \mu\text{m} < O_{90} < 2000 \mu\text{m}$ and $5\text{mm} < t_{\text{JGT}} < 20$ mm.

JGT acts as a drain allowing transmission of water along its plane (transmissivity). For JGT, if permittivity criteria are satisfied, transmissivity criteria are usually fulfilled. For survivability, JGT shall have the minimum average roll values (MARV) for armor layer as shown in Table 1 considering weight of individual stone about 50 kg with drop height of 1 m.

Table 1: MARV for Survivability of JGT

Sl. No.	Property	ASTM	Units	Values
1.	Wide Width tensile Strength	D 4595	kN/m	20
2.	Puncture Strength	D 4833	kN	400 ($\pm 10\%$)
3.	Burst Strength	D 3786	kPa	3100 ($\pm 10\%$)

To obviate probability of clogging and blocking of JGT, Gradient Ratio Test (GR Test) or Hydraulic Conductivity Test (HCR Test) as per ASTM-D 5567 or GR (Gradient Ratio) test as per ASTM-D5101-90 should be conducted

prior to deciding on the fabric porometry (AOS). Indian Standard IS: 14262:1995 (Planning & Design of Revetments-Guidelines) recommends the following regarding criteria for selection of geotextiles. For granular materials containing 50% or less fines by weight, the following relation is to be satisfied.

$$\frac{85\% \text{ passing size of bed material (mm)}}{\text{Equivalent opening size of fabric (mm)}} \geq 1.0$$

The said Standard also recommends that the minimum allowable opening size of the geotextile shall be 0.149 mm. When the bed material size is between 50% and 85% by weight, maximum allowable opening size of the geotextile should be 0.211 mm. If the bed material contains fines with more than 85% by weight, it is advisable to use non-woven geotextiles. However the recommendations require modification considering the fact that physical features of JGT and man-made geotextiles have inherent physical dissimilarities.

Design of riprap involves determination of thickness of pitching, weight and also diameter of individual boulders. The Standard published by Bureau of Indian Standards IS: 14262-1995 provides guidelines for determination of the said parameters. The aforesaid Indian Standard also presents a nomograph for calculation of the weight of stone.

Type of Jute Geotextile for Use in River Bank

Only woven treated JGT is to be used in river bank applications. Typical specifications of untreated woven JGT may be seen in Table 2 below. The grey JGT has to be smeared with a suitable eco-friendly water-repellent additive to enhance its durability.

Table 2: Typical Specification of Untreated/Grey Woven JGT

Nomenclature	Woven JGT 20 kN/m (Untreated)
Construction	1/1 DW Plain Weave
Weight (gsm) at 20% MR \geq	627
Width (cm) \geq	100
Ends \times Picks/dm \geq	85 \times 32
Thickness (mm at 2 kPa)	1.7 \pm 10%
Tensile Strength (kN/m) MD \times CD \geq	20 \times 20
Elongation at break (%) MD \times CD \geq	12 \times 12
Puncture Resistance (kN)	0.400 \pm 10%
Burst Strength (KPa)	3100 \pm 10%
Permittivity at 50 mm constant head (/sec)	350 $\times 10^{-3} \pm 10\%$
A O S (micron) O_{95}	150-400

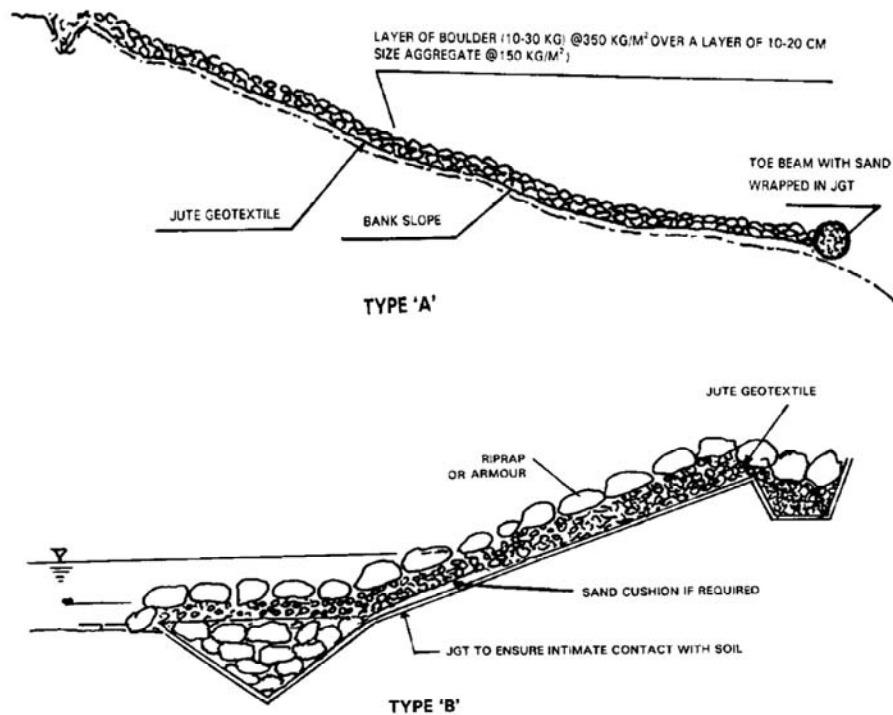


Fig. 1: Method of Installation of JGT on River bank

The specifications of woven JGT shown in Table 2 are supposed to satisfy the hydraulic design principles on permissible shear stress on the bank. Care should be taken to decide on the pore size of the fabric. Water-repellent treatment in all river-related applications is a must. For unidirectional waterways woven JGT with the above features may be adopted. In rivers with two-way flows (tidal rivers) it is advisable to use a heavier type JGT—say of weight 760 gsm which proved effective in a field application in the Hugli estuary. Overall stability of the bank with Jute Geotextiles may be checked with the help of any suitable software (say BSTEM Version 5.0) by inserting values of several critical bank-related and hydraulic parameters to determine the Factor of Safety.

Types of Vegetation for Soil-Bind

Geotextile supplements action of appropriate species of vegetation for binding bank-soil. Species of vegetation thus warrants careful selection considering the type of bank soil and salinity of river water which wets the bank. The critical factor in the choice of vegetation is the volume of its roots, the depth of its penetration in soil and its salt tolerance in the case of tidal rivers. Vetiver is considered the best choice in this regard for rivers with sweet water flow. Vetiver grass, a type of perennial grass with deep root system and tall densely tufted grass blades, could be the ideal species of

grass if the soil type and climatic conditions suit (Figure 2). The grass provides a cover on bank slope protecting it from direct impact of flow and helps moderate the velocity of flow. For tidal rivers the consideration should be on the range of salt-tolerance of the species. The ideal vegetation is mangroves which thrive in coastal regions. There are about 64 species of mangroves with varying limits of salt-tolerance. The range of salinity in the tidal river should therefore be considered before deciding on the mangrove species. Advice of agronomists/botanists will guide the planner to select the right type of mangrove. One striking feature of mangroves is that they have stilt roots which help in silt accretion when silt-laden water passes through them (Figure 3).



Fig. 2: Vetiver Grass



Fig. 3: Mangroves with Stilt Roots

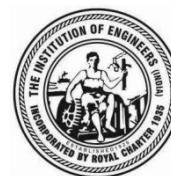
It has been the experience of the author in the Hugli estuary that silt accretion could sometimes exceed the growth-rate of some of the mangrove species. Therefore estimation of silt accretion on the bank vis-à-vis growth-rate of a species of mangrove has to be tested in simulated conditions before deciding on the species of mangroves. Mangroves will also help in attenuation of flow velocity. An intensive study on this aspect is needed for objective evaluation.

Conclusion

In developed countries such as the USA, Japan effectiveness of different types of vegetation in attenuation of fluvial velocity is being studied. Instead of spending huge sums on mining of rich mineral resources for river bank protection with the attendant pollution hazards, bio-engineering interventions as indicated is certainly worth trying. For this laboratory simulation studies should be taken up followed by field trials to lend a strong convincing scientific footing to the concept.

References

- [1] Bureau of Indian Standards: Guidelines for river bank protection with JGT: (IS 14715 Part II: 2016) Guidelines– Planning and Design of revetments (IS 14262: 1995).
- [2] Ingold, T.S. (1994). *Geotextiles and Geomembrane Manual*: 1st Ed: Oxford, Elsevier Science, UK.
- [3] Sanyal, T. (1992). A pilot project in Nayachar island in the river Hugli: Central Board of Irrigation & Power, New Delhi, January 1992 Publication.
- [4] Sanyal, T. and Chakravarty, K. (1993). Application of bitumen-coated Jute Geotextile in bank protection work in the Hugli estuary, *Geotextiles and Geomembranes*, UK.
- [5] Sanyal, T. and Khastagir, A.K. (2012). Preponderance of Jute as Geotextiles, *Geosynthetics Asia*, 2012 December, Bangkok, Thailand.
- [6] Sanyal, T. and Chakravarty, K. (1994). Performance evaluation of geotextile-Indicator of its viability in the river training measures in the Hugli estuary, *Proc. of 59th R & D Session of Central Board of Irrgn. & Power*, Vol. 2.
- [7] Sanyal, T., Das, M. and Khanra, S. (2016). Case Studies on Application of Jute Geotextiles for River Bank Protection, *Indian Journal of Geosynthetics and Ground Improvement*, Vol. 5, No. 2, July 2016.
- [8] Sanyal, T. (2016). *Jute Geotextiles and Their Application in Civil Engineering*, Book on Jute Geotextiles, Springer, Oct. 2016.



Development of Eco-Friendly and Sustainable Feminine Hygiene Products from Lignocellulosic Jute Fibre

S.N. Chattopadhyay^{*1}, R.K. Ghosh¹, S. Bhattacharyya² and S. Bhowmick¹

Abstract: Jute has multifarious uses in a variety of areas. However, the possibility of using jute as crucial components for health and hygiene products, particularly sanitary hygiene products has not been explored in details in India. Menstrual Hygiene is one of the prime health concerns at global levels at present. In India, the policy makers at the central as well as state levels have included this agenda in the public health programmes. According to a survey conducted by A.C. Nielson, only 12% of the Indian women use sanitary napkins. They mostly use cloth which exposes them to a variety of infections. One of the main reasons of low usage of napkins is high price which makes the beyond the affordable range. There are yet another group of manufacturers, the members of Self Help Groups (SHG) which have started manufacturing sanitary napkins using low cost technology. The smaller manufacturers also face some problems in procurement of raw materials, particularly the absorbent materials. NIRJAFT is engaged in development of absorbent raw materials from Jute for use in production of sanitary protection materials. The absorbent pulp which is mainly used for manufacturing sanitary napkins is wood pulp which is becoming a scare commodity as deforestation is punishable. There have been a number of attempts in India as well as outside to develop absorbent materials from various materials like banana fibre, water hyacinth etc. However, none of the materials have been promoted or marketed widely. Jute pulp as an absorbent material was developed keeping the above issues in mind. After development of the pulp, certain numbers of sanitary napkin packets were manufactured in two manufacturing units and the products were field tested in two locations with the objective of upgrade the quality of the jute pulp further. After preparation at the SHG manufacturing units, the napkins were evaluated. The tests were carried out using the following parameters as per specifications of Bureau of Indian Standards (BIS). With reference to the performance of the samples with respect to absorbance, retention of fluid, disposability after use, pH of the product, sensitivity to skin and microbiological susceptibility, the product is better than those available in the market. Moreover, the product prepared from virgin jute pulp is economic, hygienic and sustainable in character.

Keywords: Sanitary Napkins, Jute Pulp, Super Absorbent Polymer, Hygiene, Woodgel.

Introduction

Menstrual Hygiene is one of the prime health concerns at global levels at present [1–5]. In India, the policy makers at the central as well as at the state levels have included this agenda in the public health programmes. This has some reasons. According to a survey conducted by A.C. Nielson, only 12% of the Indian women use sanitary napkins [6]. They mostly use cloth which exposes them to a variety of infections [7]. One of the main reasons of low usage of napkins is high price which makes the beyond the affordable range. Another reason may be lack of availability in the remote and hard to reach areas. The napkins are mostly

manufactured by the big multinational Corporations like Johnson and Johnson, Kimberly Clarke, etc. However, there are some local companies which serve the niche market. There are yet another group of manufacturers, the members of Self Help Groups (SHG) which have started manufacturing sanitary napkins using low cost technology. The smaller manufacturers also face some problems in procurement of raw materials, particularly the absorbent materials.

However, availability of quality raw materials, particularly wood gel is a problem area especially for the small and SHG manufacturers. First of all, since both production capacity and market reach of the SHG manufacturers are limited, the

¹ Department of Chemical and Biochemical Processing, ICAR-National Institute of Research on Jute and Allied Fibre Technology, 12 Regent Park, Kolkata-700040, India. ✉ *sambhu_in@yahoo.com

² Fulcrum Consortium, Kolkata-700010, India.



procurement amount is not substantial. Therefore, the procurement price is on the higher side. Second and more importantly, most of the materials are 'seconds' or production rejects of the reputed companies. Third, none of suppliers of quality products are located in West Bengal. Most of them are either in Maharashtra or in Gujarat. This causes uncertainty in the supply schedule of raw materials. Most of the wood pulp used for the purpose is imported, and therefore expensive, increasing the overall cost of a sanitary napkin. Cotton is seen as a major fiber poised to replace wood pulp especially in the feminine hygiene products where less bulky is preferred and thinner is better. The high cost of cotton is the reason why it has not been able to replace pulp. The absorbent pulp which is mainly used for manufacturing sanitary napkins is wood. This is mixed with a chemical popularly known as Super Absorbent Polymer (SAP) which enhances the absorbency power of the pulp considerably. This mixed material, when comes in the contact of liquid (menstrual blood) takes a gel form and that is the reason why this is called 'wood gel'. There have been attempts to use alternative materials in place of wood gel. The materials include banana fibre, water hyacinth etc. in various parts of the world, mainly in the African countries. However, all these attempts have been carried out at a small level. There has been little or no attempt to scale up of these initiatives so that these materials can be used by a sizeable number of manufacturers as alternatives to wood gel. In view of scenario on availability of wood gel described in the section above, availability of similar absorbent material on the basis of locally available fibre materials would be immensely helpful. First of all, the materials will be virgin and will be free from impurities. Second, if production of pulp is encouraged, the timely supply will be assured and this will create another livelihood opportunity since jute is abundantly available in some districts of the state. Third, the price is expected to be lower than the wood gel. Jute being lignocellulosic in nature, is a very good alternative raw material for making pulp and several pulping methods have been developed [8–11]. Jute fibre consists of 60% α -cellulose which can be used to replace wood pulp and save our forests. Taking these factors into consideration it was thought that jute pulp cellulose can very well replace the imported and costly wood pulp. A sanitary napkin basically comprises of three layers; top layer, absorbent layer and barrier sheet. The absorbent layer is the key component of the napkin (cellulose pulp) and the extent to which this layer is able to absorb and retain the fluid determines the efficiency of the napkin. So, the pulps thus produced may be utilised for use as absorbent material for making sanitary napkins. In the present work some studies have been done for production of pulps by different methods and their utilisation as absorbent material. The process has been

optimized and evaluation of the final product was done with respect to performance, comfort and hygiene parameters. The quality of the developed product was compared using specified parameters with two major brands of sanitary napkins in the Indian markets. In order to conduct the survey, a structured questionnaire was prepared. The samples, along with a questionnaire were distributed in two locations. The main objective was to get a comparative assessment of the products used by them at present and the samples given to them for feedback. A detailed analysis of the feedback revealed that the samples prepared from jute pulp is equally good and sometimes better than the products used by them at present.

Materials and Methods

Materials

Jute fibre: Jute fibre of low quality was cut into 2–4 cm pieces and used for pulping.

Chemicals: The following chemicals of analytical grade were used in the experiment : sodium hydroxide, sodium silicate, trisodium phosphate, hydrogen peroxide, acetic acid, non-ionic detergent, super absorbent polymer (commercial grade), sodium carbonate, sodium sulphite, anthraquinone and methanol.

Methods

Pulping

1. High chemical, high temperature ASAM pulping-Jute fibres were treated in a solution containing sodium hydroxide (5%, owf), sodium sulphite (20%), anthraquinone (0.1%) and methanol (15%) using a liquor ratio of 1:12 for 3 hours at 160°C. The pulps were washed thoroughly after pulping.
2. Pulping with caustic, sulphite and anthraquinone at 160°C-Jute fibres were treated in a solution containing sodium hydroxide (5%, owf), sodium sulphite (20%) and anthraquinone (0.1%) using a liquor ratio of 1:12 for 3 hours at 160°C. The pulps were washed thoroughly after pulping.
3. Pulping with caustic, sulphite at 160°C-Jute fibres were treated in a solution containing sodium hydroxide (5%, owf) and sodium sulphite (20%) using a liquor ratio of 1:12 for 3 hours at 160°C. The pulps were washed thoroughly after pulping.
4. Pulping with caustic, sulphite and Methanol at 160°C-Jute fibres were treated in a solution containing sodium hydroxide (5%, owf), sodium sulphite (20%) and methanol (15%) using a liquor ratio of 1:12 for 3 hours at 160°C. The pulps were washed thoroughly after pulping.



5. Pulping with caustic, sulphite and anthraquinone by open cooking-Jute fibres were treated in a solution containing sodium hydroxide (5%, owf), sodium sulphite (20%) and anthraquinone (0.1%) using a liquor ratio of 1:12 for 3 hours at boil. The pulps were washed thoroughly after pulping.
6. Low chemical ASAM pulping at 115°C-Jute fibres were treated in a solution containing sodium hydroxide (1.2%, owf), sodium sulphite (5%), anthraquinone (0.1%) and methanol (5%) using a liquor ratio of 1:12 for 3 hours at 115°C. The pulps were washed thoroughly after pulping.

Bleaching of Pulp

All the pulps were bleached separately in a covered vessel using H₂O₂ (20 ml/l), trisodium phosphate (5 g/l), NaOH (1 g/l), sodium silicate (10 g/l) and nonionic detergent (2 g/l) at 1: 20 material to liquor ratio for 1.5 h at 90–95°C. The pH was maintained at around 10. The bleached pulp was washed in normal water and neutralized with dilute acetic acid (2 g/l) and was given a final wash for further processing.

Beating: All the pulps were subjected to beating separately in laboratory scale valley type beater for different durations to produce pulp of 40°SR freeness.

Preparation of Samples

The samples were manufactured using standard methods adopted by the SHG. The manufacturing mode was semi-manual with machines are used for grinding, pressing and sealing. Jute pulps were mixed with SAP, 2% on the weight of fibre and samples weighing 10gms were pressed under pressure of 100 kg/cm² to form mat of 20 cm × 7.5 cm × 1.5 cm. The samples were finally treated under U.V light.

Evaluation of Samples

Qualitative Fibre Analysis and Optical Properties

The diameters of the grey, pulped and pulped-bleached fibres were done using a light Microscope; the longitudinal view of the fibres was viewed under the microscope. The chemical composition of the jute fibre was done using standard procedure. The Whiteness Index in HUNTER scale, Yellowness Index in the ASTM D1925 scale and Brightness Index in TAPPI 452 scale of different pulps produced were determined by Spectrascan 5100 computerised colour matching system using relevant software.

Determination of pH

Determination of pH of Jute based sanitary napkin ingredients as per IS: 1390–1983 procedure. Each test

specimen is prepared by taking 2.0 ± 0.05 gms of sample in 100 ml of deionised water in to stoppered glass bottle. The flask was then agitated mechanically using a mechanical laboratory based agitator for 20 mins. Then pH was measured using pH paper (Merck, India), online pH meter (Eutech Instruments, Singapore), dipping electrode based pH meter (Mettler Toledo, USA).

Determination of Absorbency and Ability to withstand Pressure after Absorption.

This test was conducted as per the IS: 5405–1981. The time taken for the fluid to get completely absorbed by the napkin and the area of the spread of the fluid was noted. The sides and back of the napkin were observed for any fluid leaking through after placing a one kg weight on it.

Disposability

The disposability of the napkins was tested as per IS: 5405–1981. The napkin with the top and back covering removed was immersed in 15 liters of water and time taken to completely disperse in water was noted.

Results and Discussion

Jute being lignocellulosic in nature is an ideal raw material for pulping. The chemical composition of fibres were evaluated and tabulated in Table 1. The α-cellulose content of the fibre is maximum whereas lignin content is minimum.

Table 1: Chemical Composition of Jute Fibres

Raw Material	α-Cellulose	Hemicellulose	Holocellulose	Lignin
Jute fibre	66.6	19.8	86.4	12.6

The pulping of the fibres were carried out by the following methods:

1. High chemical, high temperature ASAM pulping
2. Pulping with caustic, sulphite and anthraquinone at 160°C
3. Pulping with caustic, sulphite at 160°C
4. Pulping with caustic, sulphite and methanol at 160°C
5. Pulping with caustic, sulphite and anthraquinone by open cooking
6. Low chemical ASAM pulping at 115°C.

All these pulps were bleached by hydrogen peroxide bleaching process. The yield of the pulps were evaluated at every steps along with optical properties of bleached pulp which are tabulated in Table 2.



Table 2: Effect of Different Pulping Methods on Yield and Optical Properties

Sample	Yield (%)	Whiteness Index	Yellowness Index	Brightness Index	K/S Value
A	57.20	88.27	11.28	68.71	0.09
B	57.95	85.79	12.78	69.90	0.10
C	60.8	81.19	16.58	61.40	0.18
D	61.8	80.09	25.23	61.07	0.28
E	80.75	82.42	17.58	60.40	0.19
F	71.44	79.43	23.83	57.23	0.31

Yield and appearance of the pulp is very important. Removals of non-cellulosic materials are maximum in case of high temperature and high chemical pulping resulting in lower yield. Whereas, in case of low chemical low temperature pulping and open cooking, weight loss is minimum and yield is very high. In all the cases whiteness and brightness obtained after bleaching is very good.

The diameters of the fibres were evaluated under microscope, they are as follows:

- grey fibre - 0.11 mm
- pulped fibre - 0.08 mm
- bleached pulp fibre - 0.06 mm

As the diameter of the fibre decreases, surface area of the bleached pulp fibre increases, this is needed for better absorption and retention of fluid. The disintegration of pulp was carried out in the laboratory which separates the individual fibres in the pulp and volume increases. This material is then mixed with super absorbent polymer (SAP) in mass mixture. The super absorbent pulp produced in the laboratory was taken to two NGO at Howrah, where sanitary napkins were produced.

- Sampriti Mahila Mahasangha. Amta, Howrah (NGO-1)
- Nari-O-Sishu Kalyan Kendra. Panchla, Howrah (NGO-2)

Sanitary napkins were prepared following the steps as mentioned below:

1. Weighing of 10 gm samples
2. Preparation of mat of 20 cm × 7.5 cm × 1.5 cm.
3. Compacting the mass using 100 kg/cm² pressure.
4. U.V. treatment of the sample.

All the samples produced from jute pulps (experimental samples), regular samples produced by two NGO's (NGO-1 and NGO-2) and two multinational product samples were evaluated for its absorbance and fluid retention properties and tabulated in Table 3.

From Table 3, it is clear that the all the samples produced from the jute pulp performs well and better than that obtained from commercial samples. All the commercial napkins as well as the napkin developed from jute pulp conformed to absorbency standards of BIS. 30 ml of test fluid flowed @15 ml/minute onto the samples was fully absorbed by all the napkins except one commercial sample. The time taken for the fluid to get completely absorbed ranged from 5 seconds to 30 seconds among the various brands. Positioning of the napkin was found to be a critical factor in observing leak-through property. With a slight shift in position of the flow point, from the centre towards the sides, some napkins tended to leak through the sides and the fluid showed up at the back. The study of pH of the pulps after mixing with SAP is important parameters. All the samples have been evaluated and have been tabulated in Table 4. It is found that the pH values of all the samples lie between 7 to 7.5. So, pH of all the samples was found to be within the range (6 to 8.5) suitable to the human skin.

Table 3: Comparative Study of Different Sanitary Napkins

Sample	Amount of SAP Added (%)	Quantity of Testing Liquid Added (ml)	Area Absorbed by Sanitary Napkin (after 2 min)	Area Absorbed by Sanitary Napkin (after putting 1 kg wt for 1 min)	Feeling of Upper Surface by Hand
A	2	15	4.5 cm × 5 cm	5 cm × 5.5 cm	Very good
B	2	30	6 cm × 6.5 cm	6.5 cm × 8 cm	Good
C	2	30	6 cm × 6.5 cm	6.5 cm × 8.5 cm	Moderate
D	2	30	6 cm × 7.5 cm	7 cm × 8.5 cm	Good
E	2	30	6.5 cm × 8 cm	7 cm × 10.5 cm	Good
F	2	30	7 cm × 10 cm	7 cm × 11 cm	Good
NGO-1	Unknown	30	7 cm × 8 cm	7 cm × 11 cm	Moderate
NGO-2	Unknown	30	6 cm × 7 cm	6 cm × 7.5 cm	Good
Carefree	Unknown	30	6.5 cm × 8 cm	7 cm × 9 cm	Moderate
Stayfree	Unknown	30	-	-	Very bad



Table 4: Determination of pH of Jute based Sanitary Napkin as per IS: 1390–1983 Procedure

Sample Code	pH Paper (Merck, India)	Online pH Meter (Eutech Instruments, Singapore)	Dipping Electrode Based pH Meter (Mettler Toledo, USA)
A	7	6.96	7.38
B	7	7.07	7.21
C	7.5	7.61	7.58
D	7	7.00	7.03
E	7.5	7.46	7.12
F	7.5	7.45	7.46
NGO-1	7	7.01	7.32
NGO-2	7	6.68	6.72
Carefree	7	7.08	7.01
Stayfree	7	7.21	7.58

Disposability in water was seen in less than 5 minutes for almost all regular type napkins, with fluff pulp as the middle layer. The middle layer of jute pulp napkin also dispersed in water within 5 minutes.

In order to conduct the survey, a structured questionnaire was prepared before the survey. The main objective was to get a comparative assessment of the products used by them at present and the samples given to them for feedback. The samples, along with a questionnaire were distributed in two locations. The girls were told to hand over the questionnaire after duly filling up their opinion on the sample napkins after use.

A number of samples has been prepared and distributed to end users in two locations:

1. Howrah–semi urban area
2. Purulia–Tribal dominated areas
3. Questionnaire has also been prepared and distributed with sanitary napkin sample pack.

One set of samples was distributed to 56 adolescent girls in Bauria, Howrah. All the girls were school students. The samples were distributed in a programme organized in the Nari O Shishu Shiksha Kendra. Another set of samples were given to 39 students in Bongabari, Purulia II Block, Purulia. The napkins prepared in Amta I was distributed in Purulia. The distribution took place in Sathi Production Centre, one of the first production centres of sanitary napkins in West Bengal.

Regarding performance of the sample napkins as compared to the napkins used at present, the findings bring out almost similar scenario for Howrah and Purulia. While 84% of

respondents in Howrah report that the sample napkins are better, this percentage in Purulia is slightly lower. This is clearly evident from Figure 1.

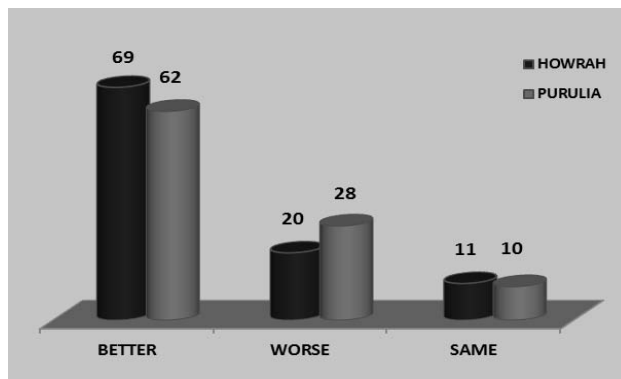


Fig. 1: Performance of the Sample Napkins vis-à-vis Napkins used at Present (%)

The finding on the absorbency power is in tune with the findings from earlier figure. While the majority of the respondents feel the absorbency power of the sample napkins is superior to the napkins used currently, the percentage is marginally lower in Purulia than in Howrah as depicted in Figure 2.

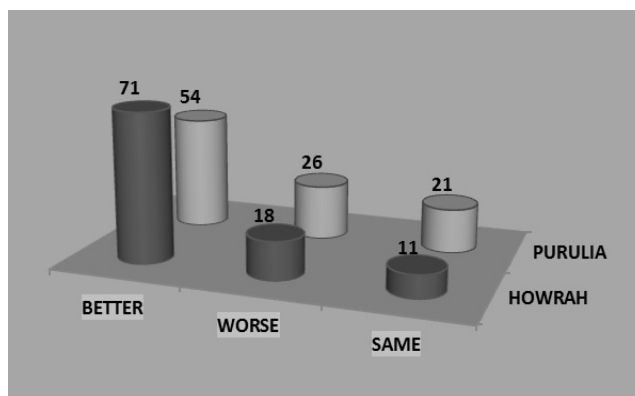


Fig. 2: Absorbency Power of the Sample Napkins (%)

Conclusion

- Pulps produced by Low Chemical ASAM process produce very white pulp after bleaching. The yield of the pulp and performance of the product is good.
- Pulping by open digestion following alkaline sulphite-anthraquinone process also produces good yield and white pulp after bleaching. The performance of the product produced from this pulp is also good.
- The performance of the product during field trial clearly shows that the sample prepared from jute pulp is preferred by most of the respondents.



References

- [1] Sommer, M. and Sahin, M., Overcoming the taboo: Advancing the global agenda for menstrual hygiene management for schoolgirls, *Am J Public Health*, 103,1556–1559 (2013).
- [2] Mahon, T. and Fernandes, M., Menstrual hygiene in South Asia: a neglected issue for WASH (water, sanitation and hygiene) programmes. *Gend Dev*, 18, 99–113 (2010).
- [3] Bodat, S., Ghate, M.M. and Majumdar, J.R., School absenteeism during menstruation among rural adolescent girls in Pune, *Natl J Community Med* 4, 212–216 (2013).
- [4] Sahin, M., Tackling the stigma and gender marginalization related to menstruation via WASH in schools programmes, *Waterlines*, 34, 3–6 (2015).
- [5] Anand, E., Singh, J. and Unisa, S., Menstrual hygiene practices and its association with reproductive tract infections and abnormal vaginal discharge among women in India, *Sex Reprod Healthc*, 6, 249–54 (2015)
- [6] Nielsen, A.C. *Plan India*. Sanitary protection: every woman's health right. New Delhi, India: Nielsen A.C., Plan India, 2010.
- [7] National Rural Health Mission, Ministry of Health and Family Welfare, Government of India. *Operational guidelines: promotion of menstrual hygiene among adolescent girls (10–19 years) in rural areas*. New Delhi, India: National Rural Health Mission, 2010.
- [8] Roy, A.K., Ghosh, I.N. and Chattopadhyay, S.N., A. Day, Jute an alternative raw material for rural based handmade paper unit, *Advances in Agro Processing and rural empowerment–Institution of Engineers, Kolkata*, 17–18 Feb. 2006.
- [9] Roy, A.K. and Chattopadhyay, S.N., Effect of accelerated ageing on paper from cold soda pulp of jute *IPPTA J*, 20(2) 81–83 (2008).
- [10] Roy, A.K., Chattopadhyay, S.N., Environment friendly pulping of jute, *IPPTA J*, 23(2), 197–199 (2011).
- [11] Roy, A.K., Chattopadhyay, S.N., Jute–An alternative Raw material for packaging Paper, *IPPTA J*, 24(3), 121–124, (2012).



Author Index

A

Adak, Asima	267
Aditya, G.	57
Agarwal, Madhu	293
Agarwal, S.C.	278
Agrawal, Kamalesh M.	73
Alam, M.	126
Arora, A.	233

B

Balaji, R.	132
Balasubramanian, V.	162
Basu, Nabanita	109, 115
Behara, Dilip Kumar	297
Belokar, R.M.	224
Bera, Supriya	274
Bhaskar, D.	87
Bhaskaran, E.	209
Bhattacharjee, K.	79
Bhattacharyya, Bidyut Kumar	215
Bhattacharyya, S.	328
Bhowmick, S.	328
Biswas, Jayanta K.	73
Brahma, N.K.	317

C

Chabri, Sumit	274
Chakraborty, S.	26, 32
Chandra, P. Sathees	187
Chatterjee, Arunava	149
Chatterjee, Debashis	149
Chattopadhyay, S.N.	328
Chaudhari, Nikhil	162
Chaudhuri, A.S.	122
Chaudhuri, B.	246, 258
Chaudhuri, Mahua Ghosh	267
Choubey, M.	79
Chowdhury, Amit Roy	274
Coumarane, M.	132

D

Dalai, A.K.	293
Das, Mitun	274
Das, Payel	171
Das, S.	252
De, R.K.	181
Debmallik, Pathik	38
Debmallik, Pramit	38
Debnath, A.	26
Dhara, Subhra	233

G

Ganguly, A.	181
Ganguly, R.I.	241
Ghosh, Anindya	171
Ghosh, D.	252
Ghosh, Mahua	311
Ghosh, R.K.	328
Ghosh, Soumyajit	149
Goyal, Akarsh	162
Gupta, A.	79
Gupta, Biman Gati	73
Gupta, Jharna	293
Gupta, Surashree Sen	311

I

Islam, T.	32
----------------	----

J

Jain, Ashok K.	141
Jalajakshi, T.	297
Jha, A.K.	79
Jha, S.K.	233
Jose, Shaji	187

K

Kandekar, S.B.	53
Kansal, Mitthan Lal	14
Karmakar, Samit	167
Kishore, Kumar Abhishek	14



Kishore, Nanda	303	Ramya, K.	132
Kolhe, S.B.	53	Rao, A. Narayana	43
Kumar, Prashant	14	Rao, G.S.	241
Kumar, R. Sai Kiran	198	Rao, K.M. Lakshmana	43
Kumar, Sanjeev	224	Ray, C.	32
Kumar, Shalendra	204	Ray, Pranab	258
Kumar, Vinod	193	Reddy, D. Madhurima	303
Kundu, Soumik Kumar	167	Reddy, G. Paavan Kumar	7
M		Reddy, K. Yella	7
Madhavi, M.	43	Reddy, L. Narayan	7
Maheswari, M. Sudha	297	Roy, M.K. Ghosh	69, 177
Maity, Shubhadeep	274	S	
Mazumder, S. Mitra	79	Samanta, A.K.	246
Mitra, S.K.	252	Sanyal, T.	323
Mitra, Sujata	95	Saraf, Rajendrakumar V.	63
Mondal, Debasish	136	Sarkar, Alope	158
Mukherjee, Siddhartha	267	Sarkar, Antariksha	215
Mukherjee, Soumya	267	Sarkar, Debashis	258
Mukherjee, Suchandra	171	Sarkar, Mili	167
Muthu, Gopal Sonai	95	Sarker, Goutam	99
N		Sharma, Amit	224
Nag, Amitava	105	Shil, Anupam	21
Nag, Sanjay	115	Singh, Alok Kumar	284
Naresh, K.	162	Singh, G.	87
P		Singh, Rajeev	284
Pal, Anindya	274	Sinha, Arijit	274
Pal, Arindrajit	105	Sinha, Ranjit	141
Panigrahi, M.K.	241	Sneha, Ch.	7
Patil, Ashish	3	Srinivas, J.	198
Patowary, D.J.	144	Subbaiah, K. Venkata	219
R		Sudhakar, K.	154
Rai, Prerna	204	Sukumaran, Sreenath	154
Rajalakshmi, N.	132	Suresh, Ch.	219
Raju, Ch.	219	T	
Raju, R.S.S.	241	Taki, G.S.	167
Ramarao, G.V.	57	Talikoti, R.S.	53
Rambabu, P.V.	57	Tiwari, K.N.	3
		Tomar, Anuj	193

Technical Volume

31st Indian Engineering Congress

Kolkata, December 15-18, 2016



The Institution of Engineers (India)

8 Gokhale Road, Kolkata 700 020

Ph : +91 (033) 2223-8311/14/15/16, 2223-8333/34, 4010-6299

Fax : +91 (033) 2223-8345

E-mail : technical@ieindia.org, iei.technical@gmail.com

Website : <http://www.ieindia.org>

ISBN 978-93-85926-15-0



Allied Publishers Pvt. Ltd.

visit us at: www.alliedpublishers.com